



Instytut Fizyki Jadrowej
im. Henryka Niewodniczańskiego Polskiej Akademii Nauk

HIGH-ENERGY FACTORIZATION,
TMD, off-shell amplitudes and nuclear effects.

defended by :
Etienne Blanco

Supervisor :
prof. dr. hab. Krzysztof Kutak

Secondary supervisor :
dr. hab. Piotr Kotko

November 2022

À mon parrain.

Acknowledgements

I'm extremely grateful to my supervisor Krzysztof Kutak for the opportunities he gave me to work on a broad range of topics, for his patience, his help and his valuable advices. I would like to extend my sincere thanks to Piotr Kotko for his guidance and patience throughout the duration of my Ph.D.

I would also like to thank Andreas van Hameren, Wiesław Płaczek, Martin Rohmoser, Alessandro Giachino, Hannes Jung, Aleksander Kusina, Konrad Tywoniuk, and Robert Straka, all the collaborators I had the pleasure to work with.

I also wish to thank Krzysztof Golec-Biernat for the fruitful discussions.

Many thanks to my friends and colleagues Tomoki, Rajeev, Gabriel, Souvik, Marcin, Sergii, and Stéphane.

Finally, special thanks to my family for their unwavering support.

Abstract

In this thesis, we explore the factorization of hadronic processes in heavy-ion collision at high energy with a focus on accounting for transverse momentum. This exploration is separated into three stages : the study of nuclear Transverse Momentum Dependant PDFs (nTMD), the presentation of a method to calculate gauge invariant off-shell amplitudes, and the study of jet evolution in Quark-Gluon Plasma (QGP), following Blaizot-Dominguez-Iancu-Mehtar-Tani (BDIM) equations.

In the first part, a set of nTMD has been obtained using the Parton Branching (PB) method (which solves the Dokshitzer-Gribov-Lipatov-Altarelli-Parisi (DGLAP) equation, keeping track of the transverse momentum during the evolution). It was the first lead (Pb) Transverse Momentum Dependant PDF (TMD) set obtained through this method. This set has been tested with the Monte-Carlo (MC) generator KATIE to reproduce CMS data for Drell-Yann Z -boson production (where k_T -factorization holds). It worked surprisingly well considering that the (off-shell) matrix elements were only calculated at tree level. This was also the occasion to test, in this context, nuclear effects and different factorization formulas (high energy, hybrid, collinear).

The method used to obtain the off-shell matrix elements is the focus of the next part. The auxiliary parton method is based on embedding the considered off-shell process into a larger one, on-shell, to guarantee gauge invariance and to benefit from our knowledge of on-shell amplitudes. Originally, it was developed for tree-level calculation only. In this thesis, one of the first steps to generalize the auxiliary parton method at loop-level has been done through the calculation of the one-loop amplitude for one off-shell-gluon and an arbitrary number of plus helicity gluons. Also, some of the difficulties related to the application of this method to other one-loop amplitudes were studied.

The last topic concerns the evolution of jet fragmentation functions (describing the energy and transverse momentum component of its constituents) in a dense medium, through the BDIM equation. These equations describe the jet energy loss through jet broadening and medium-induced splitting, accounting for gluons only and considering the medium static. We first developed several methods to solve the integrated BDIM before accounting for transverse momentum in branching. Finally, we have generalized the BDIM to account for quarks.

This thesis is based on the following publications :

- E. Blanco, A. van Hameren, H. Jung, A. Kusina, and K. Kutak, “ Z boson production in proton-lead collisions at the LHC accounting for transverse momenta of initial partons,” *Phys. Rev. D*, vol. 100, no. 5, p. 054023, 2019. DOI: [10.1103/PhysRevD.100.054023](https://doi.org/10.1103/PhysRevD.100.054023). arXiv: [1905.07331](https://arxiv.org/abs/1905.07331) [[hep-ph](#)]
- E. Blanco, A. van Hameren, P. Kotko, and K. Kutak, “All-plus helicity off-shell gauge invariant multigluon amplitudes at one loop,” *JHEP*, vol. 12, p. 158, 2020. DOI: [10.1007/JHEP12\(2020\)158](https://doi.org/10.1007/JHEP12(2020)158). arXiv: [2008.07916](https://arxiv.org/abs/2008.07916) [[hep-ph](#)]

- E. Blanco, K. Kutak, W. Placzek, M. Rohrmoser, and R. Straka, “Medium induced QCD cascades: broadening and rescattering during branching,” *JHEP*, vol. 04, p. 014, 2021. DOI: [10.1007/JHEP04\(2021\)014](https://doi.org/10.1007/JHEP04(2021)014). arXiv: [2009.03876](https://arxiv.org/abs/2009.03876) [hep-ph]
- E. Blanco, K. Kutak, W. Placzek, M. Rohrmoser, and K. Tywoniuk, “System of evolution equations for quark and gluon jet quenching with broadening,” *Eur. Phys. J. C*, vol. 82, no. 4, p. 355, 2022. DOI: [10.1140/epjc/s10052-022-10311-2](https://doi.org/10.1140/epjc/s10052-022-10311-2). arXiv: [2109.05918](https://arxiv.org/abs/2109.05918) [hep-ph].

The more general topics in this thesis are based on the following textbooks :

- F. Halzen and A. D. Martin, *Quarks and Leptons: An Introductory Course in Modern Particle Physics*. 1984, ISBN: 978-0-471-88741-6
- Y. V. Kovchegov and E. Levin, *Quantum chromodynamics at high energy*. Cambridge University Press, Aug. 2012, vol. 33, ISBN: 978-0-521-11257-4. DOI: [10.1017/CB09781139022187](https://doi.org/10.1017/CB09781139022187)
- H. Nastase, *Classical Field Theory*. Cambridge University Press, Mar. 2019, ISBN: 978-1-108-47701-7
- M. D. Schwartz, *Quantum Field Theory and the Standard Model*. Cambridge University Press, Mar. 2014, ISBN: 978-1-107-03473-0

Moreover, the following theses were highly useful :

- M. Bury, “Phenomenology of transverse-momentum dependent factorizations in hadronic collisions,” Ph.D. dissertation, IFJ-PAN, 2020
- F. Van der Veken, “Wilson lines : applications in QCD,” Ph.D. dissertation, Antwerp U., 2014
- A. Lelek, “Determination of TMD parton densities from HERA data and application to pp processes,” Ph.D. dissertation, Hamburg U., Hamburg, 2018. DOI: [10.3204/PUBDB-2018-02949](https://doi.org/10.3204/PUBDB-2018-02949)
- V. Vila Perez, “Jet quenching and heavy ion collisions,” Ph.D. dissertation, Santiago de Compostela U., 2020
- M. De Angelis, “QCD Evolution At Amplitude Level,” Ph.D. dissertation, The University of Manchester, 2021.

Streszczenie

W niniejszej rozprawie badamy faktoryzację procesów hadronowych w wysokoenergetycznych zderzeniach hadronów, ze szczególnym uwzględnieniem pedu poprzecznego. Praca jest podzielona na trzy etapy : badanie n TMDs, przedstawienie metody otrzymywania amplitud poza powłoką masy amplitud niezmienniczych ze względu na cechowanie oraz badanie ewolucji dżetów w QGP, zgodnie z równaniami BDIM.

W pierwszej części otrzymano rozkłady n TMD metoda PB. Był to pierwszy zestaw rozkładów partonowych (Pb) TMD uzyskany tą metodą. Ten rozkład partonów został użyty z generatorem MC KATIE w celu opisu danych CMS na produkcję bozonów Z Drell-Yann (gdzie zachodzi faktoryzacja k_T). Działało to zaskakująco dobrze, biorąc pod uwagę, że elementy macierzowe poza powłoką masy były obliczane tylko na poziomie drzewiastym. Była to również okazja do oszacowania efektów jądrowych i różnych wzorów faktoryzacji (faktoryzacja wysokoenergetyczna, hybrydowa, kolinearna).

Technika obliczeń elementów macierzowych poza powłoką masy jest tematem kolejnego rozdziału. Metoda partonów pomocniczych opiera się na wprowadzeniu rozważanego procesu poza powłoką masy w większym procesie na powłoce masy, aby zagwarantować niezmiennosć cechowania i skorzystać z szerokiej wiedzy o amplitudach na powłoce masy. Pierwotnie ta metoda została opracowana do obliczeń na poziomie drzewiastym. W przedstawionej pracy jeden z pierwszych kroków w celu uogólnienia metody partonów pomocniczych na poziomie petli został wykonany przez obliczenie amplitudy jedno-petlowej dla jednego gluonu poza powłoką masy i dowolnej liczby gluonów o dodatniej skretności. Analizowano również możliwość zastosowania tej metody do otrzymania innych amplitud jednopetlowych.

Ostatni temat dotyczy ewolucji funkcji fragmentacji dżetu (opisujących rozkład energii i pedu poprzecznego jego składowej) w gestym ośrodku, z wykorzystaniem równania BDIM. Równania te opisują utratę energii dżetu przez oddziaływanie dżetu z plazmą oraz rozszczepienie wywołane przez ośrodek, biorąc pod uwagę tylko gluony oraz zakładając że plazma jest statyczna. W pierwszym kroku opracowaliśmy kilka metod rozwiązywania równania BDIM, zanim rozważyliśmy ped poprzeczny w funkcjach rozszczepień. Na etapie końcowym uogólniliśmy równanie BDIM, aby uwzględnić wkład kwarków do ewolucji.

Niniejsza praca opiera się na następujących publikacjach :

- E. Blanco, A. van Hameren, H. Jung, A. Kusina, and K. Kutak, “ Z boson production in proton-lead collisions at the LHC accounting for transverse momenta of initial partons,” *Phys. Rev. D*, vol. 100, no. 5, p. 054023, 2019. DOI: [10.1103/PhysRevD.100.054023](https://doi.org/10.1103/PhysRevD.100.054023). arXiv: [1905.07331](https://arxiv.org/abs/1905.07331) [[hep-ph](#)]
- E. Blanco, A. van Hameren, P. Kotko, and K. Kutak, “All-plus helicity off-shell gauge invariant multigluon amplitudes at one loop,” *JHEP*, vol. 12, p. 158, 2020. DOI: [10.1007/JHEP12\(2020\)158](https://doi.org/10.1007/JHEP12(2020)158). arXiv: [2008.07916](https://arxiv.org/abs/2008.07916) [[hep-ph](#)]

- E. Blanco, K. Kutak, W. Placzek, M. Rohrmoser, and R. Straka, “Medium induced QCD cascades: broadening and rescattering during branching,” *JHEP*, vol. 04, p. 014, 2021. DOI: [10.1007/JHEP04\(2021\)014](https://doi.org/10.1007/JHEP04(2021)014). arXiv: [2009.03876](https://arxiv.org/abs/2009.03876) [hep-ph]
- E. Blanco, K. Kutak, W. Placzek, M. Rohrmoser, and K. Tywoniuk, “System of evolution equations for quark and gluon jet quenching with broadening,” *Eur. Phys. J. C*, vol. 82, no. 4, p. 355, 2022. DOI: [10.1140/epjc/s10052-022-10311-2](https://doi.org/10.1140/epjc/s10052-022-10311-2). arXiv: [2109.05918](https://arxiv.org/abs/2109.05918) [hep-ph].

Bardziej ogólne tematy w tej pracy oparte są na następujących podręcznikach :

- F. Halzen and A. D. Martin, *Quarks and Leptons: An Introductory Course in Modern Particle Physics*. 1984, ISBN: 978-0-471-88741-6
- Y. V. Kovchegov and E. Levin, *Quantum chromodynamics at high energy*. Cambridge University Press, Aug. 2012, vol. 33, ISBN: 978-0-521-11257-4. DOI: [10.1017/CB09781139022187](https://doi.org/10.1017/CB09781139022187)
- H. Nastase, *Classical Field Theory*. Cambridge University Press, Mar. 2019, ISBN: 978-1-108-47701-7
- M. D. Schwartz, *Quantum Field Theory and the Standard Model*. Cambridge University Press, Mar. 2014, ISBN: 978-1-107-03473-0

Ponadto bardzo przydatne okazały się następujące tezy :

- M. Bury, “Phenomenology of transverse-momentum dependent factorizations in hadronic collisions,” Ph.D. dissertation, IFJ-PAN, 2020
- F. Van der Veken, “Wilson lines : applications in QCD,” Ph.D. dissertation, Antwerp U., 2014
- A. Lelek, “Determination of TMD parton densities from HERA data and application to pp processes,” Ph.D. dissertation, Hamburg U., Hamburg, 2018. DOI: [10.3204/PUBDB-2018-02949](https://doi.org/10.3204/PUBDB-2018-02949)
- V. Vila Perez, “Jet quenching and heavy ion collisions,” Ph.D. dissertation, Santiago de Compostela U., 2020
- M. De Angelis, “QCD Evolution At Amplitude Level,” Ph.D. dissertation, The University of Manchester, 2021.

Contents

Abstract	iii
Acronyms	xiii
1 Introduction	1
1.1 QCD basics	2
1.2 QCD Lagrangian	3
1.3 QCD running constant	5
1.4 Quark model	7
1.5 Parton model	7
1.6 Factorization	9
1.7 Conciliate calculations and experimental data	12
2 Parton Distribution Function	16
2.1 Deep Inelastic Scattering	18
2.2 Collinear Parton Distribution Function	24
2.3 Transverse Momentum Dependant PDF	31
2.4 Saturation	38
2.5 The Parton Branching method	40
2.6 Nuclear PB-TMD phenomenology	45
2.7 Chapter summary	61
3 Amplitudes	62
3.1 On-shell amplitudes	64
3.2 Gauge invariant off-shell amplitudes	97
3.3 Results	110
3.4 Loop-level hybrid factorization	120
3.5 Chapter summary	121
4 Jets in heavy ion collisions	123
4.1 Jet physics	125
4.2 BDMPS-Z formalism	131
4.3 BDIM equations	143
4.4 Resolution of the BDIM equations	154

4.5	Solutions of the BDIM equations	174
4.6	Chapter summary	192
5	Conclusion and outlook	194
A	Appendices related to Parton Distribution Functions	196
A.1	Light-cone perturbation theory	196
A.2	Splitting functions	202
A.3	DGLAP solution through Mellin transform	210
B	Appendices related to amplitudes	213
B.1	QCD Feynman rules	213
B.2	Colored ordered QCD Feynman rules	215
B.3	Dirac equation	216
B.4	$\bar{q}qg\gamma$ – detailed calculation	217
B.5	Master integrals	219
B.6	5-point amplitude – detailed calculation	222
B.7	On-shell limit calculation	225
C	Appendices related to jet quenching	228
C.1	BDIM solved with Chebyshev method : Code in details	228
C.2	BDIM solutions, different approaches comparison	238

List of Figures

1.1	The six flavors of quarks.	2
1.2	The running constant of QCD.	6
1.3	$udsc$ spin $\frac{1}{2}$ and $\frac{3}{2}$ Baryons.	8
1.4	$udsc$ pseudoscalar (spin 0, odd parity) and vector (spin 1, odd parity) Mesons.	8
1.5	PDF of the different partons in the proton.	9
1.6	Structure function for different models of proton.	10
1.7	Artist's view of the proton structure.	11
1.8	Representation of a collision event.	13
1.9	Collision vent in the CMS detector.	14
2.1	e^-p^+ deep inelastic scattering.	18
2.2	Diagrammatic representation of DIS cross-section with separation of the contribution to the leptonic tensor and to the hadronic tensor.	21
2.3	Virtual photon-proton scattering.	22
2.4	Diagrammatic representation of the quark and gluon PDFs.	25
2.5	Collinear factorization.	27
2.6	1st order real correction to the quark PDF.	28
2.7	Ladder diagram describing DGLAP evolution.	31
2.8	Ladder diagram describing DLA DGLAP evolution.	32
2.9	Illustration of the DGLAP evolution equation.	32
2.10	Ladder diagram describing BFKL evolution.	34
2.11	The Reggeized gluon.	34
2.12	Lipatov vertex.	35
2.13	Illustration of the BFKL evolution equation.	35
2.14	Ladder diagram describing CCFM evolution equation.	38
2.15	Illustration of the dipole model.	39
2.16	Evolution equations in the $\ln \frac{1}{x}, \ln Q^2$ plane.	40
2.17	Illustration of the Parton-Branching iteration solution.	43
2.18	Branching $j \rightarrow i + k$	44
2.19	EPPS16 fit of the nuclear modification $R_{i/A}(x, \mu_0^2)$	47
2.20	Comparison of the nuclear modification $R_{i/A}(x, \mu_0^2)$ obtained in nCTEQ15 and EPPS16.	48

2.21	x distribution obtained by integration over k_{\perp} of Parton-Branching TMDs.	50
2.22	x distribution of the up quark from nCTEQ15 and by integration over k_{\perp} of PB-nCTEQ15FullNuc_208_82.	51
2.23	x distribution of gluons at fixed k_{\perp} from Parton-Branching TMDs.	52
2.24	x distribution of up quarks at fixed k_{\perp} from Parton-Branching TMDs.	53
2.25	k_{\perp} distribution of gluons at fixed x from Parton-Branching TMDs.	54
2.26	k_{\perp} distribution of up quarks at fixed x from Parton-Branching TMDs.	55
2.27	k_{\perp} distribution of the up quark with the uncertainties of PB-nCTEQ15-FullNuc_208_82.	56
2.28	Comparison of y^* and p_t distributions using different TMDs Set.	57
2.29	Comparison of y^* and p_t distributions using different TMDs.	57
2.30	Uncertainties of y^* and p_t distributions for PB-nCTEQ15FullNuc_208_82.	58
2.31	y^* and p_t distributions for PB-nCTEQ15FullNuc_208_82 when varying scale.	59
2.32	Comparison of y^* and p_t distributions for PB-nCTEQ15FullNuc_208_82 for different scales.	59
2.33	Comparison of y^* and p_t distributions for PB-nCTEQ15FullNuc_208_82 for different factorization schemes.	60
3.1	Diagrams from the first terms of the perturbative series of $\mathcal{A}_{gg \rightarrow gg}$.	65
3.2	Diagrammatic representation of the equations leading to color ordering.	67
3.3	Diagrammatic representation of the color decomposition of a Feynman diagram contributing to $gggg$.	68
3.4	Diagrammatic representation of the factorization of an amplitudes when two of its legs become collinear.	79
3.5	Diagrammatic representation of the factorization of an amplitudes when a gluon leg becomes soft.	81
3.6	Diagrammatic representation of the Berends-Giele recursion on off-shell currents.	82
3.7	Diagrammatic representation of the Britto-Cachazo-Feng-Witten (BCFW) recursion.	85
3.8	Master integrals.	90
3.9	Path used when performing a Wick rotation.	91
3.10	Unitarity cut of a one-loop amplitude.	93
3.11	Color-order gluonic amplitude with one off-shell leg $A(1^*, 2, \dots, n)$. The crossed circle represents the eikonal coupling.	102
3.12	Diagrammatic representation of the Slavnov-Taylor identity.	102
3.13	Application of the Slavnov-Taylor identity to amplitudes with one off-shell leg contracted with eikonal vertex.	103
3.14	Gauge restoring term calculation.	104
3.15	Scheme of the Λ -prescription : calculation of an off-shell amplitude from an on-shell one with auxiliary gluons.	105
4.1	Jets obtained by several jet algorithms : SIScone, Cambridge/Aachen, k_t and anti- k_t .	129

4.2	Back to back dijet event from CMS in pp collision and in PbPb collision. .	130
4.3	The QCD phase diagram.	130
4.4	BDMPS-Z energy spectrum.	132
4.5	Illustration of the 2-point function $S^{(2)}$	135
4.6	Illustration of the $1 \rightarrow 2$ in-medium amplitude and its complex conjugate. .	137
4.7	Illustration of the 3-point function $S^{(3)}$	140
4.8	Analytical solution $\sqrt{x}D_a(x, \tau)$	156
4.9	Comparison of results obtained with the Chebyshev method for the simplified BDIM equation with its analytical solution.	168
4.10	Comparison of results obtained with the Chebyshev method for the integrated BDIM equation with its simplified version.	169
4.11	Comparison of results obtained with the Chebyshev method for different time steps.	169
4.12	Comparison of results obtained with the Chebyshev method for different cutoff.	170
4.13	Comparison of results obtained with the Chebyshev method for different numbers of nodes.	171
4.14	Solutions of the integrated BDIM equation obtained with the Chebyshev method for a jet initiated by a gluon.	174
4.15	Solutions of the integrated BDIM equation obtained with the Chebyshev method for a jet initiated by a quark.	175
4.16	Solution of the integrated BDIM equation for gluons dominated cascade .	177
4.17	Comparison of the energy distribution of the BDIM equation to the one of the simplified case.	177
4.18	Comparison of the energy distribution of the BDIM equation for several models.	178
4.19	2D transverse momentum distribution (k_x, k_y) of the solution of the BDIM equation for gluons.	179
4.20	2D transverse momentum distribution (k_x, k_y) of the Gaussian approximation.	180
4.21	The k_T distributions for different kernels.	181
4.22	The $\langle k_T \rangle$ vs. $\log_{10} x$ distributions for different kernels.	182
4.23	The k_T distributions for different \hat{q} and different kernels.	183
4.24	2D distribution in the (x, k_T) of the solutions of the BDIM equations. . .	184
4.25	The $\sqrt{x}D(x, t)$ distributions for cascades initiated by a gluon or a quark. .	184
4.26	The $\tilde{D}(k_T, t)$ distributions for cascades initiated by a gluon or a quark. . .	185
4.27	The gluon and quark k_T vs. x distributions for cascades initiated by gluons. .	186
4.28	The gluon and quark k_T vs. x distributions for cascades initiated by quarks. .	187
4.29	The average transverse momentum $\langle k_T \rangle$ versus $\log_{10} x$	188
4.30	Energy in cone for an initial gluon jet and an initial quark jet.	189
4.31	Time evolution of the jet energy in a fixed cone for an initial gluon jet and an initial quark jet.	190
4.32	The $\sqrt{x}D(x, t)$ distributions for cascades initiated by a gluon or a quark. .	191

4.33	The $\tilde{D}(k_T, t)$ distributions for cascades initiated by a gluon or a quark. . .	191
4.34	Dijet energy imbalance in function of the jet angle Θ for back-to-back gluon jets, back-to-back quark jets and for the Gaussian approximation in gluon dominated cascade.	193
A.1	Diagrams contributing to P_{qq}	203
A.2	Diagram contributing to P_{gq}	206
A.3	Diagram contributing to P_{qg}	207
A.4	Diagrams contributing to P_{gg}	208
A.5	1st order real correction to the quark PDF	209
B.1	Master integrals.	220
C.1	Comparison of energy distributions obtained with MINCAS, TMDICE and the Chebyshev method.	239
C.2	Comparison of transverse momentum distribution obtained with the MINCAS and TMDICE.	240

Acronyms

\overline{MHV} Maximally helicity violating bar

AMY Arnold-Moore-Yaffe

ASW Armesto-Salgado-Wiedemann

BCFW Britto-Cachazo-Feng-Witten

BCJ Bern-Carraso-Johanson

BDIM Blaizot-Dominguez-Iancu-Mehtar-Tani

BDMPS-Z Baier-Dokshitzer-Mueller-Peigne-Schiff Zakharov

BFKL Balitsky-Fadin-Kuraev-Lipatov

BK Balitsky-Kovchegov

CCFM Catani-Ciafaloni-Fiorani-Marchesini

CGC Color-Glass Condensate

CMS Compact Muon Solenoid

CSS Collins-Soper-Sterman

DGLAP Dokshitzer-Gribov-Lipatov-Altarelli-Parisi

DIS Deep Inelastic Scattering

DLA Double Logarithmic Approximation

DY Drell-Yann

FF Fragmentation Function

GLR Gribov-Levin-Ryskin

GLV Gyulassy-Levai-Vitev

HT Higher-Twist

IMF Infinite Momentum Frame

IR Infra-Red

JIMWLK Jalilian-Marian, Iancu, McLerran, Weigert, Leonidov and Kovner

LCPT Light Cone Perturbation Theory

LHC Large Hadron Collider

LLA Leading Logarithmic Approximation

LO Leading Order

MC Monte-Carlo

MCMC Markov Chain Monte-Carlo

MHV Maximally helicity violating

NLO Next to Leading Order

NMHV Next to MHV

nPDF nuclear Parton Distribution Function

nTMD nuclear Transverse Momentum Dependant PDF

p.d.f Probability Distribution Function

PB Parton Branching

PDF Parton Distribution Function

PLM Lando-Pomeranchuk-Migdal

pQCD perturbative QCD

QCD Quantum Chromodynamics

QED Quantum Electrodynamics

QFT Quantum Field Theory

QGP Quark-Gluon Plasma

SIDIS Semi-Inclusive Deep Inelastic Scattering

SM Standard Model

TMD Transverse Momentum Dependant PDF

uPDF unintegrated Parton Distribution Function

UV Ultra-Violet

Chapter 1

Introduction

The [Standard Model \(SM\)](#), as formulated in the 70s, has been successfully used to describe 3 (out of 4) fundamental interactions : the electromagnetism, the weak interaction, and the strong interaction (the two first can be even merged into the electroweak interaction). While it leads to precise predictions, it has some failures : it doesn't explain baryon asymmetry (imbalance between matter and anti-matter), it can't fully incorporate the theory of gravitation, there is no candidate to dark matter within the SM and it doesn't account for the neutrino masses (among other considerations). Then, it seems natural to look beyond the standard model physics. But this needs a great understanding of the interaction it describes, meaning high precision predictions. This is particularly true in high energy collisions that we have access to at [Large Hadron Collider \(LHC\)](#) CERN where we need a precise understanding of the strong interaction and the related sector of the standard model : [Quantum Chromodynamics \(QCD\)](#). This complex branch of the Standard Model is the focus of the work presented here. This introductory chapter intends to bring the basics of QCD needed to position the works presented in further chapters.

Remark : In the present discussion, we consider natural units i.e $\hbar = c = 1$.

Contents

1.1	QCD basics	2
1.2	QCD Lagrangian	3
1.3	QCD running constant	5
1.4	Quark model	7
1.5	Parton model	7
1.6	Factorization	9
1.7	Conciliate calculations and experimental data	12

1.1 QCD basics

QCD describes the physics of quarks and gluons. Those are constituents of what we call hadrons (such as protons or neutrons, among others). The quarks are charged spin $\frac{1}{2}$ fermions, carrying a fraction of the elementary charge (charge of the electron) equal to either $+\frac{2}{3}$ (up type quarks) or $-\frac{1}{3}$ (down type quark) and antiquarks carry opposite charge. There is a total of $N_f = 6$ flavors of quarks arranged in 3 generations, as shown in Fig. 1.1 (modified from [14]), each generation gathering a down type and an up type quark of same mass scale. The 1st generation of quarks (up and down), the lightest, are present in ordinary matter (forming protons and neutrons for instance) while the other generations form unstable particles which decay to hadrons made of 1st generation quarks.

mass	2.4 MeV/c ²	1.27 GeV/c ²	171.2 GeV/c ²
charge	$\frac{2}{3}$	$\frac{2}{3}$	$\frac{2}{3}$
spin	$\frac{1}{2}$	$\frac{1}{2}$	$\frac{1}{2}$
	u	c	t
	up	charm	top
	4.8 MeV/c ²	104 MeV/c ²	4.2 GeV/c ²
	$-\frac{1}{3}$	$-\frac{1}{3}$	$-\frac{1}{3}$
	$\frac{1}{2}$	$\frac{1}{2}$	$\frac{1}{2}$
	d	s	b
	down	strange	bottom
	1st generation	2nd generation	3rd generation

Figure 1.1: The six flavors of quarks (modified from [14]).

Gluons are spin 1 gauge bosons of the strong interaction (they are massless and electrically neutral). Actually, the strong interaction happens between what we call color charges (hence the name “*chromodynamics*”). They are named this way because adding the 3 different color charges (so-called red, blue, and green) nullifies the color charge (like for the primary colors in additive mixing), leaving a colorless state (white in the same terminology). There are also 3 anti-colors, that have the same behavior (adding all three leaves a null color charge) and that also cancel their equivalent color charge (for instance, red and anti-red nullify each other).

1.2 QCD Lagrangian

To be precise, QCD is a Quantum Field Theory (QFT), a non-abelian gauge theory ($SU(3)$ Yang-Mills theory) that is described by the following Lagrangian density [15] :

$$\begin{aligned}\mathcal{L}_{QCD} &= \sum_f \bar{\psi}_i^f(x) [i\gamma^\mu D_\mu - m_f]_{ij} \psi_j^f(x) - F_{\mu\nu}^a F^{a\mu\nu}, \\ \text{with : } D_\mu &= \partial_\mu - ig_s t^a A_\mu^a \\ F_{\mu\nu} &= \frac{i}{g_s} [D_\mu, D_\nu] = \partial_\mu A_\nu^a - \partial_\nu A_\mu^a + g_s f^{abc} A_\mu^b A_\nu^c,\end{aligned}\tag{1.1}$$

where ψ_q^f ($\bar{\psi}_q^f$) are the (anti-)quark Dirac fields (of flavor f , mass m_f and color i), A_μ^a is the gluon field (of color index a in the adjoint representation), $F_{\mu\nu}$ is the gluon field strength tensor, D_μ is the covariant derivative, f^{abc} are the structure constants of $SU(3)$ and t^a its generators, g_s the coupling constant of QCD and γ^μ are the Dirac gamma matrices that satisfy the anti-commutation relation :

$$\{\gamma^\mu, \gamma^\nu\} = 2\eta^{\mu\nu},\tag{1.2}$$

where $\eta^{\mu\nu}$ is the metric tensor for which we will adopt the ‘‘mainly -’’ convention $\eta^{\mu\nu} = \text{diag}(1, -1, -1, -1)$. To see more easily the interactions encoded in the Lagrangian in Eq. (1.1), let’s expand it :

$$\begin{aligned}\mathcal{L}_{QCD} &= \sum_f \bar{\psi}_i^f(x) [i(\not{\partial} - ig_s t^a A^a) - m_f]_{ij} \psi_j^f(x) \\ &\quad - \frac{1}{4} (\partial_\mu A_\nu^a - \partial_\nu A_\mu^a) (\partial_\mu A_\nu^a - \partial_\nu A_\mu^a) \\ &\quad + g_s f^{abc} (\partial_\mu A_\nu^a) A^{b,\mu} A^{c,\nu} - \frac{g_s^2}{4} f^{abc} f^{ade} A^{b,\mu} A^{c,\nu} A_\mu^d A_\nu^e,\end{aligned}\tag{1.3}$$

where we adopted the notation, for any tensor O^μ , $\not{O} = \gamma^\mu O_\mu$. From this formulation, we see the following interactions :

- the quark-antiquark gluon vertex, coming from the 2nd term in the bracket in the 1st line. It describes quark-antiquark annihilation (or creation) similar to the electron-positron photon vertex in Quantum Electrodynamics (QED).
- the triple and quadruple gluon vertices in the 3rd line. This implies that, contrary to the photon, the gluon self-interacts.

To be complete, we need to add some terms to the Lagrangian Eq. (1.1). This Lagrangian is invariant under local gauge transformations [16] :

$$\begin{aligned}\forall i, f, \psi_j^f(x) &\rightarrow U(x) \psi_j^f(x) \\ \forall i, f, \bar{\psi}_j^f(x) &\rightarrow \bar{\psi}_j^f(x) U^{-1}(x) \\ t^a A_\mu^a &\rightarrow U(x) t^a A_\mu^a U^{-1}(x) + \frac{i}{g_s} (\partial_\mu U(x)) U^{-1}(x), \\ \text{with } U(x) &= e^{ig_s t^a \theta^a(x)} \text{ and } \theta \text{ an arbitrary real function.}\end{aligned}\tag{1.4}$$

Also, this leads to an indetermination of the gluon propagator (as the term in the second line of Eq. (1.3) cannot be inverted to obtain it). This comes from the fact that A_μ^a is not uniquely defined. To solve this problem, we need a gauge fixing term in the Lagrangian [17] :

$$\mathcal{L}_{gauge-fixing} = -\frac{1}{\xi}(\partial^\mu A_\mu^a)^2. \quad (1.5)$$

By fixing ξ , we fix the gauge. Usual choices are :

- $\xi = 1$, the Feynman gauge,
- $\xi = 0$, the Lorentz gauge,
- $\xi \rightarrow \infty$, the unitarity gauge.

Due to the self-interaction of the gluon field, such gauge fixing (that is covariant) has to be accompanied by the inclusion (in a gauge invariant way) of some unphysical particles to compensate for unphysical propagation modes of the gluons. These particles are the Faddeev-Popov ghosts [18] (and anti-ghosts), described by the anticommuting Lorentz scalar fields c^a and \bar{c}^a . They are added to the Lagrangian through the term :

$$\mathcal{L}_{ghost} = (\partial_\mu \bar{c}^a) \left(\delta^{ac} \partial_\mu + g_s f^{abc} A_\mu^b \right) c^c. \quad (1.6)$$

Actually, the inclusion of the ghost fields can be avoided using a non-covariant gauge condition (at the price of the Lorentz invariance). *Axial gauge* is such a gauge :

$$n^\mu A_\mu^a = 0, \quad (1.7)$$

with an arbitrary (non-zero) 4-vector n^μ . Then, the gauge fixing term reads :

$$\mathcal{L}_{axial} = -\frac{1}{2\xi}(n^\mu A_\mu^a)^2. \quad (1.8)$$

The specific choice of n^μ set light-like ($n^2 = 0$), is named *light cone gauge*.

This Lagrangian (and then QCD) can be approached in several ways. Lattice QCD solve QCD by formulating it on a discretized Euclidian space characterized by a *lattice* (a grid) of points in spacetime. In the limit where the lattice is infinitely large while it is at the same time infinitely fine (continuum limit), QCD is recovered. If this method is applicable to calculate non-perturbative effects, it is very heavy computationally. Effective theories, based on the Lagrangian symmetries or specific regimes are often used. For instance, chiral perturbation theory expands, at low energy, the spontaneous chiral symmetry breaking appearing in QCD to light quarks (u , d and s), while it is an exact symmetry only for massless quarks. Heavy quark effective theory, on the contrary, set the mass of the quarks (heavy quarks) to infinity. Other approaches are possible but we will now focus on probably the most successful approach so far : *perturbative QCD* (pQCD). But to justify this approach, we first need to verify if a perturbative approach to QCD is possible.

1.3 QCD running constant

When working in perturbative theory, one has to be careful regarding the parameters used to proceed with the perturbative expansion. For instance, it is usual to define :

$$\alpha_s = \frac{g_s^2}{4\pi}, \quad (1.9)$$

which is also named the coupling constant. This constant determines the coupling between quark and gluon (i.e the color charge coupling). Then it might be possible to determine it experimentally (since we do not observe free quarks, it is not as direct as in QED). If we perform a perturbative expansion of QCD in powers of this constant we might end up with calculations leading to many infinities. Indeed, we will be tempted to obtain it by matching fixed-order theoretical calculations to experimental data that are actually sensitive to the full expansion. It is still useful to write the Lagrangian as in Eq. (1.1), with what we call bare parameters and fields. To work with physically measurable (and then finite) quantities, it is necessary to perform what is called a *renormalization* of the parameters and the fields. However, this renormalization comes with a renormalization scale, μ_R on which depend the renormalized quantities. Of course, any observable must be independent of the choice of μ_R , which condition is set by the renormalization group equation. For an observable $|\mathfrak{D}|^2$, it reads :

$$\mu_R \frac{d\mathfrak{D}}{d\mu_R} = \mu_R \left(\mu_R \frac{\partial}{\partial \mu_R} + \frac{d\alpha_s}{d\mu_R} \frac{\partial}{\partial \alpha_s} + \frac{dm}{d\mu_R} \frac{\partial}{\partial m} \right) \mathfrak{D} = 0. \quad (1.10)$$

This leads to the definition of the beta function and the anomalous dimension as :

$$\beta(\alpha_s) \equiv -\mu_R \frac{\partial \alpha_s}{\partial \mu_R^2}, \quad \gamma(\alpha_s) \equiv -\frac{\mu_R}{m} \frac{\partial m}{\partial \mu_R^2}. \quad (1.11)$$

$\beta(\alpha_s)$ is calculable perturbatively and, at Next to Leading Order (NLO), it is evaluated as [19, 20] :

$$\beta(\alpha_s) = \frac{1}{12\pi} (11N_c - 2N_f) \alpha_s^2. \quad (1.12)$$

It follows that the so-called *running* constant of QCD verifies :

$$\alpha_s(Q^2) = \frac{\alpha_s(\mu_R^2)}{1 + \frac{\alpha_s(\mu_R^2)}{12\pi} (3N_c - 2N_f) \log \frac{Q^2}{\mu_R^2}}. \quad (1.13)$$

More on the determination of the running constant and the function β and γ is summarized in [21]. With $N_c = 3$ and $N_f = 6$, we see that $\alpha_s(Q^2)$ decreases with increasing Q^2 leading to an important concept in QCD : *asymptotic freedom*. At high energy (Q^2), which is equivalent to short distances, the running constant becomes small and strong interaction becomes very weak. This means that, at short distances, a group of quarks and gluons can be considered free (for the strong interaction, quarks might interact electromagnetically). On the other hand, at low energy (i.e. at long distance), the running

constant increases, to a point where it is no more small enough to perform perturbative theory. This is another important feature of QCD : *color confinement*. Indeed, at low energy, color charges are strongly coupled to form colorless states called hadrons (implying that we cannot observe free quarks or gluons). We characterize this limit by the scale $\mu^2 = \Lambda_{QCD}$ that separates the perturbative regime from the non-perturbative one. It can be written as :

$$\Lambda(QCD) = \mu_R^2 \exp \left[\frac{-12\pi}{(3N_c - 2N_f)\alpha_s(\mu_R^2)} \right]. \quad (1.14)$$

It turns out Λ_{QCD} is of the order of 0.2GeV (it depends on the number of active quark flavors, i.e on the quarks that can be produced during the considered process). Fig. 1.2 (taken from [22]) shows the perfect agreement between the running coupling as obtained with $\beta(\alpha_s)$ expanded at 4th order to experimental data.

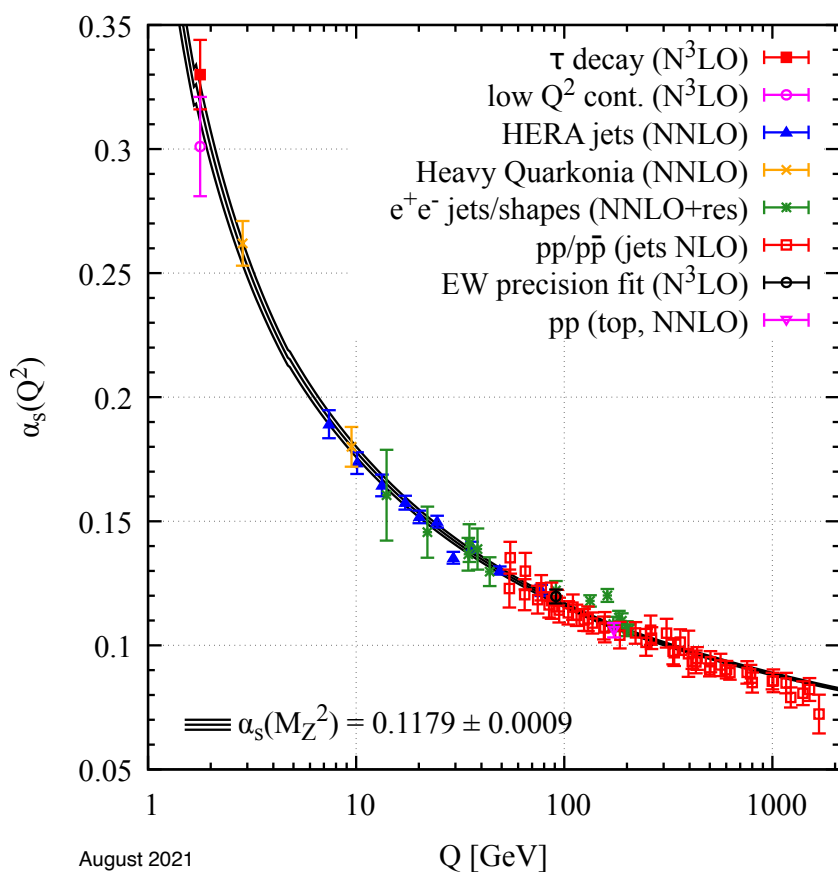


Figure 1.2: The running constant of QCD (from [22]).

1.4 Quark model

One of the strengths of QCD, as a theory, has been to predict some particles (not elementary), hadrons, before they were discovered experimentally. This was the case for instance with the Ω^- baryon, predicted, among others, by Murray Gell-Mann in 1961 (through his *eightfold way* [23]) and discovered experimentally 3 years later [24]. Gell-Mann was awarded a Nobel prize in 1969 for his work on elementary particle classification.

Based on the properties of QCD and its constraints, one can build hadrons in several ways and produce what we call the *quark model*. Due to color confinement, the main idea is to build colorless groups of quarks whose states follow the rules of quantum mechanics (especially the Pauli principle). We won't specify all the details of the quark model and all the quantum numbers used to classify hadrons in this model but just give a simple approach to it.

The first idea to construct a hadron (a colorless state) is to add 2 partons, one carrying a color and the other its anti-colors. Such particles are called *mesons*¹ and due to the rules of quantum dynamics, there are limited ways to build them, that are presented in Fig. 1.4 (taken from [22]) when accounting only for the 2 first generations of quarks (u, d, c, s).

The other main possibility is to gather 3 partons carrying the 3 colors (or the 3 anti-colors), those are named *baryon*, and they are the main constituents of matter. The different baryons obtainable from the 2 first generations of quarks are presented in Fig. 1.3 (taken from [22]).

More complex mixes can be constructed, and are actually observed². They are called “exotic hadrons” (such as tetraquarks or pentaquarks) but, describing such states with pure QCD is out of our range nowadays. For these particles, we have adopted some effective field theories [26].

The picture of hadrons described as just a few quarks, the valence quarks (that give the hadron its quantum numbers), has to be refined. A first step is to consider these quarks as bound states, interacting through gluon exchange (maintaining them in the hadron, as a colorless entity). However, this is not enough to describe properly an interacting hadron.

1.5 Parton model

The *parton model* was proposed by Richard Feynman in 1969 [27] to describe hadrons when doing calculations involving them (at high energy). In this context, the content of hadrons is described by its point-like constituents : the partons (which are quarks and gluons). Then, the idea is that an interaction with a hadron is actually depicted as an interaction with one of its constituents. If we consider a lepton-hadron collision, say

¹To be exact, Mesons are hadronic particles composed of an equal number of quark and antiquark (leading to a null baryon number).

²As for instance $Z(4430)^-$, a tetra quark made of $\bar{c}d\bar{u}$ [25]

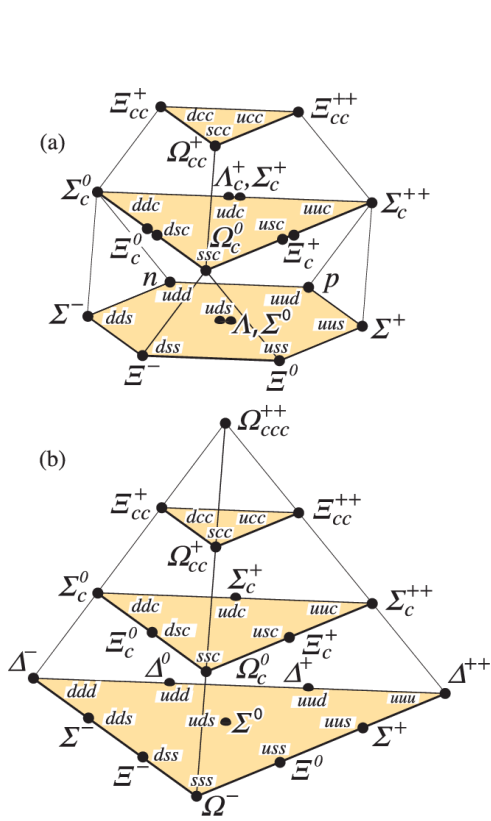


Figure 1.3: $udsc$ spin $\frac{1}{2}$ (a) and spin $\frac{3}{2}$ (b) Baryons (from [22]).

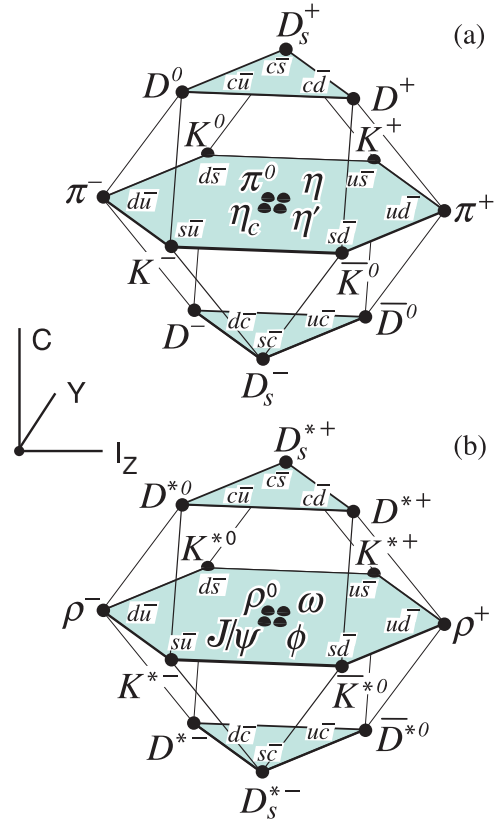


Figure 1.4: $udsc$ pseudoscalar (spin 0, odd parity) in (a) and vector (spin 1, odd parity) Mesons in (b) (from [22]).

electron-proton (ep), this can be viewed as the exchange of a photon between the electron and a quark inside the proton (as a charge constituent of the proton). In this interaction, the other partons inside the proton are only spectators. Indeed, the time scale of the interaction between the photon and the struck quark is much shorter than the time scale of interaction between the partons hence the quark interacting with the photon is viewed as a free quark. Then, a hadron can be characterized by its constituent partons through what we call a **Parton Distribution Function (PDF)** $f_{i/h}(x)$ that describe, at glsLO in $alpha_s$, the probability, in a collision, that the interaction is done with the parton of type i carrying the energy fraction (of the hadron) x . This PDF can then be accessed through the experiment. If the hadron was interacting through only its valence quarks, the PDF of a baryon (say a proton) would be a Dirac delta functions centered in $\frac{1}{3}$ (each quark carrying $\frac{1}{3}$ of the energy of the hadron)³. When we consider 3 bound quarks (interacting with each other through gluon exchange), then the picture is much more realistic with a broadened distribution peaked around $x = \frac{1}{3}$. Still, this does not correspond to what

³for a single quark, the PDF would trivially be Dirac delta function centered in 1.

is observed, which is shown in Fig. 1.5 (from [28]).

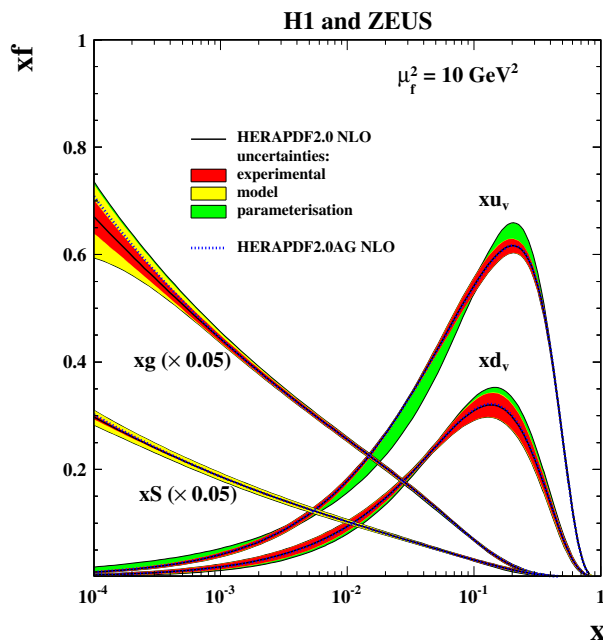


Figure 1.5: PDF of the different partons (valence quarks, sea quarks, and gluons) in the proton (from [28]).

Indeed, at low- x , the quark PDF of the proton behaves differently with an important contribution from what we call *sea quarks*. The sea quarks are pairs of quark-antiquark that are constantly created (from gluons) and annihilated (into gluons) inside the hadron (and that do not contribute to its quantum numbers). These different models for the quark PDF of the proton are summarized in Fig. 1.6⁴. This figure comes from Chap.9 of [5] devoted to partons.

The PDFs reflect the complex structure of the hadron that I remember being compared by Ignazio Scimemi (in one first seminar I attended during my Ph.D.) to Paëlla (with grains of rice, and other ingredients, playing the role of the quarks while the sauce plays the role of the gluons). The representation of the proton structure is depicted in Fig. 1.7 (credited to D. Dominguez from CERN).

1.6 Factorization

In the previous section, we introduced the PDF of a specific parton in a hadron as the probability for a probe hitting a hadron to strike this specific parton (characterized by its type and the fraction of energy of the hadron it carries). If the PDFs describe

⁴In this figure, the structure-function F_2 appears instead of the PDF, but this function is directly related to the quark PDF as we will see in Chap. 2.

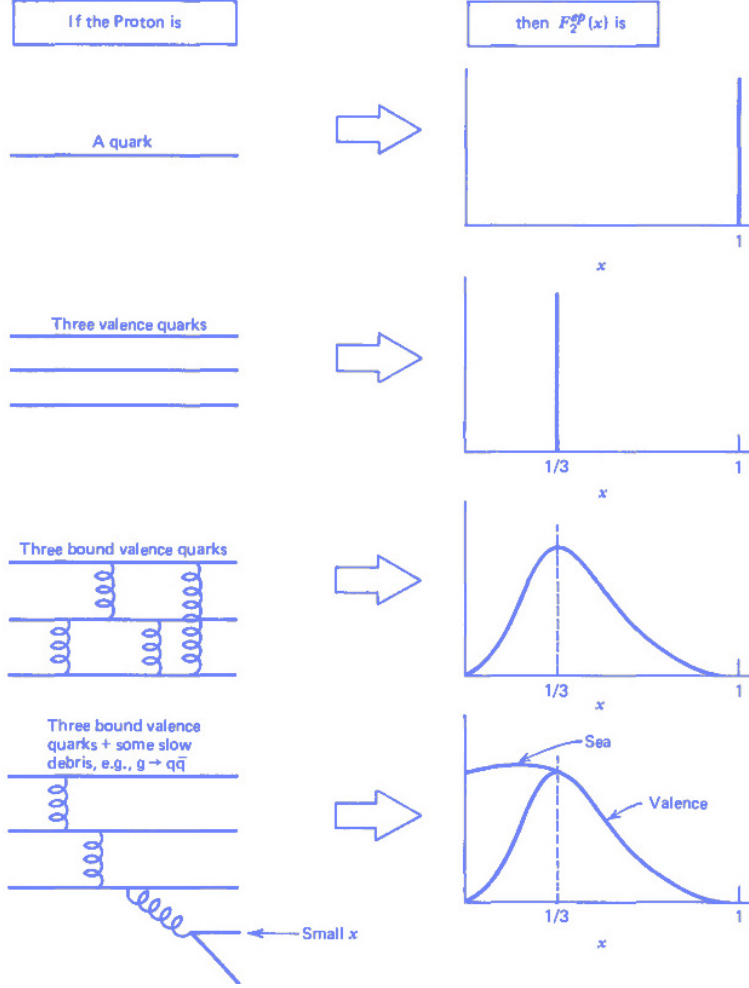


Figure 1.6: Structure function for different models of proton (from [5]).

the structure of hadrons, they also permit to calculate hadronic process (through the calculation of its cross-section). Indeed, when calculating a hadronic cross-section, we separate the partonic collision (which is calculable perturbatively) from the description of the hadron given by PDFs (that contains non-perturbative effects). The PDFs encode color confinement (where the running constant is large). Then, the cross-section of a hadronic collision is the incoherent sum over the different partons constituting the hadron of the convolution of the corresponding PDF and partonic cross-section. This can be written as :

$$d\sigma_{ab} = \sum_{i,j} \int dx_i dx_j f_{i/a}(x_i) f_{j/b}(x_j) d\hat{\sigma}_{ij}(x_i, x_j) \quad (1.15)$$

where $\hat{\sigma}$ denotes a partonic cross-section. This is a simplified picture of what we call factorization, stating that calculations in hadronic collisions can be split between the non-

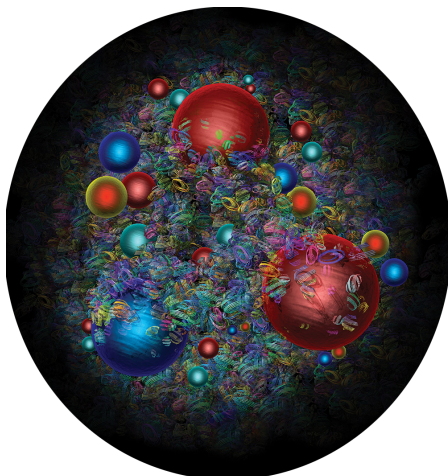


Figure 1.7: Artist's view of the proton structure (credited to D. Dominguez from CERN).

perturbative part (corresponding to long-distance interaction, involving PDFs and called soft part) and a fully perturbative part (with the partonic cross-section, corresponding to short distance interaction, called the hard part). An important feature of factorization is the fact that the PDFs describing a hadron are universal (in the sense of being process independent). Then, the idea is to obtain them through experiments⁵ and to apply them to evaluate, for instance, the glsqcd background of some specific processes. On the other hand, the hard cross-section $d\hat{\sigma}_{ij\rightarrow c}(x_i, x_j)$ is perfectly calculable perturbatively from the square of the corresponding amplitudes as we will see in Chap. 3. Actually, factorization theorems (that demonstrate the application of factorization), have only been proven for a few classes of processes (that we will list in Chap. 2).

In the basic picture of Eq. (1.15), some pieces are missing. In particular, PDFs not only depend on the energy fraction x but also on the energy scale μ^2 of the collision (the energy at which the partons are probed inside the hadron). Hopefully, this dependence on the scale μ^2 is calculable in perturbation theory and leads to what we call *evolution equations*. We might also precise the final state parton in the hard collision, denoted by X . Taking all this into account leads to the following description of $a + b \rightarrow X$ process [16] :

$$d\sigma_{ab\rightarrow X} = \sum_{i,j} \int dx_i dx_j f_{i/a}(x_i, \mu^2) f_{j/b}(x_j, \mu^2) d\hat{\sigma}_{ij}(x_i, x_j, \mu^2). \quad (1.16)$$

In this scheme (and in the one of Eq. (1.15)), we characterize the partons with the fraction of the hadron energy they carry. This means that we see them as going all in the direction of the hadron, each carrying a fraction of its momentum, hence we call this scheme *collinear factorization*.

⁵It is also possible to obtain them through lattice QCD but this is extremely calculation heavy and the present results are still far from matching all the results obtained through experiments.

In the following, we will be interested in some peculiar kinematic region where this factorization fails. Indeed, we will study the limit where the center of mass energy \sqrt{s} of the process is much larger than any other scale. In this case, the initial partons follow the high energy kinematics :

$$k_i = x_i p_a + k_{\perp,i}, \quad \text{and} \quad k_j = x_j p_b + k_{\perp,j}, \quad (1.17)$$

where $p_{a,b}$ are the momenta of the hadrons a and b , and k_{\perp} denotes an intrinsic transverse momentum. It can be shown (see Chap. 2) that in the high energy limit, $p_{a,b}$ can be considered light-like and that $x_{i,j} \rightarrow 0$ (hence, we refer to the physics in this limit to as “small- x ” physics). Then, the transverse momentum k_{\perp} (often note k_T) is not negligible. This dependence has then to be taken into account in both the PDF (that are then *transverse momentum dependent*) but also in the hard the following way :

$$\begin{aligned} d\sigma_{ab \rightarrow X} & \int \frac{d^2 \mathbf{k}_{\perp,i}}{\pi} \frac{d^2 \mathbf{k}_{\perp,j}}{\pi} dx_i dx_j \mathcal{F}_{i/a}(x_i, \mathbf{k}_{\perp,i}, \mu^2) \times \\ & \times \mathcal{F}_{j/b}(x_j, \mathbf{k}_{\perp,j}, \mu^2) d\hat{\sigma}_{i^*j^* \rightarrow X}(x_i, \mathbf{k}_{\perp,i}, x_j, \mathbf{k}_{\perp,j}, \mu^2). \end{aligned} \quad (1.18)$$

We call this factorization scheme either k_T -factorization or high-energy factorization [29, 30]. Note that this implies the calculation of off-shell amplitudes (amplitudes with 1 or 2 off-shell legs, denoted by $*$). Calculated with the usual method, those amplitudes are not gauge invariant but we will present in Chap. 3 a method to calculate them in a gauge invariant way.

1.7 Conciliate calculations and experimental data

The factorization theorems seen in the previous section give an intuitive vision of hadronic collisions. That being said, we are still far from a representation of what happens in a detector. There are several other phenomena to consider to produce results comparable to data and pretend to phenomenology. Still, this idea of factorization can be kept due to the difference in the time scale of these phenomena.

A complete description is depicted in Fig. 1.8 (from [31]). We already described two elements in this picture. First, the PDFs (the 2 green blobs in the beam axis) that separate the interacting partons from the spectators’ ones (which are staying in the beam axis). Secondly, the hard collision described by the amplitudes (in red) left us with free partons. One may note that the partons interacting in the hard process emit radiation before interacting. We have not mentioned it for simplicity, but this is taken into account in the PDFs (evolving the initial parton from the soft scale in the hadron to the hard scale of the collision through radiations). Back to our free partons, we saw that color confinement does not allow them⁶ and this leads to complex phenomena that eventually will leave us with hadrons. First, the partons (especially if they are energetic) will initiate a parton shower creating a large number of partons following the

⁶Except in quark-gluon plasma, that will be discussed later.

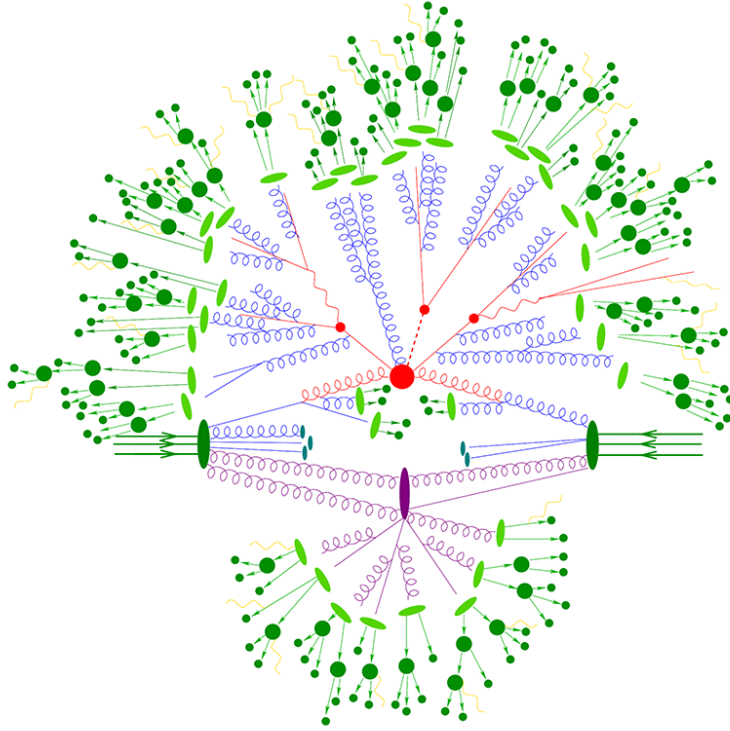


Figure 1.8: Representation of a collision event (from [31]).

QCD rules (with quarks emitting gluons and gluon creating quark-antiquark pairs). If the initial parton is energetic enough, the parton in the shower will be collimated in a cone around the momentum of the initial parton. These partons define what we call a jet. This “showering” can be calculated perturbatively and is based on the splitting functions that rule QCD (and describe the emission probabilities).

Then, on a larger time scale, the partons created in the parton shower will recombine into hadrons. This phenomenon is called hadronization and it is not yet well understood (it is a non-perturbative process). So far, to make calculations, we use phenomenological models (such as the *cluster model* [32, 33] and the *string model* [34, 35]). Hadronization can be characterized by what we call fragmentation functions. They describe the probability of observing a hadron from a given parton and they factorize from PDFs and the hard cross-section. Also, the produced hadrons are not necessarily stable and will then decay into stable ones. This hadronization (light green blobs) and hadron decay (dark green round blobs) happen for partons coming from the final state shower but also for spectators and for partons coming from the initial state shower (governed by PDF evolution).

That being said, we still need to take into account gluon emission (in yellow) and sec-

ondary interactions (in purple).

Taking all these phenomena into account eventually leads to what we actually see in a detector, which is shown in Fig. 1.9 (from [36]).

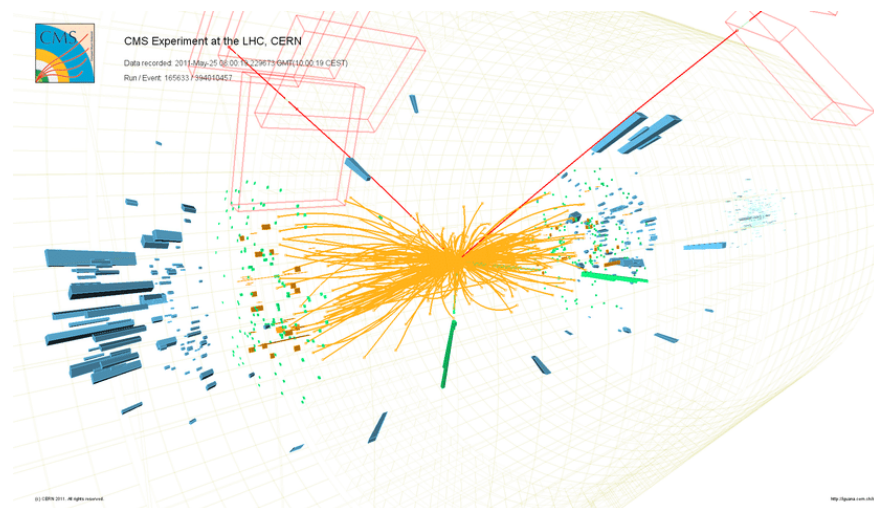


Figure 1.9: Collision vent in the CMS detector (from [36]).

Experimentally, we mainly have access to the charge (from trajectories) and the energy (through energy deposit) of a detected particle (hadron). Also, we are interested in the signature of final state partons of the hard process, then, it is more convenient to study jets (in their hadronized form) than a single hadron. This leads to a whole new physic of these jets that we will introduce in Chap. 4.

However, in the present work, we won't describe a full event as pictured in Fig. 1.8. Instead, we will consider the factorization formula Eq. (1.18) and add to it a factor describing the evolution of jet (initiated by a final state parton of the hard process) in the QGP. Indeed, we will study nuclear effects in heavy-ion collisions (say lead) within k_T -factorization. We will first study those effects on TMDs (or so-called nTMDs) and this will conclude Chap. 2. However, it also affects the final state parton shower. In fact, in a heavy-ion collision, a QGP is formed and, when traversing it, a jet will be quenched (through medium-induced radiations and multiple scattering), hence the importance of studying jet evolution in QGP in heavy-ion collisions. This leads to the following factorization formula :

$$\begin{aligned}
d\sigma_{ab\rightarrow c\mathcal{X}} = & \sum_{i,j} \int \frac{d^2\mathbf{k}_{\perp,i}}{\pi} \frac{d^2\mathbf{k}_{\perp,j}}{\pi} \frac{d^2\mathbf{q}_{\perp,c}}{\pi} dx_i dx_j dx_c \times \\
& \times \mathcal{F}_{i/a}(x_i, \mathbf{k}_{\perp,i}, \mu^2) \mathcal{F}_{j/b}(x_j, \mathbf{k}_{\perp,j}, \mu^2) \times \\
& \times d\hat{\sigma}_{i^*j^*\rightarrow c\mathcal{X}}(x_i, \mathbf{k}_{\perp,i}, x_j, \mathbf{k}_{\perp,j}, \mu^2) D_c(x_c, \mathbf{q}_{\perp,c}, t_c),
\end{aligned} \tag{1.19}$$

where D_c are the in-medium jet fragmentation functions⁷ that describe the evolution of a jet c (meaning initiated by a parton c) in the QGP. Getting these fragmentation functions (in some specific frame) and studying them will be the focus of Chap. 4. Then, by the end of Chap. 4, we will have at our disposition nTMDs, off-shell amplitudes and fragmentation functions which, all together, can describe heavy-ion collisions at small- x .

⁷Be careful with this term, not to be confused with fragmentation functions describing hadronization.

Chapter 2

Parton Distribution Function

In this chapter, we will study **Parton Distribution Functions (PDF)**. As seen in the introduction, they are needed to provide predictions for hadronic collisions and describe the structure of hadrons.

The first two sections (Sec. 2.1 and 2.2) will present the main steps to define properly PDFs in the context of collinear factorization. This will lead to the famous **DGLAP** evolution equations¹. Sec. 2.3 will present **Transverse Momentum Dependant PDFs (TMD)** first through the **BFKL** equation (where it is actually a question of unintegrated PDF), and the **CCFM** equation afterward. This will lead to the determination of different factorization schemes : k_T -factorization and hybrid factorization. We will see that the **BFKL** equation actually violates unitarity at high energy because it doesn't account for *saturation*. This phenomenon and the corrections to **BFKL** that take it into account are the subjects of Sec. 2.4. Then, in Sec. 2.5, the parton branching method, used to calculate these **TMDs**, will be presented. Finally, in Sec. 2.6, results of this method to produce **nTMDs** for lead will be presented and studied in the context of Z boson production in p Pb collisions at the **LHC**.

Contents

2.1	Deep Inelastic Scattering	18
2.2	Collinear Parton Distribution Function	24
2.3	Transverse Momentum Dependant PDF	31
2.3.1	Unintegrated PDF and BFKL	32
2.3.2	TMDs and CCFM	36
2.4	Saturation	38
2.5	The Parton Branching method	40
2.6	Nuclear PB-TMD phenomenology	45
2.6.1	Application of the Parton Branching method	45
2.6.2	Nuclear PDF used	46
2.6.3	Obtaining nuclear TMDs	48

¹The definition of the PDF and the determination of the **DGLAP** summarize the steps given in [6].

2.6.4 Z boson production in $p\text{Pb}$ collisions at the LHC	51
2.7 Chapter summary	61

2.1 Deep Inelastic Scattering

We saw briefly in the introduction that, in order to describe a collision involving hadrons, we invoke factorization theorems that decompose the collision into PDFs (the soft part) and a partonic cross-section (the hard part). To introduce these PDFs, we will first study the simplest process probing hadrons : Deep Inelastic Scattering (DIS)². What we call DIS is the collision between hadron (say a proton p) and a lepton pair (say an electron e^-) written as follows :

$$e^-(p) + p^+(P) \rightarrow e^-(p') + X(P_X) \quad (2.1)$$

where the letters in parenthesis label 4-momenta. In this process, a virtual photon (γ^* with 4-momentum q) is exchanged between the electron and the hadron. The virtual photon probes the constituents of the hadron if its wavelength λ is small enough compared to the radius of the hadron r_h , i.e if $\lambda \ll r_h$ ³. Also, if its energy $Q \sim \frac{1}{\lambda}$ ⁴ is much greater than the hadron mass, i.e if $Q^2 = -(p' - p)^2 \gg m_h^2$ (hence the term *deep*) and if the invariant mass is much greater than the mass of the hadron, i.e if $m_X^2 = (P + q)^2 \gg m_h^2$ (hence the term *inelastic*) then the hadron breaks, leaving, at the end of the process, new hadrons represented by X . This process and its kinematics are depicted in Fig. 2.1. With the conditions described just before, we consider that the photon interacts with one quark in the hadron.

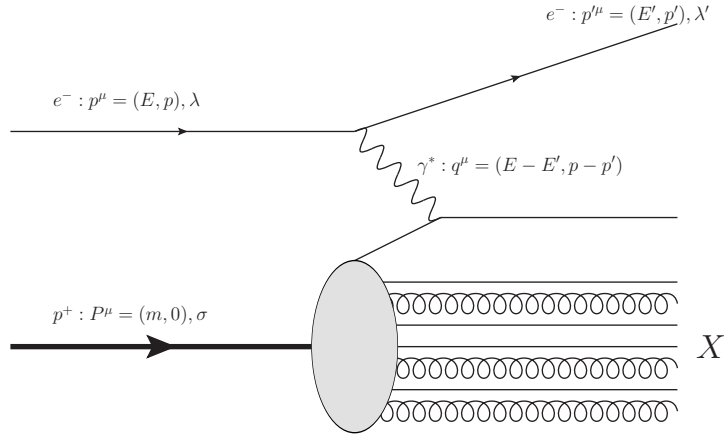


Figure 2.1: $e^- p^+$ deep inelastic scattering.

Experimentally, this corresponds to bombarding a fixed target with an electron beam and detecting the scattered electron.

To study this process (*ep DIS*), we need to parametrize its kinematics. We introduce

²This introduction, done through Sec. 2.1 and Sec. 2.2 follows the presentation done in Sec. 2 of [6]

³On the contrary case, the photon will see the hadron has a point-like particle leading to an elastic scattering described by QED.

⁴Actually, Q is defined by $Q^2 = -q^2 > 0$ and Q^2 is called the virtuality of the photon

the following invariants :

$$x_{Bj} \equiv \frac{Q^2}{2P \cdot q}, \quad y \equiv \frac{P \cdot q}{P \cdot p}, \quad \nu \equiv \frac{P \cdot q}{m_p}, \quad s = (P + p)^2, \quad (2.2)$$

where x_{Bj} is called the Bjorken-x variable, m_p is the mass of the proton and s the center-of-mass energy squared of the ep scattering. From these definitions, we see that high energy (large s) is equivalent to small- x (small- x_{Bj} for the moment) by noting :

$$x_{Bj} \sim \frac{Q^2}{ys}, \quad \text{for } s \gg m_p. \quad (2.3)$$

In the rest frame of the proton, we have :

$$P^\mu = (E, \vec{p}), \quad p^\mu = (E, \vec{p}), \quad p'^\mu = (E', \vec{p}'), \quad q^\mu = (E - E', \vec{p} - \vec{p}'), \quad (2.4)$$

which leads to (in this frame) $y = \frac{E-E'}{E}$ being the fraction of the energy transferred from the electron to the proton and $\nu = E - E'$ the part of the electron's energy transferred to the proton. We also have $Q^2 = 4EE' \sin^2 \frac{\theta}{2}$ with θ the electron scattering angle (between \vec{p} and \vec{p}').

However, it will be convenient also to work in the [Infinite Momentum Frame \(IMF\)](#)⁵ of the proton, where it is relativistic. In this frame, we have :

$$P^\mu \approx (P + \frac{m_p^2}{2P}, 0, 0, P), \quad q^\mu = (q^0, q^1, q^2, 0), \quad (2.5)$$

with $P \gg m_p$. Then, in this frame $x_{Bj} = \frac{Q^2}{2P \cdot q} \approx \frac{Q^2}{2Pq^0}$. Also, q^0 is inverse proportional to the time scale of the interaction, leading to :

$$t_{DIS} \approx \frac{1}{q^0} \approx \frac{2x_{Bj}P}{Q^2}. \quad (2.6)$$

On the other hand, the typical time for interaction between partons inside the proton is given by the scale of the non-perturbative [QCD](#) interactions $\sim m_p \sim \lambda_{QCD}$ in the proton rest frame. In the [IMF](#), it is boosted by a factor $\frac{P}{m_p}$ leading to :

$$t_{partons} \approx \frac{1}{m_p} \frac{P}{m_p}. \quad (2.7)$$

With $Q^2 \gg m_p^2$ and $x_{Bj} \leq 1$, it is clear that :

$$t_{DIS} \ll t_{partons}, \quad (2.8)$$

which justifies the assumption that, during the time of the interaction between the photon and the hit quark, the partons do not interact with each other⁶.

⁵It is also sometimes called *Bjorken frame*.

⁶Also, accounting for interaction(s) between the struck parton and the spectator partons is known as higher twist corrections. Those corrections are suppressed by powers of $\frac{m_p^2}{Q^2}$.

For the next expressions, we will go back to the rest frame of the proton (to write things in terms of E and E'). The amplitude of the DIS process can be written, taking the covariant gauge for the photon, as :

$$iM_{\sigma,\lambda,\lambda'}(X) = \frac{ie^2}{q^2} \bar{u}_{\lambda'}(p') \gamma_\mu u_\lambda(p) \langle X | J^\mu(0) | P, \sigma \rangle, \quad (2.9)$$

where λ and λ' are the polarizations of the electron (before and after the collision respectively) while σ is the polarization of the proton. $|P, \sigma\rangle$ denotes the initial state of the proton and $|X\rangle$ the final state of the many hadrons X while $J^\mu(x)$ is the quark electromagnetic current, defined as :

$$J^\mu(x) = \sum_f e_f \bar{q}^f(x) \gamma^\mu q^f(x), \quad (2.10)$$

with e_f the electric charge of the quark of flavor f (in unit of the electron charge e) and $q^f(x)$ is the quark field operator. Then, to obtain the total DIS cross-section, one has to square the amplitude in Eq. (2.9), integrate over the final-state phase-space, sum over the final-state quantum numbers, average over the initial-state quantum numbers, divide by the flux factor and implement (4-)momentum conservation (through Dirac delta function). This leads to (see [37]) :

$$\sigma^{ep} = \int \frac{d^3 p'}{(2\pi)^3 2E 2E'} \frac{1}{4} \sum_{\sigma,\lambda,\lambda'} \sum_X |M_{\sigma,\lambda,\lambda'}(X)|^2 (2\pi)^4 \delta^4(P + q - P_X). \quad (2.11)$$

An interesting feature of Eq. (2.11) is that it can be written as the product of a leptonic tensor $L_{\mu\nu}$ on one side, describing the emission of the photon by the electron, and a hadronic tensor $W^{\mu\nu}$ describing the interaction between the virtual photon and the hadron. It reads :

$$\frac{d\sigma}{d^3 p'} = \frac{\alpha_{EM}^2}{EE'Q^4} L_{\mu\nu} W^{\mu\nu}, \quad (2.12)$$

with :

$$\begin{aligned} L_{\mu\nu} &= \frac{1}{2} \sum_{\lambda=\pm 1} \sum_{\lambda'=\pm 1} \bar{u}_{\lambda'}(p') \gamma_\mu u_\lambda(p) [\bar{u}_{\lambda'}(p') \gamma_\nu u_\lambda(p)]^* \\ &= 2 (p_\mu p'_\nu + p_\nu p'_\mu - p \cdot q \eta_{\mu\nu} + m_e \eta_{\mu\nu}), \end{aligned} \quad (2.13)$$

and :

$$\begin{aligned} W^{\mu\nu} &= \frac{1}{8\pi m_p} \sum_{\sigma=\pm 1} \sum_X \langle P, \sigma | J^\mu(0) | X \rangle \langle X | J^\nu(0) | P, \sigma \rangle (2\pi)^4 \delta^4(P + q - P_X) \\ &= \frac{1}{8\pi m_p} \int d^4 x e^{iq \cdot x} \sum_{\sigma=\pm 1} \langle P, \sigma | J^\mu(x) J^\nu(0) | P, \sigma \rangle. \end{aligned} \quad (2.14)$$

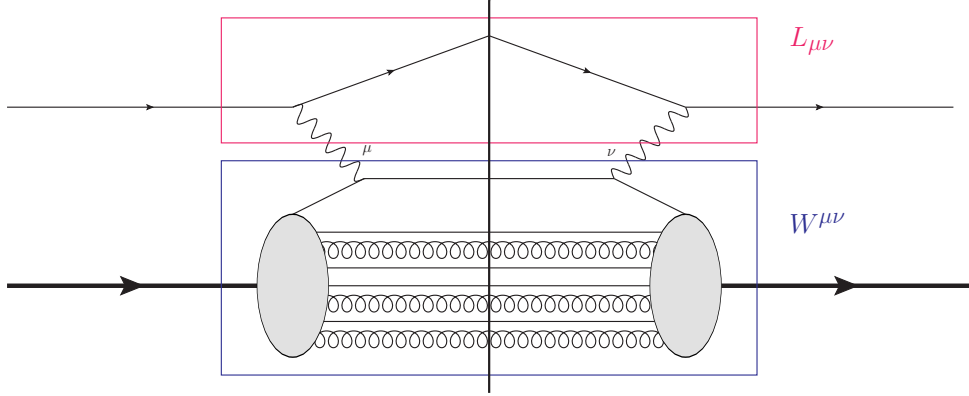


Figure 2.2: Diagrammatic representation of DIS cross-section with separation of the contribution to the leptonic tensor $L_{\mu\nu}$ (in red) and to the hadronic tensor $W^{\mu\nu}$ (in blue).

This hadronic tensor characterizes all the strong interaction dynamics in DIS and consequently contains some non-perturbative effects, making it hard to calculate. Still, we can go further in its structure, first by imposing the conservation of the electromagnetic current :

$$q_\mu W^{\mu\nu} = 0, \text{ and } q_\nu W^{\mu\nu} = 0. \quad (2.15)$$

This condition can be satisfied only in 2 inequivalent ways (with the 4-momenta appearing in the hadronic part, i.e P and q) leading to the following decomposition :

$$W^{\mu\nu} = -W_1(x_{Bj}, Q^2) \left(\eta^{\mu\nu} - \frac{q^\mu q^\nu}{q^2} \right) + \frac{W_2(x_{Bj}, Q^2)}{m_p^2} \left(P^\mu - \frac{P \cdot q}{q^2} q^\mu \right) \left(P^\nu - \frac{P \cdot q}{q^2} q^\nu \right). \quad (2.16)$$

The dependence of the function W_1 and W_2 is completely general (Q^2 and x_{Bj} are the 2 independent invariants in the hadronic part of the problem). One can show (see Chap. 8 in [5]) that the differential ep cross-section can be written as :

$$\frac{d\sigma^{ep}}{dE' d\Omega} = \frac{\alpha_{EM}^2}{4E^2 \sin^4 \frac{\theta}{2}} \left[W_2(x_{Bj}, Q^2) \cos^2 \frac{\theta}{2} + 2W_1(x_{Bj}, Q^2) \sin^2 \frac{\theta}{2} \right]. \quad (2.17)$$

Then, the functions W_1 and W_2 can be studied experimentally through only the electron scattering angle θ . Also, W_1 and W_2 have the dimension of inverse of mass so it is more convenient to work with the following dimensionless functions :

$$F_1(x_{Bj}, Q^2) \equiv m_p W_1(x_{Bj}, Q^2) \\ F_2(x_{Bj}, Q^2) \equiv \nu W_2(x_{Bj}, Q^2) = \frac{Q^2}{2m_p x_{Bj}} W_2(x_{Bj}, Q^2). \quad (2.18)$$

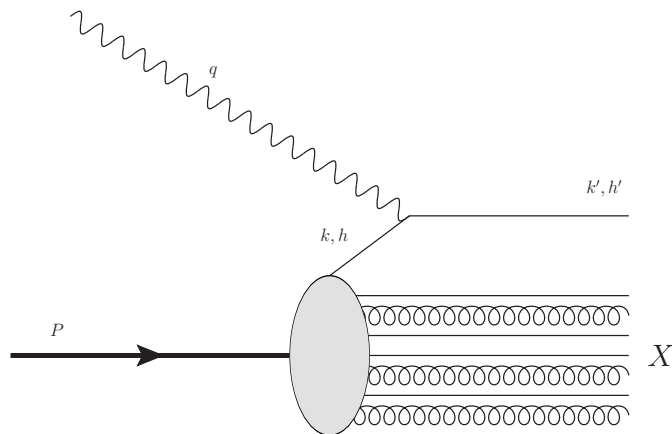


Figure 2.3: Virtual photon-proton scattering.

F_1 and F_2 are called the *structure functions*⁷ and they describe all the QCD physics in DIS.

To go further, we abandon the full picture of DIS to focus on virtual photon-proton ($\gamma^* p$) scattering (as shown in Fig. 2.3) and also, we write momenta in light cone coordinates (see details in App. A.1), such as :

$$P^\mu \approx (P^+, 0, 0_\perp), \quad k^\mu = \left(k^+, \frac{k_\perp^2}{k^+}, k_\perp \right), \quad k'^\mu = \left(k'^+, \frac{k_\perp'^2}{k'^+}, k'_\perp \right), \quad (2.19)$$

where k^μ (k'^μ) is the momentum of the struck quark before (after) interacting with the photon and h (h') its helicity. We have $P^+ \approx 2P$ very large and k^+ large. Also, to write k^μ and k'^μ , we consider the quark to be massless (since m_q is negligible compared to the hard scale of the process Q^2 and also to k^+). We also introduce the Feynman- x variable as the fraction of $+$ momentum of the proton carried by the quark :

$$x \equiv \frac{k^+}{P^+}. \quad (2.20)$$

For the virtual photon, to write its momentum within the Light Cone Perturbation Theory (LCPT) formalism (where particles are on-shell), we translate its virtuality in terms of imaginary mass :

$$q^\mu = \left(q^+, \frac{\vec{q}_\perp^2 - Q^2}{q^+}, \vec{q}_\perp \right). \quad (2.21)$$

For the following discussion, we also need to parametrize the kinematics of all partons in X . We will also assume them to be massless. Then, for a final state X with $n + 1$

⁷ W_1 and W_2 are usually called structure functions too and the distinction with F_1 and F_2 is sometimes underlined by the adjective “dimensionless”. Anyway, in the present manuscript, “structure functions” will refer only to F_1 and F_2 .

partons ($n \in \mathbb{N}$), we will write k_i the momentum of the parton i , with :

$$\forall i \in \llbracket 1, n \rrbracket, \quad k_i^\mu = \left(x_i P^+, \frac{k_{i,\perp}^2}{x_i P^+}, k_{i,\perp} \right), \quad (2.22)$$

where $\forall a, b \in \mathbb{Z}$, $\llbracket a, b \rrbracket = [a, b] \cap \mathbb{Z}$ i.e it is the set of integers between a and b .

Now, we can define the light cone wave function of the state X (described as the Fock state of the n spectator partons and the struck quark of the proton) as $\psi_n^f(\{x_i, k_{i,\perp}\}; x, k_\perp; h)$. We do not explicitly write the partons helicity and flavor for simplicity since they are summed over as soon as the light cone wave function is squared. Now, an important step to rewrite the hadronic tensor $W^{\mu\nu}$ with ψ_n^f is to determine the phase space represented by the sum over the X states in Eq. (2.14) :

$$\sum_X = \int \frac{dk'^+}{k'^+} \frac{d^2 k'_\perp}{2(2\pi)^3} \frac{1}{S_n} \sum_{h'=\pm 1} \prod_{i=1}^n \frac{dx_i}{x_i} \frac{d^2 k_{i,\perp}}{2(2\pi)^3}, \quad (2.23)$$

with the integral on k'^+ performed over $[0, P^+]$, the integral on x_i over $[0, 1]$ and the integrals over $2k'_\perp$ and $k_{i,\perp}$ over \mathbb{R}^+ . We can then rewrite Eq. (2.14) as :

$$\begin{aligned} W_{\mu\nu} &= \frac{1}{8m_p} \sum_{\sigma=\pm 1} \sum_{f,n} \int \frac{dk'^+}{k'^+} \frac{d^2 k'_\perp}{(2\pi)^3} \frac{1}{S_n} \sum_{h,h',h''} \prod_{i=1}^n \frac{dx_i}{x_i} \frac{d^2 k_{i,\perp}}{2(2\pi)^3} \\ &\quad \times e_f^2 \frac{P^+}{k^+} \psi_n^f(\{x_i, k_{i,\perp}\}; x, k_\perp; h) \left[\frac{P^+}{k^+} \psi_n^f(\{x_i, k_{i,\perp}\}; x, k_\perp; h'') \right]^* \\ &\quad \times \bar{u}_{h'}(k') \gamma_\mu u_h(k) [\bar{u}_{h'}(k') \gamma_\nu u_{h''}(k)]^* (2\pi)^4 \delta^4 \left(P + q - k' - \sum_{j=1}^n k_j \right). \end{aligned} \quad (2.24)$$

Playing with kinematics and some assumptions (that we have massless quarks and that Q^2 is the only hard scale with $\forall i$, $Q^2 \gg k_\perp, k_{i,\perp}$), we can rewrite the $+$ component of the Dirac delta function in Eq. (2.24) as :

$$\frac{1}{k'^+} \delta^4 \left(P^- + q^- - k'^- - \sum_{j=1}^n k_j^- \right) \approx \frac{x_{Bj}}{Q^2} \delta(x - x_{Bj}), \quad (2.25)$$

giving another interpretation of the Bjorken- x variable as the fraction of the light cone momentum of the proton carried by the struck quark.

Studying the transverse components of $W_{\mu\nu}$ from Eq. (2.24), and using the decomposition

of Eq. (2.16), one may show two things.

$$\begin{aligned}
W_1(x_{Bj}, Q^2) &= \frac{1}{8m_p} \sum_{f,n} e_f^2 \int dk^+ d^2k_\perp \frac{1}{S_n} \sum_h \prod_{i=1}^n \frac{dx_i}{x_i} \frac{d^2k_{i,\perp}}{(2\pi)^3} \\
&\times \left| \psi_n^f(\{x_i, k_{i,\perp}\}; x, k_\perp; h) \right|^2 \delta(x_{Bj} - x) \\
&\times \delta \left(P^+ + q^+ - k'^+ - \sum_{j=1}^n k_j^+ \right) \delta^2 \left(k_\perp + \sum_{j=1}^n k_{j,\perp} \right).
\end{aligned} \tag{2.26}$$

Then, that W_1 and W_2 are linked by what is called the *Callan-Gross relation* [38] :

$$\nu W_2(x_{Bj}, Q^2) = 2m_p x_{Bj} W_1(x_{Bj}, Q^2), \tag{2.27}$$

which translates into the structure functions :

$$F_2(x_{Bj}, Q^2) = 2x_{Bj} F_1(x_{Bj}, Q^2). \tag{2.28}$$

This shows that, in fact, the QCD dynamics in DIS can be reduced to one function of the Bjorken- x variable and of the hard scale Q^2 .

2.2 Collinear Parton Distribution Function

In this section, we will define the PDFs and relate them to the structure functions F_1 and F_2 defined in the previous section to show that factorization holds in DIS. Then we will explore the behavior of these PDFs leading us to the so-called DGLAP evolution equations. Basically, all the work to factorize the DIS process has been done in the previous section, we now need to identify the PDF. Let's first define $f_{f/p}$, the distribution function of quarks of flavor f in the proton (p) in terms of the light cone wave function ψ_n^{f8} :

$$\begin{aligned}
f_{f/p}(x, \mu_R^2) &= \sum_n \frac{1}{x} \int \frac{d^2k_\perp}{2(2\pi)^3} \frac{1}{S_n} \sum_{h=\pm 1} \prod_{i=1}^n \frac{dx_i}{x_i} \frac{d^2k_{i,\perp}}{(2\pi)^3} \\
&\times \left| \psi_n^f(\{x_i, k_{i,\perp}\}; x, k_\perp; h) \right|^2 \\
&\times (2\pi)^3 \delta^2 \left(k_\perp + \sum_{j=1}^n k_{j,\perp} \right) \delta \left(1 - x - \sum_{l=1}^n x_l \right),
\end{aligned} \tag{2.29}$$

where μ_R^2 is the renormalization scale, that appears as a UV cutoff in the transverse momentum integrals. We see that it can be interpreted as the sum of the probabilities of having a state with n spectators partons with an observed quark of flavor f (with the

⁸See App. A.1 for more details.

corresponding phase-space integrals and imposing momentum conservation) in a proton. Overall, this distribution represents the probability to find (during an interaction with a proton) a quark of flavor f carrying a fraction x of the proton's longitudinal momentum while μ_R^2 is directly related to the energy of the probe in DIS (Q^2). When it is not explicit enough, this type of distribution is called *collinear PDF*, stressing the fact that, in this picture, the partons in a hadron are seen as all following the same direction (the direction of the hadron) and then carry a fraction of the longitudinal momentum of the hadron x (that can be interpreted as a fraction of energy). In the same way, we can define the gluon distribution function $f_{g/p}$:

$$\begin{aligned}
f_{g/p}(x, \mu_R^2) &= \sum_n \frac{1}{x} \int \frac{d^2 k_\perp}{2(2\pi)^3} \frac{1}{S_n} \sum_{h=\pm 1} \prod_{i=1}^n \frac{dx_i}{x_i} \frac{d^2 k_{i,\perp}}{(2\pi)^3} \\
&\times |\psi_n(\{x_i, k_{i,\perp}\}; x, k_\perp; h)|^2 \\
&\times (2\pi)^3 \delta^2 \left(k_\perp + \sum_{j=1}^n k_{j,\perp} \right) \delta^2 \left(1 - x - \sum_{l=1}^n x_l \right),
\end{aligned} \tag{2.30}$$

where ψ_n is this time the light cone wave function of the proton with an observed gluon and n spectators partons. A diagrammatic representation of both quark and gluon PDFs is shown in Fig. 2.4 where the blob represents the squared light-cone wave function (and the solid line the separation between the “normal” and the complex conjugate part).

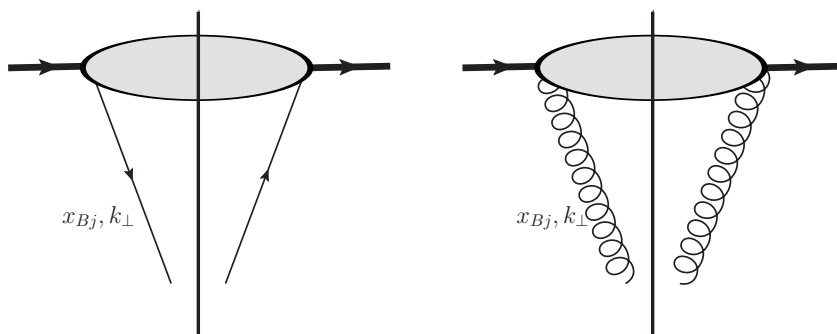


Figure 2.4: Diagrammatic representation of the quark (left) PDF and the gluon PDF (right).

We see, using the expression for $f_{f/p}$ that Eq. (2.26), becomes :

$$W_1(x_{Bj}, Q^2) = \frac{1}{m_p} \sum_f e_f^2 f_{f/p}(x_{Bj}, Q^2), \tag{2.31}$$

which implies, from the definition of the structure functions in Eq. (2.18) and with the

Callan-Gross relation in Eq. (2.28), that :

$$\begin{aligned} F_1(x_{Bj}, Q^2) &= \frac{1}{2} \sum_f e_f^2 f_{f/p}(x_{Bj}, Q^2), \\ F_2(x_{Bj}, Q^2) &= \sum_f e_f^2 x_{Bj} f_{f/p}(x_{Bj}, Q^2). \end{aligned} \quad (2.32)$$

Reassembling all the elements presented in these 2 first sections, one can show that the total cross-section of the virtual photon-proton scattering can be factorized between the PDFs describing the proton structure on one side and the partonic cross-section (virtual photon-quark scattering) on the other side as :

$$\sigma_{tot}^{\gamma^* p}(x_{Bj}, Q^2) = \sum_f \int_0^1 \frac{dz}{z} z f_{f/p}(z, Q^2) \hat{\sigma}^{\gamma^* q(f)}\left(\frac{x_{Bj}}{z}, Q^2\right). \quad (2.33)$$

This result is a cornerstone of pQCD as it permits us to do prediction for hadronic collisions, in DIS, by separating the perturbative part (the partonic cross section, or hard part, involving short distance interaction) and the non-perturbative part (represented by the PDF, the soft part, describing long-distance interactions). Also, the PDF can be seen as a description of how the state of many non-interacting partons is produced “from” a fast-moving hadron before interacting with a probe. Hence, PDFs only depend on the QCD dynamics of the hadron itself and are then universal. This means that, if we can determine for a specific process, we can use them for any process where factorization (actually, collinear factorization) holds, giving to pQCD an important predictive power. The goal of the presented developments was to give insights into how factorization arises in hadronic collisions with a diagrammatic approach. Factorization theorems have been proved to all orders (see [39–42] with an interesting overview in [43]) on several processes :

- inclusive Deep Inelastic Scattering (DIS),
- Semi-Inclusive Deep Inelastic Scattering (SIDIS),
- Drell-Yann (DY) in pp or $p\bar{p}$ collisions.

SIDIS are DIS processes where we observe one of the final state hadrons, it can be schematized as $c + b \rightarrow c + X$ (where a , b and c are hadrons). DY processes consist of the collision of 2 hadrons through the annihilation of a quark-antiquark pair into a virtual photon or a Z boson (which decays into a lepton pair). It can be schematized $a + b \rightarrow Z/\gamma^* \rightarrow l^- + l^+$. Formal demonstration of these factorization theorems is based on the characterization of the Infra-Red (IR) divergences of the Feynman diagrams (involving pinch surfaces and Landau equation), which is out of the range of this discussion. Still, we will note that these demonstrations also need a gauge invariant definition of the PDFs of a hadron h :

$$\begin{aligned} f_{f/h}(x) &= \int \frac{d\xi^-}{4\pi} e^{-xP^+\xi^-} \langle P | \bar{\psi}(0^+, 0^-, 0_\perp) \mathcal{U}^n(0; \xi^-) \gamma^+ \psi(0^+, \xi^-, 0_\perp) | P \rangle, \\ f_{g/h}(x) &= \int \frac{d\xi^-}{2\pi} e^{-xP^+\xi^-} \langle P | F_a^{+j} \mathcal{U}_{ab}^n(0; \xi^-) F_a^{+j}(0^+, \xi^-, 0_\perp) | P \rangle, \end{aligned} \quad (2.34)$$

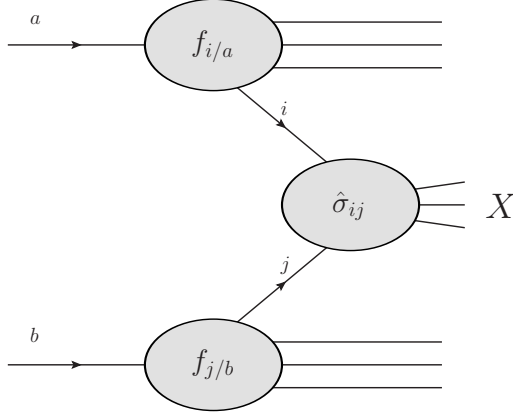


Figure 2.5: Collinear factorization.

with ψ a Dirac field, F the gluon field strength tensor. The gauge invariance is guaranteed by the inclusion of gauge links, the *Wilson lines* \mathcal{U} defined, for a path \mathcal{C} , by :

$$\mathcal{U}_{\mathcal{C}}(x; y) = \mathcal{P} e^{-\int_{\mathcal{C}} dz_{\mu} A^{\mu}(z)}, \quad (2.35)$$

with the path order operator \mathcal{P} . This Wilson line permits the parallel transport from x to y along the path \mathcal{C} . Expanding the exponential leads to the physical interpretation of a Wilson line as the resummation of all possible radiation of the gluon field A along the path.

In the following, the *collinear* factorization will refer to the factorization of a process using PDFs (dependent only on the momentum fraction x and some factorization scale μ_F) to describe partons coming from hadrons. It may even be used as an ansatz for processes where factorization has not (yet) been proved. In the case of the collision of 2 hadrons a and b (what we will be interested in), it reads :

Collinear Factorization

$$d\sigma_{ab \rightarrow X}(P_a, P_b) = \sum_{i,j} \int dx_i dx_j f_{i/a}(x_i, \mu_F^2) f_{j/b}(x_j, \mu_F^2) d\hat{\sigma}_{ij \rightarrow X}(x_i P_a, x_j P_b, \mu_R^2), \quad (2.36)$$

where i and j stand for either quark flavors or gluon and X represent final state (spectators are not denoted). This factorization is schematized in Fig. 2.5. One may notice the two scales appearing in Eq. (2.36), μ_F , the *factorization scale*, which is actually the renormalization scale of the PDF, and μ_R the *renormalization scale* of the running constant (on which depends the perturbative expansion of the partonic cross-section $\hat{\sigma}_{ij}$). Usually, both scales are set equal to the hard scale of the process : $\mu_F^2 = \mu_R^2 = \mu^2 = Q^2$.

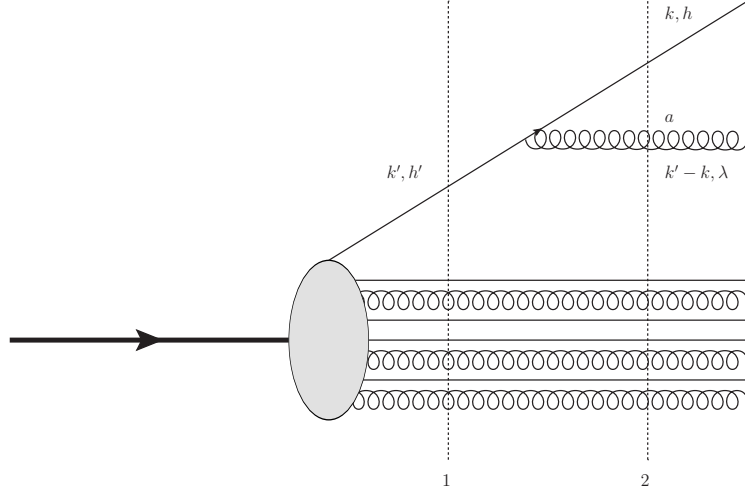


Figure 2.6: 1st order real correction to the quark PDF.

We saw that PDFs encode the non-perturbative part of a hadronic process. Still, the dependence on the scale $\mu_F^2 = Q^2$ is perturbative when Q is larger than the soft scale, i.e the QCD scale Λ_{QCD} . This dependence can then be evaluated through corrections to the PDF that we will describe diagrammatically. Looking, for instance, at the real corrections to the light cone wave function, one can relate the wave function with $n - 1$ spectators (line 1 in Fig. 2.6) with the one with n spectators (line 2 in Fig. 2.6) by applying light-cone QCD rules (see App. A.1) to describe the emission of the gluon in between.

Then, the obtained relation has to be squared to include it in the quark PDF definition of Eq. (2.29). Assuming the quark to be massless and that the transverse momenta are strongly ordered, i.e :

$$Q^2 \gg k_{\perp}^2 \gg k_{n-1,\perp}^2 \gg \dots \gg k_{1,\perp}^2 \sim \Lambda_{QCD}, \quad (2.37)$$

one can write an integral relation between $f_{f/h}(x, Q^2)$ and $f_{f/h}(x', k_{\perp}^2)$ that can be expressed as a differential integral equation (more details on this derivation are given in App. A.2). If you account for all corrections (all diagrams), for both quarks and gluons (including diagrams relating the quark wave function to the gluon one and vice versa), you may arrive at the system of equations :

DGLAP Evolution Equations

$$Q^2 \frac{\partial}{\partial Q^2} \begin{pmatrix} f_S(x, Q^2) \\ f_g(x, Q^2) \end{pmatrix} = \frac{\alpha_s(Q^2)}{2\pi} \int_x^1 \frac{dz}{z} \begin{pmatrix} P_{qq}(z) & P_{qg}(z) \\ P_{gq}(z) & P_{gg}(z) \end{pmatrix} \begin{pmatrix} f_S(x/z, Q^2) \\ f_g(x/z, Q^2) \end{pmatrix} \quad (2.38)$$

$$Q^2 \frac{\partial f_{NS}(x, Q^2)}{\partial Q^2} = \frac{\alpha_s(Q^2)}{2\pi} \int_x^1 \frac{dz}{z} P_{qq}(z) f_{NS}(x/z, Q^2).$$

These equations are the **DGLAP** equations. Gribov and Lipatov derived an equivalent equation in **QED** in 1972 [44] while this **QCD** version was derived independently by Altarelli and Parisi [45] and by Dokshitzer [46] (both in 1977). For simplicity, we have omitted the mention of the hadron in the **PDF** index. f_S and f_{NS} refer respectively to the flavor singlet **PDF** (related to sea quarks) and the flavor non-singlet **PDF** (related to valence quarks), defined by :

$$\begin{aligned} f_S(x, Q^2) &= \sum_f \left[f_f(x, Q^2) + f_{\bar{f}}(x, Q^2) \right], \\ f_{NS}(x, Q^2) &= \sum_f \left[f_f(x, Q^2) - f_{\bar{f}}(x, Q^2) \right]. \end{aligned} \quad (2.39)$$

The functions P are called Altarelli–Parisi splitting functions. P_{ij} represent the probability that a parton j emit a collinear parton i with the momentum fraction $z = \frac{p_j^+}{p_i^+}$. At **Leading Order (LO)**, we have :

$$\begin{aligned} P_{qq}(z) &= C_F \left[\frac{1+z^2}{(1-z)_+} + \frac{3}{2} \delta(1-z) \right], \\ P_{qg}(z) &= C_F \frac{1+(1-z)^2}{z}, \\ P_{gq}(z) &= N_f \left[z^2 + (1-z)^2 \right], \\ P_{gg}(z) &= 2N_c \left[\frac{z}{(1-z)_+} + \frac{1-z}{z} + z(1-z) \right] + \frac{11N_c - 2N_f}{6} \delta(1-z), \end{aligned} \quad (2.40)$$

where the “+” prescription is adopted for regularization purpose, with [47] :

$$\int_x^1 \frac{dz}{(1-z)_+} f(z) = \int_x^1 \frac{dz}{1-z} [f(z) - f(1)] + f(1) \ln(1-x), \quad (2.41)$$

and :

$$C_F = \frac{N_c^2 - 1}{2N_c}. \quad (2.42)$$

The calculation of the splitting functions is described in App. [A.2](#).

The **DGLAP** evolution equations are actually renormalization equations for the **PDFs** (involving that observables, in an all-order calculation, do not depend on the scale choice of Q^2). These equations give us a way to *evolve* the **PDFs** from an initial scale Q_0^2 to any other scale $Q^2 > \Lambda_{QCD}$ (such that the perturbative approach holds). If we take $Q_0^2 = \Lambda_{QCD}$ and Q^2 our hard scale, then, the **DGLAP** equations describe how the parton interacting in a hadronic collision evolves from the soft scale (inside the hadron) to the hard scale of the collision. This evolution is explained (perturbatively) by successive emission of partons (corresponding to the real corrections to the light-cone wave functions, while the virtual corrections are the splitting function corrections).

Then, the **DGLAP** equations can be pictured as what we call a ladder diagram (see Fig. 2.7), with n partons emitted (in this diagram, the solid line are undefined partons). Each rung j implies a contribution of the form :

$$\alpha_s(Q^2) \int \frac{dk_{j,\perp}^2}{k_{j,\perp}^2} \int \frac{dx_j}{x_j} \dots, \quad (2.43)$$

with the dots representing some function describing the vertex j . In the approximation of Eq. (2.37), i.e with strong transverse momenta ordering, the nested integral (coming from the integration over all n rungs) results in :

$$\alpha_s^n(Q^2) \int_{Q_0^2}^{Q^2} \frac{dk_{n,\perp}^2}{k_{n,\perp}^2} \int_{Q_0^2}^{k_{n,\perp}^2} \frac{dk_{n-1,\perp}^2}{k_{n-1,\perp}^2} \dots \int_{Q_0^2}^{k_{2,\perp}^2} \frac{dk_{1,\perp}^2}{k_{1,\perp}^2} = \left(\alpha_s(Q^2) \ln \frac{Q^2}{\Lambda_{QCD}^2} \right)^n. \quad (2.44)$$

We call then the regime presented in Eq. (2.37) the **Leading Logarithmic Approximation (LLA)** in Q^2 , due to the resummation parameter being $\alpha_s(Q^2) \ln \frac{Q^2}{\Lambda_{QCD}^2}$. This regime is viable when Q^2 is large and x not too small (such that the integrals in x in Eq. (2.43) are not dominating), i.e when :

$$\alpha_s(Q^2) \ln \frac{1}{x} \ll \alpha_s(Q^2) \ln \frac{Q^2}{\Lambda_{QCD}^2} \sim 1. \quad (2.45)$$

The **DGLAP** equations can also be studied in the regime where x are also strongly ordered, i.e when :

$$x \ll x_n \ll \dots \ll x_1 \ll x_0. \quad (2.46)$$

In this regime, the resummation parameter is $\alpha_s(Q^2) \ln \frac{Q^2}{\Lambda_{QCD}^2} \ln \frac{1}{x}$ hence it is called **Double Logarithmic Approximation (DLA)**, and it is valid for :

$$\alpha_s(Q^2) \ln \frac{1}{x}, \alpha_s(Q^2) \ln \frac{Q^2}{\Lambda_{QCD}^2} \ll \alpha_s(Q^2) \ln \frac{Q^2}{\Lambda_{QCD}^2} \ln \frac{1}{x} \sim 1. \quad (2.47)$$

In this approximation, i.e the small- x limit of the **DGLAP** equation, we notice that the splitting functions P_{gg} and P_{qg} dominate (due to the term $\frac{1}{z}$), which means that the gluons dominate. In this region, the **DGLAP** evolution equations simplify to :

$$Q^2 \frac{\partial f_g(x, Q^2)}{\partial Q^2} = \frac{\alpha_s(Q^2)}{2\pi} \int_x^1 \frac{dz}{z} \frac{2N_c}{z} f_g(x/z, Q^2), \quad (2.48)$$

which can be differentiated into (after the change of variable $z \rightarrow \frac{x}{x'}$...) :

$$\frac{\partial x f_g(x, Q^2)}{\partial \ln(Q^2/\Lambda_{QCD}^2) \partial \ln(1/x)} = \frac{\alpha_s(Q^2) N_c}{\pi} x f_g(x, Q^2). \quad (2.49)$$

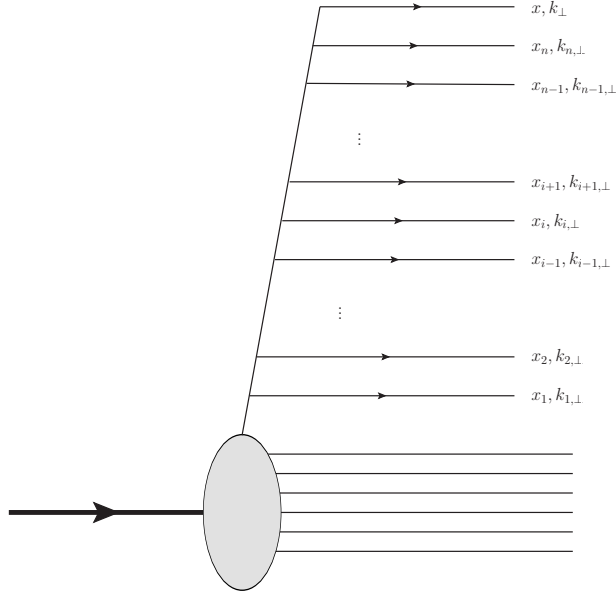


Figure 2.7: Ladder diagram describing DGLAP evolution.

The **DLA** of **DGLAP** can be represented by a ladder with only gluons, such as in Fig. 2.8.

It is usual to solve the **DGLAP** equation in moment space (using the Mellin transform, more about it and the **DGLAP** in moment space can be found in App. A.3). Using this method in the present limit (**DLA**), one can show (see [6] Sec. 2.4.6) :

$$xf_g(x, Q^2) \sim \exp \left[2 \sqrt{\frac{N_c}{\pi\beta_2} \frac{\ln(Q^2/\Lambda_{QCD})}{\ln(Q_0^2/\Lambda_{QCD})} \ln \frac{1}{x}} \right]. \quad (2.50)$$

This solution predicts the growth of the gluon **PDF** at low- x (as observed in Fig. 1.5). Also, since the virtuality Q of the photon corresponds to its transverse resolution (Δx_\perp), we can picture the **DGLAP** evolution as illustrated in Fig. 2.9 (from [6]), where the photon probes more partons of smaller transverse size when its energy increases.

2.3 Transverse Momentum Dependant PDF

In this section, we will discuss several distributions describing the parton content of hadrons, taking into account their transverse momentum. This will lead us to the **uPDFs** that follow the **BFKL** equation on one side and to the **TMDs** that follow the **CCFM** equation on the other side.

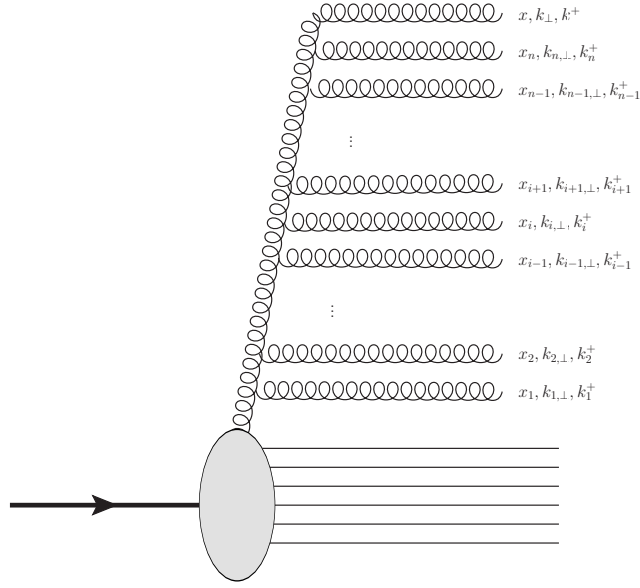


Figure 2.8: Ladder diagram describing DLA DGLAP evolution.

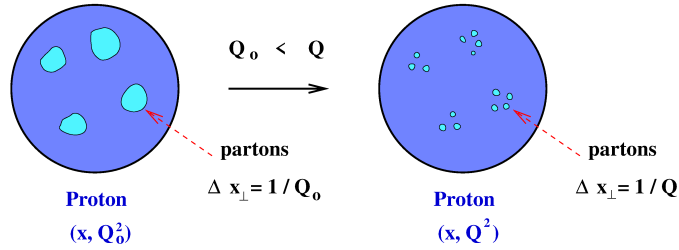


Figure 2.9: Illustration of the DGLAP evolution equation (from [6]).

2.3.1 Unintegrated PDF and BFKL

To study high-energy physics, we need to consider the small- x limit without the strong transverse momentum ordering, i.e the limit in which we resum the parameter $\alpha_s(Q^2) \ln \frac{1}{x}$, valid when :

$$\alpha_s(Q^2) \ln \frac{Q^2}{\Lambda_{QCD}^2} \ln \frac{1}{x}, \alpha_s(Q^2) \ln \frac{Q^2}{\Lambda_{QCD}^2} \ll \alpha_s(Q^2) \ln \frac{1}{x} \sim 1, \quad (2.51)$$

i.e. valid when the integrals in $x \in Eq.$ (2.43) dominate. What is particular in this limit is that, since there is no ordering in transverse momentum, we need to integrate the transverse momenta (for each emission) over their full range which implies the use of *unintegrated* PDFs (denoted uPDFs) $\mathcal{F}_{i/a}(x, k_{\perp}^2)$. In the DLA limit, such distributions

integrate into the collinear PDFs through the relation :

$$f_{i/a}(x, \mu_F^2) = \int^{\mu_F^2} dk_{\perp}^2 \mathcal{F}_{i/a}(x, k_{\perp}^2). \quad (2.52)$$

These uPDFs can be understood as the probability to hit a parton i of longitudinal transverse momentum x and transverse momentum k_{\perp} . Since gluon dominates at small- x ⁹, we will only consider the gluon uPDF $\mathcal{F}_{g/a}$.

It is still possible to evaluate the dependence in x of the gluon uPDF through the emission of gluons. While there is no ordering in k_{\perp} , the ordering in the transverse momentum fraction x impose ordering in the + and - component, such as :

$$\begin{aligned} k_1^+ &\gg k_2^+ \gg \dots \gg k_n^+, \\ k_1^- &\ll k_2^- \ll \dots \ll k_n^-, \\ k_{1,\perp} &\sim k_{2,\perp} \sim \dots \sim k_{n,\perp}, \end{aligned} \quad (2.53)$$

these conditions are referred as *multi-Regge kinematics* and they also imply rapidity ordering :

$$y_1 \gg y_2 \gg \dots \gg y_n, \quad (2.54)$$

where the rapidity is defined as $y = \frac{1}{2} \ln \frac{k^+}{k^-}$. In this conditions, the gluon uPDF follow the Balitsky-Fadin-Kuraev-Lipatov (BFKL) equation [48-50] :

BFKL Evolution Equation

$$\begin{aligned} \frac{\partial \mathcal{F}_{g/a}(x, k_{\perp}^2)}{\partial \ln(1/x)} = \frac{\alpha_s N_c}{\pi^2} \int \frac{d^2 q_{\perp}}{q_{\perp}^2} \left(\frac{q_{\perp}^2 \mathcal{F}_{g/a}(x, q_{\perp}^2) - k_{\perp}^2 \mathcal{F}_{g/a}(x, k_{\perp}^2)}{|q_{\perp}^2 - k_{\perp}^2|} \right. \\ \left. + \frac{k_{\perp}^2 \mathcal{F}_{g/a}(x, k_{\perp}^2)}{\sqrt{4q_{\perp}^4 + k_{\perp}^4}} \right), \end{aligned} \quad (2.55)$$

which evolves the gluon uPDF from a value x_0 to a smaller x ¹⁰ and can be schematized as a ladder diagram, as shown in Fig. 2.10.

In this ladder, appear Reggeized gluons (double corkscrew lines) and Lipatov vertices (large solid circles). The Reggeized gluons represent the sum of exchanges of any number of gluons, in any order, as shown in Fig. 2.11. All these gluon exchanges contribute at some power of $\alpha_s \ln s \sim \alpha_s \ln \frac{1}{x}$, hence have to be resummed at low- x . The Lipatov vertex arises from no ordering of the transverse momentum and summation the real corrections coming from any part of the ladder, as shown in Fig. 2.12.

The expression for the Reggeized gluon propagator and the Lipatov vertex will be given later, in Sec. 3.2.1.

⁹Because of the form of the splitting functions (which doesn't depend on the transverse momentum ordering).

¹⁰since the equation holds at small- x ...

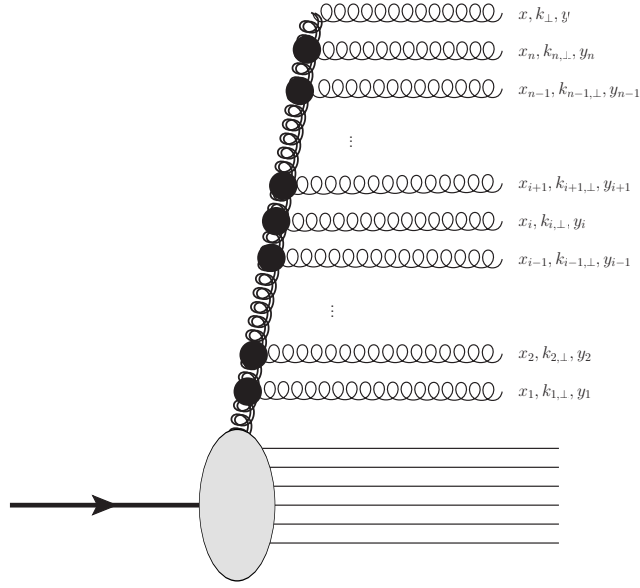


Figure 2.10: Ladder diagram describing BFKL evolution.

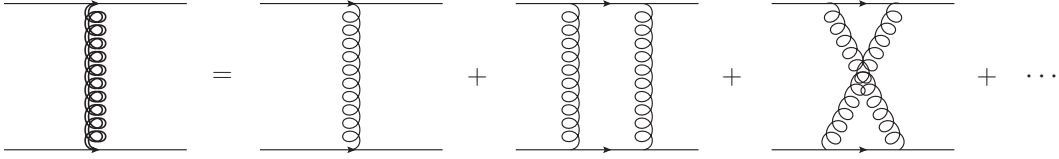


Figure 2.11: The Reggeized gluon.

At fixed running constant α_s and in the saddle point approximation[51], an analytic solution of the BFKL can be found [50]. It reads :

$$\mathcal{F}_{g/a}(x, k_{\perp}^2) \simeq \left(\frac{x}{x_0}\right)^{-\lambda} \frac{(k_{\perp}^2)^{\frac{3}{2}}}{\sqrt{56N_c\alpha_s\zeta(3)\ln(x_0/x)}} \exp\left[-\frac{\pi\ln^2(k_{\perp}^2/k_{0,\perp}^2)}{56N_c\alpha_s\zeta(3)\ln(x_0/x)}\right] \quad (2.56)$$

$$\sim \left(\frac{x}{x_0}\right)^{-\lambda},$$

with $\lambda = \frac{N_c\alpha_s}{\pi}4\ln 2$ and ζ the Riemann Zeta function. We observe then that the gluon density increases as x decreases (as the inverse power of x). This stiff growth is actually a problem, it violates unitarity. Indeed, it lead to cross-section behaving like $\sigma_{tot} \sim s^{\lambda}$, which contradicts the Froissart-Martin bound [52, 53] that states, for any QCD cross-section :

$$\sigma_{tot} \lesssim \ln s^{11}. \quad (2.57)$$

¹¹The symbol \lesssim expresses here the fact that, for simplicity, we have dropped a constant term

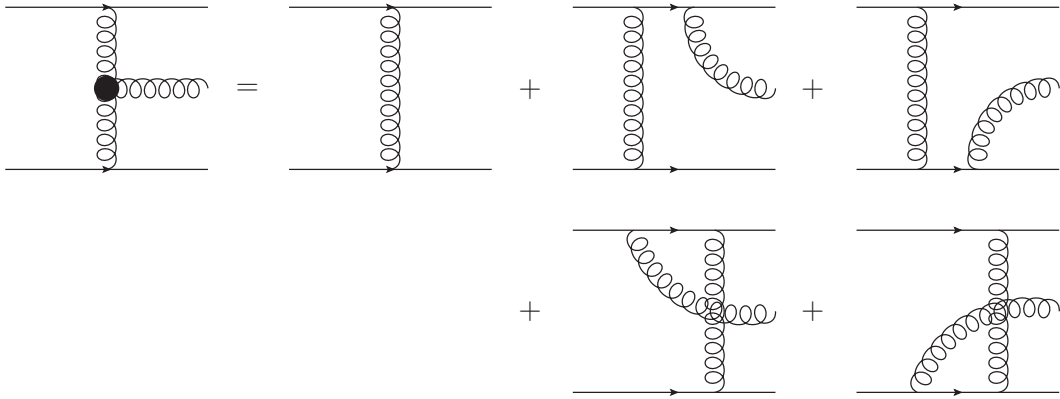


Figure 2.12: Lipatov vertex.

Also, Eq. (2.56) clearly demonstrates a diffusion behavior in transverse momentum, as a Gaussian in $\ln k_{\perp}^2$ of width proportional to $\ln(x_0/x)$. This behavior directly comes from the no-ordering in transverse momentum, which can assimilate the BFKL evolution to a random walk in k_{\perp} . The problem is then that partons can diffuse to transverse momentum $k_{\perp} < \Lambda_{QCD}$ (infrared region) where pQCD fails [54, 55] limiting the applicability of BFKL equation. This issue can be avoided by setting a lower cutoff $k_{\perp,min}$.

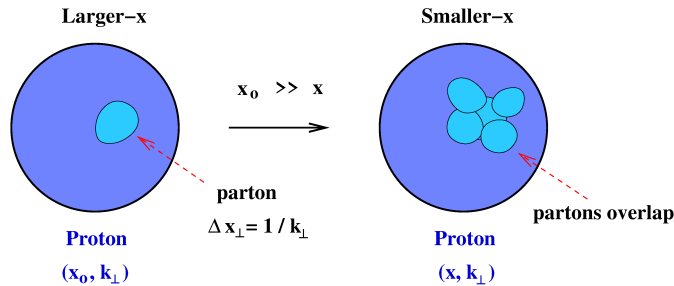


Figure 2.13: Illustration of the BFKL evolution equation (from [6]).

The typical transverse size x_{\perp} is the same for every emitted parton $\sim 1/k_{\perp}$ (due to no k_{\perp} ordering). Then we can visualize the BFKL equation as the growth of the number of partons (correlated to $x\mathcal{F}_{g/a}$) of the same size when x decreases. This description is illustrated in Fig. 2.13 from [6], and shows that at small- x , the wave functions of the partons may overlap which brings us to the idea of *saturation* (see Sec. 2.4).

The uPDF derived from the BFKL equation can be used in a factorization approach,

the *High Energy Factorization* or k_T -factorization [29, 30] :

$$\begin{aligned} d\sigma_{ab \rightarrow X}(P_a, P_b) = & \sum_{i,j} \int \frac{dx_i}{x_i} \frac{dx_j}{x_j} \int dk_{i,\perp} dk_{j,\perp} \mathcal{F}_{i/a}(x_i, k_{i,\perp}) \\ & \times \mathcal{F}_{j/b}(x_j, k_{j,\perp}) d\hat{\sigma}_{i^*j^* \rightarrow X}(x_i P_a, x_j P_b, k_{i,\perp}, k_{j,\perp}). \end{aligned} \quad (2.58)$$

This factorization has been proven for heavy quark production and holds for $s \gg Q$. The partonic cross-section in this case has 2 off-shell legs (the calculation of the amplitudes needed to calculate it will be the goal of Chap. 3).

2.3.2 TMDs and CCFM

The BFKL equation resums the singularities coming from the term in $\frac{1}{z}$ (dominating at small- x) in the splitting function. It is possible to resum in the same time the singularities coming from the $\frac{1}{1-z}$ terms (due to soft gluon emission) through coherent emission, i.e for angular ordering :

$$\theta_1 < \theta_2 < \dots < \theta_n. \quad (2.59)$$

This region is described by the Catani-Ciafaloni-Fiorani-Marchesini (CCFM) equation [56–58] which resums both $\alpha_s \ln \frac{1}{x}$ and $\alpha_s \ln \frac{1}{1-x}$ terms. This equation describes the scale evolution of the gluon TMD $\mathcal{A}_g(x, k_\perp^2, \mu^2)$, both dependent on k_\perp and a scale μ (contrary to the uPDF $\mathcal{F}_{i/a}(x, k_\perp)$), as a solution of this equation.

Remark : Here, we should precise that the term “TMD” was originally used in the context of *TMD factorization* [59, 60], valid for low transverse momentum $k_\perp^2 \ll Q^2$ and where the parton distributions follow the Collins-Soper-Sterman (CSS) evolution equations [61, 62]. This approach is especially useful to study observables sensitive to the initial parton transverse momentum (such as the transverse-momentum imbalance or transverse spin asymmetry in DY process...). Now, the term is also used in the context of small- x physics, and we will use it in this sense.

The CCFM equation can be written in a form comparable to DGLAP :

CCFM Evolution Equation

$$\bar{q}^2 \frac{d}{d\bar{q}^2} \frac{x \mathcal{A}_g(x, k_\perp^2, \bar{q}^2)}{\Delta_s(\bar{q}^2, Q_0^2)} = \int dz \frac{d\phi}{2\pi} \frac{\tilde{P}_{gg}\left(z, \left(\frac{\bar{q}}{z}\right)^2, k_\perp^2\right)}{\Delta_s(\bar{q}^2, Q_0^2)} x' \mathcal{A}_g\left(x', k_\perp'^2, \left(\frac{\bar{q}}{z}\right)^2\right), \quad (2.60)$$

with $k_\perp' = |k_\perp + \frac{1-z}{z}q|$ (where q is at azimuthal angle ϕ), $z = \frac{x}{x'}$ and $\bar{q} = \frac{|q|}{1-z}$ is the rescaled transverse momentum. The $\mathcal{A}_{g/a}(x, k_\perp^2, \mu^2)$ describe the probability to find a gluon in hadron a carrying the longitudinal momentum fraction x at scale μ^2 and having

a transverse momentum k_\perp . The Sudakov form factor is defined as :

$$\Delta_s(\bar{q}^2, Q_0^2) = \exp \left(- \int_{Q_0^2}^{\bar{q}^2} \frac{d\bar{q}'^2}{\bar{q}'^2} \int_0^{1-\frac{Q_0}{\bar{q}'}} dz \frac{\bar{\alpha}(\bar{q}'^2(1-z)^2)}{1-z} \right), \quad (2.61)$$

with $\bar{\alpha} = \frac{N_c \alpha_s}{2\pi}$. The modified splitting function \tilde{P}_{gg} reads :

$$\tilde{P}_{gg} \left(z, \left(\frac{\bar{q}}{z} \right)^2, k_\perp^2 \right) = \frac{\bar{\alpha}(\bar{q}^2(1-z)^2)}{1-z} + \frac{\alpha_s(k_\perp^2)}{z} \Delta_{NS} \left(z, \left(\frac{\bar{q}}{z} \right)^2, k_\perp^2 \right), \quad (2.62)$$

in which the so-called non-Sudakov factor appears :

$$\Delta_{NS} \left(z, \bar{q}^2, k_\perp^2 \right) = \exp \left(-\alpha_s(k_\perp^2) \int_0^{1-\frac{Q_0}{\bar{q}}} \frac{dz'}{z'} \int \frac{d\bar{q}'^2}{\bar{q}'^2} \theta(k_\perp^2 - \bar{q}'^2) \theta(\bar{q}'^2 - z'^2 \bar{q}^2) \right). \quad (2.63)$$

The Sudakov form factor resums contribution from large z region while the non-Sudakov form factor resums small z contributions.

The CCFM equation is equivalent to DGLAP (for gluon only) at large x while it reduces to BFKL at small- x . This evolution can be schematized as a ladder diagram (see Fig. 2.14).

The rescaled transverse momentum is related to the emission angle by :

$$\frac{\bar{q}_{i+1}}{\bar{q}_i} = \frac{\theta_{i+1}}{\theta_i}. \quad (2.64)$$

Then, the angular ordering $\theta_i < \theta_{i+1}$ implies :

$$\bar{q}_{i+1} > z_i \bar{q}_i. \quad (2.65)$$

In this equation, we regain the transverse momentum ordering at large z (like in DGLAP) while we also see the random walk at $z \rightarrow 0$ (like in BFKL).

Like with the uPDFs (see Eq. (2.58)) it is possible to use the TMDs to redefine k_T -factorization :

k_T -factorization

$$\begin{aligned} d\sigma_{ab \rightarrow X}(P_a, P_b) &= \sum_{i,j} \int \frac{dx_i}{x_i} \frac{dx_j}{x_j} \int dk_{i,\perp} dk_{j,\perp} \mathcal{A}_{i/a}(x_i, k_{i,\perp}, \mu_F^2) \\ &\quad \times \mathcal{A}_{j/b}(x_j, k_{j,\perp}, \mu_F^2) d\hat{\sigma}_{i^*j^* \rightarrow X}(x_i P_a, x_j P_b, k_{i,\perp}, k_{j,\perp}, \mu_R^2). \end{aligned} \quad (2.66)$$

We will be particularly interested in this factorization scheme in the following.

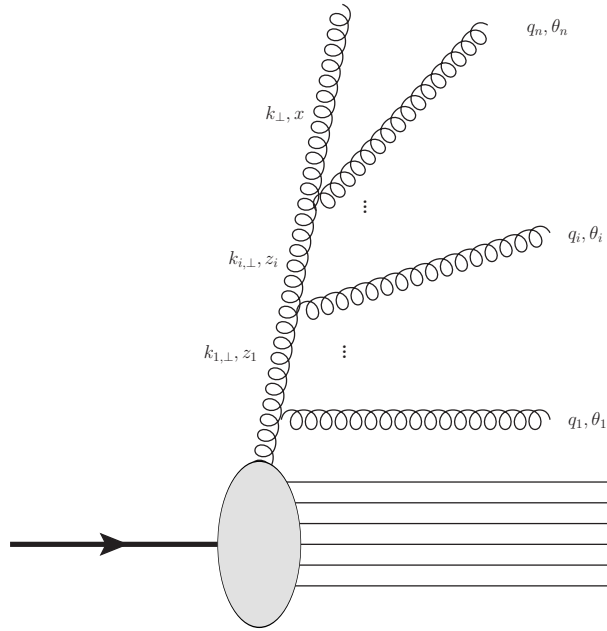


Figure 2.14: Ladder diagram describing CCFM evolution equation, showing the angular ordering of Eq. (2.59).

When there is an asymmetry in the initial state configuration, which reflects, by momentum conservation, on final states (that is the case for forward jets), it is actually suitable to use what we will refer to as *hybrid factorization* [63–67] :

Hybrid Factorization

$$\begin{aligned}
 d\sigma_{ab \rightarrow X}(P_a, P_b) = & \sum_{i,j} \int \frac{dx_i}{x_i} \frac{dx_j}{x_j} \int dk_{i,\perp} dk_{j,\perp} f_{i/a}(x_i, \mu_F^2) \\
 & \times \mathcal{A}_{j/b}(x_j, k_{j,\perp}, \mu_F^2) d\hat{\sigma}_{ij^* \rightarrow X}(x_i P_a, x_j P_b, k_{j,\perp}, \mu_R^2).
 \end{aligned} \tag{2.67}$$

where the initial state asymmetry is characterized by $x_i \sim 1$ and $x_j \ll 1$ and $d\hat{\sigma}_{ij^*}$ is calculable from amplitudes with one off-shell leg. This approach is used to describe forward jet hadroproduction, where the transverse momentum of parton i is negligible.

2.4 Saturation

We saw in Sec. 2.3.1 that the BFKL equation violates unitarity at small- x . Actually, when the gluon density becomes too high, the wave functions of the gluons overlap and then gluons can *recombine* (and not only split). When these recombinations are no more negligible compared to the splittings, we say that the gluons *saturates*.

The recombination implies corrections to the BFKL equation quadratic in the gluon PDF $\mathcal{F}_{g/a}$. This has first been implemented by considering recombination of BFKL ladders, which led to the Gribov-Levin-Ryskin (GLR) equation [68]. Another approach to saturation, in DIS, consists in boosting the frame of the struck parton such that the virtual photon appears as a dipole (a created pair, see illustration in Fig. 2.15).

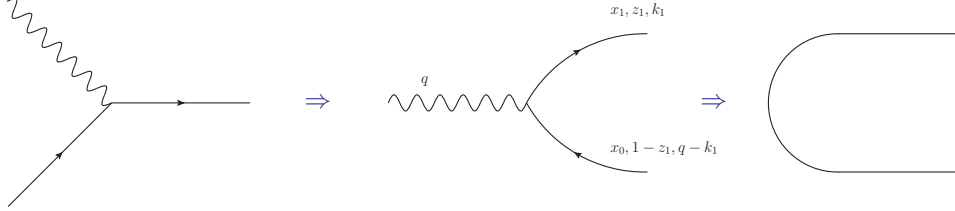


Figure 2.15: Illustration of the dipole model.

Considering single dipole scattering leads to the BFKL equation written in terms of the dipole amplitude \mathcal{N} :

$$\frac{\partial \mathcal{N}}{\partial \ln(1/x)} = \frac{\alpha_s N_c}{2\pi^2 \sigma_0} \int d^2 z_{\perp} \frac{r_{\perp}^2}{r_{1,\perp}^2 r_{2,\perp}^2} [\mathcal{N}_1 + \mathcal{N}_2 - \mathcal{N}] , \quad (2.68)$$

with :

$$\begin{aligned} \mathcal{N} &= \mathcal{N}(x_{1,\perp} - x_{0,\perp}, (x_{1,\perp} + x_{0,\perp})/2, x), \\ \mathcal{N}_1 &= \mathcal{N}(x_{1,\perp} - z_{\perp}, (x_{1,\perp} + z_{\perp})/2, x), \\ \mathcal{N}_2 &= \mathcal{N}(z_{\perp} - x_{0,\perp}, (x_{0,\perp} + z_{\perp})/2, x), \end{aligned} \quad (2.69)$$

σ_0 is the born level dipole cross-section and :

$$\begin{aligned} \mathcal{N}(r_{\perp}, x) &= \frac{4\pi\alpha_s}{3} \int \frac{d^2 k_{\perp}}{k_{\perp}^4} \mathcal{F}_{g/a}(x, k_{\perp}^2) (1 - e^{ik_{\perp} \cdot r_{\perp}}) \\ &= 2\pi \int_0^{+\infty} db^2 \mathcal{N}(r_{\perp}, b^2, x). \end{aligned} \quad (2.70)$$

Considering multiple dipole scattering introduces a quadratic term which, in the large N_c limit, leads to the Balitsky-Kovchegov (BK) equation [69–71] :

$$\frac{\partial \mathcal{N}}{\partial \ln(1/x)} = \frac{\alpha_s N_c}{2\pi^2 \sigma_0} \int d^2 z_{\perp} \frac{r_{\perp}^2}{r_{1,\perp}^2 r_{2,\perp}^2} [\mathcal{N}_1 + \mathcal{N}_2 - \mathcal{N} - \mathcal{N}_1 \mathcal{N}_2]. \quad (2.71)$$

This equation introduces a saturation scale $Q_s(x)$ at which saturation effects become important. Incorporating sub-leading N_c correction would lead us to the Color-Glass Condensate (CGC) domain [72] and the Jalilian-Marian, Iancu, McLerran, Weigert, Leonidov and Kovner (JIMWLK) equation [73–75] that we won't introduce here.

We have now a wide picture of the parton distribution function evolution in the perturbative regime, in the $(\ln \frac{1}{x}, \ln Q^2)$ plane, as summarized in Fig. 2.16 (from [76]).

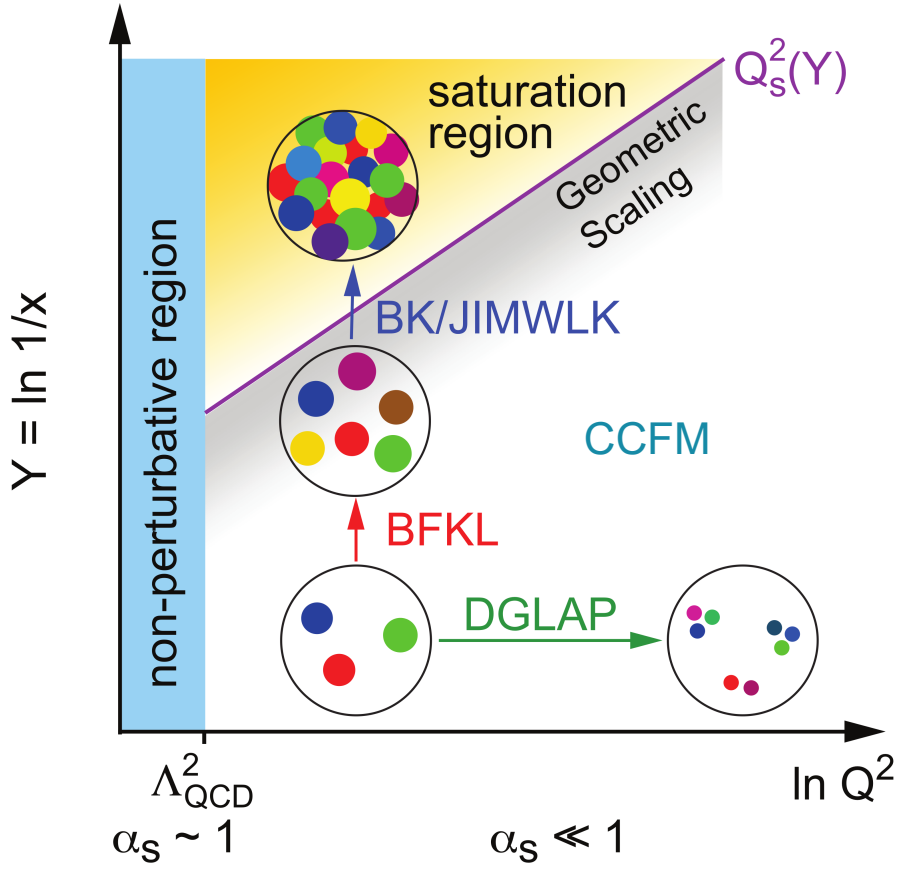


Figure 2.16: Evolution equations in the $\ln \frac{1}{x}$, $\ln Q^2$ plane (from [76]).

2.5 The Parton Branching method

One method to obtain the TMDs $\mathcal{A}_{i/a}$ is the so-called parton-branching method [77–80]. This method is based on an iterative resolution of the DGLAP equations where on each step the transverse momentum is tracked. But before going into this iterative solution, we first introduce a higher cutoff z_M on the integral over z such that $1 - z_M \sim \frac{\Lambda_{QCD}}{Q^2}$. This cutoff translates the fact that emissions with a momentum fraction too close to 1 cannot be resolved (when the resolution scale in the transverse distance between radiations is finite). When accounting for resolvable radiation only, it is possible to show¹², that the

¹²See the demonstration in [77].

DGLAP equation write :

$$\frac{\partial f_i(x, \mu_F^2)}{\partial \ln \mu_F^2} = \sum_j \left[\int_x^{z_M} \frac{dz}{z} P_{ij}^{(Re)}(z, \mu_F^2) f_j(x/z, \mu_F^2) - \int_0^{z_M} dz P_{ji}^{(Re)}(z, \mu_F^2) f_j(x/z, \mu_F^2) \right] + \mathcal{O}(1 - z_M), \quad (2.72)$$

where $P_{ji}^{(Re)}$ represents the real emission contribution to the splitting function P_{ji} . Note that the running coupling has been absorbed in the splitting function to make it more convenient to generalize at any order. We write :

$$P_{ji}(z, \mu^2) = \sum_{n \in \mathbb{N}} \left(\frac{\alpha_s(\mu^2)}{2\pi} \right)^n P_{ji}^{(n-1)}(z), \quad (2.73)$$

and an equivalent decomposition for $P_{ji}^{(Re)}$. Note that the functions $P_{ji}^{(0)}(z)$ corresponds to the splitting functions in Eq. (2.40). At LO, we have :

$$\begin{aligned} P_{qq}^{(Re,0)}(z) &= C_F [1 - z], \\ P_{qg}^{(Re,0)}(z) &= C_F \frac{1 + (1 - z)^2}{z}, \\ P_{gq}^{(Re,0)}(z) &= N_f [z^2 + (1 - z)^2], \\ P_{gg}^{(Re,0)}(z) &= 2N_c \left[\frac{1}{1 - z} + \frac{1 - z}{z} + z(1 - z) - 1 \right]. \end{aligned} \quad (2.74)$$

The evolution equation in Eq. (2.72) can be solved using an iterative MC procedure by introducing the Sudakov form factor $\Delta_i(z_M, \mu^2, \mu_0^2)$ defined as :

$$\Delta_i(z_M, \mu^2, \mu_0^2) = \exp \left(- \sum_j \int_{\mu_0^2}^{\mu^2} \frac{d\mu'^2}{\mu'^2} \int_0^{z_M} dz z P_{ji}^{(Re)}(z, \mu'^2) \right). \quad (2.75)$$

$\Delta_i(z_M, \mu^2, \mu_0^2)$ represents the probability that a parton i evolves from scale μ_0^2 to scale μ^2 without resolvable emission (no branching). Note that this Sudakov form factors is equivalent, when the pole in $z = 1$ in the splitting function dominates, to the one appearing in the CCFM equation (see Eq. (2.61)) with an upper cutoff on the integral over z set by hand and a different choice of scale for the running constant. With this Sudakov form factor, we can rewrite Eq. (2.72) as :

$$\begin{aligned} \frac{\partial f_i(x, \mu^2)}{\partial \ln \mu_F^2} &= \sum_j \int_x^{z_M} \frac{dz}{z} P_{ij}^{(Re)}(z, \mu^2) f_j(x/z, \mu^2) \\ &\quad + \frac{1}{\Delta_i(\mu^2)} \frac{\partial \Delta_i(\mu^2)}{\partial \mu^2} f_j(x, \mu^2). \end{aligned} \quad (2.76)$$

We have dropped z_M and μ_0^2 from the Sudakov form factor argument for simplicity (since it doesn't change). Integrating this equation leads (using $\Delta_a(\mu_0^2, \mu_0^2) = 0$) to :

$$f_i(x, \mu^2) = \Delta_i(\mu^2) f_i(x, \mu_0^2) + \sum_j \int_{\mu_0^2}^{\mu^2} \frac{d\mu'^2}{\mu'^2} \frac{\Delta_i(\mu^2)}{\Delta_i(\mu'^2)} \int_0^{z_M} \frac{dz}{z} P_{ij}^{(Re)}(z, \mu'^2) f_j(x/z, \mu'^2), \quad (2.77)$$

which is a Fredholm-type integral equation that can be solved by iteration. Indeed, in Eq. (2.77), one can use the expression of $f_i(x, \mu^2)$ (i.e the right-hand side of the equation) and use it to express $f_j(x/z, \mu'^2)$ under the integral (2nd term of the right-hand side of the equation). This can be done again and again, leading to :

$$\begin{aligned} f_i(x, \mu^2) &= \Delta_i(\mu^2) f_i(x, \mu_0^2) \\ &+ \sum_{i_1} \int_{\mu_0^2}^{\mu^2} \frac{d\mu_1^2}{\mu_1^2} \frac{\Delta_i(\mu^2)}{\Delta_i(\mu_1^2)} \int_x^{z_M} \frac{dz_1}{z_1} P_{ij}^{(Re)}(z_1, \mu_1^2) \Delta_{i_1}(\mu_1^2) f_j(x/z_1, \mu_0^2) \\ &+ \sum_{i_1, i_2} \int_{\mu_0^2}^{\mu^2} \frac{d\mu_1^2}{\mu_1^2} \frac{\Delta_i(\mu^2)}{\Delta_i(\mu_1^2)} \int_{\mu_0^2}^{\mu_1^2} \frac{d\mu_1'^2}{\mu_1'^2} \frac{\Delta_{i_1}(\mu_1^2)}{\Delta_{i_1}(\mu_1'^2)} \Delta_{i_1}(\mu_1'^2) \\ &\quad \times \int_x^{z_M} \frac{dz_1}{z_1} P_{ii_1}^{(Re)}(z_1, \mu_1^2) \int_x^{z_M} \frac{dz_2}{z_2} P_{i_1 i_2}^{(Re)}(z_2, \mu_2^2) \Delta_{i_2}(\mu_2^2) f_k(x/(z_1 z_2), \mu_0^2) \\ &\vdots \\ &+ \sum_{i_1, i_2, \dots, i_n} \int_{\mu_0^2}^{\mu^2} \frac{d\mu_1^2}{\mu_1^2} \frac{\Delta_i(\mu^2)}{\Delta_i(\mu_1^2)} \int_{\mu_0^2}^{\mu_1^2} \frac{d\mu_2^2}{\mu_2^2} \frac{\Delta_{i_1}(\mu_1^2)}{\Delta_{i_1}(\mu_2^2)} \int_{\mu_0^2}^{\mu_2^2} \frac{d\mu_2'^2}{\mu_2'^2} \frac{\Delta_{i_2}(\mu_2^2)}{\Delta_{i_2}(\mu_2'^2)} \dots \\ &\quad \times \int_x^{z_M} \frac{dz_1}{z_1} P_{ii_1}^{(Re)}(z_1, \mu_1^2) \int_x^{z_M} \frac{dz_2}{z_2} P_{i_1 i_2}^{(Re)}(z_2, \mu_2^2) \dots \\ &\quad \times \Delta_{i_n}(\mu_n^2) f_k \left(\frac{x}{\prod_{i=1}^n z_i}, \mu_0^2 \right) \\ &\vdots \end{aligned} \quad (2.78)$$

This way, it is possible to determine $f_i(x, \mu^2)$ from $f_i(x, \mu_0^2)$ at any order in this iterative procedure, i.e it is possible to evolve f_i from the scale μ_0^2 to the scale μ^2 . In the previous sum, it is interesting to note that the first term corresponds to the evolution between μ_0^2 and μ^2 without branching, the second is with one branching, and so on.

This equation (Eq. (2.77)) can be solved with a MC approach that reduces the problem to generating the splitting variables z_i and the scales μ_i . The scale for the $i + 1$ th branching μ_{i+1} is obtained solving :

$$r_0 \int_{\mu_i}^{\mu} d\Delta_i(z_M, \mu^2, \mu_0^2) = \int_{\mu_i}^{\mu_{i+1}} d\Delta_i(z_M, \mu^2, \mu_0^2), \quad (2.79)$$

with $r_0 \in [0, 1]$ a random number. This equation reflects the definition of the Sudakov form factor (Eq. (2.75)). In the same way, the splitting variables z_i are obtained by solving :

$$\int_{z_{min}}^{z_{i+1}} dz' P_{ij}^{(Re)}(z', \mu_{i+1}^2) = r_1 \int_{z_{min}}^{z_M} dz' P_{ij}^{(Re)}(z', \mu_{i+1}^2), \quad (2.80)$$

with $r_1 \in [0, 1]$ a random number and z_{min} the lowest kinematics allowed. Then, the iterative procedure to solve Eq. (2.77) can be schematized as is in Fig. 2.17.

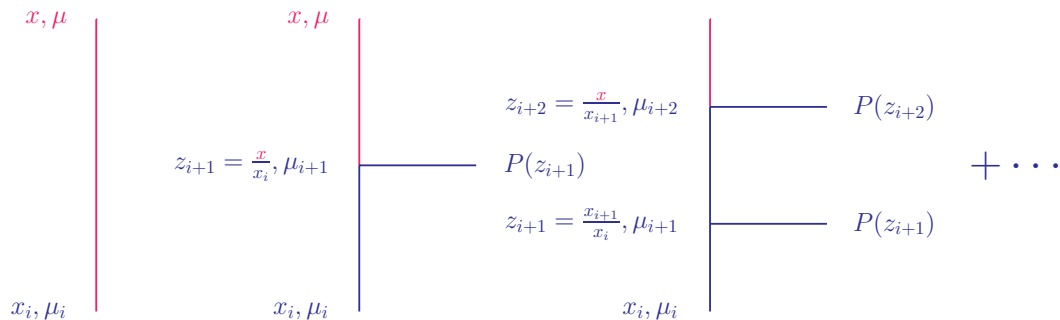


Figure 2.17: Illustration of the iteration solution : a parton can evolve from scale μ_i to scale μ without branching (left), with one (middle), two (right), or more branching.

So far, it is a method to solve DGLAP equations, i.e to evolve collinear PDFs. Actually, in the MC approach, it is possible to keep track of the kinematics in each vertex, especially of the transverse momentum. We consider the branching in Fig. 2.18. Then, the transverse momentum q_k can be associated with the scale μ through the angular ordering¹³ relation [81–83] :

$$\mu = \frac{|q_k|}{1-z}. \quad (2.81)$$

So, the transverse momentum of the evolved parton k_\perp , after n emissions, is the opposite of the sum of the transverse momenta of the emitted partons, i.e :

$$k_\perp = - \sum_k q_k. \quad (2.82)$$

This angular ordering permits to construct the TMDs $\mathcal{A}_i(x, k_\perp, \mu^2)$ in a consistent way¹⁴ [84], that integrates into f_i :

$$\int \frac{d^2 k_\perp}{\pi} \mathcal{A}_i(x, k_\perp, \mu^2) = f_i(x, \mu^2). \quad (2.83)$$

¹³This relation implies that the emissions angles are ordered.

¹⁴It can be shown that \mathcal{A}_i does not depend on z_M , as long as it is large enough (with this ordering).

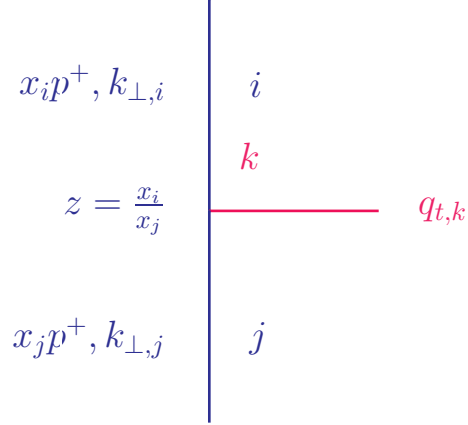


Figure 2.18: Branching $j \rightarrow i + k$.

The evolution of the TMDs is then implied by Eq. (2.77) and reads :

Parton Branching Evolution Equation

$$\begin{aligned}
\mathcal{A}_i(x, k_{\perp}, \mu^2) &= \Delta_i(\mu^2) \mathcal{A}_i(x, k_{\perp}, \mu_0^2) \\
&+ \sum_j \int \frac{dq'^2}{\pi q'^2} \frac{\Delta_i(\mu^2)}{\Delta_i(q'^2)} \Theta(\mu^2 - q'^2) \Theta(q'^2 - \mu_0^2) \\
&\times \int_x^{z_M} \frac{dz}{z} P_{ij}^{(Re)}(z, q'^2) \mathcal{A}_j(x/z, k_{\perp} + (1-z)q', q'^2).
\end{aligned} \tag{2.84}$$

Similar to PDF, this equation can also be solved by iteration :

$$\begin{aligned}
\mathcal{A}_i(x, k_\perp, \mu^2) &= \Delta_i(\mu^2) \mathcal{A}_i(x, k_\perp, \mu_0^2) \\
&+ \sum_j \int \frac{dq_1^2}{\pi q_1^2} \Theta(\mu^2 - q_1^2) \Theta(q_1^2 - \mu_0^2) \frac{\Delta_i(\mu^2)}{\Delta_i(q_1^2)} \\
&\quad \times \int_x^{z_M} \frac{dz_1}{z_1} P_{ij}^{(Re)}(z_1, q_1^2) \Delta_j(q_1^2) \mathcal{A}_j(x/z_1, k_\perp + (1 - z_1)q_1, q_1^2) \\
&+ \sum_{jk} \int \frac{dq_1^2}{\pi q_1^2} \Theta(q_1^2 - q_2^2) \Theta(q_2^2 - \mu_0^2) \frac{\Delta_i(\mu^2)}{\Delta_i(q_1^2)} \\
&\quad \times \int \frac{dq_2^2}{\pi q_2^2} \Theta(\mu^2 - q_2^2) \Theta(q_2^2 - \mu_0^2) \frac{\Delta_j(q_1^2)}{\Delta_j(q_2^2)} \Delta_i(q_2^2) \\
&\quad \times \int_x^{z_M} \frac{dz_1}{z_1} P_{ij}^{(Re)}(z_1, q_1^2) \int_x^{z_M} \frac{dz_2}{z_2} P_{jk}^{(Re)}(z_2, q_2^2) \Delta_j(q_2^2) \\
&\quad \times \mathcal{A}_j(x/(z_1 z_2), k_\perp + (1 - z_1)q_1 + (1 - z_2)q_2, q_2^2) \\
&+ \dots
\end{aligned} \tag{2.85}$$

Again, given a TMD at some initial scale $\mathcal{A}_i(x, k_\perp, \mu_0^2)$, we can evolve it at any scale with this method (usually, the initial scale is taken low).

As shown in [79], it is possible to rewrite the evolution equations of both f_i and \mathcal{A}_i as the convolution of an evolution kernel \mathcal{K} and a starting distribution (at scale μ_0 :

$$\begin{aligned}
\mathcal{A}_i(x, k_\perp, \mu^2) &= \int dx' \mathcal{A}_{0,j}(x', k_{0,\perp}, \mu_0^2) \frac{1}{x'} \mathcal{K}_{ji} \left(\frac{x}{x'}, k_{0,\perp}, k_\perp, \mu_0^2, \mu^2 \right), \\
f_i(x, \mu^2) &= \int dx' f_{0,j}(x', \mu_0^2) \frac{1}{x'} \mathcal{K}_{ji}^{int} \left(\frac{x}{x'}, \mu_0^2, \mu^2 \right).
\end{aligned} \tag{2.86}$$

In a recent work [85], this method has been extended with the use of transverse momentum dependent splitting functions.

2.6 Nuclear PB-TMD phenomenology

This section aims to present TMDs obtained (by collaborators) for lead nucleus from the PB method just presented (here with NLO splitting functions)¹⁵. We will study them, and test them to reproduce Z boson production Compact Muon Solenoid (CMS) data for p Pb collision. The results presented here have been published in [1].

2.6.1 Application of the Parton Branching method

We have seen in the previous section (Sec. 2.5) that we can use the PB method to obtain a TMD at any (perturbative) scale, evolving a TMD from a fixed scale μ_0 . We then

¹⁵It was the first application of the PB method on nTMD.

need a starting TMD. Actually, we use a known collinear PDF at scale μ_0 ($f_{0,i}(x, \mu_0^2)$) on top of which we add an independent (in the sense factorized) transverse momentum dependence. We take this dependence Gaussian (reproducing the diffusive behavior we saw in the BFKL solutions Eq. (2.56)), leading to :

$$\mathcal{A}_{0,i}(x, k_{0,\perp}, \mu_0^2) = f_{0,i}(x, \mu_0^2) \cdot e^{\frac{-|k_{0,\perp}^2|}{\sigma^2}}, \quad (2.87)$$

with $\sigma^0 = q_0^2/2$ and $q_0 = 0.5\text{GeV}$. This initial distribution is then convoluted with the evolution kernel \mathcal{K} (as in the first line of Eq. (2.86)) on fixed values of x , k_\perp , and μ , to fill a 3-dimensional grid (of size 50x50x50). The points on the grid are logarithmically spaced in the range $0.01 < k_\perp < 14.10^{-3}\text{GeV}$, $\mu_0 < \mu < 14.10^{-3}\text{GeV}$ (different values of μ_0 will be used) and $10^{-6} < x < 1$.

2.6.2 Nuclear PDF used

To initiate our PB method, we need a starting PDF. In practice, to obtain a PDF, one uses a phenomenological model with parameters that are fitted to data at a given scale and then evolves it through the DGLAP evolution equation. Many groups work on data analysis to provide PDFs with increasing precision such as MMHT [86, 87], NNPDF[88], CTEQ-TEA [89], HERAPDF [28, 90] or MSTW [91]. Their approaches may differ from the data used, the phenomenological model fitted, the evaluation of the uncertainties, or the treatment of heavy flavors, but they are all based on DGLAP evolution using the same renormalization scale.

Since we aim at studying $p\text{Pb}$ collision in Sec. 2.6.4, we need both proton and lead starting PDFs (we will mention the latter as nuclear Parton Distribution Function (nPDF)). For the proton, PDFs from HERAPDF2.0 [28] will be used while for the lead, we will compare results using the 2 following sets ;

- nCTEQ15 [92] nPDFs,
- EPPS16 [93] nPDFs.

Also, in Sec. 2.6.4, we will compare results obtained not only using k_T -factorization but also hybrid and collinear factorization. Then, the PDF used in the latter cases will be the one used to initiate the parton branching method (see above).

An important difference between these 2 nPDFs is that, in nCTEQ15, they parametrize the nPDF at initial scale in the same fashion as the proton PDF (like in [94]) with (for a parton i from a proton in the nucleus A) :

$$x f_{i/A}(x, \mu_0^2) = c_0 x^{c_1} (1-x)^{c_2} e^{c_3 x} (1 + e^{c_4 x})^{c_5}, \quad (2.88)$$

where $\{c_i\}_{i \in [0,5]} \in \mathbb{R}$ are the parameters that are fitted. On the other end, in EPPS16, they do not parametrize directly the nPDF but instead, they parametrize the nuclear

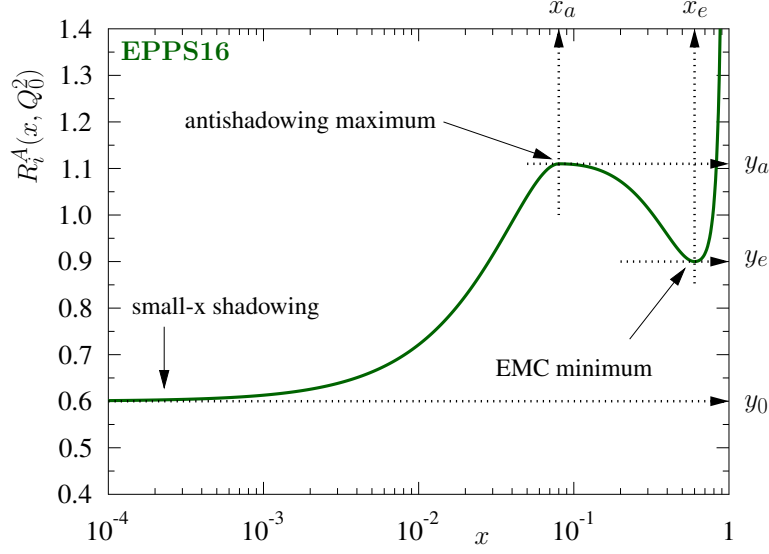


Figure 2.19: EPPS16 fit of the nuclear modification $R_{i/A}(x, \mu_0^2)$ (from [93]).

modification factor :

$$f_{i/A}(x, \mu^2) = R_{i/A}(x, \mu^2) f_{i/p}(x, \mu^2)$$

$$R_{i/A}(x, \mu_0^2) = \begin{cases} a_0 + a_1(x - x_a)^2, & \text{for } x \leq x_a, \\ b_0 + b_1 x^\alpha + b_2 x^{2\alpha} + b_3 x^{3\alpha}, & \text{for } x_a \leq x \leq x_e, \\ c_0 + (c_1 - c_2 x)(1 - x)^\beta, & \text{for } x_e \leq x \leq 1, \end{cases} \quad (2.89)$$

where the free proton PDF $f_{i/p}(x, \mu^2)$ is taken as CT14NLO [95]. This parameterization allows the description of observed nuclear effects such as shadowing at small- x (due to multiple scattering inside the nucleus), anti-shadowing (explained through sum rules) in the intermediate region characterized by x_a and EMC effect (named after the group that observed it : European Muon Collaboration), characterized by x_e , the EMC minimum (all these effects are not yet completely understood, for a review, see [96]). This nuclear modification, fitted at $\mu_0^2 = m_c^2 = (1.3)^2 \text{ GeV}$ (where m_c is the mass of the charm quark), is presented in Fig. 2.19 (from [93]), stressing the different nuclear effects observed.

This nuclear modification can be obtained also with nCTEQ15 results doing the ratio of the nCTEQ15 nPDF to a toy model of nPDF constructed from a proton PDF the following way :

$$f_{i/A_{free}}(x, \mu^2) = \frac{Z}{A} f_{i/p}(x, \mu^2) + \frac{A - Z}{A} f_{i/n}(x, \mu^2), \quad (2.90)$$

where $f_{i/n}$ is obtained from $f_{i/p}$ assuming isospin symmetry. $f_{i/A_{free}}$ is then the PDF of a nucleus without nuclear effects, where the nucleon (protons and neutrons) are free. The

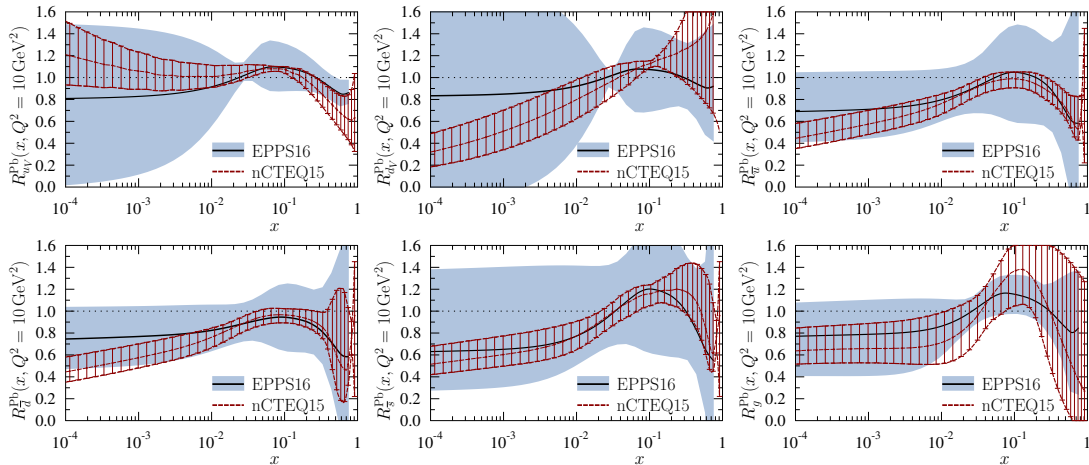


Figure 2.20: Comparison of the nuclear modification $R_{i/A}(x, \mu_0^2)$ obtained in nCTEQ15 (red) and EPPS16 (blue) for g , u_V , \bar{u} , d_V , \bar{d} and \bar{s} distributions, at $\mu^2 = 10\text{GeV}$ (from [93]).

comparison between nCTEQ15 and EPPS16 lead PDFs, in terms of nuclear modification, is shown in Fig. 2.20 (from [93], \bar{s} represent the sea quarks).

There is a relatively good agreement between the 2 approaches, but this is not really discriminant since the uncertainties are high. We can observe different tendencies of the central value of the valence quarks (u_V and d_V) and antiquark (\bar{u} and \bar{d}) distributions at low- x . Also, if the uncertainties are larger in the EPPS16 case, it is mainly because of the broader data used.

On its side, the proton PDF set, HERAPDF2.0, that we will also use was parametrized the following way :

$$x f_{i/p}(x, \mu_0^2) = c_0 x^{c_1} (1-x)^{c_2} (1 + c_3 x + c_4 x^2), \quad (2.91)$$

with some specific choice of the parameters depending on the parton i (see Eq. (26-31) in [90]). The resulting distributions are shown in Fig. 1.5 (used in the introduction).

2.6.3 Obtaining nuclear TMDs

The PDFs presented in the previous section were used to produce the TMDs¹⁶ (and especially *nuclear* TMDs or nTMDs) that we present in this section. But before discussing the obtained TMDs, we first define 2 sets (for each initial distribution). **Set2** corresponds straightforwardly to Eq. (2.84) where the scale of α_s (hidden inside the splitting functions) is taken as the transverse momentum of the radiations (q ; this choice implies angular ordering). In **Set1** however, the scale of the running constant is set to μ , which implies transverse momentum ordering. Another difference comes from the choice of

¹⁶Actually to produce starting distribution, needed in Eq. (2.87)

initial scale μ_0 for those sets. **Set1** starts its evolution at $\mu_0^2 = 1.9\text{GeV}^2$ while **Set2** starts at $\mu_0^2 = 1.4\text{GeV}^2$.

We derive 3 sets of **PB nTMDs** from the **nPDF** presented in the previous section :

- PB-nCTEQ15FullNuc_208.82 based on the starting nCTEQ15 nPDFs,
- PB-EPPS16nlo_CT14nl_Pb208 based on the starting EPPS16 nPDFs,
- PB-NLO_ptoPb208, that uses the free nucleon model presented in Eq. (2.90),

we will also use PB-TMDNLO-HERAI+II-2018-aspt to describe the proton (obtained in [80]). All these **TMDs** sets are included in **TMDLIB** [97] and can be studied through **TMDPLOTTER** (a graphics showing the **TMDs** distributions in x or k_\perp can be produced thanks to this online tool).

Let's first have a look at the x distribution of these **TMDs**. The valence quark (“up-val” and “down-val”), sea quark (“sea”), and gluon (divided by 20 for readability) distributions of the listed above **TMDs**, for both **Set1** and **Set2** are presented in Fig. 2.21.

First, we can see that the number of neutrons and protons in lead (126 and 82 respectively for Pb^{208}) is reflected in the valence quarks distribution (comparing from the free proton **TMD** in the rightmost column). We also already see that **Set1** and **Set2** do not integrate into the same **PDF**. Let's investigate this by comparing nCTEQ15 nPDF to the 2 sets of n**TMDs** obtained using it as initial distribution (for the x dependence). As shown in Fig. 2.22, for the up quark distribution, **Set1 TMD** perfectly integrates into the initial **PDF** while **Set2** do not. This was predictable since nCTEQ15 nPDF is evolved with **DGLAP** equation and the version of the **PB** method used for **Set1**, i.e with μ^2 as the scale of the running constant, is completely equivalent to **DGLAP** (at **NLO**). Then, we might keep in mind that, while **Set2** is suitable to a consistent definition of **TMDs**, it doesn't reproduce **PDFs** once integrated over k_\perp .

If we compare the integrated distributions of the different sets (see Fig. 2.23 for the gluon distributions and Fig. 2.24 for the up quark distributions), then we see that PB-nCTEQ15FullNuc_208.82 and PB-EPPS16nlo_CT14nl_Pb208 are relatively close, except for low scale and transverse momentum where they have different behavior at low- x . Comparing them with PB-NLO_ptoPb208 shows the importance of nuclear effects on **TMDs**. It is interesting to see how the choice of the scale of the running coupling (define by the choice of set) affects these nuclear effects (in the sense that it offers a different description). For instance, if we look at the gluon distribution at $k_\perp = 1\text{GeV}$, $\mu = 10\text{GeV}$, for **Set1**, PB-NLO_ptoPb208 and PB-nCTEQ15FullNuc_208.82 are comparable at mid to large x (say in $[0.03, 1]$) while for **Set2** it is nearly the contrary. As suggested in [80], while they do not integrate to known **PDFs**, **Set2 TMDs** might be more appropriate for phenomenology (something that we will test in the next section). When we look at the up quark distribution at low k_\perp , comparing, for instance, PB-nCTEQ15FullNuc_208.82 **Set2** with the free nucleon model, we can observe, as in the **PDF** case, the shadowing region at low- x , an anti-shadowing region at intermediate x (around 0.025) and the EMC region.

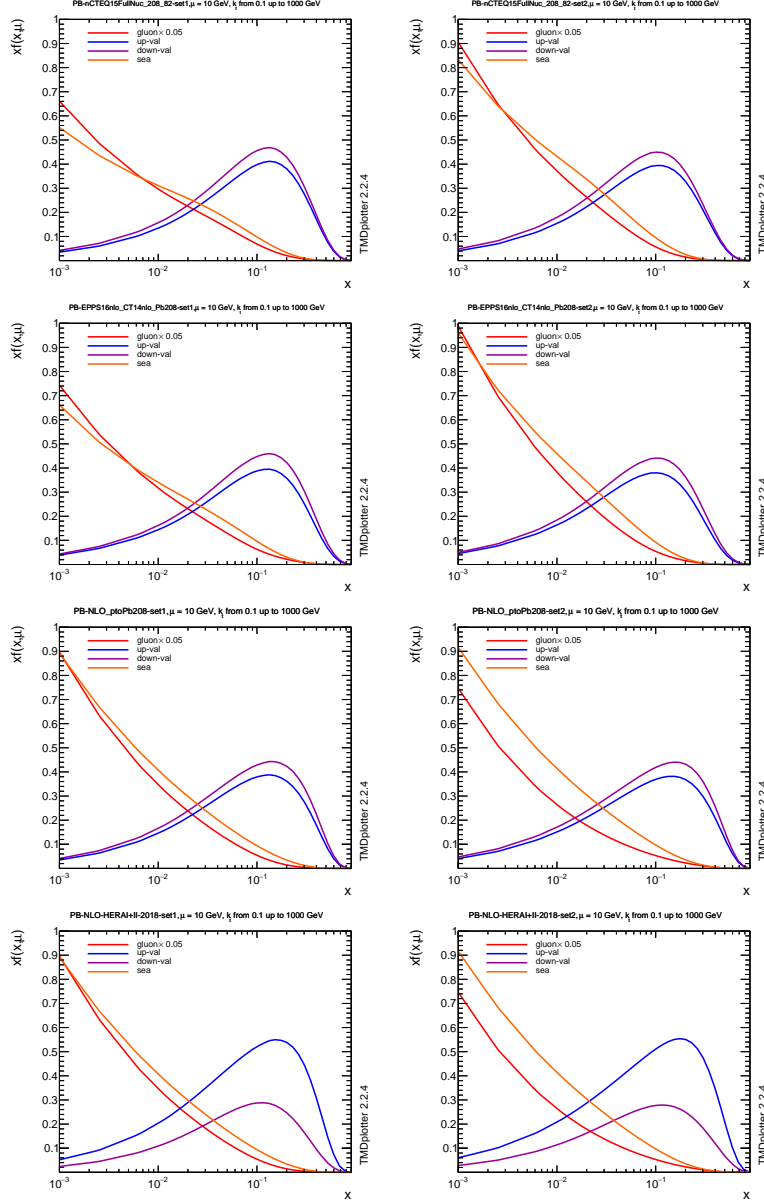


Figure 2.21: x distribution of valence quarks (blue for u_V and purple for d_V), sea quarks (orange) and gluons (red, distribution divided by 20), at $\mu = 10\text{GeV}$ obtained by integration over k_\perp of the TMD PB-nCTEQ15FullNuc_208.82 (1st line), PB-EPPS16nlo.-CT14nl_Pb208 (2nd line), PB-NLO_ptoPb208 (3rd line) and PB-TMDNLO-HERAI+II-2018-aspt (last line), for **Set1** on the 1st column and **Set2** on the 2nd.

Of course, the gluon distributions for the free parton (PB-TMDNLO-HERAI+II-2018-aspt) and for the model of lead composed of free nucleons (PB-NLO_ptoPb208) are the

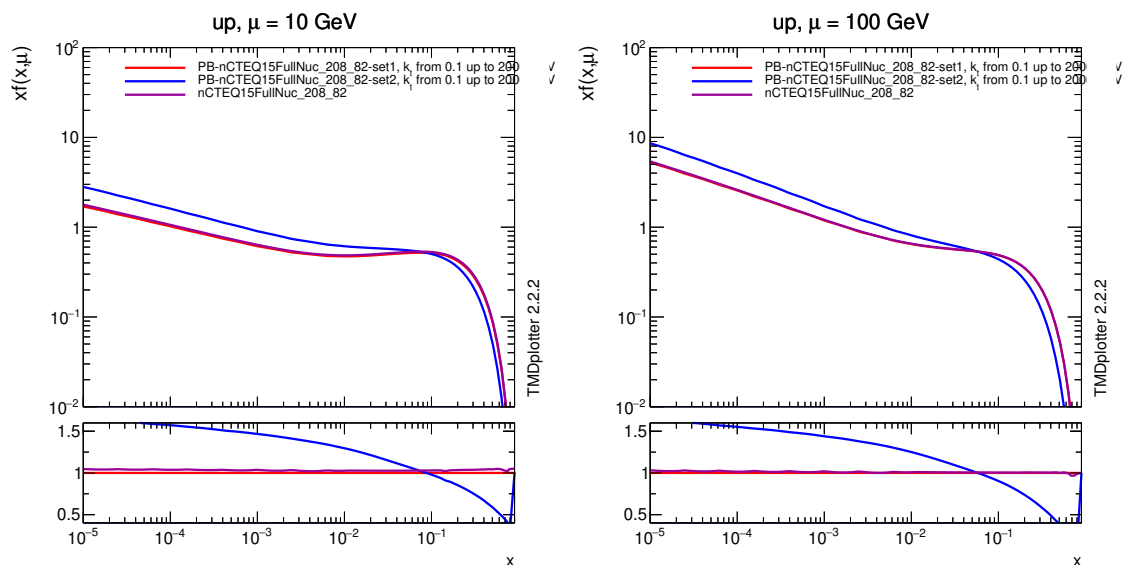


Figure 2.22: x distribution of the up quark at $\mu = 10\text{GeV}$ (left) and $\mu = 100\text{GeV}$ (right) from the nCTEQ15 (purple) and the integration over k_{\perp} of PB-nCTEQ15FullNuc_208.82 Set1 (red) and Set2 (blue).

same since the gluon distribution in the proton and in the neutron (obtained by isospin symmetry, which only affects u and d quarks) are the same.

Comparing now the transverse momentum distributions (at fixed x and scale μ), as shown in Fig. 2.25 for gluons and Fig. 2.26 for up quarks, we note that PB-nCTEQ15-FullNuc_208.82 and PB-EPPS16nlo_CT14nl_Pb208 have the same behavior at large k_{\perp} which differs from the one of the proton and of the lead with free nucleons. The later (PB-NLO_ptoPb208 and PB-TMDNLO-HERAI+II-2018-aspt) often show a similar shape (for the u distribution, they are again equal for the gluon distribution).

Finally, Fig. 2.27 shows the uncertainties for the up quark at $x = 0.01$ for 2 scales : $\mu = 10\text{GeV}$ and $\mu = 100\text{GeV}$ (with a linear scale for better readability). Those uncertainties are of the order of 10% for the shown distributions. For other flavors they are of the same order (around 10 – 15%). We observe a limited reduction of the uncertainties with the scale, especially at large k_{\perp} . Concerning the gluon TMDs, the uncertainties are much larger, of the order of 50% at low k_{\perp} .

While not necessarily well constrained (especially concerning the gluon distributions), we will see in the next section that these TMDs can precisely describe data and highlight nuclear effects (comparing results from nTMDs to our free nucleons model).

2.6.4 Z boson production in $p\text{Pb}$ collisions at the LHC

In this section, we present predictions for the inclusive Z boson production in $p\text{Pb}$ at the LHC through the DY process :

$$p\text{Pb} \rightarrow (Z/\gamma^*) \rightarrow \ell\bar{\ell}, \quad (2.92)$$

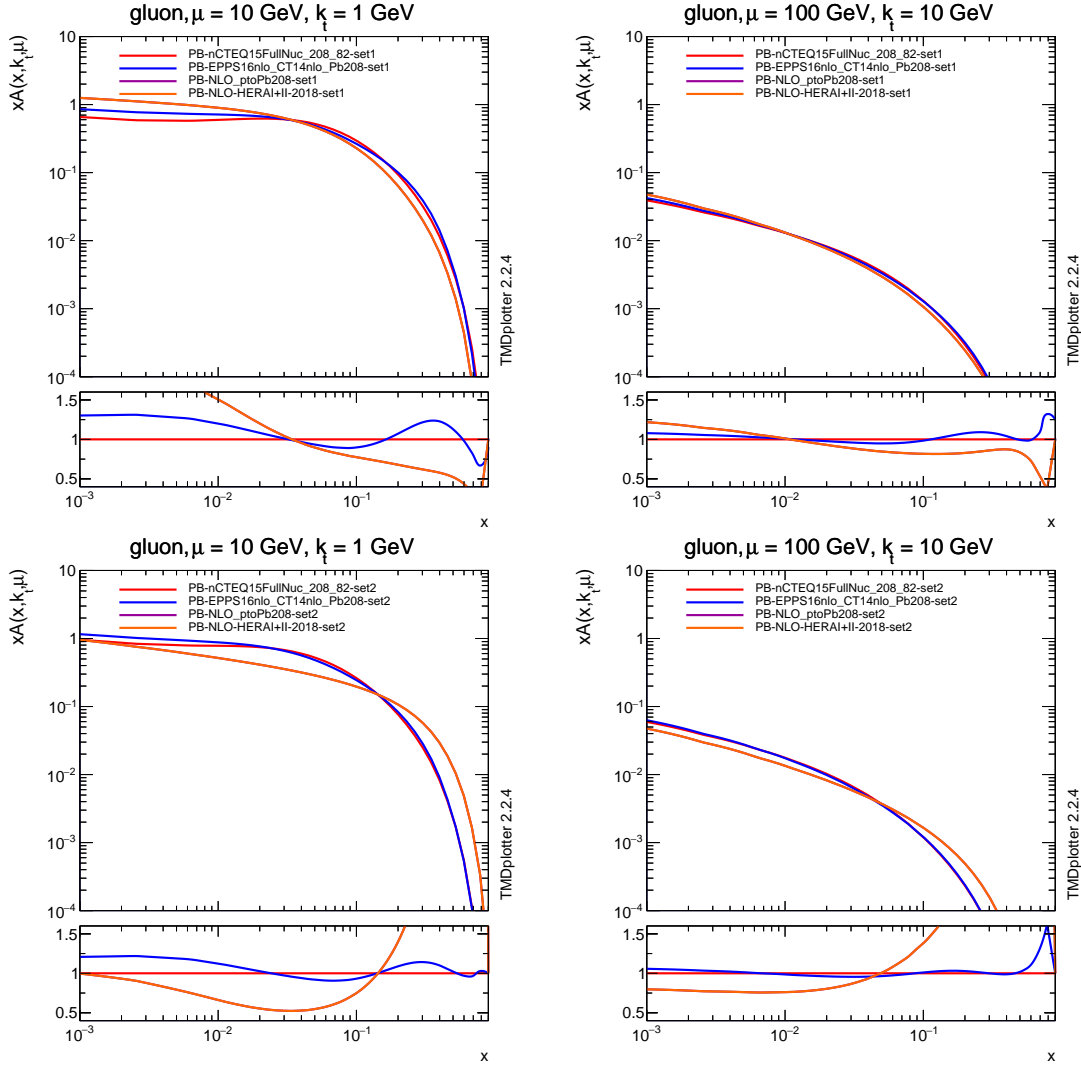


Figure 2.23: x distribution of gluons, for **Set1** (1st line) and **Set2** (2nd line) at $k_{\perp} = 1\text{GeV}$, $\mu = 10\text{GeV}$ (left) and $k_{\perp} = 10\text{GeV}$, $\mu = 100\text{GeV}$ (right) from PB-nCTEQ15-FullNuc_208.82 (red), PB-EPPS16nlo_CT14nlo_Pb208 (purple), PB-NLO_ptoPb208 (orange), PB-TMDNLO-HERAI+II-2018-aspt (orange).

where the intermediate vector boson decays into either an electron or a muon pair (denoted by $\ell\bar{\ell}$). We will compare our predictions to CMS data (presented in [98]) with the following fiducial region :

- $\sqrt{s} = 5.02\text{TeV}$,
- $p_T^{\ell} > 20\text{GeV}$,
- $|\eta_{\text{lab}}^{\ell}| < 2.4$,
- $60 < m_{\ell\ell} < 120\text{GeV}$.

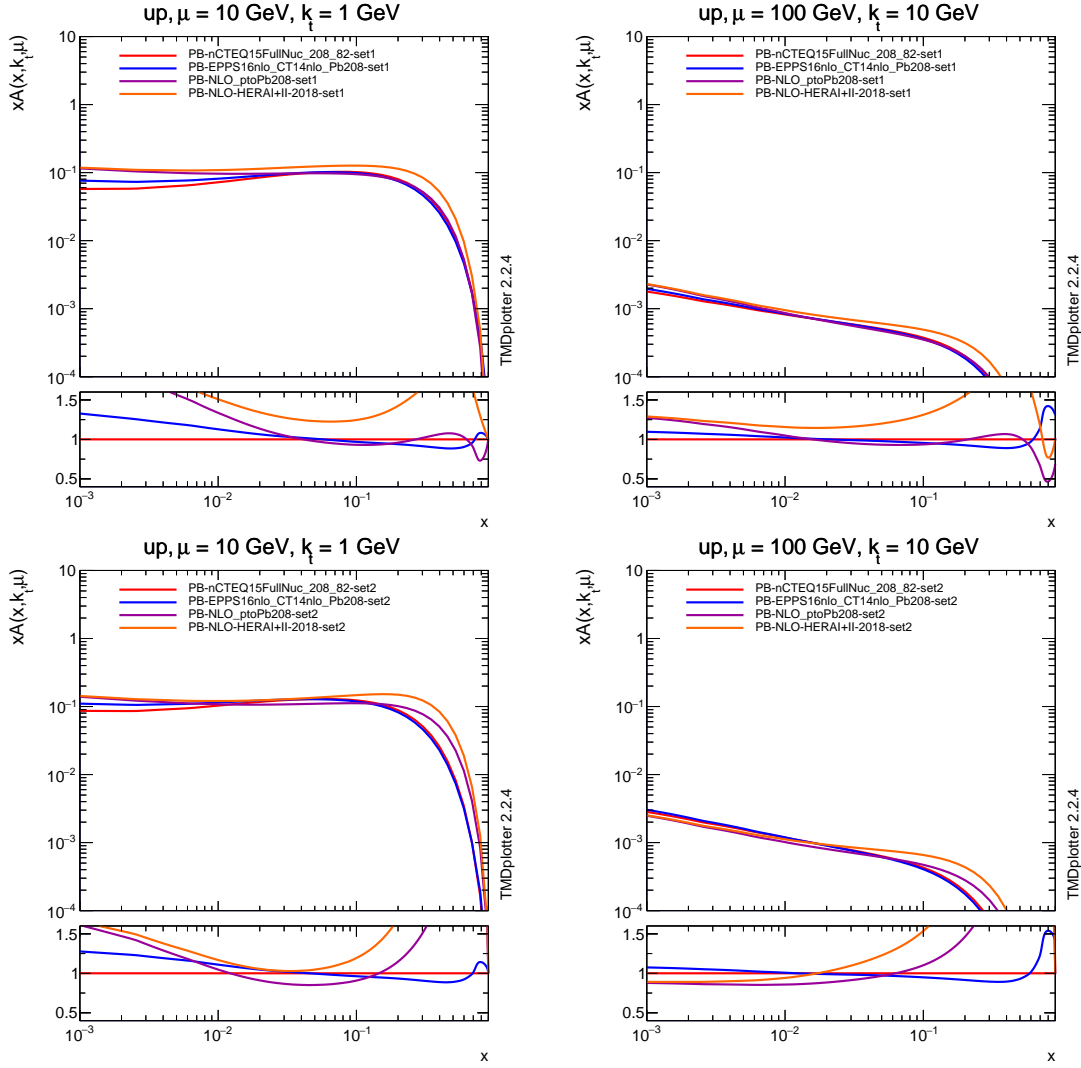


Figure 2.24: x distribution of up quarks, for **Set1** (1st line) and **Set2** (2nd line) at $k_{\perp} = 1\text{GeV}$, $\mu = 10\text{GeV}$ (left) and $k_{\perp} = 10\text{GeV}$, $\mu = 100\text{GeV}$ (right) from PB-nCTEQ15FullNuc_208_82 (red), PB-EPPS16nlo_CT14nl_Pb208 (purple), PB-NLO_ptoPb208 (orange), PB-TMDNLO-HERAI+II-2018-aspt (orange).

where \sqrt{s} is the center of mass energy, p_T^{ℓ} the transverse momentum of the lepton, η_{lab}^{ℓ} its rapidity (in the lab frame) and $m_{\ell\ell}$ the mass of the lepton pair. To perform our calculations, we used the TMDs and PDFs presented in the previous sections (Sec. 2.6.2 and Sec. 2.6.3) and LO off-shell matrix elements calculated by the MC event generator KATIE [99] (which also performs the phase-space integration). We have applied k_T -factorization (and also, for comparison purposes, hybrid and collinear factorization) with the factorization and renormalization scales set to the mass of the Z boson : $\mu_R = \mu_F = \mu = m_Z$. We present our predictions in terms of the Z boson center of mass rapidity y^*

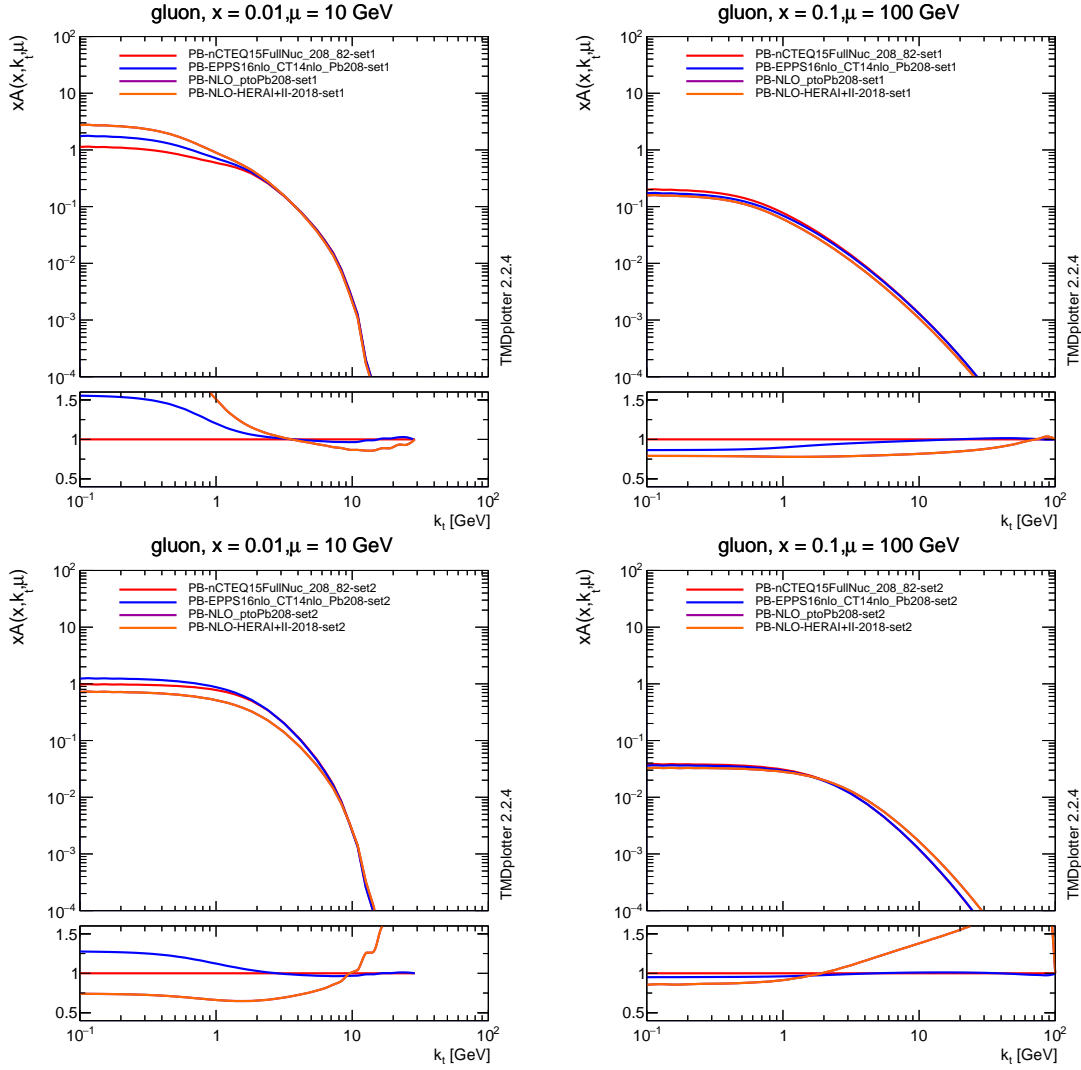


Figure 2.25: k_{\perp} distribution of gluon, for **Set1** (1st line) and **Set2** (2nd line) at $x = 0.01$, $\mu = 10\text{GeV}$ (left) and $x = 0.1\text{GeV}$, $\mu = 100\text{GeV}$ (right) from PB-nCTEQ15FullNuc-208.82 (red), PB-EPPS16nlo_CT14nlo_Pb208 (purple), PB-NLO_ptoPb208 (orange), PB-TMDNLO-HERAI+II-2018-aspt (orange).

and transverse momentum p_t distributions of the differential cross section (meaning, we present $\frac{d\sigma}{dy^*}$ and $\frac{d\sigma}{dp_t}$).

We stated that **Set2** TMDs were more suitable to reproduce data and we verify it on Fig. 2.28 where are shown predictions for the different set used (here nCTEQ15 and EPPS16 for lead and HERAPDF for the proton¹⁷), comparing results obtained

¹⁷In this section, for readability, we name PB TMDs simply by the name of the PDFs used to initiate them (if there is no ambiguity between the PDF and the TMD). We will then use nCTEQ15 instead of PB-

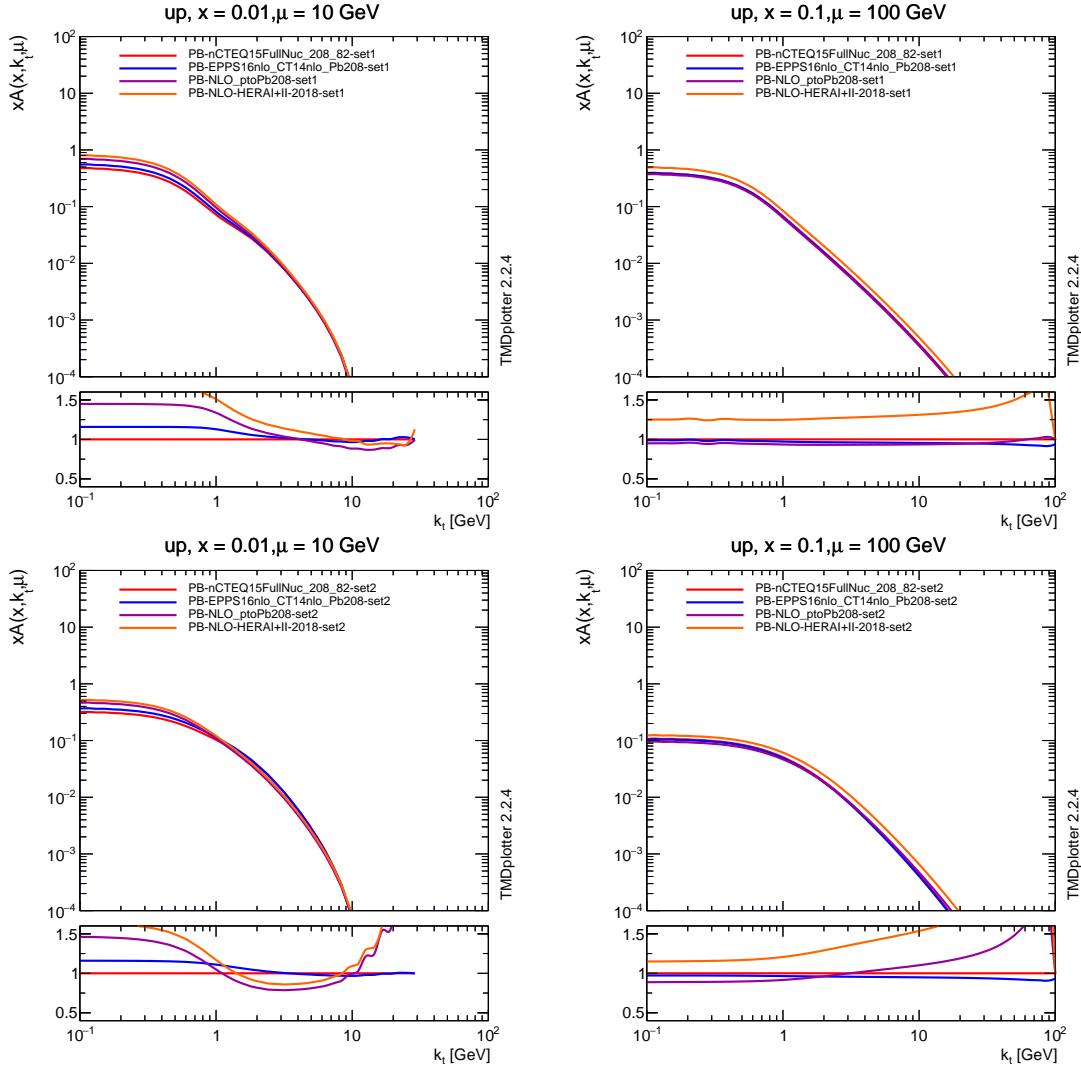


Figure 2.26: k_{\perp} distribution of up quarks, for **Set1** (1st line) and **Set2** (2nd line) at $x = 0.01$, $\mu = 10\text{GeV}$ (left) and $x = 0.1\text{GeV}$, $\mu = 100\text{GeV}$ (right) from PB-nCTEQ15-FullNuc_208.82 (red), PB-EPPS16nlo_CT14nl_Pb208 (purple), PB-NLO_ptoPb208 (orange), PB-TMDNLO-HERAI+II-2018-aspt (orange).

in k_T -factorization with **Set1** and **Set2** TMDs and in collinear factorization (with the corresponding PDFs).

The observations we can do are general for both nCTEQ15 and EPP16 sets. First, results with **Set2** show a very good agreement with CMS data (we will refine the comparison with the calculation of the uncertainties in the following), for both y^* and p_t

nCTEQ15FullNuc_208.82, EPPS16 instead of PB-EPPS16nlo_CT14nl_Pb208 and HERAPDF instead of PB-TMDNLO-HERAI+II-2018-aspt.

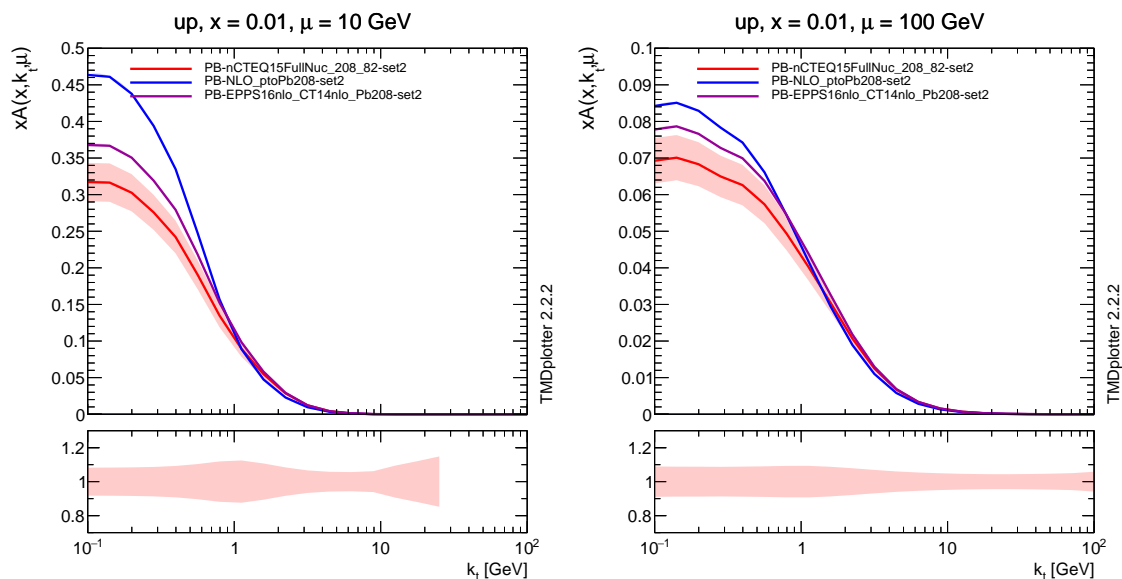


Figure 2.27: k_{\perp} distribution of the up quark with the uncertainties of PB-nCTEQ15-FullNuc_208.82 Set2 nTMD at $x = 0.01$ and $\mu = 10\text{GeV}$ (left), $\mu = 100\text{GeV}$ (right).

distributions while **Set1** exhibit behavior comparable to the collinear case (for the y^* distribution), underestimating the differential cross-section at low and negative rapidity (this underestimate is also visible in the p_t distribution). The similarity of the collinear and **Set1** results is not surprising considering that **Set1** PB TMDs integrate to the corresponding PDFs. Also, the asymmetry of the collision ($p\text{Pb}$) reflects on the rapidity distribution. The CMS points are, by the way, surprisingly symmetric but we observe that the high asymmetry of the y^* distribution predicted by both collinear factorization and **Set1** TMD is softened in **Set2** results. Concerning the p_t distribution, that collinear factorization cannot describe, we see again that **Set2** nTMD describes the data well where **Set1** fails. Also, the shape obtained for both sets is the same if we impose a higher low p_t cut. Based on these observations, we will continue our study accounting only for **Set2** TMDs.

If we compare results for the different sets used, as in Fig. 2.29, we observe that all nTMDs lead to similar results, in good agreement with CMS data. You may notice in this figure that the TMD set PB-gluon_D.c.ncteq1568CL_Pb (which is based on a nPDF improved from nCTEQ15 and EPPS16 by including data for heavy-flavor production in $p\text{Pb}$ collision), leads to better constraints on the gluon PDF (the resulting nPDF is presented in [100]). This being said, the results obtained with this TMD are very close to those obtained with PB-nCTEQ15FullNuc_208.82 and we won't study it in detail here.

Looking carefully, we observe that nCTEQ15 and EPPS16 TMDs lead to slightly different behavior in mid-negative rapidity y^* and in the low- p_t regions, results using EPPS16 are closer to the data points. Also, we saw in Sec. 2.6.2 that nCTEQ15 PDF were better constrained, and hence, we will focus on these distributions in the following

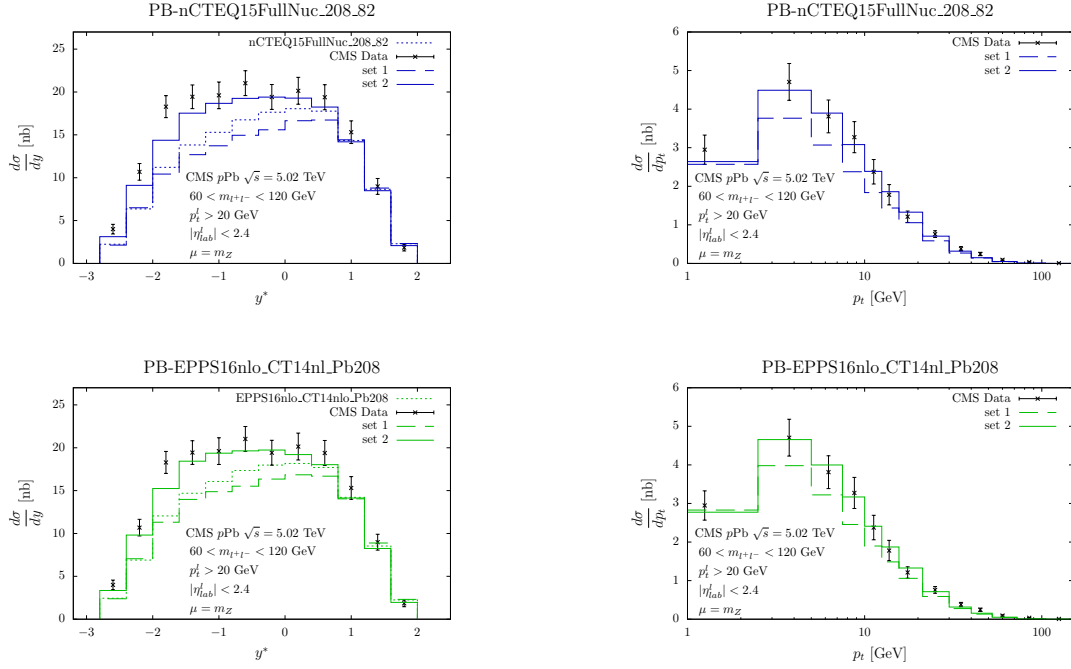


Figure 2.28: Comparison of y^* (left) and p_t (right) distributions using **Set2** (solid line), **Set1** (dashed line) or collinear factorization (dotted line) for PB-nCTEQ15FullNuc.-208.82 (1st line) and PB-EPPS16nlo_CT14nl_Pb208 (2nd line) with CMS data (black dots).

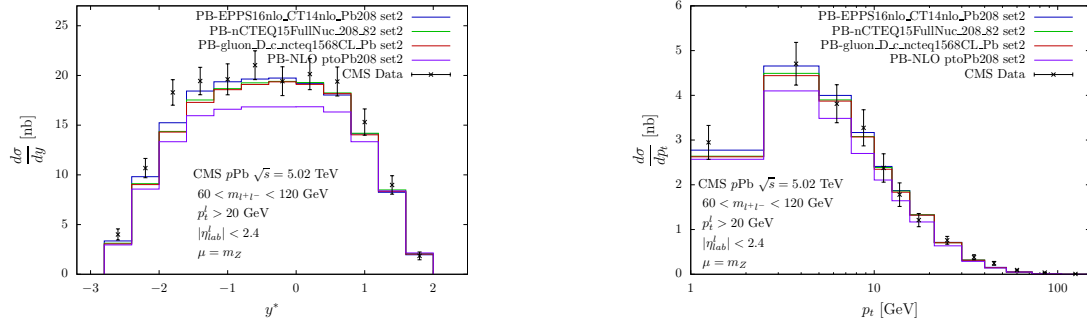


Figure 2.29: Comparison of y^* (left) and p_t (right) distributions for PB-nCTEQ15-FullNuc_208.82 (green), PB-EPPS16nlo_CT14nl_Pb208 (blue), PB-NLO_ptoPb208 (purple) and PB-gluon_D_c_ncteq1568CL_Pb (red) with CMS data (black dots).

(the PDF and the corresponding TMD).

Another interesting point of Fig. 2.29 is that it brings out the nuclear effect when comparing results with, say nCTEQ15, to those of the free nucleus model (PB-NLO_ptoPb208). This effect is clearly visible in the y^* distribution, at mid-rapidity, where the differential

cross section is greatly enhanced by nuclear effects. This enhancement is also visible in the p_t distribution but less localized and less visible (still important for $p_t \sim 3\text{GeV}$). The uncertainties, coming from the **TMDs**, on such predictions are directly related to the precision of the fit of the initial **PDFs** (at their initial scale). Indeed, to evaluate these uncertainties, we do the same calculation using what we call *error PDFs* or *error TMDs*. Each error **PDF** corresponds to the **PDF** obtained by varying one of the fitted parameters by the precision of the fit. Then, 2 **PDFs** are produced for each parameter used. In the case of nCTEQ15, we vary the parameters c_i (see Eq. (2.88)) by the error $\pm\delta c_i$, leading to the error **PDF** :

$$f_{c_i}^{\pm} \equiv f_{c_i \rightarrow c_i \pm \delta c_i}. \quad (2.93)$$

Thereby, the error made on the calculation of an observable \mathfrak{D} , $\Delta\mathfrak{D}$, is determined by adding quadratic errors as follows [92] :

$$\Delta\mathfrak{D} = \frac{1}{2} \sqrt{\sum_i \left(\mathfrak{D}(f_{c_i}^+) - \mathfrak{D}(f_{c_i}^-) \right)^2}. \quad (2.94)$$

For the Z boson production in $p\text{Pb}$ collision, the uncertainties (for nCTEQ15) are shown in Fig. 2.30.

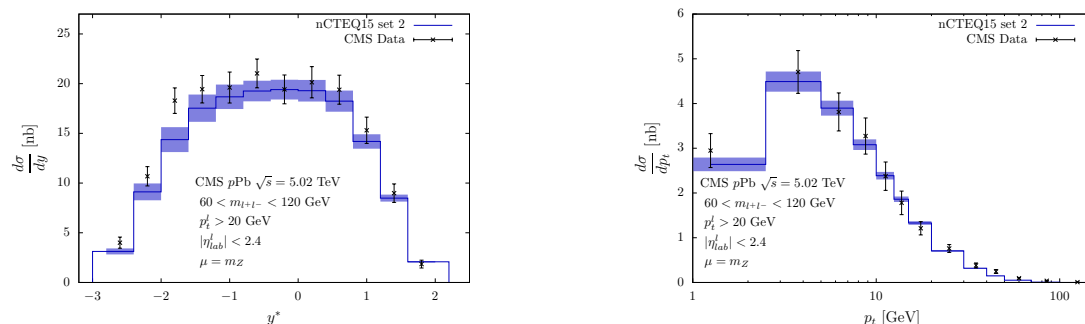


Figure 2.30: Uncertainties of y^* (left) and p_t (right) distributions for PB-nCTEQ15-FullNuc_208.82.

These uncertainties are larger than the difference between the results obtained from the different **nTMDs**, justifying our focus on nCTEQ15-based results. Also, they are small enough to clearly identify the nuclear effect and discriminating results from **nTMDs** and from the free nucleons model, and quantitatively smaller than the experimental errors. Overall, it underlines the importance of nuclear modification even if it is still secondary at the current experimental precision.

The approximations due to missing orders can also be evaluated. We know that our results in **pQCD**, for any observable, should be independent of the renormalization scale μ . Also, this is only true for the full-order calculation, hence, looking at the dependence of our results on μ tells us about the higher-order corrections. It is usual to vary this scale by a factor of 2 (multiplying and dividing it by 2) to estimate these corrections. However,

the higher order corrections in our case would come from emissions of additional partons and depend on the transverse momentum of the Z boson. At $p_t = 0$ no real emission is possible while those emissions become significant when p_t grows (giving more angle for branching). Therefore, we introduce the scale $\mu^2 = m_Z^2 + p_t^2$ (suggested by angular ordering) and we vary only the transverse momentum part (by a factor of 2). More on this scale variation choice can be found in [101]. The results of the proposed scale variation are presented in Fig. 2.31 where we observe that these variations are of the order of the uncertainties (presented in Fig. 2.30) in the y^* distribution but are much smaller in the p_t distribution.

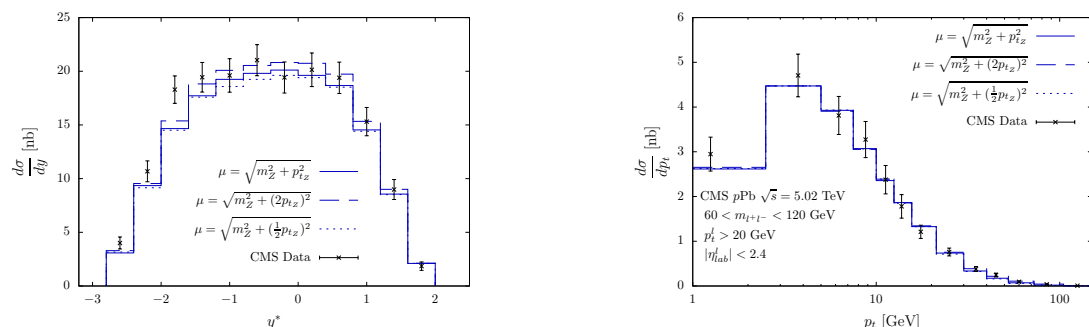


Figure 2.31: y^* (left) and p_t (right) distributions for PB-nCTEQ15FullNuc_208.82 when varying scale ($\mu^2 = m_Z^2 + p_t^2$ in solid line, $\mu^2 = m_Z^2 + (2p_t)^2$ in dashed line and $\mu^2 = m_Z^2 + (\frac{1}{2}p_t)^2$ in dotted line) with CMS data (black dots).

Also, we mentioned that angular ordering suggests the choice of scale $\mu^2 = m_Z^2 + p_t^2$ while in the presented result, we have used $\mu = m_Z$. Actually, this is justified by the very small difference between the two choices, much under the uncertainties and scale variation bands, as shown in Fig. 2.32.

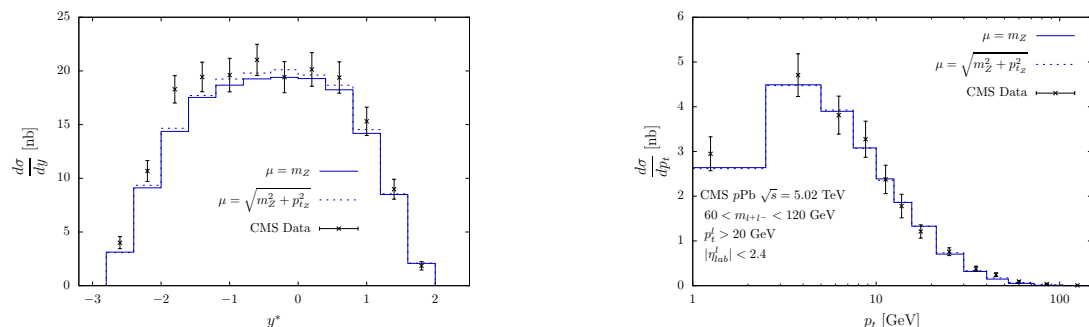


Figure 2.32: Comparison of y^* (left) and p_t (right) distributions for PB-nCTEQ15-FullNuc_208.82 for different scales ($\mu = m_Z$ in solid line and $\mu^2 = m_Z^2 + p_t^2$ in dotted line) with CMS data (black dots).

To study the importance of the factorization scheme, hence of the k_\perp dependence

of the initial parton of the hard process in the final cross-section, we have produced results within hybrid and collinear factorization to compare to those of k_T -factorization. For the hybrid factorization, we tested both possible configurations : lead described by TMD and proton by PDF and vice versa. The results are presented in Fig. 2.33 where * denotes the hadrons described by a TMD (the notation suggests the off-shellness of the corresponding parton).

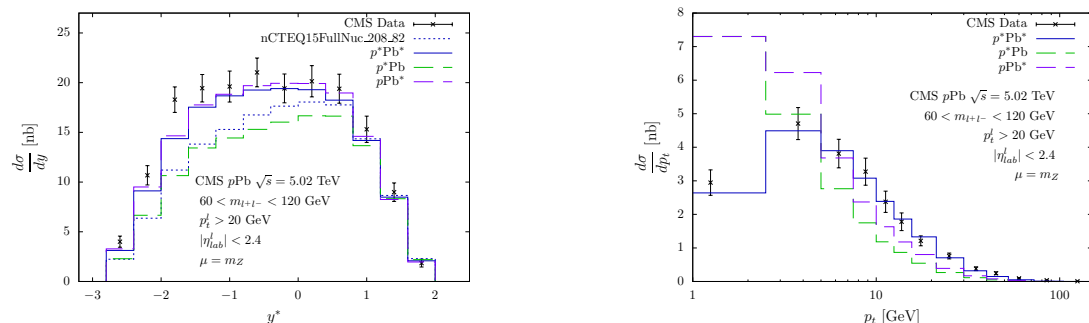


Figure 2.33: Comparison of y^* (left) and p_t (right) distributions for PB-nCTEQ15-FullNuc_208.82 for different factorization schemes (k_T in solid line, hybrid in dashed line and collinear in dotted line) with CMS data (black dots).

We see then that both hybrid factorizations fail to describe the p_t distribution (overestimating the low- p_t region while underestimating the high- p_t region). But something interesting happens for the rapidity distribution. We see that it is enough to take into account only the transverse momentum of the parton coming from the lead (in the hard process) to describe the y^* distribution. For this purpose, the intrinsic transverse momentum of the parton coming from the proton is negligible. On the other hand, treating only the proton with TMDs leads to a rapidity distribution comparable to the one obtained in the collinear case.

2.7 Chapter summary

Throughout this chapter, we have studied different parton distribution functions, objects that both describe the structure of hadrons and that are crucial to pQCD predictions. Indeed, these distributions encode the non-perturbative physics of long-distance QCD that keeps partons in colorless bound states (i.e color confinement). Hopefully, these PDFs are universal, meaning that we can obtain them from experiments on a specific process and use them to predict other processes. This is possible when factorization theorems apply i.e when it is possible to separate long-distance effects (soft part) from short-distance ones (hard part). We saw how the factorization appears in the case of DIS processes (in Sec. 2.1) leading us to collinear factorization, where the partons are described only by the fraction x of the hadron momentum they carry. In this case, the “collinear” PDFs depend on x but also on a renormalization scale μ (that we relate to the energy scale at which the hadron is probed). Hopefully, the dependence of the PDFs on the scale can be calculated perturbatively (in the range $\mu > \Lambda_{QCD}$) which leads us to the DGLAP equations, that govern this scale dependence. We then introduced uPDFs (dependent on x and on an intrinsic transverse momentum k_{\perp}) in some kinematics region that PDFs cannot describe. The x dependence of these uPDFs is governed by the BFKL equations. Both the regions described by DGLAP and BFKL can be unified with the introduction of TMDs (dependent on x , k_{\perp} and μ) which evolution is governed by the CCFM equation. This led us to a way of applying DGLAP equation in the kinematics region of application of CCFM (to evolve TMDs) called the PB method.

In the meantime, we defined two factorization schemes : k_T -factorization and hybrid factorization and had an overview of BK equation which expands BFKL equation accounting for saturation (where recombination of gluons is no more negligible). Finally, we used the Parton Branching method to produce nuclear nTMDs (TMDs for the lead nucleus) and tested them (with success) through prediction of Z boson production at LHC against CMS data. These TMDs (PB-nCTEQ15FullNuc.208.82, PB-EPPS16nlo-CT14nl_Pb208 and PB-gluon_D.c.ncteq1568CL_Pb) are available in the TMDLIB [97] library.

Chapter 3

Amplitudes

This chapter is devoted to amplitudes in QCD, meaning amplitudes describing partonic processes. In Sec. 3.1, we will describe some general features of amplitudes, beginning with their classical construction from Feynman diagrams. Then we will present tools used to simplify their calculation such as color ordering and the spinor-helicity formalism which lead to modern approaches to amplitudes, based on their properties. After reviewing some recursive techniques and properties of QCD amplitudes inherited from supersymmetry, we will focus on loop-amplitudes and the related loop-integrand calculations.

After this review on on-shell amplitudes, in Sec. 3.2, we will then describe how to calculate off-shell amplitudes (i.e amplitudes with one or two off-shell legs, useful in hybrid and k_T -factorization). The first way to do it is based on Lipatov's high energy effective action, an effective theory that describes reggeons (as appearing in the BFKL equation). While we won't make calculations within Lipatov's high-energy effective action, we present a short overview of this theory as we want to use some of the resulting amplitudes for comparison purposes.

Afterward, we will present an alternative method to calculate off-shell amplitudes, the auxiliary parton method. This method is based on the explicit reconstruction of the gauge invariance of off-shell amplitudes calculated in a naive way (indeed, calculating an amplitude with off-shell leg by simply applying Feynman rules will lead, in general, to non gauge invariant results). Finally, in Sec. 3.3, we will try to apply this method at NLO to see if it breaks and we will actually provide expressions for $g^* g^+ \dots g^+$, which exhibits the correct behavior. We will also apply it on $g^* gg$, in particular on $g^* g^- g^+$, and observe that the method breaks when dealing with dimensional regularization. This breaking has recently been understood and solved [102], which we will review shortly before summarizing the chapter.

Contents

3.1	On-shell amplitudes	64
3.1.1	Feynman diagrams	64
3.1.2	Color ordering	66
3.1.3	Helicity amplitudes	73

3.1.4	Soft and collinear factorization	79
3.1.5	Recursive techniques	81
3.1.6	Supersymmetry	86
3.1.7	Loop amplitudes	88
3.2	Gauge invariant off-shell amplitudes	97
3.2.1	Lipatov's high-energy effective action	97
3.2.2	The auxiliary parton method	101
3.3	Results	110
3.3.1	$g^* g^+ \dots g^+$ amplitudes	111
3.3.2	$g^* gg$	118
3.4	Loop-level hybrid factorization	120
3.5	Chapter summary	121

3.1 On-shell amplitudes

The hard cross section $\hat{\sigma}_{\mathcal{X}\rightarrow\mathcal{Y}}$ describes, once integrated over the phase-space considered for \mathcal{Y} , the probability to go from a state \mathcal{X} (a set of particles, at $t \rightarrow -\infty$) to a state \mathcal{Y} (at $t \rightarrow +\infty$). This differential cross section is calculated from the probability amplitude $\mathcal{A}_{\mathcal{X}\rightarrow\mathcal{Y}}$ (also called *matrix element*) as :

$$\begin{aligned} \hat{\sigma}_{\mathcal{X}\rightarrow\mathcal{Y}} &= |\mathcal{A}_{\mathcal{X}\rightarrow\mathcal{Y}}|^2, \\ \text{with } \mathcal{A}_{\mathcal{X}\rightarrow\mathcal{Y}} &= \langle \psi_{\mathcal{Y}} | S - \mathbf{1} | \psi_{\mathcal{X}} \rangle, \end{aligned} \quad (3.1)$$

with $\psi_{\mathcal{X}}$ ($\psi_{\mathcal{Y}}$) the wave function of the initial (final) state and S the *scattering matrix* (often referred to as the S -matrix), which describes the evolution from \mathcal{X} (at $t \rightarrow -\infty$) to \mathcal{Y} (at $t \rightarrow +\infty$) according to the considered QFT. The subtraction of the identity matrix permits the elimination of the non-interacting part in S . If these states are partons, this amplitude follows from the QCD Lagrangian (see Eq. (1.1)).

3.1.1 Feynman diagrams

As seen in the introduction, the QCD Lagrangian encodes free propagator (through kinematics terms) and vertices (through interaction terms). Then, calculating a scattering amplitude (probability amplitude for a scattering process) consists in calculating all possible configurations of propagators and vertices to go from the initial state to the final state. Each possibility is pictured by what is called a *Feynman diagram*. The building blocks of these diagrams are obtained by inverting the corresponding terms in the Lagrangian, which lead to the Feynman rules described in App. B.1. These rules permit to translate the Feynman diagrams into amplitudes expressions (actually, into the considered diagram contribution to the amplitude, all possible diagrams have then to be summed).

However, the number of configuration for going from an initial state \mathcal{X} to a final state \mathcal{Y} , using these building blocks, is infinite. Hopefully, they can be ordered by power of the coupling constant α_s (determined basically by the number and type of vertices). Hence, since this coupling constant is evaluated at the hard scale of the collision, it is small enough and this decomposition is actually a perturbative expansion of the amplitude (in α_s) :

$$\mathcal{A}_{\mathcal{X}\rightarrow\mathcal{Y}} = \sum_{i=i_{min}}^{+\infty} \mathcal{A}_{\mathcal{X}\rightarrow\mathcal{Y}}^i, \text{ with } \forall i, \mathcal{A}_{\mathcal{X}\rightarrow\mathcal{Y}}^i = \mathcal{O}(\alpha_s^i), \quad (3.2)$$

i_{min} depending on the process considered and actually on the number of particles n of the process¹. Considering the simplest Feynman diagrams with an increasing number of particles leads to $i_{min} = n - 2$. Then $i = i_{min}$ corresponds to the LO amplitude, called *tree level amplitude*, $i = i_{min+1}$ to the 1st order correction, and so forth. Also, when considering a specific process (say $qq \rightarrow gg$), going from the tree-level diagrams to its first correction in perturbation theory (i.e to diagrams with one more power of α_s) need

¹i.e $n = n_i + n_f$ sums the number of particles in the initial and the final state

the inclusion of two other 3-partons vertices (or a 4-gluon vertex). With fixed initial and final states, this implies the creation of a loop in the diagram, hence we call corrections to the tree-level amplitude, loop-level amplitudes. It is actually usual to denote amplitudes by their number of loops (instead of their power in α_s , as in Eq. (3.2)) :

$$\mathcal{A}_{\mathcal{X} \rightarrow \mathcal{Y}} = \sum_{l=0}^{+\infty} \mathcal{A}_{\mathcal{X} \rightarrow \mathcal{Y}}^{(l)}. \quad (3.3)$$

With the tree level amplitude usually noted $\mathcal{A}^{(0)} = \mathcal{A}^{tree}$. An example of the diagrams appearing at the first orders in perturbation theory of $\mathcal{A}_{gg \rightarrow gg}$ is presented in Fig. 3.1.

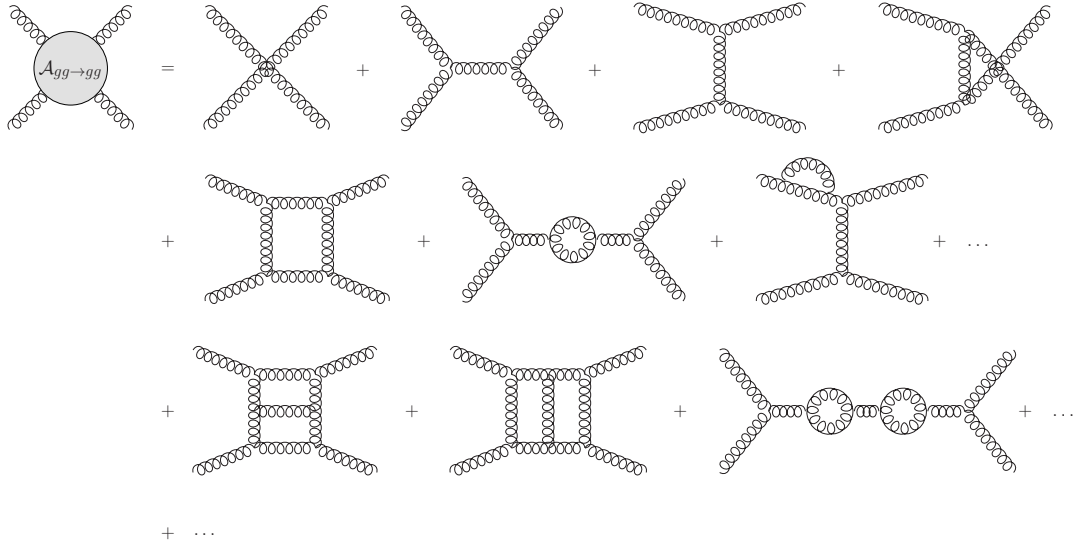


Figure 3.1: Diagrams from the first terms of the perturbative series of $\mathcal{A}_{gg \rightarrow gg}$. The 1st line corresponds to tree-level diagrams, the 2nd line to (one) loop diagrams, and the 3rd to 2-loops diagrams.

And here we can foresee the problems rising when calculating amplitudes with Feynman rules : the number of diagrams quickly grows with both the number of loops l and the number of external particles n . As an example, the number of tree-level diagrams contributing to $gg \rightarrow g \dots g$, with n overall gluons is given in table. 3.1 [103].

n	4	5	6	7	8	9	10
# of diagrams	4	25	220	2485	34 300	559 405	10 525 900

Table 3.1: Number of tree-level diagrams for n gluons amplitudes.

However, this apparent complexity leads to remarkably simple expressions (even in a non-Abelian gauge theory as QCD) when using proper variables. In the next sections, we

will present some used techniques to simplify amplitude calculation. These sections are based on [104–106], and are far from being exhaustive on the subject (a more complete review on on-shell scattering amplitudes can be found in [107, 108]). Also, the study of on-shell amplitudes and their properties (attempting to calculate them avoiding the direct calculation of the S-matrix implied by the Lagrangian formulation) is still an important subject of research, especially in QCD, where high-order amplitudes are needed to constrain theoretical errors.

In the following, for a process $p_1 p_2 \rightarrow p_3 \dots p_n$ (where p_i are partons i.e simply g, q or \bar{q}), we will adopt the notation :

$$\mathcal{A}(1_{p_1}, 2_{p_2} \dots n_{p_n}) \equiv \mathcal{A}_{p_1 p_2 \rightarrow p_3 \dots p_n}(\{k_i, \mathfrak{l}_i; \mathfrak{a}_i\}_{i \in \llbracket 1; n \rrbracket}). \quad (3.4)$$

where \mathfrak{l}_i and \mathfrak{a}_i are respectively the polarization and the adjoint color index when p_i is a gluon and the helicity and the fundamental color index when p_i is a quark. Actually, we will even drop the index p_i for gluons. When we need to specify helicities and polarizations, we write them explicitly in superscript.

Remark : We consider, by convention, all momenta outgoing.

3.1.2 Color ordering

In QCD, it is possible to arrange amplitudes according to their color structure, decomposing them into simpler gauge-invariant pieces that are free from the corresponding color factors [109–112]. These pieces are called *color-ordered amplitudes* or *partial amplitudes* and we will present how they are defined in this section, but first, we need to recall properties of QCD color factors.

QCD is a non-abelian gauge theory based on the $SU(N_c)$ group symmetry (associated to color charge), with N_c the number of color charges. Actually, for QCD, N_c is fixed to 3, but it can be interesting to keep explicit the dependence of N_c (which makes it possible to simplify expressions in the “large N_c limit”, i.e considering leading color contributions). Hence, the color factors appearing in QCD amplitudes are the Lie Algebra structure constants f^{abc} (appearing in 3 and 4 gluons vertices) and the generators $(t^a)_i^{\bar{j}}$ (appearing in gluon-quark-antiquark vertices). The indices a, b, c correspond to gluons color in adjoint representation ($a \in \llbracket 1, N_c^2 - 1 \rrbracket$) while the indices i corresponds to a quark color in fundamental representation ($i \in \llbracket 1, N_c \rrbracket$), an equivalently, \bar{j} correspond to an antiquark anticolor in fundamental representation ($\bar{j} \in \llbracket 1, N_c \rrbracket$). Also the $SU(N_c)$ generators in fundamental representation $(t^a)_i^{\bar{j}}$ are traceless hermitian $N_c \times N_c$ matrices that are normalized using :

$$\text{Tr}(t^a t^b) = \delta^{ab}. \quad (3.5)$$

Actually, the standard way of normalizing $SU(N_c)$ generators is : $\text{Tr}(t^a t^b) = \frac{\delta^{ab}}{2}$, but this leads to proliferation of $\sqrt{2}$ factors in the partial amplitudes, avoided using Eq. (3.5).

In this convention, the Casimir operator reads :

$$\sum_a t^a t^a = C_F \mathbb{1} \text{ leading to } C_F = \frac{N_c^2 - 1}{N_c}, \quad (3.6)$$

where the 2nd equality is obtained by taking the trace of the 1st one. Then, the color structure constants are defined by :

$$[t^a, t^b] = i\sqrt{2} f^{abc} t^c. \quad (3.7)$$

Then, the first step to rearrange amplitudes according to their color structure is to write the color structure functions in terms of the generators. Following from the definition Eq. (3.7), we have :

$$f^{abc} = -\frac{i}{\sqrt{2}} [\text{Tr}(t^a t^b t^c) - \text{Tr}(t^a t^c t^b)]. \quad (3.8)$$

This leads, at the amplitude level to numerous terms containing products of traces over (products of) generators and also generators strings of the form $(t^{a_1} t^{a_2} \dots t^{a_n})_{\bar{i}}^{\bar{j}}$ (if quarks are present). All these terms can be rearranged using the $SU(N_c)$ *Fierz identity* :

$$\sum_a (t^a)_{i_1}^{\bar{j}_1} (t^a)_{i_2}^{\bar{j}_2} = \delta_{i_1}^{\bar{j}_2} \delta_{i_2}^{\bar{j}_1} - \frac{1}{N_c} \delta_{i_1}^{\bar{j}_1} \delta_{i_2}^{\bar{j}_2}. \quad (3.9)$$

This equation reflects the fact that the generators t^a form a complete set of hermitian matrices, with the 2nd term in the r.h.s. of the equation expressing their tracelessness. Also, Eq. (3.8) and Eq. (3.9) can be represented diagrammatically, as shown in Fig. 3.2.

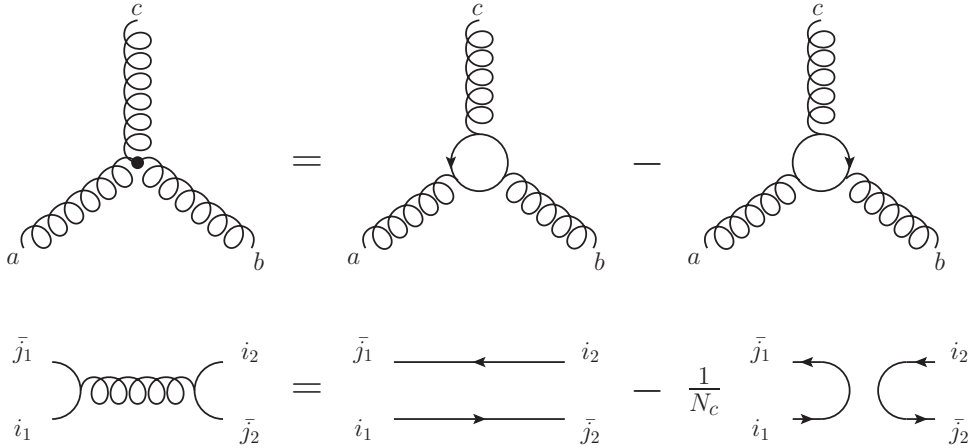


Figure 3.2: Diagrammatic representation of the equations leading to color ordering (Eq. (3.8) and Eq. (3.9)).

Applying these two equations to a QCD amplitude (i.e transforming structure functions into generator traces, expressed with explicit indices² and applying the Fierz identity) leads to the amplitude *color decomposition*. This color decomposition can be schematized diagrammatically [113, 114], as shown in Fig. 3.3 for $gggg$ tree-level amplitude (actually for one diagram contributing to this amplitude, but the other one follow the same decomposition).

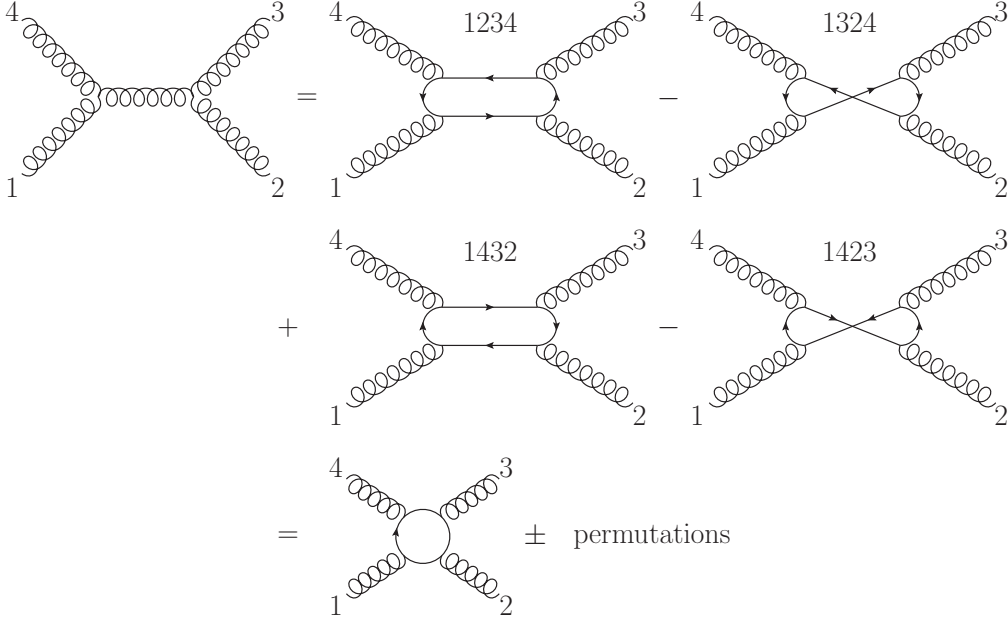


Figure 3.3: Diagrammatic representation of the color decomposition of a Feynman diagram contributing to $gggg$. The numbers on top of the diagrams represent cyclic ordering.

More generally, for the tree-level gluon amplitudes, the color factor always reduces to single traces. For $gg \dots g$ (with n gluons) \mathcal{A}_n^{tree} , the color decomposition reads [109–111] :

$$\mathcal{A}_n^{tree}(1, 2, \dots, n) = g_s^{n-2} \sum_{\sigma \in S_n / \mathbb{Z}_n} \text{Tr} \left[\prod_{k=1}^n t^{a_{\sigma(k)}} \right] A_n^{tree}(\sigma(1), \sigma(2), \dots, \sigma(n)) . \quad (3.10)$$

where A_n^{tree} are the partial amplitudes (denoted by a capital A). S_n / \mathbb{Z}_n is the set of cyclically inequivalent permutations³ (such that each traces in the sum are distinct), then the partial amplitudes appearing in Eq. (3.10) have each a particular leg ordering

²Which means writing $\text{Tr}(t^a t^b t^c) = (t^a)_{ii_1} (t^b)_{i_1 i_2} (t^c)_{i_2 i}$.

³With S_n the set of permutation over a set of size n while \mathbb{Z}_n is the subset of cyclic permutations in S_n .

(simplifying the amplitude calculation). This is a feature of partial amplitudes that led to the name *color-ordered amplitudes*. Besides, this ordering implies that only planar diagrams contribute to partial amplitudes. Note that the $-\frac{1}{N_c}$ term in the Fierz identity do not contribute. (Eq. (3.9)). This term would contribute only if a “photon” could couple to the gluon (an $U(1)$ auxiliary gauge field, that would need a readjustment of its coupling to be the photon of QED). An interesting feature of partial amplitude is that, at tree level and leading color (leading order in N_c), cross section can be expressed as incoherent sum of partial amplitudes square. Indeed, one can see by applying the Fierz identity on the color-summed cross-section leads to :

$$\begin{aligned} d\sigma^{tree} &\propto \sum_{\{a_i\}} \left| \mathcal{A}_n^{tree}(1_{\bar{q}}, 2_q, 3, \dots, n) \right|^2 \\ &\propto N_c^n \left[\sum_{\sigma \in S_{n-2}} \left| A_n^{tree}(1_{\bar{q}}, 2_q, \sigma(3), \dots, \sigma(n)) \right|^2 + \mathcal{O}\left(\frac{1}{N_c^2}\right) \right]. \end{aligned} \quad (3.11)$$

An equivalent decomposition exists for $\bar{q}qg \dots g$, which reads :

$$\mathcal{A}_n^{tree}(1_{\bar{q}}, 2_q, 3, \dots, n) = g_s^{n-2} \sum_{\sigma \in S_{n-2}} \left(\prod_{k=3}^n t^{a_{\sigma(k)}} \right)_{i_2}^{\bar{j}_1} A_n^{tree}(1_{\bar{q}}, 2_q, \sigma(3), \dots, \sigma(n)). \quad (3.12)$$

In this case, instead of single traces of $SU(N_c)$ generators, we have generator strings (which are no more equivalent by cyclic permutation, hence the sum is over all the permutations of the gluons S_{n-2}). One can similarly obtain color decomposition for loop-level amplitudes. The method stays the same but the results involve more terms. In the case of gluon amplitudes, we have [112] :

gg...g loop color decomposition

$$\begin{aligned} \mathcal{A}_n^{(1)}(1, 2, \dots, n) &= g_s^n \left[\sum_{\sigma \in S_n/\mathbb{Z}} N_c \text{Tr} \left(\prod_{k=1}^n t^{a_{\sigma(k)}} \right) A_{n;1}(\sigma(1), \sigma(2), \dots, \sigma(n)) \right. \\ &\quad + \sum_{c=2}^{\lfloor \frac{n}{2} \rfloor + 1} \sum_{\sigma \in S_n/S_{n;c}} \text{Tr} \left(\prod_{k=1}^{c-1} t^{a_{\sigma(k)}} \right) \text{Tr} \left(\prod_{k'=c}^n t^{a_{\sigma(k')}} \right) \\ &\quad \left. \times A_{n;c}(\sigma(1), \sigma(2), \dots, \sigma(n)) \right], \end{aligned} \quad (3.13)$$

where $A_{n;c}$ are the partial amplitudes and $S_{n;c}$ is the subset of permutations (in S_n) that leaves invariant the corresponding double trace. Due to the factor N_c , $A_{n;1}$ is called the leading-color partial amplitude (which are color while $A_{n;c}$, for $c > 1$, are the subleading-color partial amplitudes. An important feature of these specific partial

amplitudes is that they can all be generated from $A_{n;1}$, following the identity :

$$A_{n;c}(1, 2, \dots, c-1; c, c+1, \dots, n) = (-1)^n \sum_{\sigma \in S_{n;\alpha_c, \beta_c}} A_{n;1}(\sigma(1), \sigma(2), \dots, \sigma(n)) \quad (3.14)$$

where $\alpha_c = {}^t \llbracket 1, c-1 \rrbracket$ (reverse-ordered set) with t reversing the set order, $\beta_c = \llbracket c, n \rrbracket$ (ordered set) and $S_{n;\alpha_c, \beta_c}$ is the subset of permutations of $\{1, 2, \dots, n\}$ which fixes 1 and preserves the cyclic order in both α_c and in β_c ⁴. Overall, the previous decompositions imply that the calculation of tree and one-loop gluonic amplitudes and of tree amplitudes with a quark pair and any number of gluons reduces to the calculation of a single partial amplitude, with fixed leg order (hence planar). Of course, we actually need to calculate it for the different helicity (and polarization) configurations, but the number of diagrams is already well reduced compared to a direct calculation.

The case of $\bar{q}qg \dots g$ amplitude at loop order is slightly more complicated. Still, a color decomposition can be described, in a general fashion as [115] :

$\bar{q}qg \dots g$ loop color decomposition

$$\begin{aligned} \mathcal{A}_n^{(1)}(1_{\bar{q}}, 2_q, 3, \dots, n) &= g_s^n \sum_{c=1}^{n-1} \sum_{\sigma \in S_n/S_{n;c}} C_{n;c}(1_{\bar{q}}, 2_q, \sigma(3), \sigma(4), \dots, \sigma(n)) \\ &\quad \times A_{n;c}(1_{\bar{q}}, 2_q, \sigma(3), \dots, \sigma(n)), \end{aligned} \quad (3.15)$$

with $C_{n;c}$ the color structures that are in this specific case :

$$\begin{aligned} C_{n;1}(1_{\bar{q}}, 2_q, 3, \dots, n) &= \left(\prod_{k=3}^n t^{a_{\sigma(k)}} \right)_{i_2}^{\bar{j}_1} \\ C_{n;2}(1_{\bar{q}}, 2_q, 3; 4, \dots, n) &= 0 \\ C_{n;c}(1_{\bar{q}}, 2_q, 3, \dots, c+1; c+2, \dots, n) &= \text{Tr} \left(\prod_{k=3}^{c+1} t^{a_{\sigma(k)}} \right) \left(\prod_{k=c+2}^n t^{a_{\sigma(k)}} \right)_{i_2}^{\bar{j}_1}, \\ C_{n;n-1}(1_{\bar{q}}, 2_q, 3, \dots, n) &= \text{Tr} \left(\prod_{k=3}^n t^{a_{\sigma(k)}} \right) \delta_{i_2}^{\bar{j}_1}. \end{aligned} \quad (3.16)$$

where, in the third line, $3 \leq c \leq n-2$. Again, $S_{n;c}$ is the set of permutations that keeps the color factor in front of $A_{n;c}$ (i.e $C_{n;c}$) invariant. In this case, it is possible to

⁴As an example, let's consider $n=5$ and $c=3$, then $\alpha_3 = \{2, 1\}$ and $\beta_3 = \{3, 4, 5\}$. In this case, $S_{4;\alpha_3, \beta_3}$ contains :

$$\begin{aligned} (1, 2, 3, 4, 5), (1, 2, 4, 5, 3), (1, 2, 5, 3, 4), & \quad (1, 3, 2, 4, 5), (1, 4, 2, 5, 3), (1, 5, 2, 3, 4), \\ (1, 3, 4, 2, 5), (1, 4, 5, 2, 3), (1, 5, 3, 2, 4), & \quad (1, 3, 4, 5, 2), (1, 4, 5, 3, 2), (1, 5, 3, 4, 2). \end{aligned}$$

construct both leading and subleading partial amplitudes from common gauge-invariant pieces called *primitive amplitudes* (which are color-ordered and gauge invariant). These primitive amplitudes decompose partial amplitudes considering the quark line⁵ direction which can be either L (“Left”) or R (“Right”) (compared to the loop⁶). The corresponding primitive amplitudes when the quark line participates to the loop are denoted A^L and A^R . In the case where the quark line does not participate to the loop, we define the primitive amplitudes $A^{L,[J]}$ and $A^{R,[J]}$ where $J \in \{0, \frac{1}{2}, 1\}$ denotes the spin of the particle in the loop. Actually, these two amplitudes are not independent and are related by reflection (of the gluon legs) as :

$$A_n^{R,[J]}(1_{\bar{q}}, 3, 4, \dots, 2_q, \dots, n-1, n) = (-1)^n A_n^{L,[J]}(1_{\bar{q}}, n, n-1, \dots, 2_q, \dots, 4, 3). \quad (3.17)$$

It can then be shown [115] that the leading-color partial amplitude takes the form :

$$\begin{aligned} A_{n,1}(1_{\bar{q}}, 2_q, 3, \dots, n) &= A_n^L(1_{\bar{q}}, 2_q, 3, \dots, n) - \frac{1}{N_c^2} A_{n,1}^R(1_{\bar{q}}, 2_q, 3, \dots, n) \\ &+ \frac{n_f}{N_c} A_n^{L, [\frac{1}{2}]}(1_{\bar{q}}, 2_q, 3, \dots, n) + \frac{n_s}{N_c} A_n^{L, [0]}(1_{\bar{q}}, 2_q, 3, \dots, n), \end{aligned} \quad (3.18)$$

where n_f is the number of fermions circulating in the loop (the number of flavors of massless quarks considered) and n_s the number of complex massless scalars. The subleading-color partial amplitudes can also be determined from primitive amplitudes, following an identity similar to the one for gluon amplitudes :

$$\begin{aligned} A_{n;c}(1_{\bar{q}}, 2_q, 3, \dots, c+1; c+2, c+3, \dots, n) &= \\ (-1)^{c-1} \sum_{\sigma \in S_{n; \alpha_c, \beta_c}} &\left[A_n^{L, [1]}(\sigma(1_{\bar{q}}), \sigma(2_q), \sigma(3), \dots, \sigma(n)) \right. \\ &- \frac{n_f}{N_c} A_n^{R, [\frac{1}{2}]}(\sigma(1_{\bar{q}}), \sigma(2_q), \sigma(3), \dots, \sigma(n)) \\ &\left. - \frac{n_s}{N_c} A_n^{R, [0]}(\sigma(1_{\bar{q}}), \sigma(2_q), \sigma(3), \dots, \sigma(n)) \right], \end{aligned} \quad (3.19)$$

where actually, α_c and β_c are defined slightly differently than in the gluonic case. Indeed, here, $\alpha_c = {}^t\llbracket 3, c+1 \rrbracket$, $\beta_c = \{1, 2, c+2, c+3, \dots, n\}$ ⁷. So, again, the amplitude is fully determined by a limited number of gauge invariant, color-ordered (hence planar) pieces :

⁵By quark line, we mean the quark line linking the external quark to the external antiquark.

⁶We won’t enter into the full details of this distinction, described in [115], focusing on result relevant for the following.

⁷As an example, let’s consider $n = 5$ and $c = 3$, then $\alpha_3 = \{4, 3\}$ and $\beta_3 = \{1, 2, 5\}$. In this case, $S_{4; \alpha_3, \beta_3}$ contains :

$$\begin{aligned} &(1, 2, 5, 4, 3), (1, 2, 4, 5, 3), (1, 2, 4, 3, 5), (1, 4, 2, 5, 3), (1, 4, 2, 3, 5), (1, 4, 3, 2, 5), \\ &(1, 2, 5, 3, 4), (1, 2, 3, 5, 4), (1, 2, 3, 4, 5), (1, 3, 2, 5, 4), (1, 3, 2, 4, 5), (1, 3, 4, 2, 5). \end{aligned}$$

the *primitive amplitudes*.

We should mention that the calculation of the partial (and primitive) amplitudes does not follow the classical Feynman rules (presented in App. B.1) but rather *color-ordered Feynman rules* (presented in App. B.2). These rules are obtained by expanding the structure functions in traces of generators and using the Fierz identity on the classical Feynman rules while selecting a specific color factor.

Also, while we will use the decompositions presented above, we should mention that different color ordering exist. Actually, the color bases used are not unique. If we consider for instance the trace-basis appearing in the color decomposition of tree level gluonic amplitudes (see Eq. (3.10)), it is over-complete, which leads to relations between the tree-level partial amplitudes, the *Kleiss-Kuijff relations* [103, 116, 117] :

$$A_n^{tree}(1, \alpha, n, {}^t\beta) = (-1)^{|\beta|} \sum_{\sigma \in OP(\alpha, {}^t\beta)} A_n^{tree}(1, \sigma(\alpha \cup {}^t\beta), n), \quad (3.20)$$

where α and β are two sets verifying $\alpha \cup \beta = \llbracket 2, n-1 \rrbracket$, $\alpha \cap \beta = \emptyset$, $|\beta|$ is the cardinal of β and $OP(\alpha, \beta)$ is the set of ordered permutations, preserving ordering within α and β . Further relations exist upon partial amplitudes, especially gluonic ones, such as the *Bern-Carrasco-Johanson (BCJ)* relations that reveal the color-kinematics duality of Yang-Mills amplitudes. In their simplest form, referred to as *fundamental BCJ* relations, they read [117] :

$$\sum_{i=3}^n \left(\sum_{j=3}^i s_{2j} \right) A_n^{tree}(1, 3, \dots, i, 2, i+1, \dots, n) = 0. \quad (3.21)$$

Then, it is possible to consider different color-ordering using the same partial amplitudes. If Eq. (3.10) is based on the fundamental decomposition, it is possible to write a decomposition based on adjoint representation [118] :

$$\mathcal{A}_n^{tree}(1, 2, \dots, n) = g_s^{n-2} \sum_{\sigma \in S_{n-2}/\mathbb{Z}_n} \left(\prod_{k=2}^{n-1} T^{a_{\sigma(k)}} \right)_{a_1 a_n} A_n^{tree}(1, \sigma(2), \dots, n), \quad (3.22)$$

where $(T^a)_{bc} = if^{abc}$. This can be expanded at loop-level and also for amplitudes with one quark-antiquark pair. A last decomposition we should mention is the *color-flow decomposition* where gluons are characterized by a pair of fundamental anti-fundamental color indices, leading to [116] :

$$\mathcal{A}_n^{tree}(1, 2, \dots, n) = g_s^{n-2} 2^{-\frac{n}{2}} \sum_{\sigma \in S_{n-1}/\mathbb{Z}_n} \delta_{j\sigma(2)}^{i_1} \left[\prod_{k=2}^{n-1} \delta_{j\sigma(k+1)}^{i_{\sigma(k)}} \right] \delta_{j_1}^{i_{\sigma(n)}} A_n^{tree}(1, \sigma(2), \dots, n). \quad (3.23)$$

This way, quarks and gluons are treated on equal footing.

Finally, we should mention some properties of partial amplitudes, based on symmetries they follow. Those are particularly useful since they reduce the number of helicity configurations leading to independent amplitudes. These symmetries are :

- *Cyclicity*, as a consequence of partial amplitude definition :

$$A_n(\{i\}) = A_n(\{(i+1 \pmod n)\}). \quad (3.24)$$

- *Parity*, where all the helicities are flipped, that implies :

$$A_n(\{i^{\lambda_i}\}) = A_n(\{i^{-\lambda_i}\}). \quad (3.25)$$

- *Charge conjugation*, i.e the transformation of quark into antiquark and vice versa. From the color-ordered quark-gluon vertex, it implies :

$$A_n(1_{\bar{q}}, 2_q, 3, \dots, n) = -A_n(1_q, 2_{\bar{q}}, 3, \dots, n). \quad (3.26)$$

- At tree level, the anti-symmetry of the color-ordered Feynman rules under *reflection* leads to :

$$A_n^{tree}(1, 2, \dots, n) = -A_n^{tree}(n, n-1, \dots, 1). \quad (3.27)$$

Lastly, for gluon partial amplitudes at tree level, another interesting relation exists [112, 119] :

$$0 = A_n^{tree}(1, 2, \dots, n) + A_n^{tree}(2, 1, 3, \dots, n) + \dots + A_n^{tree}(2, 3, \dots, 1, n). \quad (3.28)$$

This property can be obtained either from string theory techniques or considering the color decomposition of Eq. (3.10), which is also valid when adding a $U(1)$ photons, which generator is the identity. Such amplitude vanishes and, considering a specific color factor, leads to Eq. (3.28). Consequently, this relation is called *photon decoupling relation* or *dual Ward identity*.

3.1.3 Helicity amplitudes

It is natural to use, as kinematic variables, the 4-momenta of the external particles $\{k_i\}$ and the Lorentz invariant products (generalizing 4-point amplitudes Mandelstam variables) defined as :

$$s_{ij} = (k_i + k_j)^2. \quad (3.29)$$

However, since the particles we deal with have spin, this is not the most suitable choice. Actually, the helicity⁸ basis has been proved an effective choice leading to the *spinor helicity formalism* [120–125]. Indeed, we will see that this basis is adapted to the amplitudes' behavior and that it avoids some redundancy in the expressions (with, for

⁸Helicity is the projection of a particle spin along its momentum.

instance, the way to write polarization vectors). Also, by considering massless quarks (adapted to describe high-energy collision), their helicities and chiralities are equivalent hence, in this case, helicity is a conserved quantity.

The massless Dirac equation (see App. B.3 for a short review on the Dirac equation and its solutions), which characterizes our on-shell quarks, leads to identical⁹ positive and negative energy solutions (u and v respectively). From “these” solutions, we construct the right-handed (+ helicity) and left-handed (− helicity) spinors (in 4-component Dirac notation) :

$$\begin{aligned} u_{\pm}(k) &= \frac{1}{2}(1 \pm \gamma_5)u(k), \\ v_{\mp}(k) &= \frac{1}{2}(1 \pm \gamma_5)v(k) = \frac{1}{2}(1 \pm \gamma_5)u(k), \end{aligned} \quad (3.30)$$

for any null 4-vector k . Equivalently, the conjugate spinor read :

$$\begin{aligned} \bar{u}_{\pm}(k) &= \bar{u}(k)\frac{1}{2}(1 \mp \gamma_5), \\ \bar{v}_{\mp}(k_i) &= \bar{v}(k)\frac{1}{2}(1 \mp \gamma_5) = \bar{u}(k)\frac{1}{2}(1 \mp \gamma_5), \end{aligned} \quad (3.31)$$

Note that, since we have adopted the outgoing momenta convention, the helicity of an outgoing particle is its physical helicity while for an incoming particle, it is opposite to its physical helicity. Then, when considering the momenta $\{k_i\}_{i \in [1;n]}$ entering an amplitude (with all legs on-shell), we will adopt the notation :

$$\begin{aligned} |i^{\pm}\rangle &= |k_i^{\pm}\rangle = u_{\pm}(k_i) = v_{\mp}(k_i), \\ \langle i^{\pm}| &= \langle k_i^{\pm}| = \bar{u}_{\pm}(k_i) = \bar{v}_{\mp}(k_i). \end{aligned} \quad (3.32)$$

This way, we can write the spinor products as :

$$\begin{aligned} \langle ij \rangle &= \langle i^- | j^+ \rangle = \bar{u}_-(k_i)u_+(k_j), \\ [ij] &= \langle i^+ | j^- \rangle = \bar{u}_+(k_i)u_-(k_j). \end{aligned} \quad (3.33)$$

This leads to an even shorter notation for the spinors :

$$\langle i| \equiv \langle i^-|, \quad |i\rangle \equiv |i^+\rangle, \quad |i] \equiv |i^-\rangle, \quad [i| \equiv \langle i^+|. \quad (3.34)$$

These spinor products are antisymmetric :

$$\langle ij \rangle = -\langle ji \rangle, \quad \langle ii \rangle = 0, \quad [ij] = -[ji], \quad [ii] = 0, \quad (3.35)$$

and the other possible configurations vanish :

$$\langle ij \rangle = [ji] = 0, \quad (3.36)$$

⁹At least up to normalization (which can be set equal).

which can be easily seen by reinserting the adequate helicity projectors. All these spinors follow the Dirac massless equation which can then be written as :

$$\langle i|\not{k}_i = 0, \quad \not{k}_i|i\rangle = 0, \quad \not{k}_i|i\rangle = 0, \quad [i|\not{k}_i = 0. \quad (3.37)$$

The 4-momenta can be reconstructed from these spinors using the *Gordon identity* (for massless spinors) :

Gordon identity

$$\langle i|\gamma^\mu|i\rangle = [i|\gamma^\mu|i\rangle = 2k_i^\mu, \quad (3.38)$$

and the invariants s_{ij} read :

$$\langle ij\rangle[ji] = \text{Tr} \left(\frac{1}{2}(1 - \gamma_5)\not{k}_i\not{k}_j \right) = 2k_i \cdot k_j = s_{ij}. \quad (3.39)$$

The first equality in Eq. (3.39) can be inferred from the spinor completeness relation :

$$|i\rangle[i] + |i\rangle\langle i| = \not{k}_i, \quad (3.40)$$

which can be split into two with the helicity projectors as :

$$|i\rangle[i] = \frac{1}{2}(1 + \gamma_5)\not{k}_i, \quad |i\rangle\langle i| = \frac{1}{2}(1 - \gamma_5)\not{k}_i. \quad (3.41)$$

Also, we will use the abusive notation :

$$\langle i|p|j\rangle \equiv \langle i|\not{p}|j\rangle, \quad (3.42)$$

for any 4-momentum p . If p is light-like, the relation can be expressed :

$$\langle i|p|j\rangle = \langle ip\rangle[pj]. \quad (3.43)$$

Furthermore, the charge conjugation of current implies :

$$\langle i|\gamma^\mu|j\rangle = [i|\gamma^\mu|j\rangle. \quad (3.44)$$

An important relation in obtaining amplitudes in terms of spinor products is the *Fierz identity* on spinors which reads :

Fierz identity

$$[i|\gamma^\mu|j\rangle[k|\gamma_\mu|l\rangle = 2[ik\rangle\langle lj]. \quad (3.45)$$

Finally, simplifying a helicity amplitude expression is mainly achieved by playing around two relations. First, the *Schouten identity* :

Schouten identity

$$\begin{aligned}
 [ij][kl] + [ik][lj] + [il][jk] &= 0, \\
 \langle ij \rangle \langle kl \rangle + \langle ik \rangle \langle lj \rangle + \langle il \rangle \langle jk \rangle &= 0,
 \end{aligned}
 \tag{3.46}$$

which follows from the fact that helicity spinors are actually 2-component vectors (for which an antisymmetric expression as in Eq. (3.46) vanishes). Thus, even if it is efficient mainly with a small number of particles (entering an amplitude), we should mention the

momentum conservation $\sum_{i=1}^n k_i^\mu = 0$, which implies the spinor product identity :

Momentum conservation

$$\sum_{i=1}^n \langle ji \rangle [ik] = 0.
 \tag{3.47}$$

We might refer to this relation as simply ‘‘momentum conservation’’. Besides, the development of the spinor helicity method is possible thanks to the possibility of writing polarization vectors (for massless vector bosons of momentum k with defined helicity) in terms of massless spinors [122, 124, 125] :

Polarization vectors

$$\epsilon_\mu^+(k, q) = \frac{\langle q | \gamma_\mu | k \rangle}{\sqrt{2} \langle qk \rangle}, \quad \text{and} \quad \epsilon_\mu^-(k, q) = -\frac{[q | \gamma_\mu | k \rangle}{\sqrt{2} [qk]},
 \tag{3.48}$$

where q is an auxiliary null vector, named *reference momentum*, which can be fixed freely (for each boson) due to gauge freedom (but different than k). Indeed, a shift in the reference momentum is a gauge invariance transformation, which can be written as :

$$\epsilon_\mu^+(q') - \epsilon_\mu^+(q) = \frac{\langle q | \not{k} \gamma_\mu + \gamma_\mu \not{k} | q' \rangle}{\sqrt{2} \langle q'k \rangle \langle qk \rangle} = \frac{\sqrt{2} \langle qq' \rangle}{\langle q'k \rangle \langle qk \rangle} k_\mu,
 \tag{3.49}$$

leading to a vanishing contribution in the amplitude (or partial amplitude), as stated by the *Ward–Takahashi identity* (for an amplitude \mathcal{A} involving a vector boson with momentum k and polarization vector ϵ) :

Ward–Takahashi identity

$$k_\mu \mathcal{A}^\mu = 0,
 \tag{3.50}$$

for $\mathcal{A} = \epsilon_\mu \mathcal{A}^\mu$. This identity is a consequence of gauge invariance, implying that the polarization of a vector boson parallel to its momentum does not contribute to the amplitude. Furthermore, such polarization vector satisfies the transverse condition :

$$\forall i, k_i \cdot \epsilon_i^\pm = 0, \quad \text{with } i \text{ a gluon},
 \tag{3.51}$$

where we have used the short notation $\epsilon_i^{\pm\mu} = \epsilon_i^{\pm\mu}(k_i, q_i)$. In the following, we will also use the notation $\epsilon_i^{\pm\mu}(q_i) = \epsilon_i^{\pm\mu}(k_i, q_i)$, when fixing the reference momentum to some specific value. These polarization vectors are also transverse to the reference momentum :

$$q_i \cdot \epsilon_i^{\pm} = 0, \text{ with } i \text{ a gluon.} \quad (3.52)$$

One can notice that complex conjugation reduces to a helicity flip :

$$(\epsilon_\mu^+)^* = \epsilon_\mu^-. \quad (3.53)$$

Also, the polarization vectors follow standard normalization :

$$\epsilon^\pm \cdot (\epsilon^\pm)^* = \epsilon^\pm \cdot \epsilon^\mp = -1, \text{ and } \epsilon^\pm \cdot (\epsilon^\mp)^* = \epsilon^\pm \cdot \epsilon^\pm = 0. \quad (3.54)$$

In this form, it can be shown that the polarization vectors follow the completeness relation as in a light-cone gauge :

$$\begin{aligned} \sum_{\lambda=\pm} \epsilon_\mu^\lambda(k, q) (\epsilon_\nu^\lambda(k, q))^* &= \sum_{\lambda=\pm} \epsilon_\mu^\lambda(k, q) \epsilon_\nu^{-\lambda}(k, q) = -\frac{1}{2} \sum_{\lambda=\pm} \frac{\langle k^\lambda | \gamma_\mu | q^\lambda \rangle \langle q^\lambda | \gamma_\nu | k^\lambda \rangle}{\langle q | k \rangle [qk]} \\ &= -\frac{1}{2} \sum_{\lambda=\pm} \frac{\langle k^\lambda | \gamma_\mu \not{q} \gamma_\nu | k^\lambda \rangle}{\langle q | k \rangle [qk]} \\ &= -\frac{1}{2} \sum_{\lambda=\pm} \frac{\langle k^\lambda | q_\mu \gamma_\nu + q_\nu \gamma_\mu - \eta_{\mu\nu} \not{q} | k^\lambda \rangle}{k \cdot q} \\ &= -\eta_{\mu\nu} + \frac{k_\mu q_\nu + k_\nu q_\mu}{k \cdot q}, \end{aligned} \quad (3.55)$$

where we have used $\gamma_\mu \gamma_\alpha \gamma_\nu = \eta_{\mu\alpha} \gamma_\nu + \eta_{\alpha\nu} \gamma_\mu - \eta_{\mu\nu} \gamma_\alpha - i \epsilon_{\mu\alpha\nu}^\beta \gamma_\beta \gamma^5$. Numerous simplifications can be applied when fixing the reference momenta, such as :

- $\epsilon_i^+(q) \cdot \epsilon_j^+(q) = \epsilon_i^-(q) \cdot \epsilon_j^-(q) = 0$.
- $\epsilon_i^+(k_j) \cdot \epsilon_j^-(q) = \epsilon_i^+(q) \Big|_{q_i=q} \cdot \epsilon_j^-(k_i) = 0$.
- $\not{\epsilon}_i^+(k_j) |j\rangle = \not{\epsilon}_i^-(k_j) |j\rangle = 0$.
- $|j\rangle \not{\epsilon}_i^-(k_j) = \langle j | \not{\epsilon}_i^+(k_j) = 0$.

Then, considerations based on the helicity configurations of an amplitude and a clever fixing of the reference momenta can greatly simplify the calculation of a partial amplitude. Also, if we consider the different products appearing in amplitudes :

$$\begin{aligned} \epsilon_i^+ \cdot \epsilon_j^+ &= \frac{[k_i k_j] \langle q_j q_i \rangle}{\langle q_i k_i \rangle \langle q_j k_j \rangle}, & \epsilon_i^+ \cdot \epsilon_j^- &= -\frac{[k_i q_j] \langle k_j q_i \rangle}{\langle q_i k_i \rangle [q_j k_j]}, \\ \epsilon_i^+ \cdot k &= \frac{[k_i k] \langle k q_i \rangle}{\sqrt{2} \langle q_i k_i \rangle}, & \epsilon_i^- \cdot k &= -\frac{[q_i k] \langle k k_i \rangle}{\sqrt{2} [q_i k_i]}, \\ k_i \cdot k_j &= \frac{1}{2} \langle ij \rangle [ji], \end{aligned} \quad (3.56)$$

we observe that we are left with rational functions of the spinor products (characteristic of the compactness of the helicity amplitudes).

To illustrate how spinor helicity can simplify an amplitude calculation, let's consider the simple example of the 4-point gluonic partial amplitude at tree level $A_4^{tree}(1, 2, 3, 4)$ (here, we will stress the vanishing contribution, for a more detailed example, see App. B.4). In this amplitude, and more exactly in every diagram contributing to it, will appear products of the type $\epsilon_i^{\lambda_i} \cdot \epsilon_j^{\lambda_j}$. For the all plus helicity configuration $A_4^{tree}(1^+, 2^+, 3^+, 4^+)$, it is clear that, setting the reference momenta $q_1 = q_2 = q_3 = q_4 = q$ leads to $A_4^{tree}(1^+, 2^+, 3^+, 4^+) = 0$ (using $\epsilon_i^+(q) \cdot \epsilon_j^+(q) = 0$). In the same way, for the case where the first gluon has opposite helicity with respect to the others, by choosing $q_2 = q_3 = q_4 = k_1$, we conclude that $A_4^{tree}(1^-, 2^+, 3^+, 4^+) = 0$. From the properties of partial amplitudes, only one more independent partial amplitude needs to be calculated : $A_4^{tree}(1^-, 2^-, 3^+, 4^+)$. Indeed we have :

- $A_4^{tree}(1^-, 2^-, 3^-, 4^-) = A_4^{tree}(1^+, 2^+, 3^+, 4^+) = 0$ and
 $A_4^{tree}(1^+, 2^-, 3^-, 4^+) = A_4^{tree}(1^-, 2^+, 3^+, 4^+) = 0$ by parity,
- $A_4^{tree}(1^-, 2^+, 3^+, 4^+) = A_4^{tree}(4^+, 1^-, 2^+, 3^+)$
 $= A_4^{tree}(3^+, 4^+, 1^-, 2^+) = A_4^{tree}(2^+, 3^+, 4^+, 1^-) = 0$,
 $A_4^{tree}(1^+, 2^-, 3^-, 4^-) = A_4^{tree}(4^-, 1^+, 2^-, 3^-)$
 $= A_4^{tree}(3^-, 4^-, 1^+, 2^-) = A_4^{tree}(2^-, 3^-, 4^-, 1^+) = 0$ and
 $A_4^{tree}(1^+, 2^-, 3^-, 4^+) = A_4^{tree}(2^-, 3^-, 4^+, 1^+)$ by cyclicity,
- and finally $A_4^{tree}(1^-, 2^+, 3^-, 4^+) = A_4^{tree}(1^+, 2^-, 3^+, 4^-)^\dagger$
 $= -A_4^{tree}(1^-, 3^-, 2^+, 4^+) - A_4^{tree}(1^-, 3^-, 4^+, 2^+)$ using the dual Ward identity of Eq. (3.28).

Note that, once written in terms of spinor products, the relation Eq. (3.25) actually implies :

$$A_n(\{i^{-\lambda_i}\}) = (-1)^n A_n(\{i^{\lambda_i}\}) \Big|_{\langle \rangle \leftrightarrow []} = (-1)^n A_n(\{i^{\lambda_i}\})^\dagger. \quad (3.57)$$

Choosing the reference momenta $q_1 = q_2 = k_4$ and $q_3 = q_4 = k_1$ reduces $A_4^{tree}(1^-, 2^-, 3^+, 4^+)$ to a single diagram leading to :

$$A_4^{tree}(1^-, 2^-, 3^+, 4^+) = i \frac{\langle 12 \rangle^3}{\langle 12 \rangle \langle 23 \rangle \langle 34 \rangle \langle 41 \rangle}, \quad (3.58)$$

which is the only partial amplitude one has to calculate to obtain the 4-point tree-level gluon amplitude (and the corresponding unpolarized cross-section).

Actually, with the same considerations, we can show that the tree level partial amplitude for n -gluons, with all plus helicity configuration or with one helicity opposite to the other vanish :

$$\begin{aligned} A_n^{tree}(1^+, \dots, n^+) &= A_n^{tree}(1^-, \dots, n^-) = 0, \\ A_n^{tree}(1^-, 2^+, \dots, n^+) &= A_n^{tree}(1^+, 2^-, \dots, n^-) = 0. \end{aligned} \quad (3.59)$$

3.1.4 Soft and collinear factorization

If the helicity basis permit reduction of the amplitude calculation to simpler objects (polarized partial amplitudes), the spinor products are also well suited to describe amplitude behavior. This can be foreseen when considering real momenta. In this case, angle and square bracket spinor products are related by complex conjugation :

$$[ij] = \langle ij \rangle^* . \quad (3.60)$$

Combined with Eq. (3.39), it implies that the spinor products are defined as :

$$[ij] = \sqrt{s_{ij}} e^{\phi_{ij}} , \quad \langle ij \rangle = \sqrt{s_{ij}} e^{-\phi_{ij}} , \quad (3.61)$$

i.e that, up to a phase ϕ_{ij} , spinor products are square roots of the invariants s_{ij} . Also, these square roots are the poles of the amplitudes when two particles become collinear. Indeed, if we consider the limit in which parton a and parton b become collinear (or parallel), and we define $P_{a,b} = k_a + k_b$, then :

$$P_{a,b}^2 = 2k_a \cdot k_b \xrightarrow{a\parallel b} 0 , \quad (3.62)$$

the internal momentum $P_{a,b}$ becomes on-shell, leading to a singularity in the amplitude. By defining, in this limit, z as :

$$k_a \xrightarrow{a\parallel b} zP_{a,b} , \quad k_b \xrightarrow{a\parallel b} (1-z)P_{a,b} , \quad (3.63)$$

we can write the (partial) amplitude in a factorized form [126, 127] :

$$A_n^{tree}(1, \dots, a^{\lambda_a}, b^{\lambda_b}, \dots, n) \xrightarrow{a\parallel b} \sum_{\lambda=\pm} Split_{-\lambda}^{tree}(z, a^{\lambda_a}, b^{\lambda_b}) \times \quad (3.64)$$

$$\times A_{n-1}^{tree}(1, \dots, a-1, P_{a,b}^\lambda, b+1, \dots, n) .$$

This factorization is illustrated on Fig. 3.4.

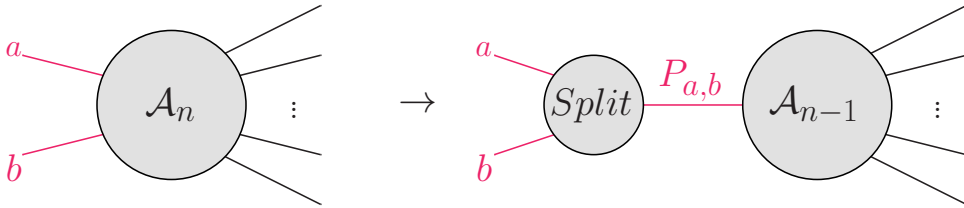


Figure 3.4: Diagrammatic representation of the factorization of an amplitudes when two of its legs become collinear.

Note that, since we consider color-ordered amplitudes, a and b have to be cyclically adjacent. The functions $Split_{-\lambda}^{tree}$ are polarized tree-level splitting functions, defined as :

$$\begin{aligned} Split_{-}^{tree}(a^{-}, b^{-}) &= 0, & Split_{-}^{tree}(a^{+}, b^{+}) &= \frac{1}{\sqrt{z(1-z)}\langle ab \rangle}, \\ Split_{+}^{tree}(a^{+}, b^{-}) &= \frac{(1-z)^2}{\sqrt{z(1-z)}\langle ab \rangle}, & Split_{-}^{tree}(a^{+}, b^{-}) &= \frac{-z^2}{\sqrt{z(1-z)}[ab]}, \end{aligned} \quad (3.65)$$

for an intermediate state of momentum $P_{a,b}$ and helicity λ . This factorization property hold also in presence of quarks, with the following splitting functions :

$$\begin{aligned} Split_{-}^{tree}(a_q^{+}, b^{+}) &= \frac{1}{\sqrt{1-z}\langle ab \rangle}, & Split_{-}^{tree}(a_q^{+}, b^{-}) &= \frac{-z}{\sqrt{1-z}[ab]}, \\ Split_{-}^{tree}(a^{+}, b_q^{+}) &= \frac{1}{\sqrt{z}\langle ab \rangle}, & Split_{-}^{tree}(a^{-}, b_q^{+}) &= \frac{z-1}{\sqrt{z}[ab]}. \end{aligned} \quad (3.66)$$

The rest of the splitting function can be obtained by parity or by charge conjugation. In Eq. (3.64), the opposite sign of the helicity of the ‘‘collinear state’’ ($a+b$) is due to the outgoing momenta convention (that we also apply on the splitting functions). One may notice that summing these splitting functions over their helicities (for all 3 legs) and squaring them, we recover the Altarelli-Parissi splitting functions¹⁰ (polarized and unregularized).

This factorization of collinear singularities, appearing when two cyclically adjacent particles become collinear, can be generalized. Indeed, we saw that the singularity was coming from the intermediate line $P_{a,b}$ going on-shell (implying a pole in the corresponding propagator). Actually, this factorization also holds when any intermediate propagator goes on-shell, i.e when $P_{i,j}^2 \rightarrow 0$ for $P_{i,j} = \sum_i^j k_i$. It is referred to as *multi-particle channel*. In fact, with color-ordered amplitudes, only poles of the form $P_{1,j}^2$ can develop, leading to :

$$A_n^{tree}(1, \dots, n) \sim \sum_{\lambda} A_{m+1}^{tree}(1, \dots, m, P^{\lambda}) \frac{i}{P_{1,m}^2} A_{n-m}^{tree}(m+1, \dots, n, P^{-\lambda}). \quad (3.67)$$

In this limit, one propagator goes on-shell hence it links two on-shell amplitudes just as described by Eq. (3.67).

The same kind of factorization holds when one of the gluons becomes soft (i.e its momentum vanishes), as shown in Fig. 3.5.

In this limit, we have :

$$A_n^{tree}(1, \dots, a, s^{\pm}, b, \dots, n) \xrightarrow{k_s \rightarrow 0} \mathcal{S}(a, s^{\pm}, b) A_{n-1}^{tree}(1, \dots, a-, b, \dots, n), \quad (3.68)$$

¹⁰Actually, the real contributions.

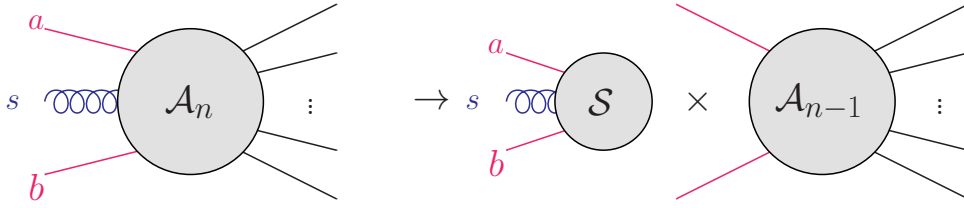


Figure 3.5: Diagrammatic representation of the factorization of an amplitudes when a gluon leg becomes soft.

with the *soft factor* (or *eikonal factor*) given by :

$$\mathcal{S}(a, s^+, b) = \frac{\langle ab \rangle}{\langle as \rangle \langle sb \rangle}, \quad \mathcal{S}(a, s^-, b) = \frac{[ab]}{[as][sb]}. \quad (3.69)$$

These soft factors are independent of the helicity of a and b and whether they are quarks or gluons but it only depends on their angular direction.

In the factorization of soft and collinear singularities, always appears at least one spinor product (in either the soft factor or the different polarized splitting functions). This shows how suitable is the helicity formalism to describe amplitudes and their divergences.

3.1.5 Recursive techniques

Even with the techniques presented (color decomposition and spinor helicity formalism), when the number of legs increases, the calculation of an amplitude stays complex due to the number of (color-ordered) diagrams quickly growing. Some recursive techniques have been developed to calculate tree-level amplitudes. We will present two, the Berends-Giele recursion, particularly suitable for numerical calculations, and the [BCFW](#) recursion that leads to compact expressions.

Berends-Giele recursion

One idea to build tree-level partial amplitudes recursively is to consider what is called the *off-shell current* as a building block. This off-shell current is similar to an amplitude but with an off-shell leg, not contracted then denoted by a Lorentz index (say μ). For n on-shell gluon legs (and one off-shell gluon), we note it $J^\mu(1, \dots, n)$. It corresponds to the sum of diagrams with n on-shell gluons and one off-shell (including its propagator). This off-shell current isn't gauge invariant, in particular, one should be careful, keeping track of the auxiliary momenta (of the on-shell gluons) used when calculating it and keep them till a gauge invariant expression is obtained. Then, the recursion is obtained

by following the off-shell leg of our n legs current. The off-shell gluon line necessarily enters either in a 3-gluon vertex or in a 4-gluon vertex. Then, each leg of these vertices is related to an off-shell current (with necessary less than n legs). This leads to the *Berends-Giele* recursion formula [128] :

Berends-Giele recursion

$$J^\mu(1, \dots, n) = -\frac{i}{P_{1,n}^2} \left[\sum_{i=1}^{n-1} V_3^{\mu\nu\rho}(P_{1,i}, P_{i+1,n}) J_\nu(1, \dots, i) J_\rho(i+1, \dots, n) + \sum_{i=1}^{n-2} \sum_{j=i+1}^{n-1} V_4^{\mu\nu\rho\sigma} J_\nu(1, \dots, i) J_\rho(i+1, \dots, j) J_\sigma(j+1, \dots, n) \right], \quad (3.70)$$

where $V_3^{\mu\nu\rho}$ and $V_4^{\mu\nu\rho\sigma}$ are respectively the 3-gluon and 4-gluon color ordered vertices, given by :

$$V_3^{\mu\nu\rho}(P, Q) = \frac{i}{\sqrt{2}} [\eta^{\nu\rho}(P - Q)^\mu + 2\eta^{\rho\mu}Q^\nu - 2\eta^{\mu\nu}P^\rho] \quad (3.71)$$

$$V_4^{\mu\nu\rho\sigma} = \frac{1}{2} (2\eta^{\mu\rho}\eta_{\sigma\delta} - \eta^{\mu\nu}\eta^{\rho\sigma} - \eta_{\mu\sigma}\eta_{\nu\rho}) .$$

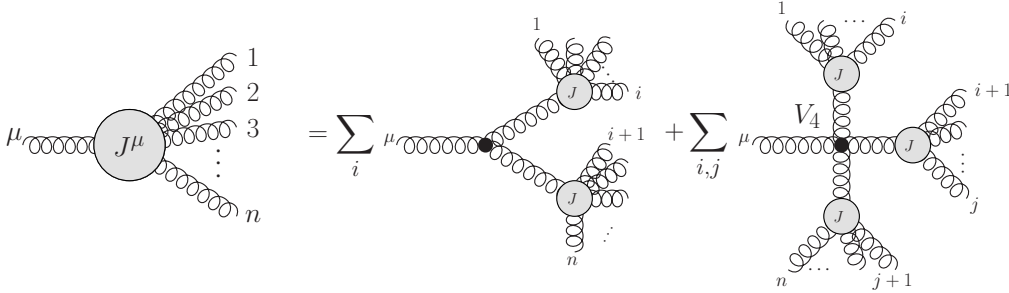


Figure 3.6: Diagrammatic representation of the Berends-Giele recursion on off-shell currents.

This recursion, summarized in Fig. 3.6, allows us to calculate the off-shell current for any number of legs. Furthermore, to obtain the n -point partial amplitude from the off-shell current $J^\mu(1, \dots, n-1)$, one needs to multiply it by $P_{1,n-1}^2$ (canceling the propagator) and contract it with the appropriate polarization vector (ϵ_n^μ). Then, the amplitude is recovered by taking the on-shell limit $k_n^2 = P_{1,n-1}^2 \rightarrow 0$. Nevertheless, the off-shell current satisfies the dual Ward identity :

$$0 = J^\mu(1, 2, 3, \dots, n) + J^\mu(2, 1, 3, \dots, n) + \dots + J^\mu(1, 2, 3, \dots, n, 1), \quad (3.72)$$

the reflection identity :

$$J^\mu(1, 2, 3, \dots, n) = (-1)^{n+1} J^\mu(n, \dots, 3, 2, 1), \quad (3.73)$$

and also, current conservation reads :

$$P_{1,n}^\mu J_\mu(1, \dots, n) = 0. \quad (3.74)$$

Overall, the Berends-Giele recursion is very efficient for numerical calculation and even leads to analytical expression for some specific helicity configurations. For instance, the all-plus off-shell current and the one with 1 negative helicity and $n - 1$ positive ones are given by [128, 129] :

$$\begin{aligned} J_\mu(1^+, 2^+, \dots, n^+) &= \frac{\langle q | \gamma^\mu \not{P}_{1,n} | q \rangle}{\sqrt{2} \langle q1 \rangle \langle 12 \rangle \cdots \langle n-1, 1 \rangle \langle nq \rangle} \\ J_\mu(1^-, 2^+, \dots, n^+) &= \frac{\langle q | \gamma^\mu \not{P}_{2,n} | q \rangle}{\sqrt{2} \langle 12 \rangle \langle 23 \rangle \cdots \langle n-1, 1 \rangle \langle n1 \rangle} \sum_{i=1}^n \frac{\langle 1i \rangle \langle 1 | P_{1,i} | i \rangle}{P_{1,i-1}^2 P_{1,i}^2}. \end{aligned} \quad (3.75)$$

where the reference momenta for all gluons have been fixed to q . An equivalent construction can be done by accounting for quarks, but it is much less compact. This recursion can be used to calculate what is called the **Maximally helicity violating (MHV)** amplitudes. Those are polarized partial gluon amplitudes where 2 gluons have negative helicity while the others have positive helicity. Amplitudes with one more “-” helicity are called **Next to MHV (NMHV)** (and so on). In a $2 \rightarrow (n - 2)$ process, $A(1^+, 2^+, \dots, n^+)$ correspond to the case where the incoming gluons have - helicity (physical one) while the outgoing ones all have + helicity. Hence, it is “helicity violating”, but the corresponding amplitude, as we have seen it, vanishes (see Eq. (3.59)). When one of the outgoing states has a - helicity, it is less violating. But again, this amplitude vanishes. The first non-zero amplitude (ordered by helicity violation) is then the one with two outgoing legs with - helicity. Parke and Taylor have conjectured a formula for **MHV** amplitudes, based on their behavior. Indeed, such amplitudes do not have multi-particle poles, as one can see from Eq. (3.67). When only two gluons have - helicity, a multi-particle pole would imply a factorization of the amplitude into two amplitudes with one that has necessarily only 1 or even no gluon with a - helicity, hence vanishing. This has lead to the Parke-Taylor formula for **MHV** amplitudes [126] :

$$\forall j, k, A_{jk}^{tree \text{ MHV}} = A_n^{tree}(1^+, \dots, j^-, \dots, k^-, \dots, n^+) = i \frac{\langle jk \rangle^4}{\langle 12 \rangle \langle 23 \rangle \cdots \langle n1 \rangle}. \quad (3.76)$$

While conjectured by Parke and Taylor, this formula has been proved by Berends and Giele using the recursion above [128]. The **Maximally helicity violating bar ($\overline{\text{MHV}}$)** amplitudes (where helicities are flipped) can be obtained by parity :

$$\forall j, k, A_{jk}^{tree \overline{\text{MHV}}} = A_n^{tree}(1^-, \dots, j^+, \dots, k^+, \dots, n^-) = i(-1)^n \frac{[jk]^4}{[12][23] \cdots [n1]}. \quad (3.77)$$

BCFW recursion

Another way of constructing recursively amplitudes is to use *linear momentum shifts*. This method is based on complex analysis, where complex momenta are considered. Let's first consider the momentum shift :

$$k_1(z) = k_1 - zq, \quad k_n(z) = k_n + zq, \quad (3.78)$$

applied on legs 1 and n (cyclically adjacent). We will note with a hat the shifted legs ($\hat{1}$ and \hat{n} here). This choice maintains momentum conservation. Also, to keep the on-shellness of the legs, q must satisfy :

$$q^2 = 0, \quad q \cdot k_1 = 0, \quad q \cdot k_n = 0. \quad (3.79)$$

This leads to two solutions (up to normalization), that can be written as :

$$q_1^\mu = \langle 1 | \gamma^\mu | n \rangle, \quad q_2^\mu = \langle n | \gamma^\mu | 1 \rangle. \quad (3.80)$$

We should also mention that the shift of Eq. (3.78) can be expressed at the spinor level as :

$$\begin{aligned} \langle 1 | (z) &= \langle 1 |, & [1 | (z) &= [1 | - z | n |, \\ \langle n | (z) &= \langle n | + z \langle 1 |, & [n | (z) &= [n |. \end{aligned} \quad (3.81)$$

Then, we consider the partial amplitude for n gluons as a complex function of z :

$$A_n(z) \equiv A_n(\hat{1}, 2, \dots, \hat{n}). \quad (3.82)$$

Using Cauchy's theorem, we can write :

$$\frac{1}{2i\pi} \oint_{\mathcal{C}_\infty} dz \frac{A_n(z)}{z} = A_n(0) + \sum_k \text{Res} \left[\frac{A_n(z)}{z} \right] \Big|_{z=z_k}, \quad (3.83)$$

where \mathcal{C}_∞ is the circle centered at the origin, with infinite radius; $\{z_k\}$ are the poles of $A_n(z)$. Note that these poles originate from propagators and are then simple poles. If $A_n(z)$ vanishes at infinity, then the closed integral in Eq. (3.83) vanishes, and we can directly express the wanted amplitude ($A_n(0)$, the amplitude without shift) with the residues of $A_n(z)$:

$$A_n(0) = - \sum_k \text{Res} \left[\frac{A_n(z)}{z} \right] \Big|_{z=z_k} \quad \text{if} \quad \lim_{z \rightarrow \infty} A(z) = 0. \quad (3.84)$$

Hopefully, this condition is satisfied when taking $q^\mu = q_1^\mu = \langle 1 | \gamma^\mu | n \rangle$, when $\{\lambda_1, \lambda_n\} \in \{(+, +), (-, -), (-, +)\}$ (see [130] for details). Now, we have to identify the residue part. The poles of $A_n(z)$ are located where the propagators go on-shell. Any momentum $P_{1,i}$ has a dependence on z after the shift (since it separates the shifted legs). We write it

$P_{1,i}(z) = P_{1,i} - zq$. Then, the on-shell condition at the pole z_i , i.e $P_{1,i}(z_i)^2 = 0$, implies :

$$z_i = \frac{P_{1,i}^2}{\langle 1|P_{1,i}|n \rangle}. \quad (3.85)$$

We can then evaluate the residues from the factorization property (of Eq. (3.67)), leading to :

$$\text{Res} \left[\frac{A_n(z)}{z} \right] \Big|_{z=z_i} = A_{i+1} \left(\hat{1}, 2, \dots, i, -\hat{P}_{1,i}^\lambda \right) \frac{-i}{P_{1,i}^2} A_{n-i+1} \left(\hat{P}_{1,i}^{-\lambda}, i+1, \dots, \hat{n} \right). \quad (3.86)$$

Overall, the BCFW recursion relation for QCD amplitudes reads [130] :

BCFW recursion

$$A_n = \sum_{i=2}^{n-2} \sum_{h=\pm} A_{i+1} \left(\hat{1}, 2, \dots, i, -\hat{P}_{1,i}^\lambda \right) \frac{-i}{P_{1,i}^2} A_{n-i+1} \left(\hat{P}_{1,i}^{-\lambda}, i+1, \dots, \hat{n} \right), \quad (3.87)$$

with the shifted momenta that can be expressed in terms of spinors as :

$$\begin{aligned} \hat{k}_1^\mu &= k_1^\mu - \frac{P_{1,i}^2}{\langle 1|P_{1,i}|n \rangle} \langle 1|\gamma^\mu|n \rangle, & \hat{k}_n^\mu &= k_n^\mu + \frac{P_{1,i}^2}{\langle 1|P_{1,i}|n \rangle} \langle 1|\gamma^\mu|n \rangle, \\ \hat{P}_{1,i}^\mu &= P_{1,i}^\mu - \frac{P_{1,i}^2}{\langle 1|P_{1,i}|n \rangle} \langle 1|\gamma^\mu|n \rangle. \end{aligned} \quad (3.88)$$

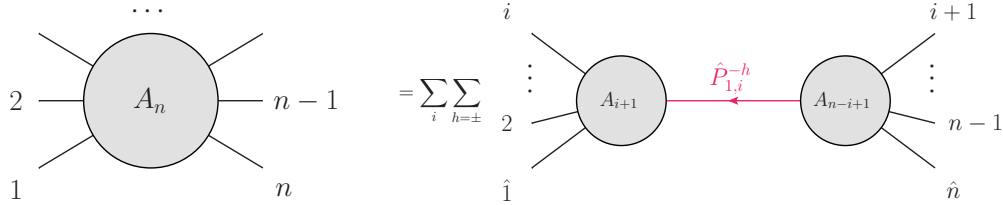


Figure 3.7: Diagrammatic representation of the BCFW recursion, where the momentum shift is applied on the hatted legs.

This recursion is sometimes referred to as simply *on-shell recursion*. Note that this recursion relation can be generalized to other theories (as long as a condition for the amplitude vanishing at infinity is satisfied), for different momentum shifts (not only on adjacent legs) and it might even be generalized at loop order (the generalization has been done for supersymmetric theories in the planar limit [131–133] and some of the difficulties arising at loop level have been already solved [134, 135]).

To initiate the **BCFW** recursion, we need 3-point amplitudes. In the massless approximation, we follow, those amplitudes are pathological. Indeed, momentum conservation and on-shellness imply that all the Lorentz invariants are null :

$$k_1 + k_2 + k_3 = 0, \quad \forall i \in \llbracket 1, 3 \rrbracket, \quad k_i^2 = 0, \quad \forall \{i, j, l\} = \{1, 2, 3\}, \quad s_{ij} = k_l^2 = 0. \quad (3.89)$$

Then, using Eq. (3.39) and Eq. (3.60) we conclude that all spinor products are null. Actually, the latter expression holds only for real momenta. If we consider complex momenta, then we can choose either angle or square brackets to vanish. If we keep non-vanishing angle spinor products, we can write the 3-point **MHV** amplitude as :

$$A_n^{tree}(1^-, 2^-, 3^+) = i \frac{\langle 12 \rangle^4}{\langle 12 \rangle \langle 23 \rangle \langle 31 \rangle}. \quad (3.90)$$

If we keep the square spinors, we can write the 3-point $\overline{\text{MHV}}$ amplitude as :

$$A_n^{tree}(1^+, 2^+, 3^-) = i \frac{[12]^4}{[12][23][31]}. \quad (3.91)$$

Of course, in the physical limit, where momenta are real, these amplitudes vanish. Still, they initiate the **BCFW** construction where momenta are shifted in the complex plane. It is interesting to note that the polarized splitting function (appearing in Eq. (3.64)) are approximations of these amplitudes (the approximation being done at the level of the kinematics).

3.1.6 Supersymmetry

While we are not concerned here by supersymmetric amplitudes, some of their properties can be used to calculate **QCD** amplitudes. We have already mentioned that the photon decoupling identity (Eq. (3.28)) can be obtained as a supersymmetric Ward identity. In fact, tree-level **QCD** partial amplitudes are effectively supersymmetric [136, 137]. Indeed, in partial tree level amplitude, since the color factors are not present, nothing differs between a quark and a gluino. Then it is possible to apply tree-level supersymmetric identity to **QCD** amplitudes. For instance, it can be shown that the supersymmetric amplitudes (denoted by a super index SUSY) follow the *supersymmetric Ward Identity* [138, 139] :

supersymmetric Ward Identity

$$A_n^{tree \text{ SUSY}}(1^-, 2^-, 3^+, \dots, n^+) = \frac{\langle 12 \rangle}{\langle 13 \rangle} A_n^{tree \text{ SUSY}}(1^-, 2_{\tilde{g}}^-, 3_{\tilde{g}}^+, 4^+, \dots, n^+), \quad (3.92)$$

where the index \tilde{g} denotes a gluino. This identity is true to all orders, however, we can apply it in **QCD** to obtain only tree-level partial amplitude (which are effectively

supersymmetric). It is in particular useful to directly obtain amplitudes with a pair of quark-antiquark (with a single gluon with negative helicity) from MHV amplitudes as :

$$\begin{aligned} A_n^{tree}(1_{\bar{q}}^-, 2_q^+, 3^+, \dots, i^-, \dots, n^+) &= \frac{\langle 2i \rangle}{\langle 1i \rangle} A_n^{tree}(1^-, 2^+, 3^+, \dots, i^-, \dots, n^+) \\ &= i \frac{\langle 1i \rangle^3 \langle 2i \rangle}{\langle 12 \rangle \langle 23 \rangle \dots \langle n1 \rangle}. \end{aligned} \quad (3.93)$$

At loop-level however, QCD partial amplitudes are no more supersymmetric. Still, gluon and fermion loops can be decomposed into supersymmetric contributions and a scalar field contribution. In the case of gluonic amplitude, we have :

$$\begin{aligned} g &= (g + 4f + 3s) - 4(f + s) + s = A^{\text{SUSY}} - 4A^{N=1} + A^s \\ f &= (f + s) - s = A^{N=1} - A^s, \end{aligned} \quad (3.94)$$

where g , f and s denotes respectively a gluon, fermion, and scalar loop. A^{SUSY} is the supersymmetric amplitude ($N = 4$ super Yang-Mills) which multiplet is formed of a gluon, four gluinos, and three complex scalars. $A^{N=1}$ is the contribution of a $N = 1$ chiral matter supermultiplet (composed of one fermion and one complex scalar). Finally, A^s corresponds to the scalar contribution. All those contributions are much simpler than the gluon loop (especially the SUSY part). For the case with a quark-antiquark pair in the amplitude, we will use similar relations to rewrite the decomposition in primitive amplitudes given in Eq. (3.18). In terms of the “left” and “right” primitive amplitudes, we have [115] :

$$\begin{aligned} A_{n;1}^{\text{SUSY}} &= A_n^L + A_n^R + A_n^{L, [\frac{1}{2}]} + A_n^{L, [\frac{1}{2}]} \\ A_n^{N=1} &= -A_n^{L, [0]} - A_n^{L, [\frac{1}{2}]} \\ A_n^s &= A_n^{L, [0]}, \end{aligned} \quad (3.95)$$

where all the cyclic orders are identical and where $A_{n;1}^{\text{SUSY}}$, is the leading color supersymmetric partial amplitudes where quarks are replaced by gluinos. In particular, with this new set of primitive amplitudes, the decomposition in Eq. (3.18) rewrites :

Primitive amplitudes

$$\begin{aligned} A_{n;1}(1_{\bar{q}}, 2_q, 3, \dots, n) &= \left(1 + \frac{1}{N_c^2}\right) A_n^L(1_{\bar{q}}, 2_q, 3, \dots, n) - \frac{1}{N_c^2} A_{n;1}^{\text{SUSY}}(1_{\bar{g}}, 2_{\bar{g}}, 3, \dots, n) \\ &\quad - \left(\frac{n_f}{N_c} + \frac{1}{N_c^2}\right) A_n^{N=1}(1_{\bar{q}}, 2_q, 3, \dots, n) \\ &\quad + \left(\frac{n_s - n_f}{N_c} - \frac{1}{N_c^2}\right) A_n^s(1_{\bar{q}}, 2_q, 3, \dots, n). \end{aligned} \quad (3.96)$$

Some amplitudes, in the following, will be written according to this decomposition.

3.1.7 Loop amplitudes

So far, we have treated mainly tree-level amplitude and mentioned some generalizations to loop level without really giving the specifics of beyond tree-level calculations. We will focus on 1-loop amplitudes in this section (because, for off-shell amplitudes presented afterward, we won't go further). Also, the need for higher order correction is justified when studying high-energy collisions at LHC where QCD dominates. Tree-level calculation in QCD can lead to uncertainties of order of unity. This is due mainly to the running constant whose dependence on the scale is hidden in higher-order correction. It is then crucial to calculate higher order corrections (1-loop calculations reduce typically these uncertainties to around 10%).

Loop integrand

At the second order in perturbation theory, diagrams participating to the amplitude draw a closed loop (of internal propagators). This loop is parametrized with a loop 4-momenta l that has to be integrated to evaluate the amplitude (or the contribution of a diagram). Then, in 1-loop amplitudes (with massless internal particles), integrals of the following form appear :

$$\mathcal{I}_{n_i}[P(l^\mu)] = \int \frac{d^4 l}{(2\pi)^4} \frac{P(l^\mu)}{l^2(l-p_1)^2(l-p_1-p_2)^2 \cdots (l-p_1-p_2-\cdots-p_n)^2}, \quad (3.97)$$

where P is a polynomial and $\{p_i\}_{i \in \llbracket 1, n_i \rrbracket}$ are momenta flowing out of the loop (cyclically ordered, they can be expressed with the external momenta $\{k_i\}_{i \in \llbracket 1, n \rrbracket}$). We call these integrals *tensor integrals*, except when the degree of P is 0, in which case we call them *scalar integrals*. Such integrals are **Ultra-Violet (UV)** divergent (i.e they diverge for high energy of the loop momentum). Actually, these divergences are absorbed into the renormalization of the bare parameters of the Lagrangian. This is done in practice through the regularization of these integrals. The most natural method would be to impose a **UV** cutoff. However, the standard regularization scheme consists in continuing analytically the loop integral in $D = 4 - 2\epsilon$ dimensions¹¹, which then depends on ϵ , and then take the limit $\epsilon \rightarrow 0$. *Dimensional regularization* has the advantage to preserve gauge invariance, Lorentz invariance, translational invariance, unitarity, and chirality invariance. However, the change of dimension implied by this technique gives a mass dimension to the coupling constant g , dependent on ϵ (such that the action is dimensionless). This is explicitly expressed through the renormalization scale μ_R (which has a mass dimension), replacing :

$$g \rightarrow \mu^\epsilon g \quad (3.98)$$

Then, the calculation of the loop integrals (see Eq. (3.97)) goes through several steps. First, the loop integrand in the numerator is expressed in terms of 4 independent momenta (constructed from the ones entering the loop), such that the decomposition of l

¹¹Sometimes, the factor 2 is absorbed in ϵ , but then, factors 2 propagates in the results. Anyway, the idea is to calculate the integral in a dimension D "around" 4 (and take the limit $D \rightarrow 4$).

makes appear the propagators present in Eq. (3.97) (that build its denominator). To this end, we introduce the 4-momenta :

$$p'_1 = p_1, \quad p'_2 = p_1 + p_2, \quad p'_3 = p_1 + p_2 + p_3, \quad p'_4 = p_1 + p_2 + p_3 + p_4, \quad (3.99)$$

and build from them a set of dual vectors :

$$\begin{aligned} K_1^\mu &= \epsilon_{\nu\sigma\rho}^\mu p_2^\nu p_3^\sigma p_4^\rho, & K_2^\mu &= \epsilon_{\nu\sigma\rho}^\mu p_1^\nu p_3^\sigma p_4^\rho, \\ K_3^\mu &= \epsilon_{\nu\sigma\rho}^\mu p_1^\nu p_2^\sigma p_4^\rho, & K_4^\mu &= \epsilon_{\nu\sigma\rho}^\mu p_1^\nu p_2^\sigma p_3^\rho, \end{aligned} \quad (3.100)$$

with ϵ the Levi-Civita tensor. This way, the loop integrand can be expressed (when appearing in the numerator) as :

$$\begin{aligned} l^\mu &= \frac{1}{\epsilon_{\mu\nu\sigma\rho} p_1^\nu p_2^\sigma p_3^\rho p_4^\rho} \sum_{i=1}^4 K_i^\mu l \cdot p'_i \\ &= \frac{1}{2\epsilon_{\mu\nu\sigma\rho} p_1^\nu p_2^\sigma p_3^\rho p_4^\rho} \sum_{i=1}^4 K_i^\mu \left[l^2 - (l - p'_i)^2 + p_i'^2 \right], \end{aligned} \quad (3.101)$$

where we have used $K_i \cdot p'_j = \epsilon_{\mu\nu\sigma\rho} p_1^\mu p_2^\nu p_3^\sigma p_4^\rho \delta_{ij}$ in the first equality. Inserting this decomposition in the integral of Eq. (3.97), we observe that the first term in the bracket of the second line of Eq. (3.101) cancels the “first” denominator, the second term cancel the i -th propagator and the third term is independent of l . In summary, this turns an n -point integral (with a polynomial in the numerator) of degree m into a sum of 2 $n - 1$ -point integrals of degree $m - 1$ and one n -point integral of degree $m - 1$. Such techniques, and their iteration, are called *loop integral reduction* [140–143] (such as the *Passarino-Veltman* [144–146], or the use of dual vector basis [147]) and permit to express any loop integral in dimensional regularization in terms of a very limited set of integrals. Those integrals consist of bubble ($n = 2$), triangle ($n = 3$), and box ($n = 4$) scalar integrals (eventually tadpole, for $n = 1$ when we allow particles in the loop to have a mass) and are referred to as *master integrals*. We will note them :

$$\begin{aligned} I_2(\{p_1\}) &= \int \frac{d^4 l}{(2\pi)^4} \frac{1}{l^2 (l - p_1)^2}, \\ I_3(\{p_1, p_2\}) &= \int \frac{d^4 l}{(2\pi)^4} \frac{1}{l^2 (l - p_1)^2 (l - p_1 - p_2)^2}, \\ I_4(\{p_1, p_2, p_3\}) &= \int \frac{d^4 l}{(2\pi)^4} \frac{1}{l^2 (l - p_1)^2 (l - p_1 - p_2)^2 (l - p_1 - p_2 - p_3)^2}, \end{aligned} \quad (3.102)$$

with the momenta $\{p_i\}$ cyclically ordered (the dependence on the last 4-momentum is dropped by momentum conservation), as shown in Fig. 3.8.

To calculate such integrals, the usual approach is first to use *Feynman parametrization* to rewrite the propagator product (in the denominator) into a single parametrized denominator. One can see that :

$$\forall a, b \in \mathbb{C}, \quad \frac{1}{ab} = \int_0^1 \frac{dx}{[ax + b(1-x)]^2}. \quad (3.103)$$

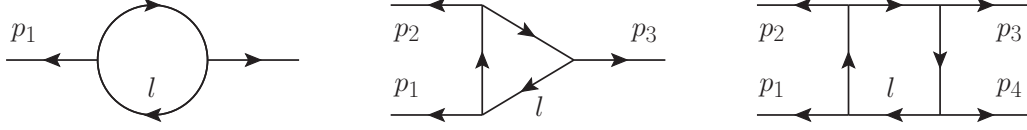


Figure 3.8: Master integrals (with the outgoing momenta convention). In order : bubble, triangle, and box scalar integral.

Deriving this expression (with respect to a and b) leads to :

$$\forall a, b \in \mathbb{C}, \forall m, n \in \mathbb{N}, \quad \frac{1}{a^m b^n} = \frac{\Gamma(m+n)}{\Gamma(m)\Gamma(n)} \int_0^1 dx \frac{x^{m-1}(x-1)^{n-1}}{[ax + b(1-x)]^{m+n}}, \quad (3.104)$$

with the gamma function defined as :

$$\forall z \in \mathbb{C}, \quad \Gamma(z) = \int_0^{+\infty} dt t^{z-1} e^{-t} \quad \text{Re}(z) > 0. \quad (3.105)$$

This is an extension of the factorial to the complex numbers which follow the properties :

$$\forall n \in \mathbb{N}, \Gamma(n+1) = n!, \quad \forall z, \Gamma(z+1) = z\Gamma(z) \quad \text{and} \quad \Gamma\left(\frac{1}{2}\right) = \sqrt{\pi}. \quad (3.106)$$

It follows from Eq. (3.104), in all generality :

$$\forall n \in \mathbb{N}, \forall \{a_i\}_{i \in \llbracket 1, n \rrbracket}, \quad \left[\prod_{i=1}^n a_i \right]^{-1} = \Gamma(n) \int_0^1 dx_1 \int_0^{1-x_1} dx_2 \cdots \\ \times \int_0^{1-\sum_{i=1}^{n-2} x_i} \frac{dx_{n-1}}{\left[a_1 x_1 + a_2 x_2 + \cdots + a_n \left(1 - \sum_{i=1}^{n-1} x_i \right) \right]^n}. \quad (3.107)$$

Another possibility is the *Schwinger parametrization* which consists in rewriting a denominator as an exponential using :

$$\forall a \in \mathbb{C}, \forall n \in \mathbb{N}, \quad \frac{1}{a^n} = \frac{1}{\Gamma(n)} \int_0^{+\infty} d\alpha \alpha^{n-1} e^{-\alpha a}, \quad (3.108)$$

which can be applied to :

$$\int \frac{dl}{a(l)^n} = \frac{1}{\Gamma(n)} \int_0^{+\infty} d\alpha \alpha^{n-1} \int dl e^{-\alpha a(l)}. \quad (3.109)$$

In particular, denominators with the *Feynman prescription* rewrite :

$$\forall k \in \mathbb{R}, \quad \int \frac{1}{k \pm i\epsilon} = \mp i \int_0^{+\infty} d\alpha e^{\pm i(k \pm i\epsilon)\alpha}. \quad (3.110)$$

Note that Feynman's parametrization can be obtained from Schwinger's one. Using Feynman parametrization, the calculation of master integrals involves the evaluation of integrals of the form :

$$I_n = \int \frac{d^4 l}{(2\pi)^4} \frac{1}{[l^2 - M]^n}, \quad (3.111)$$

where M would depend on $\{p_i\}$ and on the parameters $\{x_i\}$ for the integral I_i . The evaluation of such integral in dimensional regularization is performed using a *Wick rotation*. This consists in making a rotation, in the complex plane, of the energy component of the 4-momentum (l , in the loop) such that it is then *Euclidian* (that we then note l_E). This is done by multiplying the energy component by $-i$:

$$l_E^0 \equiv -il^0, \quad \forall i \in \{1, 2, 3\}, \quad l_E^i \equiv l^i. \quad (3.112)$$

Note that $l_E^2 = -l^2$. Then, the Euclidian integral is related to the Minkowskian one using complex analysis based on one of the paths shown in Fig. 3.9 (which is chosen depending on the pole of the integrand, here related to the sign of M).

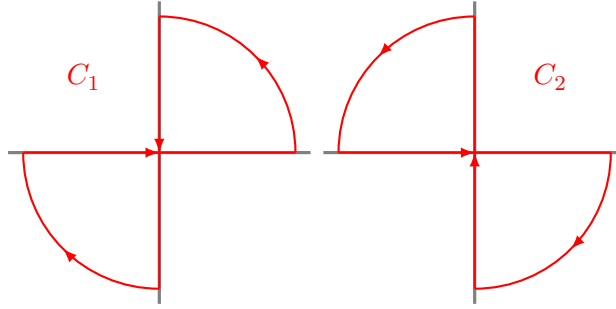


Figure 3.9: Path used when performing a Wick rotation (the arcs are at infinity).

For $M > 0$, applying the Wick rotation to l_i leads to :

$$I_n = (-1)^n i \int \frac{d^4 l_E}{(2\pi)^4} \frac{1}{[l_E^2 + M]^i} = (-1)^n i \int \frac{d^4 l_E}{(2\pi)^4} \frac{1}{[l_0^2 - |\vec{l}|^2 + M]^i}, \quad (3.113)$$

where we have used the path C_1 . Since it is now in Euclidian space, the integral can be written in spherical coordinates using :

$$d^4 l_E = d^3 \Omega dl_E l_E^3, \quad \int d^3 \Omega = 2\pi^2, \quad (3.114)$$

which leads to :

$$I_n = (-1)^n \frac{i}{8\pi^2} \int_0^{+\infty} dl_E \frac{l_E^3}{[l_E^2 + M]^i}, \quad (3.115)$$

a divergent integral for $n = 1$ and $n = 2$. Still, it can be evaluated in dimensional regularization where the passage to spherical coordinates now reads :

$$d^D l_E = d^{D-1} \Omega dl_E l_E^{D-1}, \quad \int d^{D-1} \Omega = \frac{2\pi^{D/2}}{\Gamma(\frac{D}{2})}. \quad (3.116)$$

This result can be obtained considering a Gaussian in D dimensions. Then, the Wick rotation on the integral I_n reads :

$$\begin{aligned} I_n &= \lim_{\epsilon \rightarrow 0} (-1)^n \frac{2i}{(4\pi)^{D/2} \Gamma(\frac{D}{2})} \int_0^{+\infty} dl_E \frac{l_E^{D-1}}{[l_E^2 + M]^i} \\ &= \lim_{\epsilon \rightarrow 0} (-1)^n \frac{iM^{D-2n}}{(4\pi)^{D/2}} \left(\frac{4\pi}{M^2} \right)^\epsilon \frac{\Gamma(n - \frac{D}{2} + \epsilon)}{\Gamma(n)}, \end{aligned} \quad (3.117)$$

with :

$$\forall n \in \mathbb{N}, \quad \Gamma(\epsilon - n) = \frac{(-1)^n}{n!} \left(\frac{1}{\epsilon} + \psi^{(0)}(n+1) + \mathcal{O}(\epsilon) \right), \quad (3.118)$$

where :

$$\forall z \in \mathbb{C}, \quad \psi^{(0)}(z) = \frac{\Gamma'(z)}{\Gamma(z)}, \quad (3.119)$$

The resulting master integrals are given in App. B.5, based on [148]. Once the master integrals are known, calculation of a loop-level amplitude boils down to the determination of the coefficient in the master integral decomposition :

$$A_n^{(1)}(\{k_i\}) = \sum_{i=2}^4 \sum_{\{p_j\}} c_i(\{p_j\}) I_i(\{p_j\}), \quad (3.120)$$

where the coefficients are calculated during the reduction and where $\{p_j\}$ define the possible loop kinematics. Actually, in dimensional regularization, the coefficients $\{c_i\}$ are also depending on ϵ . And, with the poles in ϵ of some of the master integrals, higher orders in the coefficient are needed (up to order $\mathcal{O}(\epsilon^2)$). Then, it is usual to rewrite this decomposition with a constant coefficient (in epsilon) and separate the rational term produced by the higher order coefficients :

Master integral decomposition

$$A_n^{(1)}(\{k_i\}) = \sum_{i=2}^4 \sum_{\{p_j\}} c_i(\{p_j\}) I_i(\{p_j\}) + \sum_{\{p_j\}} R(\{p_j\}), \quad (3.121)$$

Also, to work with the helicity formalism, we use a specific scheme of dimensional regularization where only the loop momentum is in dimension D , called *dimensional reduction*. In particular, the polarization vectors are kept in 4 dimensions.

Unitarity

While we have seen that the loop-integrand can be decomposed in a small number of master integrals, the loop-level calculation can also be simplified using the unitarity of the S -matrix. Indeed, if we write $S = \mathbb{1} + iT$, separating its free part from its interaction part T , unitarity implies :

$$S^\dagger S = \mathbb{1}, \text{ then } 2 \text{Im} T = T^\dagger T. \quad (3.122)$$

Then, when performing the perturbative expansion of T in the coupling constant, we observe that one-loop amplitude can be expressed as a product of two tree-level ones. These tree-level amplitudes correspond to cuts in the loop amplitude where two loop propagators are set on-shell. This cut (noted by a Δ) can be pictured as in Fig. 3.10 and it follows the *Cutkosky* rules :

Cutkosky rules

$$\Delta A^{(1)} \equiv \int d\mu A_{left}^{tree} A_{right}^{tree}. \quad (3.123)$$

where $d\mu$ is the Lorentz-invariant phase space.

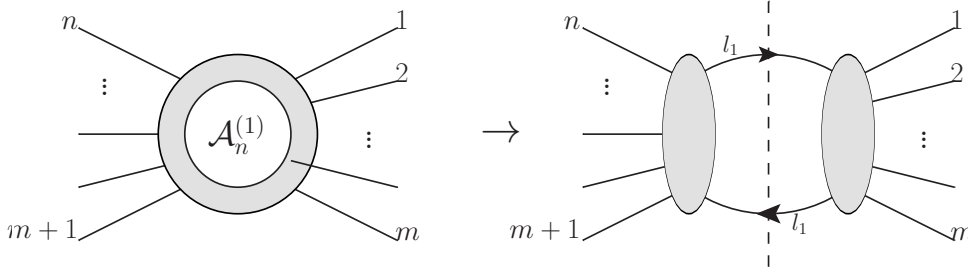


Figure 3.10: Unitarity cut of a one-loop amplitude where the propagator on the cut (dotted lines) is forced to be on-shell.

Then, the cut amplitudes can be used to reconstruct the full amplitudes. Indeed, when considering the expansion of Eq. (3.120) for cut amplitude, we observe that the branch cuts are located in the master integrals hence cut amplitudes follow the decomposition :

$$\Delta A_n^{(1)}(\{k_i\}) = \sum_{i=2}^4 \sum_{\{p_j\}} c_i(\{p_j\}) \Delta I_i(\{p_j\}), \quad (3.124)$$

where the coefficients $\{c_i\}$ are the same as for the amplitude $A_n^{(1)}(\{k_i\})$. Then, the coefficients $\{c_i\}$ are constrained by the equation of the form of Eq. (3.124), for all the

possible branch cuts. Actually, one-loop amplitudes are *cut-constructible* which means that they are fully determined by their branch cuts [149]. However, in D dimension, the reconstruction of the rational term (as explicitly written in Eq. (3.121)) can be tedious and this method is usually used in 4 dimensions (where no rational term is needed). Overall, using branch cuts to determine loop amplitudes is called the *unitarity method* [150–153].

Dipole subtraction

So far, we have treated amplitudes and reviewed methods useful to calculate them at NLO. In particular, we saw that loop integrals may involve poles (in ϵ). Those poles have to be canceled when calculating physical quantities (such that the limit $\epsilon \rightarrow 0$ can be safely taken). More precisely, the *Kinoshita–Lee–Nauenberg theorem* states that the standard model is perturbatively IR finite. To understand how it is achieved, we will consider cross-section calculations at NLO for which loop order amplitudes are not the only important component. Indeed, if we consider the cross-section of a given process \mathcal{P} with an initial state consisting of two leptons (for simplicity) and a final state characterized by n particles with momenta $\{p_i\}_{i \in [1, n]}$, we can write at LO :

$$\sigma_{\mathcal{P}}^{LO}(\{p_i\}) = \int d\sigma^B = \int d\phi(\{p_i\}) \left| \mathcal{A}_{\mathcal{P}}^{tree}(\{p_i\}) \right|^2 J(\{p_i\}), \quad (3.125)$$

where $d\sigma^B$ is called the *Born-level cross-section*, $d\phi$ is the phase space of the final state and J the jet function (that includes experimental cuts). Indeed, experimentally, instead of the momenta of the partons in the final states, we have access to the momenta of jets. The cross-section should then be soft and collinear safe. The first order corrections to the LO calculation should then include loop amplitudes for n final particles on one side, but also tree-level amplitudes for $n+1$ particles in a degenerate configuration (the added particle being either soft or collinear to another one). The former contribution is called *virtual correction* and the latter one *real correction*. We will denote this degenerate configuration $\{p'_i\}_{i \in [1, n+1]}$, which verifies :

$$\begin{aligned} \exists i \in [1, n], \{p'_1, \dots, p'_i + p'_{n+1}, \dots, p'_n\} &= \{p_i\}, \\ \text{or } \{p'_1, \dots, p'_{i-1}, p'_{i+1}, \dots, p'_n\} &= \{p_i\}. \end{aligned} \quad (3.126)$$

Thereby, the NLO cross-section reads :

$$\sigma_{\mathcal{P}} = \sigma_{\mathcal{P}}^{LO} + \sigma_{\mathcal{P}}^{NLO}, \quad (3.127)$$

with the following decomposition for the NLO cross-section :

$$\sigma_{\mathcal{P}}^{NLO} = \int_{n+1} d\sigma_{\mathcal{P}}^R + \int_n d\sigma_{\mathcal{P}}^V, \quad (3.128)$$

where the integral \int_{n+1} indicates an integration over the phase space for the degenerate state characterized by $\{p'_i\}$ and \int_n over the phase space of the final state $\{p_i\}$. Then,

the real and virtual contributions to the **NLO** cross section can be expressed :

$$\begin{aligned} d\sigma_{\mathcal{P}}^R &= \int d\phi(\{p'_i\}) \left| \mathcal{A}_{\mathcal{P}}^{tree}(\{p'_i\}) \right|^2 J(\{p'_i\}) , \\ d\sigma_{\mathcal{P}}^V &= \int d\phi(\{p_i\}) \left| \mathcal{A}_{\mathcal{P}}^{(1)}(\{p_i\}) \right|^2 J(\{p_i\}) . \end{aligned} \quad (3.129)$$

We already mentioned that the **UV** divergences originating from the loop integration in the virtual correction are carried out through the renormalization procedure. Still, the soft and collinear singularities remain¹². They appear in both real and virtual correction and cancel each other (due to soft and collinear safety of the cross-section). The problem is that this cancellation is not done at the integrand level, since each contribution involves a different phase space. Then, the numerical evaluation of such integrals is unsafe and an analytical approach can be quickly hopeless with an increasing number of particles and because of the experimental cuts leading to complicated phase space integration. To solve this problem, one possibility is to treat the divergences analytically and integrate the remainder numerically. To do so, we will follow the *subtraction method* [154] where an intermediate cross-section $d\sigma^A$ is introduced :

$$\sigma_{\mathcal{P}}^{NLO} = \int_{n+1} \left[d\sigma_{\mathcal{P}}^R - d\sigma_{\mathcal{P}}^A \right] + \int_{n+1} d\sigma_{\mathcal{P}}^A + \int_n d\sigma_{\mathcal{P}}^V , \quad (3.130)$$

$d\sigma^A$ has the same singular behavior, in D dimension, as $d\sigma^R$, such that the integration over their difference can be evaluated after performing the limit $\epsilon \rightarrow 0$. Another property of $d\sigma^A$ is that it is analytically integrable over the parton subspace leading to the soft and collinear divergences. This way, it also cancels the poles of the virtual correction under the integral over the n final state particles phase space. This is schematized as :

$$\sigma_{\mathcal{P}}^{NLO} = \int_{n+1} \left[d\sigma_{\mathcal{P}}^R - d\sigma_{\mathcal{P}}^A \right]_{\epsilon=0} + \int_n \left[d\sigma_{\mathcal{P}}^V + \int_1 d\sigma_{\mathcal{P}}^A \right]_{\epsilon=0} , \quad (3.131)$$

and the final integration can be implemented numerically. $d\sigma^A$ can be constructed in a process-independent way as the convolution of the Born-level cross-section to some dipole factors dV_{dipole} that characterized the soft and collinear divergences :

$$d\sigma_{\mathcal{P}}^A = \sum_{dipoles} d\sigma_{\mathcal{P}}^B dV_{dipole} . \quad (3.132)$$

This subtraction method and the determination of $d\sigma^A$ through the dipole formalism (based on the soft and collinear behavior of the amplitudes) is presented in [155] (with a shorter review in [156]). We won't go further in the construction of $d\sigma^A$. However, we still have to consider hadronic collisions. In the case of collinear factorization, also presented in [155], corrections to the **PDF** have to be taken into account too. Indeed,

¹²In dimensional regularization, double poles in ϵ reflect soft *and* collinear divergences while simple poles originate from soft *or* collinear divergences.

these correction will absorb the IR divergences due to initial state emissions. This leads to :

$$\begin{aligned} \sigma_{ab}(P_a, P_b) &= \sum_{i,j} \int dx_i dx_j f_{i/a}(x_i, \mu_F^2) f_{j/b}(x_j, \mu_F^2) \\ &\times \left[\hat{\sigma}_{ij}^{LO}(x_i P_a, x_j P_b) + \hat{\sigma}_{ij}^{NLO}(x_i P_a, x_j P_b, \mu_F^2) \right] \end{aligned} \quad (3.133)$$

where we have dropped the process subscript and the partonic cross-sections follow :

$$\begin{aligned} \forall i, j, \sigma_{ij}^{LO}(x_i P_a, x_j P_b) &= \int_n d\sigma_{ij}^B(x_i P_a, x_j P_b), \\ \forall i, j, \sigma_{ij}^{NLO}(x_i P_a, x_j P_b, \mu_F^2) &= \int_{n+1} d\sigma_{ij}^R(x_i P_a, x_j P_b) + \int_n d\sigma_{ij}^V(x_i P_a, x_j P_b) \\ &+ \int_n d\sigma_{ij}^C(x_i P_a, x_j P_b, \mu_F^2), \end{aligned} \quad (3.134)$$

where σ^C is a *collinear subtraction counter-term* (note that it depends on the factorization scale). A similar subtraction procedure applies in this case (also shown in [155]), but what we want to underline here is the intrication of the divergences of the real and virtual correction and of the corrections to the PDF that depend on the factorization scheme (that we will discuss a little further in the case of hybrid factorization).

In this section, we gave an overview of the techniques used to simplify the calculation of amplitudes, with a focus on loop-level QCD amplitudes. We saw that the complex calculations involved by the classical Feynman diagrams approach can be sorely simplified by decomposing QCD amplitudes into color-ordered amplitudes (which are still gauge invariant and are free from the color Lie algebra) and using the helicity formalism (where the kinematics is encoded in the spinors rather than directly in the 4-momenta, which is more suitable to reflect the amplitudes symmetries). At loop-level, the color-ordered amplitudes can be further decomposed into supersymmetric and non-supersymmetric primitive amplitudes (simpler to calculate than the partial amplitudes). Besides, the loop integrands appearing in loop integrals can be decomposed in a few master integrals simplifying again the calculation of loop amplitude. Furthermore, these coefficients can be obtained from unitarity methods i.e, from tree-level calculation. We have also seen that amplitudes can be calculated through different recursive methods. All these methods tend to explain the relative simplicity and compactness of amplitudes expressions. Actually, this was just an overview of the tools available when calculating amplitudes, enough to appreciate the on-shell amplitudes that we will use later. In particular, we have not presented the *generalized unitarity method* [150, 151, 157] (where more than two propagators are set on-shell simultaneously), which can be generalized to higher-order calculation [158], we have not discussed the determination of cut integrals nor the determination of the rational term in Eq. (3.121) (through some recursive techniques [159–163]). Also, Feynman integrals are studied through differential equations they follow [164, 165], and the logarithm and (multiple) polylogarithms that constitute

them, leading to the use of symbols [166–169] to simplify their expressions. Another approach should probably be mentioned, based on the geometric construction of amplitudes in the kinematics space, the *amplituhedron* citeArkani-Hamed:2013jha,Arkani-Hamed:2017mur,Arkani-Hamed:2017tmz,Ferro:2020ygk. In the end, we have discussed the treatment of the IR divergences through the subtraction and the dipole formalisms. Now, we will review what changes when we consider off-shell amplitudes.

3.2 Gauge invariant off-shell amplitudes

We have seen in the previous chapter that, when interested in small- x physics, we need to use either k_T -factorization (Eq. (2.66)) or hybrid factorization (Eq. (2.67)). In both cases, we need amplitudes with off-shell leg(s) (respectively 2 and 1) to calculate the hard cross-section. Such amplitudes, if calculated naively by applying classical methods would lead to non gauge-invariant expressions (like the off-shell current presented in Sec. 3.1.5). However, at high energy, new degrees of freedom arise : the reggeized gluon. We saw that they appear when deriving the BFKL equation. In the following, we will introduce Lipatov’s high-energy effective action which describes these reggeized gluons, and briefly discuss loop-level amplitude calculation within this approach. Afterward, we will introduce the auxiliary parton method, a way to calculate off-shell amplitudes which is based on on-shell calculation (making it relatively simple to apply). This method can be demonstrated to be equivalent to high energy Lipatov’s effective action at tree level and has been incorporated in the Monte-Carlo generator KATIE [99] (suitable for collinear, hybrid, and k_T -factorization). After this presentation, we will focus on generalizing this method at loop-level. To this end, as a first step toward this generalization, we will apply the auxiliary parton method to the finite all-plus helicity gluonic amplitude with one off-shell leg and verify that it has the correct behavior. We will also apply it to the 3-point g^*gg amplitude and compare it to one of the only calculations made so far within high energy Lipatov’s effective action at loop-level.

3.2.1 Lipatov’s high-energy effective action

In this section, we introduce briefly Lipatov’s high-energy effective action, following the report [170] to introduce some results that will be used later for comparison purposes. When considering a collision between two hadron A and B , in the high energy limit (or the *Regge limit*)¹³, their momenta p_A and p_B can then be considered, as a good approximation, on the opposite sides of the light-cone. Then, it is convenient to define the light-cone vectors as :

$$n_{\pm} = \frac{2}{\sqrt{s}}p_{A,B}, \quad n_+ \cdot n_- = 2. \quad (3.135)$$

¹³Explicitly, for any mass scale, μ and with $s = (p_A + p_B)^2$ the center of mass energy, this limit is characterized by $\lim \frac{\mu^2}{s} = 0$

Particles produced at high energy are then ordered in rapidity (hence local in rapidity), following the multi-Regge kinematics, presented in Eq. (2.53). The couple between separated rapidity sectors is done through the reggeized gluon (as illustrated for the BFKL ladder of Fig. 2.10). Those are described in the Lipatov's high-energy effective action.

High-energy effective action

In this effective theory, we decompose the complete gluon field into a regular, local in rapidity, gluon field (described by QCD) $a_\mu^{(s)} = -it^a a_\mu^{a,(s)}$ and a non-local one, $R_\mu^{(s)} = -it^a R_\mu^{a,(s)}$, referred to as the reggeized gluon field. The index s denotes the rapidity sector in which lives the gluon, or, for the reggeized gluon, a sector at which it couples. In the latter case, only the reference to one sector is needed due to the strong rapidity ordering. This strong ordering also implies that it has no transverse component, i.e it can be written :

$$R^{\mu,(s)}(x) = R_+^{(s)} \frac{n_-^\mu}{2} + R_-^{(s)} \frac{n_+^\mu}{2}, \quad (3.136)$$

and that its dependence on light-cone coordinates is frozen, following :

$$\partial_+ R_+^{(s)} = 0, \quad \partial_- R_-^{(s)} = 0. \quad (3.137)$$

Finally, the effective Lagrangian of this theory is the sum of the QCD Lagrangian (governing quark fields and the gluon field $a^{(s)}$) and an *induced* Lagrangian, governing the coupling of the reggeized gluon field $R_\pm^{(s)}$ to the gluon field $a^{(s)}$:

$$\mathcal{L}_{eff} = \mathcal{L}_{QCD} \left[a^{(s)}, \left\{ \bar{\psi}^{f,(s)} \right\}, \left\{ \psi^{f,(s)} \right\} \right] + \mathcal{L}_{ind} \left[a^{(s)}, R_+^{(s)}, R_-^{(s)} \right]. \quad (3.138)$$

The simplest expression for the induced Lagrangian, satisfying gauge-invariance, having the right normalization and insuring that the reggeized gluon decouples from QCD dynamics when it becomes on-shell (such that it cannot be an asymptotic state), is of the form :

$$\begin{aligned} \mathcal{L}_{ind} \left[a^{(s)}, R_+^{(s)}, R_-^{(s)} \right] &= \text{Tr} \left[(T_-[a(x)] - R_-(x)) \partial_\perp^2 R_+(x) \right] \\ &+ \text{Tr} \left[(T_+[a(x)] - R_+(x)) \partial_\perp^2 R_-(x) \right], \end{aligned} \quad (3.139)$$

where :

$$T_\pm[a] = -\frac{1}{g} \partial_\pm \frac{1}{1 + \frac{g}{\partial_\pm} a_\pm} = a_\pm \left[\sum_{n \in \mathbb{N}} \left(-\frac{g}{\partial_\pm} a_\pm \right)^n \right], \quad (3.140)$$

and :

$$\frac{1}{\partial_\pm} a_\pm = \frac{1}{2} \int_{-\infty}^{x^\pm} dx'^\pm a_\pm(x'). \quad (3.141)$$

More details on this effective action and the justifications for the form of the induced Lagrangian can be directly found in Lipatov's papers [171, 172]. Also, it is possible to consider, the same way, reggeized quarks. We don't need it in the present discussion, but details can be found in [173–175].

Feynman rules

From the effective Lagrangian presented in the previous section, it is possible to derive Feynman rules involving reggeized gluon(s), that we might also call a *reggeon*. However, Lipatov's high-energy effective action implies an infinite number of possible vertices between a reggeon and gluons. The propagators and the LO induced vertices are the following :

- the reggeon propagator :

$$+, a \text{ --- } \underset{q}{\text{wavy}} \text{ --- } -, b = \delta^{ab} \frac{2i}{q^2}, \quad (3.142)$$

- the reggeon-gluon (Rg) transition vertex¹⁴ :

$$\underset{q, \pm, a}{\text{wavy}} \text{ --- } \bullet \text{ --- } \underset{k, \mu, b}{\text{coiled}} = -\frac{i}{2} q^2 \delta^{ab} (n^\pm)^\mu, \quad k^\pm = 0, \quad (3.143)$$

- the *Rgg* vertex :

$$\begin{aligned} & \underset{q, \pm, a}{\text{wavy}} \text{ --- } \bullet \text{ --- } \begin{matrix} \text{coiled} \\ k_1, \mu_1, b_1 \\ \text{coiled} \\ k_2, \mu_2, b_2 \end{matrix} \\ & = f^{ab_1 b_2} \frac{g_s}{2} \frac{q^2}{k_1^\pm} (n^\pm)^{\mu_1} (n^\pm)^{\mu_2}, \quad (3.144) \\ & \text{with } k_1^\pm + k_2^\pm = 0, \end{aligned}$$

- the *Rggg* vertex :

$$\begin{aligned} & \underset{q, \pm, a}{\text{wavy}} \text{ --- } \bullet \text{ --- } \begin{matrix} \text{coiled} \\ k_1, \mu_1, b_1 \\ \text{coiled} \\ k_2, \mu_2, b_2 \\ \text{coiled} \\ k_3, \mu_3, b_3 \end{matrix} \\ & = i \frac{g_s}{2} q^2 \left(\frac{f^{b_3 b_2 x} f^{b_1 x a}}{k_3^\pm k_1^\pm} + \frac{f^{b_3 b_1 x} f^{b_2 x a}}{k_3^\pm k_2^\pm} \right), \quad (3.145) \\ & \text{with } k_1^\pm + k_2^\pm + k_3^\pm = 0. \end{aligned}$$

¹⁴Actually, this transition vertex vanishes when considering $a_\pm \rightarrow a_\pm + R_\pm$ in the effective action.

One has to take some care when applying these Feynman rules keeping in mind that the reggeons link sectors separated in rapidity (hence, when calculating an amplitude local in rapidity, it is needed to subtract diagrams with disconnected sectors, i.e with internal reggeon). Another subtlety comes from the pole prescription for the light-cone denominators which, if settled in a usual way, breaks the unitarity of the effective theory. Some details on these calculation subtleties, not needed for the present discussion, are reviewed in [170].

Rapidity divergences

At loop-level, another problem arises when using Lipatov's high-energy effective action, the appearance of rapidity divergences. Those divergences come from eikonal propagators of the form $n^\pm \cdot l$ (with l , the loop momentum) and they are not regulated by dimensional regularization. Hopefully, the problem can be solved through the use of *tilted Wilson lines* [174–181]¹⁵ i.e by shifting the light cone direction as :

$$n_\mu^\pm \rightarrow \tilde{n}_\mu^\pm = n_\mu^\pm + r n_\mu^\mp, \quad \text{with } r \in \mathbb{R}. \quad (3.146)$$

This regulator preserves gauge invariance.

Results

We can now present results that have been calculated with Lipatov's high-energy effective action, in particular the one-loop 3-point amplitude, given in [182] for any helicity configuration. Actually, the results are given in terms of one-loop vertices and can be used to express the 3-point partial amplitudes R_{gg} , with the spinor helicity formalism as :

$$\begin{aligned} A(R, 3^+, 4^+) &= i \frac{g_s^3}{24\pi^2} p \cdot k_3 \left(1 - \frac{n_f}{N_c}\right) \frac{|k_\perp|}{\kappa^{*2}} \frac{[p3][p4]}{\langle p3 \rangle \langle p4 \rangle} \\ A(R, 3^-, 4^+) &= -i \mu^{-2\epsilon} g_s^3 c_\Gamma \frac{p \cdot k_3}{|k_\perp|} \frac{\langle p3 \rangle [p4]}{[p3] \langle p4 \rangle} \times \\ &\quad \times \left[\left(\frac{-\mu^2}{k_\perp^2} \right)^\epsilon \left[\frac{2}{\epsilon^2} + \frac{1}{\epsilon} \left(1 + \ln r + i\pi - \ln \frac{-|p \cdot k_3|^2}{k_\perp^2} \right) \right] + 2 - \frac{\pi^2}{2} \right], \end{aligned} \quad (3.147)$$

where c_Γ is defined in Eq. (B.29). These results are obtained replacing the light-cone n_- appearing in [182] by $p^\mu = \frac{|k_\perp|}{2} n_-^\mu$ (which implies that k_{i-} is replaced by $\frac{2}{|k_\perp|} k_{i-}$), where k_\perp is the transverse momentum of the reggeon. Written this way, these amplitudes will compare straightforwardly to the one presented in Sec. 3.3.

¹⁵Actually, the functional T can be expressed in terms of Wilson lines stretching along the light-cone. The substitution of Eq. (3.146) is the result of tilting the Wilson lines appearing in the Lagrangian.

3.2.2 The auxiliary parton method

Calculating off-shell amplitudes from Lipatov’s high-energy effective action is quite demanding and only a few results have been calculated so far at loop-level [174, 175, 179–181, 183–185]. However, it is possible to obtain off-shell amplitudes from on-shell ones using the auxiliary parton method, that we may also call the Λ prescription. This method has been demonstrated to be equivalent to Lipatov’s high-energy effective action at tree level and has proven efficient [186–189]. Besides, it is implemented in the Monte-Carlo event generator KATIE [99] to obtain results within both hybrid and k_T -factorization. In this section, we will present the first results obtained applying the Λ prescription to loop-level amplitudes, the all plus off-shell multigluon amplitude $g^*g \cdots g$. This result has been published in [2]. We will also present the 3-point off-shell gluon amplitude g^*gg for all helicity configurations.

Reconstructing gauge invariance explicitly

We will see in this section that it is actually possible to calculate off-shell amplitudes starting from a classical approach and requiring them, in a later stage, to be gauge invariant. To this end, we will summarize the demonstration provided in [187].

For simplicity, let’s consider the n -point gluonic amplitude with one off-shell leg, at tree level, $\mathcal{A}^{tree}(1^*, 2, \cdots, n)$. It can be defined [29, 30, 190, 191] from the momentum space Green function G (Fourier transform of the vacuum matrix element) as :

$$\mathcal{A}^{tree}(1^*, 2, \cdots, n) = \epsilon^{*,\mu_1} \prod_{i=2}^n \frac{\epsilon_i^{\mu_i}}{S(k_i)} G_{\mu_1 \cdots \mu_n}(k_1, \cdots, \mu_n), \quad (3.148)$$

where we consider the high energy kinematics :

$$\begin{aligned} k^\mu &= xn_A^\mu + k_\perp, & n_A \cdot k_\perp &= 0, & k^2 &= k_\perp^2 = -|k_\perp|^2, \\ & & \forall i > 1, & k_i^2 &= 0, \end{aligned} \quad (3.149)$$

and where $\{\epsilon_i\}_{i \in \llbracket 2, n \rrbracket}$ are the polarization vectors of the external on-shell legs and $\epsilon^{*,\mu} = |k_\perp| n^\mu$ represents the eikonal coupling to the off-shell leg, with n_A a light-like momentum corresponding to the incident hadron. $S(k) = \frac{-i}{k^2 + i\epsilon}$ is the scalar part of the gluon propagator. So, contrary to the other external (on-shell) lines, the propagator of the off-shell line is not amputated from the Green function. To simplify further the problem, we will consider the corresponding color ordered amplitude, $A(1^*, 2, \cdots, n)$ (which follows the decomposition of Eq. (3.10)) represented diagrammatically in Fig. 3.11 (we drop the *tree* superscript in this section for convenience).

Such expression is, as already mentioned, not gauge invariant and, in particular, it doesn’t verify the Ward-Takahashi identity (see Eq. (3.50)). However, it is possible to construct a gauge invariant amplitude $A^*(1^*, 2, \cdots, n)$ using a *gauge restoring amplitude* W in the following way :

$$A^*(1^*, 2, \cdots, n) = A(1^*, 2, \cdots, n) + W^*(1^*, 2, \cdots, n), \quad (3.150)$$

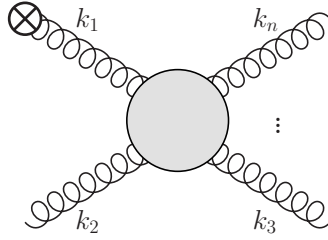


Figure 3.11: Color-order gluonic amplitude with one off-shell leg $A(1^*, 2, \dots, n)$. The crossed circle represents the eikonal coupling.

and imposing the Ward-Takahashi identity :

$$\forall i \in \llbracket 2, n \rrbracket, \quad A^*(1^*, 2, \dots, n) |_{\epsilon_i \rightarrow k_i} = 0, \quad (3.151)$$

or, in other words, that :

$$\forall i \in \llbracket 2, n \rrbracket, \quad W(1^*, 2, \dots, n) |_{\epsilon_i \rightarrow k_i} = -A(1^*, 2, \dots, n) |_{\epsilon_i \rightarrow k_i}. \quad (3.152)$$

Actually, to guarantee local gauge invariance in a non-abelian field theory as QCD, one should rather consider the Slavnov-Taylor identity which generalizes the Ward-Takahashi identity. This identity relates Green functions where one leg is contracted with its momentum to diagrams involving ghosts as represented in Fig. 3.12. Note that all diagrams are tree-level ones (the curvy gluon lines do not represent loops, but a gluon line entering the blob).

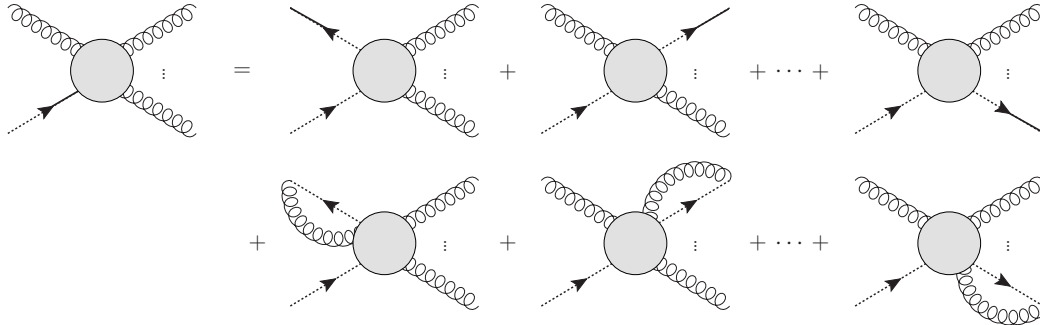


Figure 3.12: Diagrammatic representation of the Slavnov-Taylor identity. The dashed lines transforming into solid lines represent contraction with the momentum of the corresponding leg (instead of the polarization vector).

The Slavnov-Taylor identity can be applied on gluonic amplitudes with one off-shell leg and permits to evaluate the different limits “ $\epsilon_i \rightarrow k_i''$ ” of Eq. (3.152). Actually,

it simplifies to directly relate $A(1^*, 2, \dots, n) |_{\epsilon_i \rightarrow k_i}$ to an amplitude with a ghost, as depicted in Fig. 3.13.

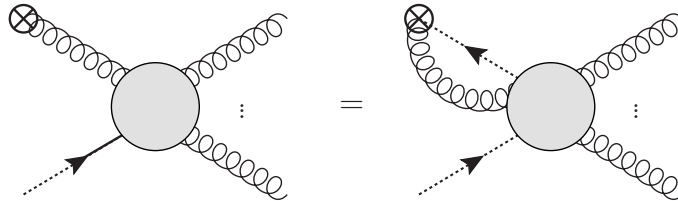


Figure 3.13: Application of the Slavnov-Taylor identity to amplitudes with one off-shell leg contracted with eikonal vertex.

This way, it is possible to calculate all the limits :

$$\forall i \in \llbracket 2, n \rrbracket, \quad W_i(1^*, 2, \dots, n) \equiv W(1^*, 2, \dots, n) |_{\epsilon_i \rightarrow k_i}, \quad (3.153)$$

from diagrams including ghosts. Then, the gauge restoring term W is reconstructed using :

$$W(1^*, 2, \dots, n) \equiv \sum_{i=2}^n W_i(1^*, 2, \dots, n) \alpha_i, \quad (3.154)$$

where $\alpha_i = \frac{\epsilon_i \cdot n_A}{k_i \cdot n_A}$. This way, the amplitude A^* verifies the Ward-Takahashi identity. This gauge restoring term can be calculated explicitly, applying the Slavnov-Taylor identity on the Green function where all on-shell legs are contracted with the corresponding momenta, as shown in Fig. 3.14, leading to the following expression :

$$\begin{aligned} W(1^*, 2, \dots, n) &= -A(1^*, 2, \dots, n) |_{\epsilon_i \rightarrow k_i} \prod_{i=2}^n \alpha_i \\ &= - \left(\frac{-g_s}{\sqrt{2}} \right)^{n-2} |k_{\perp}| \frac{k_3 \cdot n_A \dots k_n \cdot n_A}{(k_2 - k_3) \cdot n_A \dots (k_2 - \dots - k_{n-1}) \cdot n_A}. \end{aligned} \quad (3.155)$$

First, we note that this expression can be interpreted as the on-shell gluons being attached to an infinite Wilson line in the direction n_A . Actually, it is possible to calculate gauge invariant off-shell amplitudes using matrix elements of straight infinite Wilson lines [192]. Then, we can observe that this gauge restoring term vanishes if any of the reference momenta of the polarization vector related to an on-shell leg is set to n_A . It follows that, by projecting any reference momenta of an on-shell leg to n_A , one can directly obtain a gauge invariant amplitude :

$$\forall i \in \llbracket 2, n \rrbracket, \quad A^*(1^*, 2, \dots, n) = A(1^*, 2, \dots, n) |_{\epsilon_i \rightarrow \epsilon_i(n_A)}, \quad (3.156)$$

This also works when projecting several or even all on-shell legs. Besides, W vanishes when $|k_{\perp}| \rightarrow 0$, insuring that A^* has the correct on-shell limit.

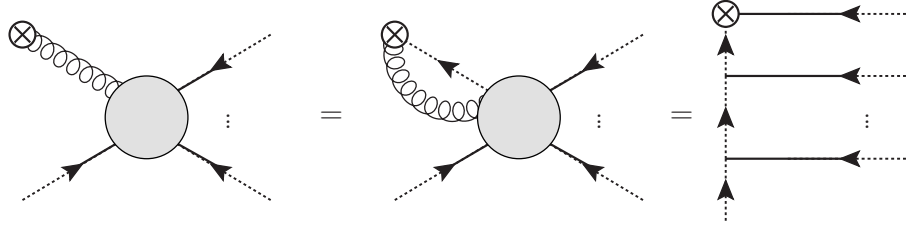


Figure 3.14: Gauge restoring term calculation.

Furthermore, this construction has been proven to be equivalent to Lipatov's effective action (comparing the different terms appearing in the Rgg vertex presented in [193] written in the axial gauge to terms contributing to A and W in the present method). In the following, we might refer to this method as the *gauge restoring method*.

The auxiliary parton method

In this section, we introduce a method to calculate amplitudes with one or two off-shell legs, based on previous observations. The idea is to extract off-shell amplitudes from on-shell ones to guarantee gauge invariance on one hand (in a way equivalent to the introduction of the gauge restoring term just presented) and to take advantage of our knowledge on on-shell amplitudes on the other hand. Let's first introduce this method, the *auxiliary parton method*, for an amplitude with one off-shell gluon and $n - 2$ on-shell particles $\mathcal{A}_{n-1}^*(g^*(k)\mathcal{X})$. It was first presented in [187], but in the following, we will introduce a variant proposed in [194] (explaining shortly the differences). The off-shell gluon follows the high energy kinematics (or quasi-multi-Regge kinematics) :

$$k^\mu = xp^\mu + k_\perp^\mu, \quad (3.157)$$

where p^μ is the light-like momentum associated with the colliding hadron, x is the fraction of this momentum carried by off-shell gluon, and k_\perp^μ is the transverse component (which verifies $k_\perp \cdot p = 0$).

The main idea consists in embedding the considered process ($g^*\mathcal{X}$) in an on-shell, bigger one in which we take some specific kinematics to extract it. Here, we will consider an on-shell process with an auxiliary quarks-antiquark pair, more precisely, we will obtain our off-shell amplitude from the on-shell amplitude $\mathcal{A}_n(\bar{q}(k_1)q(k_2)\mathcal{X})$. Finally, we parametrize the kinematics of the auxiliary quarks momenta k_1 and k_2 through a scalar Λ such that obtaining the off-shell amplitude involves taking the limit :

Auxiliary parton method

$$\lim_{\Lambda \rightarrow +\infty} \left(\frac{x|k_\perp|}{g_s \Lambda} \mathcal{A}(\bar{q}(k_1)q(k_2)\mathcal{X}) \right) = \mathcal{A}^*(g^*(k)\mathcal{X}), \quad (3.158)$$

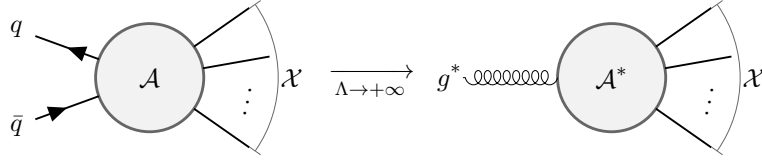


Figure 3.15: Scheme of the Λ -prescription : calculation of an off-shell amplitude from an on-shell one with auxiliary gluons.

which is schematized in Fig. 3.15. We might refer to this method as the Λ -prescription. The factor $1/g_s$ and the factor $|k_\perp|$ make sure the amplitude is finite for $|k_\perp| \rightarrow 0$ (we will enter more details later).

To go further, we need to detail the kinematics of the auxiliary quarks. We require their momenta to be light-like and to add up to the off-shell gluon momentum :

$$\begin{aligned} k_1^2 = k_2^2 = 0, \\ k_1^\mu + k_2^\mu = k^\mu, \end{aligned} \quad (3.159)$$

Several choices can be done to fulfill this requirement. Here, we will use the following Sudakov decomposition :

Auxiliary partons kinematics

$$\begin{aligned} k_1^\mu &= \Lambda p^\mu + \alpha q^\mu + \beta k_\perp^\mu, \\ k_2^\mu &= (x - \Lambda)p^\mu - \alpha q^\mu + (1 - \beta)k_\perp^\mu, \end{aligned} \quad (3.160)$$

where q^μ is an arbitrary light-like momentum such that $q \cdot k_\perp = 0$, $q \cdot p > 0$ and where :

$$\alpha = \frac{-\beta^2 k_\perp^2}{2\Lambda p \cdot q}, \quad \beta = \frac{1}{1 + \sqrt{1 - x/\Lambda}}. \quad (3.161)$$

This way, k_1 and k_2 verify Eq. (3.159) for any value of the real Λ , i.e guarantee the high energy form of the off-shell gluon. This parametrization is different from the one presented in [187] which consisted in taking $k_1^\mu = k$ and $k_2^\mu = 0$. This had the convenience to lead to simple spinor expression (for k_1 and k_2), but implied that momenta k_1 and k_2 were complex (recovering physical momenta in the limit $\Lambda \rightarrow +\infty$). Here, we lose the simplicity of the spinors but we have real momenta. Now, the key point is that, in the limit $\Lambda \rightarrow +\infty$ the coupling of gluons to the quark line becomes eikonal, consistent with the high energy limit, as in Eq. (3.148)¹⁶. Indeed, in the limit $\Lambda \rightarrow +\infty$, momenta flowing in the quark line (due to the auxiliary quarks) are dominated by Λp^μ . Let's consider such momenta $k_q = k_1 + K_q$ where K_q can be expressed as a sum of momenta of the on-shell legs (hence, it is negligible in the limit $\Lambda \rightarrow +\infty$). Then, the related

¹⁶In [187], this was set by hand, forcing eikonal Feynman rules for the quark line

propagator behaves as :

$$i \frac{k'_q}{k_q^2} = i \frac{k'_1 + K_q}{(k_1 + K_q)^2} \xrightarrow{\Lambda \rightarrow +\infty} i \frac{\not{p}}{2p \cdot k_q}. \quad (3.162)$$

Now, concerning the spinor chain of this quark line (involving the numerator of the quarks propagators, quark gluon vertices, and the auxiliary quarks spinors), we have :

$$\langle 1 | \prod_{i=1}^{v-1} \left[i\sqrt{2}\gamma^{\mu_i} k'_{\mu_i} \right] | 1 \rangle \xrightarrow{\Lambda \rightarrow +\infty} \Lambda \prod_{i=1}^v i\sqrt{2} \langle p | \gamma^{\mu_i} | p \rangle = \prod_{i=1}^v i2\sqrt{2} p^{\mu_i}. \quad (3.163)$$

where v is the number of vertices on the quark line. This corresponds to an eikonal coupling to the quark line (after canceling the factors 2 brought by the propagator and by the vertices).

In practice, instead of using the above definitions of k_1^μ and k_2^μ , we will use their expansion in Λ :

$$\begin{aligned} k_1^\mu &= \Lambda p^\mu + \left(\frac{1}{2} + \frac{x}{8\Lambda} \right) k_\perp^\mu - \frac{k_\perp^2}{8\Lambda p \cdot q} q^\mu + \mathcal{O}(\Lambda^{-2}), \\ k_2^\mu &= (x - \Lambda) p^\mu + \left(\frac{1}{2} - \frac{x}{8\Lambda} \right) k_\perp^\mu + \frac{k_\perp^2}{8\Lambda p \cdot q} q^\mu + \mathcal{O}(\Lambda^{-2}). \end{aligned} \quad (3.164)$$

In order to use the helicity method, we can express k_\perp^μ in terms of spinors as follows :

$$k_\perp^\mu = -\frac{\kappa}{\sqrt{2}} \varepsilon_-^\mu(p, q) - \frac{\kappa^*}{\sqrt{2}} \varepsilon_+^\mu(p, q), \quad (3.165)$$

with polarization vectors

$$\varepsilon_-^\mu(p, q) = \frac{\langle p | \gamma^\mu | q \rangle}{\sqrt{2} [pq]}, \quad \varepsilon_+^\mu(p, q) = \frac{\langle q | \gamma^\mu | p \rangle}{\sqrt{2} \langle qp \rangle}. \quad (3.166)$$

and

$$\kappa = \frac{\langle q | \not{k} | p \rangle}{\langle qp \rangle}, \quad \kappa^* = \frac{\langle p | \not{k} | q \rangle}{[pq]}. \quad (3.167)$$

In particular, we have :

$$k_\perp^2 = -\kappa \kappa^*. \quad (3.168)$$

With this decomposition, it is then possible to express k_1^μ and k_2^μ spinors in terms of those of p^μ and q^μ :

$$|1\rangle = \sqrt{\Lambda} |p\rangle - \frac{\beta \bar{\kappa}^*}{\sqrt{\Lambda}} |q\rangle, \quad |1] = \sqrt{\Lambda} |p] - \frac{\beta \bar{\kappa}}{\sqrt{\Lambda}} |q] \quad (3.169)$$

$$|2\rangle = \sqrt{\Lambda - x} |p\rangle + \frac{\beta \bar{\kappa}^*}{\sqrt{\Lambda}} |q\rangle, \quad |2] = -\sqrt{\Lambda - x} |p] - \frac{\beta \bar{\kappa}}{\sqrt{\Lambda}} |q]. \quad (3.170)$$

These expressions are valid at $\mathcal{O}\left(\Lambda^{-\frac{1}{2}}\right)$, which is sufficient in practice. Also, we observe that the external spinors associated to the auxiliary quarks bring an overall factor Λ , which is compensated in Eq. (3.158). Notice that $\sqrt{(\Lambda-x)/\Lambda}\beta = 1-\beta$ and that the spinor products involving both auxiliary quarks do not depend on Λ and reduce to :

$$\langle 12 \rangle = -\kappa^* \quad , \quad [12] = -\kappa . \quad (3.171)$$

Also, in the limit of interest, $\Lambda \rightarrow +\infty$, the spinors for auxiliary quarks behave as :

$$|1\rangle \rightarrow \sqrt{\Lambda} |p\rangle \quad , \quad |1] \rightarrow \sqrt{\Lambda} |p] \quad , \quad |2\rangle \rightarrow \sqrt{\Lambda} |p\rangle \quad , \quad |2] \rightarrow -\sqrt{\Lambda} |p] . \quad (3.172)$$

Overall, the auxiliary parton method reduces the evaluation of the off-shell amplitude for $g^*\mathcal{X}$ to the application of the kinematics just presented to the helicity on-shell amplitude for $qq\mathcal{X}$. This means replacing spinor products involving both auxiliary quarks, using Eq. (3.171), replacing the leftover auxiliary spinors by their approximation at large Λ (most of the time, the leading behavior, as in Eq. (3.172) is sufficient) and finally, expressing Lorentz invariant by applying Eq. (3.164) (for which, most of the time, only the $\mathcal{O}\left(\Lambda^{-1}\right)$ part is necessary) and finally, taking the limit presented in Eq. (3.158). Then, applying such kinematics to the embedding amplitude already guarantees gauge invariance and the expected collinear and soft behavior of the result (inherited from the on-shell amplitude), and also the expected high energy kinematic of the off-shell gluon (with the form of k for any Λ and the eikonal coupling of the quark line in the limit $\Lambda \rightarrow +\infty$).

Another important property of the obtained amplitudes is that they reduce to the expected on-shell limit (i.e. the limit $|k_\perp| \rightarrow 0$). To demonstrate it, we first consider an off-shell current J^μ attached to the auxiliary quark line via a gluon propagator $\frac{d_\mu^\nu(l,n)}{l^2}$ in the an axial gauge with gauge vector n^μ :

$$d^{\mu\nu}(k,n) = \eta^{\mu\nu} - \frac{k^\mu n^\nu + k^\nu n^\mu}{k \cdot n} + n^2 \frac{k^\mu k^\nu}{(k \cdot n)^2} , \quad (3.173)$$

$$p^\mu i\sqrt{2} \frac{d_\mu^\nu(l,n)}{l^2} J_\nu = -i\sqrt{2} \frac{p \cdot J_l}{l^2} + i\sqrt{2} \frac{p \cdot l}{n \cdot l} \frac{n \cdot J_l}{l^2} . \quad (3.174)$$

For $l^\mu = k^\mu = xp^\mu + k_\perp$, we observe that the corresponding off-shell current J couples to the auxiliary quark line as $-i\sqrt{2} \frac{p \cdot J}{k_\perp^2}$, independently of the gauge choice. Also, charge conservation reads :

$$k \cdot J = 0 , \quad (3.175)$$

and implies :

$$p \cdot J = -\frac{1}{x} k_\perp \cdot J . \quad (3.176)$$

For any other off-shell current J_l (with $l^\mu \neq k^\mu$), we can see that, by fixing the gauge with $n^\mu = p^\mu$, $p^\mu i \frac{d_\mu^\nu(l,n)}{l^2} J_\nu = 0$. This means that, the only off-shell current that can be

attached to the auxiliary quark line is k_μ . In other words, the only graphs contributing to the off-shell amplitude are those where only one gluon of momentum k^μ is attached to the quark line or those where all gluons attached to the quark line are on-shell (this latter case is only possible when \mathcal{X} consists only in gluons). If we consider off-shell amplitudes with only gluons, like in Sec. 3.2.2, then, the former case corresponds to the amplitude A in Eq. (3.150) while the former case is the gauge restoring amplitude W , filling the gap between the two methods. However, this only proves the expected on-shell limit for \mathcal{X} consisting of only gluons. For the more general case, we need to go a few steps back. When considering the limit $k_\perp \rightarrow 0$, the contributions with a propagator denominator $k_\perp^2 = -\kappa\kappa^*$ dominate. Those contributions have the form :

$$i\sqrt{2}\frac{p \cdot J}{k_\perp^2} = i\sqrt{2}\frac{k_\perp \cdot J}{x\kappa\kappa^*} = i\sqrt{2}\frac{k_\perp \cdot J}{x\kappa\kappa^*}. \quad (3.177)$$

The second term shows the importance of the factor x in Eq. (3.158). To continue, we consider Eq. (3.177) multiplied by $x|\mathbf{k}_\perp|$ (again, as in Eq. (3.158)¹⁷) to see that it leads to the right on-shell limit :

$$i\sqrt{2}\frac{|\mathbf{k}_\perp|}{\kappa\kappa^*}k_\perp \cdot J. \quad (3.178)$$

Using Eq. (3.165), we conclude that the projection on k_\perp means a projection on the polarization vectors ε_\pm ; leading to :

On-shell limit

$$\lim_{|k_\perp| \rightarrow 0} \mathcal{A}_n^*(g^* \mathcal{X}) = \frac{|k_\perp|}{\kappa^*} \mathcal{A}(g^- \mathcal{X}) + \frac{|k_\perp|}{\kappa} \mathcal{A}(g^+ \mathcal{X}), \quad (3.179)$$

where $\mathcal{A}(g^\pm \mathcal{X}) = \varepsilon_\pm \cdot J$. It is possible to express $|k_\perp|/\kappa^* = e^{i\phi}$ for some angle ϕ , and $|k_\perp|/\kappa$ its complex conjugate. Then, we see that the on-shell limit of the off-shell amplitude obtained applying the auxiliary parton method is the sum of two on-shell amplitudes, where the off-shell gluon becomes on-shell and acquires either a + or - polarization, multiplied by some phase factor. Actually, the matching of the on-shell result for $g\mathcal{X}$ and the on-shell limit of $g^*\mathcal{X}$ using the auxiliary parton method is achieved at the level of amplitude square, after summation over initial-state helicities for the on-shell process and averaged over the azimuthal angle ϕ for the off-shell one :

$$\sum_{\lambda=\pm} \left| \mathcal{A}(g^\lambda \mathcal{X}) \right|^2 = \left\langle \left| \lim_{|k_\perp| \rightarrow 0} \mathcal{A}(g^* \mathcal{X}) \right|^2 \right\rangle_\phi. \quad (3.180)$$

Indeed, if we square our on-shell limit Eq. (3.179), we obtain :

$$\begin{aligned} \left| \lim_{|k_\perp| \rightarrow 0} \mathcal{A}^*(g^* \mathcal{X}) \right|^2 &= \left| e^{i\phi} \mathcal{A}(g^- \mathcal{X}) + e^{-i\phi} \mathcal{A}(g^+ \mathcal{X}) \right|^2 \\ &= \left| \mathcal{A}(g^- \mathcal{X}) \right|^2 + \left| \mathcal{A}(g^+ \mathcal{X}) \right|^2 \\ &\quad + e^{2i\phi} \mathcal{A}(g^- \mathcal{X}) \mathcal{A}(g^+ \mathcal{X})^* + e^{-2i\phi} \mathcal{A}(g^+ \mathcal{X}) \mathcal{A}(g^- \mathcal{X})^*, \end{aligned} \quad (3.181)$$

¹⁷The other factors are considered to be absorbed in the off-shell current for this demonstration.

implying, after the average over ϕ :

$$\left\langle \left| \lim_{|k_\perp| \rightarrow 0} \mathcal{A}(g^* \mathcal{X}) \right|^2 \right\rangle_\phi = \left| \mathcal{A}(g^- \mathcal{X}) \right|^2 + \left| \mathcal{A}(g^+ \mathcal{X}) \right|^2 . \quad (3.182)$$

We see that the phase factors in Eq. (3.181) lead to an incoherent sum of the squared amplitude, justifying the proper on-shell limit (after averaging over ϕ).

Finally, the auxiliary parton method is a generalization of the gauge restoration method to any process with one off-shell gluon. It has been proved to be equivalent to Lipatov's high energy action [187] (by showing that it reproduces the effective vertices involving reggeized gluons). Also, directly using eikonal Feynman rules to describe the auxiliary partons is possible. Actually, any method that reproduces the eikonal coupling to the off-shell gluon (with high energy kinematics), that ensures gauge invariance, the proper soft and collinear behavior, and finally the proper on-shell limit would be acceptable (and indeed, variations on the method and more precisely deviations from the kinematics proposed here exist).

This method can easily be generalized for processes with 2 off-shell gluons [187], needed in k_T -factorization. This would involve 2 pairs of auxiliary quarks and the corresponding kinematics. It may also be used, in a modified version, for off-shell quarks [195] (using an auxiliary quark and an auxiliary photon this time). Alternatively, the auxiliary parton method can be used with an auxiliary gluon line, instead of the quark line (this has been proven in [194]). The idea is to project the color decomposition of a $(n-2)$ -gluon amplitude with a quark-antiquark pair onto a $(n-1)$ -gluon amplitude by a contraction with $(t^{a_*})_{ji}$, where a_* represents the color index of the off-shell gluon. In practice, it means that, for an auxiliary gluon pair, one simply needs to select contributions that retain the order of gluons 1 and 2 and substitute $t^{a_1} t^{a_2} \rightarrow t^{a_*}$.

Loop-level

The auxiliary parton method presented above has been developed and demonstrated for tree-level calculations. It is useful in automated calculations and, as already mentioned, has been implemented in the Monte Carlo generator KATIE [99] (used, for instance, in the study proposed in Sec. 2.6.4). Recently, a proof of concept was proposed for its generalization at one-loop in [194] (summarized in [196]). We will shortly present the arguments advanced there but also present the difficulties linked to this one-loop generalization.

Like in Lipatov's high energy effective action, the first problem arising at loop level comes from the regularization of the eikonal propagators. Such denominator would contain momentum of the form $P_i = k_1 + K_i$, where K_i is a sum of a subset of the on-shell momenta. These denominators imply integrands of the form :

$$\frac{\Lambda}{(l + k_1 + K_i)^2} \xrightarrow{\Lambda \rightarrow +\infty} \frac{1}{2p \cdot (l + K_i)^2} , \quad (3.183)$$

where the factor Λ comes from the spinor of the auxiliary quarks and l is the loop momentum. However, with the presented auxiliary parton method, the parameter Λ regularize such divergences. Indeed, at fixed Λ , there is no eikonal propagators and the usual techniques to calculate loop integrands can be used (like those presented in Sec. 3.1.7). Then, the idea is to take the limit $\Lambda \rightarrow +\infty$ after the loop integration (i.e. after taking the limit $\epsilon \rightarrow 0$). This means expanding in (logarithm of) Λ the loop integrals expanded in ϵ . However, this is possible only if the divergences are not power-like (i.e. they are balanced by the factor $\frac{1}{\Lambda}$ in Eq. (3.158)). This is actually the case (see [194] for the demonstration), the loop amplitudes diverge at most like $\log^2 \Lambda$. Also, the expansion in Λ can become quickly complicated with increasing multiplicity so one might want to use master integral reduction (and calculate the coefficients numerically). The question is then if the coefficients of this reduction (see Eq. (3.121)) can be calculated in the limit $\Lambda \rightarrow +\infty$. Without entering the details, it is possible for most loop integrals but 2, the *anomalous bubble* :

$$\int \frac{d^4 l}{(l + P_0)^2 (l + k_1 + P_1)^2} = -\ln \Lambda + \frac{1}{\epsilon} + 2 + \ln \left(\frac{2p \cdot (P_1 - P_0)}{-\mu^2} \right) + \mathcal{O}(\epsilon) , \quad (3.184)$$

and *anomalous triangle* :

$$\int \frac{d^4 l}{l^2 (l + k_1)^2 (l + k)^2} = \frac{1}{k_\perp^2} \left[\frac{1}{\epsilon^2} - \frac{1}{\epsilon} \ln \left(\frac{k_\perp^2}{-\mu^2} \right) + \frac{1}{2} \ln^2 \left(\frac{k_\perp^2}{-\mu^2} \right) \right] + \mathcal{O}(\epsilon) . \quad (3.185)$$

Then, to calculate an off-shell amplitude at loop level using the auxiliary parton method, one should :

- Choose a momentum routing such that the divergent components of the auxiliary quark (linear in Λ) flow through the internal auxiliary quark line,
- consider only contributions with, at most, one momentum of the auxiliary quark line in the denominator (other contributions either vanish or reduce to these ones),
- apply master integral reduction except for the anomalous integrals
- obtain the anomalous integral contribution by using auxiliary gluons instead of auxiliary quarks.

To go further in the application of the auxiliary parton method at loop level, we will test its application and see if the resulting amplitude verifies the properties observed at tree level.

3.3 Results

To validate the proof of concept given in [99], we will apply the auxiliary parton method to simple one-loop amplitudes and study the obtained result. In particular, we will verify the correctness of the on-shell limit, we will test the equivalence with Lipatov's

high energy effective action and the equivalence between the use of auxiliary quarks and auxiliary gluons. As a very first step, we want to consider the simplest one-loop helicity amplitudes. Gluonic amplitudes with all helicities being the same vanish at tree level while are non-zero at loop-level but are still free from divergences (avoiding the anomalous integrals mentioned previously). Thus, we have chosen to study the one-loop amplitudes with all-plus helicity gluons and one off-shell gluon (for arbitrary number of gluons n). Later, we will apply our method to the one off-shell gluon two on-shell one loop amplitude since equivalent Lipatov's high energy effective action results are known in this case.

3.3.1 $g^*g^+ \dots g^+$ amplitudes

In this section we present our results for the one loop amplitudes for one off-shell gluon and $n - 1$ on-shell positive helicity gluons. These results were published in [2]. Such amplitudes are primarily used for forward particle production.

We begin with several low multiplicity examples, starting with the simplest cases: $n = 3$ (the vertex). We continue with $n = 4$ and $n = 5$ before presenting a result for arbitrary n . For each case, we apply the auxiliary parton method for auxiliary quarks and also for auxiliary gluons. This means that we shall use the existing one-loop results for $(-+\dots+)$ helicity on-shell amplitudes, where the first pair of particles is either gluon pair or quark-antiquark pair. One may notice that result are only one partial amplitude is given, the other ones being obtained through Eq. (3.14).

3-point vertex

We first consider the 3-point vertex with one off-shell gluon and two positive helicity on-shell gluons at one loop. Such vertex has been calculated for arbitrary helicity projection in [175] from the Lipatov's effective action (as reported in Eq. (3.147)).

In order to calculate it from the auxiliary parton method, we need the 4-point amplitude for quark, antiquark and two gluons. At one loop it has the following form [115] :

$$A_{4;1}^{(1)}(1_{\bar{q}}^-, 2_q^+, 3^+, 4^+) = -\frac{ig_s^4}{16\pi^2} \left[\frac{1}{2} \left(1 + \frac{1}{N_c^2} \right) + \frac{1}{3} \left(1 + \frac{n_s - n_f}{N_c} \right) \frac{s_{23}}{s_{12}} \right] \frac{\langle 12 \rangle [24]}{\langle 23 \rangle \langle 34 \rangle}, \quad (3.186)$$

where n_f accounts for the number of Weyl fermions circulating in the loop, n_s the number of complex scalars. Applying the Λ prescription we get :

$g^*g^+g^+$ loop-amplitude

$$\begin{aligned} \mathcal{A}_3^{*(1)}(g^*, 3^+, 4^+) &= -\frac{ig_s^3}{24\pi^2} \left(1 + \frac{n_s - n_f}{N_c} \right) x|k_\perp| \frac{p \cdot k_3}{k_\perp^2} \frac{\kappa^*[p4]}{\langle p3 \rangle \langle 34 \rangle} \\ &= -\frac{ig_s^3}{24\pi^2} \left(1 + \frac{n_s - n_f}{N_c} \right) \frac{x|k_\perp|}{\kappa^2} p \cdot k_3 \frac{[p3][p4]}{\langle p3 \rangle \langle p4 \rangle}, \end{aligned} \quad (3.187)$$

where we used that $k_{\perp}^2 = -\kappa\kappa^*$, $\kappa = \langle 4|\not{k}|p\rangle/\langle 4p\rangle$ and $k^{\mu} = -k_3^{\mu} - k_4^{\mu}$. We observe that, for $n_s = 0$ the above result agrees with Lipatov high energy effective action (see Eq. (3.147)).

Now, we can test the equivalence in the auxiliary parton used. For this, we need the 4-point one loop amplitude for one negative helicity gluon and three positive helicity gluons which is given by [115] :

$$A_{4;1}^{(1)}(1^-, 2^+, 3^+, 4^+) = \frac{ig_s^4}{48\pi^2} \left(1 + \frac{n_s - n_f}{N_c}\right) \frac{\langle 24\rangle[24]^3}{[12]\langle 23\rangle\langle 34\rangle[41]}. \quad (3.188)$$

After applying the Λ prescription we indeed find that it leads to the same result as before :

$$\mathcal{A}_3^{*(1)}(g^*, 3^+, 4^+) = -\frac{ig_s^3 x|k_{\perp}|}{24\pi^2} \left(1 + \frac{n_s - n_f}{N_c}\right) \frac{p \cdot k_3}{k_{\perp}^2} \frac{\kappa^*[p4]}{\langle p3\rangle\langle 34\rangle}, \quad (3.189)$$

where we have used $p \cdot k_3 = -p \cdot k_4$ since $0 = p \cdot k = p \cdot (-k_3 - k_4)$.

4-point amplitude

For the 4-point off-shell amplitude, we need the 5-leg amplitude with auxiliary quark pair which is given by [115] :

$$\begin{aligned} A_{5;1}^{(1)}(1_{\bar{q}}^-, 2_q^+, 3^+, 4^+, 5^+) &= -\frac{ig_s^5}{32\pi^2} \left(1 + \frac{1}{N_c^2}\right) \frac{\langle 12\rangle[23]\langle 31\rangle + \langle 14\rangle[45]\langle 51\rangle}{\langle 23\rangle\langle 34\rangle\langle 45\rangle\langle 51\rangle} \\ &- \frac{ig_s^5}{48\pi^2} \left(1 + \frac{n_s - n_f}{N_c}\right) \left(\frac{\langle 13\rangle[34]\langle 41\rangle^2}{\langle 12\rangle\langle 34\rangle^2\langle 45\rangle\langle 51\rangle} + \frac{\langle 14\rangle\langle 24\rangle[45]\langle 51\rangle}{\langle 12\rangle\langle 23\rangle\langle 34\rangle\langle 45\rangle^2} + \frac{[23][25]}{[12]\langle 34\rangle\langle 45\rangle} \right). \end{aligned} \quad (3.190)$$

Applying the Λ prescription we find that the first term is of the order Λ^{-1} and thus vanishes. Further calculation leads to the following result :

$g^* g^+ g^+ g^+$ loop-amplitude

$$\begin{aligned} A_{4;1}^{*(1)}(g^*, 3^+, 4^+, 5^+) &= -\frac{ig_s^4}{48\pi^2} \frac{x|k_{\perp}|}{\kappa^*\langle p3\rangle\langle 34\rangle\langle 45\rangle\langle 5p\rangle} \left(1 + \frac{n_s - n_f}{N_c}\right) \\ &\times \left[\langle p3\rangle^2 \langle p4\rangle^2 \frac{[34]}{\langle 34\rangle} + \langle p4\rangle^2 \langle p5\rangle^2 \frac{[45]}{\langle 45\rangle} - \frac{\kappa^*}{\kappa} s_{p3} s_{p5} \right]. \end{aligned} \quad (3.191)$$

The 5-point on-shell gluon amplitude we need (with auxiliary gluons) is given

by [197] :

$$A_{5;1}^{(1)}(1^-, 2^+, 3^+, 4^+, 5^+) = \frac{ig_s^5}{48\pi^2} \frac{\left(1 + \frac{n_s - n_f}{N_c}\right)}{[12]\langle 23 \rangle \langle 34 \rangle \langle 45 \rangle [51]} \times \left[(s_{23} + s_{34} + s_{45}) [25]^2 \right. \\ \left. - [24] \langle 43 \rangle [35] [25] - \frac{[12][15]}{\langle 12 \rangle \langle 15 \rangle} \left(\langle 12 \rangle^2 \langle 13 \rangle^2 \frac{[23]}{\langle 23 \rangle} + \langle 13 \rangle^2 \langle 14 \rangle^2 \frac{[34]}{\langle 34 \rangle} + \langle 14 \rangle^2 \langle 15 \rangle^2 \frac{[45]}{\langle 45 \rangle} \right) \right]. \quad (3.192)$$

Applying the same procedure as before leads to the following off-shell amplitude :

$$A_{4;1}^{*(1)}(g^*, 3^+, 4^+, 5^+) = \frac{ig_s^4}{48\pi^2} \frac{x|k_\perp| \left(1 + \frac{n_s - n_f}{N_c}\right)}{\kappa^* \langle p3 \rangle \langle 34 \rangle \langle 45 \rangle [5p]} \times \left[s_{p3} [p5]^2 \right. \\ \left. - \frac{\kappa [p5]}{\kappa^* \langle p5 \rangle} \left(\langle p3 \rangle^2 \langle p4 \rangle^2 \frac{[34]}{\langle 34 \rangle} + \langle p4 \rangle^2 \langle p5 \rangle^2 \frac{[45]}{\langle 45 \rangle} \right) \right], \quad (3.193)$$

which turns out to be equal to Eq. (3.191).

5-point amplitude

Here, the amplitude with the auxiliary quark pair is given by [198] :

$$A_{6;1}^{(1)}(1_{\bar{q}}^-, 2_q^+, 3^+, 4^+, 5^+, 6^+) = \frac{ig_s^6}{32\pi^2} \left(1 + \frac{1}{N_c^2}\right) \frac{\sum_{i=3}^5 \langle 1 | \not{K}_{2\dots i} k_i | 1 \rangle}{\langle 23 \rangle \langle 34 \rangle \langle 45 \rangle \langle 56 \rangle \langle 61 \rangle} \\ + \frac{ig_s^6}{48\pi^2} \left(1 + \frac{n_s - n_f}{N_c}\right) \left[\frac{\langle 14 \rangle \langle 1 | (2+3)(3+4) | 1 \rangle}{\langle 12 \rangle \langle 34 \rangle^2 \langle 45 \rangle \langle 56 \rangle \langle 61 \rangle} + \frac{\langle 24 \rangle \langle 15 \rangle \langle 1 | (4+5)(5+6) | 1 \rangle}{\langle 12 \rangle \langle 23 \rangle \langle 34 \rangle \langle 45 \rangle^2 \langle 56 \rangle \langle 61 \rangle} \right. \\ - \frac{\langle 25 \rangle \langle 1 | 56 | 1 \rangle}{\langle 12 \rangle \langle 23 \rangle \langle 34 \rangle \langle 45 \rangle \langle 56 \rangle^2} + \frac{\langle 1 | 3+4 | 2 \rangle^2}{\langle 34 \rangle^2 \langle 56 \rangle \langle 61 \rangle \langle 5 | 3+4 | 2 \rangle} \\ + \frac{\langle 2 | 4+5 | 6 \rangle \langle 1 | 4+5 | 6 \rangle^2}{\langle 12 \rangle \langle 23 \rangle \langle 45 \rangle^2 \langle 3 | 4+5 | 6 \rangle s_{456}} \\ \left. - \frac{[26]^2 [2 | (3+4)(4+5)(3+4)(4+5) | 6]}{[12] \langle 34 \rangle \langle 45 \rangle \langle 5 | 3+4 | 2 \rangle \langle 3 | 4+5 | 6 \rangle s_{345}} \right], \quad (3.194)$$

where we defined :

$$\not{K}_{a\dots b} = \sum_{i=a}^b \not{k}_i, \quad (3.195)$$

$$s_{ijk} = (k_i + k_j + k_k)^2, \quad (3.196)$$

and used :

$$\langle a | (i+j) | b \rangle = \langle ai \rangle [ib] + \langle aj \rangle [jb] \quad (3.197)$$

$$\langle a | (i+j)(k+l) | b \rangle = \langle ai \rangle [i(k+l)|b] + \langle aj \rangle [j(k+l)|b]. \quad (3.198)$$

Above $a, b, i, j, k, l \in \llbracket 1, n \rrbracket$, where $n = 6$ in the present section.

After we apply the Λ prescription we find that the term proportional to $\left(1 + \frac{1}{N_c^2}\right)$ vanishes, leading to :

$g^* g^+ g^+ g^+ g^+$ loop-amplitude

$$\begin{aligned}
A_{5;1}^{*(1)}(g^*, 3^+, 4^+, 5^+, 6^+) &= \left(1 + \frac{n_s - n_f}{N_c}\right) \times \\
&\times \frac{ig_s^5 x |k_\perp|}{48\pi^2} \left[\frac{\langle p4 \rangle (\kappa^* [p3 + 4|p] + \langle p3 \rangle [34] \langle 4p \rangle)}{\kappa^* \langle 34 \rangle^2 \langle 45 \rangle \langle 56 \rangle \langle 6p \rangle} + \frac{\langle p4 \rangle \langle p5 \rangle \langle p | (4 + 5) (5 + 6) | p \rangle}{\kappa^* \langle p3 \rangle \langle 34 \rangle \langle 45 \rangle^2 \langle 56 \rangle \langle 6p \rangle} \right. \\
&\quad - \frac{\langle p5 \rangle \langle p | 56 | p \rangle}{\kappa^* \langle p3 \rangle \langle 34 \rangle \langle 45 \rangle \langle 56 \rangle^2} + \frac{\langle p | 3 + 4 | p \rangle^2}{\langle 34 \rangle^2 \langle 56 \rangle \langle 6p \rangle \langle 5 | 3 + 4 | p \rangle} \\
&\quad \left. + \frac{\langle p | 4 + 5 | 6 \rangle^3}{\kappa^* \langle p3 \rangle \langle 45 \rangle^2 \langle 3 | 4 + 5 | 6 \rangle s_{456}} - \frac{[p6]^2 [p] (3 + 4) (4 + 5) (3 + 4) (4 + 5) [6]}{\kappa \langle 34 \rangle \langle 45 \rangle \langle 5 | 3 + 4 | p \rangle \langle 3 | 4 + 5 | 6 \rangle s_{345}} \right].
\end{aligned} \tag{3.199}$$

In order to derive 5-point off-shell amplitude from auxiliary gluons, we use the following 6-point on-shell one loop amplitude [198] :

$$\begin{aligned}
A_{6;1}^{(1)}(1^-, 2^+, 3^+, 4^+, 5^+, 6^+) &= \frac{ig_s^6}{48\pi^2} \left(1 + \frac{n_s - n_f}{N_c}\right) \times \\
&\times \left[\frac{\langle 1 | 2 + 3 | 6 \rangle^3}{\langle 12 \rangle \langle 23 \rangle \langle 45 \rangle^2 s_{123} \langle 3 | 1 + 2 | 6 \rangle} + \frac{\langle 1 | 3 + 4 | 2 \rangle^3}{\langle 34 \rangle^2 \langle 56 \rangle \langle 61 \rangle s_{234} \langle 5 | 3 + 4 | 2 \rangle} \right. \\
&\quad + \frac{[26]^3}{[12][61] s_{345}} \left(\frac{[23][34]}{\langle 45 \rangle \langle 5 | 3 + 4 | 2 \rangle} - \frac{[45][56]}{\langle 34 \rangle \langle 3 | 1 + 2 | 6 \rangle} + \frac{[35]}{\langle 34 \rangle \langle 45 \rangle} \right) \\
&\quad - \frac{\langle 13 \rangle^3 [23] \langle 24 \rangle}{\langle 23 \rangle^2 \langle 34 \rangle^2 \langle 45 \rangle \langle 56 \rangle \langle 61 \rangle} + \frac{\langle 15 \rangle^3 \langle 46 \rangle [56]}{\langle 12 \rangle \langle 23 \rangle \langle 34 \rangle \langle 45 \rangle^2 \langle 56 \rangle^2} \\
&\quad \left. - \frac{\langle 14 \rangle^3 \langle 35 \rangle \langle 1 | 2 + 3 | 4 \rangle}{\langle 12 \rangle \langle 23 \rangle \langle 34 \rangle^2 \langle 45 \rangle^2 \langle 56 \rangle \langle 61 \rangle} \right].
\end{aligned} \tag{3.200}$$

Applying the Λ prescription to the above on-shell result gives :

$$\begin{aligned}
A_{5;1}^{*(1)}(g^*, 3^+, 4^+, 5^+, 6^+) &= \frac{ig_s^5 x |k_\perp|}{48\pi^2} \left(1 + \frac{n_s - n_f}{N_c} \right) \times \\
&\times \left[\frac{(\kappa^* [p6] + \langle p3 \rangle [36])^3}{\kappa^* \langle p3 \rangle \langle 45 \rangle^2 s_{k3} \langle 3|k|6 \rangle} + \frac{\langle p|3+4|p \rangle^3}{\langle 34 \rangle^2 \langle 56 \rangle \langle 6p \rangle (s_{p3} + s_{p4}) \langle 5|3+4|p \rangle} \right. \\
&+ \frac{[p6]^2}{\kappa^* s_{345}} \left(\frac{[p3][34]}{\langle 45 \rangle \langle 5|3+4|p \rangle} - \frac{[45][56]}{\langle 34 \rangle \langle 3|k|6 \rangle} + \frac{[35]}{\langle 34 \rangle \langle 45 \rangle} \right) \\
&- \frac{\langle p3 \rangle [p3] \langle p4 \rangle}{\langle 34 \rangle^2 \langle 45 \rangle \langle 56 \rangle \langle 6p \rangle} + \frac{\langle p5 \rangle^3 \langle 46 \rangle [56]}{\kappa^* \langle p3 \rangle \langle 34 \rangle \langle 45 \rangle^2 \langle 56 \rangle^2} \\
&\left. - \frac{\langle p4 \rangle^3 \langle 35 \rangle (\kappa^* [p4] + \langle p3 \rangle [34])}{\kappa^* \langle p3 \rangle \langle 34 \rangle^2 \langle 45 \rangle^2 \langle 56 \rangle \langle 6p \rangle} \right].
\end{aligned} \tag{3.201}$$

This amplitude turns out to be equal to the one obtained with auxiliary quark line, Eq. (3.194). The comparison is detailed in Appendix B.6.

n -point amplitude

Finally, in the following section we shall derive the general expression for one-loop amplitude for one off-shell gluon and $n - 1$ on-shell gluons with all helicities positive. To this end, we need the one loop amplitude for a quark-antiquark pair and $n - 1$ positive helicity gluons. A suitable expression has been derived in [198]. It reads :

$$\begin{aligned}
\mathcal{A}_{n+1}^{(1)}(1_{\bar{q}}^-, 2_q^+, 3^+, \dots, (n+1)^+) &= \frac{ig_s^{n+1}}{32\pi^2} \left(1 + \frac{1}{N_c^2} \right) \frac{\sum_{l=3}^n \langle 1|K_{2\dots l}k_l|1 \rangle}{\langle 23 \rangle \dots \langle (n+1)1 \rangle} \\
&+ \frac{ig_s^{n+1}}{48\pi^2} \left(1 + \frac{n_s - n_f}{N_c} \right) \frac{S_1 + S_2}{\langle 12 \rangle \langle 23 \rangle \dots \langle (n+1)1 \rangle},
\end{aligned} \tag{3.202}$$

with :

$$\begin{aligned}
S_1 &= \sum_{j=3}^n \frac{\langle 2j \rangle \langle 1(j+1) \rangle \langle 1|K_{j,j+1}K_{(j+1)\dots(n+1)}|1 \rangle}{\langle j(j+1) \rangle}, \\
S_2 &= \sum_{j=3}^{n-1} \sum_{l=j+1}^n \frac{\langle 1|K_{j\dots l}K_{(l+1)\dots(n+1)}|1 \rangle^2 \langle 2|K_{j\dots l}K_{(l+1)\dots(n+1)}|1 \rangle}{\langle 1|K_{(l+1)\dots(n+1)}K_{j\dots l}|(j-1) \rangle \langle 1|K_{(l+1)\dots(n+1)}K_{j\dots l}|j \rangle} \\
&\times \frac{\langle (j-1)j \rangle \langle l(l+1) \rangle \langle 1|K_{2\dots(j-1)}[\mathcal{F}(j,l)]^2 K_{(l+1)\dots(n+1)}|1 \rangle}{\langle 1|K_{2\dots(j-1)}K_{j\dots l}|l \rangle \langle 1|K_{2\dots(j-1)}K_{j\dots l}|(l+1) \rangle s_{j\dots l}},
\end{aligned} \tag{3.203}$$

where :

$$\mathcal{F}(j,l) = \sum_{i=j}^{l-1} \sum_{m=i+1}^l k_i k_m. \tag{3.204}$$

After applying the Λ prescription we find that the term proportional to $\left(1 + \frac{1}{N_c}\right)$ is of the order Λ^{-1} , whereas the other term is of order 1 and is the one contributing to the off-shell amplitude. Eventually, we obtain the following expression for the off-shell amplitude :

$g^* g^+ \cdots g^+$ loop-amplitude

$$A_{n;1}^{*(1)}(g^*, 3^+, \dots, (n+1)^+) = \frac{ig_s^n x |k_\perp|}{48\pi^2} \left(1 + \frac{n_s - n_f}{N_c}\right) \frac{U_1^* + U_2^* + U_3^*}{\kappa^* \langle p3 \rangle \langle 34 \rangle \cdots \langle np \rangle}, \quad (3.205)$$

with :

$$\begin{aligned} U_1^* &= \sum_{j=3}^n \frac{\langle pj \rangle \langle p(j+1) \rangle \langle p | \mathcal{K}_{j,j+1} \mathcal{K}_{(j+1)\dots(n+1)} | p \rangle}{\langle j(j+1) \rangle}, \\ U_2^* &= \sum_{j=4}^{n-1} \sum_{l=j+1}^n \frac{\langle p | \mathcal{K}_{j\dots l} \mathcal{K}_{(l+1)\dots(n+1)} | p \rangle^3}{\langle p | \mathcal{K}_{(l+1)\dots(n+1)} \mathcal{K}_{j\dots l} | (j-1) \rangle \langle p | \mathcal{K}_{(l+1)\dots(n+1)} \mathcal{K}_{j\dots l} | j \rangle} \\ &\quad \times \frac{\langle (j-1)j \rangle \langle l(l+1) \rangle \langle p | \mathcal{K}'_{3\dots(j-1)} [\mathcal{F}(j,l)]^2 \mathcal{K}_{(l+1)\dots(n+1)} | p \rangle}{\langle p | \mathcal{K}_{3\dots(j-1)} \mathcal{K}_{j\dots l} | l \rangle \langle p | \mathcal{K}_{3\dots(j-1)} \mathcal{K}_{j\dots l} | (l+1) \rangle s_{j\dots l}}, \quad (3.206) \\ U_3^* &= \sum_{l=4}^n \frac{\langle p | \mathcal{K}_{3\dots l} \mathcal{K}_{(l+1)\dots(n+1)} | p \rangle^3}{\langle p | \mathcal{K}_{(l+1)\dots(n+1)} \mathcal{K}_{3\dots l} | p \rangle \langle p | \mathcal{K}_{(l+1)\dots(n+1)} \mathcal{K}_{3\dots l} | 3 \rangle} \\ &\quad \times \frac{\langle p3 \rangle \langle l(l+1) \rangle [p | \mathcal{F}(3,l)]^2 \mathcal{K}_{(l+1)\dots(n+1)} | p \rangle}{\kappa^* [p | \mathcal{K}_{3\dots l} | l] [p | \mathcal{K}_{3\dots l} | (l+1)] s_{3\dots l}}. \end{aligned}$$

It can be readily checked that the above expression recovers the amplitudes calculated previously for $n = 3, 4, 5$ in an independent way.

Now, using auxiliary quarks, we need the on-shell gluonic amplitude taken from [198] :

$$\mathcal{A}_{n+1}^{(1)}(1^-, 2^+, 3^+, \dots, (n+1)^+) = \frac{ig_s^{n+1}}{48\pi^2} \left(1 + \frac{n_s - n_f}{N_c}\right) \frac{T_1 + T_2}{\langle 12 \rangle \langle 23 \rangle \cdots \langle n1 \rangle}, \quad (3.207)$$

with :

$$\begin{aligned} T_1 &= \sum_{j=2}^n \frac{\langle 1j \rangle \langle 1(j+1) \rangle \langle 1 | \mathcal{K}_{j,j+1} \mathcal{K}_{(j+1)\dots(n+1)} | 1 \rangle}{\langle j(j+1) \rangle}, \\ T_2 &= \sum_{j=3}^{n-1} \sum_{l=j+1}^n \frac{\langle 1 | \mathcal{K}_{j\dots l} \mathcal{K}_{(l+1)\dots(n+1)} | 1 \rangle^3}{\langle 1 | \mathcal{K}_{(l+1)\dots(n+1)} \mathcal{K}_{j\dots l} | (j-1) \rangle \langle 1 | \mathcal{K}_{(l+1)\dots(n+1)} \mathcal{K}_{j\dots l} | j \rangle} \\ &\quad \times \frac{\langle (j-1)j \rangle \langle l(l+1) \rangle \langle 1 | \mathcal{K}_{2\dots(j-1)} [\mathcal{F}(j,l)]^2 \mathcal{K}_{(l+1)\dots(n+1)} | 1 \rangle}{\langle 1 | \mathcal{K}_{2\dots(j-1)} \mathcal{K}_{j\dots l} | l \rangle \langle 1 | \mathcal{K}_{2\dots(j-1)} \mathcal{K}_{j\dots l} | (l+1) \rangle s_{j\dots l}}. \quad (3.208) \end{aligned}$$

Applying the Λ prescription to T_2 gives the same result as for S_2 in Eq. (3.203). It turns out that T_1 is equal to S_1 within the Λ description once you realize that the first term in the sum over j in T_1 is of the order Λ^{-1} . In the end, applying the Λ prescription to $\bar{q}^- q^+ g^+ \cdots g^+$ or $g^- g^+ g^+ \cdots g^+$ gives the same expression, given by Eq. (3.205).

On-shell limit

Now, that we have obtained the expression for $A_{n;1}^{*(1)}(g^*, 3^+, \dots, (n+1)^+)$, we should verify that in the on-shell limit, i.e. when $|k_\perp| \rightarrow 0$, we obtain the incoherent sum of one loop on-shell amplitude with the first gluon having the momentum xp^μ and helicity either “+” or “-” (as described in Eq. (3.179)). Rather than doing it for each multiplicity separately, we directly use our result for an arbitrary number of gluons (see Eq. (3.205)).

First, one can notice that $U_1^* \xrightarrow{|k_\perp| \rightarrow 0} T^1$ and $U_2^* \xrightarrow{|k_\perp| \rightarrow 0} T^2$, which implies :

$$\begin{aligned} \lim_{|k_\perp| \rightarrow 0} A_{n;1}^{*(1)}(g^*, 3^+, \dots, (n+1)^+) &= \frac{|k_\perp|}{\kappa^*} \mathcal{A}_n^{(1)}(xp^-, 3^+, \dots, (n+1)^+) \\ &+ \frac{ig_s^n x \lim_{k_\perp \rightarrow 0} (U_3^* |k_\perp| / \kappa^*)}{48\pi^2 \langle p3 \rangle \langle 34 \rangle \cdots \langle (n+1)p \rangle}. \end{aligned} \quad (3.209)$$

So we already have the contribution from the amplitude with negative helicity gluon (the first term in the expression above). We now need to show that the second term is actually the contribution from the amplitude with a positive helicity gluon, i.e. :

$$A_{n;1}^{(1)}(1^+, \dots, n^+) = \frac{ig_s^n}{48\pi^2} \left(1 + \frac{n_s - n_f}{N_c} \right) \sum_{1 \leq i < j < k < l \leq n} \frac{\langle ij \rangle [jk] \langle kl \rangle [li]}{\langle 12 \rangle \cdots \langle n1 \rangle}. \quad (3.210)$$

To this end, we have to manipulate on the expression U_3^* . One can show that :

$$\begin{aligned} U_3^* \xrightarrow{|k_\perp| \rightarrow 0} \frac{\kappa^*}{\kappa [p(n+1)]} [p | \mathcal{F}(3, n)]^2 | (n+1)] &= \frac{\kappa^*}{\kappa} \sum_{3 \leq i < j < k < l \leq (n+1)} \langle ij \rangle [jk] \langle kl \rangle [li] \\ &+ \frac{\kappa^*}{\kappa} \sum_{3 \leq j < k < l \leq (n+1)} \langle pj \rangle [jk] \langle kl \rangle [lp]. \end{aligned} \quad (3.211)$$

Inserting this into Eq. (3.209) leads to :

$$\begin{aligned} \lim_{k_\perp \rightarrow 0} A_{n;1}^{*(1)}(g^*, 3^+, \dots, (n+1)^+) &= \frac{|k_\perp|}{\kappa^*} \mathcal{A}_n^{(1)}(xp^-, 3^+, \dots, (n+1)^+) \\ &+ \frac{|k_\perp|}{\kappa} \mathcal{A}_n^{(1)}(xp^+, 3^+, \dots, (n+1)^+). \end{aligned} \quad (3.212)$$

More details on the above rather non-trivial calculation are given in App. B.7. This is exactly what we expect from the on-shell limit, as presented in Eq. (3.179).

We see that, for the all-plus gluonic amplitude with one gluon off-shell, the auxiliary parton method keeps the same properties at loop-level as at tree-level. In particular, we respect the on-shell limit, we keep the equivalence between using auxiliary quark and auxiliary gluons and, for the one we could verify (the 3-point vertex), we even find agreement with Lipatov's high energy effective action. Then, we can conclude that the auxiliary parton method works at one-loop level, at least for amplitudes with same helicities.

3.3.2 g^*gg

We have also calculated g^*gg amplitudes, this time for any helicity configuration, in particular $g^*g^-g^+$ ¹⁸, which will be our first loop amplitude with divergences. This calculation had also been performed within high energy Lipatov effective action, making the comparison possible. We will also compare the results when using either auxiliary quark or auxiliary gluon. However, we won't be able to verify the on-shell limit since the helicity amplitudes ggg vanish for real momenta (as discussed in Sec. 3.1.5).

$g^*g^-g^+$

For this amplitude, we use the result for $\bar{q}^-q^+g^-g^+$ given in [115] in the form of primitive amplitudes :

$$\begin{aligned}
A_4^L(1_{\bar{q}}^-, 2_q^+, 3^-, 4^+) &= c_\Gamma A_4^{tree}(1_{\bar{q}}^-, 2_q^+, 3^-, 4^+) \times \\
&\times \left[-\frac{2+3\epsilon}{2\epsilon^2} \left(\frac{-\mu^2}{s_{12}} \right)^\epsilon - \frac{2}{\epsilon^2} \left(\frac{-\mu^2}{s_{23}} \right)^\epsilon \right. \\
&\quad + \left(\ln^2 \frac{s_{12}}{s_{23}} + \pi^2 \right) \left(1 + \frac{1}{2} \frac{s_{12}^3}{s_{13}^3} - \frac{3}{2} \frac{s_{12}s_{23}}{s_{13}^2} \right) \\
&\quad \left. + \frac{s_{12}}{s_{13}} \left(\frac{3}{2} - \frac{s_{23}}{s_{13}} \right) \ln \frac{s_{12}}{s_{23}} + \frac{s_{12}}{2s_{13}} - \frac{5}{2} \right] \\
A_4^{SUSY}(1_{\bar{q}}^-, 2_q^+, 3^-, 4^+) &= c_\Gamma A_4^{tree}(1_{\bar{q}}^-, 2_q^+, 3^-, 4^+) \times \\
&\times \left[-\frac{4+3\epsilon}{2\epsilon^2} \left[\left(\frac{-\mu^2}{s_{12}} \right)^\epsilon + \left(\frac{-\mu^2}{s_{23}} \right)^\epsilon \right] \right. \\
&\quad + \left(\ln^2 \frac{s_{12}}{s_{23}} + \pi^2 \right) \left(1 - \frac{3}{2} \frac{s_{12}s_{23}}{s_{13}^2} \right) \\
&\quad \left. + \frac{3}{2} \frac{s_{12}}{s_{13}} \left(1 - \frac{s_{23}}{s_{12}} \right) \ln \frac{s_{12}}{s_{23}} + \frac{s_{12}}{2s_{13}} - 6 \right] \\
A_4^{N=1}(1_{\bar{q}}^-, 2_q^+, 3^-, 4^+) &= A_4^s(1_{\bar{q}}^-, 2_q^+, 3^-, 4^+) = 0,
\end{aligned} \tag{3.213}$$

¹⁸ $g^*g^+g^+$ has already been presented ion the precedent result, and $g^*g^+g^-$ can simply be obtained from $g^*g^+g^+$ by using parity (see Eq. (3.57)).

with the tree level amplitude :

$$A_4^{tree}(1_{\bar{q}}^-, 2_q^+, 3^-, 4^+) = i \frac{\langle 13 \rangle^3 \langle 23 \rangle}{\langle 12 \rangle \langle 23 \rangle \langle 34 \rangle \langle 41 \rangle}. \quad (3.214)$$

We can now apply the auxiliary parton method, which leads to (we have used Eq. (3.96)) :

$$A_{4;1}(1_{\bar{q}}^-, 2_q^+, 3^-, 4^+) \underset{\Lambda\text{-presc.}}{=} -ix|k_\perp|g_s^3 \frac{c_\Gamma \langle p3 \rangle^3}{\kappa^* \langle 34 \rangle \langle p4 \rangle} \left(\frac{-\mu^2}{k_\perp^2} \right)^\epsilon \times \left[\begin{aligned} & \frac{-1}{\epsilon^2} \left(3 - \frac{1}{N_c^2} \right) - \frac{3}{2\epsilon} \left(1 - \frac{1}{N_c^2} \right) \\ & - \frac{2}{\epsilon} \ln \frac{k_\perp^2}{2\Lambda k_{3-}} + \pi^2 - \frac{5}{2} + \frac{7}{2N_c^2} \end{aligned} \right] \quad (3.215)$$

$$A_{4;3}(1_{\bar{q}}^-, 2_q^+, 3^-, 4^+) \underset{\Lambda\text{-presc.}}{=} -ix|k_\perp|g_s^3 \frac{c_\Gamma \langle p3 \rangle^3}{\kappa^* \langle 34 \rangle \langle p4 \rangle} \cdot \frac{-2 \ln(-1)}{\epsilon} \left(\frac{-\mu^2}{k_\perp^2} \right)^\epsilon \quad (3.216)$$

Comparing this result to Lipatov high energy action (see Eq. (3.147)) we see that the results differ, with no relation between the regulator Λ and r that would let these results match. Actually, from a diagrammatic point of view, it isn't surprising. Indeed, when looking at the loop diagrams contributing to $\bar{q}^- q^+ g^- g^+$, we observe diagrams that, even considering the auxiliary parton in the eikonal approximation, has no equivalent in $Rg^- g^+$. This stressed the difference in the regularization of the rapidity divergences between these two approaches. Actually, we will see in the next section that, to apply properly the auxiliary parton method at loop-level, we should refine the factorization formula for NLO calculation (in particular, by defining IR subtraction scheme).

To use auxiliary gluons, we need the following amplitude :

$$A_4^g(1^-, 2^+, 3^-, 4^+) = c_\Gamma A_4^{tree} \left[-\frac{2}{\epsilon^2} \left[\left(\frac{-\mu^2}{s_{12}} \right)^\epsilon + \left(\frac{-\mu^2}{s_{23}} \right)^\epsilon \right] + \ln^2 \frac{s_{12}}{s_{23}} + \pi^2 \right]$$

$$A_4^{N=1}(1^-, 2^+, 3^-, 4^+) = c_\Gamma A_4^{tree} \left[\frac{-1}{2\epsilon} \left[\left(\frac{-\mu^2}{s_{12}} \right)^\epsilon + \left(\frac{-\mu^2}{s_{23}} \right)^\epsilon \right] - 2 \right. \\ \left. - \frac{s_{12}s_{23}}{2s_{13}^2} \left(\ln^2 \frac{s_{12}}{s_{23}} + \pi^2 \right) + \frac{s_{12} - s_{23}}{2s_{13}} \ln \frac{s_{12}}{s_{23}} \right] \quad (3.217)$$

$$A_4^s(1^-, 2^+, 3^-, 4^+) = c_\Gamma A_4^{tree} \left[\frac{1}{6\epsilon} \left[\left(\frac{-\mu^2}{s_{12}} \right)^\epsilon + \left(\frac{-\mu^2}{s_{23}} \right)^\epsilon \right] + \frac{8}{9} \right. \\ \left. + \frac{s_{12}s_{23}}{s_{13}^2} \left[\frac{s_{12}s_{23}}{s_{13}^2} \left(\ln^2 \frac{s_{12}}{s_{23}} + \pi^2 \right) \right] \right. \\ \left. - \frac{s_{12} - s_{23}}{s_{13}} \left(1 + \frac{s_{13}^2}{6s_{12}s_{23}} \right) \ln \frac{s_{12}}{s_{23}} - 1 \right],$$

which leaves, after applying the Λ prescription :

$$\begin{aligned}
A_{4;1}(1^-, 2^+, 3^-, 4^+) \Big|_{\Lambda\text{-presc.}} &= -ix|k_\perp|g_s^3 \frac{c_\Gamma \langle p3 \rangle^3}{\kappa^* \langle 34 \rangle \langle p4 \rangle} \left(\frac{-\mu^2}{k_\perp^2} \right)^\epsilon \times \\
&\times \left[-\frac{4}{\epsilon^2} + \frac{1}{\epsilon} \left(-\frac{11}{3} + \frac{n_s + 2n_f}{3N_c} - 2 \ln \frac{k_\perp^2}{2\Lambda k_{3-}} \right) \right. \\
&\quad \left. + \pi^2 - \frac{64}{9} + \frac{8n_s + 10n_f}{9N_c} \right]
\end{aligned} \tag{3.218}$$

Then, the difference between auxiliary quarks and auxiliary gluons (for $n_s = 0$) reads :

$$\begin{aligned}
A_{4;1}(1_{\bar{q}}^-, 2_q^+, 3^-, 4^+) - A_{4;1}(1^-, 2^+, 3^-, 4^+) \\
&= \Big|_{\Lambda\text{-presc.}} ix|k_\perp|g_s^3 \frac{c_\Gamma \langle p3 \rangle^3}{\kappa^* \langle 34 \rangle \langle 4p \rangle} \left[\frac{1}{\epsilon^2} + \frac{113}{\epsilon} + \frac{83}{18} + \frac{1}{N_c^2} \left(\frac{1}{\epsilon^2} + \frac{3}{2\epsilon} + \frac{7}{2} \right) \right. \\
&\quad \left. - \frac{n_f}{N_c} \left(\frac{2}{3\epsilon} + \frac{10}{9} \right) \right]
\end{aligned} \tag{3.219}$$

So, the equivalence between using auxiliary quarks or auxiliary gluons also breaks. Besides, other (unpublished yet) calculations exhibit the same difference.

3.4 Loop-level hybrid factorization

The differences observed between high-energy Lipatov effective action and the Λ -prescription at loop-level are not really surprising, the regularization of the rapidity divergences being different. In fact, using the Λ -prescription at loop-level implies a refinement of the high energy hybrid factorization scheme used, as recently proposed in [102] (that we briefly summarize here). In particular, the dipole subtraction, as presented in Sec. 3.1.7, does not hold when using the auxiliary parton model at NLO, due to so-called *unfamiliar* real and virtual contribution. The former appears due to the possibility that the radiative gluon takes an important momentum component p in the limit $\Lambda \rightarrow +\infty$. The unfamiliar virtual correction is, on its side, due to the anomalous integrals presented in Sec. 3.2.2. The interesting point is that these contributions only depend on the choice of auxiliary momenta. Then, the Λ dependence of the one-loop partial amplitudes using either auxiliary partons (quarks or gluons) has been determined

in [102] and follow :

$$\begin{aligned}
A_{aux-g}^{(1)} &= A^{(1)} + c_{\Gamma} A^{tree} \left(\frac{-\mu^2}{k_{\perp}^2} \right)^{\epsilon} \left[\frac{1}{\epsilon} (2 \ln \Lambda - i\pi) - \frac{1}{\epsilon^2} + \frac{\pi^2}{3} \right], \\
A_{aux-q}^{(1)} &= A^{(1)} + c_{\Gamma} A^{tree} \left(\frac{-\mu^2}{k_{\perp}^2} \right)^{\epsilon} \left[\frac{1}{\epsilon} (2 \ln \Lambda - i\pi) + \frac{1}{\epsilon} \frac{13}{6} + \frac{\pi^2}{3} + \frac{83}{18} \right. \\
&\quad \left. + \frac{1}{N_c^2} \left(\frac{1}{\epsilon^2} + \frac{3}{2\epsilon} + \frac{7}{2} \right) - \frac{n_f}{N_c} \left(\frac{2}{3\epsilon} + \frac{10}{9} \right) \right],
\end{aligned} \tag{3.220}$$

such that :

$$A_{aux-q}^{(1)} - A_{aux-g}^{(1)} = c_{\Gamma} A^{tree} \left(\frac{-\mu^2}{k_{\perp}^2} \right)^{\epsilon} \left[\frac{1}{\epsilon^2} + \frac{1}{\epsilon} \frac{13}{6} + \frac{83}{18} + \frac{1}{N_c^2} \left(\frac{1}{\epsilon^2} + \frac{3}{2\epsilon} + \frac{7}{2} \right) - \frac{n_f}{N_c} \left(\frac{2}{3\epsilon} + \frac{10}{9} \right) \right], \tag{3.221}$$

which justifies the observation of Eq. (3.219). Then, when applying the auxiliary parton method at NLO, one should subtract to the obtained amplitude the second term in the r.h.s of Eq. (3.220) (choising the one corresponding to the auxiliary parton used) to get IR-subtracted amplitudes.

3.5 Chapter summary

In this chapter, we introduced a broad set of tools useful to calculate amplitudes. The simplicity of these amplitudes contrasts with the extreme complexity of their description through Feynman diagrams which makes them an important subject of study. A lot of work is put into simplifying their calculation based on their properties and the methods mentioned in Sec. 3.1 are relatively basic ones (but powerful). The evaluation of the higher order corrections to QCD amplitudes is needed for precision calculation of the QCD noise in collision hence for precision collider physics. This is also the case in small-x physics, for which the special kinematics (the multi-Regge kinematics) demands the construction of off-shell amplitudes. Calculation of such objects is usually done through the use of Lipatov's high energy effective action, an effective theory suitable for this kinematics. However, while on-shell amplitudes are well known at NLO, only a few processes have been calculated with Lipatov's high energy effective action at NLO. Then, having a method to extract an off-shell amplitude from an on-shell one seems very appealing. This justifies the interest of the auxiliary parton method, as we presented it. However, this method was only proven for tree-level calculation. The goal of the work presented in this chapter was to perform the first steps towards the generalization of the auxiliary parton method at loop level. We have successfully calculated the loop amplitude for one off-shell gluon and any number of plus helicity gluons and proven

its proper on-shell limit. On the other hand, we also have observed its limits when it has to deal with virtual poles (loop integration). Also, this problem has been solved (in parallel to the work of this thesis) and it opens the path to new possible plans : determination of an NLO k_T -factorization formula (for two off-shell gluons), addressing off-shell quarks and ultimately automatize the NLO calculations in k_T -factorization as well as the small- x improved TMD factorization (ITMD) [199, 200].

Chapter 4

Jets in heavy ion collisions

In this chapter, we will be interested in the evolution of jets, initiated by a parton coming from the hard scattering, in a dense medium. Indeed, in heavy-ion collisions, a **Quark-Gluon Plasma (QGP)** is formed and it will influence the jet evolution.

But first, in Sec. 4.1, we will have a closer look at jets and how they are defined both theoretically and experimentally. Then we will overview their evolution in vacuum before studying the medium influence on this evolution. This will lead us to the **BDMPS-Z** formalism presented in Sec. 4.2. This formalism sets how jets interact with the **QGP**. Then, it is possible, with some simple medium model, to derive evolution equations for jets in a **QGP**, the **BDIM** equations. These equations have been derived for gluon-dominated cascades and we will generalize them to the case where both quarks and gluons are present in the parton shower (see Sec. 4.3.2).

In the following, we present 2 methods to solve the **BDIM** equations : a **Monte-Carlo (MC)** approach (see Sec. 4.4.2) and a semi-analytical approach based on Chebyshev polynomials (see Sec. 4.4.3).

Ultimately, we present and study the solutions of the different versions of the **BDIM** equation presented (in Sec. 4.5).

Remark : In this chapter, we will use bold letters to label transverse momenta (instead of using the index “ \perp ”).

Contents

4.1	Jet physics	125
4.2	BDMPS-Z formalism	131
4.2.1	Collision kernel	134
4.2.2	Splitting kernel	137
4.3	BDIM equations	143
4.3.1	Pure gluons	143
4.3.2	System of equations	145
4.3.3	Energy distribution	148

4.3.4	Approximations	150
4.4	Resolution of the BDIM equations	154
4.4.1	Analytical solution	155
4.4.2	Resolution with Monte-Carlo approach	155
4.4.3	Resolution with Chebyshev method	160
4.5	Solutions of the BDIM equations	174
4.5.1	Results for the pure gluon case	176
4.5.2	Results for the system case	182
4.6	Chapter summary	192

4.1 Jet physics

Due to color confinement, we do not have direct access to the hard partons produced in the hard scattering. Indeed, those partons evolve from the hard scale to the hadronization scale (around 1GeV) by the emission of partons (gluons or quark-antiquark pairs), themselves initiating radiations. This series of radiation is called *parton shower* (or cascade). Then, all the partons produced in the shower hadronize. The produced hadrons are often unstable and eventually decay into stable and metastable hadrons (mainly pions in high-energy hadronic collisions). To study the hard parton (i.e energetic) initiating a shower, we introduce what we call a jet. A jet will link the hard parton (as described in the final state of the scattering amplitude) to what we actually observe in our detectors : a bunch of hadrons. Hopefully, what we really observe at high energy are collimated particles (hadrons). This is because of color coherence, the successive emission in a shower are ordered in angle (this can be seen through the soft and collinear divergences of the splitting functions). Then, it is natural to define a jet as a group of observed particles, that we can set inside a cone, with the initial hard parton as the rotation axis. This is one possible definition of a jet which is, in all generality, a way to cluster observed particles in a detector event (a collision) such that they can be interpreted as the result of the cascade of one hard parton (and can then be used as proxies of this parton). The idea is to simplify the problem of describing the initial partons through the properties of a single object, the jet, instead of numerous particles (and their kinematics). Studying jets and their physics permit also to recognize detector events in terms of their underlying hard process (and so, to select and class events of interest observed in a detector...). The way we characterize and define a jet, in other words how we cluster final hadrons and how we combine momenta inside it, is called *jet algorithm*. A jet algorithm must be simple to implement in experimental analysis but also in theoretical calculations. It has to be sensitive to the initial parton (its nature and dynamics)¹. This implies that a jet should not be sensitive to hadronization nor to showering (i.e it should be soft and collinear safe²). Also, depending on our jet definition, we might account for losses due to hadrons or radiations going outside our jet (while initiated by the same hard parton) and for contamination (from other final state parton shower, initial state parton shower, or underlying event).

Before entering the main jet algorithms, we should introduce some kinematics variables. To a particle with 4-momentum $p = (E, p_x, p_y, p_z)$ and mass m , we associate the rapidity y and the transverse mass m_t defined as :

$$y = \frac{1}{2} \ln \frac{E + p_z}{E - p_z}, \quad m_t = \sqrt{m^2 + p_t^2}, \quad (4.1)$$

where $\phi = \arctan \frac{p_y}{p_x}$ is the azimuth and $p_t = \sqrt{p_x^2 + p_y^2}$ the transverse momentum. It leads to $p = (m_t \cosh y, p_t \cos \phi, p_t \sin \phi, m_t \sinh y)$. It is also usual to define the pseudo-

¹Because we use it as a proxy of this hard parton.

²Adding a collinear or a soft radiation to an event should not change how hadrons are clustered in this event

rapidity η as :

$$\eta = -\ln \tan \frac{\theta}{2} = \frac{1}{2} \ln \frac{|p| + p_z}{|p| - p_z}, \quad (4.2)$$

where $\theta = \arccos \frac{p_z}{|p|}$ is the polar angle. For massless particles, $\eta = y$.

Jets and angular ordering

As already mentioned, the idea of clustering hadrons into jets comes from the experimental observation of collimated hadrons in high-energy collisions. This idea is also justified by the theory (QCD, but that's actually a feature of QFT). Let's consider as an illuminating example with the amplitude $\gamma^* \rightarrow \bar{q}q$:

$$\mathcal{M}_{\bar{q}q} = -\bar{u}(p_1) e_q \gamma^\mu v(p_2). \quad (4.3)$$

Then, if we consider the final state emission of a gluon of momentum k , polarization vector ϵ and color a (like the first emission in a final state shower that gives rise to a jet), we have to consider the amplitude :

$$\mathcal{M}_{\bar{q}qg} = \bar{u}(p_1) i g_s \not{\epsilon} t^a \frac{i}{\not{p}_1 + \not{k}} i e_q \gamma^\mu v(p_2) - \bar{u}(p_1) i e_q \gamma^\mu \frac{i}{\not{p}_2 + \not{k}} i g_s \not{\epsilon} t^a v(p_2). \quad (4.4)$$

Once squared (implying the sum over polarization and color of the emitted gluon), this amplitude factorized in $\mathcal{M}_{\bar{q}q}^2$ and a soft factor as :

$$|\mathcal{M}_{\bar{q}qg}|^2 = |\mathcal{M}_{\bar{q}q}|^2 C_F g_s^2 \frac{2p_1 \cdot p_2}{(p_1 \cdot k)(p_2 \cdot k)} = |\mathcal{M}_{\bar{q}q}|^2 C_F g_s^2 \frac{1}{E^2 (1 - \cos^2 \theta)}. \quad (4.5)$$

This factorization hold when we consider also the phase space :

$$d\phi_{\bar{q}qg} |\mathcal{M}_{\bar{q}qg}|^2 = d\phi_{\bar{q}q} |\mathcal{M}_{\bar{q}q}|^2 \frac{d^3 k}{2E(2\pi)^3} C_F g_s^2 \frac{1}{E^2 (1 - \cos^2 \theta)} = d\phi_{\bar{q}q} |\mathcal{M}_{\bar{q}q}|^2 d\mathcal{S}, \quad (4.6)$$

with the soft factor :

$$d\mathcal{S} = \frac{d^3 k}{2E(2\pi)^3} C_F g_s^2 \frac{1}{E^2 (1 - \cos^2 \theta)} = \frac{2\alpha_s C_F}{\pi} \frac{dE}{E} \frac{d\theta}{\sin \theta} \frac{d\phi}{2\pi}. \quad (4.7)$$

This soft factor is general to the emission of a gluon from a quark pair. For a gluon pair emitting a gluon, only the color factor C_F would change for $C_A = N_c$. In any case, the emission probability is enhanced³ in both the collinear limit (where $\theta \rightarrow 0$) and the soft limit (where $E \rightarrow 0$). This means that, in vacuum, the partons in a cascade will be ordered in angle, leading to a collimated cascade of partons that can be identified as a jet.

We should also mention that the jets follow, in vacuum the DGLAP equation to evolve from the hard scale of the collision to the soft scale of hadronization (a backward evolution compared to the initial state one).

³It is actually divergent, but compensated by virtual corrections.

Jet algorithms

A jet algorithm is an algorithm that takes a set of (hadron) momenta $\{p_i\}$ (describing an event) to produce a set of jets $\{j_i\}$. As mentioned, the first idea to define a jet, based on the fact that branching doesn't modify the energy flow's direction (i.e angular ordering), is to cluster final hadrons in cones defined by a radius R^4 in the rapidity-azimuth plane (y, ϕ) . This class of jet algorithms is called *cone algorithms* [201]. After choosing some cone size, the first step is to order the hadrons $\{p_i\}$ in an event according to their transverse momentum. A cone is centered on the hardest particle, called seed (s). Then, all particles in the cone, i.e the particles i that verify $\Delta R_{is} = (y_i - y_s)^2 + (\phi_i - \phi_s)^2 < R$ are associated to this cone. The procedure is repeated till there is no hadron left and if two cones overlap, they are merged.

Unfortunately, this procedure is not soft nor collinear safe. Indeed; when you add a soft emission between two hard hadrons, the associated cones could merge. Also, if one of the hardest particles is split into 2 collinear radiation, then the associated cone could move to a nearby less hard hadron. This algorithm has been improved with the concept of *stable cone*. Once a cone is set, all the 4-momenta of the particles inside the cone are summed to verify that they point to the center of the cone. If it is the case, the cone is stable and the procedure continues the same way as previously. If not, then, the cone is re-centered in the direction pointed (and the procedure repeats). However, this improvement does not solve the problems of soft and collinear safety.

The other main class of jet algorithms are the *sequential recombination algorithms*. They try to reconstruct, backward, the branching process. They all follow the same principle :

- Compute all distances between particles d_{ij} and all distances between a particle and the beam axis d_{iB} .
- Find the smallest distance in $\{d_{ij}\} \cup \{d_{iB}\}$
 - if it is d_{ij} , merge i and j into a proto-jet $p_{(ij)}$ and combine momenta $p_{(ij)}^\mu = p_i^\mu + p_j^\mu$,
 - if it is d_{iB} , remove i from the set $\{p_i\}$ and place it in the set of jets $\{j\}$ ⁵.
- Return to step 1 as long as $\{p_i\}$ is not empty.

So basically, this algorithm sorts all hadrons by distances (between them and with the beam axis) and considers that the nearest particles come from a branching. Of course, the notion of jet is then highly dependent on the notion of distance used. One could think of the invariant $s_{ij} = p_i \cdot p_j$, but this doesn't work well. Actually, to recover the

⁴Which is actually the angular reach of the cone.

⁵Instead of using the distance to the beam axis, it is also possible to impose a higher threshold in the distance [202].

branching process, the distance should be based on the properties of this branching. Let's recall the emission probability in the soft and collinear limit (noted $S\&C$) :

$$\begin{aligned} d\omega_{g\rightarrow gg}^{S\&C} &= \frac{2\alpha_s}{\pi} C_F \frac{dE}{E} \frac{d\theta}{\theta} \frac{d\phi}{2\pi}, \\ d\omega_{q\rightarrow qg}^{S\&C} &= \frac{2\alpha_s}{\pi} C_A \frac{dE}{E} \frac{d\theta}{\theta} \frac{d\phi}{2\pi}. \end{aligned} \quad (4.8)$$

Then, when the soft particle isn't determined (between 2 emission i and j), we need to rewrite $\frac{dE}{E} \frac{d\theta}{\theta} \rightarrow \frac{dE_i}{\min(E_i, E_j)} \frac{d\theta_{ij}}{\theta_{ij}}$. It leads to define the distance $d_{ij} = \frac{2}{Q^2} \min(E_i, E_j) \theta_{ij}$ [202]

that reduces (modulo normalization) in the collinear limit to $d_{ij} = \min(p_{i,t}^2, p_{j,t}^2) \frac{\Delta R_{ij}^2}{R^2}$ [203, 204], where R is a parameter (whose role is similar to the radius in the cone algorithms). The distance to the beam is then defined as $d_{iB} = p_{i,t}^2$. This distance is used in the so-called k_t -algorithm. The problem with it is that it clusters soft radiation first, hence it is not soft-safe. Also, it leads to irregular shapes that complicate calibration.

The previous algorithm can be generalized by introducing the distance :

$$\begin{aligned} d_{ij} &= \min(p_{i,t}^{2\alpha}, p_{j,t}^{2\alpha}) \frac{\Delta R_{ij}^2}{R^2}, \\ d_{iB} &= p_{i,t}^{2\alpha}. \end{aligned} \quad (4.9)$$

Different choices for α have been used. For $\alpha = 1$, we recognize k_t -algorithm. $\alpha = 0$ correspond to the *Cambridge/Aachen algorithm* [205, 206], where is only left the geometrical dependency. Finally, the most used jet algorithm nowadays is the so-called *anti- k_t algorithm* [207, 208], where α is set to -1 ⁶ (it is implemented in the `FastJet` package [209, 210]). This might be counter-intuitive but, by clustering hard hadron first, it leads to round-shaped jets (like with cone algorithm) and it is collinear and soft safe! The anti- k_t algorithm is then both easy to calibrate on the experimental side and suitable for theoretical calculations since it tries to reconstruct the successive branching appearing in the parton shower. A comparison of the results of the use of the k_t , Cambridge/Aachen, anti- k_t and a cone algorithm (named `SISCone` [211]) is shown in Fig. 4.1 (taken from [208]).

Jet and QGP

While jets are well described by (vacuum) parton shower in the case of pp collisions, it has been observed that, in heavy-ion collisions, high- p_t jets are suppressed [212–218]. This is particularly clear in some back-to-back dijet events where one jet is strongly suppressed compared to the other, as shown in Fig. 4.2 (where are presented 2 back-to-back dijet events, one for pp collision one for PbPb collision, both from the `CMS` experiment).

This suppression, named *jet quenching*, is understood as the result of the interaction between the jet and the medium formed during the collision. Indeed, contrary to pp

⁶It means that, instead of defining your distance according to the emission probability of Eq. (4.8), you consider the angular distance scaled (divided) by the energy of the hardest of the two partons.

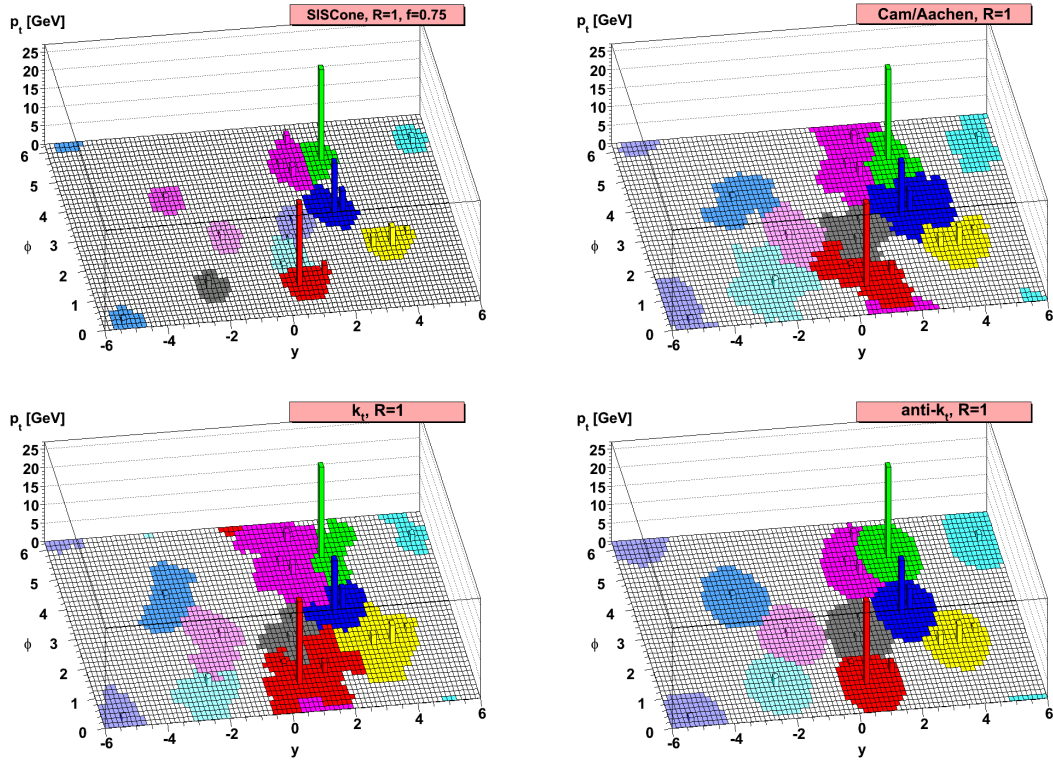


Figure 4.1: Jets obtained, from the same event, in the (y, ϕ) plane, by several jet algorithms : SIScone (top left), Cambridge/Aachen (top right), k_t (bottom left) and anti- k_t (bottom right) algorithms (from [208]).

collisions, heavy-ion collisions involve the formation of a highly dense and hot state of matter, the QGP [221]. QGP is a state, predicted by asymptotic freedom, of highly dense nuclear matter made of deconfined quarks and gluons (a color plasma). It appears not only in heavy-ion collisions but also in neutron stars and it describes the matter a few microseconds after the Big Bang. A phase diagram of QCD is depicted in Fig. 4.3 (from [222]), showing the phase transition between ordinary hadron phase and QGP (in the temperature / baryon density plane).

Also studying it may lead us to a better understanding of quarks and gluon confinement. Then, the jet can be used as a hard probe of the QGP, and investigating their interactions is a key to understand QGP (an overview on jet quenching is given in [223]). Jet quenching is explained mainly by energy loss through two processes, elastic and inelastic collisions with the medium constituents. The former process is also called *collisional energy loss* (first proposed by Bjorken [224], the model has been improved in [225–229]) where it is usual to consider heavy scattering centers (i.e neglecting recoils effects). The latter is called *radiative energy loss* and consists of multiple scattering with the medium constituent leading to (induced) radiations transporting a fraction of the

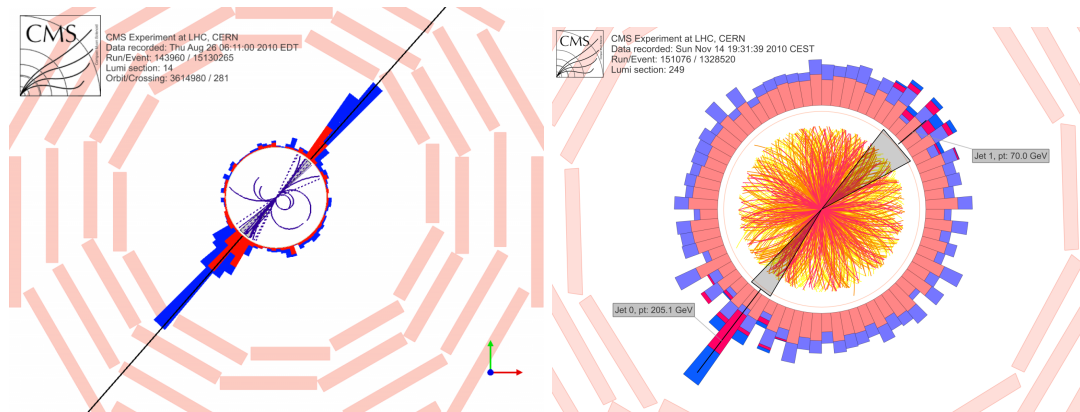


Figure 4.2: Back to back dijet event from CMS in pp collision (left, taken from [219]) and in PbPb collision (right, taken from [220]).

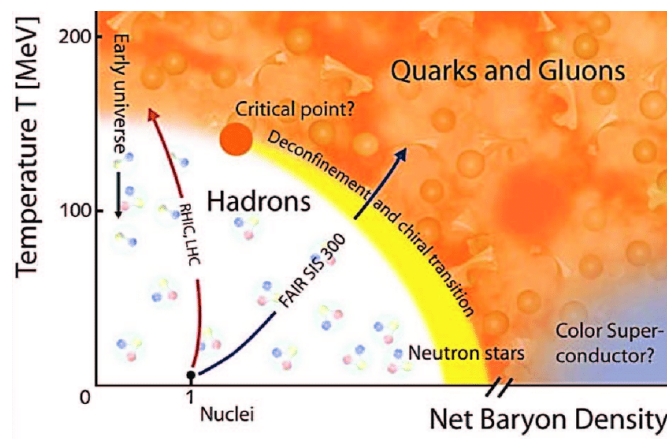


Figure 4.3: The QCD phase diagram (from [222]).

initial parton energy outside the jet (breaking the angular ordering of vacuum cascades). Radiative energy loss in QCD are the equivalent of Lando-Pomeranchuk-Migdal (PLM) effect [230, 231] in QED which states that the bremsstrahlung spectrum of a highly relativistic particle in dense media is suppressed (as compared to the Bethe-Heitler spectrum [232], where incoherent rescattering is assumed) by interference appearing in multiple medium scattering. Several models exist for the QCD equivalent and we will study the very first one formulated : the Baier-Dokshitzer-Mueller-Peigne-Schiff Zakharov (BDMPS-Z) formalism [233–237]. It is based on a path-integral formulation of the multiple (resummed) scattering on heavy and static color centers. Other standing out formalisms include Armesto-Salgado-Wiedemann (ASW) [238–242], Gyulassy-Levai-Vitev (GLV) [243–246], Arnold-Moore-Yaffe (AMY) [247–249] and Higher-Twist (HT) [250–254]. These models may differ in their treatment of the in-medium splitting of the hard parton, their description of the medium, and by the assumed kinematics of

the medium-parton interaction. A detailed comparison of these models is given in [255].

4.2 BDMPS-Z formalism

In this section, we will set up the next calculations by introducing useful notions and results from the BDMPS-Z formalism [256, 257]. In particular, we will introduce the splitting function (that are altered by the medium), as presented in [258] (going actually beyond one of the hypotheses of the BDMPS-Z formalism).

In this model, the medium is viewed as a collection of static scattering colored centers characterize by their density n along the (hard) parton path (this density may vary along this path, in particular, a decreasing density would reflect the medium expansion). The recoils of the scattering centers are neglected hence there is no collision energy loss in this model. Also, the interaction of both the hard parton and its radiations to the medium are considered eikonal. This means that partons propagate at a fixed transverse position. This translates, for a parton of energy E emitting a parton of energy ω and exchanging a transverse momentum q_\perp with the medium as :

$$E \gg q_\perp, \quad \omega \gg k_t. \quad (4.10)$$

In other words, the radiations are considered collinear. For an emitted parton of energy ω and transverse momentum k_t ⁷, it means :

$$\omega \gg q_\perp. \quad (4.11)$$

Then, when a high energy parton (of energy ω and transverse momentum k_\perp) propagates through the QGP, it can radiate parton over a typical time scale :

$$\tau_f \sim \frac{2\omega}{k_\perp^2}. \quad (4.12)$$

τ_f is called the *formation time*. Its inverse represents the energy required to set it on-shell. This energy is gained through multiple scattering with the medium constituents. Also, the most important parameter of the BDMPS-Z formalism is the transport coefficient that measures the transverse momentum Δk_\perp^2 accumulated by a parton when passing through a length Δl of medium. It is called the *quenching parameter* :

$$\hat{q} = \frac{\Delta k_\perp^2}{\Delta l}, \quad (4.13)$$

which can equivalently be written in terms of the time passed in the medium Δt : $\hat{q} = \frac{\Delta k_\perp^2}{\Delta t}$ (since we are working in natural units). Then, it is possible to evaluate the

⁷The index t refers to the transverse plane of the parent parton (while \perp is used for the transverse plane of the beam axis / the initial hadron direction).

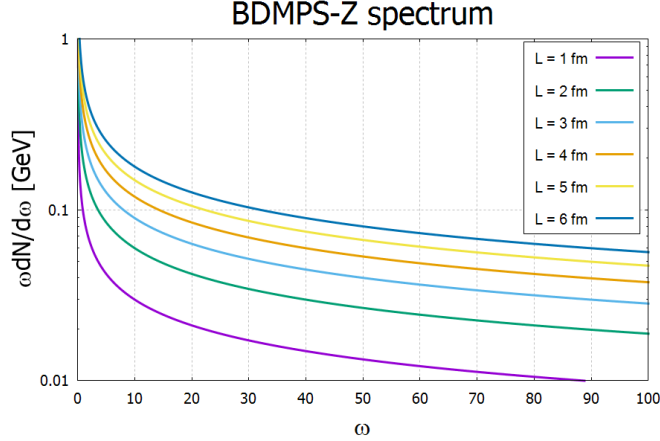


Figure 4.4: BDMPS-Z energy spectrum for $\bar{\alpha} = 0.3$, $\hat{q} = 1 \text{ GeV}^2/\text{fm}$ for different medium length ($L \in \{1, 2, 3, 4, 5, 6\}$ fm).

time scale for in-medium splitting (or branching) as the formation time that verifies Eq. (4.13) (identifying Δt with τ_l and Δk_{\perp}^2 with $2\omega/\tau_f$) :

$$\tau_{br}(\omega) \sim \sqrt{\frac{2\omega}{\hat{q}}}. \quad (4.14)$$

The related typical transverse momentum acquired during τ_{br} is then $k_{br}^2 = \hat{q}\tau_{br} = (2\omega\hat{q})^{1/4}$. We can also evaluate a typical emission angle $\theta_{br} \sim \frac{k_{br}}{\omega}$, learning us that the softer the parton the larger is its emission angle. This emission angle has minimum fixed by $\tau_{br} = L$ at $\theta_c = (\hat{q}L^3)^{-1/2}$ (where L is the length of the medium). Then, the BDMPS-Z energy spectrum of radiated gluons follows :

$$\omega \frac{dN}{d\omega} \simeq \bar{\alpha} \sqrt{\frac{\omega_c}{\omega}} = \bar{\alpha} \sqrt{\frac{L}{\tau_{br}(\omega)}}, \quad (4.15)$$

where N is the number of radiated gluons, $\tau_{br}(\omega_c) \sim L$ and $\bar{\alpha} = \frac{\alpha_s N_c}{\pi}$. This spectrum (illustrated in Fig. 4.4) holds for $\omega \lesssim \omega_c$. But, when $\tau_{br}(\omega)$ is of the order of the mean free path λ the radiations are in fact produced by incoherent collision (multiple scattering is negligible) and the above spectrum should then be replaced by the Bethe-Heitler (bremsstrahlung) spectrum [232]. We characterize this limit by the frequency ω_{BH} (such that $\tau_{br}(\omega) \sim \lambda$). So, to consider medium-induced radiations, we need $\omega_{BH} \ll \omega \lesssim \omega_c$. In this range, the number of scattering centers coherently participating in the emission is large (as $\frac{\tau_{br}(\omega)}{\lambda} \gg 1$). We can translate this condition over energy into a condition on transverse momentum exchange by introducing the Debye (screening) mass that characterizes the collision with a screened one parton exchange : $m_D^2 = \hat{q}\lambda$. Then $\omega_{BH} \ll \omega$ translates into $k_{br}^2 \gg m_D^2$. It is then possible to evaluate the energy loss as :

$$\Delta E = \int_{\omega_0}^{\omega_c} d\omega \omega \frac{dN}{d\omega} \sim \bar{\alpha} \hat{q} L^2. \quad (4.16)$$

This gives a simple estimation for the energy loss based on the intuitive parameter \hat{q} . Then, we can dwell on the average number of partons emitted, with an energy $\omega' \in [\omega, \omega_c]$:

$$\Delta N(\omega) = \int_{\omega}^{\omega_c} d\omega' \frac{dN}{d\omega'} \sim \bar{\alpha} \frac{L}{\tau_f(\omega)} 2. \quad (4.17)$$

For relatively hard emissions (say $\omega \gtrsim \bar{\alpha}\omega_c$), $\Delta N(\omega) \lesssim 1$, meaning that the probability of having multiple emissions is small. On the contrary, for relatively soft emissions ($\omega \lesssim \bar{\alpha}\omega_c \equiv \omega_s$), $\Delta N(\omega) \gtrsim 1$, and multiple emissions become important. Overall, it means that the regime where $\omega_{BH} \ll \omega \ll \omega_c$ is dominated by medium-induced radiations with an important contribution from multiple emissions. Finally, if we consider the probability of emitting one parton of energy $\omega \geq \omega_0$:

$$P(\Delta t; \omega_0) \sim \bar{\alpha} \frac{\Delta t}{\tau_{br}(\omega_0)}. \quad (4.18)$$

we can define the typical time interval $\tau_{rad}(\omega_0)$ that the a parton of energy ω does not radiate in the range $[\omega_0, \omega]$ as $P(\tau_{rad}(\omega_0); \omega_0) = 1$, leading to :

$$\tau_{rad}(\omega_0) = \frac{\tau_{br}(\omega_0)}{\bar{\alpha}} = \frac{1}{\bar{\alpha}} \sqrt{\frac{2\omega_0}{\hat{q}}}. \quad (4.19)$$

This means that the typical time interval between radiations in the cascade is larger than the formation time, hence that the successive emissions are independent (and color coherence is lost). In other words, the “single (medium-induced) splitting” can be used as a building block of the full cascade.

Now that the time scale considerations have been done, we need to better characterize the problem. We consider a hard relativistic gluon propagating in the z direction and, for simplicity, we consider only gluon radiations (quark will be reintroduced later). It travels through the QGP over a distance L , from time t_0 to time t_L . The medium is parametrized through a random color field \mathcal{A}_\perp^- (in the light-cone gauge $A^+ = 0$). Due to the eikonal approximation, the gluons couple only to the $-$ component of the gauge field which is probed only around x^- , justifying that we drop its x^- dependence. From now on, we will note t the light-cone time (i.e the x^+) and we will indicate transverse variables with bold letters the (i.e $x_\perp \rightarrow \mathbf{x}$). Assuming homogeneity in the transverse plane and a constant color charge density n (i.e a static medium), we can describe this medium field through a correlation function γ verifying :

$$\langle A_a^-(\mathbf{q}, t) A_b^{\dagger -}(\mathbf{q}', t') \rangle = n \delta_{ab} \delta(t - t') (2\pi)^2 \delta^{(2)}(\mathbf{q} - \mathbf{q}') \gamma(\mathbf{q}), \quad (4.20)$$

where the angle brackets denotes the *medium average*. As an example, the correlation function can be written, for a QGP at equilibrium (we will come back to the medium model used in a few steps) using the screened Coulomb propagator $\frac{1}{(\mathbf{q}^2 + m_D^2)^2}$ with :

$$\gamma(\mathbf{q}) = \frac{g^2 n}{(\mathbf{q}^2 + m_D^2)^2}. \quad (4.21)$$

The gluon propagator G , in presence of the background field A^- verifies the equation [259, 260] :

$$\left[2\partial_x^+ \mathcal{D}_x^- - \nabla_\perp^2\right]_{ac} G_{cb}(x, y) = \delta_{ab} \delta(x - y), \quad (4.22)$$

with $\mathcal{D}_x^- = \partial^- - igA^- \cdot T$.

Actually, due to the form of A^- (independent on x^-), it is convenient to introduce another Green function, \mathcal{G} through :

$$G_{ab}(x, y) = \int \frac{dk^+}{2\pi} e^{-ik^+(x^+ - y^+)} \frac{i}{2k^+} \mathcal{G}_{ab}(\mathbf{x}, x^+, \mathbf{y}, y^+; k^+). \quad (4.23)$$

\mathcal{G} satisfies the Schrödinger equation :

$$\left[i\mathcal{D}^- - \frac{\nabla_\perp^2}{2k^+}\right]_{ac} \mathcal{G}_{cb}(\mathbf{x}, x^+, \mathbf{y}, y^+) = i\delta_{ab} \delta(x^+ - y^+) \delta(\mathbf{x} - \mathbf{y}), \quad (4.24)$$

with $\mathcal{D}^- = i\partial^- + g_s A^-$.

\mathcal{G} can then be written in the form of a path integral :

$$\mathcal{G}(\mathbf{x}, x^+, \mathbf{y}, y^+) = \int_{\mathbf{r}(y^+) = \mathbf{y}}^{\mathbf{r}(x^+) = \mathbf{x}} \mathcal{D}\mathbf{r} \exp \left\{ i \frac{k^+}{2} \int_{y^+}^{x^+} dt \dot{\mathbf{r}}^2 \right\} \mathcal{U}(x^+, y^+; \mathbf{r}), \quad (4.25)$$

with $\mathcal{U}(x^+, y^+; \mathbf{r}) = T \exp \left\{ ig_s \int_{y^+}^{x^+} dt A_a^-(t, \mathbf{r}(t)) t^a \right\}$.

We will actually write it in momentum space as :

$$\mathcal{G}(\mathbf{k}, t, \mathbf{p}_0, t_0) = \int d\mathbf{x} d\mathbf{y} e^{-i\mathbf{k} \cdot \mathbf{y}} e^{-ip_0 \cdot \mathbf{x}} \mathcal{G}(\mathbf{x}, x^+, \mathbf{y}, y^+). \quad (4.26)$$

We are now set up for the calculation of the collision and in-medium splitting kernels needed to derive the [Blaizot-Dominguez-Iancu-Mehtar-Tani \(BDIM\)](#) equations in the next section. Also, the medium will be better characterized when studying scattering with the medium color charges.

4.2.1 Collision kernel

Let's now study in-medium multiple scattering by introducing the probability $P_1(k; t_L, t_0) d\Omega_k$ to observe a gluon at t_L with momentum in the phase space element $d\Omega_k$ while it was in $d\Omega_{p_0}$ at time t_0 (with energy p_0^+ , that we may also note E). The invariant phase space element reads :

$$d\Omega_k = \frac{d^2 \mathbf{k} dk^+}{(2\pi)^3 k^+}. \quad (4.27)$$

Also, with the conservation of the + component of the momentum, it is convenient to introduce \mathcal{P} as :

$$P_1(k; t_L, t_0) = 2p_0^+ 2\pi\delta(k^+ - p_0^+) \mathcal{P}(\mathbf{k}; t_L, t_0). \quad (4.28)$$

\mathcal{P} is then the probability, for gluon propagating in the medium, to acquire a transverse momentum $\mathbf{k} - \mathbf{p}_0$ during the time $t_L - t_0$. It is calculable as an amplitude squared, with the help of the propagator \mathcal{G} or more directly with the 2-point function $S^{(2)}$ (in momentum space) :

$$(2\pi)^2 \delta^{(2)}(\mathbf{p}_0 - \bar{\mathbf{p}}_0) \mathcal{P}(\mathbf{k} - \mathbf{p}_0; t_L, t_0) = S^{(2)}(\mathbf{k}, \bar{\mathbf{k}}, t_L; \mathbf{p}_0, \bar{\mathbf{p}}_0, t_0), \quad (4.29)$$

with $S^{(2)}(\mathbf{k}, \bar{\mathbf{k}}, t_L; \mathbf{p}_0, \bar{\mathbf{p}}_0, t_0) = \left\langle \mathcal{G}^\dagger(\bar{\mathbf{p}}_0, t_0, \bar{\mathbf{k}}, t_L) \mathcal{G}(\mathbf{k}, t_L, \mathbf{p}_0, t_0) \right\rangle,$

which is pictured in Fig. 4.5 where the amplitude is in blue and its complex conjugate in red. The notation \bar{a} indicates that a is in the complex conjugate part.

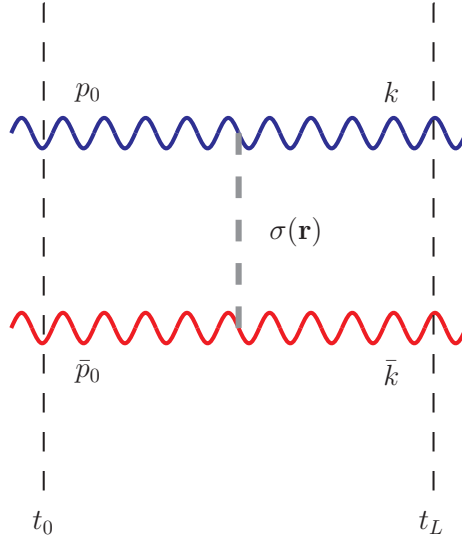


Figure 4.5: Illustration of the 2-point function $S^{(2)}$ with amplitude in blue and its complex conjugate in red. The grey dash line denotes the dipole involved in $S^{(2)}$.

The 2-point function can be evaluated, expressing the Green function with their path integral form and performing the medium average, as :

$$S^{(2)}(\mathbf{k}, \bar{\mathbf{k}}, t_L; \mathbf{p}_0, \bar{\mathbf{p}}_0, t_0) = (2\pi)^2 \delta^{(2)}(\mathbf{p}_0 - \bar{\mathbf{p}}_0) \int d^2\mathbf{r} e^{-i(\mathbf{k}-\mathbf{p}_0)\cdot\mathbf{r}} e^{-\frac{N_c n}{2}(t_L-t_0)\sigma(\mathbf{r})}, \quad (4.30)$$

with σ the *dipole cross section* defined as :

$$\sigma(\mathbf{r}) = 2g_s^2 \int \frac{d^2\mathbf{q}}{(2\pi)^2} \left(1 - e^{i\mathbf{q}\cdot\mathbf{r}}\right) \gamma(\mathbf{q}), \quad (4.31)$$

which Fourier transform reads :

$$\sigma(\mathbf{l}) = \int d\mathbf{r} e^{-i\mathbf{l}\cdot\mathbf{r}} \sigma(\mathbf{r}) = -2g_s^2 \left[\gamma(\mathbf{l}) - (2\pi)^2 \delta^{(2)}(\mathbf{l}) \int \frac{d^2\mathbf{q}}{(2\pi)^2} \gamma(\mathbf{q}) \right]. \quad (4.32)$$

It is usual to define the collision kernel \mathcal{C}_g , which describes transverse momentum broadening due to multiple scattering (without branching) as :

$$\mathcal{C}_g(\mathbf{l}) = -\frac{1}{2} N_c n \sigma(\mathbf{l}) = 4\pi\alpha_S N_c n \left[\gamma(\mathbf{l}) - (2\pi)^2 \delta^{(2)}(\mathbf{l}) \int \frac{d^2\mathbf{q}}{(2\pi)^2} \gamma(\mathbf{q}) \right], \quad (4.33)$$

such as (combining Eq. (4.29), Eq. (4.30) and Eq. (4.33)) :

$$\mathcal{P}(\mathbf{k} - \mathbf{p}_0; t_L, t_0) = \int d^2\mathbf{r} e^{-i(\mathbf{k}-\mathbf{p}_0)\cdot\mathbf{r} + (t_L-t_0)\mathcal{C}_g(\mathbf{l})}. \quad (4.34)$$

It is also usual to set the medium model in a function $w(\mathbf{q})$, the in-medium potential (as it would appear in the Hamiltonian of the problem), defined such that :

$$\mathcal{C}_g(\mathbf{l}) = \left[w(\mathbf{l}) - (2\pi)^2 \delta^{(2)}(\mathbf{l}) \int \frac{d^2\mathbf{q}}{(2\pi)^2} w(\mathbf{q}) \right], \quad (4.35)$$

meaning $w(\mathbf{l}) = 4\pi\alpha_S N_c n \gamma(\mathbf{l})$. For a weakly coupled QGP in thermal equilibrium at high temperature T , this function can be obtained from hard thermal loop calculation (out of the reach of this work) and reads [261] :

$$w(\mathbf{l}) = \frac{g_s^4 n N_c}{\mathbf{l}^2 (\mathbf{l}^2 + m_D^2)}. \quad (4.36)$$

The Debye mass m_D and the color charge density n can be related to the temperature of the medium through :

$$m_D^2 = \left(\frac{N_c}{3} + \frac{N_f}{6} \right) g^2 T^2, \text{ and } n = m_D^2 \frac{T}{g} \propto T^3, \quad (4.37)$$

where the coupling constant g is evaluated at the temperature of the medium. As already mentioned, we consider a constant color charge density, this can be understood also as keeping a constant temperature for the medium.

We will also be interested in the function w for out-of-equilibrium plasma (without screening) in the form :

$$w(\mathbf{l}) = \frac{g_s^4 n N_c}{\mathbf{l}^4}. \quad (4.38)$$

Back to \mathcal{P} , we see, deriving Eq. (4.34), that it follows the equation :

$$\frac{\partial}{\partial t} \mathcal{P}(\mathbf{k} - \mathbf{p}_0; t, t_0) = \int \frac{d^2\mathbf{l}}{(2\pi)^2} \mathcal{C}_g(\mathbf{l}) \mathcal{P}(\mathbf{k} - \mathbf{p}_0 - \mathbf{l}; t, t_0). \quad (4.39)$$

This equation will be useful in the derivation of the BDIM equations (in the next section).

4.2.2 Splitting kernel

Let's now have a look at the medium-induced splitting process for which we will actually go beyond the eikonal limit of the BDMPS-Z formalism (non-neglecting the transverse momentum transfer during splitting). Similarly to P_1 (Eq. (4.28)), we can define the probability $P_2(k_a, k_b; t_L, t_0) d\Omega_{k_a} d\Omega_{k_b}$ to observe 2 gluons at t_L (in the phase space elements $d\Omega_{k_a}$ and $d\Omega_{k_b}$ respectively) given a single gluon at t_0 (in $d\Omega_{p_0}$). The same way, we introduce \mathcal{P}_2 as :

$$P_2(k_a, k_b; t_L, t_0) = 2p_0^+ 2\pi\delta(k_a^+ + k_b^+ - p_0^+) \mathcal{P}_2(\mathbf{k}_a, \mathbf{k}_b, z; t_L, t_0). \quad (4.40)$$

This probability can be expressed in terms of n-point functions (their Fourier transform), when looking at the $1 \rightarrow 2$ amplitude between t_0 and t_L , as pictured in Fig. 4.6, where the splitting happens at t_1 in the amplitude and at t_2 in its complex conjugate.

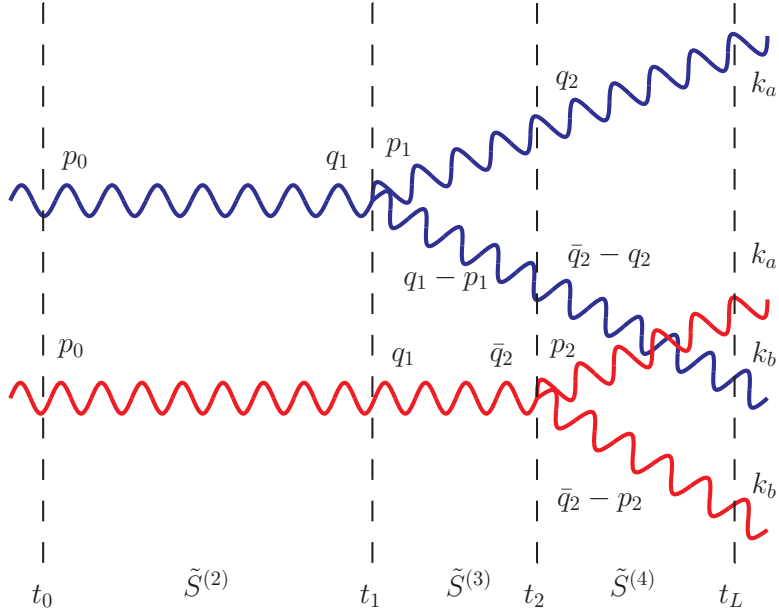


Figure 4.6: Illustration of the $1 \rightarrow 2$ in-medium amplitude, in blue, and its complex conjugate, in red with the regions described by $S^{(2)}$ ($[t_0, t_1]$), $S^{(3)}$ ($[t_1, t_2]$), $S^{(4)}$ ($[t_2, t_L]$).

Then, after summing over polarization and averaging over the azimuthal angle at the

vertices, \mathcal{P}_2 reads :

$$\begin{aligned}
\mathcal{P}_2(\mathbf{k}_a, \mathbf{k}_b, z; t_L, t_0) &= \frac{g_s^2 P_{gg}(z)}{z(1-z)(p_0^+)^2} 2\text{Re} \int_{t_0}^{t_L} dt_2 \int_{t_0}^{t_2} dt_1 \\
&\times \int \frac{d\mathbf{p}_1}{(2\pi)^2} \frac{d\mathbf{q}_1}{(2\pi)^2} \frac{d\bar{\mathbf{q}}_2}{(2\pi)^2} \frac{d\mathbf{p}_2}{(2\pi)^2} \frac{d\mathbf{q}_2}{(2\pi)^2} (\mathbf{P} \cdot \mathbf{Q}) \\
&\times \tilde{S}^{(4)}(\mathbf{q}_2, \bar{\mathbf{q}}_2 - \mathbf{q}_2, \mathbf{p}_2, \bar{\mathbf{q}}_2 - \mathbf{q}_2, t_2; \mathbf{k}_a, \mathbf{k}_b, \mathbf{k}_a, \mathbf{k}_b, t_L) \\
&\times \tilde{S}^{(3)}(\mathbf{p}_1, \mathbf{q}_1 - \mathbf{p}_1, \mathbf{q}_1, t_1; \mathbf{q}_2, \bar{\mathbf{q}}_2 - \mathbf{q}_2, \bar{\mathbf{q}}_2, t_2) \\
&\times \tilde{S}^{(2)}(\mathbf{q}_1, \mathbf{q}_1, t_1; \mathbf{p}_0, \mathbf{p}_0, t_0),
\end{aligned} \tag{4.41}$$

with $\mathbf{P} = \mathbf{p}_1 - z\mathbf{q}_1$ and $\mathbf{Q} = \mathbf{p}_2 - z\bar{\mathbf{q}}_2$. The regions between $[t_0, t_1]$, $[t_1, t_2]$ and $[t_2, t_L]$ are respectively covered by the following n-point functions $\tilde{S}^{(2)}$, $\tilde{S}^{(3)}$ and $\tilde{S}^{(4)}$ and the Altarelli-Parisi splitting function comes from the square of the 2 vertices (in the amplitude and its complex conjugate). Taking two times the real part of the integral written with the time order $t_1 < t_2$ permits taking into account the reverse order $t_2 < t_1$. The momenta notations follow from the fact that, at each time, the sum of momenta in the amplitude equals the sum in its complex conjugate (implied by the n-point functions and the correlator form). This transverse momentum conservation is held by the Dirac delta functions in the n-point functions which, when we use the momenta as labeled in Fig. 4.6, have already been applied. This means that we use n-point functions stripped of their Dirac delta, which is denoted by a tilde. In the regime where $\tau_{br} \ll t_L - t_0$, several approximations can be done. First, the 4-point functions can be factorized into two 2-point functions (the non-factorizable part being of order $\frac{\tau_{br}}{L}$ [258]), hence, can be written using \mathcal{P} as :

$$\begin{aligned}
&\tilde{S}^{(4)}(\mathbf{q}_2, \bar{\mathbf{q}}_2 - \mathbf{q}_2, \mathbf{p}_2, \bar{\mathbf{q}}_2 - \mathbf{q}_2, t_2; \mathbf{k}_a, \mathbf{k}_b, \mathbf{k}_a, \mathbf{k}_b, t_L) \\
&= (2\pi)^2 \delta^{(2)}(\mathbf{p}_2 - \mathbf{q}_2) \mathcal{P}(\mathbf{k}_a - \mathbf{q}_2; t_L, t_2) \mathcal{P}(\mathbf{k}_b - \bar{\mathbf{q}}_2 + \mathbf{q}_2; t_L, t_2).
\end{aligned} \tag{4.42}$$

If we use the time integration variables t_1 (that we will rename t) and $\Delta t = t_2 - t_1$, the other approximation consists in neglecting the dependence in Δt in the 4-point function (i.e in the corresponding \mathcal{P}). This way, it is possible to perform the integral over Δt , on $\tilde{S}^{(3)}$, apart. Overall, it leaves :

$$\begin{aligned}
\mathcal{P}_2(\mathbf{k}_a, \mathbf{k}_b, z; t_L, t_0) &= 2g_s^2 z(1-z) \int_{t_0}^{t_L} dt \int \frac{d\mathbf{q}_1}{(2\pi)^2} \frac{d\mathbf{Q}}{(2\pi)^2} \frac{d\mathbf{l}}{(2\pi)^2} \\
&\times \mathcal{P}(\mathbf{k}_a - \mathbf{q}_2; t_L, t) \mathcal{P}(\mathbf{k}_b - \mathbf{q}_1 - \mathbf{l} + \mathbf{q}_2; t_L, t) \\
&\times \frac{P_{gg}(z)}{(z(1-z)p_0^+)^2} \text{Re} \left[\int d\Delta t \int \frac{d\mathbf{P}}{(2\pi)^2} (\mathbf{P} \cdot \mathbf{Q}) \tilde{S}^{(3)}(\mathbf{P}, \mathbf{Q}, \mathbf{l}, z, \Delta t) \right] \\
&\times \mathcal{P}(\mathbf{q}_1 - \mathbf{p}_0; t, t_0),
\end{aligned} \tag{4.43}$$

with the 3-point function $\tilde{S}^{(3)}$ written in terms of the natural momentum variable \mathbf{Q}, \mathbf{P}

and $\mathbf{l} = \bar{\mathbf{q}}_2 - \mathbf{q}_1$ ⁸ :

$$\tilde{S}^{(3)}(\mathbf{P}, \mathbf{Q}, \mathbf{l}, z, t_2 - t_1) = \tilde{S}^{(3)}(\mathbf{p}_1, \mathbf{q}_1 - \mathbf{p}_1, \mathbf{q}_1, t_1; \mathbf{q}_2, \bar{\mathbf{q}}_2 - \mathbf{q}_2, \bar{\mathbf{q}}_2, t_2). \quad (4.44)$$

This way, we can define the in-medium splitting kernel as the part of Eq. (4.43) related to the region between t_1 and t_2 (i.e the part described by $\tilde{S}^{(3)}$ but also the vertices) :

$$\mathcal{K}_{gg}(\mathbf{Q}, \mathbf{l}, z, t) \equiv \frac{P_{gg}(z)}{(z(1-z)p_0^+)^2} \text{Re} \left[\int d\Delta t \int \frac{d\mathbf{P}}{(2\pi)^2} (\mathbf{P} \cdot \mathbf{Q}) \tilde{S}^{(3)}(\mathbf{P}, \mathbf{Q}, \mathbf{l}, z, \Delta t) \right]. \quad (4.45)$$

We will come back to the calculation of the 3-point function and then of this splitting kernel in a few steps. With this splitting kernel, \mathcal{P}_2 verifies :

$$\begin{aligned} \mathcal{P}_2(\mathbf{k}_a, \mathbf{k}_b, z; t_L, t_0) &= 2g_s^2 z(1-z) \int_{t_0}^{t_L} dt \int \frac{d\mathbf{q}_1}{(2\pi)^2} \frac{d\mathbf{Q}}{(2\pi)^2} \frac{d\mathbf{l}}{(2\pi)^2} \\ &\times \mathcal{P}(\mathbf{k}_a - \mathbf{q}_2; t_L, t) \mathcal{P}(\mathbf{k}_b - \mathbf{q}_1 - \mathbf{l} + \mathbf{q}_2; t_L, t) \mathcal{K}_{gg}(\mathbf{Q}, \mathbf{l}, z, t) \mathcal{P}(\mathbf{q}_1 - \mathbf{p}_0; t, t_0). \end{aligned} \quad (4.46)$$

Also, the transverse momentum \mathbf{l} can be neglected in the factors \mathcal{P} . Indeed, it represents the typical transverse momentum acquired during branching and is of order $\mathbf{l} \sim \hat{q}\tau_{br}$, negligible compared to \mathbf{k}_a or \mathbf{k}_b . We can then rewrite Eq. (4.47) as :

$$\begin{aligned} \mathcal{P}_2(\mathbf{k}_a, \mathbf{k}_b, z; t_L, t_0) &= 2g_s^2 z(1-z) \int_{t_0}^{t_L} dt \int \frac{d\mathbf{q}_1}{(2\pi)^2} \frac{d\mathbf{Q}}{(2\pi)^2} \\ &\times \mathcal{P}(\mathbf{k}_a - \mathbf{Q} - z\mathbf{q}_1; t_L, t) \mathcal{P}(\mathbf{k}_b + \mathbf{Q} - (1-z)\mathbf{q}_1; t_L, t) \\ &\times \mathcal{K}_{gg}(\mathbf{Q}, z, t) \mathcal{P}(\mathbf{q}_1 - \mathbf{p}_0; t, t_0), \end{aligned} \quad (4.47)$$

with $\mathcal{K}_{gg}(\mathbf{Q}, z, t) = \int \frac{d\mathbf{l}}{(2\pi)^2} \mathcal{K}_{gg}(\mathbf{Q}, \mathbf{P}, \mathbf{l}, z, t)$ and rewriting $\mathbf{q}_2 = \mathbf{Q} + z(\mathbf{l} + \mathbf{q}_1) \sim \mathbf{Q} + z\mathbf{q}_1$. Taking the time derivative, we obtain the equation :

$$\begin{aligned} \partial_t \mathcal{P}_2(\mathbf{k}_a, \mathbf{k}_b, z; t, t_0) &= 2g_s^2 z(1-z) \int \frac{d\mathbf{q}_1}{(2\pi)^2} \frac{d\mathbf{Q}}{(2\pi)^2} \frac{d\mathbf{l}}{(2\pi)^2} \\ &\times (2\pi)^4 \delta^{(2)}(\mathbf{k}_a - \mathbf{Q} - z\mathbf{q}_1) \delta^{(2)}(\mathbf{k}_b + \mathbf{Q} - (1-z)\mathbf{q}_1) \\ &\times \mathcal{K}_{gg}(\mathbf{Q}, \mathbf{P}, z, t) \mathcal{P}(\mathbf{q}_1 - \mathbf{p}_0; t, t_0), \end{aligned} \quad (4.48)$$

where we have used $\mathcal{P}(\mathbf{p}; t, t) = (2\pi)^2 \delta^{(2)}(\mathbf{p})$. This equation, with the one for \mathcal{P} (Eq. (4.39)) are the roots of the equations derived in the following section.

Now, we need to determine the in-medium splitting kernel \mathcal{K}_{gg} which means that we have to evaluate the 3-point function $\tilde{S}^{(3)}$. Like for the 2-point function, $S^{(3)}$ can be written in terms of the medium average of 3 Green functions \mathcal{G} :

$$\begin{aligned} S^{(3)}(\mathbf{p}_1, \mathbf{q}_1 - \mathbf{p}_1, \mathbf{q}_1, t_1; \mathbf{q}_2, \bar{\mathbf{q}}_2 - \mathbf{q}_2, \bar{\mathbf{q}}_2, t_2) &= \\ &\left\langle \mathcal{G}^\dagger(\mathbf{q}_1, t_1, \bar{\mathbf{q}}_2, t_2) \mathcal{G}(\bar{\mathbf{q}}_2 - \mathbf{q}_2, t_2, \mathbf{q}_1 - \mathbf{p}_1, t_1) \mathcal{G}(\mathbf{q}_2, t_2, \mathbf{p}_1, t_1) \right\rangle. \end{aligned} \quad (4.49)$$

⁸Also, $\tilde{S}^{(3)}$ depends only on the time difference $t_2 - t_1$ and not on t_2 and t_1 independently.

Again, writing the Green functions \mathcal{G} as path integrals and performing the medium average leads to (in coordinate space first, for simplicity, notations follow those of Fig. 4.7) :

$$\begin{aligned}
S^{(3)}(\mathbf{x}_i, \mathbf{x}_k, \bar{\mathbf{x}}_j, t_1; \mathbf{y}_i, \mathbf{y}_k, \bar{\mathbf{y}}_j, t_2) = & \\
& \int \mathcal{D}\mathbf{r}_i \mathcal{D}\mathbf{r}_j \mathcal{D}\mathbf{r}_k \exp \left\{ \frac{i}{2} \int_{t_1}^{t_2} dt (\omega_i \dot{\mathbf{r}}_i^2 + \omega_k \dot{\mathbf{r}}_k^2 - \omega_j \dot{\mathbf{r}}_j^2) \right\} \\
& \times \exp \left\{ -\frac{N_c n}{4} \int_{t_1}^{t_2} dt [\sigma(\mathbf{r}_i - \mathbf{r}_j) + \sigma(\mathbf{r}_k - \mathbf{r}_j) + \sigma(\mathbf{r}_k - \mathbf{r}_i)] \right\}, \tag{4.50}
\end{aligned}$$

where all the possible dipoles that can be formed between the 3 gluons appear, as pictured in Fig. 4.7.

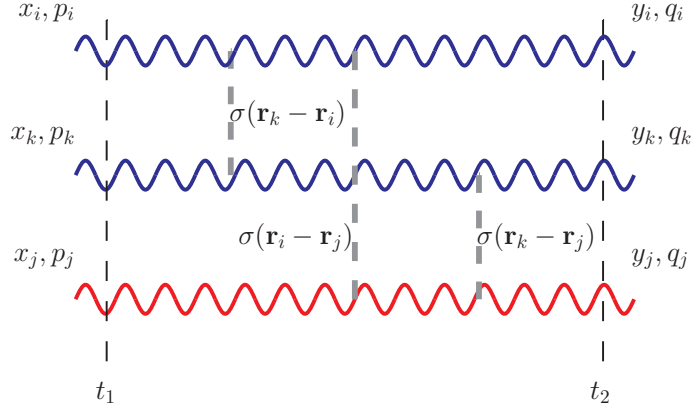


Figure 4.7: Illustration of the 3-point function $S^{(3)}$ with amplitude in blue and its complex conjugate in red. The grey dash line denotes the dipole involved in $S^{(3)}$.

Then, we perform a change of variable, using $\mathbf{u} = \mathbf{r}_i - \mathbf{r}_k$ and $\mathbf{v} = z\mathbf{r}_i + (1-z)\mathbf{r}_k - \mathbf{r}_j$. Considering also $\omega_i = z\omega_j$ and $\omega_k = (1-z)\omega_j$ we obtain :

$$\begin{aligned}
S^{(3)}(\mathbf{x}_i, \mathbf{x}_k, \bar{\mathbf{x}}_j, t_1; \mathbf{y}_i, \mathbf{y}_k, \bar{\mathbf{y}}_j, t_2) = & \\
& \int \mathcal{D}\mathbf{u} \mathcal{D}\mathbf{v} \mathcal{D}\mathbf{r}_j \exp \left\{ \frac{i\omega_j}{2} \int_{t_1}^{t_2} dt (\dot{\mathbf{v}}^2 + 2\dot{\mathbf{v}} \cdot \dot{\mathbf{r}}_j + z(1-z)\dot{\mathbf{u}}^2) \right\} \\
& \times \exp \left\{ -\frac{N_c n}{4} \int_{t_1}^{t_2} dt [\sigma(\mathbf{u}) + \sigma(\mathbf{v} - z\mathbf{u}) + \sigma(\mathbf{v} + (1-z)\mathbf{u})] \right\}. \tag{4.51}
\end{aligned}$$

\mathbf{v} is the distance between the gluon j and the “center of mass” of gluon i and k and it follows a straight line, making the kinetics integral over the path \mathbf{v} and \mathbf{r}_j possible and

leaving :

$$S^{(3)}(\mathbf{x}_i, \mathbf{x}_k, \bar{\mathbf{x}}_j, t_1; \mathbf{y}_i, \mathbf{y}_k, \bar{\mathbf{y}}_j, t_2) = \left(\frac{\omega_j}{2\pi\Delta t} \right)^2 \exp \left\{ \frac{i\omega_j}{2} \frac{\Delta \mathbf{v}}{\Delta t} \cdot (\Delta \mathbf{v} + 2\Delta \mathbf{r}_j) \right\} \int \mathcal{D}\mathbf{u} \\ \times \exp \left\{ \frac{i\omega_0}{2} \int_{t_1}^{t_2} dt \dot{\mathbf{u}}^2 - \frac{N_c n}{4} \int_{t_1}^{t_2} dt [\sigma(\mathbf{u}) + \sigma(\mathbf{v} - z\mathbf{u}) + \sigma(\mathbf{v} + (1-z)\mathbf{u})] \right\}. \quad (4.52)$$

with $\Delta \mathbf{v} = \mathbf{v}(t_2) - \mathbf{v}(t_1)$, $\Delta \mathbf{r}_j = \bar{\mathbf{y}}_j - \bar{\mathbf{x}}_j$, $\omega_0 = z(1-z)\omega_j$ and $\Delta t = t_2 - t_1$. We need now to take the Fourier transform of $S^{(3)}$ as :

$$S^{(3)}(\mathbf{p}_i, \mathbf{p}_k, \bar{\mathbf{p}}_j, t_1; \mathbf{q}_i, \mathbf{q}_k, \bar{\mathbf{q}}_j, t_2) = \int \frac{d^2 \mathbf{x}_i}{(2\pi)^2} \frac{d^2 \mathbf{x}_k}{(2\pi)^2} \frac{d^2 \bar{\mathbf{x}}}{(2\pi)^2} \frac{d^2 \mathbf{y}_i}{(2\pi)^2} \frac{d^2 \mathbf{y}_k}{(2\pi)^2} \frac{d^2 \bar{\mathbf{y}}}{(2\pi)^2} \\ \times e^{-i\mathbf{q}_i \cdot \mathbf{y}_i} e^{-i\mathbf{q}_k \cdot \mathbf{y}_k} e^{i\bar{\mathbf{q}}_j \cdot \bar{\mathbf{y}}_j} e^{i\mathbf{p}_i \cdot \mathbf{x}_i} e^{i\mathbf{p}_k \cdot \mathbf{x}_k} e^{-i\bar{\mathbf{p}}_j \cdot \bar{\mathbf{x}}_j} \quad (4.53) \\ \times S^{(3)}(\mathbf{x}_i, \mathbf{x}_k, \bar{\mathbf{x}}_j, t_1; \mathbf{y}_i, \mathbf{y}_k, \bar{\mathbf{y}}_j, t_2).$$

Then, using the notations introduced earlier, it is possible to write $\tilde{S}^{(3)}$ as :

$$\tilde{S}^{(3)}(\mathbf{P}, \mathbf{Q}, \mathbf{l}, z, \Delta t, t) = \int d^2 \mathbf{u}_1 d^2 \mathbf{u}_2 d^2 \mathbf{v} e^{i\mathbf{u}_1 \cdot \mathbf{P} - i\mathbf{u}_2 \cdot \mathbf{Q} - i\mathbf{v} \cdot \mathbf{l}} \int \mathcal{D}\mathbf{u} \\ \times \exp \left\{ i \frac{\omega_0}{2} \int_{t_1}^{t_2} dt \dot{\mathbf{u}}^2 - \frac{N_c n}{4} \int_{t_1}^{t_2} dt [\sigma(\mathbf{u}) + \sigma(\mathbf{v} - z\mathbf{u}) + \sigma(\mathbf{v} + (1-z)\mathbf{u})] \right\}. \quad (4.54)$$

To achieve it, one needs to rewrite the space coordinates x_i and x_k in terms of the endpoint of the path \mathbf{u} and \mathbf{v} (with $\mathbf{u}(t_i) = \mathbf{u}_i$ for $i \in \{1, 2\}$ and equivalently for \mathbf{v}). Also, the other integrals introduced by the Fourier transform reduce to Dirac deltas that are implicit with the notations used (those of Fig. 4.7), as explained when we introduced the tilde notation. Then, we notice that the integral over \mathbf{l} (that appears in front of $\tilde{S}^{(3)}$ in \mathcal{K}_{gg}) leaves a Dirac delta function that let simplify the involved dipoles as :

$$\int \frac{d\mathbf{l}}{(2\pi)^2} \tilde{S}^{(3)}(\mathbf{P}, \mathbf{Q}, \mathbf{l}, z, \Delta t, t) = \int d^2 \mathbf{u}_1 d^2 \mathbf{u}_2 e^{i\mathbf{u}_1 \cdot \mathbf{P} - i\mathbf{u}_2 \cdot \mathbf{Q}} \int \mathcal{D}\mathbf{u} \\ \times \exp \left\{ i \frac{\omega_0}{2} \int_{t_1}^{t_2} dt \dot{\mathbf{u}}^2 - \frac{N_c n}{4} \int_{t_1}^{t_2} dt [\sigma(\mathbf{u}) + \sigma(-z\mathbf{u}) + \sigma((1-z)\mathbf{u})] \right\}. \quad (4.55)$$

Actually, the integral over \mathbf{v} could be done without performing the integral on \mathbf{l} first (as shown in [258]), but it is simpler this way (since we aim at an expression for $\mathcal{K}_{gg}(\mathbf{Q}, z, t)$). To go further, we will focus on the integral :

$$\mathcal{I}(\mathbf{u}_1, t_1, \mathbf{u}_2, t_2) = \int \mathcal{D}\mathbf{u} \exp \left\{ \begin{array}{l} i \frac{\omega_0}{2} \int_{t_1}^{t_2} dt \dot{\mathbf{u}}^2 \\ - \frac{N_c n}{4} \int_{t_1}^{t_2} dt [\sigma(\mathbf{u}) + \sigma(-z\mathbf{u}) + \sigma((1-z)\mathbf{u})] \end{array} \right\}. \quad (4.56)$$

To calculate it, we need to evaluate the dipole cross-section in the harmonic approximation, i.e by expanding it at quadratic order in the dipole size :

$$N_c n \sigma(\mathbf{r}) \simeq \frac{1}{2} \hat{q} \mathbf{r}^2. \quad (4.57)$$

Note that, considering \hat{q} constant is also part of the harmonic approximation. Then, the integral \mathcal{I} can be written as :

$$\mathcal{I}(\mathbf{u}_1, t_1, \mathbf{u}_2, t_2) = \int \mathcal{D}\mathbf{u} \exp \left\{ i\omega_0 \int_{t_1}^{t_2} dt \left[\frac{\dot{\mathbf{u}}^2}{2} + i\omega_{br}^2 \mathbf{u}^2 \right] \right\}. \quad (4.58)$$

where we define a typical branching time τ_{br} , a typical branching energy ω_{br} and an effective quenching parameter \hat{q}_{eff} :

$$\tau_{br} \equiv \sqrt{\frac{\omega_0}{\hat{q}_{\text{eff}}}}, \quad \omega_{br} \equiv \frac{1}{2\tau_{br}}, \quad \hat{q}_{\text{eff}} \equiv \frac{\hat{q}}{2} \left[1 + z^2 + (1-z)^2 \right]. \quad (4.59)$$

We see that \mathcal{I} (and then $\tilde{S}^{(3)}$) is exponentially suppressed for large time $\Delta t > \tau_{br}$, limiting Δt to small times. This justifies the approximation made for $\tilde{S}^{(4)}$, where we neglected the time dependence on Δt . Also, we recognize a classical path integral for the harmonic oscillator that yields :

$$\begin{aligned} \mathcal{I}(\mathbf{u}_1, t_1, \mathbf{u}_2, t_2) &= \frac{(1-i)k_{br}^2}{4\pi \sinh(\Omega\Delta t)} \exp \left\{ \frac{(i-1)k_{br}^2}{4 \sinh \Omega\Delta t} \left((\mathbf{u}_1^2 + \mathbf{u}_2^2) \cosh \Omega\Delta t - 2\mathbf{u}_1 \cdot \mathbf{u}_2 \right) \right\} \\ &= \frac{(1-i)k_{br}^2}{4\pi \sinh(\Omega\Delta t)} \exp \left\{ \frac{(i-1)k_{br}^2}{2} \left((\mathbf{u}_1 + \mathbf{u}_2)^2 \tanh \frac{\Omega\Delta t}{2} \right. \right. \\ &\quad \left. \left. + (\mathbf{u}_1 - \mathbf{u}_2)^2 \coth \frac{\Omega\Delta t}{2} \right) \right\}. \end{aligned} \quad (4.60)$$

with $\Omega = (1+i)\omega_{br}$ and $k_{br} = \hat{q}_{\text{eff}}\tau_{br}$. In this form, it is possible to perform the left Fourier integrals (on \mathbf{u}_1 and \mathbf{u}_2) in $\tilde{S}^{(3)}$ leading to :

$$\begin{aligned} \int \frac{d\mathbf{l}}{(2\pi)^2} \tilde{S}^{(3)}(\mathbf{P}, \mathbf{Q}, \mathbf{l}, z, \Delta t, t) &= \\ &= \frac{2\pi(1+i)}{k_{br}^2 \sinh(\Omega\Delta t)} \exp \left\{ -\frac{(i+1)}{4k_{br}^2} \left((\mathbf{P} + \mathbf{Q})^2 \tanh \frac{\Omega\Delta t}{2} \right. \right. \\ &\quad \left. \left. + (\mathbf{P} - \mathbf{Q})^2 \coth \frac{\Omega\Delta t}{2} \right) \right\}. \end{aligned} \quad (4.61)$$

Finally, after performing the Gaussian integral on \mathbf{P} , one obtain the splitting kernel :

$$\begin{aligned} \mathcal{K}_{gg}(\mathbf{Q}, z, t) &= \\ &= \frac{P_{gg}(z)}{(z(1-z)p_0^+)^2} \text{Re} \left[\int d\Delta t \cosh^{-2}(\Omega\Delta t) \exp \left\{ -\frac{i\mathbf{Q}^2}{2z(1-z)p_0^+\Omega} \tanh(\Omega\Delta t) \right\} \right]. \end{aligned} \quad (4.62)$$

The last step to determine the in-medium splitting kernel in the harmonic approximation is to perform the time integral :

$$\begin{aligned}\mathcal{K}_{gg}(\mathbf{Q}, z, t) &= \frac{P_{gg}(z)}{z(1-z)p_0^+} \operatorname{Re} \left[i \int_0^{t_2-t_0} d\Delta t \frac{d}{d\Delta t} \exp \left\{ -\frac{i\mathbf{Q}^2}{2z(1-z)p_0^+\Omega} \tanh(\Omega\Delta t) \right\} \right] \\ &= \frac{P_{gg}(z)}{z(1-z)p_0^+} \operatorname{Re} \left[i \exp \left\{ -\frac{i\mathbf{Q}^2}{2z(1-z)p_0^+\Omega} \tanh(\Omega(t_2-t_0)) - i \right\} \right].\end{aligned}\tag{4.63}$$

Also, when $t_2 - t_0 \gg \tau_{br}$, $\tanh(\Omega(t_2 - t_0)) \sim 1$ and if we neglect the region $t_2 - t_0 \lesssim \tau_{br}$, we obtain a time independent kernel :

In-medium splitting kernel for gluon

$$\mathcal{K}_{gg}(\mathbf{Q}, z, p_0^+) \simeq 2 \frac{P_{gg}(z)}{z(1-z)p_0^+} \sin \frac{\mathbf{Q}^2}{2k_{br}^2} \exp -\frac{\mathbf{Q}^2}{2k_{br}^2}.\tag{4.64}$$

It is worth mentioning that this kernel can be negative. If this is a hint on the limits of the approximations made to obtain it, it hopefully happens only for large momentum transfer $\mathbf{Q} > \pi k_{br}$ where the exponential crushes the expression.

4.3 BDIM equations

In this section, we will derive the equation governing the inclusive one gluon distributions (in the in-medium cascade) depending on both the fraction of the initial parton energy x and the transverse momentum \mathbf{k} . This equation goes beyond the [BDMPS-Z](#) formalism since the transverse momentum transferred during branching is taken into account (with the in-medium splitting functions introduced in the previous section). The energy distribution will be obtained by integrating the transverse momentum component of the inclusive gluon distribution. It describes the radiative energy loss of a jet when passing through a QGP following the [BDMPS-Z](#) formalism. Also, these distributions describe the medium-induced parton shower of hard jets, hence we may call them (in-medium jet) [Fragmentation Functions \(FF\)](#) in the current work (like in [Eq. \(1.19\)](#)). Describing the evolution of jet in the medium through [FFs](#) implies that we assume factorization in heavy-ion collisions (which is not proved but is motivated by time scale considerations). The evolution equations describing these [FFs](#) are referred to as [Blaizot-Dominguez-Iancu-Mehtar-Tani \(BDIM\)](#) equations (and were originally derived in [\[258, 262\]](#)).

4.3.1 Pure gluons

As a first derivation of the [BDIM](#) equation, we will consider the pure gluonic case (i.e with only gluons populating the medium-induced parton shower), that follows from

Sec. 4.2. Let's begin by defining the fragmentation function D , i.e the inclusive one gluon distribution function :

$$\begin{aligned}
D_g(x, \mathbf{k}, t) &= k^+ \frac{dN_g}{dk^+ d\mathbf{k}} \equiv k^+ \left\langle \sum_{n \in \mathbb{N}_+^*} \sum_{i=1}^n \delta^{(3)}(k_j - k) \right\rangle \\
&= \frac{1}{(2\pi)^3} \sum_{n \in \mathbb{N}_+^*} \frac{1}{n!} \left(\prod_{i=1}^{n-1} d\Omega_{k_i} \right) n P_n(k, k_1, k_2, \dots, k_{n-1}; t, t_0),
\end{aligned} \tag{4.65}$$

with the convention $\prod_{i=1}^{n-1} d\Omega_{k_i} = 1$. This fragmentation function counts all the possibilities to have one gluon at t_0 initiating the cascade and any number n of gluons at time t . Then, the formal derivation of the **BDIM** equation needs the introduction of a generating functional [262], not needed for the present discussion. The main steps will be summarized here. The main idea is to consider, for an infinitesimal time δt , that the **FF** D can only evolve through scattering with the medium and through a single medium-induced emission (at leading order in perturbation theory). This means that $D(t_0 + \delta t)$ depends only on $P_1(t_0 + \delta t)$ and $P_2(t_0 + \delta t)$:

$$D_g(x, \mathbf{k}, t_0 + \delta t) = \frac{1}{(2\pi)^3} n \left(P_1(k, ; t + \delta t, t_0) + \frac{1}{2} \int d\Omega_{k_2} P_2(k_1, k_2; t + \delta t, t_0) \right). \tag{4.66}$$

Then, the **BDIM** equation for gluon-dominated cascades is obtained using the equations for \mathcal{P} and \mathcal{P}_2 (Eq. (4.39) and Eq. (4.48) respectively). Actually, the equation on \mathcal{P}_1 (Eq. (4.39)) required to be corrected by order of α_s term (to have the same order in perturbation theory as Eq. (4.48)) :

$$\begin{aligned}
\frac{\partial}{\partial t} \mathcal{P}(\mathbf{k} - \mathbf{p}_0; t, t_0) &= \int \frac{d^2 \mathbf{l}}{(2\pi)^2} \mathcal{C}_g(\mathbf{l}) \mathcal{P}(\mathbf{k} - \mathbf{p}_0 - \mathbf{l}; t, t_0) \\
&\quad - \alpha_s \int_0^1 dz \mathcal{K}(z, p_0^+, t) \mathcal{P}(\mathbf{k} - \mathbf{p}_0; t, t_0).
\end{aligned} \tag{4.67}$$

This correction takes into account the probability of the gluon not to undergo branching. All together, it leads to the **BDIM** equation :

BDIM equation for gluons

$$\begin{aligned}
\frac{\partial}{\partial t} D_g(x, \mathbf{k}, t) &= \int_0^1 dz \int \frac{d^2 \mathbf{q}}{(2\pi)^2} \alpha_s \left[2\mathcal{K}_{gg} \left(\mathbf{Q}, z, \frac{x}{z} p_0^+ \right) D_g \left(\frac{x}{z}, \mathbf{q}, t \right) \right. \\
&\quad \left. - \mathcal{K}_{gg}(\mathbf{q}, z, x p_0^+) D_g(x, \mathbf{k}, t) \right] \\
&\quad + \int \frac{d^2 \mathbf{l}}{(2\pi)^2} C_g(\mathbf{l}) D_g(x, \mathbf{k} - \mathbf{l}, t).
\end{aligned} \tag{4.68}$$

This equation has a simple interpretation. The FF for in-medium jet $D_g(x, \mathbf{k}, t)$ (accounting for gluons only) can evolve through 3 possible processes (3 elementary blocks of the parton shower in the medium). A gluon can be emitted with a fraction of energy x and transverse momentum \mathbf{k} at time t from a parent gluon at $(\frac{x}{z}, \mathbf{q}, t)$ (for any $z \in [0, 1]$ and any \mathbf{q}), leading to a gain term (first line of the r.h.s). A gluon at (x, \mathbf{k}, t) can split, leading to a loss term (2nd line) and finally, a gluon can gain transverse momentum to reach \mathbf{k} leading to the collision term (3rd line). Also, one should understand that in this equation, the integral over z goes implicitly from 0 to 1 for the loss term while it goes from x to 1 in the gain term (such that $\frac{x}{z} \in [0, 1]$). This could be written explicitly by adding Heaviside θ functions (and setting the integral on z from 0 to 1), but it has been chosen to keep it implicit for readability. We should remind that the solutions of this equation should be used to describe the evolution of jets in a collision involving the formation of a QGP (basically, a heavy-ion collision) where this evolution can be factorized⁹ from the rest of the cross-section, i.e the initial state shower and the hard part. This means that we want to solve the BDIM equation for an initial high energy parton (a final state of the hard process), in the present case, an on-shell gluon. This is represented by the product of two Dirac's delta functions :

$$D_g(x, \mathbf{k}, t_0) = \delta(1-x)\delta^{(2)}(\mathbf{k}). \quad (4.69)$$

The solutions of this equation will be studied in Sec. 4.5.1, but for now, we will present different forms of BDIM equations.

4.3.2 System of equations

The BDIM equation (Eq. (4.68)) presented for gluon-dominated cascades in the previous section can be extended to a cascade accounting for both quarks and gluons. This generalization, with the calculation of the needed kernels (and the study of the solutions) were published in [4]. What changes are the possible building blocks to be used in the cascade with, in particular, different color factors. In this sense, we define a quenching parameter stripped off its color factor :

$$\hat{q} = \frac{\hat{q}}{N_c}. \quad (4.70)$$

If, for instance, we consider the gluon FF $D_g(x, \mathbf{k}, t)$, it can now evolve through the emission of a gluon at (x, \mathbf{k}, t) from either a gluon parent or a quark parent (there are now 2 gain terms), through gluon at (x, \mathbf{k}, t) emitting either a gluon or forming a quark-antiquark pair (leading to two loss terms) and finally, the elastic scattering term does not change. Doing the same exercise for the quark leads to the BDIM system of equation for both gluon distribution D_g and quark distributions D_{q_i} (with i the flavor of the quark) :

⁹At least, is considered to factorize, like in Eq. (1.19).

BDIM equations

$$\begin{aligned}
\frac{\partial}{\partial t} D_g(x, \mathbf{k}, t) &= \int_0^1 dz \int \frac{d^2 \mathbf{q}}{(2\pi)^2} \alpha_s \left\{ 2\mathcal{K}_{gg} \left(\mathbf{Q}, z, \frac{x}{z} p_0^+ \right) D_g \left(\frac{x}{z}, \mathbf{q}, t \right) \right. \\
&\quad + \mathcal{K}_{gq} \left(\mathbf{Q}, z, \frac{x}{z} p_0^+ \right) \sum_i D_{q_i} \left(\frac{x}{z}, \mathbf{q}, t \right) \\
&\quad \left. - \left[\mathcal{K}_{gg}(\mathbf{q}, z, xp_0^+) + \mathcal{K}_{qg}(\mathbf{q}, z, xp_0^+) \right] D_g(x, \mathbf{k}, t) \right\} \\
&\quad + \int \frac{d^2 \mathbf{l}}{(2\pi)^2} C_g(\mathbf{l}) D_g(x, \mathbf{k} - \mathbf{l}, t), \\
\frac{\partial}{\partial t} D_{q_i}(x, \mathbf{k}, t) &= \int_0^1 dz \int \frac{d^2 \mathbf{q}}{(2\pi)^2} \alpha_s \left\{ \mathcal{K}_{qq} \left(\mathbf{Q}, z, \frac{x}{z} p_0^+ \right) D_{q_i} \left(\frac{x}{z}, \mathbf{q}, t \right) \right. \\
&\quad + \frac{1}{N_f} \mathcal{K}_{qg} \left(\mathbf{Q}, z, \frac{x}{z} p_0^+ \right) D_g \left(\frac{x}{z}, \mathbf{q}, t \right) \\
&\quad \left. - \mathcal{K}_{qq}(\mathbf{q}, z, xp_0^+) D_{q_i}(x, \mathbf{k}, t) \right\} \\
&\quad + \int \frac{d^2 \mathbf{l}}{(2\pi)^2} C_q(\mathbf{l}) D_{q_i}(x, \mathbf{k} - \mathbf{l}, t),
\end{aligned} \tag{4.71}$$

where the collision kernels C_g and C_q differ only from the color factor used (set inside the in-medium potential $w_{q(g)}$) :

$$C_{q(g)}(\mathbf{l}) = w_{q(g)}(\mathbf{l}) - \delta(\mathbf{l}) \int d^2 \mathbf{l}' w_{q(g)}(\mathbf{l}'), \tag{4.72}$$

with :

$$w_g(\mathbf{l}) = \frac{N_c g_s^4 n}{\mathbf{l}^2 (\mathbf{l}^2 + m_D^2)}, \quad w_q(\mathbf{l}) = \frac{C_F g_s^4 n}{\mathbf{l}^2 (\mathbf{l}^2 + m_D^2)}. \tag{4.73}$$

Note that we consider here the in-medium potential for a weakly coupled QGP in thermal equilibrium at high temperature T . Contrary to the gluon-dominated cascade, we won't treat the out-of-equilibrium case (without screening), focusing, when using this system of equations, on the difference between quark and gluon jets and their composition (rather than on different medium models).

For the splitting kernel \mathcal{K}_{ij} (for an emitted parton i , from a parent parton j), we need to go some steps backward to determine them properly. Basically, their derivation follows the same steps as for \mathcal{K}_{gg} but different dipole cross-sections appear when writing $\tilde{S}^{(3)}$. Indeed, these dipoles can now be between a gluon and a quark (with a quark spectator) and between 2 quarks (with a gluon spectator) in addition to the case with only gluons

which impacts the color factors used. In all generality, the splitting kernels read :

$$\begin{aligned}\mathcal{K}_{ij}(\mathbf{Q}, z, p_0^+) &= \frac{P_{ij}^{(k)}(z)}{\omega_0^2} \text{Re} \int_0^{+\infty} d\Delta t \int \frac{d^2\mathbf{P}}{(2\pi)^2} \frac{d^2\mathbf{l}}{(2\pi)^2} (\mathbf{P} \cdot \mathbf{Q}) \tilde{S}_{ij}^{(3)}(\mathbf{P}, \mathbf{Q}, \mathbf{l}, z, \Delta t, t), \\ S_{ij}^{(3)}(\mathbf{P}, \mathbf{Q}, \mathbf{l}, z, \Delta t, t) &= \int d^2\mathbf{u}_1 d^2\mathbf{u}_2 d^2\mathbf{v} e^{i\mathbf{u}_1 \cdot \mathbf{P} - i\mathbf{u}_2 \cdot \mathbf{Q} - i\mathbf{v} \cdot \mathbf{l}} \\ &\quad \times \int_{\mathbf{u}(t_1)=\mathbf{u}_1}^{\mathbf{u}(t_2)=\mathbf{u}_2} \mathcal{D}\mathbf{u} e^{i\frac{\omega_0}{2} \int_{t_1}^{t_2} ds \dot{\mathbf{u}}^2(s) - \int_{t_1}^{t_2} ds n(s) \sigma_{ij,\text{eff}}(\mathbf{u}(s), \mathbf{v})},\end{aligned}\tag{4.74}$$

where $\omega_0 = z(1-z)p_0^+$, and $P_{ij}^{(k)}(z)$ are the (unregularised) Altarelli-Parisi splitting functions. $\sigma_{ij,\text{eff}}$ gathered the 3 dipoles cross-sections participating in $S_{ij}^{(3)}$, it is defined as :

$$\begin{aligned}\sigma_{ij,\text{eff}}(\mathbf{u}, \mathbf{v}) &= \frac{C_i + C_k - C_j}{2} \bar{\sigma}(\mathbf{u}) + \frac{C_i + C_j - C_k}{2} \bar{\sigma}(\mathbf{v} + (1-z)\mathbf{u}) \\ &\quad + \frac{C_k + C_j - C_i}{2} \bar{\sigma}(\mathbf{v} - z\mathbf{u}).\end{aligned}\tag{4.75}$$

where C_i is the squared Casimir operators of the color representation of the particle i and $\bar{\sigma}$ is the dipole cross-section stripped of its color factor. The form of the color factors follows from color conservation arguments [263, 264]. Again, we have stripped off the dipole cross-section from their color factor to obtain these expressions, with $\bar{\sigma}(\mathbf{r}) \equiv \frac{\sigma(\mathbf{r})}{N_c}$ (considering σ defined in the pure gluon case). Then, the calculation follows the same steps as in the gluon-dominated case (calculation of \mathcal{K}_{gg}). In particular, once the harmonic approximation is applied, it leads to the following effective quenching parameter :

$$\hat{q}_{ij}(z) = f_{ij}(z) \hat{q},\tag{4.76}$$

where :

$$f_{ij}(z) = \frac{C_i + C_k - C_j}{2} + \frac{C_i + C_j - C_k}{2} (1-z)^2 + \frac{C_k + C_j - C_i}{2} z^2.\tag{4.77}$$

Explicitly, this gives :

$$\begin{aligned}f_{gg}(z) &= (1-z)C_A + z^2C_A, \\ f_{qg}(z) &= C_F - z(1-z)C_A, \\ f_{gq}(z) &= (1-z)C_A + z^2C_F, \\ f_{qq}(z) &= zC_A + (1-z)^2C_F.\end{aligned}\tag{4.78}$$

Then, we can write the in-medium splitting kernel the same way as in Eq. (4.64) :

In-medium splitting kernels

$$\mathcal{K}_{ij}(\mathbf{Q}, z, p_0^+) = 2 \frac{P_{ij}(z)}{z(1-z)p_0^+} \sin \frac{Q^2}{2k_{ij,br}^2} \exp - \frac{Q^2}{2k_{ij,br}^2},\tag{4.79}$$

with $k_{ij,br}^2 = \sqrt{z(1-z)p_0^+ \hat{q}_{ij}(z)}$. We recall the unregularized Altarelli-Parisi splitting functions :

$$\begin{aligned}
P_{gg}(z) &= C_A \frac{[1-z(1-z)]^2}{z(1-z)}, \\
P_{q_i g}(z) &= \frac{1}{N_f} P_{qg}(z) = \frac{1}{2} [z^2 + (1-z)^2], \\
P_{gq_i}(z) &= P_{gq}(z) = C_F \frac{1+(1-z)^2}{z}, \\
P_{q_i q_j}(z) &= \delta_{ij} P_{qq}(z), \quad P_{qq}(z) = C_F \frac{1+z^2}{1-z}.
\end{aligned} \tag{4.80}$$

4.3.3 Energy distribution

The precedent versions of the **BDIM** equation permit to follow the transverse momentum evolution of the partons in an in-medium cascade, i.e it makes possible the study of jet broadening. Also, these equations are well suited to study (alone) radiative energy loss. To this end, one might integrate the **BDIM** equations (hence we will call them *integrated BDIM* equations) along the transverse momentum \mathbf{k} . This leads then to equations on the energy distributions $D_{g(q_i)}(x, t) = \int \frac{d\mathbf{k}}{(2\pi)^2} D_{g(q_i)}(x, \mathbf{k}, t)$ (if it isn't ambiguous, we might also call them in-medium jet **FF**). The integrated **BDIM** equation for gluon dominated cascade is then :

$$\frac{\partial}{\partial t} D_g(x, t) = \alpha_s \int dz \left[2\mathcal{K}_{gg} \left(z, \frac{x}{z} p_0^+ \right) D_g \left(\frac{x}{z}, t \right) - \mathcal{K}_{gg}(z, x p_0^+) D_g(x, t) \right], \tag{4.81}$$

where the integrated in-medium branching kernel reads :

$$\mathcal{K}_{gg}(z, p_0^+) \equiv \int \frac{d\mathbf{Q}}{(2\pi)^2} \mathcal{K}_{gg}(\mathbf{Q}, z, p_0^+) = \frac{P_{gg}(z)}{2\pi\tau_{br}}. \tag{4.82}$$

This recalls that, in the **BDMPS-Z** formalism, the scattering with the medium color charges is elastic and hence does not involve energy loss (implying that $\int \frac{d\mathbf{l}}{(2\pi)^2} C_g(\mathbf{l}) = 0$).

Eq. (4.81) can be further simplified using the dimensionless quantities :

$$t^* \equiv \frac{\pi}{\alpha_s N_c} \sqrt{\frac{p_0^+}{\hat{q}}}, \quad \tau \equiv \frac{t - t_0}{t^*}, \quad \mathcal{K}_{gg}(z) \equiv 2t^* \alpha_s \mathcal{K}_{gg}(z, p_0^+) = \frac{[1-z(1-z)]^{\frac{5}{2}}}{[z(1-z)]^{\frac{3}{2}}}, \tag{4.83}$$

where t^* is the stopping time (typical time spent in the medium for a hard parton to thermalize) and τ is called proper time. Then, Eq. (4.81) can be put in the form :

Integrated BDIM equation for gluons

$$\frac{\partial}{\partial \tau} D_g(x, \tau) = \int dz \mathcal{K}_{gg}(z) \left[\sqrt{\frac{z}{x}} D_g \left(\frac{x}{z}, \tau \right) - \frac{z}{\sqrt{x}} D_g(x, \tau) \right]. \tag{4.84}$$

It is interesting to note that the collinear kernel encodes the gluon spectrum produced via a single medium-induced radiation which can be recognized as the BDMPS-Z spectrum [233–235, 237] :

$$z \frac{dN}{dz} = \frac{\alpha_s}{\pi} z t_L \mathcal{K}_{gg}(z) = \frac{\alpha_s}{\pi} t_L P_{gg}(z) \sqrt{\frac{\hat{q}_{\text{eff}}}{z(1-z)p_0^+}}. \quad (4.85)$$

This is expected since when integrating the BDIM equations over the transverse momentum, we recover the eikonal limit of the BDMPS-Z formalism. We should mention that this equation, describing energy loss within BDMPS-Z formalism, was already known (meaning, before the establishment of the BDIM equation) and proposed heuristically in [225, 265]. It also has been implemented in the MC event generator MARTINI [266]. The same procedure can be used for the “full” cascade (accounting for quarks), however, one has to define a stopping time stripped of its usual color factor : $\bar{t}^* = \frac{\pi}{\alpha_s} \sqrt{\frac{p_0^+}{\hat{q}}}$. and it leads to the system of equations :

Integrated BDIM equations

$$\begin{aligned} \frac{\partial}{\partial t} D_g(x, \tau) &= \int dz 2\mathcal{K}_{gg}(z) \left[\sqrt{\frac{z}{x}} D_g\left(\frac{x}{z}, \tau\right) - \frac{z}{\sqrt{x}} D_g(x, \tau) \right] \\ &\quad - \int dz 2\mathcal{K}_{qg}(z) \frac{z}{\sqrt{x}} D_g(x, \tau) \\ &\quad + \int dz \mathcal{K}_{gq}(z) \sqrt{\frac{z}{x}} \sum_i D_{q_i}\left(\frac{x}{z}, \tau\right), \quad (4.86) \\ \frac{\partial}{\partial t} D_q(x, \tau) &= \int dz \mathcal{K}_{qq}(z) \left[\sqrt{\frac{z}{x}} D_q\left(\frac{x}{z}, \tau\right) - \frac{1}{\sqrt{x}} D_q(x, \tau) \right] \\ &\quad + \frac{1}{N_f} \int dz \mathcal{K}_{qg}(z) \sqrt{\frac{z}{x}} D_g\left(\frac{x}{z}, \tau\right), \end{aligned}$$

where the collinear splitting kernels are defined as :

In-medium collinear splitting kernels

$$\mathcal{K}_{ij}(z) = \frac{P_{ij}(z)}{2} \sqrt{\frac{f_{ij}(z)}{z(1-z)}}. \quad (4.87)$$

It is also convenient to rewrite the latter equations in the quark singlet/non-singlet

basis [267] (characterizing respectively sea and valence quarks), where we find :

$$\begin{aligned}
\frac{\partial}{\partial t} D_g(x, \tau) &= \int dz 2\mathcal{K}_{gg}(z) \left[\sqrt{\frac{z}{x}} D_g\left(\frac{x}{z}, \tau\right) - \frac{z}{\sqrt{x}} D_g(x, \tau) \right] \\
&\quad - \int dz 2\mathcal{K}_{qq}(z) \frac{z}{\sqrt{x}} D_g(x, \tau) \\
&\quad + \int dz \mathcal{K}_{gq}(z) \sqrt{\frac{z}{x}} D_S\left(\frac{x}{z}, \tau\right), \\
\frac{\partial}{\partial t} D_S(x, \tau) &= \int dz \mathcal{K}_{qq}(z) \left[\sqrt{\frac{z}{x}} D_S\left(\frac{x}{z}, \tau\right) \right. \\
&\quad \left. - \frac{1}{\sqrt{x}} D_S(x, \tau) \right] + \int dz 2\mathcal{K}_{gg}(z) \sqrt{\frac{z}{x}} D_g\left(\frac{x}{z}, \tau\right), \\
\frac{\partial}{\partial t} D_{NS}^{(i)}(x, \tau) &= \int dz \mathcal{K}_{qq}(z) \left[\sqrt{\frac{z}{x}} D_{NS}^{(i)}\left(\frac{x}{z}, \tau\right) - \frac{1}{\sqrt{x}} D_{NS}^{(i)}(x, \tau) \right],
\end{aligned} \tag{4.88}$$

with :

$$D_S = \sum_{i=1}^{N_f} [D_{q_i} + D_{\bar{q}_i}], \quad D_{NS}^{(i)} = D_{q_i} - D_{\bar{q}_i}. \tag{4.89}$$

4.3.4 Approximations

Collinear approximation

If we go back to the BDIM equations (Eq. (4.68) or Eq. (4.71) for the gluon dominated case), several approximations can be done on either the branching kernel or the scattering one. Actually, the typical momentum k_{br}^2 transferred during branching is small (compared to the transverse momentum acquired through scattering) and then often neglected. In this case, the collinear splitting kernels, as seen in the integrated BDIM equation (see Eq. (4.86) and Eq. (4.81)) might be used also in what we will call *collinear* BDIM equation :

Collinear BDIM equation for gluons

$$\begin{aligned}
\frac{\partial}{\partial t} D_g(x, \mathbf{k}, \tau) &= \int dz 2\mathcal{K}_{gg}(z) \left[\frac{1}{z^2} \sqrt{\frac{z}{x}} D_g\left(\frac{x}{z}, \frac{\mathbf{k}}{z}, \tau\right) - \frac{z}{\sqrt{x}} D_g(x, \mathbf{k}, \tau) \right] \\
&\quad + t^* \int \frac{d^2\mathbf{l}}{(2\pi)^2} C_g(\mathbf{l}) D(x, \mathbf{k} - \mathbf{l}, \tau),
\end{aligned} \tag{4.90}$$

for the pure gluon case, and, when accounting for quarks :

Collinear BDIM equations

$$\begin{aligned}
\frac{\partial}{\partial t} D_g(x, \mathbf{k}, \tau) &= \int dz 2\mathcal{K}_{gg}(z) \left[\frac{1}{z^2} \sqrt{\frac{z}{x}} D_g \left(\frac{x}{z}, \frac{\mathbf{k}}{z}, \tau \right) - \frac{z}{\sqrt{x}} D_g(x, \mathbf{k}, \tau) \right] \\
&\quad - \int dz 2\mathcal{K}_{qg}(z) \frac{z}{\sqrt{x}} D_g(x, \mathbf{k}, \tau) \\
&\quad + \int dz \mathcal{K}_{gq}(z) \frac{1}{z^2} \sqrt{\frac{z}{x}} \sum_i D_{q_i} \left(\frac{x}{z}, \frac{\mathbf{k}}{z}, \tau \right) \\
&\quad + \bar{t}^* \int \frac{d^2 \mathbf{l}}{(2\pi)^2} C_g(\mathbf{l}) D(x, \mathbf{k} - \mathbf{l}, \tau), \tag{4.91} \\
\frac{\partial}{\partial t} D_q(x, \mathbf{k}, \tau) &= \int dz \mathcal{K}_{qq}(z) \left[\frac{1}{z^2} \sqrt{\frac{z}{x}} D_q \left(\frac{x}{z}, \frac{\mathbf{k}}{z}, \tau \right) - \frac{1}{\sqrt{x}} D_q(x, \mathbf{k}, \tau) \right] \\
&\quad + \frac{1}{N_f} \int dz \mathcal{K}_{qg}(z) \frac{1}{z^2} \sqrt{\frac{z}{x}} D_g \left(\frac{x}{z}, \frac{\mathbf{k}}{z}, \tau \right) \\
&\quad + \bar{t}^* \int \frac{d^2 \mathbf{l}}{(2\pi)^2} C_q(\mathbf{l}) D_q(x, \mathbf{k} - \mathbf{l}, \tau).
\end{aligned}$$

Diffusion approximation

The BDIM equation can be simplified further considering another interesting approximation which concerns the collision term this time. For simplicity in the discussion, we consider first the gluon-dominated case. So, the typical momentum transferred during a collision is of order m_D , which is much smaller than the momentum transferred during the propagation over a distance $l \sim L$, which would be $\sqrt{\hat{q}l}$. With this in mind, we can rewrite the equation followed by \mathcal{P} (see Eq. (4.39)) as a Fokker-Plank equation [262]¹⁰ :

$$\frac{\partial}{\partial t} \mathcal{P}(\mathbf{k} - \mathbf{p}_0; t, t_0) = \frac{\hat{q}}{4} \frac{\partial^2}{\partial \mathbf{k}^2} \mathcal{P}(\mathbf{k} - \mathbf{p}_0; t, t_0), \tag{4.92}$$

where the quenching parameter \hat{q} plays the role of a diffusion parameter. This directly translates in the collinear BDIM equation through a diffusion term :

Collinear BDIM equation for gluons with diffusive approximation

$$\begin{aligned}
\frac{\partial}{\partial t} D_g(x, \mathbf{k}, \tau) &= \int dz 2\mathcal{K}_{gg}(z) \left[\frac{1}{z^2} \sqrt{\frac{z}{x}} D_g \left(\frac{x}{z}, \frac{\mathbf{k}}{z}, \tau \right) - \frac{z}{\sqrt{x}} D_g(x, \mathbf{k}, \tau) \right] \\
&\quad + \frac{\bar{t}^*}{4} \hat{q} \nabla_{\mathbf{k}}^2 \left[D(x, \mathbf{k}, t) \right]. \tag{4.93}
\end{aligned}$$

The same could be done when accounting for quarks :

¹⁰Actually, the quenching parameter in this case should be logarithmic in \mathbf{k} , but we have neglected this dependence here.

Collinear BDIM equations with diffusive approximation

$$\begin{aligned}
\frac{\partial}{\partial t} D_g(x, \mathbf{k}, \tau) &= \int dz 2\mathcal{K}_{gg}(z) \left[\frac{1}{z^2} \sqrt{\frac{z}{x}} D_g \left(\frac{x}{z}, \frac{\mathbf{k}}{z}, \tau \right) - \frac{z}{\sqrt{x}} D_g(x, \mathbf{k}, \tau) \right] \\
&\quad - \int dz 2\mathcal{K}_{qg}(z) \frac{z}{\sqrt{x}} D_g(x, \mathbf{k}, \tau) \\
&\quad + \int dz \mathcal{K}_{gq}(z) \frac{1}{z^2} \sqrt{\frac{z}{x}} \sum_i D_{q_i} \left(\frac{x}{z}, \frac{\mathbf{k}}{z}, \tau \right) \\
&\quad + \frac{\bar{t}^*}{4} \hat{q} \nabla_k^2 \left[D(x, \mathbf{k}, t) \right], \tag{4.94} \\
\frac{\partial}{\partial t} D_q(x, \mathbf{k}, \tau) &= \int dz \mathcal{K}_{qq}(z) \left[\frac{1}{z^2} \sqrt{\frac{z}{x}} D_q \left(\frac{x}{z}, \frac{\mathbf{k}}{z}, \tau \right) - \frac{1}{\sqrt{x}} D_q(x, \mathbf{k}, \tau) \right] \\
&\quad + \frac{1}{N_f} \int dz \mathcal{K}_{qg}(z) \frac{1}{z^2} \sqrt{\frac{z}{x}} D_g \left(\frac{x}{z}, \frac{\mathbf{k}}{z}, \tau \right) \\
&\quad + \frac{\bar{t}^*}{4} \hat{q} \nabla_k^2 \left[D(x, \mathbf{k}, t) \right].
\end{aligned}$$

Gaussian approximation

In this last approximation, for the gluon-dominated case, it is possible to approach the solution considering that its dependence on the transverse momentum remains Gaussian all along the evolution in the medium. Then, the estimation of the mean transverse momentum leads to a solution that we will call the *Gaussian approximation* [268] :

$$D_G(x, \mathbf{k}, t) = D(x, t) \frac{4\pi}{\langle k_\perp^2 \rangle} \exp \left[-\frac{\mathbf{k}^2}{\langle k_\perp^2 \rangle} \right], \tag{4.95}$$

where

$$\langle k_\perp^2 \rangle_{x,t} \equiv \frac{\int \frac{d\mathbf{k}}{(2\pi)^2} |\mathbf{k}| D(x, \mathbf{k}, t)}{\int \frac{d\mathbf{k}}{(2\pi)^2} D(x, \mathbf{k}, t)} = \min \left\{ \frac{1}{2} \hat{q} t (1 + x^2), \frac{k_{br}^2(x)}{4\bar{\alpha}}, (xE)^2 \right\}, \tag{4.96}$$

with E the energy of the initial hard gluon and $k_{br}^2(x) = \sqrt{x E \hat{q}}$. In this approximation, the solution takes the factorized form of the solution of the integrated BDIM equation (for gluons, Eq. (4.84)) times a Gaussian dependence on the transverse momentum. This Gaussian dependence, characterized by $\langle k_\perp^2 \rangle$, is obtained in different regimes. The first term in Eq. (4.96) (in the min function) corresponds to the regime where single medium-induced radiations dominate (it is obtained as a perturbative estimate of the solution) while the second term corresponds to the regime dominated by multiple scattering. Finally, the last term is actually a condition for the approximation done to estimate $\langle k_\perp^2 \rangle$ to be valid.

Perturbative estimate

Finally, we should consider the 1st-order perturbative estimation of the **BDIM** equation (to approach its solution) which is equivalent to considering a single in-medium splitting or scattering. We derive this estimation for the most general case.

Let's begin with a (hard) gluon initiator :

$$D_g^{(0)}(x, \mathbf{k}) = x\delta(1-x)\delta^{(2)}(\mathbf{k}), \quad \text{and} \quad D_q^{(0)}(x, \mathbf{k}) = 0. \quad (4.97)$$

We introduce this initial solution in the **BDIM** equation Eq. (4.71) in order to find the first-order perturbative estimate :

$$\begin{aligned} D_g^{(1)}(x, \mathbf{k}, \delta t) &= D_g^{(0)}(x, \mathbf{k}) \times \\ &\times \left\{ 1 - \delta t \left[\alpha_s \int_0^1 dz \left(\mathcal{K}_{gg}(z, p_0^+) + \mathcal{K}_{qg}(z, p_0^+) \right) + \int \frac{d^2 \mathbf{q}}{(2\pi)^2} w_g(\mathbf{q}) \right] \right\} \\ &+ \frac{\delta t}{(2\pi)^2} \left[2\alpha_s x \mathcal{K}_{gg}(\mathbf{k}, x, p_0^+) + x\delta(1-x)w_g(\mathbf{k}) \right], \\ D_q^{(1)}(x, \mathbf{k}, \delta t) &= \frac{\delta t}{(2\pi)^2} \frac{\alpha_s}{N_F} x \mathcal{K}_{qq}(\mathbf{k}, x, p_0^+), \end{aligned} \quad (4.98)$$

where $\mathcal{K}_{ij}(x, p_0^+) = \int \frac{d^2 \mathbf{k}}{(2\pi)^2} \mathcal{K}_{ij}(\mathbf{k}, x, p_0^+)$. The term in curly brackets next to the initial condition $D_g^{(0)}(x, \mathbf{k})$ is responsible for probability conservation. Now, integrating out the transverse momentum \mathbf{k} or the momentum fraction x , respectively, we get the following distributions:

$$D(x, t) \equiv \int d^2 \mathbf{k} D(x, \mathbf{k}, t), \quad D(\mathbf{k}, t) = \int_0^1 dx D(x, \mathbf{k}, t), \quad (4.99)$$

which respects $\int_0^1 dx D(x, t) = 1$ and $\int d^2 \mathbf{k} D(\mathbf{k}, t) = 1$. The expressions for these distributions take the form :

$$\begin{aligned} D_g^{(1)}(x, \delta t) &= \delta t 2\alpha_s x \mathcal{K}_{gg}(x, p_0^+), \\ D_q^{(1)}(x, \delta t) &= \delta t \frac{\alpha_s}{N_F} x \mathcal{K}_{qq}(x, p_0^+), \end{aligned} \quad (4.100)$$

and, finally :

$$\begin{aligned} D_g^{(1)}(\mathbf{k}, \delta t) &= \frac{\delta t}{(2\pi)^2} \int_0^1 dx 2\alpha_s x \mathcal{K}_{gg}(\mathbf{k}, x, p_0^+) + \frac{\delta t}{(2\pi)^2} w_g(\mathbf{k}), \\ D_q^{(1)}(\mathbf{k}, \delta t) &= \frac{\delta t}{(2\pi)^2} \frac{\alpha_s}{N_F} \int_0^1 dx x \mathcal{K}_{qq}(\mathbf{k}, x, p_0^+). \end{aligned} \quad (4.101)$$

For readability, we have dropped terms that are proportional to the initial condition. They are however crucial to restore the normalization of the distributions.

Now, for the quark initiator, we have :

$$D_g^{(0)}(x, \mathbf{k}) = 0, \quad \text{and} \quad D_q^{(0)}(x, \mathbf{k}) = x\delta(1-x)\delta^{(2)}(\mathbf{k}), \quad (4.102)$$

which leads to :

$$\begin{aligned} D_g^{(1)}(x, \mathbf{k}, \delta t) &= \frac{\delta t}{(2\pi)^2} \alpha_s N_F x \mathcal{K}_{gq}(\mathbf{k}, x, p_0^+), \\ D_q^{(1)}(x, \mathbf{k}, \delta t) &= D_q^{(0)}(x, \mathbf{k}) \left\{ 1 - \delta t \left[\alpha_s \int_0^1 dz \mathcal{K}_{qq}(z, p_0^+) + \int \frac{d^2 \mathbf{q}}{(2\pi)^2} w_q(\mathbf{q}) \right] \right\} \\ &\quad + \frac{\delta t}{(2\pi)^2} x \delta(1-x) w_q(\mathbf{k}). \end{aligned} \quad (4.103)$$

The integrated distributions now read, omitting the terms proportional to the initial condition :

$$\begin{aligned} D_g^{(1)}(x, \delta t) &= \delta t \alpha_s N_F x \mathcal{K}_{gq}(x, p_0^+), \\ D_q^{(1)}(x, \delta t) &= \delta t \alpha_s x \mathcal{K}_{qq}(x, p_0^+), \end{aligned} \quad (4.104)$$

and, finally :

$$\begin{aligned} D_g^{(1)}(\mathbf{k}, \delta t) &= \frac{\delta t}{(2\pi)^2} \int_0^1 dx \alpha_s N_F x \mathcal{K}_{gq}(\mathbf{k}, x, p_0^+), \\ D_q^{(1)}(\mathbf{k}, \delta t) &= \frac{\delta t}{(2\pi)^2} \alpha_s \int_0^1 dx x \mathcal{K}_{qq}(\mathbf{k}, x, p_0^+). \end{aligned} \quad (4.105)$$

Note that these perturbative estimates imply the integral of the splitting kernel which has to be performed numerically.

4.4 Resolution of the BDIM equations

Now that we have derived equations for the evolution of jet in a QGP, we will consider different options to solve them. The BDIM equations are linear integral-differential equations (for which numerous methods exist) but the difficulty to solve these equations lies in 2 main points. First, the branching kernels diverge for $z = 0$ and $z = 1$, secondly the dependence in $\frac{x}{z}$ and $\frac{k}{z}$ of the fragmentation functions makes it non-trivial to mesh efficiently a grid for standard numerical method. Anyway, in this section, we will first consider a simplified BDIM equation for which an analytical solution exists. We will study briefly this solution to use it later as an analytical ansatz to compare it to solutions for the actual BDIM equation (in one of the forms presented in the previous section). Then, we will present 2 methods to solve them. A Markov Chain Monte-Carlo (MCMC) method (used differently by two programs, MINCAS [269] and TMDICE [270]) that has proven efficient and able to solve all the forms of BDIM equations we are interested in. A second one, semi-analytical, based on the expansion of the fragmentation functions in Chebyshev polynomials (which, while not completely adapted to the problem, successfully solved the integrated BDIM equations).

4.4.1 Analytical solution

In the simplest case, i.e the integrated **BDIM** equation for gluon-dominated cascades (see Eq. (4.84)), they are no analytical solutions. Still, it is possible to simplify the branching kernel in this case (Eq. (4.83)), setting its numerator to 1 :

$$\mathcal{K}_{simple}(z) = \frac{1}{[z(1-z)]^{\frac{3}{2}}}. \quad (4.106)$$

This does not change the divergent behavior of the kernel hence the solution of this simplified equation should keep the main features of the complete solution. With this kernel, it is possible to obtain an analytical solution to Eq. (4.84) for the starting distribution $D_g(x, 0) = \delta(1-x)$ using a Laplace transform leading to [271] :

$$D_a(x, \tau) = \frac{\tau}{\sqrt{x(1-x)^3}} e^{-\pi \frac{\tau^2}{1-x}}. \quad (4.107)$$

We can already see that this distribution scales like $\frac{1}{\sqrt{x}}$ at small- x for any time $\tau > 0$. More remarkably, at low- x , the x and τ dependence factorize :

$$D_a(x \ll 1, \tau) \simeq \frac{1}{\sqrt{x}} \tau e^{-\pi \tau^2}. \quad (4.108)$$

At small times (and small- x), if the scale is governed by a $\frac{1}{\sqrt{x}}$ shape, its amplitude increase linearly with time. The stability of the x dependence while time increases reflects that the energy flows from the initial source at $x = 1$ (the initial parton) to $x = 0$ without any accumulation at intermediate x , which is a signature of what is called *wave turbulence* [271, 272]. By the way, the total energy for gluons in the cascade with energy $0 < x < 1$ decreases with time as :

$$E_a(\tau) \equiv \int_0^1 dz D_a(x, \tau) = e^{-\pi \tau^2}. \quad (4.109)$$

The essential singularity at $x = 1$ can be understood as due to the vanishing probability of emitting no gluon at a finite time (which can be written as a Sudakov suppression factor [273]). This solution is presented in Fig. 4.8, multiplied by \sqrt{x} , for several values of τ ($\tau \in \{0.01, 0.1, 0.3, 0.5, 0.7, 0.9\}$). We clearly see the low- x scaling and also the energy flow that washes out the initial peak at $x = 1$ to leave after long evolution time a depletion in the energy distribution.

4.4.2 Resolution with Monte-Carlo approach

We will begin by presenting the method applied by the **MCMC** program **MINCAS** [269], provided by our collaborator Wieslaw Placzek, that we have used extensively to produce solutions to all the forms of **BDIM** equations presented earlier, and study them. In particular, we will detail this method directly for the most general case of Eq. (4.71)

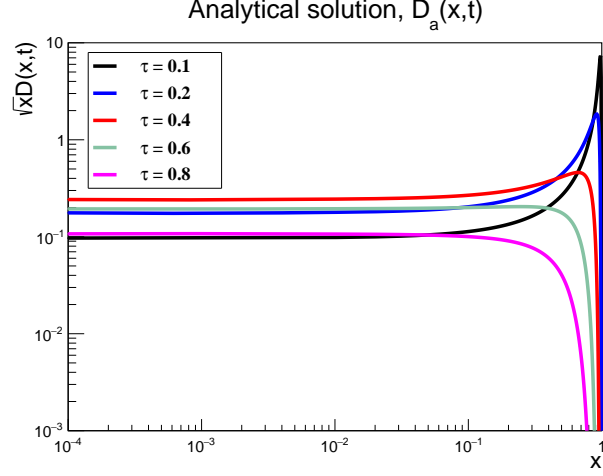


Figure 4.8: Analytical solution $\sqrt{x}D_a(x, \tau)$ for several evolution times ($\tau \in \{0.1, 0.2, 0.4, 0.6, 0.8\}$).

(complete cascade with broadening in branching).

Actually, the first step to solve the BDIM equation Eq. (4.71) with a MCMC method is to rewrite it in a Volterra type form. To this end, we have first to introduce a few notations. First, we rewrite the equations not only in terms of the partons types i, j but in terms of their precise flavor $I, J \in \{g, q_1, \dots, q_{N_f}, \bar{q}_1, \dots, \bar{q}_{N_f}\}$, leading to the definition of the kernels :

$$\mathcal{K}_{IJ}(z, y, \mathbf{Q}) = \frac{\alpha_s}{(2\pi)^2} (1 + \delta_{Ig}\delta_{Jg}) \bar{t}^* z \mathcal{K}_{IJ}(\mathbf{Q}, z, yp_0^+). \quad (4.110)$$

This leads to $\mathcal{K}_{gq_i} \equiv \mathcal{K}_{gq}$, $\mathcal{K}_{q_i g} \equiv \mathcal{K}_{qg}/N_f$, and $\mathcal{K}_{q_i q_j} \equiv \delta_{ij} \mathcal{K}_{qq}$ while the delta functions $(1 + \delta_{IG}\delta_{JG})$ accounts for the symmetry in \mathcal{K}_{gg} .

To continue, we need to introduce the Sudakov form-factor $\Psi_I(x)$ that resums all unresolved branchings and scatterings :

$$\Psi_I(x) = \Phi_I(x) + W_I, \quad (4.111)$$

where :

$$\Phi_I(x) = \sum_J \Phi_{JI}(x), \quad \Phi_{JI}(x) = \int_0^{1-\epsilon} dz \int d^2\mathbf{Q} \mathcal{K}_{JI}(z, x, \mathbf{Q}), \quad (4.112)$$

and :

$$W_I = \bar{t}^* \int_{|\mathbf{l}| > l_{\min}} \frac{d^2\mathbf{l}}{(2\pi)^2} w_I(\mathbf{l}). \quad (4.113)$$

This Sudakov form factor is defined with a higher cutoff ϵ for the integration in z (delimiting the resolvable branching) and a lower cutoff l_{\min} in the integral over the

transverse momentum \mathbf{l} (acquired through multiple scattering). Then, we can define a kernel accounting for both branching and scattering :

$$\mathcal{G}_{IJ}(z, y, \mathbf{Q}, \mathbf{l}) = \mathcal{K}_{IJ}(z, y, \mathbf{Q})\theta(1 - \epsilon - z)\delta(\mathbf{l}) + \bar{t}^* \frac{w_I(\mathbf{l})}{(2\pi)^2} \theta(|\mathbf{l}| - l_{\min}) \delta(1 - z)\delta(\mathbf{Q})\delta_{IJ}. \quad (4.114)$$

Finally, we can write the Eq. (4.71) using the introduced notations and the proper time τ as :

$$\begin{aligned} \frac{\partial}{\partial \tau} D_I(x, \mathbf{k}, \tau) + \Psi_I(x) D_I(x, \mathbf{k}, \tau) &= \int_0^1 dy \int_0^1 dz \int d^2 \mathbf{k}' \int d^2 \mathbf{Q} \int d^2 \mathbf{l} \\ &\times \delta(x - zy) \delta(\mathbf{k} - \mathbf{l} - \mathbf{Q} - z\mathbf{k}') \sum_J \mathcal{G}_{IJ}(z, y, \mathbf{Q}, \mathbf{l}) D_J(y, \mathbf{k}', \tau). \end{aligned} \quad (4.115)$$

which solution can be written as a Volterra-type equation, namely :

$$\begin{aligned} D_I(x, \mathbf{k}, \tau) &= D_I(x, \mathbf{k}, \tau_0) e^{-\Psi_I(x)(\tau - \tau_0)} \\ &+ \sum_J \int_{\tau_0}^{\tau} d\tau' \int_0^1 dy \int_0^1 dz \int d^2 \mathbf{k}' \int d^2 \mathbf{Q} \int d^2 \mathbf{l} \mathcal{G}_{IJ}(z, y, \mathbf{Q}, \mathbf{l}) \\ &\times D_J(y, \mathbf{k}', \tau') e^{-\Psi_I(x)(\tau - \tau')} \delta(x - zy) \delta(\mathbf{k} - \mathbf{l} - \mathbf{Q} - z\mathbf{k}'), \end{aligned} \quad (4.116)$$

where $\tau_0 = t_0/\bar{t}^*$ is the initial proper time for the evolution. In this equation, the first term in the r.h.s corresponds to the probability that no (resolvable) branching nor scattering occurs between τ_0 and τ . Such equations can be solved iteratively (like Fredholm equations seen in Sec. 2.5). This can be written in our case :

$$\begin{aligned} D_I(x, \mathbf{k}, \tau) &= \sum_{J_0} \int_0^1 dx_0 \int d^2 \mathbf{k}_0 \left\{ e^{-\Psi_{J_0}(x_0)(\tau - \tau_0)} \delta_{IJ_0} \delta(x - x_0) \delta(\mathbf{k} - \mathbf{k}_0) \right. \\ &+ \sum_{n=1}^{+\infty} \sum_{J_1, J_2, \dots, J_n} \prod_{i=1}^n \left[\int_{\tau_{i-1}}^{\tau} d\tau_i \int_0^1 dz_i \int d^2 \mathbf{Q}_i \int d^2 \mathbf{l}_i \right. \\ &\quad \left. \left. \mathcal{G}_{J_i J_{i-1}}(z_i, x_{i-1}, \mathbf{Q}_i, \mathbf{l}_i) e^{-\Psi_{J_{i-1}}(x_{i-1})(\tau_i - \tau_{i-1})} \right] \right. \\ &\left. \times e^{-\Psi_{J_n}(x_n)(\tau - \tau_n)} \delta_{J_n I} \delta(x - x_n) \delta(\mathbf{k} - \mathbf{k}_n) \right\} D_{J_0}(x_0, \mathbf{k}_0, \tau_0), \end{aligned} \quad (4.117)$$

where :

$$x_i = z_i x_{i-1}, \quad \mathbf{k}_i = \mathbf{Q}_i + \mathbf{l}_i + z_i \mathbf{k}_{i-1}. \quad (4.118)$$

The last step is the evaluation of this iterative solution and this is done with the help of a MCMC method. This means that we have to rewrite Eq. (4.117) in a probabilistic way, suited to MCMC. To do it, we define the Probability Distribution Function (p.d.f) for the generation of the variable τ_i :

$$\varrho_{J_{i-1}}(\tau_i) = \Psi_{J_{i-1}}(x_{i-1}) e^{-\Psi_{J_{i-1}}(x_{i-1})(\tau_i - \tau_{i-1})} \theta(\tau_i - \tau_{i-1}). \quad (4.119)$$

For the generation of the variables $(z_i, \mathbf{Q}_i, \mathbf{l}_i)$, we define :

$$\Xi_{J_i J_{i-1}}(z_i, \mathbf{Q}_i, \mathbf{l}_i) = \frac{\mathcal{G}_{J_i J_{i-1}}(z_i, x_{i-1}, \mathbf{Q}_i, \mathbf{l}_i)}{\Psi_{J_i J_{i-1}}(x_{i-1})}, \quad \Psi_{J_i J_{i-1}}(x_{i-1}) = \Phi_{J_i J_{i-1}}(x_{i-1}) + W_{J_i}. \quad (4.120)$$

And finally, the conditional probability for generating a new parton flavor J_i (given the flavor J_{i-1}) reads :

$$p_{J_i} \equiv p(J_i | J_{i-1}) = \frac{\Psi_{J_i J_{i-1}}(x_{i-1}) e^{-\Psi_{J_i J_{i-1}}(x_{i-1})(\tau_i - \tau_{i-1})}}{\varrho_{J_{i-1}}(\tau_i)}. \quad (4.121)$$

All those probability distributions are normalized to 1. Now we can write Eq. (4.117) as :

$$\begin{aligned} D_I(x, \tau) = & d(\tau_0) \int_0^1 dx_0 \int d^2 \mathbf{k}_0 \chi(x_0, \mathbf{k}_0) \sum_{J_0} p_{J_0} \left\{ \int_{\tau}^{+\infty} d\tau_1 \varrho_{J_0}(\tau_1) \delta_{J_0 I} \delta(x - x_0) \delta(\mathbf{k} - \mathbf{k}_0) \right. \\ & + \sum_{n=1}^{+\infty} \sum_{J_1, \dots, J_n} \prod_{i=1}^n \left[\int_0^{\tau} d\tau_i \varrho_{J_{i-1}}(\tau_i) p_{J_i} \int_0^1 dz_i \int d^2 \mathbf{Q}_i \int d^2 \mathbf{l}_i \Xi_{J_i J_{i-1}}(z_i, \mathbf{Q}_i, \mathbf{l}_i) \right] \\ & \left. \times \int_{\tau}^{+\infty} d\tau_{n+1} \varrho_{J_n}(\tau_{n+1}) \delta_{J_n I} \delta(x - x_n) \delta(\mathbf{k} - \mathbf{k}_n) \right\}, \end{aligned} \quad (4.122)$$

with the initial functions :

$$d(\tau_0) = \int_0^1 dx_0 \int d^2 \mathbf{k}_0 \sum_J D_J(x_0, \mathbf{k}_0, \tau_0), \quad (4.123)$$

$$\chi(x_0, \mathbf{k}_0) = \frac{\sum_J D_J(x_0, \mathbf{k}_0, \tau_0)}{d(\tau_0)}, \quad p_{J_0} = \frac{D_J(x_0, \mathbf{k}_0, \tau_0)}{\sum_J D_J(x_0, \mathbf{k}_0, \tau_0)}. \quad (4.124)$$

Eq. (4.122) can be proceeded following the MCMC algorithm :

1. Set the initial values of (x_0, \mathbf{k}_0) and J_0 or generate them according to the probabilities $\chi(x_0, \mathbf{k}_0)$ and p_{J_0} , respectively. Set $i = 1$.
2. Generate τ_i according to the p.d.f $\varrho_{J_{i-1}}(\tau_i)$.
 - 2.1 If $\tau_i > \tau$ set $x = x_{i-1}$, $\mathbf{k} = \mathbf{k}_{i-1}$, $I = J_{i-1}$ and **stop**,
 - 2.2 otherwise, i.e. if $\tau_i \leq \tau$:
 - (a) generate the parton flavour J_i according the probability p_{J_i} ,
 - (b) generate the variables $(z_i, \mathbf{Q}_i, \mathbf{l}_i)$ according to the p.d.f. $\Xi_{J_i J_{i-1}}(z_i, \mathbf{Q}_i, \mathbf{l}_i)$,
 - (c) set $x_i = z_i x_{i-1}$ and $\mathbf{k}_i = z_i \mathbf{k}_{i-1} + \mathbf{Q}_i + \mathbf{l}_i$,
 - (d) increment $i \rightarrow i + 1$ and go to step 2.

At the end of the algorithm, one get an n -leap trajectories γ_n with MC weight :

$$w_I^{\gamma_n}(x, \mathbf{k}, \tau) = d(\tau_0) \delta_{J_n I} \delta(x - x_n) \delta(\mathbf{k} - \mathbf{k}_n). \quad (4.125)$$

The expectation value of such a weight is the sought distribution function $D_I(x, \mathbf{k}, \tau)$:

$$E [w_I^{\gamma}(x, \mathbf{k}, \tau)] = D_I(x, \mathbf{k}, \tau). \quad (4.126)$$

In practice, histograms of the desired variables are filled with the described algorithm, weighted as in Eq. (4.125). However, in this algorithm, it is not trivial that the necessary random variable can be sampled from the respective probability distribution functions (ϱ and Ξ for instance). In particular, the kernels used to define them are not integrable analytically. MINCAS deals with this problem using a simplified kernel (as close as possible to the original one but which can be integrated analytically) and re-weights the event accordingly. More details on MINCAS may be found on the paper where it was used ([269] for the collinear case, where more details on the re-weighting are given, [3] in the pure gluon case, accounting for broadening in branching and finally in [4] for the most general case presented here).

Basically based on the same approach, TMDICE [270] is another MCMC based program (developped by our collaborator Martin Rohmoser) that solves the BDIM equation. Actually, TMDICE focuses on the multiplicity distributions F_i :

$$F_i(x, \mathbf{k}, t) \equiv \frac{d^3 N_a}{dx d^2 \mathbf{k}} = \frac{1}{x} D_i(x, \mathbf{k}, t), \quad (4.127)$$

and calculates solution of the BDIM equivalent equations for this multiplicity distribution :

$$\begin{aligned} \frac{\partial}{\partial t} F_g(x, \mathbf{k}, t) &= \alpha_s \int_0^1 dz \int \frac{d^2 \mathbf{q}}{(2\pi)^2} \left[2\mathcal{K}_{gg}(\mathbf{Q}, z, \frac{x}{z} p_+) \frac{1}{z} F_g\left(\frac{x}{z}, \mathbf{q}, t\right) \right. \\ &\quad + \mathcal{K}_{gq}(\mathbf{Q}, z, \frac{x}{z} p_+) \frac{1}{z} F_q\left(\frac{x}{z}, \mathbf{q}, t\right) \\ &\quad \left. - \left\{ \mathcal{K}_{gg}(\mathbf{q}, z, xp_+) + \mathcal{K}_{qg}(\mathbf{q}, z, xp_+) \right\} F_g(x, \mathbf{k}, t) \right] \\ &\quad + \int \frac{d^2 \mathbf{l}}{(2\pi)^2} C_g(\mathbf{l}) F_g(x, \mathbf{k} - \mathbf{l}, t), \quad (4.128) \\ \frac{\partial}{\partial t} F_q(x, \mathbf{k}, t) &= \alpha_s \int_0^1 dz \int \frac{d^2 \mathbf{q}}{(2\pi)^2} \left[\mathcal{K}_{qq}(\mathbf{Q}, z, \frac{x}{z} p_+) \frac{1}{z} F_q\left(\frac{x}{z}, \mathbf{q}, t\right) \right. \\ &\quad + \mathcal{K}_{qg}(\mathbf{Q}, z, \frac{x}{z} p_+) \frac{1}{z} F_g\left(\frac{x}{z}, \mathbf{q}, t\right) - \mathcal{K}_{qq}(\mathbf{q}, z, xp_+) F_q(x, \mathbf{k}, t) \left. \right] \\ &\quad + \int \frac{d^2 \mathbf{l}}{(2\pi)^2} C_q(\mathbf{l}) F_q(x, \mathbf{k} - \mathbf{l}, t). \end{aligned}$$

Basically, it leads to the iterative solution Eq. (4.122) but with some changes in the p.d.f and kernels used. Ξ and \mathcal{G} are replaced by $\tilde{\Xi}$ and $\tilde{\mathcal{G}}$, defined as :

$$\begin{aligned}\tilde{\Xi}_{J_i J_{i-1}}(z_i, \mathbf{Q}_i, \mathbf{l}_i) &= \frac{\tilde{\mathcal{G}}_{J_i J_{i-1}}(z_i, x_{i-1}, \mathbf{Q}_i, \mathbf{l}_i)}{\Psi_{J_i J_{i-1}}(x_{i-1})}, \\ \tilde{\mathcal{G}}_{IJ}(z, y, \mathbf{Q}, \mathbf{l}) &= \frac{1}{z} \mathcal{K}_{IJ}(z, y, \mathbf{Q}) \theta(1 - \epsilon - z) \delta(\mathbf{l}) \\ &\quad + \bar{t}^* \frac{w_I(\mathbf{l})}{(2\pi)^2} \theta(|\mathbf{l}| - l_{\min}) \delta(1 - z) \delta(\mathbf{Q}).\end{aligned}\tag{4.129}$$

Please note that the functions $\Phi_{J_i J_{i-1}}$, $\Psi_{J_i J_{i-1}}$, and W_{J_i} stay the same in both approaches.

Another subtle difference exists between the two MCMC programs, TMDICE deals with the non-integrable kernel (used in the p.d.f performing the sampling of the needed random variables) numerically. This might be long (especially if great numerical precision is needed) but no re-weighting is needed. More details on TMDICE can be found in [270].

Finally, we should mention that to consider collinear splitting (as in Eq. (4.91)), one only needs to perform the following substitution in the definition of \mathcal{G}_{IJ} (Eq. (4.114)) :

$$\mathcal{K}_{IJ}(z, y, \mathbf{Q}) \rightarrow \frac{1}{\sqrt{y}} z \mathcal{K}_{IJ}(z),\tag{4.130}$$

and for the energy distribution Eq. (4.86)), set also $w_I(\mathbf{l}) = 0$.

4.4.3 Resolution with Chebyshev method

Now, we will present a method to solve linear integral differential equation based on Chebyshev polynomials and apply it to the BDIM equations. This method has been developed to provide a semi-analytical approach to the resolution of the BDIM equations and then to confirm results obtains by the MCMC programs presented above. The idea is to decompose the solution in Chebyshev polynomials such that, in the end, we determine numerically the coefficients of this decomposition and can then use them to obtain the solution for any value. Also, we decompose integrands in Chebyshev polynomials to evaluate the appearing integrals. Consequently, we call this method the *Chebyshev method*. It is based on the method used in [274] to solve QCD evolution equations, adapted to our specific problem (similar method had also been used to solve BK equations [275, 276]).

So, we will first present the method (with a more general equation) and the useful properties of the Chebyshev polynomials before applying it to the integrated BDIM equations (first for gluons only then for quarks and gluons). We will then study the obtained solution and their dependence on some non-physical parameters (linked to the method) to understand the limits of the Chebyshev method on solving the BDIM equation.

General method

We consider equations of the form :

$$\frac{\partial D(x, \tau)}{\partial \tau} = \int_0^1 dz \left[\mathcal{K}_1(x, z)D(x, \tau) + \mathcal{K}_2(x, z)D\left(\frac{x}{z}, \tau\right) \right], \quad (4.131)$$

with D the distribution function we are interested in ($D(x, \tau)$ can be a vector, in the case of a system of equations), $x \in [0, 1]$, $\tau > 0$, $\mathcal{K}_{1,2}$ some kernels ($\mathcal{K}_{1,2}(x, z)$ can be matrices) that may be divergent on 0 and/or 1.

To solve the differential equation, we will use standard numerical methods (as simple as the Euler method, and maybe some higher-order Runge-Kutta).

To do so, we need to discretize the distribution function on a set of coordinates $\{x_k\}$, $\{\tau_k\}$. But, due to the term $D(\frac{x}{z}, \tau)$, we decide to expand D in Chebyshev polynomials on the x variable. This way $D(x, \tau)$ can be taken outside the integrals.

The Chebyshev expansion reads :

$$D(x, \tau) \simeq \frac{2}{N} \sum_{i=0}^{N-1} ' \sum_{j=0}^{N-1} D(x_j, \tau) T_i(y_j) T_i(y(x)), \quad (4.132)$$

where :

- $\{T_i\}_{i \in \llbracket 1; N \rrbracket}$ are the N -th first Chebyshev polynomials of the first kind ($N \in \mathbb{N}$ is the order of our decomposition). They are defined as :

$$\forall i \in \mathbb{N}, \forall z \in [-1, 1], T_i(z) = \cos(i \arccos(z)).$$

- \sum' means that the first term in the sum is divided by 2,
- $\{y_i\}_{i \in \llbracket 1; N \rrbracket}$ are the nodes (or zeros) of T_N :

$$y_i = \cos \frac{\pi}{N} \left(i + \frac{1}{2} \right), \quad i \in \llbracket 1; N \rrbracket,$$

- $y : [0, 1] \rightarrow [-1, 1]$ is an arbitrary bijection (that we will give explicitly later),
- $\{x_i\}_{i \in \llbracket 1; N \rrbracket}$ are the arguments of $\{y_i\}$ by y :

$$\forall i \in \llbracket 1; N \rrbracket, x_i = y^{-1}(y_i).$$

Some remarks :

- We note that $T_i(y_j)$ does not depend on the bijection y used to define $\{y_i\}$, we will then simply note $T_{i,j} \equiv T_i(y_j)$ as the i -th Chebyshev polynomial evaluated on the j -th node (of the N -th Chebyshev polynomial).

- The convergence of the Chebyshev expansion is only given for bounded and continuous functions (it is even exponential for infinitely smooth ones). We may still use it while this is not fulfilled by the searched function. In this case, the convergence has to be checked.
- The decomposition in Chebyshev polynomials at order N is exact on the nodes $\{x_k\}$ of the N -th polynomial, like an interpolation of the function considered over these points. Also, it may have the same defaults as a simple polynomial interpolation (oscillation around the interpolated points), what make this decomposition special is the distribution of the nodes : denser at the border of the definition set of the considered function.

The idea now is to solve the equation on the arguments of y of the N -th Chebyshev polynomial (T_N) nodes, i.e on $\{x_i\}_{i \in [1;N]}$. But before that, we should rewrite the integral (considering that $D(x, \tau)$ is only defined for $x \in [0, 1]$:

$$\frac{\partial D(x, \tau)}{\partial \tau} = \int_x^1 dz \left[\mathcal{K}_1(x, z)D(x, \tau) + \mathcal{K}_2(x, z)D\left(\frac{x}{z}, \tau\right) \right] + \int_0^x dz \mathcal{K}_1(x, z)D(x, \tau). \quad (4.133)$$

Indeed, when evaluating the integrals with the Chebyshev method, it is important that the range of integration is in the support of the integrand (if not, the precision drastically drops). This means, for instance, that the implicit Heaviside function implied by the coordinate $\frac{x}{z}$ has to be set explicit in the integration bounds. Also, keeping \mathcal{K}_1 and \mathcal{K}_2 under the same integral around 1 insures convergence in the equations we will study later (basically considering they have canceling divergences around 1). The equations on the nodes are then :

$$\begin{aligned} \frac{\partial D(x_k, \tau)}{\partial \tau} &= \frac{2}{N} \sum_{i=0}^{N-1}{}' \sum_{j=0}^{N-1} D(x_j, \tau) T_{i,j} \left[\int_{x_k}^1 dz \left[\mathcal{K}_1(x_k, z) T_{i,k} + \mathcal{K}_2(x_k, z) T_i\left(y\left(\frac{x_k}{z}\right)\right) \right] \right. \\ &\quad \left. + \int_0^{x_k} dz \mathcal{K}_1(x_k, z) T_{i,k} \right] \\ &= \frac{2}{N} \sum_{i=0}^{N-1}{}' \sum_{j=0}^{N-1} D(x_j, \tau) T_{i,j} \left[\int_{x_k}^1 dz \left[\mathcal{K}_1(x_k, z) \delta_{j,k} + \mathcal{K}_2(x_k, z) T_i\left(y\left(\frac{x_k}{z}\right)\right) \right] \right. \\ &\quad \left. + \int_0^{x_k} dz \mathcal{K}_1(x_k, z) \delta_{j,k} \right], \end{aligned} \quad (4.134)$$

where we went from the 1st line to the 2nd one using the orthogonality of the Chebyshev polynomials.

More generally, we obtain an equation of the form :

$$\frac{\partial D(x_k, \tau)}{\partial \tau} = \sum_{j=0}^{N-1} D(x_j, \tau) \mathcal{S}_j(x_k), \quad (4.135)$$

that is easily solved by an Euler method :

$$D(x_k, \tau_{t+1}) = D(x_k, \tau_t) + d\tau \sum_{j=0}^{N-1} D(x_j, \tau_t) \mathcal{S}_j(x_k), \quad (4.136)$$

with $d\tau$ a fixed time step and $\tau_t = \tau_0 + td\tau$ (with τ_0 the starting time, for which we need an initial distribution $D_0(x) = D(x, \tau_0)$ and $t \in \mathbb{N}$).

Chebyshev integration

To solve our equation with the Euler method, as presented before, we need first to calculate the matrix \mathcal{S} . This means, calculating the integrals appearing in Eq. (4.134) which will be done using another Chebyshev expansion. The idea is to expand the integrands in the Chebyshev polynomial using a bijection y going from the integrals borders to $[-1, 1]$. Then, the only integrals left are on the Chebyshev polynomials $\int_{-1}^1 dz T_i(z)$ which are perfectly known. More precisely, if we consider $f : [a, b] \rightarrow \mathbb{R}$ and a linear bijection $y : [a, b] \rightarrow [-1, 1]$, we can write :

$$\begin{aligned} \int_a^b dz f(z) &\simeq \frac{2}{N} \sum_{i=0}^{N-1} \sum_{j=0}^{N-1} f(x_j) T_i(y_j) \int_a^b dz T_i(y(z)) \\ &= \frac{b-a}{N} \sum_{i=0}^{N-1} \sum_{j=0}^{N-1} f(x_j) T_i(y_j) \int_{-1}^1 dz T_i(z). \end{aligned} \quad (4.137)$$

Here :

$$\begin{aligned} y &: [a, b] \rightarrow [-1, 1], \\ x &\mapsto \frac{2x - b - a}{b - a} \end{aligned} \quad (4.138)$$

whose inverse is (needed to calculate $\{x_k\}$) :

$$\begin{aligned} y^{-1} &: [-1, 1] \rightarrow [a, b]. \\ x &\mapsto \frac{1}{2} ((b-a)x + b+a) \end{aligned} \quad (4.139)$$

And the integrals of the Chebyshev polynomials are given by :

$$\int_{-1}^1 dz T_i(z) = \begin{cases} 0, & \text{for } i = 1, \\ \frac{1+(-1)^i}{1-i^2} & \text{otherwise} \end{cases} \quad (4.140)$$

This way of calculating integrals works better if $[a, b] \in \text{supp}(f)$. For instance, integrals of the form $\int_a^b dz f(z) \theta(z-c)$ with $c \in [a, b]$ should be written $\int_c^b dz f(z)$ before using this method (this means also that the bijection should be defined $y : [c, b] \rightarrow [-1, 1]$ in this case).

Also, a linear bijection may not be best suited for any integral. Particularly, when the integrand diverges on the border of the integral, a logarithmic bijection might be interesting :

$$\begin{aligned} y &: [a, b] \rightarrow [-1, 1], \\ x &\mapsto 1 + 2 \frac{\log \frac{x}{b}}{\log \frac{b}{a}} \end{aligned} \quad (4.141)$$

whose inverse is :

$$\begin{aligned} y^{-1} &: [-1, 1] \rightarrow [a, b], \\ x &\mapsto b \left(\frac{b}{a} \right)^{\frac{x-1}{2}} \end{aligned} \quad (4.142)$$

which leads to the following formula for the integral :

$$\int_a^b dz f(z) \simeq \frac{1}{N} \sum_{i=0}^{N-1} ' \sum_{j=0}^{N-1} f(y^{-1}(y_i)) T_{i,j} b \left(\frac{b}{a} \right)^{\frac{y_j-1}{2}} \log \frac{b}{a} \int_{-1}^1 dz T_i(z). \quad (4.143)$$

Of course, the logarithmic bijection doesn't work for $a = 0$. If we still want to use it in this case, we need to introduce a regulator $\epsilon > 0$ and integrate over $[\epsilon, b]$ rather than $[0, b]$.

In the following, we use a logarithmic bijection (from $[0, 1]$ to $[-1, 1]$) for the expansion of the distribution D (fragmentation function) and linear bijections for the integrals (either from $[x_k, 1]$ to $[-1, 1]$ or from $[0, x_k]$ to $[-1, 1]$). This choice has been done after some tests (taking logarithmic bijections for both doesn't give as good results as we thought).

Algorithm scheme

Before going through each equation we solved with this method, we will describe the general scheme of the program coded (since it follows what has been stated before, this section serves also to introduce the notations used in the program).

As described before, the distribution D is discretized in x on the Chebyshev polynomial nodes $\{x_k\}$ and linearly in τ such as :

$$D_{t,k} \equiv D(\tau_0 + td\tau, x_k), \quad (4.144)$$

with τ_0 the starting time of the Euler method (for which we provide a distribution) and $d\tau$ the time step. This way Eq. (4.136) is rewritten :

$$\Delta D_{k,t} = D_{k,t+1} - D_{k,t} \simeq \sum_{j=0}^{N-1} D_{j,t} \mathcal{S}_{k,j}. \quad (4.145)$$

Let's mention that the number of operations made during this Euler method, with the S matrix calculated in advance, grows as $n_t N^2$ with n_t the number of time steps (and N the order in the Chebyshev expansion).

We will see that even with such a simple approach to the differential equation (Euler method), results are qualitatively correct (main difficulties are elsewhere). Actually, we have also tested multistep methods (with an Adams–Bashforth method, easily implemented in the used code) to increase the accuracy but the change was completely negligible hence we have kept the Euler method for both simplicity and low calculation cost (even with a high number of time steps). Anyway, an important (and time-consuming) part of the algorithm is the calculation of the matrix S , which contain the integrals calculated via Chebyshev polynomials. We follow the decomposition of Eq. (4.134) :

$$\begin{aligned} \mathcal{S}_{k,j} &= \frac{2}{N} \sum_{i=0}^{N-1} {}'T_{i,j} \int_{x_k}^1 dz \left[\mathcal{K}_1(x_k, z) T_{i,k} + \mathcal{K}_2(x_k, z) T_i\left(y\left(\frac{x_k}{z}\right)\right) \right] \\ &\quad + \int_0^{x_k} dz \mathcal{K}_1(x_k, z) \delta_{j,k} \\ &= \frac{2}{N} \sum_{i=0}^{N-1} {}'T_i(y_j) I_{k,i}^1 + \delta_{j,k} I_k^2, \end{aligned} \tag{4.146}$$

where :

- $I_{k,i}^1 \equiv \int_{x_k}^1 dz \left[\mathcal{K}_1(x_k, z) T_{i,k} + \mathcal{K}_2(x_k, z) T_i\left(y\left(\frac{x_k}{z}\right)\right) \right]$,
- $I_k^2 \equiv \int_0^{x_k} dz \mathcal{K}_1(x_k, z)$.

Since we need to calculate integrals over $[0, x_k]$ and $[x_k, 1]$ we need to introduce 2 sets of bijections (linear ones) and the corresponding arguments of the nodes $\{x_i\}$:

- $\{y^{0k}\}_{k \in \llbracket 1; N \rrbracket}$ with :

$$\forall k \in \llbracket 1; N \rrbracket, y^{0k} : [0, x_k] \rightarrow [-1, 1],$$
- $\{x_i^{0k}\}_{i \in \llbracket 1; N \rrbracket}$ are the arguments of $\{y_i\}$ by y^{0k} :

$$\forall i \in \llbracket 1; N \rrbracket, x_i^{0k} = y^{0k^{-1}}(y_i),$$
- $\{y^{k1}\}_{k \in \llbracket 1; N \rrbracket}$ with :

$$\forall k \in \llbracket 1; N \rrbracket, y^{k1} : [x_k, 1] \rightarrow [-1, 1],$$
- $\{x_i^{k1}\}_{i \in \llbracket 1; N \rrbracket}$ are the arguments of $\{y_i\}$ by y^{k1} :

$$\forall i \in \llbracket 1; N \rrbracket, x_i^{k1} = y^{k1^{-1}}(y_i).$$

Then, we can express the integrals as :

$$\begin{aligned}
I_{k,i}^1 &\simeq \frac{1-x_k}{N} \sum_{l=0}^{N-1} \sum_{m=0}^{N-1} \left[\mathcal{K}_1(x_k, x_m^{k1}) T_{i,k} + \mathcal{K}_2(x_k, x_m^{k1}) T_i\left(y\left(\frac{x_k}{x_m^{k1}}\right)\right) \right] \\
&\quad \times T_{l,m} \int_{-1}^1 dz T_l(z), \\
I_k^2 &\simeq \frac{x_k}{N} \sum_{l=0}^{N-1} \sum_{m=0}^{N-1} \mathcal{K}_1(x_k, x_m^{0k}) T_{l,m} \int_{-1}^1 dz T_l(z).
\end{aligned} \tag{4.147}$$

Some remarks :

- The calculation of the S matrix grows as N^4 with the order in Chebyshev expansion. It can quickly become resource-demanding.
- This method provides a semi-analytical solution in the sense that the behavior in x is given by the Chebyshev decomposition (and the coefficients of this decomposition are obtained numerically). However, depending on the distribution behavior, the solutions obtained may oscillate a lot around the nodes. Then it may be interesting to consider the solution as completely numerical, meaning as a simple grid (meshed with the Chebyshev nodes), and extrapolating the values in between as if it wasn't obtained by this specific decomposition (a linear extrapolation for instance). This take on the result is possible since the coefficient of the Chebyshev expansion corresponds to the value of the distribution on the N -th Chebyshev polynomial nodes.

For those interested in the details of the code, or those who would like to modify it, a detailed review, introducing all notations and subroutines, is given in App. C.1. Also, the code itself is shared on [github](#).

Application to the integrated BDIM equation for gluons

We will first apply the Chebyshev method to the integrated **BDIM** equation for gluon-dominated cascade, which we recall (with explicit Heaviside functions) :

$$\frac{\partial D(x,t)}{\partial t} = \frac{1}{t^*} \int_0^1 dz \mathcal{K}(z) \left[\sqrt{\frac{z}{x}} D\left(\frac{x}{z}, t\right) \theta(z-x) - \frac{z}{\sqrt{x}} D(x,t) \right]. \tag{4.148}$$

The Euler method reads :

$$\Delta D_{k,t} = D_{k,t+1} - D_{k,t} \simeq \frac{dt}{t^*} \sum_{j=0}^{N-1} D_{j,t} \mathcal{S}_{k,j}, \tag{4.149}$$

with :

- $D_{t,k} \equiv D(t_0 + tdt, x_k)$ with t_0 the starting time and dt the time step (for the Euler method),

- $\mathcal{S}_{k,j} = \frac{1}{\sqrt{x_k}} \frac{2}{N} \left(\sum_{i=0}^{N-1} T_{i,j} I_{k,i}^2 - \delta_{k,j} \frac{N}{2} I_k^1 \right)$,
- $I_k^1 \equiv \int_0^{x_k} dz \mathcal{K}(z) z$,
- $I_{k,i}^2 \equiv \int_{x_k}^1 dz \mathcal{K}(z) \left(\sqrt{z} T_i \left(y \left(\frac{x_k}{z} \right) \right) - \delta_{j,k} z \right) = \int_{x_k}^1 dz \mathcal{K}(z) \left(\sqrt{z} T_i \left(y \left(\frac{x_k}{z} \right) \right) - z T_{i,k} \right)$,

and the integrals are given by :

$$\begin{aligned}
I_k^1 &\simeq \frac{x_k}{N} \sum_{l=0}^{N-1} \sum_{m=0}^{N-1} x_m^{0k} \mathcal{K}(x_m^{0k}) T_{l,m} \int_{-1}^1 dz T_l(z), \\
I_{k,i}^2 &\simeq \frac{1-x_k}{N} \sum_{l=0}^{N-1} \sum_{m=0}^{N-1} \mathcal{K}(x_m^{k1}) \left[\sqrt{x_m^{k1}} T_i \left(y \left(\frac{x_k}{x_m^{k1}} \right) \right) - x_m^{k1} T_{i,k} \right] T_{l,m} \int_{-1}^1 dz T_l(z).
\end{aligned} \tag{4.150}$$

We should mention that this method naturally avoids numerical instabilities due to the divergences of the kernel $\mathcal{K}(z)$ (for $z = 0$ and $z = 1$) with the calculations made on the nodes (which never are on the edge of the considered range). Also, the higher density of nodes near the edges helps in the precision of the integration of this kernel. Then, the Chebyshev method seems well suited to the studied equation. The problem comes from the initial distribution we need :

$$D_0(x) = D(x, \tau_0) = \delta(1-x), \tag{4.151}$$

a Dirac's delta function which is completely non-reproducible by a Chebyshev polynomial series. What we do is that we initialize our solution with a narrow Gaussian, peaked in 1 instead (to mimic the delta function), as follows :

$$D_0(x; \varepsilon) = \sqrt{\frac{2}{\pi}} \frac{1}{\varepsilon} \exp \left[-\frac{(x-1)^2}{2\varepsilon^2} \right], \tag{4.152}$$

where ε cannot be taken too small for the Chebyshev polynomials to reproduce the initial solution. Another solution would be to use the analytical solution (see Eq. (4.107)) for the simplified case at a short time $\tau_0 > 0$ or a solution obtained for some short time (with the MCMC approach for instance). Anyway, the most important problem for the Chebyshev method is the error made at the initialization (and how they propagate in the evolution).

Convergence of the results As a test, we consider the simplified BDIM equation (with the simplified kernel of Eq. (4.106)) that has an analytical solution to see if we reproduce it with the Chebyshev method. In Fig. 4.9, we compare the results obtained with $\varepsilon = 10^{-4}$, $dt = 10^{-6}$ and $N = 200$ when using either a linear bijection to decompose D or a logarithmic one.

With the linear bijection, we see that the Chebyshev polynomials completely fail to reproduce the initial distribution and undergo important oscillation that makes them

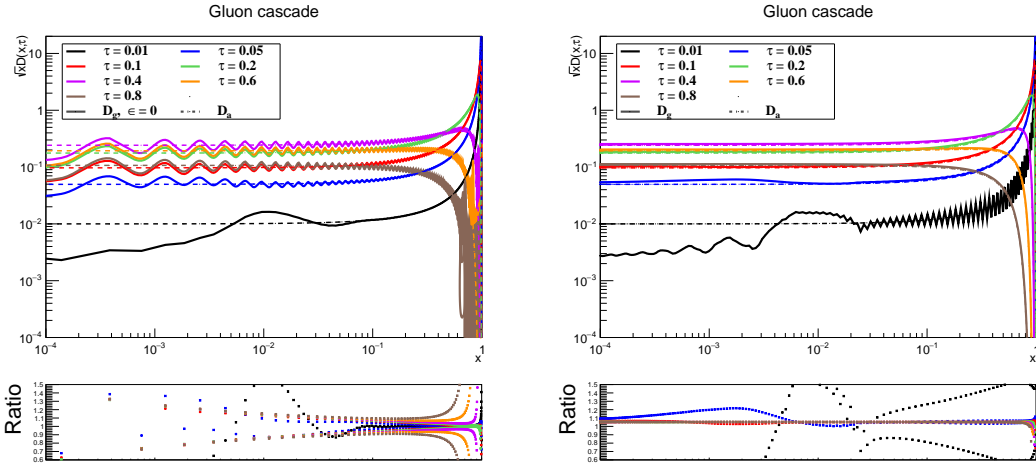


Figure 4.9: Comparison of results obtained with the Chebyshev method (solid lines) for the simplified BDIM equation with its analytical solution (dashed lines) at different evolution times ($\tau \in \{0.01, 0.05, 0.1, 0.2, 0.4, 0.6, 0.8\}$) and using either a linear bijection (left) or a logarithmic one (right). The ratio of D_{cheb}/D_a is also presented.

unusable. The evolution tends to amplify the initial oscillations due to the peaked shape of the initial distribution (not well reproduced by the Chebyshev polynomials) and propagates them at low- x . Still, the high- x distribution ($x \gtrsim 0.1$) is relatively well reproduced (especially at relatively low evolution times). Note that, in these pictures (and in the following ones), we use do not show the full decomposition but only the value of the distributions on the nodes of the Chebyshev polynomials (with this number of nodes, it doesn't make an important difference).

On the other hand, when we use a logarithmic bijection, the analytical result is recovered, for long enough evolution time (already at $\tau = 0.05$, the result is decent). In this case, the oscillations are tamed with the evolution and are important only at short times ($\tau = 0.01$), stressing again the problem due to the reproduction of the initial delta Dirac. Also, the method fails to properly describe the solution at high x in a range that becomes larger and larger with time (but, this is not too bad with this number of nodes, see the drop of the ration D_{cheb}/D_a around $x = 1$). Anyway, in the following, we should use the logarithmic bijection.

Actually, the difference with the analytical solution at long evolution time, looks like a cumulative error, mainly due to the initial distribution used, and its reproduction by the Chebyshev polynomials. Indeed, tests have been made with multistep methods (that were expected to reduce the cumulative error) but the results weren't significantly different.

In Fig. 4.10, we show the difference between our results obtained with the simplified kernel and the full one. Basically, the broadening of the peak at $x = 1$ seems slower when considering the full kernel. It is visible longer with the evolution and this makes look the evolution of the low- x distribution slower that in the simplified case.

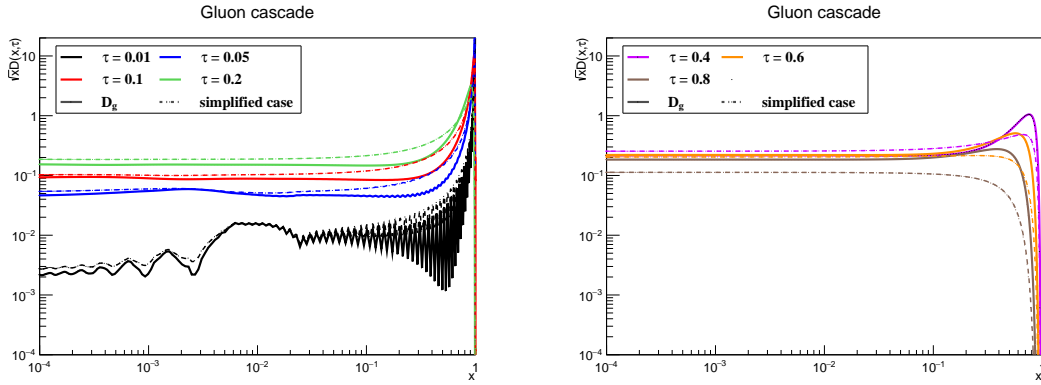


Figure 4.10: Comparison of results obtained with the Chebyshev method for the integrated BDIM equation (solid lines) with its simplified version (dashed lines) at evolution times $\tau \in \{0.01, 0.05, 0.1, 0.2\}$ (left) and $\tau \in \{0.4, 0.6, 0.8\}$ (right).

Next, we have made a series of convergence checks (important since the Chebyshev decomposition is not guaranteed to converge in the studied case). If the method is not very sensitive to the time step dt , a very small time step will help at high x for long evolution times (where unphysical oscillations appear). It is also important to very small x at small evolution times. These extreme cases are shown in Fig. 4.11 (note that here, and in the following figures, we plot the solutions at the nodes and do not use anymore the full decomposition since it has not proven relevant).

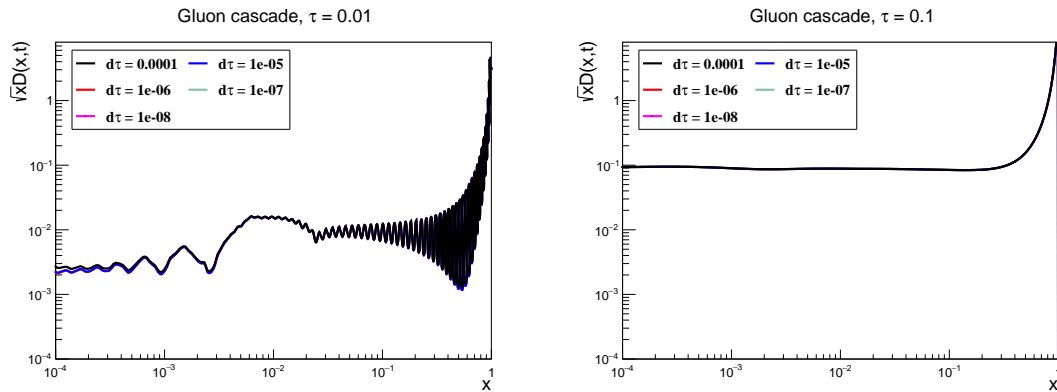


Figure 4.11: Comparison of results obtained with the Chebyshev method for different time steps ($dt \in \{10^{-4}, 10^{-5}, 10^{-6}, 10^{-7}, 10^{-8}\}$) at $\tau = 0.001$ (left) and $\tau = 0.1$ (right).

For the behavior with respect to ϵ , we can see some fluctuations at small times (see Fig. 4.12) but it converges quickly in time (at $\tau = 0.1$, the differences are negligible) to the same solution (at least for the cutoff, the linear bijection, denoted by " $\epsilon = 0$ ", exhibits the oscillations already observed).

Finally, let's review the parameter that influences the most the solutions obtained,

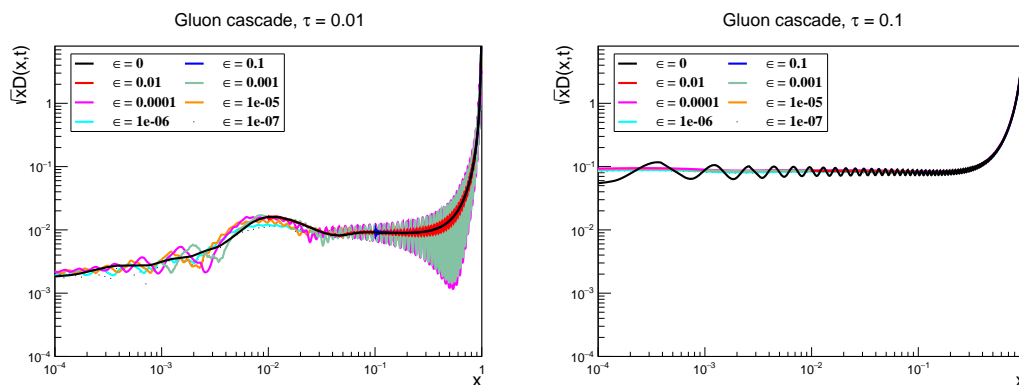


Figure 4.12: Comparison of results obtained with the Chebyshev method for different cutoff ($\epsilon \in \{0, 10^{-2}, 10^{-3}, 10^{-4}, 10^{-5}, 10^{-6}, 10^{-7}\}$) at $\tau = 0.01$ (left) and $\tau = 0.1$ (right).

the order in the Chebyshev expansion (equivalently the number of nodes) N . A priori, we might think that increasing the number of nodes should result in a more accurate result. Alas, this is mathematically proven only when it is used on bounded functions while in this method, it is used, among others, on the integrand of the integral appearing in the evolution equation, that is to say on unbounded functions (with divergences in 0 and in 1). Then, an option is to simply run the calculation with an increasing number of nodes and see if we converge to a unique solution (up to minor fluctuations). We show in the following plots (where $N \in \{50, 75, 100, 125, 150, 200\}$), that it indeed seems to converge. Indeed, The results mainly differ at small times but after a long enough evolution (for $t > 0.15$ and for $N \geq 75$), the solutions seem already in good agreement. In our example, only the solution for $N = 50$ does not converge in time to the same solution as others. Also, at $t = 0.08$, the solutions for $N \geq 75$ are nearly identical, as you can see in Fig. 4.13.

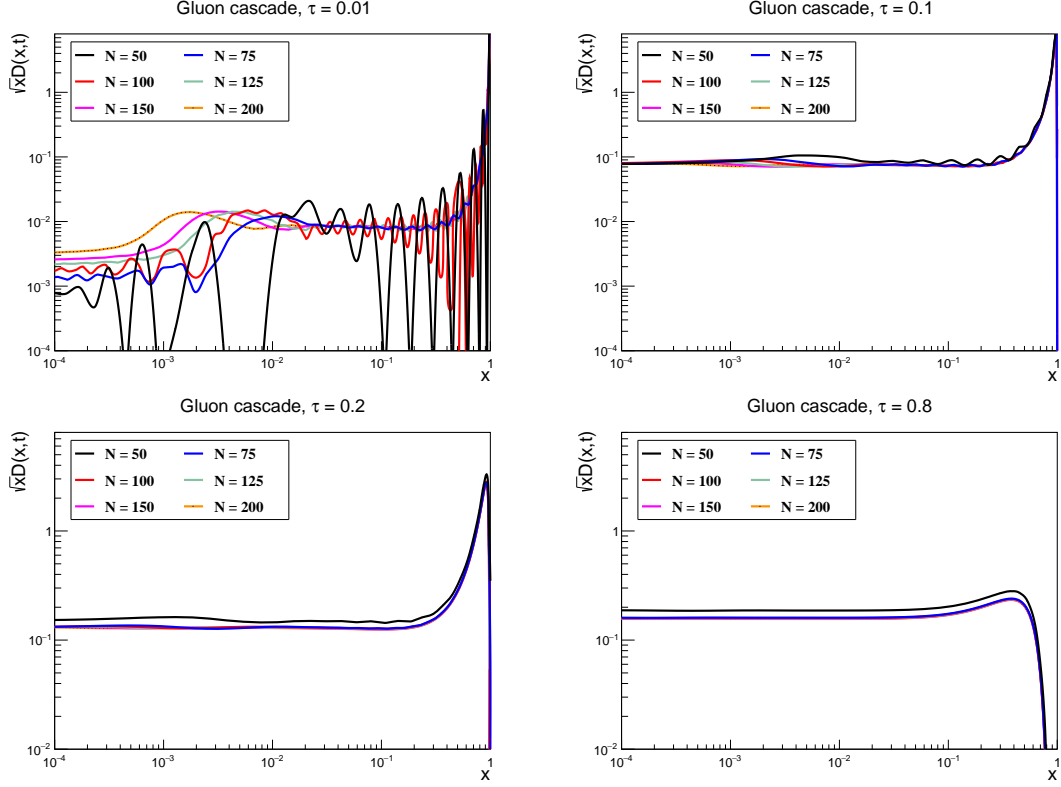


Figure 4.13: Comparison of results obtained with the Chebyshev method for different numbers of nodes ($N \in \{50, 75, 100, 125, 150, 200\}$) at $\tau = 0.01$ (top left), $\tau = 0.1$ (top right), $\tau = 0.2$ (bottom left) and $\tau = 0.8$ (bottom right).

Application to the full integrated BDIM equations

Then, we consider the coupled integrated BDIM equations for gluon, flavor singlet and non-singlet FFs (as defined in Eq. (4.89)) written with explicit Heaviside functions :

$$\begin{aligned}
\frac{\partial D^g(x,t)}{\partial \tau} &= \int_0^1 dz \mathcal{K}_{gg}(z) \left[\sqrt{\frac{z}{x}} D^g\left(\frac{x}{z}, t\right) \theta(z-x) - \frac{z}{\sqrt{x}} D^g(x,t) \right] \\
&\quad - \int_0^1 dz \mathcal{K}_{qg}(z) \frac{z}{\sqrt{x}} D^g(x,t) + \int_0^1 dz \mathcal{K}_{gq}(z) \sqrt{\frac{z}{x}} D^S\left(\frac{x}{z}, t\right) \theta(z-x), \\
\frac{\partial D^S(x,t)}{\partial \tau} &= \int_0^1 dz \mathcal{K}_{qq}(z) \left[\sqrt{\frac{z}{x}} D^S\left(\frac{x}{z}, t\right) \theta(z-x) - \frac{1}{\sqrt{x}} D^S(x,t) \right] \\
&\quad + \int_0^1 dz \mathcal{K}_{qg}(z) \sqrt{\frac{z}{x}} D^g\left(\frac{x}{z}, t\right) \theta(z-x), \\
\frac{\partial D^{NS}(x,t)}{\partial \tau} &= \int_0^1 dz \mathcal{K}_{qq}(z) \left[\sqrt{\frac{z}{x}} D^{NS}\left(\frac{x}{z}, t\right) \theta(z-x) - \frac{1}{\sqrt{x}} D^{NS}(x,t) \right].
\end{aligned} \tag{4.153}$$

This system of equations follows the same resolution scheme as the previous one, let's list the quantities appearing in this case :

- $D_{t,k}^g \equiv D^g(t_0 + tdt, x_k)$,
- $D_{t,k}^S \equiv D^S(t_0 + tdt, x_k)$,
- $D_{t,k}^{NS} \equiv D^{NS}(t_0 + tdt, x_k)$.

Then, the Euler method reads :

$$\begin{aligned}
\Delta D_{k,t}^g &= D_{k,t+1}^g - D_{k,t}^g \simeq dt \sum_{j=0}^{N-1} \left(\mathcal{S}_{k,j}^{gg} D_{j,t}^g + \mathcal{S}_{k,j}^{gS} D_{j,t}^S \right) \\
\Delta D_{k,t}^S &= D_{k,t+1}^S - D_{k,t}^S \simeq dt \sum_{j=0}^{N-1} \left(\mathcal{S}_{k,j}^{SS} D_{j,t}^S + \mathcal{S}_{k,j}^{Sg} D_{j,t}^g \right) \\
\Delta D_{k,t}^{NS} &= D_{k,t+1}^{NS} - D_{k,t}^{NS} \simeq dt \sum_{j=0}^{N-1} \mathcal{S}_{k,j}^{NSNS} D_{j,t}^{NS}
\end{aligned} \tag{4.154}$$

where all the time-independent parts are calculated in advance in the following matrices :

$$\begin{aligned}
\mathcal{S}_{k,j}^{gg} &= \frac{1}{\sqrt{x_k}} \left[\frac{2}{N} \sum_{i=0}^{N-1} {}'T_{i,j} I_{k,i}^{g,1} - \delta_{k,j} \left(I_k^{g,2} + I_k^{g,3} \right) \right] \\
\mathcal{S}_{k,j}^{gS} &= \frac{1}{\sqrt{x_k}} \frac{2}{N} \sum_{i=0}^{N-1} {}'T_{i,j} I_{k,i}^{g,4}, \\
\mathcal{S}_{k,j}^{SS} &= \frac{1}{\sqrt{x_k}} \left[\frac{2}{N} \sum_{i=0}^{N-1} {}'T_{i,j} I_{k,i}^{S,1} - \delta_{k,j} I_k^{S,2} \right] \\
\mathcal{S}_{k,j}^{Sg} &= \frac{1}{\sqrt{x_k}} \frac{2}{N} \sum_{i=0}^{N-1} {}'T_{i,j} I_{k,i}^{S,3}, \\
\mathcal{S}_{k,j}^{NSNS} &= \mathcal{S}_{k,j}^{SS}.
\end{aligned} \tag{4.155}$$

and the integrals are :

- $I_{k,i}^{g,1} \equiv \int_{x_k}^1 dz \mathcal{K}_{gg}(z) \left(\sqrt{z} T_i \left(y \left(\frac{x_k}{z} \right) \right) - z T_{i,k} \right)$,
- $I_k^{g,2} \equiv \int_0^{x_k} \mathcal{K}_{gg}(z) z$,
- $I_k^{g,3} \equiv \int_0^1 \mathcal{K}_{gg}(z) z$,

- $I_k^{g,4} \equiv \int_{x_k}^1 \mathcal{K}_{gq}(z) \sqrt{z} T_i(y(\frac{x_k}{z})),$
- $I_{k,i}^{S,1} \equiv \int_{x_k}^1 dz \mathcal{K}_{qq}(z) (\sqrt{z} T_i(y(\frac{x_k}{z})) - T_{i,k}),$
- $I_k^{S,2} \equiv \int_0^{x_k} \mathcal{K}_{qq}(z),$
- $I_k^{S,3} \equiv \int_{x_k}^1 \mathcal{K}_{gq}(z) \sqrt{z} T_i(y(\frac{x_k}{z})),$
- $I_{k,i}^{NS,1} \equiv \int_{x_k}^1 dz \mathcal{K}_{qq}(z) (\sqrt{z} T_i(y(\frac{x_k}{z})) - T_{i,k}) = I_{k,i}^{S,1},$
- $I_k^{NS,2} \equiv \int_0^{x_k} \mathcal{K}_{qq}(z) = I_k^{S,2}.$

Results test As a test, we tried to reproduce qualitatively the results presented in [267]. As presented in Fig. 4.14 for a gluon-initiated jet and in Fig. 4.15 for a quark-initiated jet, the results of the Chebyshev method agree well with these results.

We could observe that, when looking at the full decomposition (and not only the values on the nodes) the oscillations, directly due to the polynomial interpolation, quickly vanish (for $\tau > 0.02$ at worst) which is encouraging for the applicability of the method. We will come back to it later but we can already observe that quarks have a different behavior than gluons. It is especially true for the non-singlet distribution for a quark-initiated jet, which does not scale as $\frac{1}{\sqrt{x}}$.

Limits and the transverse momentum dependent case

Finally, the Chebyshev method has proved relatively efficient in solving the integrated BDIM equations. Its strength comes from the low calculation cost of the Euler method used to solve the time evolution which makes it suitable when a long evolution time is needed. However, in practice, for heavy-ion collisions, the length of the QGP is of the order of a few fm only, limiting this benefit. On the other hand, the incapacity to properly initiate the solution is an important weakness of the method. This gets worse when we try to solve the BDIM equation with transverse momentum. First, if what was taking time in the integrated case was the calculation of the matrix \mathcal{S} , it becomes much worse when a second Chebyshev decomposition, for the variable \mathbf{k} this time, is added to the method (on both the fragmentation functions and the integrands). Indeed, each decomposition implies two loops over N (so the calculation time in this case, grows like N^4).

But that is just a problem of computation time, what is worse is the fact that the initial distribution should now contain 2 delta functions. In the tests made, this led to the failure of the method and no solution to this problem has been found. Consequently, we use the Chebyshev solution only to solve the integrated BDIM equations. A last difficulty should be mentioned, the choice of range for \mathbf{k} . Indeed, cutting it too low might lead to underestimation of broadening but cutting it too high might demand a high number of nodes to reach a sufficient density at low \mathbf{k} where both the scattering

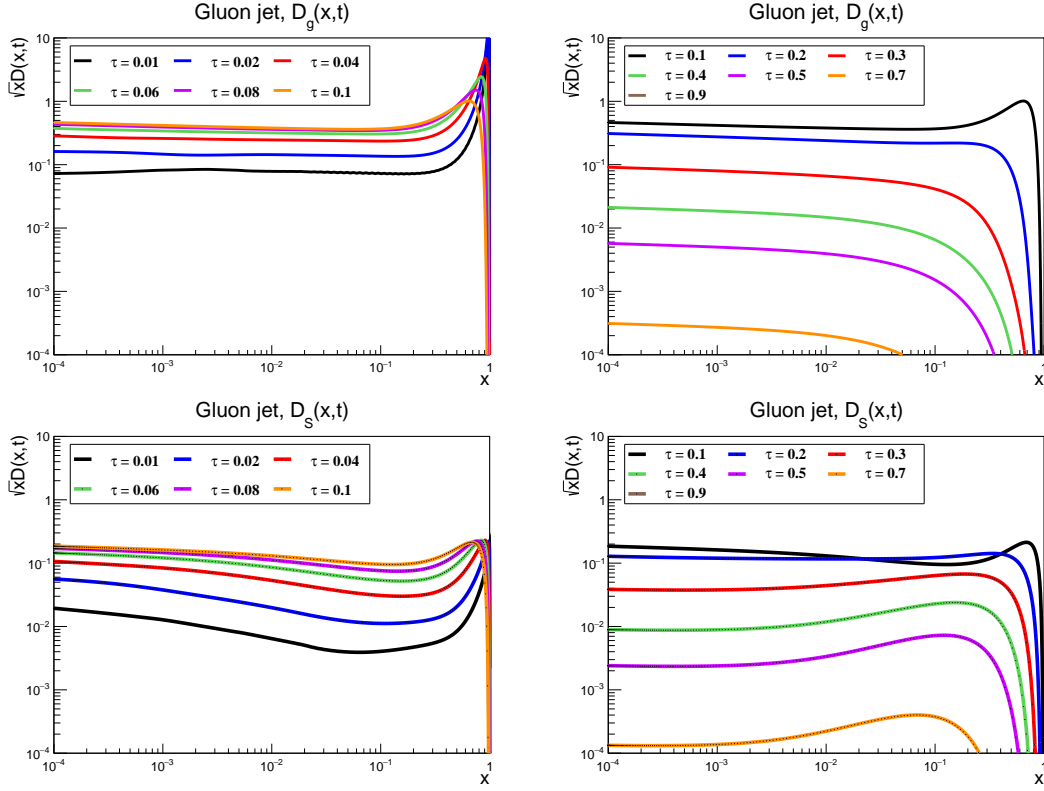


Figure 4.14: Solutions of the integrated BDIM equation obtained with the Chebyshev method for a jet initiated by a gluon. Both Gluons distribution (top) and singlet distribution (bottom) are presented for short times $\tau \in \{0.01, 0.02, 0.04, 0.06, 0.08, 0.1\}$ (left) and long times $\tau \in \{0.1, 0.2, 0.3, 0.4, 0.5, 0.7, 0.9\}$ (right).

and the branching kernel are peaked (this is also problematic when applying classical numerical method).

4.5 Solutions of the BDIM equations

In this section, we present the solutions we obtained for the different BDIM equations (that we presented in [3, 4]). First, we will have a look at the features of gluon dominated cascade described this way. We will study the energy distributions before examining broadening (through the transverse momentum distributions). The goal is to investigate the features of the solutions of the BDIM equation in different cases (different approximations for the branching and the scattering kernel). Secondly, we will account for quarks and focus on the differentiation of gluon and quark jets (and on the difference in the gluon and quark composition of such jets). This will be done at the level of the energy distribution first then in terms of broadening (with different observables).

The solutions that we will present have been obtained with the following input param-

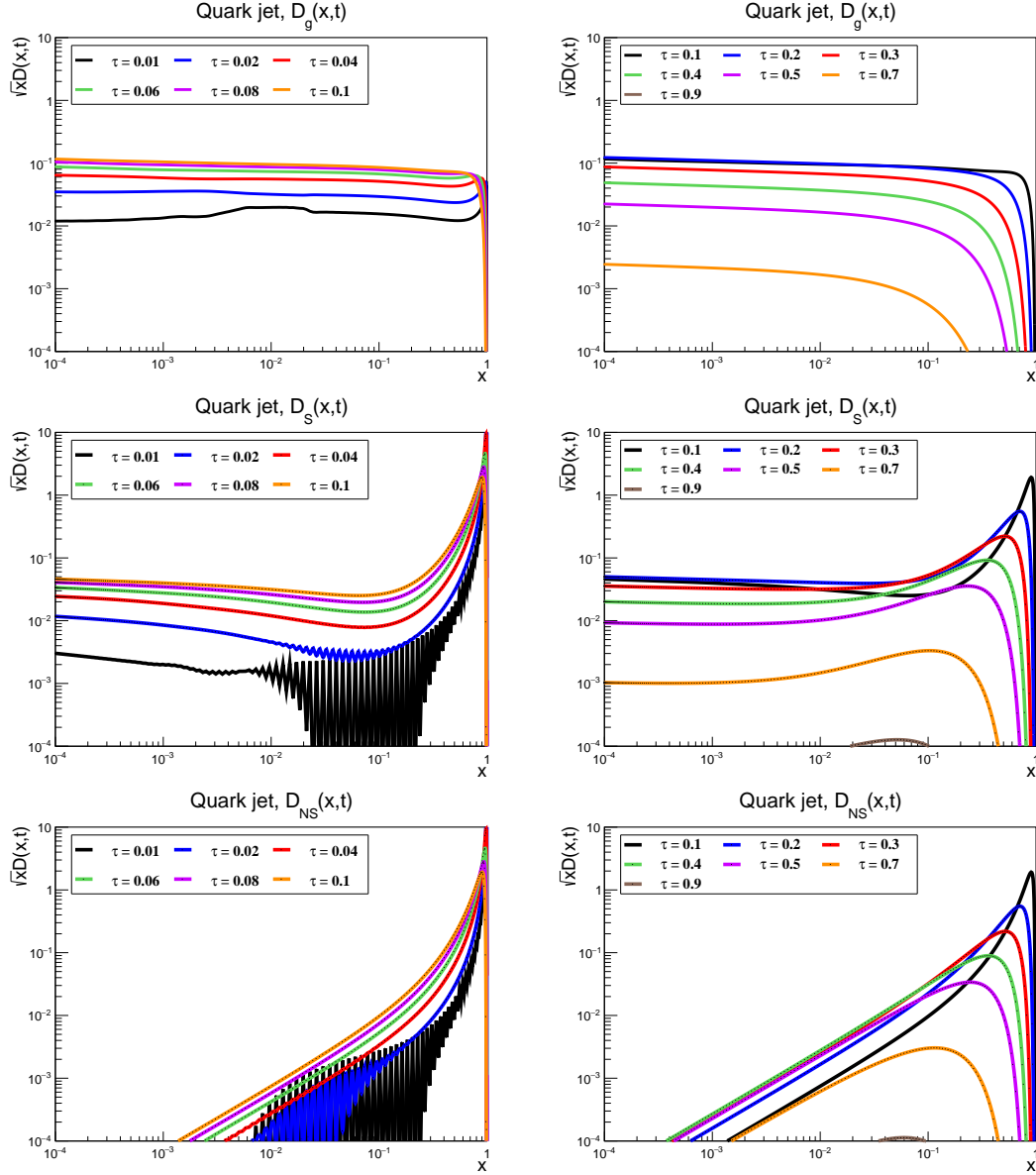


Figure 4.15: Solutions of the integrated BDIM equation obtained with the Chebyshev method for a jet initiated by a quark. The Gluons distribution (top), singlet distribution (middle), and non-singlet distribution (bottom) are presented for short times $\tau \in \{0.01, 0.02, 0.04, 0.06, 0.08, 0.1\}$ (left) and long times $\tau \in \{0.1, 0.2, 0.3, 0.4, 0.5, 0.7, 0.9\}$ (right).

eters :

$$\begin{aligned}
 x_{\min} &= 10^{-4}, & \epsilon &= 10^{-6}, & l_{\min} &= 0.1 \text{ GeV}, \\
 N_c &= 3, & N_f &= 3, & \alpha_s &= \pi/10, \\
 E &= 100 \text{ GeV}, & n &= 0.243 \text{ GeV}^3, & \hat{q} &= 1 \text{ GeV}^2/\text{fm}, & m_D &= 0.993 \text{ GeV},
 \end{aligned}
 \tag{4.156}$$

where the first line corresponds to the regulator for MINCAS [269]. Indeed, the study of the solutions of the BDIM equations proposed here will be based on those obtained through MINCAS. For a comparison of the results obtained through the different methods presented in the previous section, see App. C.2. The rest are physical parameters (already introduced). It was already mentioned, but the medium is not considered evolving hence the physical parameters (like the density of scatterers n , the Debye mass m_D and the quenching parameter \hat{q}) are here constant. Also, it is worth mentioning that the coupling to the medium (usually evaluated at the scale of the medium temperature $\sim 2\pi T$) and the coupling in the medium cascade (that should scale with k_{br}^2) are taken equal (and constant). With the parameters chosen, the stopping time is $\bar{t}^* = 14.81\text{fm}$ ¹¹. Still, we will look at the evolution up to a time of order of the usual medium length in a heavy-ion collision, i.e of order 4fm.

4.5.1 Results for the pure gluon case

In the case of gluon-dominated cascades, we will have a look in Sec. 4.5.1 at the energy distributions $D_g(x, t)$, either obtained directly solving the integrated BDIM equation Eq. (4.84) or integrating over the transverse momentum the solution of the BDIM equation for gluons Eq. (4.68). Then, in Sec. 4.5.1, we will study jet broadening and the difference of the transverse momentum distribution obtained in different limits and models.

Energy distribution

In Fig. 4.16 is presented the energy distribution $D_g(x, t)$ for evolution time $t = 0.1\text{fm}$, $t = 1\text{fm}$, $t = 2\text{fm}$, $t = 3\text{fm}$ and $t = 4\text{fm}$. We can already observe that the scaling at low- x (like $\frac{1}{\sqrt{x}}$), if still present, is less marked than in the analytical solution (of Eq. (4.107)). And actually, these solutions are well different from the analytical solution.

This can be observed in Fig. 4.17 (where we decided, to have a different point of view, plotting directly $D_g(x, t)$ on a linear scale). At low evolution times, the analytical solution is actually a good estimate of the actual solution. However, at a longer evolution time, the quenching of the peak in $x = 1$ is slower than the one predicted by the analytical solution. Also, as a consequence, the analytical solution overestimates the energy distribution at intermediate and low x .

Basically, if the energy flow going from the initial peak at $x = 1$ toward $x = 0$ is still a feature of the solution of the integrated BDIM equations, this flow is slightly slower than in the simplified case.

We obtained the BDIM equation for the energy distribution by integrating the one taking into account broadening (through both scattering and branching). If then, in theory, all the fragmentation functions $D_g(x, \mathbf{k}, t)$ obtained from different versions of the BDIM equations (the collinear one for instance, or the different approaches to the scattering part, that shouldn't play a role in the energy loss), it is interesting to verify

¹¹We count the time in fermi because it is directly related to the length of the medium crossed.

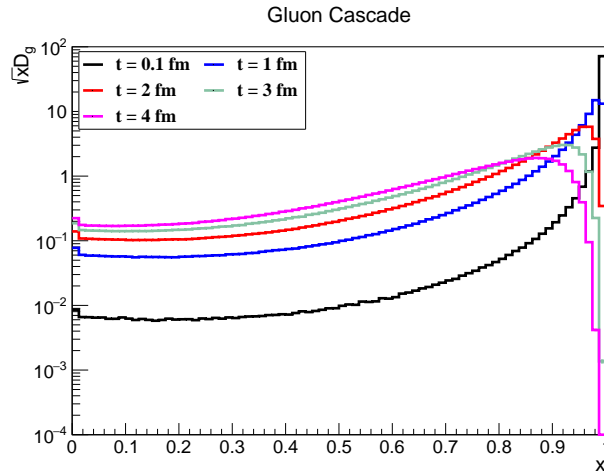


Figure 4.16: Solution of the integrated BDIM equation for gluons dominated cascade at times $t = 0.1\text{fm}$, $t = 1\text{fm}$, $t = 2\text{fm}$, $t = 3\text{fm}$ and $t = 4\text{fm}$.

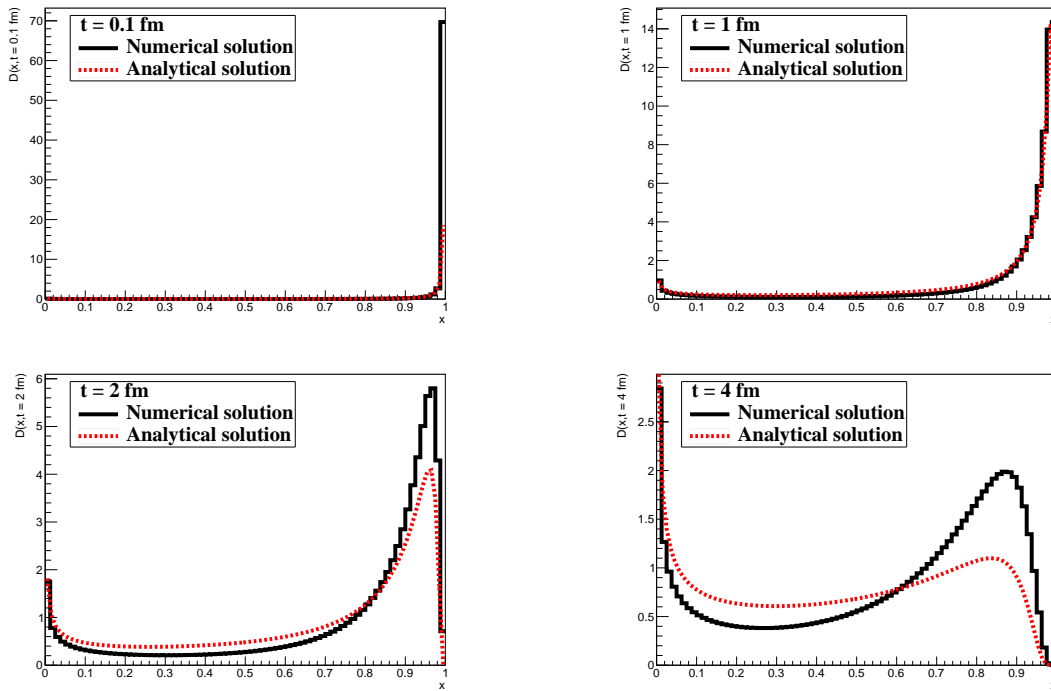


Figure 4.17: Comparison of the energy distribution of the BDIM equation (numerical solution) to the one of the simplified case (analytical solution) at different evolution times.

that the obtained fragmentation functions all integrate to the same energy distribution. This comparison is done in Fig. 4.18. For the comparison, we will consider either the full splitting kernel (of Eq. (4.64)) or the collinear one (of Eq. (4.83)). Considering the collision kernel, we will use both the one corresponding to a QGP at thermal equilibrium (defined by the in-medium potential of Eq. (4.36)) or out of equilibrium (defined by the in-medium potential of Eq. (4.38)) and we may even switch it off. We also consider the Gaussian approximation of Eq. (4.95).

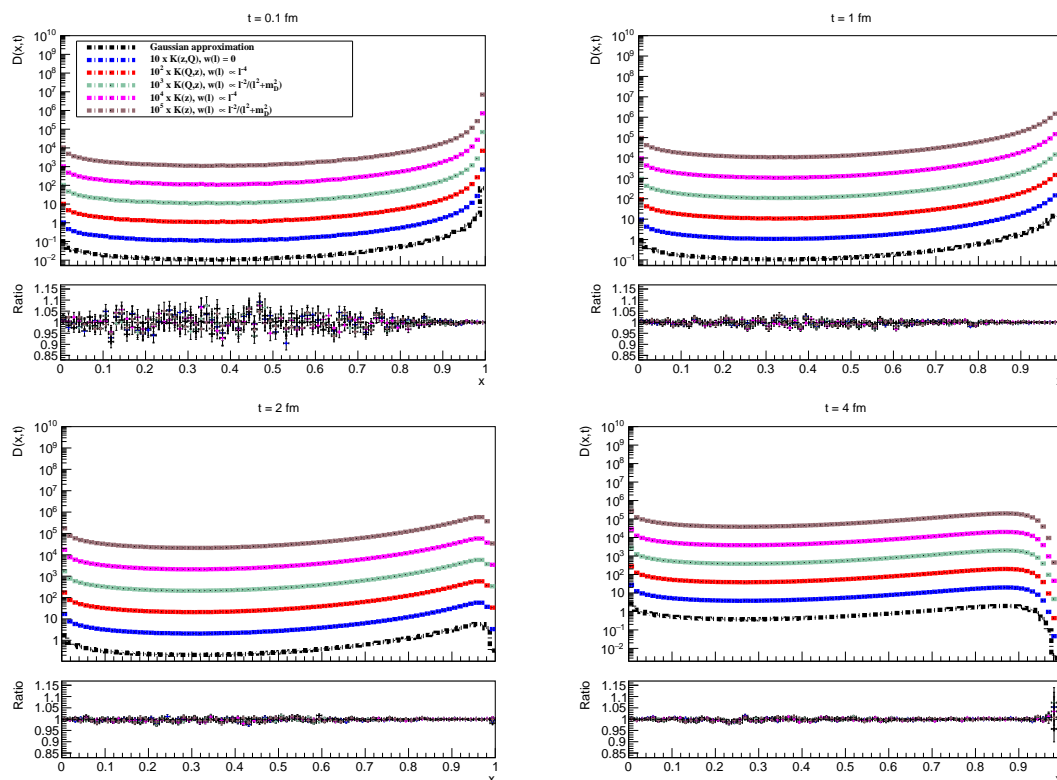


Figure 4.18: Comparison of the energy distribution of the BDIM equation for several models : full splitting kernel with equilibrium medium (in green, it serves also as the base for the ratio plot), full splitting kernel with out of equilibrium medium (red), full splitting kernel without scattering (blue), collinear splitting kernel with equilibrium medium (brown), collinear splitting kernel with out of equilibrium medium (magenta) and finally the Gaussian approximation (black).

We can see the perfect agreement between the curves (up to some statistical errors) which implies that all the models studied here describe the same energy loss, as expected¹² (by momentum conservation).

¹²Still, this is an important check of the validity of our solutions.

Broadening

Let's now turn on broadening and observe the influence of the different kernels used on the transverse momentum distribution. While we may present some results in terms of \mathbf{k} (i.e through k_x and k_y), by symmetry of the BDIM equations on the azimuthal angle, most of the results will be presented in terms of $k_T \equiv |\mathbf{k}|$ dependence. We then need to introduce the distribution :

$$\tilde{D}(x, k_T, t) = \int_0^{2\pi} d\phi k_T D(x, \mathbf{k}, t), \quad \text{such that } D(x, t) = \int dk_T \tilde{D}(x, k_T, t). \quad (4.157)$$

The \mathbf{k} distribution of the solution of the BDIM equation for gluon is presented in Fig. 4.19 (the distributions are integrated over x).

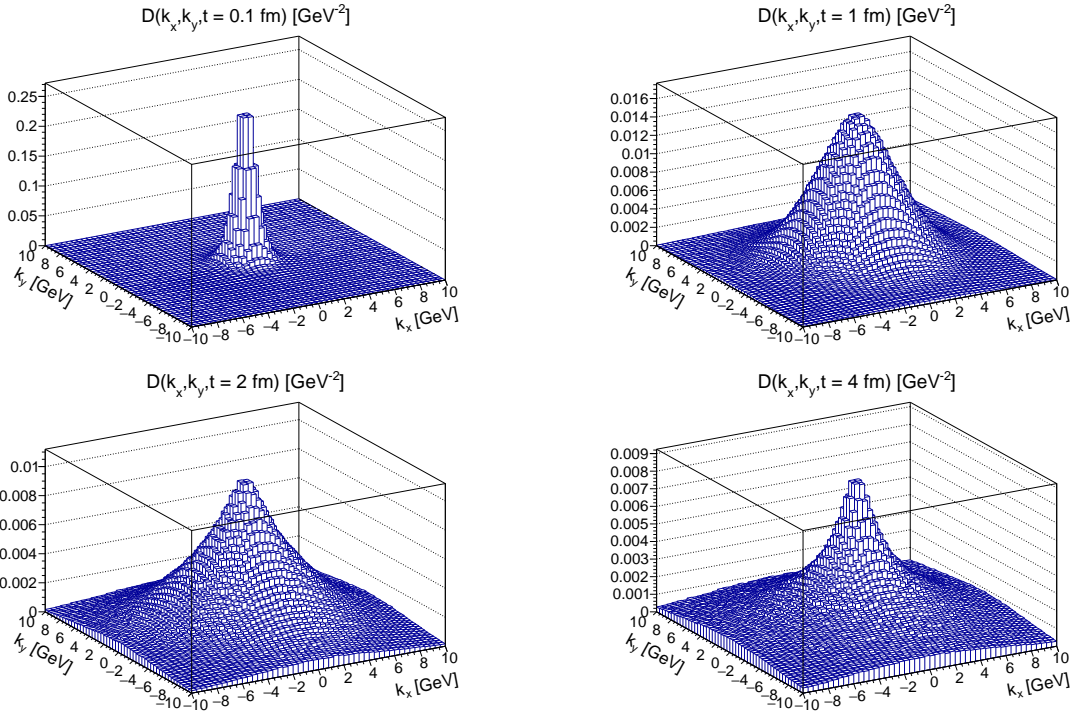


Figure 4.19: 2D transverse momentum distribution (k_x, k_y) of the solution of the BDIM equation for gluons at times $t = 0.1\text{fm}$, 1fm , 2fm and 4fm .

The broadening of the solutions with time is clearly observed with an important evolution of the shape of the distributions while time increases. This is a hint that the Gaussian approximation should fail to describe this broadening. And indeed, if we have a look at the same distribution in the case of the Gaussian approximation, as shown in Fig. 4.20, we observe important differences. As mentioned, contrary to the Gaussian approximation, the actual solution sees the shape of its transverse momentum distribution changing with time (while in the former, by construction, it stays Gaussian).

Then, it is clear that the Gaussian approximation completely underestimates broadening (with a much steeper shape than in the “actual” solution¹³).

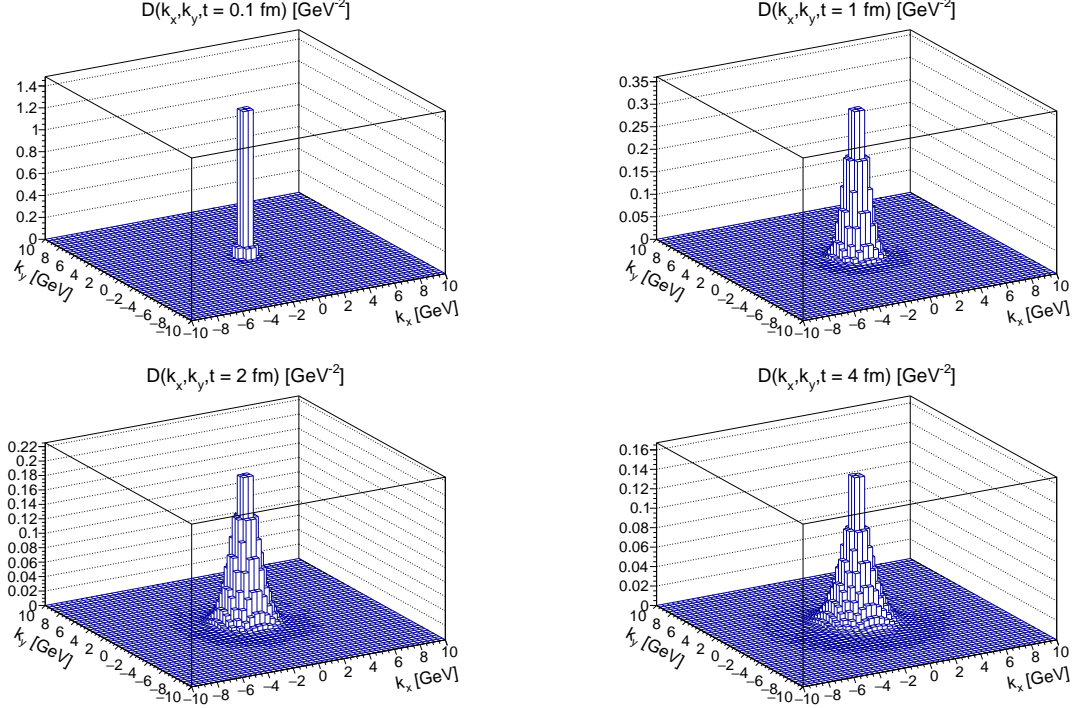


Figure 4.20: 2D transverse momentum distribution (k_x, k_y) of the Gaussian approximation at times $t = 0.1\text{fm}$, 1fm , 2fm and 4fm .

To see clearly these differences, we should study the k_T distributions. In Fig. 4.21 we show this k_T distribution for different models (the same as presented in Fig. 4.18).

This is clear that the Gaussian approximation fails to approach any of the other models. The nearest one is the solution accounting for broadening in splitting but without collision term (which is not expected since the Gaussian approximation should approximate the solution for collinear splitting and diffusion approximation). The shapes are similar, but the width of the distributions is much thinner in the Gaussian case. Then, all the other distributions show fast broadening (with similar width) but non-Gaussian shape. For the collision kernel based on out-of-equilibrium medium (without screening), we observe similar distribution when considering or not broadening in splitting (slightly wider in the former case). For the collision kernel based on medium at thermal equilibrium (with screening), overall, we observe more peaked distributions around $k_T = 0$ hence, slower broadening than when the medium is out of equilibrium. Also, in this case, there is a noticeable difference in shape when turning on or off broadening in splitting

¹³For simplicity, we may refer to the solution of the BDIM equation Eq. (4.68) for gluon, or Eq. (4.71) more generally, as “actual” solution, as opposed to the solutions of the different approximations of the BDIM equation.

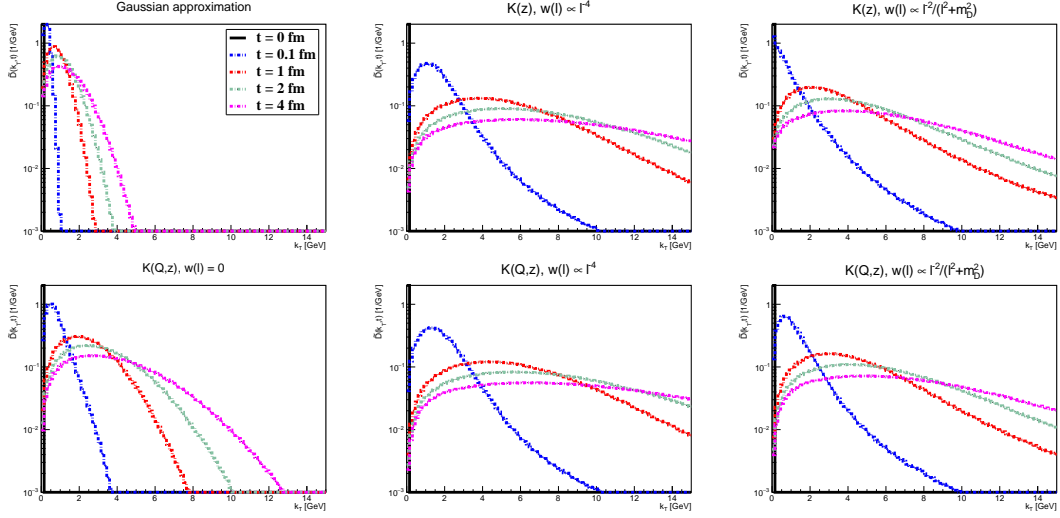


Figure 4.21: The k_T distributions for the evolution time values $t = 0, 0.1, 1, 2, 4$ fm, for different kernels: the Gaussian approximation, $\mathcal{K}(z)$ and $\mathcal{K}(\mathbf{Q}, z, p^+)$ (denoted as $\mathcal{K}(\mathbf{Q}, z)$), and different collision terms: no collision term, the collision term for an equilibrium medium and for an out of equilibrium medium.

(especially at short times).

To go further, we study the mean transverse momentum $\langle k_\perp^2 \rangle$, that can now be defined thanks to the distribution \tilde{D} :

$$\langle k_T \rangle = \frac{\int d^2\mathbf{k} |\mathbf{k}| D(x, \mathbf{k}, t)}{\int d^2\mathbf{k} D(x, \mathbf{k}, t)} = \frac{\int_0^{+\infty} dk_T k_T^2 \tilde{D}(x, k_T, t)}{\int_0^{+\infty} dk_T k_T \tilde{D}(x, k_T, t)}, \quad (4.158)$$

These distributions, for the different cases studied here, are presented in Fig. 4.22.

In every case, $\langle k_\perp^2 \rangle$ overall grows with x . The narrow k_T distribution of the Gaussian approximation reflects in the drop of the $\langle k_\perp^2 \rangle$ distribution at low- x (seen only in this case). One can notice that, for every case, the $\langle k_\perp^2 \rangle$ distribution at small- x converges quickly to some linear function (already at $t = 1$ fm, the distribution does not evolve anymore). The slopes are similar from one case to the other but are shifted in abscissa. Overall, the Gaussian approximation gives the smallest values of $\langle k_\perp^2 \rangle$, followed by the case without collision (but accounting for broadening in splitting). Then, different behavior can be observed around $x = 1$. In particular, with a collinear kernel, these distributions have a positive second derivative in this region while those obtained with the full kernel undergo a drop at $x = 1$. This drop results from the fact that the evolution starts at $x = 1$ with $k_T = 0$ and already a single soft emission with the \mathbf{Q} -dependent kernel \mathcal{K} gives to the emitter a significant k_T -kick, which is not the case for the z -only dependent emission kernel. This effect is more pronounced for the shortest evolution time $t = 0.1$ fm, when the (x, k_T) -distribution is strongly peaked at $x = 1$ and $k_T = 0$ (which is no more the case for long evolution times).

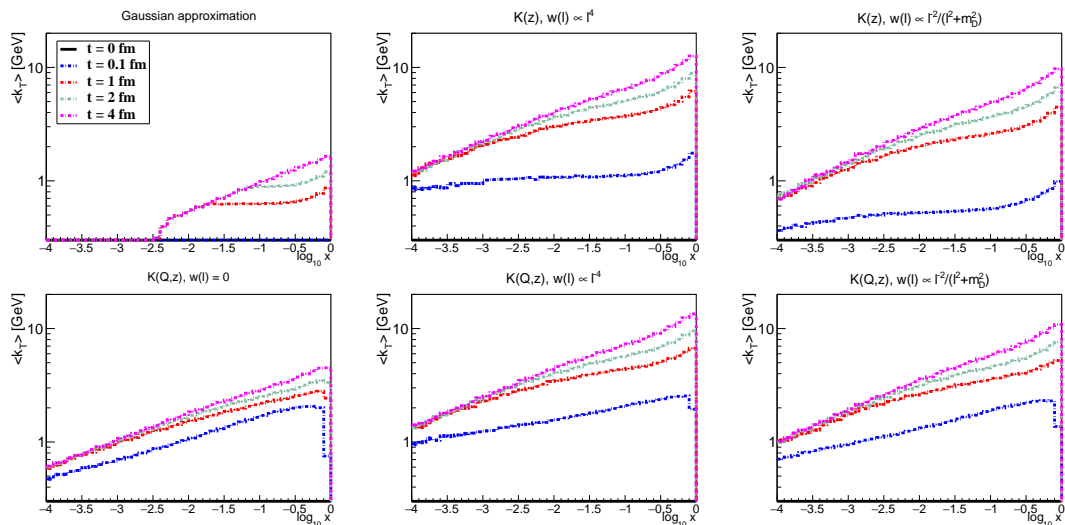


Figure 4.22: The $\langle k_T \rangle$ vs. $\log_{10} x$ distributions for the evolution time values $t = 0, 0.1, 1, 2, 4$ fm, for different kernels: the Gaussian approximation, $\mathcal{K}(z)$ and $\mathcal{K}(\mathbf{Q}, z, p^+)$ (denoted as $\mathcal{K}(\mathbf{Q}, z)$), and different collision terms: no collision term, the collision term for equilibrium and out of equilibrium medium.

In Fig. 4.23 we present the dependence of the k_T distribution on the quenching parameters. We present solutions for a double and a halved quenching parameter (compared to the one we used so far : $\hat{q} = 1\text{GeV}^2/\text{fm}$) at long evolution time (4fm).

It is worth mentioning that the dependence on the quenching parameter is not trivial (as it could have been thought from its simple interpretation in the diffusion approximation), its increase does not resumes in broaden k_T distributions. This direct translation only applies when there is no collision kernel (as in the Gaussian approximation and the case without scattering). In the remaining cases, the interplay between splitting and scattering (in which the quenching parameter enters, differently) results in non-trivial observed structures.

This study let us conclude that the Gaussian approximation is a very crude approximation that underestimates broadening and that the effect of broadening appearing in the splitting process is not negligible compared to broadening coming from scattering with the medium. The features of the BDIM equations for gluon-dominated cascade can be summarized through k_T vs. x distributions (showing both energy loss and broadening), as illustrated in Fig. 4.24.

4.5.2 Results for the system case

Now that we have studied features of the BDIM solution in the case of gluon-dominated cascades, we will look at the influence of quarks in the cascades. In particular, we will focus on the difference between jets initiated by a hard gluon and those initiated by a

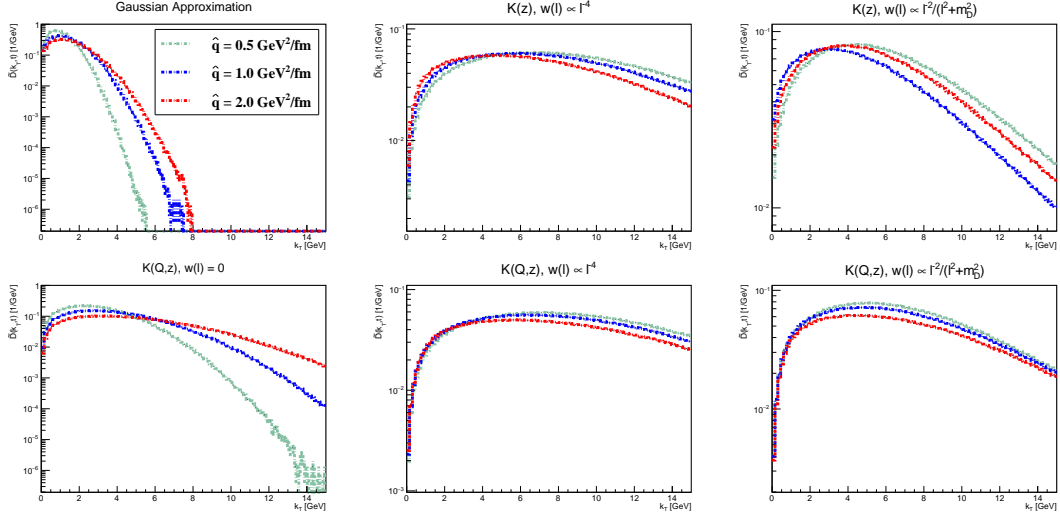


Figure 4.23: The k_T distributions for $\hat{q} = 0.5, 1, 2$ GeV²/fm and $t = 4$ fm, for different kernels: the Gaussian approximation, $\mathcal{K}(z)$ and $\mathcal{K}(\mathbf{Q}, z, p^+)$ (denoted as $K(\mathbf{Q}, z)$), and different collision terms: no collision term, the collision term for equilibrium out of equilibrium medium.

hard quark. We will begin with the energy distribution in Sec. 4.5.2 and see if gluon and quark jets can be discriminated by their in-medium energy loss. Then, in Sec. 4.5.2 we will observe the difference in the broadening of these jets (through not only the transverse momentum distribution but also the energy in-cone that we will define). And we will conclude with an evaluation of the dijet asymmetry (an important observable) in our model.

Energy distribution

The energy distributions of gluons and quarks in a gluon jet (cascade initiated by a hard gluon) and by a quark jet (cascade initiated by a hard quark) are presented in Fig. 4.25.

These results agree with those presented in [267]. We see that even with quarks in the cascade, the gluons distribution for both gluon and quark jet scales like $\frac{1}{\sqrt{x}}$ at low- x after some time. This scaling implies no accumulation of energy at intermediate or low x while the energy flows from $x = 1$ to $x = 0$, the sign of a turbulent behavior of the cascade. However, for quark jets, the quarks distribution exhibit a different behavior, going like $x^{3/2}$ at low- x , which reflects the thermalization of valence quarks. Also, the energy loss for quark jets is slower than the one for gluons (the peak at $x = 1$ smears out quickly in gluon jets, which is much slower for quark jets). In the case of the initial gluon at late times there is a region, at high x , where quarks dominate while in the case of the initial quark, gluons tend to dominate if x is low for all time scales and quarks dominate at $x > 0.5$.

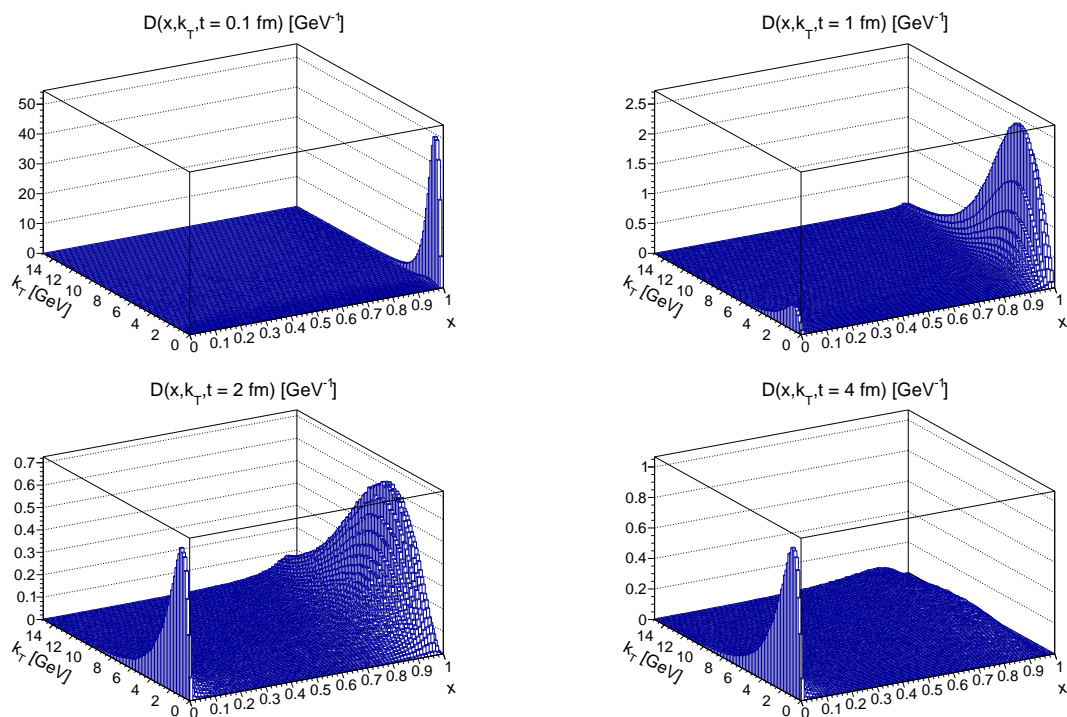


Figure 4.24: 2D distribution in the (x, k_T) of the solutions of the BDIM equations at times $t = 0.1\text{fm}$, 1fm , 2fm and 4fm .

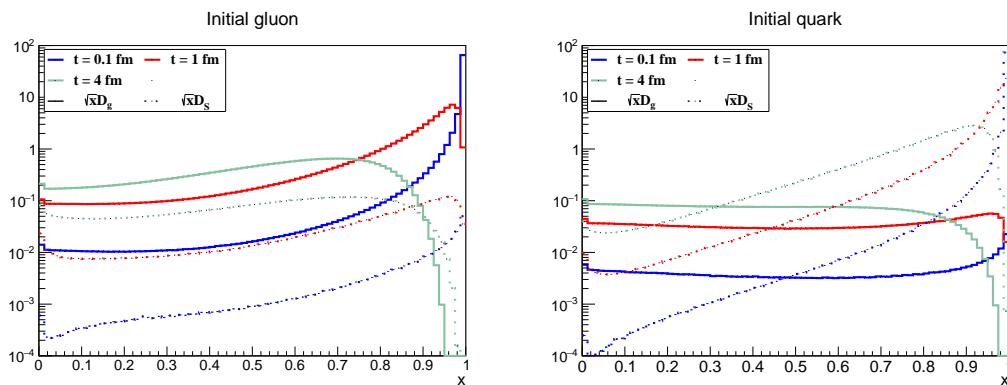


Figure 4.25: The $\sqrt{x}D(x, t)$ distributions at the time-scales $t = 0.1, 1, 4\text{fm}$: cascades initiated by a gluon (left) and a quark (right). The dashed lines correspond to the quark distributions while the solid lines to the gluon distributions.

Broadening

For the case with both quarks and gluons in the cascade, we will consider, when studying broadening, only the BDIM equation Eq. (4.71) (splitting with broadening and collision

kernel for a medium at equilibrium). Let's first have a look at the k_T distributions for either gluons or quarks in gluon jets and quark jets, as presented in Fig. 4.26 (the distributions are integrated over x).

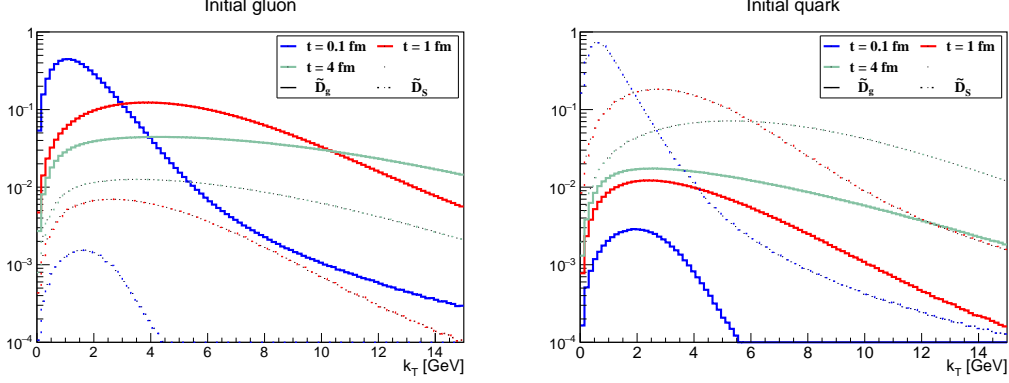


Figure 4.26: The $\tilde{D}(k_T, t)$ distributions at the time-scales $t = 0.1, 1, 4$ fm: cascades initiated by gluon (left) and quark (right). The dashed lines correspond to the quark distributions while the solid lines to the gluon distributions.

We observe that both the quarks and the gluons fragmentation functions become wider, in both gluon and quark jets. Still, gluon broadening is faster, leading to wider gluon jets (for the same time evolution). Furthermore, the distributions of gluons are higher than that of quarks if gluons are in the initial state, and similarly, the distributions of quarks are higher than that of gluons if quarks are in the initial state. To summarize (visually) the features of the solutions of the BDIM equations, we present both quarks and gluons 2D distributions on the (x, k_T) plane, for gluon jets in Fig. 4.27 and quarks jets in Fig. 4.28.

To go further in the comparison of gluon and quark jets and their composition, we will study some observables (in the formal sense). As for the gluon case, we will begin with the average transverse momentum $\langle k_T \rangle$. This average transverse momentum is presented in Fig. 4.29 as a function of x (actually in logarithmic scale) for different evolution times and for both quark and gluon components of either quark or gluon jets.

These distributions are rather similar for both gluon and quark jets. The distributions for different times tend to merge as x gets small enough (like in the gluon case). Certain differences can be observed, between the distributions for the final quark and final gluon, as time progresses, through different slopes and a more linear behavior for the gluon distributions at high x (where there is a depletion in the quark distribution). These differences suggest that gluons have harder momenta at large x .

An interesting observable to compare gluon and quark jets is the energy contained in a cone of angle Θ (that we will simply call *energy in cone*), defined as :

$$E_{\text{in-cone}}(\Theta) = \int_0^1 dx \int_0^{xE \sin \Theta} dk_T \tilde{D}(x, k_T, t). \quad (4.159)$$

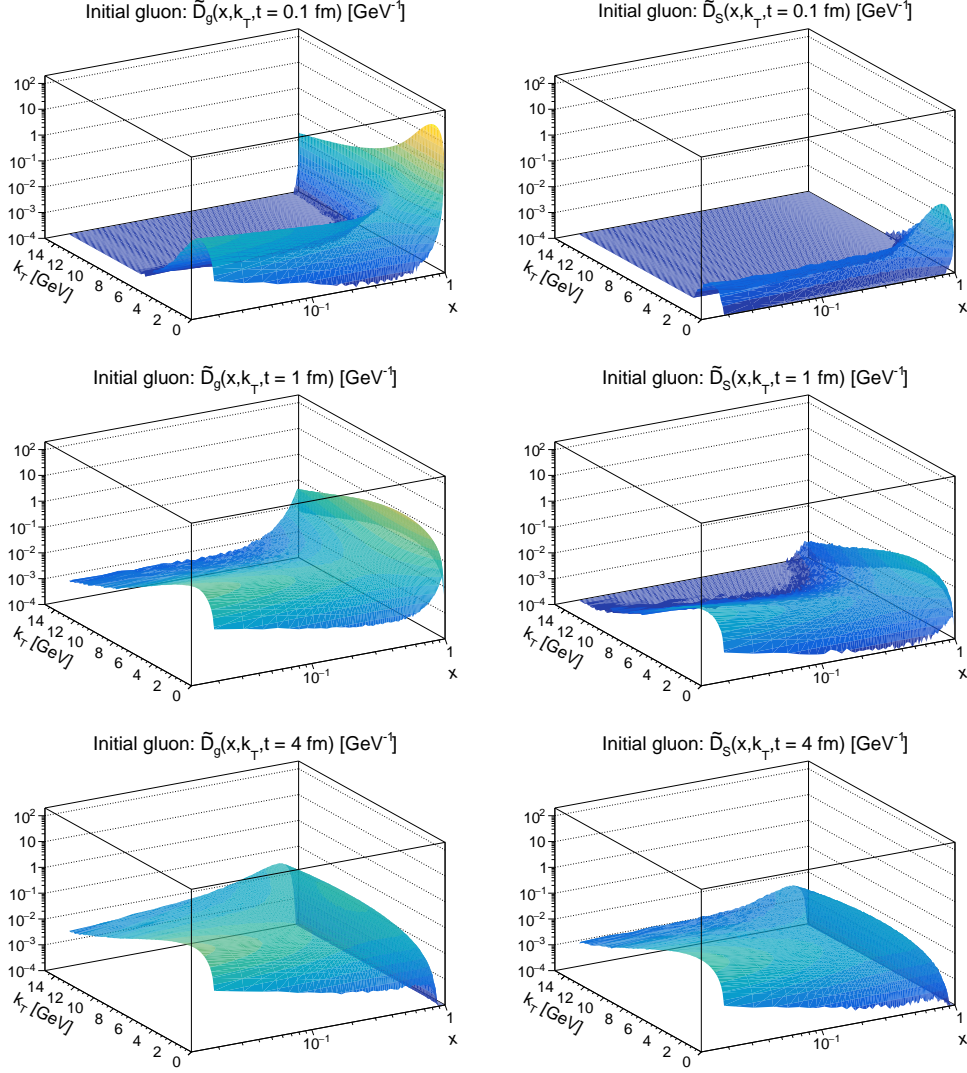


Figure 4.27: The gluon (left) and quark (right) k_T vs. x distributions for cascades initiated by gluons at the time-scales $t = 0.1, 1, 4$ fm.

This function is related to the picture of a jet as collimated particles inside a cone (hence could be seen as the “energy in the jet”). This energy in cone, as a variable of the cone angle Θ , is illustrated in Fig. 4.30 for both quark and gluon jets. The figure shows the energy coming from both quarks and gluons in the cascade independently as well as the total energy (the sum of them). Also, we compare the result for the BDIM equation to the Gaussian approximation of Eq. (4.95) and also to the analytical ansatz of Eq. (4.107) (for the simplified case).

We already noted that the Gaussian approximation was underestimating greatly broadening. This can be seen in the energy in-cone where for the Gaussian approxi-

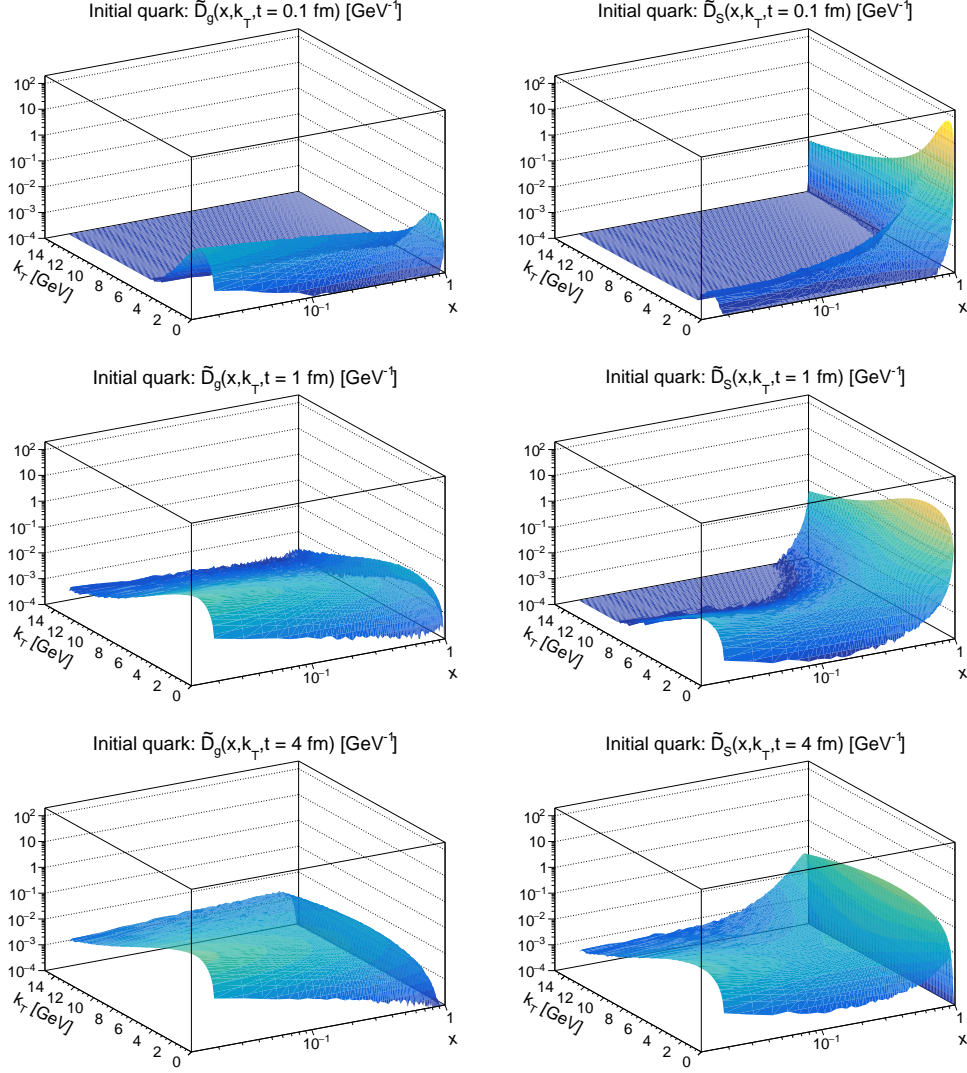


Figure 4.28: The gluon (left) and quark (right) k_T vs. x distributions for cascades initiated by quarks with at the time-scales $t = 0.1, 1, 4 \text{ fm}$.

mation, it grows faster and reaches a plateau as Θ increases before the actual solution. This implies that jets described by the Gaussian approximation are more collimated than those described by the full BDIM equation. Also, the energy in-cone in the Gaussian approximation is greater than the actual one. It is interesting to see that the analytical ansatz describes pretty well the energy in-cone of gluons for Θ large enough (greater than 0.4 roughly). Then, comparing the distributions obtained for initial quark and initial gluons, one can conclude that quark jets are more collimated than gluon ones (which is expected since quark jets broaden slower than gluon ones). Also, if the energy in cone for an initial quark quickly saturates, the one for an initial gluon keeps growing slowly

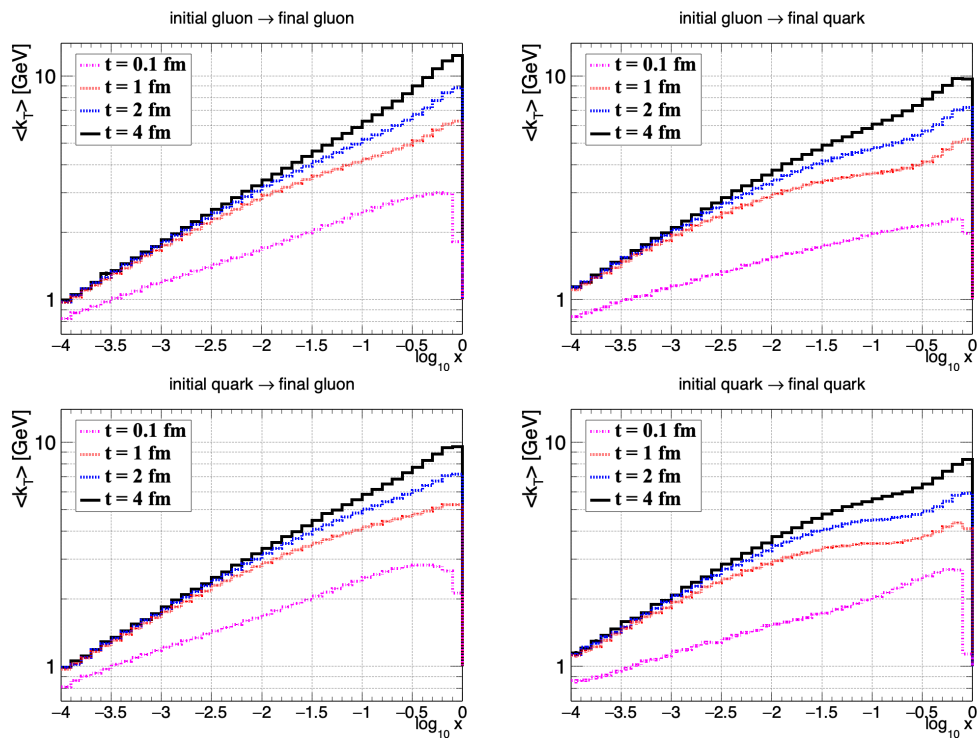


Figure 4.29: The average transverse momentum $\langle k_T \rangle$ versus $\log_{10} x$ for the time-scales $t = 0.1, 1, 2, 4$ fm.

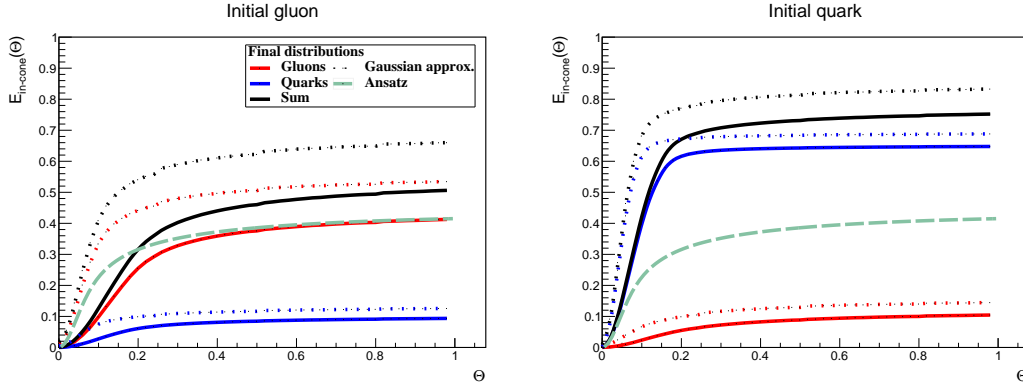


Figure 4.30: Energy in cone for an initial gluon jet (left) and an initial quark jet (right) after 4fm for the full BDIM equation (solid lines), in the Gaussian approximation (dotted lines) and for the analytical ansatz (green dashed line, only in the case of gluon jets).

with Θ . This can be rephrased as radiative energy loss in quark jets comes from very small angle (hence very soft) radiations, while for gluon jets, it is much less localized. Finally, we study the evolution of the energy in-cone with time, for fixed cone angle values (a small one $\Theta = 0.1$ and a large one $\Theta = 1$). This is presented in Fig. 4.31.

Here we remark that quarks dominate at all times in quark jets while in gluon jets, if gluon initially dominates, after a long evolution time (around 8 – 10fm), quarks becomes dominant¹⁴. Then, we see that the analytical ansatz diverges from the actual gluon distribution after a long evolution time while the Gaussian approximation roughly describes the behavior of the actual solution at large angles (better for quarks than for gluons). This last observation is expected since the Gaussian approximation integrates to the same energy distribution as the actual solution.

Perturbative estimate

It is very instructive to compare the result of the full medium evolution with a perturbative estimate which only accounts for one single emission or elastic scattering with the medium, as presented in Sec. 4.3.4. In order to write the perturbative estimate in terms of k_T , we note that $D(\mathbf{k}, \delta t) = D(\mathbf{k}^2, \delta t)$, so that :

$$\tilde{D}_i^{(1)}(k_T, \delta t) = 2\pi k_T D_i^{(1)}(k_T, \delta t). \quad (4.160)$$

The comparison between the perturbative estimate and the actual solution is done for a gluon jet in Fig. 4.32 for the energy distribution and in Fig. 4.33 for the transverse momentum distribution.

We observe that it is actually quite a crude estimate that barely reproduces the gluons energy distribution at short times but fails at reproducing the quark distribution

¹⁴Also, this is a theoretic observation, 8fm being longer than any realistic value for the medium length.

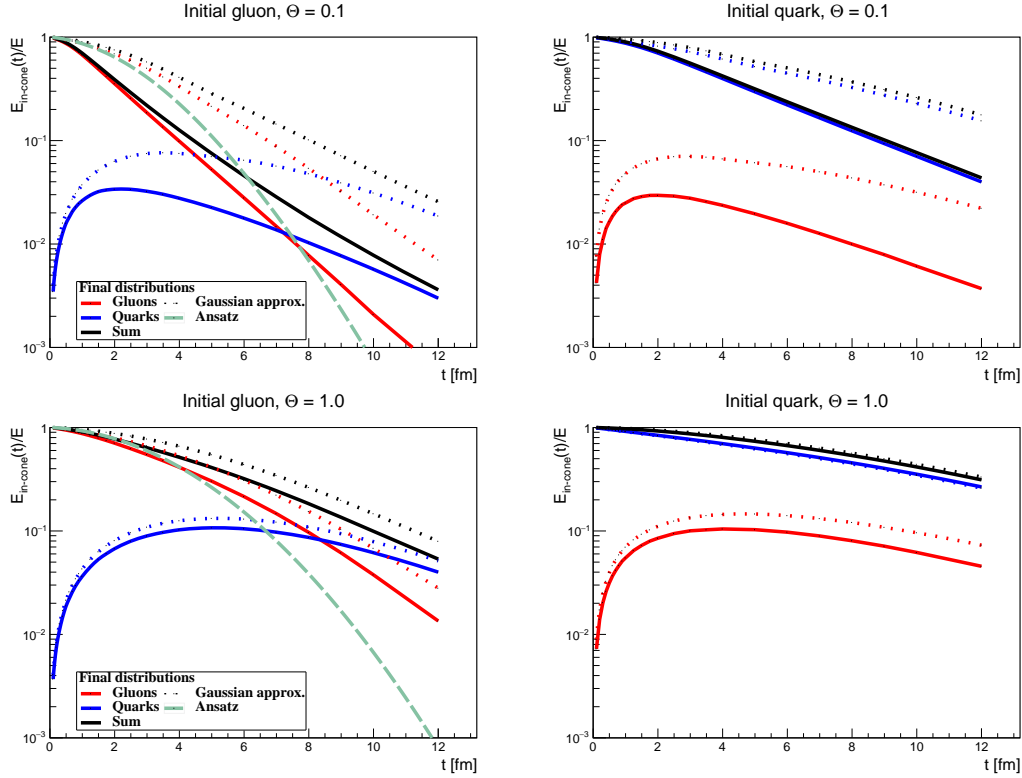


Figure 4.31: Time evolution of the jet energy in a fixed cone with $\Theta = 0.1$ (upper panels) and $\Theta = 1$ (lower panels) for the initial gluon jet (left panels) and the initial quark jet (right panels) for the full BDIM equation (solid lines), in the Gaussian approximation (dotted lines) and for the analytical ansatz (green dashed line, only in the case of gluon jets)..

and the transverse momentum distribution. This underlines the importance of multiple splitting and scattering in in-medium cascades.

Dijet asymmetry

One way to experimentally evaluate jet quenching is through the asymmetry of back-to-back jets in heavy ion collision (where jet quenching is more striking). To this end, we consider 2 back to back hard partons of the same energy $E = 100\text{GeV}$ (the simplest situation we could think of). The 1st one (leading jet) crosses 1fm of the medium while the second one (sub-leading) crosses 4fm (meaning that we evolve these hard jets through the BDIM equations for the corresponding evolution time). Then we can evaluate the dijet energy imbalance as a function of the jet (cone) angle Θ . This reads :

$$\Delta E_i(\Theta) = \int_0^1 dx \int_0^{xE \sin \Theta} dk_T x \left(\tilde{D}_i(x, k_T, t_1) - \tilde{D}_i(x, k_T, t_2) \right), \quad (4.161)$$

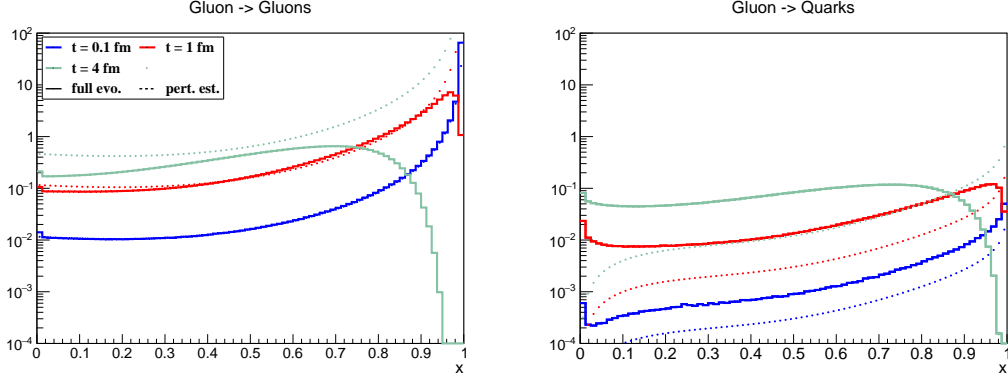


Figure 4.32: The $\sqrt{x}D(x,t)$ distributions at the time-scales $t = 0.1, 1, 4$ fm: cascades initiated by a gluon, gluons distribution on left, quarks on right. The solid lines correspond to the full medium evolution and the dotted line to the perturbative estimate.

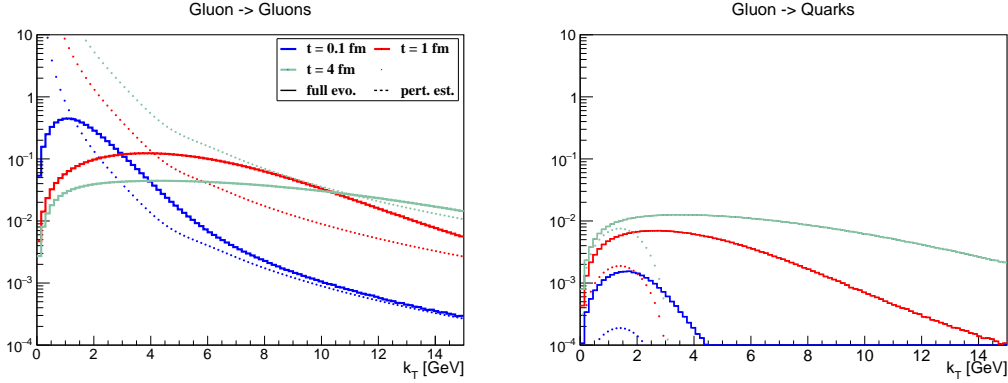


Figure 4.33: The $\tilde{D}(k_T,t)$ distributions at the time-scales $t = 0.1, 1, 4$ fm: cascades initiated by gluon, gluons distribution on left, quarks on right. The solid lines correspond to the full medium evolution and the dotted line to the perturbative estimate.

where t_1 and t_2 correspond respectively to the evolution time of the leading jet and the sub-leading jet. Results are shown in Fig. 4.34, where we have used a binning similar to those used experimentally [277] (even if the discussion will stay qualitative, since our model, with fixed medium temperature, is not phenomenology ready).

First, the steps like shapes (of the low energy bins) are due to the effective binning of the distribution in Θ (since the distributions are binned in $k_T = xE \sin \Theta$, a low energy implies an important sensibility to binning of Θ). The energy imbalance is clear at low angles (for the gluons distribution in case of back-to-back gluon jets and for the quarks distribution in case of back-to-back quark jets), for the hard particles, and is balanced at larger angles, i.e for soft particles. We can observe that the balance of the soft particles is more important for quark jets than for gluon jets (and overall, less important than in the Gaussian approximation). Also, we observe a different energy distribution in the

full **BDIM** case than in the Gaussian approximation. In the latter, the energy from low energy particle (first energy bin) decreases with the angle (but still becomes dominant at a large angle), while in the former case, it is negligible at low angles and increases with Θ .

4.6 Chapter summary

We have been interested in this chapter in jets, their definition and their evolution, with a focus on their evolution when they interact with a **QGP** (different from their vacuum evolution). The mechanisms that describe this interaction have been studied for nearly 30 years now and the 1st formalism to describe it is the well-known **BDMPS-Z** formalism. In this formalism, the interactions of a jet with the medium (a **QGP**) are described through two mechanisms : scattering with the medium color charges and medium-induced radiation. We have seen how to derive an evolution equation for gluon-dominated jets crossing a dense medium, taking into account these 2 formalisms (as building blocks of the parton cascade) and we went beyond the **BDMPS-Z** formalism by taking into account momentum transfer in branching (which goes beyond the eikonal limit of the **BDMPS-Z** formalism). This leads to the **BDIM** equation, where the jet energy loss is due to (medium-induced) splitting and jet broadening is both due to splitting and (multiple) scattering. We have then derived the equivalent equations accounting for quarks in the cascade (which also makes it possible to consider either quark or gluon jets). To this end, we calculated the different in-medium splitting kernels necessary in this case. After reviewing different forms and approximations of the **BDIM** equations, we have presented methods to solve them. We saw that an analytical solution existed in a simplified case. Then, we described a Monte-Carlo approach to solve the different forms of the **BDIM** equations presented (note that, the **MCMC** programs presented here, **MINCAS** [269] and **TMDICE** [270] were the first to propose a full treatment of broadening in splitting¹⁵). A method of resolution based on the Chebyshev polynomials has also been proposed, but it has been proven successful only for the integrated **BDIM** equations (describing the jet energy distribution). Finally, we studied the solutions of the **BDIM** equation, obtained through the program **MINCAS**, and observed the importance of the broadening coming from branching. We have also pointed out differences between quark and gluon jets, the former being more collimated than the latter. Also, there is still space for future work on the **BDIM** equations and their extensions. First, a natural next step would be to, somehow, take into account the dynamics of the medium. This could be done through some model for the temperature evolution, leading to evolving parameters (like the scatterers density, the Debye mass, and the scale of the coupling constant used in the scattering term). Another question is the role of vacuum-like emission that should be added to the model.

¹⁵Of course, other **MC** approaches have been proposed to describe jet evolution in heavy-ion collisions [278, 279], but so far without accounting for broadening in branching.

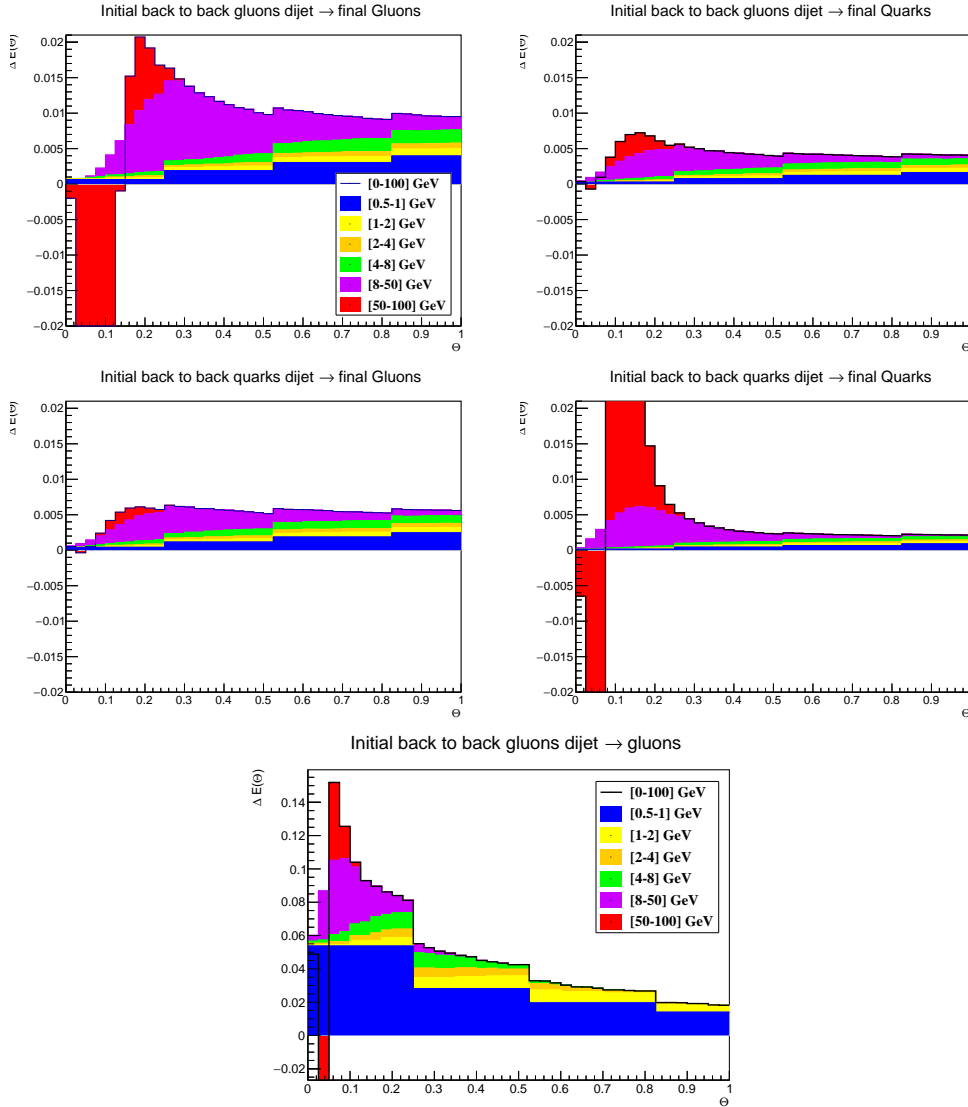


Figure 4.34: Dijet energy imbalance in function of the jet angle Θ for back-to-back gluon jets (top), back-to-back quark jets (middle) and for the Gaussian approximation in gluon dominated cascade (bottom). The energy imbalance is calculated in terms of the gluons distribution (left) and the quark distribution (right). The histogram accounts for the following binning in energy : [0.5, 1] GeV (in blue), [1, 2] GeV (in yellow), [2, 4] GeV (in orange), [4, 8] GeV (in green), [8, 50] GeV (in magenta) and [50, 100] GeV (in red).

Chapter 5

Conclusion and outlook

Along this thesis, we have explored different aspects of high-energy QCD and heavy-ion collisions. In particular, we have focused our attention on the influence of the kinematic variable k_T , the transverse momentum of an initial state hadron. We had to first introduce factorization which describes a hadronic process as the convolution of a non-perturbative part, hold by PDFs that describes universally the content of this hadron, with a perturbative part, describing the collision of two partons and hold by amplitudes. Another way to interpret PDFs is the transport of a soft parton inside the hadron (at a hadronic scale) to the scale of the collision, described by the evolution equation (that PDFs obey). In particular, we introduced k_T and hybrid factorization which involve TMDs, which permit the initial state in a collision to be off-shell. This factorization also relies on off-shell amplitudes (for one or both of the initial states legs). The Chap. 2 was dedicated to these PDF, their definition, given by factorization theorems, and their properties through the different evolution equations they follow. As our main focus was TMD, we presented a method to obtain them : the parton branching method, and studied the first PB nTMD obtained, for lead. This study ended with some comparison of results based on these nTMDs to CMS data for Z boson production in proton-lead collision i.e a DY process where k_T -factorization holds. While our predictions were based on tree-level matrix elements, they were in surprisingly good agreement with data. Also, this study has well shown the importance of the factorization scheme and the nuclear effects on the TMD. Then, we studied the calculation of QCD amplitudes in Chap. 3 with an introduction to common (but powerful) techniques to simplify the quick complexity involved by evaluating amplitude by applying Feynman rules. After a relatively long, but far from the exhaustive presentation of tools applicable to on-shell amplitudes, we focused on amplitudes with off-shell leg(s). We quickly introduced Lipatov's high energy effective theory in which reggeized gluons are new degrees of freedom. Also, the small amount of calculation made at one-loop in this theory suggests the difficulty of its application. We presented then a method to calculate off-shell gluon amplitudes based on the extraction, from specific kinematics, of this amplitude from the well-known on-shell amplitudes in a gauge invariant way : the auxiliary parton method. This method was working at tree level and the aim of the following was to generalize

it (at least, initialize its generalization) to **NLO**. We proposed an expression for the loop amplitude with one off-shell gluon and an arbitrary number of plus helicity gluons which exhibits the expected properties. However, we realized its limits when we tried to apply it to $g^*g^+g^-$. In this case, we have to apply the auxiliary parton method on (embedding) amplitudes with **IR** divergences (something new compared to the all plus helicity case). It appeared that, while the method naturally regularizes rapidity divergences, it led to expressions for them non equivalent to those calculated within Lipatov's high energy effective action. In the meantime, a solution was proposed in the form of a hybrid factorization formula at **NLO**. The last subject of this thesis was the jets and their interactions with the **QGP** formed during heavy-ion collisions. Understanding this object, a trail of collimated particles due to color confinement, is a key point to fill the gap between the partons leaving amplitudes and what is experimentally seen. Also, this gap gathers several phenomena (parton shower, hadronization, and decays). Being sensible to the medium they pass through, jets can be used as a probe. In particular, they are sensitive to the **QGP** formed in heavy-ion collision and are our key to understanding this state of matter. Especially, jets undergo energy loss when interacting with a **QGP**, which is referred to as jet quenching. This phenomenon can be described through the **BDMPS-Z** formalism which describes two kinds of interaction between the jet and the medium : scattering with the medium color charges and medium-induced radiations. From this formalism, and going beyond it (considering momentum transfer in branching) it is possible to derive the **BDIM** equations. Those equations describe the energy loss of a jet, traveling in a **QGP**, through medium-induced splitting and jet broadening (the former are more collimated). However, this equation was describing only pure gluon jets. We derived an equivalent equation accounting for quarks, such that we could evaluate their influence (greater than what is usually considered) and also observe the differences between a quark and a gluon jet. We also studied the relative importance of broadening and splitting. These studies have been possible with the help of two Monte-Carlo programs, **MINCAS** [269], **TMDICE** [270] and a Chebyshev approach (even if this last approach wasn't suitable to solve the full unintegrated **BDIM** equation). There is also room for new developments in this direction. Indeed, in these equations, the medium is considered static (which leads to an overestimation of quenching). The dynamic of the medium could be taken into account, first, through the modeled evolution of a parameter (the temperature). Another question is the role of vacuum-like emissions and how to implement them.

Also, the three elements studied here : nuclear **TMD**, off-shell amplitudes, and fragmentation functions convoluted through hybrid or k_T -factorization open the path to the study of the relative importance of saturation (taken into account at the **TMD** level) and jet quenching.

Appendix A

Appendices related to Parton Distribution Functions

A.1 Light-cone perturbation theory

Light cone perturbative theory has been introduced in [280–282] to quantize QCD on light cone coordinates (where the light-cone time takes the place of the time), suitable for the description of bound states (hadrons) in terms of quantum-mechanical (light-cone) wave functions. We won't enter the details of light-cone quantization but we will introduce light-cone coordinates to then give the QCD LCPT rules (that are some modified Feynman rules to be used in this context) to finally introduce light-cone wave function (that are used to describe hadrons).

A.1.1 Light-cone coordinates

If we consider a 4-momentum p in some frame \mathcal{F} where its *standard* coordinates read :

$$p^\mu = (p^0, p^1, p^2, p^3) = (E, p^x, p^y, p^z), \quad (\text{A.1})$$

where we have recalled 2 standard notations. Then we can rewrite p in what are called light-cone coordinates :

$$p_\mu = (p_+, p_\perp, p_-), \quad (\text{A.2})$$

where :

$$p^+ = E + p^z, \quad p_\perp = (p^x, p^y), \quad p^- = E - p^z. \quad (\text{A.3})$$

Then, the product of two 4-momenta p and k reads :

$$p \cdot k = \frac{1}{2} p^+ k^- + \frac{1}{2} p^- k^+ - p_\perp \cdot k_\perp. \quad (\text{A.4})$$

This translates in the metric, which nonzero components are :

$$\eta_{+-} = \eta_{-+} = \frac{1}{2}, \quad \eta_{xx} = \eta_{yy} = -1. \quad (\text{A.5})$$

Note that in light-cone coordinates, the metric isn't diagonal. This leads to :

$$p_- = \frac{1}{2}p^+, \quad p_+ = \frac{1}{2}p^-, \quad \text{and } \partial_- = \frac{1}{2}\partial^+, \quad \partial_+ = \frac{1}{2}\partial^-. \quad (\text{A.6})$$

We can also define Dirac matrices in light-cone coordinates as :

$$\gamma^+ = \gamma^0 + \gamma^z, \quad \gamma^- = \gamma^0 - \gamma^z. \quad (\text{A.7})$$

Then we can define a projector :

$$\Lambda_{\pm} = \frac{1}{2}\gamma^0\gamma^{\pm}. \quad (\text{A.8})$$

which satisfies :

$$\Lambda_+\Lambda_- = 0, \quad \Lambda_{\pm}^2 = \Lambda_{\pm}, \quad \text{and } \Lambda_+ + \Lambda_- = 1. \quad (\text{A.9})$$

This projector permit to separate a quark field $q(x)$ into two spinor components :

$$q_{\pm}(x) = \Lambda_{\pm}q(x). \quad (\text{A.10})$$

A.1.2 QCD light-cone perturbative theory rules

LCPT is comparable to time-ordered perturbation theory (see [47] for instance) where, in place of the time, we use the light-cone time x^+ . The QCD LCPT rules that we will present have been calculated in [280–283] in the specific light-cone gauge (see Eq. (1.7))¹ :

$$A^+ = 0. \quad (\text{A.11})$$

QCD LCPT rules are like Feynman rules describing how to calculate an amplitude in this approach. They can be written as follows :

- Draw all diagrams for the considered process and order in perturbation theory. Include all possible ordering of the vertices in the light-cone time.
- Assign an on-shell 4-momentum k to each line (of mass m) of the form :

$$k^{\mu} = \left(k^+, k_{\perp}, \frac{k_{\perp}^2 + m^2}{k^+} \right). \quad (\text{A.12})$$

This form reflects the on-shellness of the particle and the fact that only the $+$ and \perp component of the momentum are conserved at each vertex.

- Quarks on-shell spinors follow the Lepage and Brodsky [280] convention :

$$\begin{aligned} u_{\sigma}(k) &= \frac{1}{\sqrt{k^+}}\xi(\sigma) \left(k^+ + m\gamma^0 + \gamma^0\gamma_{\perp} \cdot k_{\perp} \right), \\ v_{\sigma}(k) &= \frac{1}{\sqrt{k^+}}\xi(-\sigma) \left(k^+ - m\gamma^0 + \gamma^0\gamma_{\perp} \cdot k_{\perp} \right). \end{aligned} \quad (\text{A.13})$$

¹This can be obtain choosing the light-cone vector $n^{\mu} = (0, 0_{\perp}, 2)$ when fixing the axial gauge.

where :

$$\xi(+1) = \frac{1}{\sqrt{2}} \begin{pmatrix} 1 \\ 0 \\ 1 \\ 0 \end{pmatrix}, \quad \xi(-1) = \frac{1}{\sqrt{2}} \begin{pmatrix} 0 \\ 1 \\ 0 \\ -1 \end{pmatrix}. \quad (\text{A.14})$$

- Gluon polarization vectors are of the form :

$$\epsilon_\lambda^\mu(k) = \left(0, \epsilon_\perp^\lambda, 2 \frac{\epsilon_\perp^\lambda \cdot k_\perp}{k^+} \right), \quad \text{with } \epsilon_\perp^\lambda = -\frac{1}{\sqrt{2}}(\lambda, i), \quad (\text{A.15})$$

such that it verifies $\epsilon_\lambda^+ = 0$ and $\epsilon_\lambda(k) \cdot k = 0$.

- Each intermediate state comes with the energy denominator :

$$\frac{1}{(\sum_{\text{initial}} - \sum_{\text{intermediate}}) k^- + i\epsilon}, \quad (\text{A.16})$$

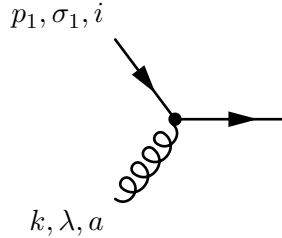
where the sums are defined respectively over the initial states of the considered diagram and over the particles over the intermediate state considered.

- Each internal lines with momentum k^+ flowing in the future light-cone direction imply a factor :

$$\frac{\theta(k^+)}{k^+}. \quad (\text{A.17})$$

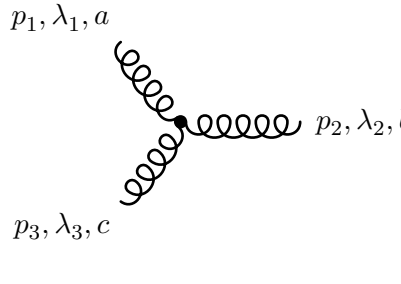
- The vertices are as follows :

– Quark-gluon vertex :



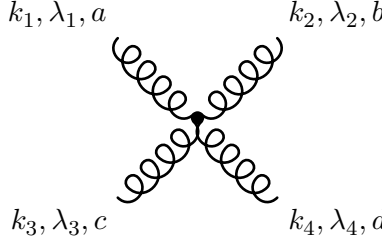
$$= -g_s \bar{u}_{\sigma_2, i_2}(p_2) \not{\epsilon}_\lambda(k) (t^a)_{ij} u_{\sigma_1, i_1}(p_1). \quad (\text{A.18})$$

– 3-gluons vertex :



$$= -ig_s f^{abc} [(k_1 - k_3) \cdot \epsilon_{\lambda_2}^*(k_2) \epsilon_{\lambda_1}(k_1) \cdot \epsilon_{\lambda_3}(k_3) \\ + (k_2 - k_1) \cdot \epsilon_{\lambda_3}(k_3) \epsilon_{\lambda_2}^*(k_2) \cdot \epsilon_{\lambda_1}(k_1) \\ + (k_3 - k_2) \cdot \epsilon_{\lambda_1}(k_1) \epsilon_{\lambda_3}(k_3) \cdot \epsilon_{\lambda_2}^*(k_2)]. \quad (\text{A.19})$$

– 4-gluons vertex :

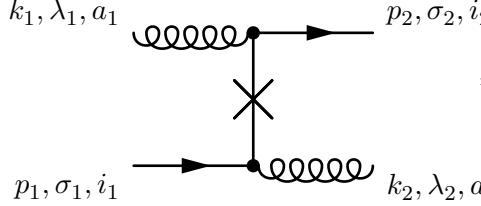


$$\begin{aligned}
&= g_s^2 [f^{abe} f^{cde} (\epsilon_{\lambda_1} \cdot \epsilon_{\lambda_3} \epsilon_{\lambda_2}^* \cdot \epsilon_{\lambda_4}^* - \epsilon_{\lambda_1} \cdot \epsilon_{\lambda_4}^* \epsilon_{\lambda_3} \cdot \epsilon_{\lambda_2}^*) \\
&\quad + f^{ace} f^{bde} (\epsilon_{\lambda_1} \cdot \epsilon_{\lambda_2}^* \epsilon_{\lambda_3} \cdot \epsilon_{\lambda_4}^* - \epsilon_{\lambda_1} \cdot \epsilon_{\lambda_4}^* \epsilon_{\lambda_3} \cdot \epsilon_{\lambda_2}^*) \\
&\quad + f^{ade} f^{bce} (\epsilon_{\lambda_1} \cdot \epsilon_{\lambda_2}^* \epsilon_{\lambda_3} \cdot \epsilon_{\lambda_4}^* - \epsilon_{\lambda_1} \cdot \epsilon_{\lambda_3} \epsilon_{\lambda_2}^* \cdot \epsilon_{\lambda_4}^*)],
\end{aligned} \tag{A.20}$$

where the momenta of the polarization vectors are implicit for readability.

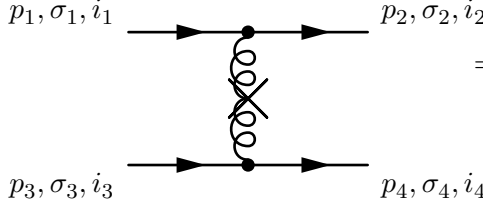
In addition to these vertices (equivalent to those of usual Feynman rules), in light-cone perturbation theory, due to the light-cone time ordering, one has to take into account the following instantaneous parton exchanges (denoted by a cross) :

– Instantaneous quark exchange :

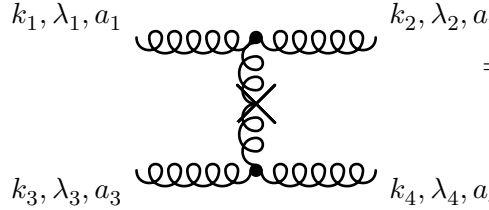


$$\begin{aligned}
&= g_s^2 \bar{u}_{\sigma_2, i_2}(p_2) \not{\epsilon}_{\lambda_1}(k_1) \frac{\gamma^+}{2(p_1^+ - k_2^+)} \not{\epsilon}_{\lambda_2}^*(k_2) \\
&\quad \times (t^{a_1} t^{a_2})_{i_1 i_2} u_{\sigma_1, i_1}(p_1).
\end{aligned} \tag{A.21}$$

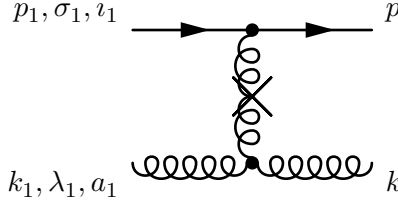
– 3 possible instantaneous gluon exchange :



$$\begin{aligned}
&= g_s^2 \bar{u}_{\sigma_2, i_2}(p_2) \gamma^+ (t^a)_{i_2 i_1} u_{\sigma_1, i_1}(p_1) \\
&\quad \times \frac{1}{(p_1^+ - p_2^+)^2} \bar{u}_{\sigma_4, i_4}(p_4) \gamma^+ (t^a)_{i_4 i_3} u_{\sigma_3, i_3}(p_3).
\end{aligned} \tag{A.22}$$



$$\begin{aligned}
&= g_s^2 f^{a_1 a_2 b} f^{a_3 a_4 b} \epsilon_{\lambda_2}^* \cdot \epsilon_{\lambda_1} \epsilon_{\lambda_4}^* \cdot \epsilon_{\lambda_3} \\
&\quad \times \frac{(k_1^+ + k_2^+)(k_3^+ + k_4^+)}{(k_1^+ - k_2^+)^2}.
\end{aligned} \tag{A.23}$$



$$\begin{aligned}
&= -g_s^2 \bar{u}_{\sigma_2, i_2}(p_2) \gamma^+ (t^b)_{i_2 i_1} u_{\sigma_1, i_1}(p_1) \\
&\quad \times \frac{k_1^+ + k_2^+}{(k_1^+ - k_2^+)^2} i f^{a_1 a_2 b} \epsilon_{\lambda_2}^* \cdot \epsilon_{\lambda_1}.
\end{aligned} \tag{A.24}$$

In these diagrams, the light cone time flows from left to right.

- Integrate, for each independent momentum k^μ , with the measure :

$$\int \frac{dk^+ d^2 k_\perp}{2(2\pi)^3}. \tag{A.25}$$

- Sum over internal quarks and gluons polarization and color.

A.1.3 Light-cone wave function

One of the strength of LCPT it is that it gives a suitable framework to characterize bounded partonic states (a hadron) in terms of quantum-mechanical wave function (and the possibility to calculate them following the QCD LCPT just presented), which is much harder with standard Feynman diagrams. Let's consider a hadron state $|\Psi\rangle$. This state is a superposition of Fock states of the form :

$$|n_g, n_Q\rangle \equiv |n_g, \{k_i^+, k_{i,\perp}, \lambda_i, a_i\}_{i \in [1, n_g]}; n_Q, \{p_j^+, p_{j,\perp}, \sigma_j, \alpha_j, f_j\}_{j \in [1, n_Q]}\rangle, \tag{A.26}$$

for a state composed of n_g gluons, n_q quarks and $n_{\bar{q}}$ antiquarks (with $n_Q = n_q + n_{\bar{q}}$), where gluons are characterized by the + and transverse component of their momentum k , their polarization λ and their color index a while quarks are characterized the + and transverse component of their momentum p , their helicity σ , their color α and their flavor f .

These Fock states form a complete basis, which translates in :

$$\sum_{n_g, n_Q} \int d\Omega_{n_g, n_Q} |n_g, n_Q\rangle \langle n_g, n_Q| = \mathbf{1}. \tag{A.27}$$

Each Fock states are normalized to 1 ($\langle n_g, n_Q | n_g, n_Q \rangle = 1$) and the phase-space integral is defined, for a hadron of momentum P , as :

$$\begin{aligned}
\int d\Omega_{n_g, n_Q} &= \frac{2P^+ (2\pi)^3}{S_n} \int \prod_{i=1}^{n_g} \sum_{\lambda_i, a_i} \frac{dk_i^+ d^2 k_{i,\perp}}{2k_i^+ (2\pi)^3} \prod_{i=j}^{n_Q} \sum_{\sigma_j, \alpha_j, f_j} \frac{dp_j^+ d^2 p_{j,\perp}}{2p_j^+ (2\pi)^3} \\
&\quad \times \delta \left(P^+ - \sum_{i^+=1}^{n_g} k_{i^+}^+ - \sum_{j^+=1}^{n_g} p_{j^+}^+ \right) \delta^{(2)} \left(P_\perp - \sum_{i_\perp=1}^{n_g} k_{i_\perp, \perp} - \sum_{j_\perp=1}^{n_g} p_{j_\perp, \perp} \right),
\end{aligned} \tag{A.28}$$

where the symmetry factor reads $S_n = n_g!n_q!n_{\bar{q}}!$. Note that the **LCPT** rules are respected with the momentum conservation of only the + and transverse components.

With this, we can define the hadron state $|\Psi\rangle$ as :

$$|\Psi\rangle = \sum_{n_g, n_Q} \int d\Omega_{n_g, n_Q} |n_g, n_Q\rangle \langle n_g, n_Q | \Psi\rangle, \quad (\text{A.29})$$

and define the *light-cone wave function* as the multi-particle wave function corresponding to the hadron Fock state with n_g gluons and n_Q quarks (antiquarks included) :

$$\Psi(n_g, n_Q) \equiv \langle n_g, n_Q | \Psi\rangle. \quad (\text{A.30})$$

We can see that this wave function is normalized to a number less or equal to 1, when writing the condition :

$$\langle \Psi | \Psi\rangle = 1 = \sum_{n_g, n_Q} \int d\Omega_{n_g, n_Q} |\Psi(n_g, n_Q)|^2. \quad (\text{A.31})$$

We mentioned that one can use the **QCD LCPT** to calculate a light-cone wave function. Actually some modification havee to be taken into account :

- The outgoing states are treated as internal (bringing an energy denominator). This is because the outgoing states in a wave-function are thought to interact further.
- Outgoing lines are treated as external and only bring a factor $\theta(k^+)$.
- Incoming external lines are treated as internal and bring a factor $\frac{1}{k^+}$ (the theta function is not necessary for these lines).

A.1.4 Light-cone “Diracology”

We will gather here some properties of the Dirac spinors in light-cone coordinates, useful when calculating light-cone wave functions. First we define the operation \times as :

$$p_{\perp} \times k_{\perp} \equiv p^x k^y - p^y k^x = \epsilon^{ij} p_{\perp}^i k_{\perp}^j. \quad (\text{A.32})$$

Then, the following relation are needed to calculate light-cone wave function :

$$\begin{aligned} \frac{\bar{u}_{\sigma'}(p')}{\sqrt{p'^+}} \gamma^+ \frac{u_{\sigma}(p)}{\sqrt{p^+}} &= 2\delta_{\sigma, \sigma'}, \\ \frac{\bar{u}_{\sigma'}(p')}{\sqrt{p'^+}} \gamma^- \frac{u_{\sigma}(p)}{\sqrt{p^+}} &= 2 \frac{\delta_{\sigma, \sigma'}}{p^+ p'^+} (p_{\perp} \cdot p'_{\perp} - i\sigma p_{\perp} \times p'_{\perp}), \\ \frac{\bar{u}_{\sigma'}(p')}{\sqrt{p'^+}} \gamma_{\perp}^i \frac{u_{\sigma}(p)}{\sqrt{p^+}} &= \delta_{\sigma, \sigma'} \left(\frac{p_{\perp}^i - i\sigma \epsilon^{ij} p_{\perp}^j}{p'^+} + \frac{p_{\perp}^i - i\sigma \epsilon^{ij} p_{\perp}^j}{p^+} \right), \end{aligned} \quad (\text{A.33})$$

for matrix elements based on massless u spinors only and :

$$\begin{aligned}
\frac{\bar{v}_{\sigma'}(p')}{\sqrt{p'^+}} \gamma^+ \frac{u_{\sigma}(p)}{\sqrt{p^+}} &= 2\delta_{\sigma, -\sigma'}, \\
\frac{\bar{v}_{\sigma'}(p')}{\sqrt{p'^+}} \gamma^- \frac{u_{\sigma}(p)}{\sqrt{p^+}} &= 2 \frac{\delta_{\sigma, -\sigma'}}{p^+ p'^+} (p_{\perp} \cdot p'_{\perp} - i\sigma p_{\perp} \times p'_{\perp}), \\
\frac{\bar{v}_{\sigma'}(p')}{\sqrt{p'^+}} \gamma_{\perp}^i \frac{u_{\sigma}(p)}{\sqrt{p^+}} &= \delta_{\sigma, -\sigma'} \left(\frac{p_{\perp}^i - i\sigma \epsilon^{ij} p_{\perp}^j}{p'^+} + \frac{p_{\perp}^i - i\sigma \epsilon^{ij} p_{\perp}^j}{p^+} \right),
\end{aligned} \tag{A.34}$$

for matrix elements mixing massless u and v spinors. The other possible matrix elements are found using :

$$\begin{aligned}
\bar{v}_{\sigma'}(p') \gamma^{\mu} v_{\sigma}(p) &= \bar{u}_{\sigma}(p) \gamma^{\mu} u_{\sigma'}(p'), \\
\bar{u}_{\sigma'}(p') \gamma^{\mu} v_{\sigma}(p) &= (\bar{v}_{\sigma}(p) \gamma^{\mu} u_{\sigma'}(p'))^*.
\end{aligned} \tag{A.35}$$

A.2 Splitting functions

We review here the derivation of the LO splitting functions. This derivation follows the one presented in [6].

A.2.1 P_{qq}

Let's begin by the splitting P_{qq} . To calculate it, we need to evaluate the first order corrections to the quark wave function. For instance, the real correction to the quark wave function ψ_n^f is presented in Fig. 2.6. This type of diagram permits to relate the wave function ψ_n^q (at the dash line 2) to the wave function ψ_{n-1}^f (at the dash line 1) using the QCD LCPT rules (see Sec. A.1.2) to describe what happens in between. Actually, P_{qq} appears when calculating the corrections to the quark parton distribution function $f_{f/p}$ which comes to LO corrections to the wave function squared $|\psi_n^f|^2$. These corrections are pictured in Fig. A.1 where diagram A represents the real correction while diagrams B and C are the virtual corrections.

Let's begin with the real correction, as depicted in Fig. 2.6. Applying the QCD LCPT rules (for a wave function, in the light-cone gauge $A^+ = 0$) leads to :

$$\begin{aligned}
\psi_n^f(\{k_i\}; x, k_{\perp}; h) &= \frac{g_s t^a \theta(k^+) \theta(k'^+ - k^+)}{(k' - k)^- + k^- + \sum_{j=1}^{n-1} k_j^- - P^-} \frac{1}{k'^+} \\
&\times \bar{u}_h(k) \not{\epsilon}_{\lambda}^*(k' - k) u_{h'}(k') \psi_{n-1}^f(\{k_i\}; x', k'_{\perp}; h'),
\end{aligned} \tag{A.36}$$

where P is the momentum of the initial hadron. Then, the energy denominator is transformed using the on-shellness of the particles in LCPT and also the LLA, which

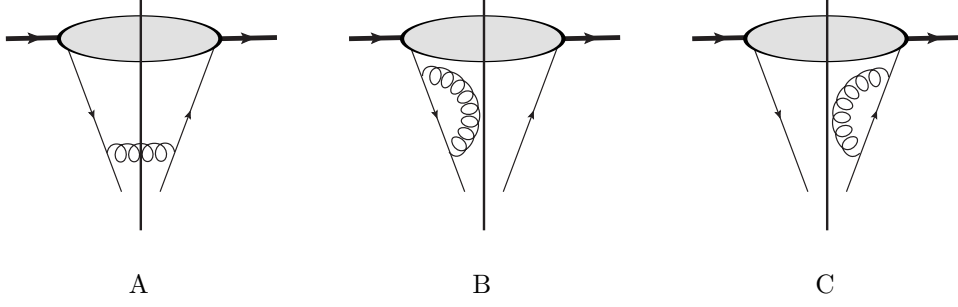


Figure A.1: Diagrams contributing to P_{qq}

permit to neglect all transverse momenta squared towards k_{\perp}^2 . It leads to :

$$\frac{1}{(k' - k)^- + k^- + \sum_{j=1}^{n-1} k_j^- - P^-} \frac{1}{k^+} = \frac{1}{\frac{(k'_{\perp} - k_{\perp})^2}{(k' - k)^+} + \frac{k_{\perp}^2}{k^+} + \sum_{j=1}^{n-1} \frac{k_{j,\perp}^2}{k_j^+} - \frac{P_{\perp}^2}{P^+}} \frac{1}{k^+} \quad (\text{A.37})$$

$$\simeq \frac{1}{\frac{k_{\perp}^2}{(k' - k)^+} + \frac{k_{\perp}^2}{k^+}} = \frac{k^+ (k' - k)^+}{k'^+ k_{\perp}^2},$$

where $z = \frac{k^+}{k'^+}$. Using the properties of spinors (see Eq. (A.33)), one can evaluate the spinor part as :

$$\begin{aligned} \bar{u}_h(k) \not{\epsilon}_{\lambda}^*(k' - k) u_{h'}(k') &= \bar{u}_h(k) \gamma^+ u_{h'}(k') \frac{\epsilon_{\perp}^{\lambda*} \cdot (k' - k)_{\perp}}{(k' - k)^+} \\ &\quad - \bar{u}_h(k) \gamma_{\perp} \cdot \epsilon_{\perp}^{\lambda*} (k' - k) \cdot u_{h'}(k') \\ &= \frac{\delta_{h,h'}}{\sqrt{z(1-z)}} \epsilon_{\perp}^{\lambda*} (k' - k) \cdot (k_{\perp} - z k'_{\perp}) [1 + z + h\lambda(1-z)], \end{aligned} \quad (\text{A.38})$$

where we have used in the first equality the form of the gluon polarization vector in LCPT (as given in Eq. (A.15)). It can be further simplified in the LLA (neglecting k'_{\perp}). In the following, we will set the momentum dependence of the polarization vector implicit (for readability). Overall, Eq. (A.36) now reads :

$$\begin{aligned} \psi_n^f(\{k_i\}; x, k_{\perp}; h) &= -g_s t^a \theta(z) \theta(1-z) \delta_{h,h'} \sqrt{z} \frac{\epsilon_{\perp}^{\lambda*} \cdot k_{\perp}}{k_{\perp}^2} \\ &\quad \times [1 + z + h\lambda(1-z)] \psi_{n-1}^f(\{k_i\}; x', k'_{\perp}; h'). \end{aligned} \quad (\text{A.39})$$

Squaring this expression and summing over the polarizations, helicities and colors (has it would appear in the PDF $f_{f/p}$), and using the expression for $\epsilon_{\perp}^{\lambda}$ (given in Eq. (A.15)),

reads :

$$\begin{aligned} \sum_{h,h',\lambda,a} \left| \psi_n^f(\{k_i\}; x, k_\perp; h) \right|^2 &= 8\pi\alpha_s C_F \theta(z) \theta(1-z) \frac{z(1+z^2)}{k_\perp^2} \\ &\times \sum_{h'=\pm} \left| \psi_{n-1}^f(\{k_i\}; x', k'_\perp; h') \right|^2. \end{aligned} \quad (\text{A.40})$$

We should then write the expression of the quark PDF at the end of our diagram (denoted by the superscript A) :

$$\begin{aligned} f_{f/p}^A(x, \mu^2) &= \sum_n \frac{1}{x} \int \frac{d^2 k_\perp}{2(2\pi)^3} \frac{d^2(k'_\perp - k_\perp)}{2(2\pi)^3} \frac{d(k'^+ - k^+)}{k'^+ - k^+} \prod_{i=1}^n \frac{dx_i}{x_i} \frac{d^2 k_{i,\perp}}{(2\pi)^3} \\ &\times \sum_{h,h',\lambda,a} \left| \psi_n^f(\{k_i\}; x, k_\perp; h) \right|^2 \\ &\times (2\pi)^3 \delta^2 \left(k'_\perp + \sum_{j=1}^{n-1} k_{j,\perp} \right) \delta \left(1 - x' - \sum_{l=1}^{n-1} x_l \right), \end{aligned} \quad (\text{A.41})$$

where, due to the momentum ordering, the partons are distinguishable hence, no symmetry factor is needed. Before introducing the formula we got for $\sum_{h,h',\lambda,a} |\psi_n^f|^2$ in this expression, we should rewrite the phase space integrals of the momentum of the emitted gluon as :

$$\begin{aligned} \int \frac{d^2(k'_\perp - k_\perp)}{2(2\pi)^3} \int_0^{P^+ - k^+} \frac{d(k'^+ - k^+)}{k'^+ - k^+} &= \int \frac{d^2 k'_\perp}{2(2\pi)^3} \int_{k^+}^{P^+} \frac{dk'^+}{k'^+ - k^+} \\ &= \int^{\mu^2} \frac{d^2 k'_\perp}{2(2\pi)^3} \int_x^1 \frac{dz}{z(1-z)}, \end{aligned} \quad (\text{A.42})$$

where we have used the fact that k^+ is fixed and that the integration over k_\perp is already performed in the expression of $f_{f/p}^A$. This leads to (introducing also Eq. (A.40)) :

$$\begin{aligned} f_{f/p}^A(x, \mu^2) &= \frac{\alpha_s C_F}{2\pi} \frac{1}{x} \int^{\mu^2} \frac{dk_\perp^2}{k_\perp^2} \int_x^1 dz \frac{1+z^2}{1-z} \sum_n \int \prod_{i=1}^n \frac{dx_i}{x_i} \frac{d^2 k_{i,\perp}}{(2\pi)^3} \frac{d^2 k'_\perp}{2(2\pi)^3} \\ &\times \sum_{h'=\pm} \left| \psi_{n-1}^f(\{k_i\}; x', k'_\perp; h') \right|^2 \\ &\times (2\pi)^3 \delta^2 \left(k'_\perp + \sum_{j=1}^{n-1} k_{j,\perp} \right) \delta \left(1 - x' - \sum_{l=1}^{n-1} x_l \right). \end{aligned} \quad (\text{A.43})$$

We recognize in this expression $x' f_{f/p}(x', k_\perp^2) = \frac{x}{z} f_{f/p} \left(\frac{x}{z}, k_\perp^2 \right)$ (from the 2nd line), which leads to the integral relation :

$$f_{f/p}^A(x, \mu^2) = \frac{\alpha_s C_F}{2\pi} \int^{\mu^2} \frac{dk_\perp^2}{k_\perp^2} \int_x^1 \frac{dz}{z} \frac{1+z^2}{1-z} f_{f/p} \left(\frac{x}{z}, k_\perp^2 \right), \quad (\text{A.44})$$

which can be differentiated as :

$$\mu^2 \frac{\partial}{\partial \mu^2} f_{f/p}^A(x, \mu^2) = \frac{\alpha_s}{2\pi} \int_x^1 \frac{dz}{z} P_{qq}^A(z) f_{f/p} \left(\frac{x}{z}, \mu^2 \right), \quad (\text{A.45})$$

where P_{qq}^A is the contribution of diagram A to P_{qq} , defined as :

$$P_{qq}^A(z) = C_F \frac{1+z^2}{1-z}. \quad (\text{A.46})$$

This is the first step in the derivation of the **DGLAP** equation, which implies to account all other possible correction (for both quark and gluon **PDF**). To obtain P_{qq} , we still need to account for the virtual correction. We can see that, directly by construction or invoking unitarity that the virtual correction (diagrams B and C) lead to the same formula (up to a sign) for the wave function as in the real corrections (see Eq. (A.36)) except that the relation linked ψ_n^f to ψ_n^f . Also, note that the dominant transverse momentum in this case is k'_\perp . This leads to :

$$\begin{aligned} \sum_{h, h', \lambda, a} \left| \psi_n^f(\{k_i\}; x, k_\perp; h) \right|^2 &= -8\pi\alpha_s C_F \theta(z) \theta(1-z) \frac{z(1+z^2)}{k'_\perp{}^2} \\ &\times \sum_{h=\pm} \left| \psi_n^f(\{k_i\}; x, k_\perp; h) \right|^2. \end{aligned} \quad (\text{A.47})$$

Then the corresponding **PDF** reads :

$$\begin{aligned} f_{f/p}^{B+C}(x, \mu^2) &= \sum_n \frac{1}{x'} \int \frac{d^2 k'_\perp}{2(2\pi)^3} \frac{d^2 k_\perp}{2(2\pi)^3} \frac{d(k^+ - k'^+)}{k^+ - k'^+} \prod_{i=1}^n \frac{dx_i}{x_i} \frac{d^2 k_{i,\perp}}{(2\pi)^3} \\ &\times \sum_{h, h', \lambda, a} \left| \psi_n^f(\{k_i\}; x', k'_\perp; h') \right|^2 \\ &\times (2\pi)^3 \delta^2 \left(k_\perp + \sum_{j=1}^n k_{j,\perp} \right) \delta \left(1 - x - \sum_{l=1}^{n-1} x_l \right). \end{aligned} \quad (\text{A.48})$$

In this case, the gluon phase space is written as (with the $\frac{1}{x}$ factor) :

$$\begin{aligned} \int \frac{d^2(k_\perp - k'_\perp)}{2(2\pi)^3} \int_0^{P^+} \frac{d(k^+ - k'^+)}{k^+ - k'^+} \frac{1}{x'} &= \int \frac{d^2 k_\perp}{2(2\pi)^3} \int_0^{k^+} \frac{dk'^+ P^+}{k'^+(k^+ - k'^+)} \\ &= \int^{\mu^2} \frac{d^2 k'_\perp}{2(2\pi)^3} \int_0^1 \frac{dz}{xz(1-z)}. \end{aligned} \quad (\text{A.49})$$

This leads to :

$$f_{f/p}^{B+C}(x, \mu^2) = -\frac{\alpha_s C_F}{2\pi} \int^{\mu^2} \frac{dk'_\perp{}^2}{k'_\perp{}^2} \int_0^1 dz \frac{1+z^2}{1-z} f_{f/p}(x, k'_\perp{}^2), \quad (\text{A.50})$$

which can be differentiated as :

$$\mu^2 \frac{\partial}{\partial \mu^2} f_{f/p}^{B+C}(x, \mu^2) = -\frac{\alpha_s C_F}{2\pi} \int_0^1 dz \frac{1+z^2}{1-z} f_{f/p}(x, \mu^2). \quad (\text{A.51})$$

Accounting for all 3 diagrams leads to the equation :

$$\mu^2 \frac{\partial}{\partial \mu^2} f_{f/p}(x, \mu^2) = \frac{\alpha_s C_F}{2\pi} \left[\int_x^1 \frac{dz}{z} \frac{1+z^2}{1-z} f_{f/p}\left(\frac{x}{z}, \mu^2\right) - \int_0^1 dz \frac{1+z^2}{1-z} f_{f/p}(x, \mu^2) \right], \quad (\text{A.52})$$

where it is possible to define P_{qq} in the form :

$$P_{qq}(z) = C_F \left[\frac{1+z^2}{(1-z)_+} + \frac{3}{2} \delta(1-z) \right], \quad (\text{A.53})$$

with the + prescription given by :

$$\int_x^1 dz \frac{f(z)}{(1-z)_+} \equiv \int_x^1 dz \frac{f(z) - f(1)}{1-z} + f(1) \ln(1-x). \quad (\text{A.54})$$

This way, we can write :

$$\mu^2 \frac{\partial}{\partial \mu^2} f_{f/p}(x, \mu^2) = \frac{\alpha_s}{2\pi} \int_x^1 \frac{dz}{z} P_{qq}(z) f_{f/p}\left(\frac{x}{z}, \mu^2\right), \quad (\text{A.55})$$

which is the form wanted for the DGLAP equations.

A.2.2 P_{gq}

To calculate P_{gq} , the only possible LO contribution is the real correction presented in Fig. A.2.

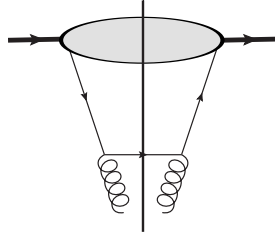


Figure A.2: Diagram contributing to P_{gq}

The calculation of this correction is very similar to the real correction of P_{qq} . Basically, the role of the outgoing quark and outgoing gluon are inverted. Then we can directly write P_{gq} as :

$$P_{gq}(z) = P_{qq}^A(1-z) = C_F \frac{1+(1-z)^2}{z}. \quad (\text{A.56})$$

A.2.3 P_{qg}

For P_{qg} , there is also an unique diagram (real correction), presented in Fig. A.3.

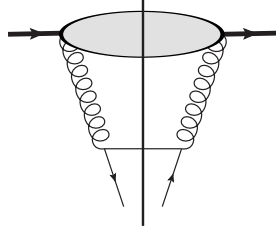


Figure A.3: Diagram contributing to P_{qg}

The calculation can be handled the same way as for the real correction to P_{qq} , starting with :

$$\begin{aligned} \psi_n^f(\{k_i\}; x, k_\perp; h) &= \frac{g_s t^a \theta(k^+) \theta(k'^+ - k^+)}{(k' - k)^- + k^- + \sum_{j=1}^{n-1} k_j^- - P^-} \frac{1}{k'^+} \\ &\times \bar{u}_h(k) \not{\epsilon}_\lambda^*(k') v_h(k' - k) \psi_{n-1}^f(\{k_i\}; x', k'_\perp; h'), \end{aligned} \quad (\text{A.57})$$

when the antiquark is observed (the case where the quark is observed has also to be taken into account, but it leads to the same contribution). Rather than performing again the same calculation, we will give arguments to obtain it from P_{qq}^A . Indeed the considered diagram differs from the real correction of P_{qq} by the fact that here, the gluon is incoming while the quark antiquark pair is outgoing which will translate into a crossing symmetry $P_{qg}(z) \propto z P_{qq}^A(1 - \frac{1}{z})$. Also, the color factor C_F is replaced by $\frac{1}{2}$, and since we sum here over the quark and antiquark flavors, we also need a factor $2N_f$. Overall P_{qg} reads :

$$P_{qg}(z) = \frac{N_f}{C_F} z P_{qq}^A \left(1 - \frac{1}{z}\right) = N_f \left[z^2 + (1 - z)^2\right]. \quad (\text{A.58})$$

A.2.4 P_{gg}

Finally, we will calculate P_{gg} . This is probably the most complex splitting function, since, as shown in Fig. A.4, we have 1 diagram for real corrections and no less than 4 diagrams for virtual corections.

Let's first have look at the real correction, as shown in Fig. A.5. Contrary to the

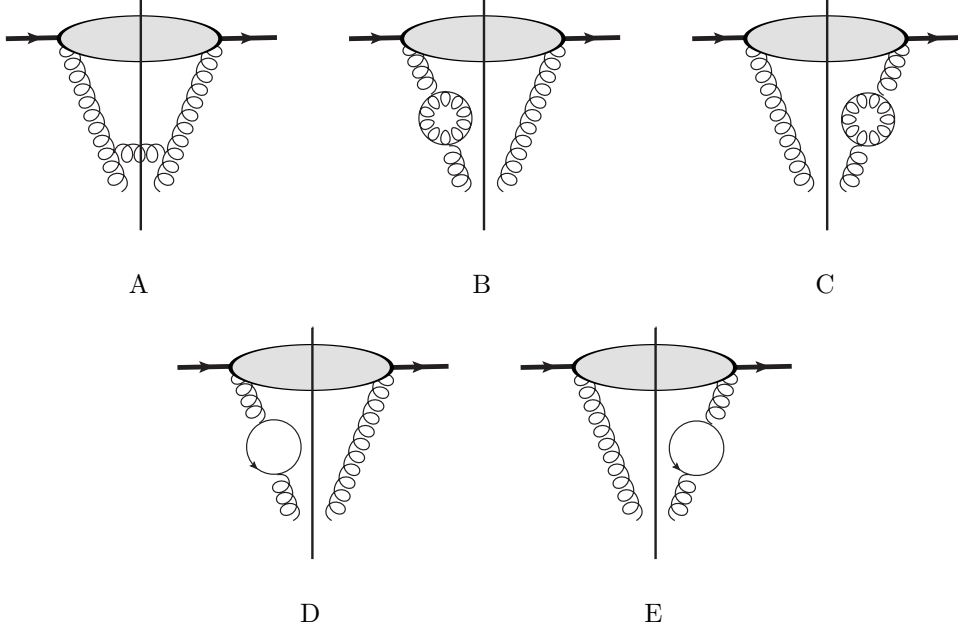


Figure A.4: Diagrams contributing to P_{gg}

other real correction calculated so far, we have here a 3-gluons vertex, which leads to :

$$\begin{aligned}
\psi_n(\{k_i\}; x, k_\perp; \lambda) &= \frac{ig_s f^{abc} \theta(k^+) \theta(k'^+ - k^+)}{(k' - k)^- + k^- + \sum_{j=1}^{n-1} k_j^- - P^-} \frac{1}{k'^+} \\
&\times \left[(k' + k) \cdot \epsilon_{\lambda''}^* \epsilon_\lambda^* \cdot \epsilon_{\lambda'} + (k - 2k') \cdot \epsilon_\lambda^* \epsilon_{\lambda'} \cdot \epsilon_{\lambda''}^* \right. \\
&\quad \left. + (k' - 2k) \cdot \epsilon_{\lambda'} \epsilon_{\lambda''}^* \cdot \epsilon_\lambda^* \right] \\
&\times \psi_{n-1}(\{k_i\}; x', k'_\perp; \lambda').
\end{aligned} \tag{A.59}$$

Using the form of the polarization vectors in LCPT (see Eq. (A.15)), applying the LLA, and using Eq. (A.37), one should obtain :

$$\begin{aligned}
\psi_n(\{k_i\}; x, k_\perp; \lambda) &= ig_s f^{abc} \theta(z) \theta(1 - z) \frac{z(1 - z)}{k_\perp^2} \\
&\times \left[\frac{2}{1 - z} k_\perp \cdot \epsilon_\perp^{\lambda''*} \epsilon_\perp^{\lambda*} \cdot \epsilon_\perp^{\lambda'} + \frac{2}{z} k_\perp \cdot \epsilon_\perp^{\lambda*} \epsilon_\perp^{\lambda'} \cdot \epsilon_\perp^{\lambda''*} \right. \\
&\quad \left. - 2k_\perp \cdot \epsilon_\perp^{\lambda'} \epsilon_\perp^{\lambda''*} \cdot \epsilon_\perp^{\lambda*} \right] \\
&\times \psi_{n-1}(\{k_i\}; x', k'_\perp; \lambda').
\end{aligned} \tag{A.60}$$

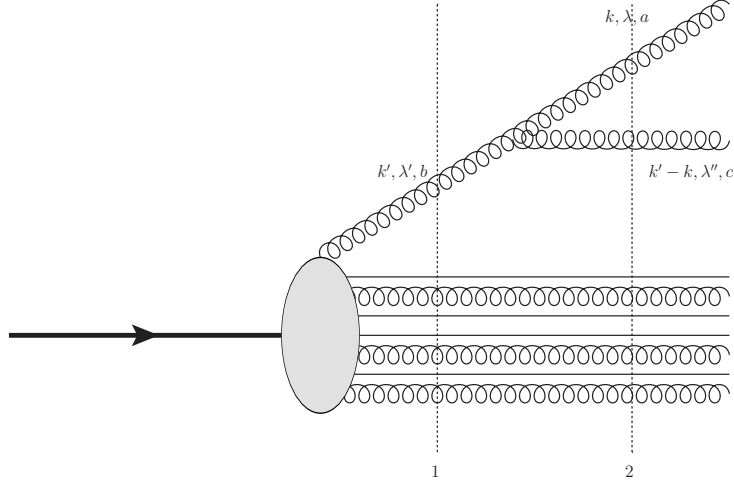


Figure A.5: 1st order real correction to the quark PDF

Once squared, and summed over color and polarization, it gives :

$$\begin{aligned}
 \sum_{\lambda, \lambda', \lambda'', a, b, b', c} |\psi_n(\{k_i\}; x, k_{\perp}; \lambda)|^2 &= 16\pi\alpha_s N_c \theta(z)\theta(1-z) \frac{1}{k_{\perp}^2} \\
 &\times \left[z^2 + (1+z^2)(1-z)^2 \right] \\
 &\times \sum_{\lambda', b} |\psi_{n-1}(\{k_i\}; x', k'_{\perp}; \lambda')|^2, \tag{A.61}
 \end{aligned}$$

where b' correspond to the color of the incoming gluon, but in the conjugate amplitude. From applying this expression to the gluon PDF in diagram D, it follows the integral relation :

$$f_g^A(x, \mu^2) = \frac{\alpha_s N_c}{\pi} \int^{\mu^2} \frac{dk_{\perp}^2}{k_{\perp}^2} \int_x^1 \frac{dz}{z^2(1-z)} \left[z^2 + (1+z^2)(1-z)^2 \right] f_g\left(\frac{z}{x}, k'_{\perp}{}^2\right), \tag{A.62}$$

which can be differentiated as :

$$\mu^2 \frac{\partial}{\partial \mu^2} f_g^A(x, \mu^2) = \frac{\alpha_s}{2\pi} \int_x^1 \frac{dz}{z} P_{gg}^A(z) f_g\left(\frac{z}{x}, k'_{\perp}{}^2\right), \tag{A.63}$$

where P_{gg}^A is the contribution from diagram A to P_{gg} , defined as :

$$P_{gg}^A(z) = 2N_c \left[\frac{z}{1-z} + \frac{1-z}{z} + z(1-z) \right]. \tag{A.64}$$

Actually, the virtual corrections can be obtained with the already derived splitting functions. Indeed, diagrams B and C corresponds to virtual corrections to the real correction

A and diagrams B and C corresponds to virtual corrections to the real correction leading to P_{gg} .

It leads to :

$$\begin{aligned}\mu^2 \frac{\partial}{\partial \mu^2} f_g^{B+C}(x, \mu^2) &= -\frac{\alpha_s N_c}{2\pi} \int_0^1 dz \left[\frac{z}{1-z} + \frac{1-z}{z} + z(1-z) \right] f_g(x, k_\perp'^2) \\ &= -\frac{\alpha_s N_c}{2\pi} \left[\int_0^1 dz \frac{2}{1-z} - \frac{11}{6} \right] f_g(x, k_\perp'^2), \\ \mu^2 \frac{\partial}{\partial \mu^2} f_g^{D+E}(x, \mu^2) &= -\frac{\alpha_s N_f}{4\pi} \int_0^1 dz \left[z^2 + (1-z)^2 \right] f_g(x, k_\perp'^2) = -\frac{\alpha_s N_f}{2\pi} \frac{1}{3} f_g(x, k_\perp'^2).\end{aligned}\tag{A.65}$$

Accounting for all contributions, it is possible to show that :

$$\mu^2 \frac{\partial}{\partial \mu^2} f_g(x, \mu^2) = \frac{\alpha_s}{2\pi} \int_x^1 \frac{dz}{z} P_{gg}(z) f_g\left(\frac{z}{x}, k_\perp'^2\right),\tag{A.66}$$

with the splitting function P_{gg} expressed as :

$$P_{gg}(z) = 2N_c \left[\frac{z}{(1-z)_+} + \frac{1-z}{z} + z(1-z) \right] + \frac{11N_c - 2N_f}{6} \delta(1-z).\tag{A.67}$$

A.3 DGLAP solution through Mellin transform

A common method to solve DGLAP equations, is to rewrite the equations in *moment space*, using the Mellin transform [284] $f_\omega(Q^2)$ of the distribution functions $f(x, Q^2)$:

$$\{\mathcal{M}f\}(\omega) = f_\omega(Q^2) \equiv \int_0^1 dx x^\omega f(x, Q^2).\tag{A.68}$$

We will note f_ω^S , f_ω^{NS} and f_ω^g the Mellin transform of f_S , f_{NS} and f_g respectively and $\gamma_{ij}(\omega)$ those of the splitting functions P_{ij} (γ_{ij} are called *anomalous dimension*). Then, it can be shown that, in moment space, the DGLAP equations reads [285, 286] :

$$\begin{aligned}\frac{\partial}{\partial \ln Q^2} \begin{pmatrix} f_\omega^S(Q^2) \\ f_\omega^g(Q^2) \end{pmatrix} &= \frac{\alpha_s(Q^2)}{2\pi} \begin{pmatrix} \gamma_{qq}(\omega) & \gamma_{qg}(\omega) \\ \gamma_{gq}(\omega) & \gamma_{gg}(\omega) \end{pmatrix} \begin{pmatrix} f_\omega^S(Q^2) \\ f_\omega^g(Q^2) \end{pmatrix} \\ \frac{\partial f_\omega^{NS}(Q^2)}{\partial \ln Q^2} &= \frac{\alpha_s(Q^2)}{2\pi} \gamma_{qq}(\omega) f_\omega^{NS}(Q^2),\end{aligned}\tag{A.69}$$

with the anomalous dimension given as :

$$\begin{aligned}
\gamma_{qq}(\omega) &= C_F \left[\frac{1}{(1+\omega)(2+\omega)} + \frac{3}{2} - 2\psi(2+\omega) + 2\psi(1) \right], \\
\gamma_{qg}(\omega) &= C_F \left[\frac{1}{2+\omega} + \frac{1}{\omega(1+\omega)} \right], \\
\gamma_{gq}(\omega) &= N_f \left[\frac{1}{1+\omega} + \frac{1}{(2+\omega)(3+\omega)} \right], \\
\gamma_{gg}(\omega) &= 2N_c \left[\frac{1}{\omega(1+\omega)} + \frac{1}{(2+\omega)(3+\omega)} - \psi(2+\omega) + \psi(1) \right] + \frac{11N_c - 2N_f}{6},
\end{aligned} \tag{A.70}$$

where $\psi(\omega) = \frac{\Gamma'(\omega)}{\Gamma(\omega)}$ is the digamma function. In this form, the solution of the DGLAP equations can be written as the following exponential :

$$\begin{aligned}
\begin{pmatrix} f_\omega^S(Q^2) \\ f_\omega^g(Q^2) \end{pmatrix} &= \exp \left\{ \int_{Q_0^2}^{Q^2} \frac{dQ'^2}{Q'^2} \frac{\alpha_s(Q'^2)}{2\pi} \begin{pmatrix} \gamma_{qq}(\omega) & \gamma_{qg}(\omega) \\ \gamma_{gq}(\omega) & \gamma_{gg}(\omega) \end{pmatrix} \right\} \begin{pmatrix} f_\omega^S(Q_0^2) \\ f_\omega^g(Q_0^2) \end{pmatrix} \\
f_\omega^{NS}(Q^2) &= \exp \left\{ \int_{Q_0^2}^{Q^2} \frac{dQ'^2}{Q'^2} \frac{\alpha_s(Q'^2)}{2\pi} \gamma_{qq}(\omega) \right\} f_\omega^{NS}(Q_0^2).
\end{aligned} \tag{A.71}$$

Then, to obtain the solution in x -space, one has to use inverse Mellin transform :

$$f(x, \mathbf{Q}^2) = \{\mathcal{M}^{-1} f_\omega\}(x, \mathbf{Q}^2) \equiv \int_{a-i\infty}^{a+i\infty} \frac{d\omega}{2i\pi} x^{-\omega-1} f_\omega(Q^2). \tag{A.72}$$

A.3.1 Mellin transform properties

Here are gathered some properties of the Mellin transform :

$$\begin{aligned}
\{\mathcal{M}x^v f(x)\} &= \{\mathcal{M}f\}(\omega + v), \\
\{\mathcal{M}f(x^v)\} &= \frac{1}{|v|} \{\mathcal{M}f\}\left(\frac{\omega}{v}\right), \\
\{\mathcal{M}f(vx)\} &= v^{-\omega} \{\mathcal{M}f\}(\omega), \\
\{\mathcal{M} \ln x f(x)\} &= \{\mathcal{M}f'\}(\omega), \\
\{\mathcal{M} \frac{d^n}{dx^n} f(x)\} &= (-1)^n \frac{\Gamma(\omega)}{\Gamma(\omega - n)} \{\mathcal{M}f\}(\omega - n), \\
\{\mathcal{M} \left(x \frac{d}{dx}\right)^n f(x)\} &= (-\omega)^n \{\mathcal{M}f\}(\omega), \\
\{\mathcal{M} \int_0^x dy f(y)\} &= -\frac{1}{\omega} \{\mathcal{M}f\}(\omega + 1), \\
\{\mathcal{M} \int_x^{+\infty} dy f(y)\} &= \frac{1}{\omega} \{\mathcal{M}f\}(\omega + 1), \\
\{\mathcal{M} \int_0^{+\infty} \frac{dy}{y} f_1\left(\frac{x}{y}\right) f_2(y)\} &= \{\mathcal{M}f_1\}(\omega) \{\mathcal{M}f_2\}(\omega), \\
\{\mathcal{M} f_1(x) f_2(x)\} &= \frac{1}{2i\pi} \int_{c-i\infty}^{c+i\infty} ds \{\mathcal{M}f_1\}(s) \{\mathcal{M}f_2\}(\omega - s).
\end{aligned} \tag{A.73}$$

Appendix B

Appendices related to amplitudes

B.1 QCD Feynman rules

We present here the Feynman rules for QCD, with massless quarks (in the presented diagrams, time flows from left to right) :

- The external lines are written as (the dot symbolise an undefined vertex) :

– Gluon :

$$\underbrace{\text{wavy line}}_{k, \lambda, a} \bullet = \epsilon_\lambda(k), \quad \bullet \underbrace{\text{wavy line}}_{k, \lambda, a} = \epsilon_\lambda(k)^*. \quad (\text{B.1})$$

– Quark :

$$\underbrace{\text{arrow}}_{p, \sigma, i} \bullet = u_\sigma(p), \quad \bullet \underbrace{\text{arrow}}_{p, \sigma, i} = \bar{u}_\sigma(p). \quad (\text{B.2})$$

– Antiquark :

$$\underbrace{\text{arrow}}_{p, \sigma, i} \bullet = \bar{v}_\sigma(p), \quad \bullet \underbrace{\text{arrow}}_{p, \sigma, i} = v_\sigma(p). \quad (\text{B.3})$$

- The propagators (internal lines) read :

– Gluon propagator (in the light cone gauge) :

$$\begin{array}{c} \mu \\ \text{-----} \\ \text{|||||} \\ \text{-----} \\ \nu \\ k, \lambda \end{array} = \frac{-i\delta_{a,b}}{k^2 + i\epsilon} \left[\eta_{\mu\nu} - \frac{n_\mu k_\nu + n_\nu k_\mu}{n \cdot k} \right]. \quad (\text{B.4})$$

– Quark propagator :

$$i \text{-----} \begin{array}{c} \blacktriangleright \\ p, \sigma \end{array} j = i\delta_{i,j} \frac{\not{p}}{p^2 + i\epsilon}. \quad (\text{B.5})$$

• The vertices are as follows :

– Quark-gluon vertex :

$$\begin{array}{c} i \\ \swarrow \\ \bullet \\ \downarrow \\ \mu, a \end{array} \text{-----} j = -ig_s \gamma^\mu (t^a)_{ij}. \quad (\text{B.6})$$

– 3-gluons vertex (with incoming momenta) :

$$\begin{array}{c} \mu, a \\ \swarrow \\ \text{|||||} \\ \nu, b \\ \searrow \\ \rho, c \end{array} \begin{array}{c} k \\ \text{-----} \\ p \\ q \end{array} = -g_s f^{abc} [\eta^{\mu\nu} (k-p)^\rho + \eta^{\nu\rho} (p-q)^\mu + \eta^{\rho\mu} (q-k)^\nu]. \quad (\text{B.7})$$

– 4-gluons vertex :

$$\begin{array}{c} \mu \\ \swarrow \\ \text{|||||} \\ \nu \\ \searrow \\ \rho \end{array} \begin{array}{c} \sigma \\ \swarrow \\ \text{|||||} \\ \rho \end{array} = -ig_s^2 [f^{abx} f^{xcd} (\eta^{\mu\rho} \eta^{\nu\sigma} - \eta^{\mu\sigma} \eta^{\nu\rho}) \\ + f^{acx} f^{xbd} (\eta^{\mu\sigma} \eta^{\nu\rho} - \eta^{\mu\nu} \eta^{\rho\sigma}) \\ + f^{adx} f^{xbc} (\eta^{\mu\rho} \eta^{\nu\sigma} - \eta^{\mu\nu} \eta^{\rho\sigma})]. \quad (\text{B.8})$$

We do not consider ghosts since we are working in the light-cone gauge.

B.2 Colored ordered QCD Feynman rules

When considering colored ordered amplitude (partial amplitudes), since the color part is treated by the color decomposition, we should used modified Feynman rules as follows (where we consider momenta outgoing) :

- The propagators (internal lines) read :

- Gluon propagator (in the light cone gauge) :

$$\begin{array}{c} \mu, a \\ \text{~~~~} \\ \text{-----} \\ \text{~~~~} \\ \nu, b \\ \text{~~~~} \\ k, \lambda \end{array} = \frac{-i}{k^2} \left[\eta_{\mu\nu} - \frac{n_\mu k_\nu + n_\nu k_\mu}{n \cdot k} \right]. \quad (\text{B.9})$$

- Quark propagator :

$$i \xrightarrow[p, \sigma]{\text{-----}} j = i \frac{\not{p}}{p^2}. \quad (\text{B.10})$$

- The vertices are as follows :

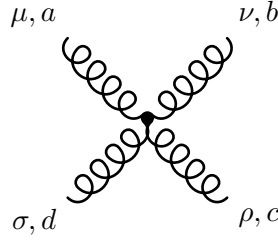
- Quark-gluon vertex :

$$\begin{array}{c} i \\ \text{-----} \\ \text{-----} \\ \text{-----} \\ \mu \end{array} = \frac{i}{\sqrt{2}} \gamma^\mu. \quad (\text{B.11})$$

- 3-gluons vertex (with incoming momenta) :

$$\begin{array}{c} \mu \\ \text{-----} \\ \text{-----} \\ \text{-----} \\ \nu \\ \text{-----} \\ \rho \end{array} = \frac{i}{\sqrt{2}} [\eta^{\mu\nu}(k-p)\rho + \eta^{\nu\rho}(p-q)^\mu + \eta^{\rho\mu}(q-k)^\nu]. \quad (\text{B.12})$$

– 4-gluons vertex :



$$= i\eta^{\mu\rho}\eta^{\nu\sigma} - \frac{i}{2}(\eta^{\mu\nu}\eta^{\rho\sigma} + \eta^{\mu\sigma}\eta^{\nu\rho}). \quad (\text{B.13})$$

For the external lines, color-ordered Feynman rules are identical to those presented in App. B.1.

B.3 Dirac equation

In this appendix, we shortly review the Dirac equation and provide a solution for the massless case, useful for numerical calculations.

The Dirac equation is the relativistic equation of motion for spin- $\frac{1}{2}$ massive particles (like quarks). It reads (in natural units) :

Dirac equation

$$(i\cancel{\partial} - m_f)\psi_i^f(x) = 0, \quad (\text{B.14})$$

for a quark of flavor f and color i . Since the color has no action in this equation, we will drop the index i in the following. For an antiquark, it would be :

$$\bar{\psi}^f(x)(-i\cancel{\partial} - m_f) = 0. \quad (\text{B.15})$$

The Dirac equation has plane-wave solutions of positive and negative energy that can be written :

$$\psi_+^f(x) = u^f(p)e^{-ip\cdot x}, \quad \text{and} \quad \psi_-^f(x) = v^f(p)e^{ip\cdot x}. \quad (\text{B.16})$$

The functions u^f and v^f are (4-components) Dirac spinors and they follow the Dirac equation in momentum space :

$$(\not{p} - m_f)u^f(p) = 0, \quad (\not{p} + m_f)v^f(p) = 0. \quad (\text{B.17})$$

Now, we are interested in the massless case. Then, both u^f and v^f follow the same equation and are equal up to normalization (we can also drop the flavor index) :

Massless Dirac equation

$$\not{p}u(p) = 0. \quad (\text{B.18})$$

Actually, in this limit, the Dirac equation is equivalent to the *Weyl equation*, which describes spin- $\frac{1}{2}$ massless particles :

$$\sigma^\mu \partial_\mu \psi(x) = 0, \quad (\text{B.19})$$

where σ^μ are the Pauli matrices. Due to this, the helicity formalism can also be described in terms of (2-components) Weyl spinors (see [105] for a review).

We conclude this appendix presenting one solution of the Dirac equation in terms of Dirac spinors. This solution is the one presented in [287] and can be used for numerical applications. For fixed helicities, we have :

$$u_+(k) = v_-(k) = \frac{1}{\sqrt{2}} \begin{bmatrix} \sqrt{k^+} \\ \sqrt{k^-} e^{i\varphi_k} \\ \sqrt{k^+} \\ \sqrt{k^-} e^{i\varphi_k} \end{bmatrix}, \quad u_-(k) = v_+(k) = \frac{1}{\sqrt{2}} \begin{bmatrix} \sqrt{k^-} e^{-i\varphi_k} \\ -\sqrt{k^+} \\ -\sqrt{k^-} e^{-i\varphi_k} \\ \sqrt{k^+} \end{bmatrix}, \quad (\text{B.20})$$

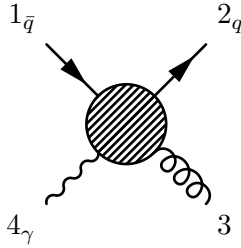
with $e^{\pm i\varphi_k} = \frac{k^1 \pm ik^2}{\sqrt{k^+ k^-}}$ and $k^\pm = k^0 \pm k^3$. Then, the spinor products can be written (for $k_{i,j} > 0$) :

$$\langle ij \rangle = \sqrt{|s_{ij}|} e^{i\phi_{ij}}, \quad [ij] = \sqrt{|s_{ij}|} e^{-i(\phi_{ij} + \pi)}, \quad (\text{B.21})$$

with $\cos \phi_{ij} = \frac{k_i^1 k_j^+ - k_j^1 k_i^+}{\sqrt{|s_{ij}| k_i^+ k_j^+}}$ and $\sin \phi_{ij} = \frac{k_i^2 k_j^+ - k_j^2 k_i^+}{\sqrt{|s_{ij}| k_i^+ k_j^+}}$. It can be checked that such solutions are indeed solution of the Dirac equation Eq. (B.18), and that they follow the properties presented in the main text.

B.4 $\bar{q}qg\gamma$ – detailed calculation

To show how to apply the helicity formalism, we consider the simple case of $\bar{q}qg\gamma$.



We consider external momenta outgoing, labeled with the letter k , the helicities are labelled λ , the polarization vectors ϵ and the corresponding reference momenta q . At tree level, the color decomposition of such amplitude is very simple since it involves only one term :

$$\mathcal{A}^{tree}(1_{\bar{q}}, 2_q, 3, 4_\gamma) = g_s \sqrt{2} e_q (t^{a_3})_{i_2}^{\bar{j}_1} A^{tree}(1_{\bar{q}}^{\lambda_1}, 2_q^{\lambda_2}, 3^{\lambda_3}, 4_\gamma^{\lambda_4}). \quad (\text{B.22})$$

Such partial amplitude is obtained with the two following diagrams :

$$\begin{aligned}
\textcircled{1} = & \begin{array}{c} 1_{\bar{q}} \\ \swarrow \\ \bullet \\ \downarrow \\ 4_{\gamma} \end{array} \text{---} \begin{array}{c} \bullet \\ \swarrow \\ 2_q \\ \downarrow \\ 3 \end{array} \\
& = \frac{-i}{2s_{14}} \langle 2^{\lambda_2} | \not{\epsilon}_3^* (k_1 + k_4) \not{\epsilon}_4^* | 1^{-\lambda_1} \rangle \\
& = \frac{i}{2s_{23}} \langle 2^{\lambda_2} | \not{\epsilon}_3^* (k_2 + k_3) \not{\epsilon}_4^* | 1^{-\lambda_1} \rangle,
\end{aligned} \tag{B.23}$$

$$\begin{aligned}
\textcircled{2} = & \begin{array}{c} 1_{\bar{q}} \\ \swarrow \\ \bullet \\ \downarrow \\ 3 \end{array} \text{---} \begin{array}{c} \bullet \\ \swarrow \\ 2_q \\ \downarrow \\ 4_{\gamma} \end{array} \\
& = \frac{-i}{2s_{13}} \langle 2^{\lambda_2} | \not{\epsilon}_4^* (k_1 + k_3) \not{\epsilon}_3^* | 1^{-\lambda_1} \rangle \\
& = \frac{i}{2s_{24}} \langle 2^{\lambda_2} | \not{\epsilon}_4^* (k_2 + k_4) \not{\epsilon}_3^* | 1^{-\lambda_1} \rangle.
\end{aligned} \tag{B.24}$$

Note that only the ordering of the partons is fixed by color-ordering, the photon can have different positions. The spinor chain involved by the quark line imposes that the quark and the anti-quark have opposite helicities $\lambda_1 = -\lambda_2 \equiv \lambda_q$. Using the properties of the polarization vectors (see Eq. (3.51) to Eq. (3.56)), we notice that :

- amplitude $\textcircled{1}$ vanishes for :
$$\begin{cases} q_4 = k_1 & \text{if } \lambda_4 = \lambda_q \\ q_3 = k_2 & \text{if } \lambda_3 = -\lambda_q \end{cases},$$
- and amplitude $\textcircled{2}$ vanishes for :
$$\begin{cases} q_3 = k_1 & \text{if } \lambda_3 = \lambda_q \\ q_4 = k_2 & \text{if } \lambda_4 = -\lambda_q \end{cases}.$$

This implies that :

$$A^{tree}(1_{\bar{q}}^{\lambda_q}, 2_q^{-\lambda_q}, 3^{-\lambda_q}, 4_{\gamma}^{-\lambda_q}) = A^{tree}(1_{\bar{q}}^{\lambda_q}, 2_q^{-\lambda_q}, 3^{\lambda_q}, 4_{\gamma}^{\lambda_q}) = 0 \tag{B.25}$$

Now, we will only consider $\lambda_1 = -$ and $\lambda_2 = +$ (i.e $\lambda_q = -$) since the opposite helicity configuration is obtained by charge conjugation. It leaves only two non-vanishing amplitudes : $A^{tree}(1_{\bar{q}}^-, 2_q^+, 3^-, 4_{\gamma}^+)$ and $A^{tree}(1_{\bar{q}}^-, 2_q^+, 3^-, 4_{\gamma}^+)$. In the former helicity configuration, if we impose $q_4 = k_1$ or $q_3 = k_2$, the contribution of diagram $\textcircled{1}$ vanishes. In the latter configuration, by imposing $q_3 = k_1$ or $q_4 = k_2$, the contribution of diagram $\textcircled{1}$ vanishes. Let's calculate these two amplitudes.

B.4.1 $A^{tree}(1_{\bar{q}}^-, 2_q^+, 3^-, 4_\gamma^+)$

For $A^{tree}(1_{\bar{q}}^-, 2_q^+, 3^-, 4_\gamma^+)$, we choose $q_4 = k_1$ (we do not fix q_3 since, as we will see, it doesn't appear in the final result). In this case, the only contribution comes from diagram $\textcircled{2}$. For the readability, we keep q_4 in the intermediate steps :

$$\begin{aligned}
A^{tree}(1_{\bar{q}}^-, 2_q^+, 3^-, 4_\gamma^+) &= \frac{-i}{2s_{13}} [2|\not{\epsilon}_4^+(k_1 + k_3)\not{\epsilon}_3^-|1\rangle \\
&= \frac{-i}{4s_{13}} \frac{1}{[q_3 3]\langle q_4 4\rangle} [2|\gamma^\mu \langle q_4^- | \gamma_\mu | 4\rangle (|1\rangle [1| + |3\rangle [3|) \gamma^\nu [q_3 | \gamma_\nu | 3\rangle |1\rangle] \\
&= \frac{-i}{4s_{13}} \frac{1}{[q_3 3]\langle q_4 4\rangle} \left[\begin{array}{l} [2|\gamma^\mu |1\rangle [4|\gamma_\mu |q_4\rangle [1|\gamma^\nu |1\rangle [q_3 | \gamma_\nu | 3\rangle \\ + [2|\gamma^\mu |3\rangle [4|\gamma_\mu |q_4\rangle [3|\gamma^\nu |1\rangle [q_3 | \gamma_\nu | 3\rangle \end{array} \right] \\
&= \frac{-i}{2s_{13}} \frac{1}{[q_3 3]\langle q_4 4\rangle} ([24]\langle q_4 1\rangle [1q_3]\langle 31\rangle + [24]\langle q_4 3\rangle [3q_3]\langle 31\rangle) \\
&= \frac{-i}{2s_{13}} \frac{[24]\langle 13\rangle^2}{\langle 14\rangle} = i \frac{[24]\langle 13\rangle}{[13]\langle 14\rangle}.
\end{aligned} \tag{B.26}$$

B.4.2 $A^{tree}(1_{\bar{q}}^-, 2_q^+, 3^-, 4_\gamma^+)$

For $A^{tree}(1_{\bar{q}}^-, 2_q^+, 3^-, 4_\gamma^+)$, we choose $q_3 = k_1$ for which only diagram $\textcircled{1}$ contributes. Note that, the expressions for $\textcircled{1}$ (Eq. (B.23)) and $\textcircled{2}$ (Eq. (B.24)) only differ by the exchange of the role of legs 3 and 4. Then, we can use the expression we get in the previous case, before fixing the auxiliary momenta, and switching $3 \leftrightarrow 4$. This leads to :

$$\begin{aligned}
A^{tree}(1_{\bar{q}}^-, 2_q^+, 3^-, 4_\gamma^+) &= \frac{-i}{2s_{14}} \frac{1}{\langle q_3 3\rangle [q_4 4]} ([23]\langle q_3 1\rangle [1q_4]\langle 41\rangle + [23]\langle q_3 4\rangle [4q_4]\langle 41\rangle) \\
&= \frac{i}{2s_{14}} \frac{[23]\langle 14\rangle^2}{\langle 13\rangle} = i \frac{[23]\langle 14\rangle}{\langle 13\rangle [14]}
\end{aligned} \tag{B.27}$$

B.5 Master integrals

We gather here master integrals for massless internal particles, based on results provided in [148] (where results accounting for massive particles are also presented). First, let's recall our notation :

$$\begin{aligned}
I_2^D(\{p_1\}) &= \frac{\mu^{4-D}}{i(4\pi)^{\frac{D}{2}}} \int \frac{d^D l}{(2\pi)^4} \frac{1}{l^2 (l-p_1)^2}, \\
I_3^D(\{p_1, p_2\}) &= \frac{\mu^{4-D}}{i(4\pi)^{\frac{D}{2}}} \int \frac{d^4 l}{(2\pi)^4} \frac{1}{l^2 (l-p_1)^2 (l-p_1-p_2)^2}, \\
I_4^D(\{p_1, p_2, p_3\}) &= \frac{\mu^{4-D}}{i(4\pi)^{\frac{D}{2}}} \int \frac{d^4 l}{(2\pi)^4} \frac{1}{l^2 (l-p_1)^2 (l-p_1-p_2)^2 (l-p_1-p_2-p_3)^2},
\end{aligned} \tag{B.28}$$

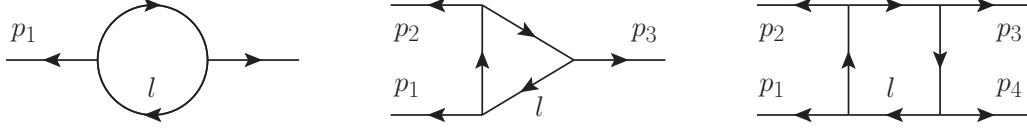


Figure B.1: Master integrals (with the outgoing momenta convention). In order : bubble, triangle, and box scalar integral.

in dimensional regularization with $D = 4 - 2\epsilon$, all momenta outgoing (as shown in Fig. B.1) and where¹ :

$$\begin{aligned}
c_\Gamma &= \frac{1}{(4\pi)^{2-\epsilon}} \frac{\Gamma(1+\epsilon)\Gamma^2(1-\epsilon)}{\Gamma(1-2\epsilon)} \\
&= \frac{1}{(4\pi)^2} \left[1 + (\ln 4\pi - \gamma)\epsilon + \frac{1}{2} \left((\ln 4\pi - \gamma)^2 - \frac{\pi^2}{6} \right) \epsilon^2 \right] + \mathcal{O}(\epsilon^3)
\end{aligned} \tag{B.29}$$

In practice, those integrals are written in terms of products of the involved momenta (momenta square p_i^2 , invariants s_{ij} , and in the massive case, squares of the masses m_i^2). We have one bubble integral :

$$I_2^D(p_1^2) = \left(\frac{\mu^2}{-p_1^2} \right)^\epsilon \left[\frac{1}{\epsilon} + 2 \right] + \mathcal{O}(\epsilon), \tag{B.30}$$

two triangle integrals $I_3^D(p_1^2, p_2^2, p_3^2)$:

$$\begin{aligned}
I_3^D(0, p_2^2, p_3^2) &= \frac{1}{p_2^2 - p_3^2} \left[\frac{1}{\epsilon} \left(\ln \left(\frac{\mu^2}{-p_2^2} \right) - \ln \left(\frac{\mu^2}{-p_3^2} \right) \right) + \frac{1}{2} \left(\ln^2 \left(\frac{\mu^2}{-p_2^2} \right) - \ln^2 \left(\frac{\mu^2}{-p_3^2} \right) \right) \right] + \mathcal{O}(\epsilon), \\
I_3^D(0, 0, p_3^2) &= \frac{1}{p_3^2} \left[\frac{1}{\epsilon} + \frac{1}{\epsilon} \ln \left(\frac{\mu^2}{-p_3^2} \right) + \frac{1}{2} \ln^2 \left(\frac{\mu^2}{-p_3^2} \right) \right] + \mathcal{O}(\epsilon),
\end{aligned} \tag{B.31}$$

¹It is also usual to write these integrals with :

$$r_\Gamma = \frac{\Gamma^2(1-\epsilon)\Gamma(1+\epsilon)}{\Gamma(1-2\epsilon)} = 1 - \gamma\epsilon + \left(\frac{\gamma^2}{2} - \frac{\pi^2}{12} \right) \epsilon^2 + \mathcal{O}(\epsilon^3)$$

instead of c_Γ .

and five box integrals $I_4^D(p_1^2, p_2^2, p_3^2, p_4^2, s_{12}, s_{23})$:

$$\begin{aligned}
I_4^D(0, p_2^2, p_3^2, p_4^2, s_{12}, s_{23}) &= \frac{\mu^{2\epsilon}}{s_{12}s_{23} - p_2^2 p_4^2} \times \\
&\times \left[\frac{2}{\epsilon^2} \left((-s_{12})^{-\epsilon} + (-s_{23})^{-\epsilon} - (-p_2^2)^{-\epsilon} - (-p_3^2)^{-\epsilon} - (-p_4^2)^{-\epsilon} \right) \right. \\
&\quad \left. + \frac{1}{\epsilon^2} \left(\left(\frac{-s_{23}}{p_2^2 p_3^2} \right)^\epsilon + \left(\frac{-s_{12}}{p_3^2 p_4^2} \right)^\epsilon \right) - \ln^2 \left(\frac{s_{12}}{s_{23}} \right) \right. \\
&\quad \left. - 2\text{Li}_2 \left(1 - \frac{p_2^2}{s_{12}} \right) - 2\text{Li}_2 \left(1 - \frac{p_4^2}{s_{23}} \right) - 2\text{Li}_2 \left(1 - \frac{p_2^2 p_4^2}{s_{12} s_{23}} \right) \right] \\
&+ \mathcal{O}(\epsilon), \\
I_4^D(0, 0, p_3^2, p_4^2, s_{12}, s_{23}) &= \frac{\mu^{2\epsilon}}{s_{12}s_{23}} \left[\frac{2}{\epsilon^2} \left((-s_{12})^{-\epsilon} + (-s_{23})^{-\epsilon} - (-p_3^2)^{-\epsilon} - (-p_4^2)^{-\epsilon} \right) \right. \\
&\quad \left. + \frac{1}{\epsilon^2} \left(\frac{-s_{12}}{p_3^2 p_4^2} \right)^\epsilon - \ln^2 \left(\frac{s_{12}}{s_{23}} \right) \right. \\
&\quad \left. - 2\text{Li}_2 \left(1 - \frac{p_3^2}{s_{23}} \right) - 2\text{Li}_2 \left(1 - \frac{p_4^2}{s_{23}} \right) \right] \\
&+ \mathcal{O}(\epsilon), \\
I_4^D(0, p_2^2, 0, p_4^2, s_{12}, s_{23}) &= \frac{\mu^{2\epsilon}}{s_{12}s_{23} - p_2^2 p_4^2} \times \\
&\times \left[\frac{2}{\epsilon^2} \left((-s_{12})^{-\epsilon} + (-s_{23})^{-\epsilon} - (-p_2^2)^{-\epsilon} - (-p_4^2)^{-\epsilon} \right) \right. \\
&\quad \left. - \ln^2 \left(\frac{s_{12}}{s_{23}} \right) - 2\text{Li}_2 \left(1 - \frac{p_2^2}{s_{12}} \right) - 2\text{Li}_2 \left(1 - \frac{p_2^2}{s_{23}} \right) \right. \\
&\quad \left. - 2\text{Li}_2 \left(1 - \frac{p_4^2}{s_{12}} \right) - 2\text{Li}_2 \left(1 - \frac{p_4^2}{s_{23}} \right) - 2\text{Li}_2 \left(1 - \frac{p_2^2 p_4^2}{s_{12} s_{23}} \right) \right] \\
&+ \mathcal{O}(\epsilon), \\
I_4^D(0, 0, 0, p_4^2, s_{12}, s_{23}) &= \frac{\mu^{2\epsilon}}{s_{12}s_{23}} \left[\frac{2}{\epsilon^2} \left((-s_{12})^{-\epsilon} + (-s_{23})^{-\epsilon} - (-p_4^2)^{-\epsilon} \right) \right. \\
&\quad \left. + 2\text{Ls}_{-1} \left(\frac{s_{12}}{p_4^2}, \frac{s_{23}}{p_4^2} \right) \right] + \mathcal{O}(\epsilon), \\
I_4^D(0, 0, 0, 0, s_{12}, s_{23}) &= \frac{\mu^{2\epsilon}}{s_{12}s_{23}} \left[\frac{2}{\epsilon^2} \left((-s_{12})^{-\epsilon} + (-s_{23})^{-\epsilon} \right) - \ln^2 \left(\frac{s_{12}}{s_{23}} \right) - \pi^2 \right] \\
&+ \mathcal{O}(\epsilon),
\end{aligned} \tag{B.32}$$

where :

$$\text{Ls}_{-1}(x, y) = \text{Li}_2(1 - x) + \text{Li}_2(1 - y) + \ln(x) \ln(y) - \frac{\pi^2}{6} \quad (\text{B.33})$$

with the dilogarithm defined as :

$$\begin{aligned} \text{Li}_2(x) &= - \int_0^x \frac{dz}{z} \ln(1 - z) \\ &= \sum_{i \in \mathbb{N}^*} \frac{x^i}{i^2}, \quad \text{for } |x| \leq 1. \end{aligned} \quad (\text{B.34})$$

B.6 5-point amplitude – detailed calculation

In order to compare the off-shell gauge invariant 5-point amplitude obtained from the auxiliary quark line $\bar{q}^- q^+ g^+ g^+ g^+$ to the one obtained from the auxiliary gluon line $g^- g^+ g^+ g^+ g^+$, we will rewrite both expressions. Let's first rewrite the first term of the amplitude with auxiliary quarks (before applying the Λ prescription, see Eq. (3.194))

$$\begin{aligned} \frac{\langle 14 \rangle \langle 1 | (2 + 3)(3 + 4) | 1 \rangle}{\langle 12 \rangle \langle 34 \rangle^2 \langle 45 \rangle \langle 56 \rangle \langle 61 \rangle} &= \frac{\langle 14 \rangle (\langle 12 \rangle [23] \langle 31 \rangle + \langle 1 | 2 + 3 | 4 \rangle \langle 41 \rangle)}{\langle 12 \rangle \langle 34 \rangle^2 \langle 45 \rangle \langle 56 \rangle \langle 61 \rangle} \\ &= - \frac{\langle 14 \rangle [23] \langle 13 \rangle}{\langle 34 \rangle^2 \langle 45 \rangle \langle 56 \rangle \langle 61 \rangle} + \frac{\langle 23 \rangle \langle 45 \rangle \langle 14 \rangle^2 \langle 1 | 5 + 6 | 4 \rangle}{\langle 12 \rangle \langle 23 \rangle \langle 34 \rangle^2 \langle 45 \rangle^2 \langle 56 \rangle \langle 61 \rangle} \\ &= - \frac{\langle 14 \rangle [23] \langle 13 \rangle}{\langle 34 \rangle^2 \langle 45 \rangle \langle 56 \rangle \langle 61 \rangle} + \frac{\langle 24 \rangle \langle 35 \rangle \langle 14 \rangle^2 \langle 1 | 5 + 6 | 4 \rangle}{\langle 12 \rangle \langle 23 \rangle \langle 34 \rangle^2 \langle 45 \rangle^2 \langle 56 \rangle \langle 61 \rangle} \\ &\quad - \frac{\langle 25 \rangle \langle 14 \rangle^2 \langle 1 | 5 + 6 | 4 \rangle}{\langle 12 \rangle \langle 23 \rangle \langle 34 \rangle \langle 45 \rangle^2 \langle 56 \rangle \langle 61 \rangle}. \end{aligned} \quad (\text{B.35})$$

Above, we have used the momentum conservation to write $\langle 1|2+3|4\rangle = -\langle 1|5+6|4\rangle$ and the Schouten identity: $\langle 23\rangle\langle 45\rangle = \langle 24\rangle\langle 35\rangle + \langle 25\rangle\langle 43\rangle$. It leads to

$$\begin{aligned}
& \mathcal{A}_5^{(1)}(g^*, 3^+, 4^+, 5^+, 6^+) \\
&= \frac{ig^5 x|k_T|}{48\pi^2} \left[-\frac{\langle p4\rangle[p3]\langle p3\rangle}{\langle 34\rangle^2\langle 45\rangle\langle 56\rangle\langle 6p\rangle} + \frac{\langle 35\rangle\langle p4\rangle^3\langle p|5+6|4\rangle}{\kappa^*\langle p3\rangle\langle 34\rangle^2\langle 45\rangle^2\langle 56\rangle\langle 6p\rangle} \right. \\
&\quad - \frac{\langle p5\rangle\langle p4\rangle^2\langle p|5+6|4\rangle}{\kappa^*\langle p3\rangle\langle 34\rangle\langle 45\rangle^2\langle 56\rangle\langle 6p\rangle} + \frac{\langle p|4+5|6\rangle^3}{\kappa^*\langle p3\rangle\langle 45\rangle^2\langle 3|4+5|6\rangle s_{k3}} \\
&\quad + \frac{\langle p4\rangle\langle p5\rangle(\langle p4\rangle[4|5+6|p] + \langle p5\rangle[56]\langle 6p\rangle)}{\kappa^*\langle p3\rangle\langle 34\rangle\langle 45\rangle^2\langle 56\rangle\langle 6p\rangle} - \frac{\langle p5\rangle\langle p|56|p\rangle}{\kappa^*\langle p3\rangle\langle 34\rangle\langle 45\rangle\langle 56\rangle^2} \\
&\quad \left. + \frac{\langle p|3+4|p\rangle^2}{\langle 34\rangle^2\langle 56\rangle\langle 6p\rangle\langle 5|3+4|p\rangle} - \frac{[p6]^2[p|(3+4)(4+5)(3+4)(4+5)|6]}{\kappa\langle 34\rangle\langle 45\rangle\langle 5|3+4|p\rangle\langle 3|4+5|6\rangle s_{k6}} \right] \\
&= \frac{ig^5 x|k_T|}{48\pi^2} \left[-\frac{\langle p4\rangle[p3]\langle p3\rangle}{\langle 34\rangle^2\langle 45\rangle\langle 56\rangle\langle 6p\rangle} + \frac{\langle 35\rangle\langle p4\rangle^3\langle p|5+6|4\rangle}{\kappa^*\langle p3\rangle\langle 34\rangle^2\langle 45\rangle^2\langle 56\rangle\langle 6p\rangle} \right. \\
&\quad + \frac{\langle p|4+5|6\rangle^3}{\kappa^*\langle p3\rangle\langle 45\rangle^2\langle 3|4+5|6\rangle s_{k3}} + \frac{\langle p4\rangle\langle p5\rangle^2[56]\langle 6p\rangle}{\kappa^*\langle p3\rangle\langle 34\rangle\langle 45\rangle^2\langle 56\rangle\langle 6p\rangle} \\
&\quad - \frac{\langle p5\rangle^2[56]\langle 6p\rangle}{\kappa^*\langle p3\rangle\langle 34\rangle\langle 45\rangle\langle 56\rangle^2} + \frac{\langle p|3+4|p\rangle^2}{\langle 34\rangle^2\langle 56\rangle\langle 6p\rangle\langle 5|3+4|p\rangle} \\
&\quad \left. - \frac{[p6]^2[p|(3+4)(4+5)(3+4)(4+5)|6]}{\kappa\langle 34\rangle\langle 45\rangle\langle 5|3+4|p\rangle\langle 3|4+5|6\rangle s_{k6}} \right]. \tag{B.36}
\end{aligned}$$

Terms 4 and 5 can be combined using the Schouten identity

$$\frac{\langle p5\rangle^2[56]}{\kappa^*\langle p3\rangle\langle 34\rangle\langle 45\rangle^2\langle 56\rangle^2}(\langle p4\rangle\langle 56\rangle - \langle 6p\rangle\langle 45\rangle) = \frac{\langle p5\rangle^3\langle 46\rangle[56]}{\kappa^*\langle p3\rangle\langle 34\rangle\langle 45\rangle^2\langle 56\rangle^2}. \tag{B.37}$$

Thus, finally, the amplitude reads

$$\begin{aligned}
& \mathcal{A}_5^{(1)}(g^*, 3^+, 4^+, 5^+, 6^+) \\
&= \frac{ig^5 x|k_T|}{48\pi^2} \left[\frac{\langle p|4+5|6\rangle^3}{\kappa^*\langle p3\rangle\langle 45\rangle^2\langle 3|4+5|6\rangle s_{k3}} + \frac{\langle p|3+4|p\rangle^2}{\langle 34\rangle^2\langle 56\rangle\langle 6p\rangle\langle 5|3+4|p\rangle} \right. \\
&\quad - \frac{[p6]^2[p|(3+4)(4+5)(3+4)(4+5)|6]}{\kappa\langle 34\rangle\langle 45\rangle\langle 5|3+4|p\rangle\langle 3|4+5|6\rangle s_{k6}} - \frac{\langle p4\rangle[p3]\langle p3\rangle}{\langle 34\rangle^2\langle 45\rangle\langle 56\rangle\langle 6p\rangle} \\
&\quad \left. + \frac{\langle p5\rangle^3\langle 46\rangle[56]}{\kappa^*\langle p3\rangle\langle 34\rangle\langle 45\rangle^2\langle 56\rangle^2} + \frac{\langle 35\rangle\langle p4\rangle^3\langle p|5+6|4\rangle}{\kappa^*\langle p3\rangle\langle 34\rangle^2\langle 45\rangle^2\langle 56\rangle\langle 6p\rangle} \right]. \tag{B.38}
\end{aligned}$$

Let us now rewrite the expression for the amplitude Eq. (3.200). In the second term

we use

$$s_{234} = s_{23} + s_{24} + s_{34} \xrightarrow{\Lambda \text{ prescr.}} \Lambda(s_{p3} + s_{p4}) + \mathcal{O}(1) = \Lambda(\langle p3 \rangle [3p] + \langle p4 \rangle [4p]) = \Lambda \langle p|3+4|p \rangle. \quad (\text{B.39})$$

In the first term we use

$$\langle 1|2+3|6 \rangle = -\langle 1|4+5|6 \rangle \xrightarrow{\Lambda \text{ prescr.}} -\Lambda \langle p|4+5|6 \rangle + \mathcal{O}(1) \quad (\text{B.40})$$

For the factorized term in the second line, we can use the momentum conservation

$$s_{345} = s_{k6}. \quad (\text{B.41})$$

For the last term, before applying Λ prescription, we use :

$$\langle 1|2+3|4 \rangle = -\langle 1|5+6|4 \rangle \xrightarrow{\Lambda \text{ prescr.}} -\Lambda \langle p|5+6|4 \rangle + \mathcal{O}(1) \quad (\text{B.42})$$

In the end, we have

$$\begin{aligned} & \mathcal{A}_5^{(1)}(g^*, 3^+, 4^+, 5^+, 6^+) \\ &= \frac{ig^5 x|k_T|}{48\pi^2} \left[-\frac{\langle p|4+5|6 \rangle^3}{\kappa^* \langle p3 \rangle \langle 45 \rangle^2 s_{k3} \langle 3|k|6 \rangle} + \frac{\langle p|3+4|p \rangle^2}{\langle 34 \rangle^2 \langle 56 \rangle \langle 6p \rangle \langle 5|3+4|p \rangle} \right. \\ & \quad + \frac{[p6]^2}{\kappa^* s_{k6}} \left(\frac{[p3][34]}{\langle 45 \rangle \langle 5|3+4|p \rangle} - \frac{[45][56]}{\langle 34 \rangle \langle 3|k|6 \rangle} + \frac{[35]}{\langle 34 \rangle \langle 45 \rangle} \right) \\ & \quad - \frac{\langle p3 \rangle [p3] \langle p4 \rangle}{\langle 34 \rangle^2 \langle 45 \rangle \langle 56 \rangle \langle 6p \rangle} + \frac{\langle p5 \rangle^3 \langle 46 \rangle [56]}{\kappa^* \langle p3 \rangle \langle 34 \rangle \langle 45 \rangle^2 \langle 56 \rangle^2} \\ & \quad \left. + \frac{\langle p4 \rangle^3 \langle 35 \rangle \langle p|5+6|4 \rangle}{\kappa^* \langle p3 \rangle \langle 34 \rangle^2 \langle 45 \rangle^2 \langle 56 \rangle \langle 6p \rangle} \right]. \quad (\text{B.43}) \end{aligned}$$

Let us now compare Eq. (B.38) and Eq. (B.43). It is clear that the terms 2, 4, 5 and 6 are the same. The first terms are also equal upon applying $\langle 3|4+5|6 \rangle = -\langle 3|k|6 \rangle$. Let us now work on the third term of Eq. (B.38):

$$\begin{aligned} & \frac{[p|(3+4)(4+5)(3+4)(4+5)|6]}{\langle 34 \rangle \langle 45 \rangle \langle 5|3+4|p \rangle \langle 3|4+5|6 \rangle} = \frac{[5|(3+4)(4+5)|6]}{\langle 34 \rangle \langle 45 \rangle \langle 3|4+5|6 \rangle} + \frac{[p|343(4+5)|6]}{\langle 34 \rangle \langle 45 \rangle \langle 5|3+4|p \rangle \langle 3|4+5|6 \rangle} \\ &= \frac{[53] \langle 3|(4+5)|6]}{\langle 34 \rangle \langle 45 \rangle \langle 3|4+5|6 \rangle} + \frac{[54] \langle 45 \rangle [56]}{\langle 34 \rangle \langle 45 \rangle \langle 3|4+5|6 \rangle} + \frac{[p3] \langle 34 \rangle [43] \langle 3|(4+5)|6]}{\langle 34 \rangle \langle 45 \rangle \langle 5|3+4|p \rangle \langle 3|4+5|6 \rangle} \\ &= -\frac{[35]}{\langle 34 \rangle \langle 45 \rangle} + \frac{[45][56]}{\langle 34 \rangle \langle 3|k|6 \rangle} - \frac{[p3][34]}{\langle 45 \rangle \langle 5|3+4|p \rangle}. \quad (\text{B.44}) \end{aligned}$$

If we put back the factor $-\frac{[p6]^2}{\kappa^* s_{k6}}$ (not written in the calculation for simplicity), we recognize the second line of Eq. (B.43). Thus, both approaches give the same result.

B.7 On-shell limit calculation

In this appendix we detail the calculation that leads to Eq. (3.211) which implies the correct on-shell limit for the n -point off-shell amplitude we presented in Eq. (3.208).

In order to rewrite the expression for U_3^* so that the on-shell limit can be utilized, let us come back to the expression for T_2 , see Eq. (3.208) before applying the Λ prescription. We focus on the first term in the sum over j (i.e. for $j = 3$), since it is the term that leads to U_3^* when applying the Λ prescription. Let us call this term T_3 :

$$T_3 = \sum_{l=4}^n \frac{\langle 1|\mathcal{K}_{3\dots l}\mathcal{K}_{(l+1)\dots(n+1)}|1\rangle^3}{\langle 1|\mathcal{K}_{(l+1)\dots(n+1)}\mathcal{K}_{3\dots l}|2\rangle\langle 1|\mathcal{K}_{(l+1)\dots(n+1)}\mathcal{K}_{3\dots l}|3\rangle} \times \frac{\langle 23\rangle\langle l(l+1)\rangle\langle 12\rangle[2|[\mathcal{F}(3,l)]^2\mathcal{K}_{(l+1)\dots(n+1)}|1\rangle}{\langle 12\rangle[2|\mathcal{K}_{3\dots l}|l\rangle\langle 12\rangle[2|\mathcal{K}_{3\dots l}|(l+1)\rangle]s_{3\dots l}}. \quad (\text{B.45})$$

We have

$$\langle 1|\mathcal{K}_{3\dots l}\mathcal{K}_{(l+1)\dots(n+1)}|1\rangle = -\langle 1|\mathcal{K}_{3\dots l}^2|1\rangle - \langle 1|\mathcal{K}_{3\dots l}|2\rangle\langle 21\rangle \xrightarrow{\Lambda \text{ prescr.}} \Lambda\kappa^* \sum_{i=3}^l s_{pi}. \quad (\text{B.46})$$

Similar, we have

$$\langle 1|\mathcal{K}_{(l+1)\dots(n+1)}\mathcal{K}_{3\dots l}|2\rangle = -\langle 12\rangle[2|\mathcal{K}_{3\dots l}|2\rangle \xrightarrow{\Lambda \text{ prescr.}} -\Lambda\kappa^* \sum_{i=3}^l s_{pi}, \quad (\text{B.47})$$

$$\begin{aligned} \langle 1|\mathcal{K}_{(l+1)\dots(n+1)}\mathcal{K}_{3\dots l}|3\rangle &= -\langle 1|\mathcal{K}_{3\dots l}^2|3\rangle - \langle 12\rangle[2|\mathcal{K}_{3\dots l}|3\rangle \\ &= \langle 13\rangle s_{3\dots l} - \langle 1|\mathcal{K}_{3\dots l}^2|3\rangle - \langle 12\rangle[2|\mathcal{K}_{3\dots l}|3\rangle, \end{aligned} \quad (\text{B.48})$$

which implies

$$\langle 1|\mathcal{K}_{(l+1)\dots(n+1)}\mathcal{K}_{3\dots l}|3\rangle \xrightarrow{\Lambda \text{ prescr.}} -\sqrt{\Lambda} (\kappa^*[p|\mathcal{K}_{3\dots l}|3\rangle + \langle p3\rangle s_{3\dots l}) \xrightarrow{k_T \rightarrow 0} -\sqrt{\Lambda}\langle p3\rangle s_{3\dots l}. \quad (\text{B.49})$$

We may also notice that, for $l = n$, we have

$$[2|\mathcal{K}_{3\dots n}|(l+1)\rangle = [2|\mathcal{K}_{3\dots n}|(n+1)\rangle = -[21]\langle 1(n+1)\rangle \xrightarrow{\Lambda \text{ prescr.}} \kappa\langle p(n+1)\rangle. \quad (\text{B.50})$$

This is the only term in the sum over l that has κ in the denominator and that is the only non vanishing term when k_T tends to 0.

Putting all this together leads to

$$\begin{aligned} T_3 \xrightarrow{\Lambda \text{ prescr.}} U_3^* &= \kappa^* \sum_{l=4}^{n-1} \frac{\left(\sum_{i=3}^l s_{pi}\right)^2 \langle l(l+1)\rangle [p|[\mathcal{F}(3,l)]^2\mathcal{K}_{(l+1)\dots(n+1)}|p\rangle}{[p|\mathcal{K}_{3\dots l}|l\rangle [p|\mathcal{K}_{3\dots l}|(l+1)\rangle] s_{3\dots l}^2} \\ &+ \kappa^* \frac{\left(\sum_{i=3}^n s_{pi}\right)^2 \langle n(n+1)\rangle [p|[\mathcal{F}(3,n)]^2|(n+1)\rangle \langle (n+1)p\rangle}{[p(n+1)] \langle (n+1)n\rangle \kappa \langle p(n+1)\rangle s_{3\dots n}^2} \\ &\xrightarrow{k_T \rightarrow 0} \frac{\kappa^* \left(\sum_{i=3}^n s_{pi}\right)^2 [p|[\mathcal{F}(3,n)]^2|(n+1)\rangle}{\kappa [p(n+1)] s_{3\dots n}^2}. \end{aligned} \quad (\text{B.51})$$

Notice that

$$s_{3\dots n} = s_{p(n+1)} = \langle p(n+1) \rangle [(n+1)p] = - \sum_{i=3}^n \langle pi \rangle [ip] = - \sum_{i=3}^n s_{pi}. \quad (\text{B.52})$$

Back to U_3^* , we have

$$\lim_{k_T \rightarrow 0} \frac{|k_T|}{\kappa^*} U_3^* = \frac{|k_T|}{\kappa [p(n+1)]} [p | \mathcal{F}(3, n) |^2 (n+1)]. \quad (\text{B.53})$$

This demonstrates the first relation in Eq. (3.211). We now have to prove the second one i.e. we need to show that the obtained expression corresponds to the numerator of the amplitude for $n-1$ gluons with positive helicity (up to some factor). Actually, we should first rewrite this numerator

$$\begin{aligned} \sum_{1 \leq i < j < k < l \leq n} \langle ij \rangle [jk] \langle kl \rangle [li] &= \frac{1}{[1n]} \sum_{1 \leq i < j < k < l \leq n} \langle ij \rangle [jk] \langle kl \rangle [li] [1n] \\ &= \frac{1}{[1n]} \sum_{1 \leq i < j < k < l \leq n} ([1l] \langle lk \rangle [kj] \langle ji \rangle [in] + [1i] \langle ij \rangle [jk] \langle kl \rangle [ln]) \\ &= \frac{1}{[1n]} \left(\sum_{2 \leq i < j < k < l < n} + \sum_{1 \leq l < k < j < i \leq n} \right) [1i] \langle ij \rangle [jk] \langle kl \rangle [ln]. \end{aligned} \quad (\text{B.54})$$

Now we can work on U_3^* . Let's first express \mathcal{F} in terms of a sum. For a direct comparison, we should also use the expression of U_3^* with the following change in the momenta label : $p \rightarrow 1, \forall i \in 3, \dots, n+1, i \rightarrow i-1$ (then momentum conservation expresses the same way i.e. $\sum_{i=1}^n k_i = 0$).

$$\begin{aligned} \lim_{k_T \rightarrow 0} \frac{|k_T|}{\kappa^*} U_3^* &= \frac{|k_T|}{\kappa [1n]} [1 | \mathcal{F}(2, n-1) |^2 |n] \\ &= \frac{|k_T|}{\kappa [1n]} \sum_{\substack{2 \leq i < j < n \\ 2 \leq k < l < n}} [1i] \langle ij \rangle [jk] \langle kl \rangle [ln] \end{aligned} \quad (\text{B.55})$$

We have then for both Eq. (B.55) and Eq. (B.54) a sum over the same expression. We can then, to shorten the demonstration, forget about the summed term (i.e. $[1i] \langle ij \rangle [jk] \langle kl \rangle [ln]$) and work directly on the sums to show that they are the same in this context.

On one side we have

$$\begin{aligned} \sum_{\substack{2 \leq i < j < n \\ 2 \leq k < l < n}} &= \sum_{2 \leq i < j < k < l < n} + \sum_{2 \leq i \leq k < j \leq l < n} + \sum_{2 \leq i \leq k < l < j < n} \\ &+ \sum_{2 \leq k < i < j \leq l < n} + \sum_{2 \leq k < i \leq l < j < n} + \sum_{2 \leq k < l < i < j < n} \end{aligned} \quad (\text{B.56})$$

on the other hand, we have

$$\begin{aligned}
\sum_{2 \leq i < j < k < l < n} + \sum_{1 \leq l < k < j < i \leq n} &= \sum_{2 \leq i < j < k < l < n} - \left(\sum_{2 \leq k < l < j < i \leq n} + \sum_{2 \leq k < j \leq l < i \leq n} + \sum_{2 \leq k < j < i \leq l < n} \right) \\
&= \sum_{2 \leq i < j < k < l < n} + \left(\sum_{2 \leq i \leq k < l < j < n} + \sum_{2 \leq k < i \leq l < j < n} + \sum_{2 \leq k < l < i < j < n} \right) \\
&\quad + \left(\sum_{2 \leq i \leq k < j \leq l < n} + \sum_{2 \leq k < i < j \leq l < n} + \sum_{2 \leq k < j < i \leq l < n} \right) \quad (\text{B.57}) \\
&\quad - \sum_{2 \leq k < j < i \leq l < n} \\
&= \sum_{\substack{2 \leq i_1 < j_1 < n \\ 2 \leq i_2 < j_2 < n}}
\end{aligned}$$

The first equality is obtained by momentum conservation on the index l (in the second term only) and the second one also by momentum conservation, on the index i this time (for terms 2 and 3). This finally proves the second relation in Eq. (3.211) which leads then to the expected on-shell limit for the amplitude in Eq. (3.205).

Appendix C

Appendices related to jet quenching

C.1 BDIM solved with Chebyshev method : Code in details

We present an overview of the code used to apply the Chebyshev method, as described in Sec. 4.4.3 (most of the variables names follow those used in this section). This program is available on [github](#). This overview will enter in the details of the usage of the program, and, for those interested in how its works or who would like to modify it, a review of the different variables and subroutines is given.

C.1.1 Usage

The program is compiled through the command :

```
$ g++ -std=c++11 -o cheb Cheb_general_main.cpp
```

or simply by running the script [compile.sh](#) (which just launch the compilation command). Then three commands can be used to launch the program :

```
$ ./cheb
```

to launch it with the default parameter file [Parameters](#), provided with the source code. The help is accessible through :

```
$ ./cheb help
```

Finally, for those who would like to prepare different parameter files, it is possible to select the parameter file [parameterfile](#) through the command :

```
$ ./cheb parameterfile
```

For the details of the input parameters used, refer to Sec. [C.1.3](#).

C.1.2 General structure

Let's begin the code overview by the structure of the program and the role of its different files. First, the main file `Cheb_general_main.cpp` (see Sec. C.1.4) organizes the code. It launches the parameter initialisation (from a file), allocates memory for arrays going from one subroutine to another, launches the calculation of the \mathcal{S} matrix, initializes the result file, launches the Euler method and finally frees memory. Also, the code is basically separated in 2 subprograms, with same structure, devoted to either the gluon dominated cascade or the one accounting for quarks.

Then, `Cheb_method_g.h` (see Sec. C.1.5) contain the subroutines of the calculation of the \mathcal{S} matrix and of the Euler method, in the pure gluon case. Similarly, `Cheb_method_g_NS.h` (see Sec. C.1.6) contain the subroutines of the calculation of the \mathcal{S} matrix and of the Euler method for the case accounting for quarks this time.

Finally, `Cheb_functions.h` (see Sec. C.1.7) contains mathematical definitions related to the Chebyshev polynomials, as well as the kernels of the BDIM equation and the initial solutions intended in the code.

C.1.3 Parameters

As already mentioned, input parameters are read from a file. This permits to rerun the program with different parameters without having to recompile it. The parameter file can be organized at will. The code will only recognize lines of the form¹ :

```
1 parametername = parametervalue
```

where “parametername” is the name of a parameter from the parameters class. And, any parameter not present in the parameter file is set to a default value. Also, after the program has read the parameters, and before launching the calculation, the parameters used are printed.

All the input parameters enter a parameter class defined in `Cheb_parameters.h`, which reads :

```
1 //Constants parameters used
2 class parameters
3 {
4     public:
5         //Result options
6         int norm;
7         bool positivity;
8
9         //Evolution used
10        int evo;
11
12        //Chebyshev method
13        int Nx;
14        double eps;
15
16        //Euler method
```

¹Actually, if it is separated by a space, anything can be put after parametervalue.

```

17     int Nt;
18     int Nt_w;
19     double t0;
20     double dt;
21
22     //Initial distributions
23     bool initgrid;
24     string initgridname;
25     double Ieps;
26     double C_g0;
27     double C_S0;
28     double C_NS0;
29
30
31     string gridname;
32
33     //internal parameters
34     bool paramfromfile;
35
36     void from_file(string filename);
37     void default_();
38     void show();
39     void write();
40 };

```

Lets review all these parameter :

- **int norm** specifies a normalization for the fragmentation function, with the following possibilities² :
 - 0 : no normalization (the default choice)
 - 1 : normalisation of the fragmentation functions $D_g(x) + D_S(x)$
 - 2 : normalisation of the multiplicity functions

$$N_g(x) + N_S(x) = \frac{1}{x}(D_g(x) + D_S(x))$$
 - 1 : normalisation of each fragmentation functions $D_i(x)$ (when not null)
 - 2 : normalisation of each multiplicity functions $N_i(x) = \frac{1}{x}D_i(x)$ (when not null)

Note that option 1 & 3 and 2 & 4 are the same in the pure gluon case.

- **bool positivity** : forces positivity of $D(x)$ when set to 1 (setting the negative values of $D(x)$ ³ to 0). When set to 0, the negative values are allowed (and may rise from the oscillation of the solution due to the polynomial expansion).
- **int evo** defines the type of evolution : pure gluon for 0, with quarks for 1 and the simplified case of (with the kernel of Eq. (4.106)) for (2).

²This choices were implemented for comparison purpose, to MC approach, testing different weighting. There are not meant to be physical (except the default choice).

³i.e the values of D on the Chebyshev nodes.

- **int Nx** is the order of the Chebyshev decomposition over the variable x of both the FF D and the integrands.
- **double eps** defines the bijection used as :
 - if **eps**= 0 : a linear bijection from $y : [0, 1] \rightarrow [-1, 1]$ as defined in Eq. (4.138).
 - if **eps**> 0 : a logarithmic bijection from $y : [\epsilon, 1] \rightarrow [-1, 1]$ as defined in Eq. (4.141).
- **int Nt** is the number of time steps⁴.
- **int Nt_w** is the number time steps saved in the result grids. This means that the Euler method can run for an high number of time steps (and hence increasing the precision of the calculation) without having the size of the grids increase dramatically (by fixing **Nt_w** at a reasonable value).
- **int t0** is the initial time of the evolution (usually set to 0, but it could be set differently when initiating the evolution with an already evolved distribution...).
- **int dt** is the time step used in the Euler method.
- **bool initgrid** defines if a grid is used as the initial solution (when set to 1) or if the initial solution is taken from an analytical formula, characterized by other parameters (when set to 0).

In the former case, the grid is loaded from the file **initgridname**. The file as to be a 1 column array of **Nx** lines, filled with the Chebyshev decomposition of the initial distribution to be used. Caution, no verification on the file formatting is done.

When **initgrid**= 0, the initial solution is defined by :

$$\begin{aligned} D_g(x, t_0) &= C_{g0} D_{init}(x, I_\epsilon), \\ D_S(x, t_0) &= C_{S0} D_{init}(x, I_\epsilon), \\ D_{NS}(x, t_0) &= C_{NS0} D_{init}(x, I_\epsilon), \end{aligned} \tag{C.1}$$

where the FF D_{init} reads :

$$D_{init}(x, I_\epsilon) = \begin{cases} D_a(x, t_0), & \text{if } I_\epsilon = 0, \\ D_0(x, I_\epsilon), & \text{if } I_\epsilon > 0, \end{cases} \tag{C.2}$$

where D_a and D_0 are respectively the analytical solution to the simplified BDIM equation, given in Eq. (4.107) and the Gaussian approaching a Dirac delta function, defined in Eq. (4.152). Note that, using D_a as the initial solution implies choosing

⁴While noted t , it is actually the proper time τ that is used in this program.

an initial time $t_0 > 0$ (and no verification in this sense are made by the program⁵). In the case of the gluon dominated cascade, Eq. (C.1) reduces to :

$$D_g(x, t_0) = D_{init}(x, I_\epsilon), \quad (\text{C.3})$$

where the factors C have no impact. Indeed, these factors are present to define the composition of the initial jet.

- **string gridname** is the time step used in the Euler method.
- **bool paramfromfile** is set to 1 when the parameter file has been found, and to 0 in the contrary case. It is use to specify, in the later case, that the parameters used are the default ones (when printing the parameters used).

Finally, some routines are attached to these parameters :

- **void from_file(string filename)** initializes the parameters of the class, first with default values then reading them from the file **filename** (if found).
- **void default_()** sets the default values of the parameters.
- **void show()** display the parameters (in the shell).
- **void write()** writes the parameters in a file (in **gridname+”_parameters”**).

Also, a set of little functions is defined to extract in a line in the parameter file the parameter (with the wanted type) :

```
1 double paramstr2double(string str);
2 int paramstr2int(string str);
3 bool paramstr2bool(string str);
4 string paramstr2str(string str);
```

While we will not enter into the details of all routines, we will just mention how the parameters are read from the parameter file. Basically the lines of the parameter file are scanned, looking for the possible parameters. Once a line with a parameter is found, we use the relevant function to extract from it the wanted parameter. In the case of **Nx**, it reads :

```
1 while (getline(parameters_file, line))
2 {
3     if (!(line[0]=='/' && line[1]=='/'))
4     {
5         if (line[0]=='N' && line[1]=='x')
6             Nx = paramstr2int(line);
7         .
8         .
9         .
10    }
11 }
```

⁵In this case, i.e when $I_\epsilon = 0$ and $t_0 = 0$, the initial solution will be null as well as the solution calculated.

As one can see, any line beginning with `//` is directly skipped.

For any modification implying a new parameter **a**, this parameter has to be correctly implemented in the parameter class and all its subroutines (which means basically answering how to read it from file, what is its default value, how to display it and to write it in a summary parameter file).

C.1.4 `Cheb_general_main.cpp` subroutines

Let's now have a look to the main file. First, some constants, not accessible through the input parameters

```

1 const long double M_PI = 3.141592...;
2 const int Nc = 3; //Number of colors
3 const int Nf = 3; //Number of active quark flavors
4 //Casimir operators
5 const double C_A = Nc;
6 const double C_F = (Nc*Nc-1)/2./Nc;
7 const double T_F = .5;

```

Then the function `int main(int argc, char** argv)` gives the possibility to set the parameter file to use when running the program (which is, without argument, 'Parameters'). It permits also to display the help message (written in `int help(void)`) and an error message when the program is run with more than one argument. When the program is run with zero or one argument (the name of the parameter file), then the routine `int program_init(string parametersfile)` is launched. It creates the parameter class used in the whole algorithm from the file `parametersfile` and, depending on the type of evolution (defined by `evo`), it launches either `int program_g_S_NS(parameters param)` or `int program_g(parameters param)` in the pure gluon case. These routine are very similar, the former reducing to the later when forgetting all the variables relative to color singlet and non singlet.

Then we will detail it for the pure gluon case. The first goal of `int program_g(parameters param)` is to allocate memory for the arrays that will be shared between the calculation of the \mathcal{S} matrix and the Euler method :

```

1 double *D = new double[Nx];
2 double **T = new double*[Nx];
3 double *X = new double[Nx];
4 double **S = new double*[Nx];
5
6 for (int i = 0; i < Nx; ++i)
7 {
8     T[i] = new double[Nx];
9     S[i] = new double[Nx];
10 }

```

where :

- `double *D` correspond to the gluon (discrete) fragmentation function $D_{t,k}$ we want to evolve. Actually, only the fragmentation at the current time (in the time loop

of the Euler method) is kept in memory (but it is written on the result grid during the time loop).

- **double **S** correspond to $\mathcal{S}_{i,j}$.
- **double **T** correspond to $T_{i,j}$.
- **double *X** is the set of used nodes $\{x_i\}$.

Then, the calculation of the matrix \mathcal{S} is hold by the routine **cheb_initilization_g(X, T, S, param)** (defined in Sec. C.1.5). Once achieved, the result grid **D_grid** is created and the Euler method can be carried out by the routine **cheb_Euler_g(X, T, D, S, D_grid, param)** (also defined in Sec. C.1.5). Finally, once the solution obtained, the memory used by the arrays defined earlier is deallocated (and the result file closed).

In the “full” case (accounting for quarks in the cascade), **int program_g_S_NS(parameters param)** has exactly the same structure, what changes are the different arrays defined. In addition to the one introduced in the gluon case, we have :

- **double *D_g** corresponds to the gluon fragmentation function $D_{t,k}^g$.
- **double *D_S** corresponds to the color singlet fragmentation function $D_{t,k}^S$.
- **double *D_NS** corresponds to the color non-singlet fragmentation function $D_{t,k}^{NS}$.
- **double **S_gg** corresponds to $\mathcal{S}_{i,j}^{gg}$.
- **double **S_gS** corresponds to $\mathcal{S}_{i,j}^{gS}$.
- **double **S_SS** corresponds to $\mathcal{S}_{i,j}^{SS}$.
- **double **S_Sg** corresponds to $\mathcal{S}_{i,j}^{Sg}$.
- **double **S_NSNS** corresponds to $\mathcal{S}_{i,j}^{NSNS}$.

This, of course implies different definitions of the routines holding the \mathcal{S} matrix calculation and the Euler method (which are written in **cheb_initilization_g_S_NS(X, T, S, param)** see Sec. C.1.6).

C.1.5 Cheb_method_g.h subroutines

Cheb_method_g.h contains the routines related to both the calculations of the \mathcal{S} matrix and and of the Euler method. Let’s review the different subroutine present :

- **cheb_initilization_g** initialize the calculation of the matrix \mathcal{S} by defining the useful Chebyshev polynomials T_{ij} . Then, it launches the subroutines where the actual calculation of the matrix \mathcal{S} takes place. This choice depends on the value of ϵ :

- for $\epsilon = 0$, the calculation is performed with a linear bijection, hold by the subroutine `cheb_init_S_chebint_g`.
- for $\epsilon > 0$, the calculation is performed with a logarithmic bijection, hold by the subroutine `cheb_init_S_chebint_glog`.
- `cheb_Euler_g` initialize the solution with the initial distribution either coming from a grid or following Eq. (C.1). Then, the Euler method is performed, given the \mathcal{S} matrix, through a loop in time t . During this loop, the derivative of the FF D is calculated using Eq. (4.149) and added to the value of D in the previous iteration. Note that the results are directly written during the Euler method. Indeed, when $t \equiv 0 \pmod{\text{int}(\frac{N \cdot t}{N \cdot t \cdot w})}$ ⁶, in addition to the actual calculation, D is added to the result grid (i.e its value on the $\mathbf{N}\mathbf{x}$ nodes).
- `normalize_Dg` is used to applied, during the Euler method, the normalization choice set by `norm`.

We will detail a little the calculation of the \mathcal{S} matrix, in the case of the logarithmic bijection (i.e, as described in `cheb_init_S_chebint_glog`). This calculation uses the following variables :

- `double **intTk` corresponds to the integral of the l -th Chebyshev polynomial between -1 and 1.
- `double *X0k` is the set of used nodes $\{x_i^{0k}\}$.
- `double *Xk1` is the set of used nodes
- `double **I1` corresponds to I_k^1 .
- `double **I2` corresponds to $I_{k,i}^2$. $\{x_i^{k1}\}$.

First, the arrays `intTk`, `X0k` and `Xk1` are evaluated. Then The calculation of both the \mathcal{S} matrix and the different integrals I are performed in the same loops (ordered in such a way that it works). If we isolate the \mathcal{S} calculation, it follows exactly the formula given in Sec. 4.4.3 :

```

1 for (int k = 0; k < N; ++k){
2   for (int i = 0; i < N; ++i){
3     for (int j = 0; j < N; ++j){
4       if (i==0)
5         S_gg[k][j] += 1./N/sqrt(X[k])*T[i][j]*I_g1[k][i];
6       else
7         S_gg[k][j] += 2./N/sqrt(X[k])*T[i][j]*I_g1[k][i];
8     }
9     S_gg[k][k] -= 1./sqrt(X[k])*(I_g2[k]+I_g3);}

```

⁶this condition insure the number of time points in the result grid to be `N.t.w`.

where the `if` loop is due to the prime prescription for the sum on i . What is less direct, is how the calculation of the integrals I is implemented in the same loop (since the loop due to the Chebyshev integration has to be performed before the calculation of \mathcal{S}). One may argue that each integral and the sum could be calculated in separated loop but, since the calculation of $I_{i,j}^2$ already implies 4 `for` loops (2 on the indices, 2 for the sums), it is faster in the proposed way :

```

1 for (int k = 0; k < N; ++k){
2     for (int i = 0; i < N; ++i){
3         for (int m = 0; m < N; ++m){
4             for (int l = 0; l < N; ++l){
5                 I = 1./N*T[l][m]*.5*(1-X[k])*intT[l];
6                 if (l==0)
7                     I_g1[k][i] += I*K_gg(Xk1[m][k])
8                                 *(sqrt(Xk1[m][k])
9                                 *cheb_T(i,y_log(X[k]/Xk1[m][k],eps,1))
10                                -Xk1[m][k]*T[i][k]);
11                else
12                    I_g1[k][i] += 2*I*K_gg(Xk1[m][k])
13                                *(sqrt(Xk1[m][k])
14                                *cheb_T(i,y_log(X[k]/Xk1[m][k],eps,1))
15                                -Xk1[m][k]*T[i][k]);
16                if (i==0){
17                    if (l==0)
18                        I_g2[k] += 1./N*K_gg(X0k[m][k])*X0k[m][k]
19                                *T[l][m]*.5*X[k]*intT[l];
20                    else
21                        I_g2[k] += 2./N*K_gg(X0k[m][k])*X0k[m][k]
22                                *T[l][m]*.5*X[k]*intT[l];}}}}

```

This basically follows the expressions given in Eq. (4.147), with some changes in the indices adapted to the loop and ordering used. Note that the integrals are initialized to 0 in advance.

C.1.6 `Cheb_method_g_S_NS.h` subroutines

`Cheb_method_g_S_NS.h` works the same way as `Cheb_method_g.h` but in the system of equation case, as presented in Sec. 4.4.3. Then, to the variables present in `Cheb_method_g.h`, we have to add :

- `double **I_g1` corresponds to $I_{k,i}^{g,1}$.
- `double *I_g2` corresponds to $I_k^{g,2}$.
- `double I_g3` corresponds to $I^{g,3}$.
- `double *I_g4` corresponds to $I_k^{g,4}$.
- `double **LS1` corresponds to $I_{k,i}^{S,1}$.
- `double *LS2` corresponds to $I_k^{S,2}$.

- `double *LS3` corresponds to $I_k^{S,3}$.
- `double **LNS1` corresponds to $I_{k,i}^{NS,1}$.
- `double *LNS2` corresponds to $I_k^{NS,2}$.

Also, the normalization of the FF is now hold by two definitions of `normalize_D` (corresponding to either the normalisation of the sum of FF or of each of them).

C.1.7 `Cheb_functions.h` subroutines

Finally, `Cheb_functions.h` contains all the “basic” function i.e mathematical definitions. First we have the definitions related to the Chebyshev polynomials.

`cheb_T` evaluates the n -th Chebyshev polynomial (of the first kind) on x .

```

1 double cheb_T(int n, double x){
2     double T;
3     if (x<-1){
4         cout << "\nError cheb_T cannot be evaluated on " << x;
5         return 0;}
6     else if (x>1){
7         cout << "\nError cheb_T cannot be evaluated on " << x;
8         return 0;}
9     T = cos(n*acos(x));
10    return T;}

```

`cheb_int` evaluates the integral of the i -th Chebyshev polynomial on the range $[-1, 1]$.

```

1 double cheb_int(int i){
2     double y;
3     if (i==1)
4         y = 0;
5     else
6         y = (pow(-1., double(i))+1)/double(1-i*i);
7     return y;}

```

`node` returns the i -th node of the N -th Chebyshev polynomial.

```

1 double node(int N, int i){
2     return cos(M_PI/N*(i+.5));}

```

`y_` defines a linear bijection $y : [a, b] \rightarrow [-1, 1]$, returning its value on x .

```

1 double y_(double x, double a, double b){
2     return (2*x-b-a)/(b-a);}

```

`y_inv` defines the inverse of the linear bijection y , $y^{-1} : [-1, 1] \rightarrow [a, b]$, returning its value on x .

```

1 double y_inv(double x, double a, double b){
2     return 0.5*((b-a)*x+b+a);}

```

`y_log` defines a logarithmic bijection $y : [a, b] \rightarrow [-1, 1]$, returning its value on x .

```

1 double y_(double x, double a, double b){
2     return 1+2*log(x/b)/log(b/a);}

```

`y_log_inv` defines the inverse of the logarithmic bijection $y, y^{-1} : [-1, 1] \rightarrow [a, b]$, returning its value on x .

```
1 double y_inv(double x, double a, double b){
2     return b*pow(b/a, .5*(x-1));}
```

Then, the kernels of the BDIM equations are defined :

```
1 double K_simpl(double x)
2     return 1./pow(x*(1-x), 1.5);
3
4 double K_gonly(double x)
5 {
6     double f;
7     f = 1-x+x*x;
8     return pow(f, 2.5)/pow(x*(1-x), 1.5);
9 }
10
11 double K_gg(double x){
12     double f;
13     f = 1-x+x*x;
14     return pow(C_A, 1.5)*pow(f, 2.5)/pow(x*(1-x), 1.5);}
15
16 double K_gq(double x){
17     return C_F/2.*(1+pow(1-x, 2))/x*sqrt(((1-x)*C_A+x*x*C_F)/(x*(1-x)));}
18
19 double K_qq(double x){
20     return C_F/2.*(1+x*x)/(1-x)*sqrt((x*C_A+pow(1-x, 2)*C_F)/(x*(1-x)));}
21
22 double K_qg(double x){
23     return Nf*T_F*(x*x+pow(1-x, 2))*sqrt((C_F-x*(1-x)*C_A)/(x*(1-x)));}
```

And finally, the possible analytical expression that can be used to define initial distribution are set. `D_t0_e` defines the narrow Gaussian peaked in 1 (as in Eq. (4.152)).

```
1 double D_t0_e(double x, double eps){
2     return sqrt(2./M_PI)/eps*exp(-pow((1-x)/eps, 2.)/2.);}
```

`D_t0_a` defines the analytical solution of the simplified BDIM equation (as in Eq. (4.107)).

```
1 double D_t0_a(double x, double tau){
2     return tau/sqrt(x*pow(1-x, 3.))*exp(-M_PI*tau*tau/(1-x));}
```

C.2 BDIM solutions, different approaches comparison

In this appendix, we compare the results obtained by the different method to solve the BDIM equations presented in Sec. 4.4. First, we will compare the energy distribution obtained with the Chebyshev method, with MINCAS and with TMDICE. The solutions

used here were obtained with the following input parameters :

$$\begin{aligned}
x_{\min} &= 10^{-4}, & \epsilon &= 10^{-6}, & l_{\min} &= 0.1 \text{ GeV}, \\
\epsilon_{Cheb} &= 10^{-4}, & dt &= 10^{-6}, & N &= 200, \\
N_c &= 3, & N_f &= 3, & \alpha_s &= \pi/10, \\
E &= 100 \text{ GeV}, & n &= 0.243 \text{ GeV}^3, & \hat{q} &= 1 \text{ GeV}^2/\text{fm}, & m_D &= 0.993 \text{ GeV}.
\end{aligned} \tag{C.4}$$

where the first line corresponds to regulator for both MCMC methods and the second lines concerns parameters specific to the Chebyshev method. They are the same as those used in Sec. 4.5 with the addition of specific parameters for the Chebyshev method (in particular, ϵ_{Cheb} is the low- x cut used for the logarithmic bijection). The comparison is presented in Fig. C.1.

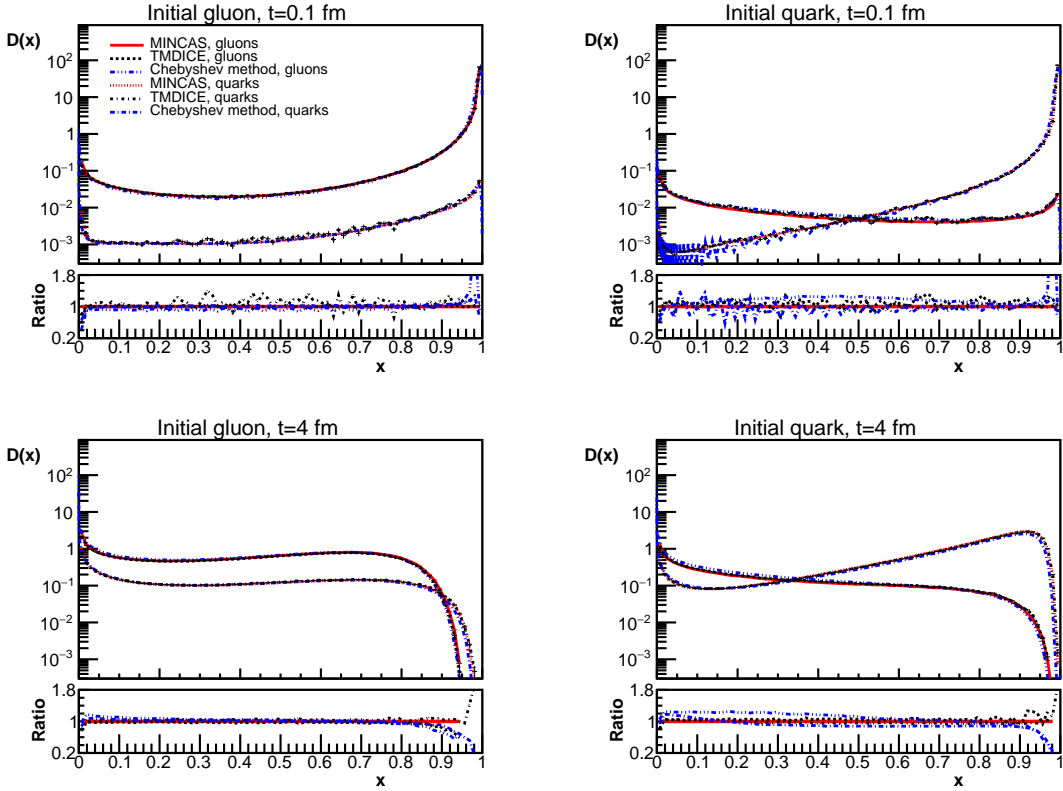


Figure C.1: Comparison of energy distribution obtained with the MINCAS (in red), TMDICE (in black) and the Chebyshev method (in blue) for an initial gluon (left) and for an initial quark (right) at 0.1fm (top) and 4fm (bottom). Ratio plots with respect to the MINCAS solution are also plotted.

We observe a very good agreement between all 3 approaches except for some statistical errors in TMDICE (which could be solved with finer numerical integration, but the

calculation time increase rapidly then) and some oscillations of the Chebyshev method (even for the nodes) at low- x in the quark distribution for quark jets at low time (where the Chebyshev expansion has difficulty to reproduce the steep peak appearing in the distribution).

We can also have a look on the transverse momentum distributions of the solutions to the “full” BDIM equation (Eq. (4.71)) obtained by MINCAS and TMDICE. This is illustrated in Fig. C.2.

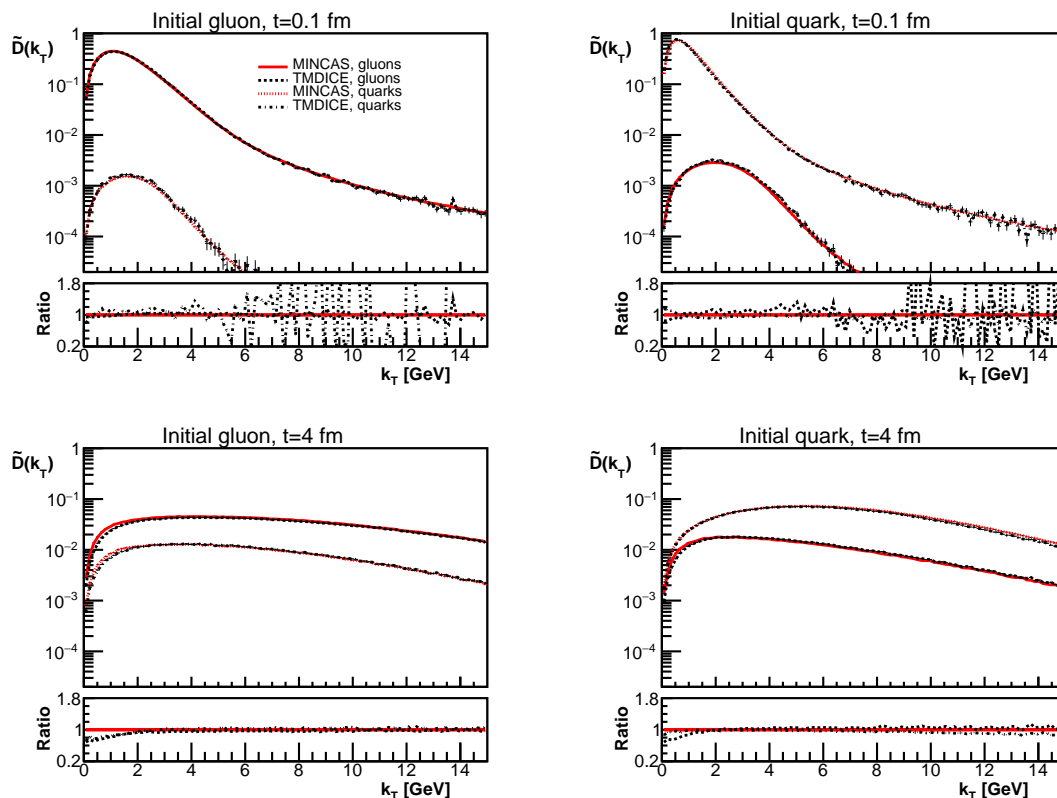


Figure C.2: Comparison of transverse momentum distribution obtained with the MINCAS (in red) and TMDICE (in black) for an initial gluon (left) and for an initial quark (right) at 0.1fm (top) and 4fm (bottom). Ratio plots with respect to the MINCAS solution are also plotted.

Again, both approaches agree well on the transverse momentum distribution, even if it is more complicated to obtain good statistics with TMDICE (due to the precision of the numerical integration...). Still, it is interesting to note a slight difference in shape (not due to statistical errors) at low- k_T for the distribution after a long evolution (4fm for instance).

Bibliography

- [1] E. Blanco, A. van Hameren, H. Jung, A. Kusina, and K. Kutak, “ Z boson production in proton-lead collisions at the LHC accounting for transverse momenta of initial partons,” *Phys. Rev. D*, vol. 100, no. 5, p. 054023, 2019. DOI: [10.1103/PhysRevD.100.054023](https://doi.org/10.1103/PhysRevD.100.054023). arXiv: [1905.07331](https://arxiv.org/abs/1905.07331) [[hep-ph](#)].
- [2] E. Blanco, A. van Hameren, P. Kotko, and K. Kutak, “All-plus helicity off-shell gauge invariant multigluon amplitudes at one loop,” *JHEP*, vol. 12, p. 158, 2020. DOI: [10.1007/JHEP12\(2020\)158](https://doi.org/10.1007/JHEP12(2020)158). arXiv: [2008.07916](https://arxiv.org/abs/2008.07916) [[hep-ph](#)].
- [3] E. Blanco, K. Kutak, W. Placzek, M. Rohrmoser, and R. Straka, “Medium induced QCD cascades: broadening and rescattering during branching,” *JHEP*, vol. 04, p. 014, 2021. DOI: [10.1007/JHEP04\(2021\)014](https://doi.org/10.1007/JHEP04(2021)014). arXiv: [2009.03876](https://arxiv.org/abs/2009.03876) [[hep-ph](#)].
- [4] E. Blanco, K. Kutak, W. Placzek, M. Rohrmoser, and K. Tywoniuk, “System of evolution equations for quark and gluon jet quenching with broadening,” *Eur. Phys. J. C*, vol. 82, no. 4, p. 355, 2022. DOI: [10.1140/epjc/s10052-022-10311-2](https://doi.org/10.1140/epjc/s10052-022-10311-2). arXiv: [2109.05918](https://arxiv.org/abs/2109.05918) [[hep-ph](#)].
- [5] F. Halzen and A. D. Martin, *Quarks and Leptons: An Introductory Course in Modern Particle Physics*. 1984, ISBN: 978-0-471-88741-6.
- [6] Y. V. Kovchegov and E. Levin, *Quantum chromodynamics at high energy*. Cambridge University Press, Aug. 2012, vol. 33, ISBN: 978-0-521-11257-4. DOI: [10.1017/CB09781139022187](https://doi.org/10.1017/CB09781139022187).
- [7] H. Nastase, *Classical Field Theory*. Cambridge University Press, Mar. 2019, ISBN: 978-1-108-47701-7.
- [8] M. D. Schwartz, *Quantum Field Theory and the Standard Model*. Cambridge University Press, Mar. 2014, ISBN: 978-1-107-03473-0.
- [9] M. Bury, “Phenomenology of transverse-momentum dependent factorizations in hadronic collisions,” Ph.D. dissertation, IFJ-PAN, 2020.
- [10] F. Van der Veken, “Wilson lines : applications in QCD,” Ph.D. dissertation, Antwerp U., 2014.
- [11] A. Lelek, “Determination of TMD parton densities from HERA data and application to pp processes,” Ph.D. dissertation, Hamburg U., Hamburg, 2018. DOI: [10.3204/PUBDB-2018-02949](https://doi.org/10.3204/PUBDB-2018-02949).

- [12] V. Vila Perez, “Jet quenching and heavy ion collisions,” Ph.D. dissertation, Santiago de Compostela U., 2020.
- [13] M. De Angelis, “QCD Evolution At Amplitude Level,” Ph.D. dissertation, The University of Manchester, 2021.
- [14] Ranjithsiji. (), [Online]. Available: <https://commons.wikimedia.org/wiki/File:Quark.svg> (visited on 05/20/2022).
- [15] T. Muta, *Foundations of quantum chromodynamics. Second edition.* 1998, vol. 57.
- [16] R. K. Ellis, W. J. Stirling, and B. R. Webber, *QCD and collider physics.* Cambridge University Press, Feb. 2011, vol. 8, ISBN: 978-0-511-82328-2. DOI: [10.1017/CBO9780511628788](https://doi.org/10.1017/CBO9780511628788).
- [17] A. G. Williams, “QCD, gauge fixing, and the Gribov problem,” *Nucl. Phys. B Proc. Suppl.*, vol. 109, A. C. Kalloniatis, D. B. Leinweber, W. Melnitchouk, and A. G. Williams, Eds., pp. 141–145, 2002. DOI: [10.1016/S0920-5632\(02\)01405-6](https://doi.org/10.1016/S0920-5632(02)01405-6). arXiv: [hep-lat/0202010](https://arxiv.org/abs/hep-lat/0202010).
- [18] L. Faddeev and V. Popov, “Feynman diagrams for the yang-mills field,” *Physics Letters B*, vol. 25, no. 1, pp. 29–30, 1967, ISSN: 0370-2693. DOI: [https://doi.org/10.1016/0370-2693\(67\)90067-6](https://doi.org/10.1016/0370-2693(67)90067-6). [Online]. Available: <https://www.sciencedirect.com/science/article/pii/0370269367900676>.
- [19] D. J. Gross and F. Wilczek, “Asymptotically Free Gauge Theories - I,” *Phys. Rev. D*, vol. 8, pp. 3633–3652, 1973. DOI: [10.1103/PhysRevD.8.3633](https://doi.org/10.1103/PhysRevD.8.3633).
- [20] H. D. Politzer, “Reliable Perturbative Results for Strong Interactions?” *Phys. Rev. Lett.*, vol. 30, J. C. Taylor, Ed., pp. 1346–1349, 1973. DOI: [10.1103/PhysRevLett.30.1346](https://doi.org/10.1103/PhysRevLett.30.1346).
- [21] M. Jamin, “Qcd and renormalisation group methods,” *Lecture presented at Herbstschule für Hochenergiephysik, Maria Laach*, 2006.
- [22] P. Zyla *et al.*, “Review of Particle Physics,” *PTEP*, vol. 2020, no. 8, p. 083C01, 2020, and 2021 update. DOI: [10.1093/ptep/ptaa104](https://doi.org/10.1093/ptep/ptaa104).
- [23] M. Gell-Mann, “The Eightfold Way: A Theory of strong interaction symmetry,” Mar. 1961. DOI: [10.2172/4008239](https://doi.org/10.2172/4008239).
- [24] V. E. Barnes *et al.*, “Observation of a Hyperon with Strangeness Minus Three,” *Phys. Rev. Lett.*, vol. 12, pp. 204–206, 1964. DOI: [10.1103/PhysRevLett.12.204](https://doi.org/10.1103/PhysRevLett.12.204).
- [25] R. Aaij *et al.*, “Observation of the resonant character of the $Z(4430)^-$ state,” *Phys. Rev. Lett.*, vol. 112, no. 22, p. 222002, 2014. DOI: [10.1103/PhysRevLett.112.222002](https://doi.org/10.1103/PhysRevLett.112.222002). arXiv: [1404.1903](https://arxiv.org/abs/1404.1903) [hep-ex].
- [26] N. Brambilla, A. Vairo, A. Polosa, and J. Soto, “Round Table on Heavy Quarkonia and Exotic States,” *Nucl. Phys. B Proc. Suppl.*, vol. 185, G. Ricciardi, G. De Nardo, D. Monorchio, and C. Sciacca, Eds., pp. 107–117, 2008. DOI: [10.1016/j.nuclphysbps.2008.10.011](https://doi.org/10.1016/j.nuclphysbps.2008.10.011).

- [27] R. P. Feynman, “The behavior of hadron collisions at extreme energies,” *Conf. Proc. C*, vol. 690905, pp. 237–258, 1969.
- [28] H. Abramowicz *et al.*, “Combination of measurements of inclusive deep inelastic $e^\pm p$ scattering cross sections and QCD analysis of HERA data,” *Eur. Phys. J. C*, vol. 75, no. 12, p. 580, 2015. DOI: [10.1140/epjc/s10052-015-3710-4](https://doi.org/10.1140/epjc/s10052-015-3710-4). arXiv: [1506.06042](https://arxiv.org/abs/1506.06042) [hep-ex].
- [29] S. Catani, M. Ciafaloni, and F. Hautmann, “Gluon contributions to small x heavy flavor production,” *Phys. Lett. B*, vol. 242, pp. 97–102, 1990. DOI: [10.1016/0370-2693\(90\)91601-7](https://doi.org/10.1016/0370-2693(90)91601-7).
- [30] ———, “High-energy factorization and small x heavy flavor production,” *Nucl. Phys. B*, vol. 366, pp. 135–188, 1991. DOI: [10.1016/0550-3213\(91\)90055-3](https://doi.org/10.1016/0550-3213(91)90055-3).
- [31] T. Gleisberg, S. Hoeche, F. Krauss, A. Schalicke, S. Schumann, and J.-C. Winter, “SHERPA 1. alpha: A Proof of concept version,” *JHEP*, vol. 02, p. 056, 2004. DOI: [10.1088/1126-6708/2004/02/056](https://doi.org/10.1088/1126-6708/2004/02/056). arXiv: [hep-ph/0311263](https://arxiv.org/abs/hep-ph/0311263).
- [32] B. R. Webber, “A QCD Model for Jet Fragmentation Including Soft Gluon Interference,” *Nucl. Phys. B*, vol. 238, pp. 492–528, 1984. DOI: [10.1016/0550-3213\(84\)90333-X](https://doi.org/10.1016/0550-3213(84)90333-X).
- [33] G. Marchesini, B. R. Webber, G. Abbiendi, I. G. Knowles, M. H. Seymour, and L. Stanco, “Herwig version 5.9,” Jul. 1996. arXiv: [hep-ph/9607393](https://arxiv.org/abs/hep-ph/9607393).
- [34] B. Andersson, G. Gustafson, G. Ingelman, and T. Sjostrand, “Parton Fragmentation and String Dynamics,” *Phys. Rept.*, vol. 97, pp. 31–145, 1983. DOI: [10.1016/0370-1573\(83\)90080-7](https://doi.org/10.1016/0370-1573(83)90080-7).
- [35] T. Sjostrand, “The Lund Monte Carlo for Jet Fragmentation and $e^+ e^-$ Physics: Jetset Version 6.2,” *Comput. Phys. Commun.*, vol. 39, pp. 347–407, 1986. DOI: [10.1016/0010-4655\(86\)90096-2](https://doi.org/10.1016/0010-4655(86)90096-2).
- [36] C. Collaboration, L. Taylor, and T. McCauley, “CMS collision events at 7 TeV: candidate ZZ to 4e,” CMS Collection., Jul. 2011. [Online]. Available: <https://cds.cern.ch/record/1378102>.
- [37] M. E. Peskin and D. V. Schroeder, *An Introduction to quantum field theory*. Reading, USA: Addison-Wesley, 1995, ISBN: 978-0-201-50397-5.
- [38] C. G. Callan Jr. and D. J. Gross, “High-energy electroproduction and the constitution of the electric current,” *Phys. Rev. Lett.*, vol. 22, pp. 156–159, 1969. DOI: [10.1103/PhysRevLett.22.156](https://doi.org/10.1103/PhysRevLett.22.156).
- [39] G. T. Bodwin, “Factorization of the Drell-Yan Cross-Section in Perturbation Theory,” *Phys. Rev. D*, vol. 31, p. 2616, 1985, [Erratum: *Phys.Rev.D* 34, 3932 (1986)]. DOI: [10.1103/PhysRevD.34.3932](https://doi.org/10.1103/PhysRevD.34.3932).
- [40] J. C. Collins, D. E. Soper, and G. F. Sterman, “Factorization for Short Distance Hadron - Hadron Scattering,” *Nucl. Phys. B*, vol. 261, pp. 104–142, 1985. DOI: [10.1016/0550-3213\(85\)90565-6](https://doi.org/10.1016/0550-3213(85)90565-6).

- [41] J. C. Collins and D. E. Soper, “The Theorems of Perturbative QCD,” *Ann. Rev. Nucl. Part. Sci.*, vol. 37, pp. 383–409, 1987. DOI: [10.1146/annurev.ns.37.120187.002123](https://doi.org/10.1146/annurev.ns.37.120187.002123).
- [42] J. C. Collins, D. E. Soper, and G. F. Sterman, “Factorization of Hard Processes in QCD,” *Adv. Ser. Direct. High Energy Phys.*, vol. 5, pp. 1–91, 1989. DOI: [10.1142/9789814503266_0001](https://doi.org/10.1142/9789814503266_0001). arXiv: [hep-ph/0409313](https://arxiv.org/abs/hep-ph/0409313).
- [43] —, “Soft Gluons and Factorization,” *Nucl. Phys. B*, vol. 308, pp. 833–856, 1988. DOI: [10.1016/0550-3213\(88\)90130-7](https://doi.org/10.1016/0550-3213(88)90130-7).
- [44] V. N. Gribov and L. N. Lipatov, “Deep inelastic e p scattering in perturbation theory,” *Sov. J. Nucl. Phys.*, vol. 15, pp. 438–450, 1972.
- [45] G. Altarelli and G. Parisi, “Asymptotic Freedom in Parton Language,” *Nucl. Phys. B*, vol. 126, pp. 298–318, 1977. DOI: [10.1016/0550-3213\(77\)90384-4](https://doi.org/10.1016/0550-3213(77)90384-4).
- [46] Y. L. Dokshitzer, “Calculation of the Structure Functions for Deep Inelastic Scattering and e+ e- Annihilation by Perturbation Theory in Quantum Chromodynamics,” *Sov. Phys. JETP*, vol. 46, pp. 641–653, 1977.
- [47] G. F. Sterman, *An Introduction to quantum field theory*. Cambridge University Press, Aug. 1993, ISBN: 978-0-521-31132-8.
- [48] L. N. Lipatov, “Reggeization of the Vector Meson and the Vacuum Singularity in Nonabelian Gauge Theories,” *Sov. J. Nucl. Phys.*, vol. 23, pp. 338–345, 1976.
- [49] E. A. Kuraev, L. N. Lipatov, and V. S. Fadin, “The Pomeranchuk Singularity in Nonabelian Gauge Theories,” *Sov. Phys. JETP*, vol. 45, pp. 199–204, 1977.
- [50] I. I. Balitsky and L. N. Lipatov, “The Pomeranchuk Singularity in Quantum Chromodynamics,” *Sov. J. Nucl. Phys.*, vol. 28, pp. 822–829, 1978.
- [51] H. E. Daniels, “Saddlepoint Approximations in Statistics,” *The Annals of Mathematical Statistics*, vol. 25, no. 4, pp. 631–650, 1954. DOI: [10.1214/aoms/1177728652](https://doi.org/10.1214/aoms/1177728652). [Online]. Available: <https://doi.org/10.1214/aoms/1177728652>.
- [52] M. Froissart, “Asymptotic behavior and subtractions in the Mandelstam representation,” *Phys. Rev.*, vol. 123, pp. 1053–1057, 1961. DOI: [10.1103/PhysRev.123.1053](https://doi.org/10.1103/PhysRev.123.1053).
- [53] A. Martin, “Extension of the axiomatic analyticity domain of scattering amplitudes by unitarity. 1.,” *Nuovo Cim. A*, vol. 42, pp. 930–953, 1965. DOI: [10.1007/BF02720568](https://doi.org/10.1007/BF02720568).
- [54] J. Bartels, “Unitarity corrections to the Lipatov pomeron and the four gluon operator in deep inelastic scattering in QCD,” *Z. Phys. C*, vol. 60, pp. 471–488, 1993. DOI: [10.1007/BF01560045](https://doi.org/10.1007/BF01560045).
- [55] J. Bartels, H. Lotter, and M. Vogt, “A Numerical estimate of the small k(T) region in the BFKL pomeron,” *Phys. Lett. B*, vol. 373, pp. 215–222, 1996. DOI: [10.1016/0370-2693\(96\)00115-3](https://doi.org/10.1016/0370-2693(96)00115-3). arXiv: [hep-ph/9511399](https://arxiv.org/abs/hep-ph/9511399).

- [56] M. Ciafaloni, “Coherence Effects in Initial Jets at Small q^2 / s ,” *Nucl. Phys. B*, vol. 296, pp. 49–74, 1988. DOI: [10.1016/0550-3213\(88\)90380-X](https://doi.org/10.1016/0550-3213(88)90380-X).
- [57] S. Catani, F. Fiorani, and G. Marchesini, “Small x Behavior of Initial State Radiation in Perturbative QCD,” *Nucl. Phys. B*, vol. 336, pp. 18–85, 1990. DOI: [10.1016/0550-3213\(90\)90342-B](https://doi.org/10.1016/0550-3213(90)90342-B).
- [58] G. Marchesini, “QCD coherence in the structure function and associated distributions at small x ,” *Nucl. Phys. B*, vol. 445, pp. 49–80, 1995. DOI: [10.1016/0550-3213\(95\)00149-M](https://doi.org/10.1016/0550-3213(95)00149-M). arXiv: [hep-ph/9412327](https://arxiv.org/abs/hep-ph/9412327).
- [59] J. C. Collins, D. E. Soper, and G. F. Sterman, “Transverse Momentum Distribution in Drell-Yan Pair and W and Z Boson Production,” *Nucl. Phys. B*, vol. 250, pp. 199–224, 1985. DOI: [10.1016/0550-3213\(85\)90479-1](https://doi.org/10.1016/0550-3213(85)90479-1).
- [60] ———, “Factorization for One Loop Corrections in the Drell-Yan Process,” *Nucl. Phys. B*, vol. 223, pp. 381–421, 1983. DOI: [10.1016/0550-3213\(83\)90062-7](https://doi.org/10.1016/0550-3213(83)90062-7).
- [61] J. C. Collins and D. E. Soper, “Parton Distribution and Decay Functions,” *Nucl. Phys. B*, vol. 194, pp. 445–492, 1982. DOI: [10.1016/0550-3213\(82\)90021-9](https://doi.org/10.1016/0550-3213(82)90021-9).
- [62] ———, “Back-To-Back Jets: Fourier Transform from B to K-Transverse,” *Nucl. Phys. B*, vol. 197, pp. 446–476, 1982. DOI: [10.1016/0550-3213\(82\)90453-9](https://doi.org/10.1016/0550-3213(82)90453-9).
- [63] M. Deak, F. Hautmann, H. Jung, and K. Kutak, “Forward Jet Production at the Large Hadron Collider,” *JHEP*, vol. 09, p. 121, 2009. DOI: [10.1088/1126-6708/2009/09/121](https://doi.org/10.1088/1126-6708/2009/09/121). arXiv: [0908.0538](https://arxiv.org/abs/0908.0538) [[hep-ph](https://arxiv.org/abs/0908.0538)].
- [64] K. Kutak and S. Sapeta, “Gluon saturation in dijet production in p-Pb collisions at Large Hadron Collider,” *Phys. Rev. D*, vol. 86, p. 094043, 2012. DOI: [10.1103/PhysRevD.86.094043](https://doi.org/10.1103/PhysRevD.86.094043). arXiv: [1205.5035](https://arxiv.org/abs/1205.5035) [[hep-ph](https://arxiv.org/abs/1205.5035)].
- [65] M. Deak, F. Hautmann, H. Jung, and K. Kutak, “Forward-Central Jet Correlations at the Large Hadron Collider,” Dec. 2010. arXiv: [1012.6037](https://arxiv.org/abs/1012.6037) [[hep-ph](https://arxiv.org/abs/1012.6037)].
- [66] A. van Hameren, P. Kotko, K. Kutak, C. Marquet, and S. Sapeta, “Saturation effects in forward-forward dijet production in p+Pb collisions,” *Phys. Rev. D*, vol. 89, no. 9, p. 094014, 2014. DOI: [10.1103/PhysRevD.89.094014](https://doi.org/10.1103/PhysRevD.89.094014). arXiv: [1402.5065](https://arxiv.org/abs/1402.5065) [[hep-ph](https://arxiv.org/abs/1402.5065)].
- [67] A. van Hameren, P. Kotko, K. Kutak, and S. Sapeta, “Small- x dynamics in forward-central dijet correlations at the lhc,” *Physics Letters B*, vol. 737, pp. 335–340, 2014, ISSN: 0370-2693. DOI: <https://doi.org/10.1016/j.physletb.2014.09.005>. [Online]. Available: <https://www.sciencedirect.com/science/article/pii/S0370269314006558>.
- [68] L. V. Gribov, E. M. Levin, and M. G. Ryskin, “Semihard Processes in QCD,” *Phys. Rept.*, vol. 100, pp. 1–150, 1983. DOI: [10.1016/0370-1573\(83\)90022-4](https://doi.org/10.1016/0370-1573(83)90022-4).
- [69] I. Balitsky, “Operator expansion for high-energy scattering,” *Nucl. Phys. B*, vol. 463, pp. 99–160, 1996. DOI: [10.1016/0550-3213\(95\)00638-9](https://doi.org/10.1016/0550-3213(95)00638-9). arXiv: [hep-ph/9509348](https://arxiv.org/abs/hep-ph/9509348).

- [70] Y. V. Kovchegov, “Small x $F(2)$ structure function of a nucleus including multiple pomeron exchanges,” *Phys. Rev. D*, vol. 60, p. 034008, 1999. DOI: [10.1103/PhysRevD.60.034008](https://doi.org/10.1103/PhysRevD.60.034008). arXiv: [hep-ph/9901281](https://arxiv.org/abs/hep-ph/9901281).
- [71] ———, “Unitarization of the BFKL pomeron on a nucleus,” *Phys. Rev. D*, vol. 61, p. 074018, 2000. DOI: [10.1103/PhysRevD.61.074018](https://doi.org/10.1103/PhysRevD.61.074018). arXiv: [hep-ph/9905214](https://arxiv.org/abs/hep-ph/9905214).
- [72] F. Gelis, E. Iancu, J. Jalilian-Marian, and R. Venugopalan, “The Color Glass Condensate,” *Ann. Rev. Nucl. Part. Sci.*, vol. 60, pp. 463–489, 2010. DOI: [10.1146/annurev.nucl.010909.083629](https://doi.org/10.1146/annurev.nucl.010909.083629). arXiv: [1002.0333 \[hep-ph\]](https://arxiv.org/abs/1002.0333).
- [73] J. Jalilian-Marian, A. Kovner, A. Leonidov, and H. Weigert, “The BFKL equation from the Wilson renormalization group,” *Nucl. Phys. B*, vol. 504, pp. 415–431, 1997. DOI: [10.1016/S0550-3213\(97\)00440-9](https://doi.org/10.1016/S0550-3213(97)00440-9). arXiv: [hep-ph/9701284](https://arxiv.org/abs/hep-ph/9701284).
- [74] H. Weigert, “Unitarity at small Bjorken x ,” *Nucl. Phys. A*, vol. 703, pp. 823–860, 2002. DOI: [10.1016/S0375-9474\(01\)01668-2](https://doi.org/10.1016/S0375-9474(01)01668-2). arXiv: [hep-ph/0004044](https://arxiv.org/abs/hep-ph/0004044).
- [75] E. Ferreiro, E. Iancu, A. Leonidov, and L. McLerran, “Nonlinear gluon evolution in the color glass condensate. 2.,” *Nucl. Phys. A*, vol. 703, pp. 489–538, 2002. DOI: [10.1016/S0375-9474\(01\)01329-X](https://doi.org/10.1016/S0375-9474(01)01329-X). arXiv: [hep-ph/0109115](https://arxiv.org/abs/hep-ph/0109115).
- [76] C. Marquet, “Open questions in QCD at high parton density,” *Nucl. Phys. A*, vol. 904-905, T. Ullrich, B. Wyslouch, and J. W. Harris, Eds., pp. 294c–301c, 2013. DOI: [10.1016/j.nuclphysa.2013.01.075](https://doi.org/10.1016/j.nuclphysa.2013.01.075). arXiv: [1212.3482 \[hep-ph\]](https://arxiv.org/abs/1212.3482).
- [77] F. Hautmann, H. Jung, A. Lelek, V. Radescu, and R. Zlebcik, “Collinear and TMD Quark and Gluon Densities from Parton Branching Solution of QCD Evolution Equations,” *JHEP*, vol. 01, p. 070, 2018. DOI: [10.1007/JHEP01\(2018\)070](https://doi.org/10.1007/JHEP01(2018)070). arXiv: [1708.03279 \[hep-ph\]](https://arxiv.org/abs/1708.03279).
- [78] ———, “Soft-gluon resolution scale in QCD evolution equations,” *Phys. Lett. B*, vol. 772, pp. 446–451, 2017. DOI: [10.1016/j.physletb.2017.07.005](https://doi.org/10.1016/j.physletb.2017.07.005). arXiv: [1704.01757 \[hep-ph\]](https://arxiv.org/abs/1704.01757).
- [79] A. Bermudez Martinez *et al.*, “Determination and application of TMD parton densities using the Parton Branching method,” *PoS*, vol. DIS2018, p. 013, 2018. DOI: [10.22323/1.316.0013](https://doi.org/10.22323/1.316.0013). arXiv: [1809.04511 \[hep-ph\]](https://arxiv.org/abs/1809.04511).
- [80] A. Bermudez Martinez *et al.*, “Collinear and TMD parton densities from fits to precision DIS measurements in the parton branching method,” *Phys. Rev. D*, vol. 99, no. 7, p. 074008, 2019. DOI: [10.1103/PhysRevD.99.074008](https://doi.org/10.1103/PhysRevD.99.074008). arXiv: [1804.11152 \[hep-ph\]](https://arxiv.org/abs/1804.11152).
- [81] B. R. Webber, “Monte Carlo Simulation of Hard Hadronic Processes,” *Ann. Rev. Nucl. Part. Sci.*, vol. 36, pp. 253–286, 1986. DOI: [10.1146/annurev.ns.36.120186.001345](https://doi.org/10.1146/annurev.ns.36.120186.001345).
- [82] S. Catani, B. R. Webber, and G. Marchesini, “QCD coherent branching and semiinclusive processes at large x ,” *Nucl. Phys. B*, vol. 349, pp. 635–654, 1991. DOI: [10.1016/0550-3213\(91\)90390-J](https://doi.org/10.1016/0550-3213(91)90390-J).

- [83] S. Gieseke, P. Stephens, and B. Webber, “New formalism for QCD parton showers,” *JHEP*, vol. 12, p. 045, 2003. DOI: [10.1088/1126-6708/2003/12/045](https://doi.org/10.1088/1126-6708/2003/12/045). arXiv: [hep-ph/0310083](https://arxiv.org/abs/hep-ph/0310083).
- [84] F. Hautmann, “Endpoint singularities in unintegrated parton distributions,” *Phys. Lett. B*, vol. 655, pp. 26–31, 2007. DOI: [10.1016/j.physletb.2007.08.081](https://doi.org/10.1016/j.physletb.2007.08.081). arXiv: [hep-ph/0702196](https://arxiv.org/abs/hep-ph/0702196).
- [85] F. Hautmann, M. Hentschinski, L. Keersmaekers, A. Kusina, K. Kutak, and A. Lelek, “A parton branching with transverse momentum dependent splitting functions,” *Phys. Lett. B*, vol. 833, p. 137276, 2022. DOI: [10.1016/j.physletb.2022.137276](https://doi.org/10.1016/j.physletb.2022.137276). arXiv: [2205.15873](https://arxiv.org/abs/2205.15873) [[hep-ph](#)].
- [86] L. A. Harland-Lang, A. D. Martin, P. Motylinski, and R. S. Thorne, “Parton distributions in the LHC era: MMHT 2014 PDFs,” *Eur. Phys. J. C*, vol. 75, no. 5, p. 204, 2015. DOI: [10.1140/epjc/s10052-015-3397-6](https://doi.org/10.1140/epjc/s10052-015-3397-6). arXiv: [1412.3989](https://arxiv.org/abs/1412.3989) [[hep-ph](#)].
- [87] S. Bailey, T. Cridge, L. A. Harland-Lang, A. D. Martin, and R. S. Thorne, “Parton distributions from LHC, HERA, Tevatron and fixed target data: MSHT20 PDFs,” *Eur. Phys. J. C*, vol. 81, no. 4, p. 341, 2021. DOI: [10.1140/epjc/s10052-021-09057-0](https://doi.org/10.1140/epjc/s10052-021-09057-0). arXiv: [2012.04684](https://arxiv.org/abs/2012.04684) [[hep-ph](#)].
- [88] R. D. Ball *et al.*, “Parton distributions for the LHC Run II,” *JHEP*, vol. 04, p. 040, 2015. DOI: [10.1007/JHEP04\(2015\)040](https://doi.org/10.1007/JHEP04(2015)040). arXiv: [1410.8849](https://arxiv.org/abs/1410.8849) [[hep-ph](#)].
- [89] J. Gao *et al.*, “CT10 next-to-next-to-leading order global analysis of QCD,” *Phys. Rev. D*, vol. 89, no. 3, p. 033009, 2014. DOI: [10.1103/PhysRevD.89.033009](https://doi.org/10.1103/PhysRevD.89.033009). arXiv: [1302.6246](https://arxiv.org/abs/1302.6246) [[hep-ph](#)].
- [90] H. Abramowicz *et al.*, “Combination and QCD analysis of charm and beauty production cross-section measurements in deep inelastic *ep* scattering at HERA,” *Eur. Phys. J. C*, vol. 78, no. 6, p. 473, 2018. DOI: [10.1140/epjc/s10052-018-5848-3](https://doi.org/10.1140/epjc/s10052-018-5848-3). arXiv: [1804.01019](https://arxiv.org/abs/1804.01019) [[hep-ex](#)].
- [91] A. D. Martin, W. J. Stirling, R. S. Thorne, and G. Watt, “Parton distributions for the LHC,” *Eur. Phys. J. C*, vol. 63, pp. 189–285, 2009. DOI: [10.1140/epjc/s10052-009-1072-5](https://doi.org/10.1140/epjc/s10052-009-1072-5). arXiv: [0901.0002](https://arxiv.org/abs/0901.0002) [[hep-ph](#)].
- [92] K. Kovarik *et al.*, “nCTEQ15 - Global analysis of nuclear parton distributions with uncertainties in the CTEQ framework,” *Phys. Rev. D*, vol. 93, no. 8, p. 085037, 2016. DOI: [10.1103/PhysRevD.93.085037](https://doi.org/10.1103/PhysRevD.93.085037). arXiv: [1509.00792](https://arxiv.org/abs/1509.00792) [[hep-ph](#)].
- [93] K. J. Eskola, P. Paakkinen, H. Paukkunen, and C. A. Salgado, “EPPS16: Nuclear parton distributions with LHC data,” *Eur. Phys. J. C*, vol. 77, no. 3, p. 163, 2017. DOI: [10.1140/epjc/s10052-017-4725-9](https://doi.org/10.1140/epjc/s10052-017-4725-9). arXiv: [1612.05741](https://arxiv.org/abs/1612.05741) [[hep-ph](#)].
- [94] J. Pumplin, D. R. Stump, J. Huston, H. L. Lai, P. M. Nadolsky, and W. K. Tung, “New generation of parton distributions with uncertainties from global QCD analysis,” *JHEP*, vol. 07, p. 012, 2002. DOI: [10.1088/1126-6708/2002/07/012](https://doi.org/10.1088/1126-6708/2002/07/012). arXiv: [hep-ph/0201195](https://arxiv.org/abs/hep-ph/0201195).

- [95] M. Krämer, F. I. Olness, and D. E. Soper, “Treatment of heavy quarks in deeply inelastic scattering,” *Phys. Rev. D*, vol. 62, p. 096007, 2000. DOI: [10.1103/PhysRevD.62.096007](https://doi.org/10.1103/PhysRevD.62.096007). arXiv: [hep-ph/0003035](https://arxiv.org/abs/hep-ph/0003035).
- [96] B. Z. Kopeliovich, J. G. Morfin, and I. Schmidt, “Nuclear Shadowing in Electro-Weak Interactions,” *Prog. Part. Nucl. Phys.*, vol. 68, pp. 314–372, 2013. DOI: [10.1016/j.pnpnp.2012.09.004](https://doi.org/10.1016/j.pnpnp.2012.09.004). arXiv: [1208.6541](https://arxiv.org/abs/1208.6541) [[hep-ph](#)].
- [97] N. A. Abdulov *et al.*, “TMDlib2 and TMDplotter: a platform for 3D hadron structure studies,” *Eur. Phys. J. C*, vol. 81, no. 8, p. 752, 2021. DOI: [10.1140/epjc/s10052-021-09508-8](https://doi.org/10.1140/epjc/s10052-021-09508-8). arXiv: [2103.09741](https://arxiv.org/abs/2103.09741) [[hep-ph](#)].
- [98] V. Khachatryan *et al.*, “Study of Z boson production in pPb collisions at $\sqrt{s_{NN}} = 5.02$ TeV,” *Phys. Lett. B*, vol. 759, pp. 36–57, 2016. DOI: [10.1016/j.physletb.2016.05.044](https://doi.org/10.1016/j.physletb.2016.05.044). arXiv: [1512.06461](https://arxiv.org/abs/1512.06461) [[hep-ex](#)].
- [99] A. van Hameren, “KaTie : For parton-level event generation with k_T -dependent initial states,” *Comput. Phys. Commun.*, vol. 224, pp. 371–380, 2018. DOI: [10.1016/j.cpc.2017.11.005](https://doi.org/10.1016/j.cpc.2017.11.005). arXiv: [1611.00680](https://arxiv.org/abs/1611.00680) [[hep-ph](#)].
- [100] A. Kusina, J.-P. Lansberg, I. Schienbein, and H.-S. Shao, “Gluon Shadowing in Heavy-Flavor Production at the LHC,” *Phys. Rev. Lett.*, vol. 121, no. 5, p. 052004, 2018. DOI: [10.1103/PhysRevLett.121.052004](https://doi.org/10.1103/PhysRevLett.121.052004). arXiv: [1712.07024](https://arxiv.org/abs/1712.07024) [[hep-ph](#)].
- [101] S. Dooling, F. Hautmann, and H. Jung, “Hadroproduction of electroweak gauge boson plus jets and TMD parton density functions,” *Phys. Lett. B*, vol. 736, pp. 293–298, 2014. DOI: [10.1016/j.physletb.2014.07.035](https://doi.org/10.1016/j.physletb.2014.07.035). arXiv: [1406.2994](https://arxiv.org/abs/1406.2994) [[hep-ph](#)].
- [102] A. van Hameren, L. Motyka, and G. Ziarko, “Hybrid k_T -factorization and impact factors at NLO,” May 2022. arXiv: [2205.09585](https://arxiv.org/abs/2205.09585) [[hep-ph](#)].
- [103] R. Kleiss and H. Kuijf, “Multi - Gluon Cross-sections and Five Jet Production at Hadron Colliders,” *Nucl. Phys. B*, vol. 312, pp. 616–644, 1989. DOI: [10.1016/0550-3213\(89\)90574-9](https://doi.org/10.1016/0550-3213(89)90574-9).
- [104] L. J. Dixon, “Calculating scattering amplitudes efficiently,” in *Theoretical Advanced Study Institute in Elementary Particle Physics (TASI 95): QCD and Beyond*, Jan. 1996, pp. 539–584. arXiv: [hep-ph/9601359](https://arxiv.org/abs/hep-ph/9601359).
- [105] R. Britto, “Introduction to scattering amplitudes,” *Lecture notes*, 2011.
- [106] L. J. Dixon, “A brief introduction to modern amplitude methods,” in *Theoretical Advanced Study Institute in Elementary Particle Physics: Particle Physics: The Higgs Boson and Beyond*, 2014, pp. 31–67. DOI: [10.5170/CERN-2014-008.31](https://doi.org/10.5170/CERN-2014-008.31). arXiv: [1310.5353](https://arxiv.org/abs/1310.5353) [[hep-ph](#)].
- [107] H. Elvang and Y.-t. Huang, “Scattering Amplitudes,” Aug. 2013. arXiv: [1308.1697](https://arxiv.org/abs/1308.1697) [[hep-th](#)].

- [108] J. M. Henn and J. C. Plefka, *Scattering Amplitudes in Gauge Theories*. Berlin: Springer, 2014, vol. 883, ISBN: 978-3-642-54021-9. DOI: [10.1007/978-3-642-54022-6](https://doi.org/10.1007/978-3-642-54022-6).
- [109] F. A. Berends and W. Giele, “The Six Gluon Process as an Example of Weyl-Van Der Waerden Spinor Calculus,” *Nucl. Phys. B*, vol. 294, pp. 700–732, 1987. DOI: [10.1016/0550-3213\(87\)90604-3](https://doi.org/10.1016/0550-3213(87)90604-3).
- [110] M. L. Mangano, S. J. Parke, and Z. Xu, “Duality and Multi - Gluon Scattering,” *Nucl. Phys. B*, vol. 298, pp. 653–672, 1988. DOI: [10.1016/0550-3213\(88\)90001-6](https://doi.org/10.1016/0550-3213(88)90001-6).
- [111] M. L. Mangano, “The Color Structure of Gluon Emission,” *Nucl. Phys. B*, vol. 309, pp. 461–475, 1988. DOI: [10.1016/0550-3213\(88\)90453-1](https://doi.org/10.1016/0550-3213(88)90453-1).
- [112] Z. Bern and D. A. Kosower, “Color decomposition of one loop amplitudes in gauge theories,” *Nucl. Phys. B*, vol. 362, pp. 389–448, 1991. DOI: [10.1016/0550-3213\(91\)90567-H](https://doi.org/10.1016/0550-3213(91)90567-H).
- [113] G. 't Hooft, “A Planar Diagram Theory for Strong Interactions,” *Nucl. Phys. B*, vol. 72, J. C. Taylor, Ed., p. 461, 1974. DOI: [10.1016/0550-3213\(74\)90154-0](https://doi.org/10.1016/0550-3213(74)90154-0).
- [114] P. Cvitanovic, *Group Theory: Part I*. Jan. 1984.
- [115] Z. Bern, L. Dixon, and D. A. Kosower, “One-loop corrections to two-quark three-gluon amplitudes,” *Nuclear Physics B*, vol. 437, no. 2, pp. 259–304, 1995.
- [116] V. Del Duca, L. J. Dixon, and F. Maltoni, “New color decompositions for gauge amplitudes at tree and loop level,” *Nucl. Phys. B*, vol. 571, pp. 51–70, 2000. DOI: [10.1016/S0550-3213\(99\)00809-3](https://doi.org/10.1016/S0550-3213(99)00809-3). arXiv: [hep-ph/9910563](https://arxiv.org/abs/hep-ph/9910563).
- [117] Z. Bern, J. J. M. Carrasco, and H. Johansson, “New Relations for Gauge-Theory Amplitudes,” *Phys. Rev. D*, vol. 78, p. 085 011, 2008. DOI: [10.1103/PhysRevD.78.085011](https://doi.org/10.1103/PhysRevD.78.085011). arXiv: [0805.3993 \[hep-ph\]](https://arxiv.org/abs/0805.3993).
- [118] F. Maltoni, K. Paul, T. Stelzer, and S. Willenbrock, “Color Flow Decomposition of QCD Amplitudes,” *Phys. Rev. D*, vol. 67, p. 014 026, 2003. DOI: [10.1103/PhysRevD.67.014026](https://doi.org/10.1103/PhysRevD.67.014026). arXiv: [hep-ph/0209271](https://arxiv.org/abs/hep-ph/0209271).
- [119] M. L. Mangano and S. J. Parke, “Multiparton amplitudes in gauge theories,” *Phys. Rept.*, vol. 200, pp. 301–367, 1991. DOI: [10.1016/0370-1573\(91\)90091-Y](https://doi.org/10.1016/0370-1573(91)90091-Y). arXiv: [hep-th/0509223](https://arxiv.org/abs/hep-th/0509223).
- [120] F. A. Berends, R. Kleiss, P. De Causmaecker, R. Gastmans, and T. T. Wu, “Single Bremsstrahlung Processes in Gauge Theories,” *Phys. Lett. B*, vol. 103, pp. 124–128, 1981. DOI: [10.1016/0370-2693\(81\)90685-7](https://doi.org/10.1016/0370-2693(81)90685-7).
- [121] P. De Causmaecker, R. Gastmans, W. Troost, and T. T. Wu, “Multiple Bremsstrahlung in Gauge Theories at High-Energies. 1. General Formalism for Quantum Electrodynamics,” *Nucl. Phys. B*, vol. 206, pp. 53–60, 1982. DOI: [10.1016/0550-3213\(82\)90488-6](https://doi.org/10.1016/0550-3213(82)90488-6).

- [122] R. Kleiss and W. J. Stirling, “Spinor Techniques for Calculating p anti- $p \rightarrow W^{+/-} / Z^0 + \text{Jets}$,” *Nucl. Phys. B*, vol. 262, pp. 235–262, 1985. DOI: [10.1016/0550-3213\(85\)90285-8](https://doi.org/10.1016/0550-3213(85)90285-8).
- [123] R. Gastmans and T. T. Wu, *The Ubiquitous photon: Helicity method for QED and QCD*. 1990, vol. 80.
- [124] Z. Xu, D.-H. Zhang, and L. Chang, “Helicity Amplitudes for Multiple Bremsstrahlung in Massless Nonabelian Gauge Theories,” *Nucl. Phys. B*, vol. 291, pp. 392–428, 1987. DOI: [10.1016/0550-3213\(87\)90479-2](https://doi.org/10.1016/0550-3213(87)90479-2).
- [125] J. F. Gunion and Z. Kunszt, “Improved Analytic Techniques for Tree Graph Calculations and the $G g q$ anti- q Lepton anti-Lepton Subprocess,” *Phys. Lett. B*, vol. 161, p. 333, 1985. DOI: [10.1016/0370-2693\(85\)90774-9](https://doi.org/10.1016/0370-2693(85)90774-9).
- [126] S. J. Parke and T. R. Taylor, “An Amplitude for n Gluon Scattering,” *Phys. Rev. Lett.*, vol. 56, p. 2459, 1986. DOI: [10.1103/PhysRevLett.56.2459](https://doi.org/10.1103/PhysRevLett.56.2459).
- [127] M. L. Mangano and S. J. Parke, “Quark - Gluon Amplitudes in the Dual Expansion,” *Nucl. Phys. B*, vol. 299, pp. 673–692, 1988. DOI: [10.1016/0550-3213\(88\)90368-9](https://doi.org/10.1016/0550-3213(88)90368-9).
- [128] F. A. Berends and W. T. Giele, “Recursive Calculations for Processes with n Gluons,” *Nucl. Phys. B*, vol. 306, pp. 759–808, 1988. DOI: [10.1016/0550-3213\(88\)90442-7](https://doi.org/10.1016/0550-3213(88)90442-7).
- [129] D. A. Kosower, “Light Cone Recurrence Relations for QCD Amplitudes,” *Nucl. Phys. B*, vol. 335, pp. 23–44, 1990. DOI: [10.1016/0550-3213\(90\)90167-C](https://doi.org/10.1016/0550-3213(90)90167-C).
- [130] R. Britto, F. Cachazo, B. Feng, and E. Witten, “Direct proof of tree-level recursion relation in Yang-Mills theory,” *Phys. Rev. Lett.*, vol. 94, p. 181602, 2005. DOI: [10.1103/PhysRevLett.94.181602](https://doi.org/10.1103/PhysRevLett.94.181602). arXiv: [hep-th/0501052](https://arxiv.org/abs/hep-th/0501052).
- [131] E. W. Nigel Glover and C. Williams, “One-Loop Gluonic Amplitudes from Single Unitarity Cuts,” *JHEP*, vol. 12, p. 067, 2008. DOI: [10.1088/1126-6708/2008/12/067](https://doi.org/10.1088/1126-6708/2008/12/067). arXiv: [0810.2964 \[hep-th\]](https://arxiv.org/abs/0810.2964).
- [132] I. Bierenbaum, S. Catani, P. Draggiotis, and G. Rodrigo, “A Tree-Loop Duality Relation at Two Loops and Beyond,” *JHEP*, vol. 10, p. 073, 2010. DOI: [10.1007/JHEP10\(2010\)073](https://doi.org/10.1007/JHEP10(2010)073). arXiv: [1007.0194 \[hep-ph\]](https://arxiv.org/abs/1007.0194).
- [133] H. Elvang, D. Z. Freedman, and M. Kiermaier, “Integrands for QCD rational terms and $N=4$ SYM from massive CSW rules,” *JHEP*, vol. 06, p. 015, 2012. DOI: [10.1007/JHEP06\(2012\)015](https://doi.org/10.1007/JHEP06(2012)015). arXiv: [1111.0635 \[hep-th\]](https://arxiv.org/abs/1111.0635).
- [134] S. Caron-Huot, “Loops and trees,” *JHEP*, vol. 05, p. 080, 2011. DOI: [10.1007/JHEP05\(2011\)080](https://doi.org/10.1007/JHEP05(2011)080). arXiv: [1007.3224 \[hep-ph\]](https://arxiv.org/abs/1007.3224).
- [135] N. Arkani-Hamed, J. L. Bourjaily, F. Cachazo, S. Caron-Huot, and J. Trnka, “The All-Loop Integrand For Scattering Amplitudes in Planar $N=4$ SYM,” *JHEP*, vol. 01, p. 041, 2011. DOI: [10.1007/JHEP01\(2011\)041](https://doi.org/10.1007/JHEP01(2011)041). arXiv: [1008.2958 \[hep-th\]](https://arxiv.org/abs/1008.2958).

- [136] S. J. Parke and T. R. Taylor, “Perturbative QCD Utilizing Extended Supersymmetry,” *Phys. Lett. B*, vol. 157, p. 81, 1985, [Erratum: *Phys.Lett.B* 174, 465 (1986)]. DOI: [10.1016/0370-2693\(85\)91216-X](https://doi.org/10.1016/0370-2693(85)91216-X).
- [137] Z. Kunszt, “Combined Use of the Calkul Method and N=1 Supersymmetry to Calculate QCD Six Parton Processes,” *Nucl. Phys. B*, vol. 271, pp. 333–348, 1986. DOI: [10.1016/0550-3213\(86\)90319-6](https://doi.org/10.1016/0550-3213(86)90319-6).
- [138] M. T. Grisaru, H. N. Pendleton, and P. van Nieuwenhuizen, “Supergravity and the S Matrix,” *Phys. Rev. D*, vol. 15, p. 996, 1977. DOI: [10.1103/PhysRevD.15.996](https://doi.org/10.1103/PhysRevD.15.996).
- [139] M. T. Grisaru and H. N. Pendleton, “Some Properties of Scattering Amplitudes in Supersymmetric Theories,” *Nucl. Phys. B*, vol. 124, pp. 81–92, 1977. DOI: [10.1016/0550-3213\(77\)90277-2](https://doi.org/10.1016/0550-3213(77)90277-2).
- [140] W. L. van Neerven and J. A. M. Vermaseren, “LARGE LOOP INTEGRALS,” *Phys. Lett. B*, vol. 137, pp. 241–244, 1984. DOI: [10.1016/0370-2693\(84\)90237-5](https://doi.org/10.1016/0370-2693(84)90237-5).
- [141] D. Melrose, “Reduction of feynman diagrams,” *Il Nuovo Cimento A (1965-1970)*, vol. 40, no. 1, pp. 181–213, 1965.
- [142] Z. Bern, L. J. Dixon, and D. A. Kosower, “Dimensionally regulated one loop integrals,” *Phys. Lett. B*, vol. 302, pp. 299–308, 1993, [Erratum: *Phys.Lett.B* 318, 649 (1993)]. DOI: [10.1016/0370-2693\(93\)90400-C](https://doi.org/10.1016/0370-2693(93)90400-C). arXiv: [hep-ph/9212308](https://arxiv.org/abs/hep-ph/9212308).
- [143] —, “Dimensionally regulated pentagon integrals,” *Nucl. Phys. B*, vol. 412, pp. 751–816, 1994. DOI: [10.1016/0550-3213\(94\)90398-0](https://doi.org/10.1016/0550-3213(94)90398-0). arXiv: [hep-ph/9306240](https://arxiv.org/abs/hep-ph/9306240).
- [144] L. M. Brown and R. P. Feynman, “Radiative corrections to Compton scattering,” *Phys. Rev.*, vol. 85, L. M. Brown, Ed., pp. 231–244, 1952. DOI: [10.1103/PhysRev.85.231](https://doi.org/10.1103/PhysRev.85.231).
- [145] G. Passarino and M. J. G. Veltman, “One Loop Corrections for e+ e- Annihilation Into mu+ mu- in the Weinberg Model,” *Nucl. Phys. B*, vol. 160, pp. 151–207, 1979. DOI: [10.1016/0550-3213\(79\)90234-7](https://doi.org/10.1016/0550-3213(79)90234-7).
- [146] G. ’t Hooft and M. J. G. Veltman, “Scalar One Loop Integrals,” *Nucl. Phys. B*, vol. 153, pp. 365–401, 1979. DOI: [10.1016/0550-3213\(79\)90605-9](https://doi.org/10.1016/0550-3213(79)90605-9).
- [147] G. J. van Oldenborgh and J. A. M. Vermaseren, “New Algorithms for One Loop Integrals,” *Z. Phys. C*, vol. 46, pp. 425–438, 1990. DOI: [10.1007/BF01621031](https://doi.org/10.1007/BF01621031).
- [148] R. K. Ellis and G. Zanderighi, “Scalar one-loop integrals for QCD,” *JHEP*, vol. 02, p. 002, 2008. DOI: [10.1088/1126-6708/2008/02/002](https://doi.org/10.1088/1126-6708/2008/02/002). arXiv: [0712.1851](https://arxiv.org/abs/0712.1851) [[hep-ph](https://arxiv.org/abs/hep-ph)].
- [149] Z. Bern, L. J. Dixon, and D. A. Kosower, “Progress in one loop QCD computations,” *Ann. Rev. Nucl. Part. Sci.*, vol. 46, pp. 109–148, 1996. DOI: [10.1146/annurev.nucl.46.1.109](https://doi.org/10.1146/annurev.nucl.46.1.109). arXiv: [hep-ph/9602280](https://arxiv.org/abs/hep-ph/9602280).

- [150] Z. Bern, L. J. Dixon, D. C. Dunbar, and D. A. Kosower, “One loop n point gauge theory amplitudes, unitarity and collinear limits,” *Nucl. Phys. B*, vol. 425, pp. 217–260, 1994. DOI: [10.1016/0550-3213\(94\)90179-1](https://doi.org/10.1016/0550-3213(94)90179-1). arXiv: [hep-ph/9403226](https://arxiv.org/abs/hep-ph/9403226).
- [151] ———, “Fusing gauge theory tree amplitudes into loop amplitudes,” *Nucl. Phys. B*, vol. 435, pp. 59–101, 1995. DOI: [10.1016/0550-3213\(94\)00488-Z](https://doi.org/10.1016/0550-3213(94)00488-Z). arXiv: [hep-ph/9409265](https://arxiv.org/abs/hep-ph/9409265).
- [152] R. Britto, F. Cachazo, and B. Feng, “Generalized unitarity and one-loop amplitudes in N=4 super-Yang-Mills,” *Nucl. Phys. B*, vol. 725, pp. 275–305, 2005. DOI: [10.1016/j.nuclphysb.2005.07.014](https://doi.org/10.1016/j.nuclphysb.2005.07.014). arXiv: [hep-th/0412103](https://arxiv.org/abs/hep-th/0412103).
- [153] R. Britto, B. Feng, and P. Mastrolia, “The Cut-constructible part of QCD amplitudes,” *Phys. Rev. D*, vol. 73, p. 105 004, 2006. DOI: [10.1103/PhysRevD.73.105004](https://doi.org/10.1103/PhysRevD.73.105004). arXiv: [hep-ph/0602178](https://arxiv.org/abs/hep-ph/0602178).
- [154] R. K. Ellis, D. A. Ross, and A. E. Terrano, “The Perturbative Calculation of Jet Structure in e+ e- Annihilation,” *Nucl. Phys. B*, vol. 178, pp. 421–456, 1981. DOI: [10.1016/0550-3213\(81\)90165-6](https://doi.org/10.1016/0550-3213(81)90165-6).
- [155] S. Catani and M. H. Seymour, “A General algorithm for calculating jet cross-sections in NLO QCD,” *Nucl. Phys. B*, vol. 485, pp. 291–419, 1997, [Erratum: *Nucl.Phys.B* 510, 503–504 (1998)]. DOI: [10.1016/S0550-3213\(96\)00589-5](https://doi.org/10.1016/S0550-3213(96)00589-5). arXiv: [hep-ph/9605323](https://arxiv.org/abs/hep-ph/9605323).
- [156] ———, “NLO calculations in QCD: A General algorithm,” *Nucl. Phys. B Proc. Suppl.*, vol. 51, J. Blumlein, F. Jegerlehner, and T. Riemann, Eds., pp. 233–242, 1996. DOI: [10.1016/S0920-5632\(96\)90030-4](https://doi.org/10.1016/S0920-5632(96)90030-4). arXiv: [hep-ph/9607318](https://arxiv.org/abs/hep-ph/9607318).
- [157] Z. Bern and Y.-t. Huang, “Basics of Generalized Unitarity,” *J. Phys. A*, vol. 44, p. 454 003, 2011. DOI: [10.1088/1751-8113/44/45/454003](https://doi.org/10.1088/1751-8113/44/45/454003). arXiv: [1103.1869](https://arxiv.org/abs/1103.1869) [[hep-th](https://arxiv.org/abs/hep-th)].
- [158] J. J. M. Carrasco and H. Johansson, “Generic multiloop methods and application to N=4 super-Yang-Mills,” *J. Phys. A*, vol. 44, p. 454 004, 2011. DOI: [10.1088/1751-8113/44/45/454004](https://doi.org/10.1088/1751-8113/44/45/454004). arXiv: [1103.3298](https://arxiv.org/abs/1103.3298) [[hep-th](https://arxiv.org/abs/hep-th)].
- [159] Z. Bern, L. J. Dixon, and D. A. Kosower, “Bootstrapping multi-parton loop amplitudes in QCD,” *Phys. Rev. D*, vol. 73, p. 065 013, 2006. DOI: [10.1103/PhysRevD.73.065013](https://doi.org/10.1103/PhysRevD.73.065013). arXiv: [hep-ph/0507005](https://arxiv.org/abs/hep-ph/0507005).
- [160] ———, “The last of the finite loop amplitudes in QCD,” *Phys. Rev. D*, vol. 72, p. 125 003, 2005. DOI: [10.1103/PhysRevD.72.125003](https://doi.org/10.1103/PhysRevD.72.125003). arXiv: [hep-ph/0505055](https://arxiv.org/abs/hep-ph/0505055).
- [161] D. Forde and D. A. Kosower, “All-multiplicity one-loop corrections to MHV amplitudes in QCD,” *Phys. Rev. D*, vol. 73, p. 061 701, 2006. DOI: [10.1103/PhysRevD.73.061701](https://doi.org/10.1103/PhysRevD.73.061701). arXiv: [hep-ph/0509358](https://arxiv.org/abs/hep-ph/0509358).
- [162] Z. Bern and A. G. Morgan, “Massive loop amplitudes from unitarity,” *Nucl. Phys. B*, vol. 467, pp. 479–509, 1996. DOI: [10.1016/0550-3213\(96\)00078-8](https://doi.org/10.1016/0550-3213(96)00078-8). arXiv: [hep-ph/9511336](https://arxiv.org/abs/hep-ph/9511336).

- [163] S. D. Badger, “Direct Extraction Of One Loop Rational Terms,” *JHEP*, vol. 01, p. 049, 2009. DOI: [10.1088/1126-6708/2009/01/049](https://doi.org/10.1088/1126-6708/2009/01/049). arXiv: [0806.4600](https://arxiv.org/abs/0806.4600) [[hep-ph](#)].
- [164] M. Argeri and P. Mastrolia, “Feynman Diagrams and Differential Equations,” *Int. J. Mod. Phys. A*, vol. 22, pp. 4375–4436, 2007. DOI: [10.1142/S0217751X07037147](https://doi.org/10.1142/S0217751X07037147). arXiv: [0707.4037](https://arxiv.org/abs/0707.4037) [[hep-ph](#)].
- [165] J. M. Henn, “Lectures on differential equations for Feynman integrals,” *J. Phys. A*, vol. 48, p. 153001, 2015. DOI: [10.1088/1751-8113/48/15/153001](https://doi.org/10.1088/1751-8113/48/15/153001). arXiv: [1412.2296](https://arxiv.org/abs/1412.2296) [[hep-ph](#)].
- [166] C. Bogner and S. Weinzierl, “Periods and Feynman integrals,” *J. Math. Phys.*, vol. 50, p. 042302, 2009. DOI: [10.1063/1.3106041](https://doi.org/10.1063/1.3106041). arXiv: [0711.4863](https://arxiv.org/abs/0711.4863) [[hep-th](#)].
- [167] A. B. Goncharov, M. Spradlin, C. Vergu, and A. Volovich, “Classical Polylogarithms for Amplitudes and Wilson Loops,” *Phys. Rev. Lett.*, vol. 105, p. 151605, 2010. DOI: [10.1103/PhysRevLett.105.151605](https://doi.org/10.1103/PhysRevLett.105.151605). arXiv: [1006.5703](https://arxiv.org/abs/1006.5703) [[hep-th](#)].
- [168] C. Duhr, H. Gangl, and J. R. Rhodes, “From polygons and symbols to polylogarithmic functions,” *JHEP*, vol. 10, p. 075, 2012. DOI: [10.1007/JHEP10\(2012\)075](https://doi.org/10.1007/JHEP10(2012)075). arXiv: [1110.0458](https://arxiv.org/abs/1110.0458) [[math-ph](#)].
- [169] M. Hidding and F. Moriello, “All orders structure and efficient computation of linearly reducible elliptic Feynman integrals,” *JHEP*, vol. 01, p. 169, 2019. DOI: [10.1007/JHEP01\(2019\)169](https://doi.org/10.1007/JHEP01(2019)169). arXiv: [1712.04441](https://arxiv.org/abs/1712.04441) [[hep-ph](#)].
- [170] M. Hentschinski, “Chapter 11: Lipatov’s QCD High Energy Effective Action: Past and Future,” in *From the Past to the Future*, J. Bartels, V. Fadin, E. Levin, A. Levy, V. Kim, and A. Sabio-Vera, Eds. 2021, pp. 283–310. DOI: [10.1142/9789811231124_0011](https://doi.org/10.1142/9789811231124_0011). arXiv: [2010.14748](https://arxiv.org/abs/2010.14748) [[hep-ph](#)].
- [171] L. N. Lipatov, “Gauge invariant effective action for high-energy processes in QCD,” *Nucl. Phys. B*, vol. 452, pp. 369–400, 1995. DOI: [10.1016/0550-3213\(95\)00390-E](https://doi.org/10.1016/0550-3213(95)00390-E). arXiv: [hep-ph/9502308](https://arxiv.org/abs/hep-ph/9502308).
- [172] —, “Small x physics in perturbative QCD,” *Phys. Rept.*, vol. 286, pp. 131–198, 1997. DOI: [10.1016/S0370-1573\(96\)00045-2](https://doi.org/10.1016/S0370-1573(96)00045-2). arXiv: [hep-ph/9610276](https://arxiv.org/abs/hep-ph/9610276).
- [173] L. N. Lipatov and M. I. Vyzovsky, “QuasimultiRegge processes with a quark exchange in the t channel,” *Nucl. Phys. B*, vol. 597, pp. 399–409, 2001. DOI: [10.1016/S0550-3213\(00\)00709-4](https://doi.org/10.1016/S0550-3213(00)00709-4). arXiv: [hep-ph/0009340](https://arxiv.org/abs/hep-ph/0009340).
- [174] M. Nefedov and V. Saleev, “On the one-loop calculations with Reggeized quarks,” *Mod. Phys. Lett. A*, vol. 32, no. 40, p. 1750207, 2017. DOI: [10.1142/S0217732317502078](https://doi.org/10.1142/S0217732317502078). arXiv: [1709.06246](https://arxiv.org/abs/1709.06246) [[hep-th](#)].
- [175] M. A. Nefedov, “Computing one-loop corrections to effective vertices with two scales in the EFT for Multi-Regge processes in QCD,” *Nucl. Phys. B*, vol. 946, p. 114715, 2019. DOI: [10.1016/j.nuclphysb.2019.114715](https://doi.org/10.1016/j.nuclphysb.2019.114715). arXiv: [1902.11030](https://arxiv.org/abs/1902.11030) [[hep-ph](#)].

- [176] J. Collins, *Foundations of perturbative QCD*. Cambridge University Press, Nov. 2013, vol. 32, ISBN: 978-1-107-64525-7, 978-1-107-64525-7, 978-0-521-85533-4, 978-1-139-09782-6.
- [177] ———, “New definition of TMD parton densities,” *Int. J. Mod. Phys. Conf. Ser.*, vol. 4, I. Balitsky, A. Prokudin, and A. Radyushkin, Eds., pp. 85–96, 2011. DOI: [10.1142/S2010194511001590](https://doi.org/10.1142/S2010194511001590). arXiv: [1107.4123](https://arxiv.org/abs/1107.4123) [[hep-ph](#)].
- [178] M. G. Echevarria, I. Scimemi, and A. Vladimirov, “Universal transverse momentum dependent soft function at NNLO,” *Phys. Rev. D*, vol. 93, no. 5, p. 054004, 2016. DOI: [10.1103/PhysRevD.93.054004](https://doi.org/10.1103/PhysRevD.93.054004). arXiv: [1511.05590](https://arxiv.org/abs/1511.05590) [[hep-ph](#)].
- [179] M. Hentschinski and A. Sabio Vera, “NLO jet vertex from Lipatov’s QCD effective action,” *Phys. Rev. D*, vol. 85, p. 056006, 2012. DOI: [10.1103/PhysRevD.85.056006](https://doi.org/10.1103/PhysRevD.85.056006). arXiv: [1110.6741](https://arxiv.org/abs/1110.6741) [[hep-ph](#)].
- [180] G. Chachamis, M. Hentschinski, J. D. Madrigal Martinez, and A. Sabio Vera, “Next-to-leading order corrections to the gluon-induced forward jet vertex from the high energy effective action,” *Phys. Rev. D*, vol. 87, no. 7, p. 076009, 2013. DOI: [10.1103/PhysRevD.87.076009](https://doi.org/10.1103/PhysRevD.87.076009). arXiv: [1212.4992](https://arxiv.org/abs/1212.4992) [[hep-ph](#)].
- [181] G. Chachamis, M. Hentschinski, J. D. Madrigal Martinez, and A. Sabio Vera, “Quark contribution to the gluon Regge trajectory at NLO from the high energy effective action,” *Nucl. Phys. B*, vol. 861, pp. 133–144, 2012. DOI: [10.1016/j.nuclphysb.2012.03.015](https://doi.org/10.1016/j.nuclphysb.2012.03.015). arXiv: [1202.0649](https://arxiv.org/abs/1202.0649) [[hep-ph](#)].
- [182] M. Nefedov, “One-loop corrections to multiscale effective vertices in the eft for multi-regge processes in qcd,” 2019. arXiv: [1905.01105](https://arxiv.org/abs/1905.01105).
- [183] M. Hentschinski, J. D. Madrigal Martinez, B. Murdaca, and A. Sabio Vera, “The next-to-leading order vertex for a forward jet plus a rapidity gap at high energies,” *Phys. Lett. B*, vol. 735, pp. 168–172, 2014. DOI: [10.1016/j.physletb.2014.06.022](https://doi.org/10.1016/j.physletb.2014.06.022). arXiv: [1404.2937](https://arxiv.org/abs/1404.2937) [[hep-ph](#)].
- [184] M. A. Nefedov, “Towards stability of NLO corrections in High-Energy Factorization via Modified Multi-Regge Kinematics approximation,” *JHEP*, vol. 08, p. 055, 2020. DOI: [10.1007/JHEP08\(2020\)055](https://doi.org/10.1007/JHEP08(2020)055). arXiv: [2003.02194](https://arxiv.org/abs/2003.02194) [[hep-ph](#)].
- [185] M. Hentschinski, K. Kutak, and A. van Hameren, “Forward Higgs production within high energy factorization in the heavy quark limit at next-to-leading order accuracy,” *Eur. Phys. J. C*, vol. 81, no. 2, p. 112, 2021, [Erratum: *Eur.Phys.J.C* 81, 262 (2021)]. DOI: [10.1140/epjc/s10052-021-08902-6](https://doi.org/10.1140/epjc/s10052-021-08902-6). arXiv: [2011.03193](https://arxiv.org/abs/2011.03193) [[hep-ph](#)].
- [186] A. van Hameren, P. Kotko, and K. Kutak, “Multi-gluon helicity amplitudes with one off-shell leg within high energy factorization,” *JHEP*, vol. 12, p. 029, 2012. DOI: [10.1007/JHEP12\(2012\)029](https://doi.org/10.1007/JHEP12(2012)029). arXiv: [1207.3332](https://arxiv.org/abs/1207.3332) [[hep-ph](#)].
- [187] A. van Hameren, P. Kotko, and K. Kutak, “Helicity amplitudes for high-energy scattering,” *JHEP*, vol. 01, p. 078, 2013. DOI: [10.1007/JHEP01\(2013\)078](https://doi.org/10.1007/JHEP01(2013)078). arXiv: [1211.0961](https://arxiv.org/abs/1211.0961) [[hep-ph](#)].

- [188] A. van Hameren, “BCFW recursion for off-shell gluons,” *JHEP*, vol. 07, p. 138, 2014. DOI: [10.1007/JHEP07\(2014\)138](https://doi.org/10.1007/JHEP07(2014)138). arXiv: [1404.7818](https://arxiv.org/abs/1404.7818) [[hep-ph](#)].
- [189] A. van Hameren and M. Serino, “BCFW recursion for TMD parton scattering,” *JHEP*, vol. 07, p. 010, 2015. DOI: [10.1007/JHEP07\(2015\)010](https://doi.org/10.1007/JHEP07(2015)010). arXiv: [1504.00315](https://arxiv.org/abs/1504.00315) [[hep-ph](#)].
- [190] S. Catani, M. Ciafaloni, and F. Hautmann, “Small x structure functions and heavy flavor production,” *Nucl. Phys. B Proc. Suppl.*, vol. 18, pp. 220–225, 1991. DOI: [10.1016/0920-5632\(91\)90109-R](https://doi.org/10.1016/0920-5632(91)90109-R).
- [191] ———, “High-energy factorization in QCD and minimal subtraction scheme,” *Phys. Lett. B*, vol. 307, pp. 147–153, 1993. DOI: [10.1016/0370-2693\(93\)90204-U](https://doi.org/10.1016/0370-2693(93)90204-U).
- [192] P. Kotko, “Wilson lines and gauge invariant off-shell amplitudes,” *JHEP*, vol. 07, p. 128, 2014. DOI: [10.1007/JHEP07\(2014\)128](https://doi.org/10.1007/JHEP07(2014)128). arXiv: [1403.4824](https://arxiv.org/abs/1403.4824) [[hep-ph](#)].
- [193] E. Antonov, I. Cherednikov, E. Kuraev, and L. Lipatov, “Feynman rules for effective regge action,” *Nuclear Physics B*, vol. 721, no. 1-3, pp. 111–135, 2005.
- [194] A. van Hameren, “Calculating off-shell one-loop amplitudes for k_T -dependent factorization: a proof of concept,” 2017. arXiv: [1710.07609](https://arxiv.org/abs/1710.07609) [[hep-ph](#)].
- [195] A. van Hameren, K. Kutak, and T. Salwa, “Scattering amplitudes with off-shell quarks,” *Phys. Lett. B*, vol. 727, pp. 226–233, 2013. DOI: [10.1016/j.physletb.2013.10.039](https://doi.org/10.1016/j.physletb.2013.10.039). arXiv: [1308.2861](https://arxiv.org/abs/1308.2861) [[hep-ph](#)].
- [196] A. Van Hameren, “One-loop amplitudes for k_T -dependent factorization,” *PoS*, vol. LL2018, p. 055, 2018. DOI: [10.22323/1.303.0055](https://doi.org/10.22323/1.303.0055). arXiv: [1807.05930](https://arxiv.org/abs/1807.05930) [[hep-ph](#)].
- [197] Z. Bern, L. Dixon, and D. A. Kosower, “One-loop corrections to five-gluon amplitudes,” *Physical Review Letters*, vol. 70, no. 18, p. 2677, 1993.
- [198] Z. Bern, L. J. Dixon, and D. A. Kosower, “Last of the finite loop amplitudes in qcd,” *Physical Review D*, vol. 72, no. 12, p. 125 003, 2005.
- [199] P. Kotko, K. Kutak, C. Marquet, E. Petreska, S. Sapeta, and A. van Hameren, “Improved TMD factorization for forward dijet production in dilute-dense hadronic collisions,” *JHEP*, vol. 09, p. 106, 2015. DOI: [10.1007/JHEP09\(2015\)106](https://doi.org/10.1007/JHEP09(2015)106). arXiv: [1503.03421](https://arxiv.org/abs/1503.03421) [[hep-ph](#)].
- [200] T. Altinoluk, R. Boussarie, and P. Kotko, “Interplay of the CGC and TMD frameworks to all orders in kinematic twist,” *JHEP*, vol. 05, p. 156, 2019. DOI: [10.1007/JHEP05\(2019\)156](https://doi.org/10.1007/JHEP05(2019)156). arXiv: [1901.01175](https://arxiv.org/abs/1901.01175) [[hep-ph](#)].
- [201] G. F. Sterman and S. Weinberg, “Jets from Quantum Chromodynamics,” *Phys. Rev. Lett.*, vol. 39, p. 1436, 1977. DOI: [10.1103/PhysRevLett.39.1436](https://doi.org/10.1103/PhysRevLett.39.1436).
- [202] S. Catani, Y. L. Dokshitzer, M. Olsson, G. Turnock, and B. R. Webber, “New clustering algorithm for multi - jet cross-sections in $e^+ e^-$ annihilation,” *Phys. Lett. B*, vol. 269, pp. 432–438, 1991. DOI: [10.1016/0370-2693\(91\)90196-W](https://doi.org/10.1016/0370-2693(91)90196-W).

- [203] S. Catani, Y. L. Dokshitzer, M. H. Seymour, and B. R. Webber, “Longitudinally invariant K_t clustering algorithms for hadron hadron collisions,” *Nucl. Phys. B*, vol. 406, pp. 187–224, 1993. DOI: [10.1016/0550-3213\(93\)90166-M](https://doi.org/10.1016/0550-3213(93)90166-M).
- [204] S. D. Ellis and D. E. Soper, “Successive combination jet algorithm for hadron collisions,” *Phys. Rev. D*, vol. 48, pp. 3160–3166, 1993. DOI: [10.1103/PhysRevD.48.3160](https://doi.org/10.1103/PhysRevD.48.3160). arXiv: [hep-ph/9305266](https://arxiv.org/abs/hep-ph/9305266).
- [205] Y. L. Dokshitzer, G. D. Leder, S. Moretti, and B. R. Webber, “Better jet clustering algorithms,” *JHEP*, vol. 08, p. 001, 1997. DOI: [10.1088/1126-6708/1997/08/001](https://doi.org/10.1088/1126-6708/1997/08/001). arXiv: [hep-ph/9707323](https://arxiv.org/abs/hep-ph/9707323).
- [206] M. Wobisch and T. Wengler, “Hadronization corrections to jet cross-sections in deep inelastic scattering,” in *Workshop on Monte Carlo Generators for HERA Physics (Plenary Starting Meeting)*, Apr. 1998, pp. 270–279. arXiv: [hep-ph/9907280](https://arxiv.org/abs/hep-ph/9907280).
- [207] M. Cacciari, G. P. Salam, and G. Soyez, “The Catchment Area of Jets,” *JHEP*, vol. 04, p. 005, 2008. DOI: [10.1088/1126-6708/2008/04/005](https://doi.org/10.1088/1126-6708/2008/04/005). arXiv: [0802.1188 \[hep-ph\]](https://arxiv.org/abs/0802.1188).
- [208] —, “The anti- k_t jet clustering algorithm,” *JHEP*, vol. 04, p. 063, 2008. DOI: [10.1088/1126-6708/2008/04/063](https://doi.org/10.1088/1126-6708/2008/04/063). arXiv: [0802.1189 \[hep-ph\]](https://arxiv.org/abs/0802.1189).
- [209] —, “FastJet User Manual,” *Eur. Phys. J. C*, vol. 72, p. 1896, 2012. DOI: [10.1140/epjc/s10052-012-1896-2](https://doi.org/10.1140/epjc/s10052-012-1896-2). arXiv: [1111.6097 \[hep-ph\]](https://arxiv.org/abs/1111.6097).
- [210] M. Cacciari and G. P. Salam, “Dispelling the N^3 myth for the k_t jet-finder,” *Phys. Lett. B*, vol. 641, pp. 57–61, 2006. DOI: [10.1016/j.physletb.2006.08.037](https://doi.org/10.1016/j.physletb.2006.08.037). arXiv: [hep-ph/0512210](https://arxiv.org/abs/hep-ph/0512210).
- [211] S. Weinzierl, “The SIScone jet algorithm optimised for low particle multiplicities,” *Comput. Phys. Commun.*, vol. 183, pp. 813–820, 2012. DOI: [10.1016/j.cpc.2011.12.007](https://doi.org/10.1016/j.cpc.2011.12.007). arXiv: [1108.1934 \[hep-ph\]](https://arxiv.org/abs/1108.1934).
- [212] K. Aamodt *et al.*, “Suppression of Charged Particle Production at Large Transverse Momentum in Central Pb-Pb Collisions at $\sqrt{s_{NN}} = 2.76$ TeV,” *Phys. Lett. B*, vol. 696, pp. 30–39, 2011. DOI: [10.1016/j.physletb.2010.12.020](https://doi.org/10.1016/j.physletb.2010.12.020). arXiv: [1012.1004 \[nucl-ex\]](https://arxiv.org/abs/1012.1004).
- [213] G. Aad *et al.*, “Observation of a Centrality-Dependent Dijet Asymmetry in Lead-Lead Collisions at $\sqrt{s_{NN}} = 2.77$ TeV with the ATLAS Detector at the LHC,” *Phys. Rev. Lett.*, vol. 105, p. 252303, 2010. DOI: [10.1103/PhysRevLett.105.252303](https://doi.org/10.1103/PhysRevLett.105.252303). arXiv: [1011.6182 \[hep-ex\]](https://arxiv.org/abs/1011.6182).
- [214] S. Chatrchyan *et al.*, “Observation and studies of jet quenching in PbPb collisions at nucleon-nucleon center-of-mass energy = 2.76 TeV,” *Phys. Rev. C*, vol. 84, p. 024906, 2011. DOI: [10.1103/PhysRevC.84.024906](https://doi.org/10.1103/PhysRevC.84.024906). arXiv: [1102.1957 \[nucl-ex\]](https://arxiv.org/abs/1102.1957).

- [215] ———, “Jet momentum dependence of jet quenching in PbPb collisions at $\sqrt{s_{NN}} = 2.76$ TeV,” *Phys. Lett. B*, vol. 712, pp. 176–197, 2012. DOI: [10.1016/j.physletb.2012.04.058](https://doi.org/10.1016/j.physletb.2012.04.058). arXiv: [1202.5022](https://arxiv.org/abs/1202.5022) [[nucl-ex](#)].
- [216] J. Putschke, “First fragmentation function measurements from full jet reconstruction in heavy-ion collisions at $s(NN)^{1/2} = 200$ -GeV by STAR,” *Eur. Phys. J. C*, vol. 61, N. Armesto, C. Pajares, C. A. Salgado, and U. A. Wiedemann, Eds., pp. 629–635, 2009. DOI: [10.1140/epjc/s10052-009-0904-7](https://doi.org/10.1140/epjc/s10052-009-0904-7). arXiv: [0809.1419](https://arxiv.org/abs/0809.1419) [[nucl-ex](#)].
- [217] S. Salur, “First Direct Measurement of Jets in $s(NN)^{1/2} = 200$ -GeV Heavy Ion Collisions by STAR,” *Eur. Phys. J. C*, vol. 61, N. Armesto, C. Pajares, C. A. Salgado, and U. A. Wiedemann, Eds., pp. 761–767, 2009. DOI: [10.1140/epjc/s10052-009-0880-y](https://doi.org/10.1140/epjc/s10052-009-0880-y). arXiv: [0809.1609](https://arxiv.org/abs/0809.1609) [[nucl-ex](#)].
- [218] Y.-S. Lai, “Probing medium-induced energy loss with direct jet reconstruction in p+p and Cu+Cu collisions at PHENIX,” *Nucl. Phys. A*, vol. 830, P. Stankus, D. Silvermyr, S. Sorensen, and V. Greene, Eds., pp. 251C–254C, 2009. DOI: [10.1016/j.nuclphysa.2009.10.139](https://doi.org/10.1016/j.nuclphysa.2009.10.139). arXiv: [0907.4725](https://arxiv.org/abs/0907.4725) [[nucl-ex](#)].
- [219] “Searches for dijet resonances in pp collisions at $\sqrt{s} = 13$ TeV using the 2016 and 2017 datasets,” CERN, Geneva, Tech. Rep., 2018. [Online]. Available: <https://cds.cern.ch/record/2637847>.
- [220] C. CMS, “CMS collision events: from lead ion collisions,” CMS Collection., Nov. 2010. [Online]. Available: <http://cds.cern.ch/record/1309898>.
- [221] J. C. Collins and M. J. Perry, “Superdense Matter: Neutrons Or Asymptotically Free Quarks?” *Phys. Rev. Lett.*, vol. 34, p. 1353, 1975. DOI: [10.1103/PhysRevLett.34.1353](https://doi.org/10.1103/PhysRevLett.34.1353).
- [222] D. GSI Helmholtzzentrum für Schwerionenforschung GmbH. (), [Online]. Available: www.gsi.de/en/start/fair/forschung_an_fair/kernmateriephysik.htm.
- [223] J. Casalderrey-Solana and C. A. Salgado, “Introductory lectures on jet quenching in heavy ion collisions,” *Acta Phys. Polon. B*, vol. 38, M. Praszalowicz, M. Kutschera, and E. Malec, Eds., pp. 3731–3794, 2007. arXiv: [0712.3443](https://arxiv.org/abs/0712.3443) [[hep-ph](#)].
- [224] J. D. Bjorken, “Energy Loss of Energetic Partons in Quark - Gluon Plasma: Possible Extinction of High p(t) Jets in Hadron - Hadron Collisions,” Aug. 1982.
- [225] S. Jeon and G. D. Moore, “Energy loss of leading partons in a thermal QCD medium,” *Phys. Rev. C*, vol. 71, p. 034901, 2005. DOI: [10.1103/PhysRevC.71.034901](https://doi.org/10.1103/PhysRevC.71.034901). arXiv: [hep-ph/0309332](https://arxiv.org/abs/hep-ph/0309332).
- [226] A. Peshier, “The QCD collisional energy loss revised,” *Phys. Rev. Lett.*, vol. 97, p. 212301, 2006. DOI: [10.1103/PhysRevLett.97.212301](https://doi.org/10.1103/PhysRevLett.97.212301). arXiv: [hep-ph/0605294](https://arxiv.org/abs/hep-ph/0605294).

- [227] S. Peigne, P.-B. Gossiaux, and T. Gousset, “Retardation effect for collisional energy loss of hard partons produced in a QGP,” *JHEP*, vol. 04, p. 011, 2006. DOI: [10.1088/1126-6708/2006/04/011](https://doi.org/10.1088/1126-6708/2006/04/011). arXiv: [hep-ph/0509185](https://arxiv.org/abs/hep-ph/0509185).
- [228] M. Djordjevic, “Collisional energy loss in a finite size QCD matter,” *Phys. Rev. C*, vol. 74, p. 064907, 2006. DOI: [10.1103/PhysRevC.74.064907](https://doi.org/10.1103/PhysRevC.74.064907). arXiv: [nucl-th/0603066](https://arxiv.org/abs/nucl-th/0603066).
- [229] S. Peigne and A. Peshier, “Collisional energy loss of a fast heavy quark in a quark-gluon plasma,” *Phys. Rev. D*, vol. 77, p. 114017, 2008. DOI: [10.1103/PhysRevD.77.114017](https://doi.org/10.1103/PhysRevD.77.114017). arXiv: [0802.4364 \[hep-ph\]](https://arxiv.org/abs/0802.4364).
- [230] L. D. Landau and I. Pomeranchuk, “Limits of applicability of the theory of bremsstrahlung electrons and pair production at high-energies,” *Dokl. Akad. Nauk Ser. Fiz.*, vol. 92, pp. 535–536, 1953.
- [231] A. B. Migdal, “Bremsstrahlung and pair production in condensed media at high-energies,” *Phys. Rev.*, vol. 103, pp. 1811–1820, 1956. DOI: [10.1103/PhysRev.103.1811](https://doi.org/10.1103/PhysRev.103.1811).
- [232] H. Bethe and W. Heitler, “On the Stopping of fast particles and on the creation of positive electrons,” *Proc. Roy. Soc. Lond. A*, vol. 146, pp. 83–112, 1934. DOI: [10.1098/rspa.1934.0140](https://doi.org/10.1098/rspa.1934.0140).
- [233] R. Baier, Y. L. Dokshitzer, A. H. Mueller, S. Peigne, and D. Schiff, “Radiative energy loss of high-energy quarks and gluons in a finite volume quark - gluon plasma,” *Nucl. Phys. B*, vol. 483, pp. 291–320, 1997. DOI: [10.1016/S0550-3213\(96\)00553-6](https://doi.org/10.1016/S0550-3213(96)00553-6). arXiv: [hep-ph/9607355](https://arxiv.org/abs/hep-ph/9607355).
- [234] —, “Radiative energy loss and $p(T)$ broadening of high-energy partons in nuclei,” *Nucl. Phys. B*, vol. 484, pp. 265–282, 1997. DOI: [10.1016/S0550-3213\(96\)00581-0](https://doi.org/10.1016/S0550-3213(96)00581-0). arXiv: [hep-ph/9608322](https://arxiv.org/abs/hep-ph/9608322).
- [235] B. G. Zakharov, “Fully quantum treatment of the Landau-Pomeranchuk-Migdal effect in QED and QCD,” *JETP Lett.*, vol. 63, pp. 952–957, 1996. DOI: [10.1134/1.567126](https://doi.org/10.1134/1.567126). arXiv: [hep-ph/9607440](https://arxiv.org/abs/hep-ph/9607440).
- [236] —, “Radiative energy loss of high-energy quarks in finite size nuclear matter and quark - gluon plasma,” *JETP Lett.*, vol. 65, pp. 615–620, 1997. DOI: [10.1134/1.567389](https://doi.org/10.1134/1.567389). arXiv: [hep-ph/9704255](https://arxiv.org/abs/hep-ph/9704255).
- [237] R. Baier, Y. L. Dokshitzer, A. H. Mueller, and D. Schiff, “Medium induced radiative energy loss: Equivalence between the BDMPS and Zakharov formalisms,” *Nucl. Phys. B*, vol. 531, pp. 403–425, 1998. DOI: [10.1016/S0550-3213\(98\)00546-X](https://doi.org/10.1016/S0550-3213(98)00546-X). arXiv: [hep-ph/9804212](https://arxiv.org/abs/hep-ph/9804212).
- [238] U. A. Wiedemann, “Transverse dynamics of hard partons in nuclear media and the QCD dipole,” *Nucl. Phys. B*, vol. 582, pp. 409–450, 2000. DOI: [10.1016/S0550-3213\(00\)00286-8](https://doi.org/10.1016/S0550-3213(00)00286-8). arXiv: [hep-ph/0003021](https://arxiv.org/abs/hep-ph/0003021).

- [239] —, “Gluon radiation off hard quarks in a nuclear environment: Opacity expansion,” *Nucl. Phys. B*, vol. 588, pp. 303–344, 2000. DOI: [10.1016/S0550-3213\(00\)00457-0](https://doi.org/10.1016/S0550-3213(00)00457-0). arXiv: [hep-ph/0005129](https://arxiv.org/abs/hep-ph/0005129).
- [240] —, “Jet quenching versus jet enhancement: A Quantitative study of the BDMPS-Z gluon radiation spectrum,” *Nucl. Phys. A*, vol. 690, pp. 731–751, 2001. DOI: [10.1016/S0375-9474\(01\)00362-1](https://doi.org/10.1016/S0375-9474(01)00362-1). arXiv: [hep-ph/0008241](https://arxiv.org/abs/hep-ph/0008241).
- [241] C. A. Salgado and U. A. Wiedemann, “Calculating quenching weights,” *Phys. Rev. D*, vol. 68, p. 014008, 2003. DOI: [10.1103/PhysRevD.68.014008](https://doi.org/10.1103/PhysRevD.68.014008). arXiv: [hep-ph/0302184](https://arxiv.org/abs/hep-ph/0302184).
- [242] N. Armesto, C. A. Salgado, and U. A. Wiedemann, “Medium induced gluon radiation off massive quarks fills the dead cone,” *Phys. Rev. D*, vol. 69, p. 114003, 2004. DOI: [10.1103/PhysRevD.69.114003](https://doi.org/10.1103/PhysRevD.69.114003). arXiv: [hep-ph/0312106](https://arxiv.org/abs/hep-ph/0312106).
- [243] M. Gyulassy, P. Levai, and I. Vitev, “Jet quenching in thin quark gluon plasmas. 1. Formalism,” *Nucl. Phys. B*, vol. 571, pp. 197–233, 2000. DOI: [10.1016/S0550-3213\(99\)00713-0](https://doi.org/10.1016/S0550-3213(99)00713-0). arXiv: [hep-ph/9907461](https://arxiv.org/abs/hep-ph/9907461).
- [244] M. Gyulassy, P. Levai, and I. Vitev, “NonAbelian energy loss at finite opacity,” *Phys. Rev. Lett.*, vol. 85, pp. 5535–5538, 2000. DOI: [10.1103/PhysRevLett.85.5535](https://doi.org/10.1103/PhysRevLett.85.5535). arXiv: [nucl-th/0005032](https://arxiv.org/abs/nucl-th/0005032).
- [245] —, “Reaction operator approach to nonAbelian energy loss,” *Nucl. Phys. B*, vol. 594, pp. 371–419, 2001. DOI: [10.1016/S0550-3213\(00\)00652-0](https://doi.org/10.1016/S0550-3213(00)00652-0). arXiv: [nucl-th/0006010](https://arxiv.org/abs/nucl-th/0006010).
- [246] —, “Jet tomography of Au+Au reactions including multigluon fluctuations,” *Phys. Lett. B*, vol. 538, pp. 282–288, 2002. DOI: [10.1016/S0370-2693\(02\)01990-1](https://doi.org/10.1016/S0370-2693(02)01990-1). arXiv: [nucl-th/0112071](https://arxiv.org/abs/nucl-th/0112071).
- [247] P. B. Arnold, G. D. Moore, and L. G. Yaffe, “Photon emission from ultrarelativistic plasmas,” *JHEP*, vol. 11, p. 057, 2001. DOI: [10.1088/1126-6708/2001/11/057](https://doi.org/10.1088/1126-6708/2001/11/057). arXiv: [hep-ph/0109064](https://arxiv.org/abs/hep-ph/0109064).
- [248] —, “Photon emission from quark gluon plasma: Complete leading order results,” *JHEP*, vol. 12, p. 009, 2001. DOI: [10.1088/1126-6708/2001/12/009](https://doi.org/10.1088/1126-6708/2001/12/009). arXiv: [hep-ph/0111107](https://arxiv.org/abs/hep-ph/0111107).
- [249] —, “Photon and gluon emission in relativistic plasmas,” *JHEP*, vol. 06, p. 030, 2002. DOI: [10.1088/1126-6708/2002/06/030](https://doi.org/10.1088/1126-6708/2002/06/030). arXiv: [hep-ph/0204343](https://arxiv.org/abs/hep-ph/0204343).
- [250] X.-F. Guo and X.-N. Wang, “Multiple scattering, parton energy loss and modified fragmentation functions in deeply inelastic e A scattering,” *Phys. Rev. Lett.*, vol. 85, pp. 3591–3594, 2000. DOI: [10.1103/PhysRevLett.85.3591](https://doi.org/10.1103/PhysRevLett.85.3591). arXiv: [hep-ph/0005044](https://arxiv.org/abs/hep-ph/0005044).
- [251] X.-N. Wang and X.-f. Guo, “Multiple parton scattering in nuclei: Parton energy loss,” *Nucl. Phys. A*, vol. 696, pp. 788–832, 2001. DOI: [10.1016/S0375-9474\(01\)01130-7](https://doi.org/10.1016/S0375-9474(01)01130-7). arXiv: [hep-ph/0102230](https://arxiv.org/abs/hep-ph/0102230).

- [252] B.-W. Zhang and X.-N. Wang, “Multiple parton scattering in nuclei: Beyond helicity amplitude approximation,” *Nucl. Phys. A*, vol. 720, pp. 429–451, 2003. DOI: [10.1016/S0375-9474\(03\)01003-0](https://doi.org/10.1016/S0375-9474(03)01003-0). arXiv: [hep-ph/0301195](https://arxiv.org/abs/hep-ph/0301195).
- [253] A. Majumder, R. J. Fries, and B. Muller, “Photon bremsstrahlung and diffusive broadening of a hard jet,” *Phys. Rev. C*, vol. 77, p. 065 209, 2008. DOI: [10.1103/PhysRevC.77.065209](https://doi.org/10.1103/PhysRevC.77.065209). arXiv: [0711.2475](https://arxiv.org/abs/0711.2475) [[nucl-th](#)].
- [254] A. Majumder, “Hard collinear gluon radiation and multiple scattering in a medium,” *Phys. Rev. D*, vol. 85, p. 014 023, 2012. DOI: [10.1103/PhysRevD.85.014023](https://doi.org/10.1103/PhysRevD.85.014023). arXiv: [0912.2987](https://arxiv.org/abs/0912.2987) [[nucl-th](#)].
- [255] N. Armesto *et al.*, “Comparison of Jet Quenching Formalisms for a Quark-Gluon Plasma ‘Brick’,” *Phys. Rev. C*, vol. 86, p. 064 904, 2012. DOI: [10.1103/PhysRevC.86.064904](https://doi.org/10.1103/PhysRevC.86.064904). arXiv: [1106.1106](https://arxiv.org/abs/1106.1106) [[hep-ph](#)].
- [256] R. Baier, D. Schiff, and B. G. Zakharov, “Energy loss in perturbative QCD,” *Ann. Rev. Nucl. Part. Sci.*, vol. 50, pp. 37–69, 2000. DOI: [10.1146/annurev.nucl.50.1.37](https://doi.org/10.1146/annurev.nucl.50.1.37). arXiv: [hep-ph/0002198](https://arxiv.org/abs/hep-ph/0002198).
- [257] M. Gyulassy, I. Vitev, X.-N. Wang, and B.-W. Zhang, “Jet quenching and radiative energy loss in dense nuclear matter,” R. C. Hwa and X. N. Wang, Eds., pp. 123–191, 2004. DOI: [10.1142/9789812795533_0003](https://doi.org/10.1142/9789812795533_0003). arXiv: [nuc1-th/0302077](https://arxiv.org/abs/nuc1-th/0302077).
- [258] J.-P. Blaizot, F. Dominguez, E. Iancu, and Y. Mehtar-Tani, “Medium-induced gluon branching,” *JHEP*, vol. 01, p. 143, 2013. DOI: [10.1007/JHEP01\(2013\)143](https://doi.org/10.1007/JHEP01(2013)143). arXiv: [1209.4585](https://arxiv.org/abs/1209.4585) [[hep-ph](#)].
- [259] Y. Mehtar-Tani, “Relating the description of gluon production in pA collisions and parton energy loss in AA collisions,” *Phys. Rev. C*, vol. 75, p. 034 908, 2007. DOI: [10.1103/PhysRevC.75.034908](https://doi.org/10.1103/PhysRevC.75.034908). arXiv: [hep-ph/0606236](https://arxiv.org/abs/hep-ph/0606236).
- [260] J. P. Blaizot, F. Gelis, and R. Venugopalan, “High-energy pA collisions in the color glass condensate approach. 1. Gluon production and the Cronin effect,” *Nucl. Phys. A*, vol. 743, pp. 13–56, 2004. DOI: [10.1016/j.nuclphysa.2004.07.005](https://doi.org/10.1016/j.nuclphysa.2004.07.005). arXiv: [hep-ph/0402256](https://arxiv.org/abs/hep-ph/0402256).
- [261] M. Gyulassy and X.-n. Wang, “Multiple collisions and induced gluon Bremsstrahlung in QCD,” *Nucl. Phys. B*, vol. 420, pp. 583–614, 1994. DOI: [10.1016/0550-3213\(94\)90079-5](https://doi.org/10.1016/0550-3213(94)90079-5). arXiv: [nuc1-th/9306003](https://arxiv.org/abs/nuc1-th/9306003).
- [262] J.-P. Blaizot, F. Dominguez, E. Iancu, and Y. Mehtar-Tani, “Probabilistic picture for medium-induced jet evolution,” *JHEP*, vol. 06, p. 075, 2014. DOI: [10.1007/JHEP06\(2014\)075](https://doi.org/10.1007/JHEP06(2014)075). arXiv: [1311.5823](https://arxiv.org/abs/1311.5823) [[hep-ph](#)].
- [263] P. Arnold and S. Iqbal, “The LPM effect in sequential bremsstrahlung,” *JHEP*, vol. 04, p. 070, 2015, [Erratum: *JHEP* 09, 072 (2016)]. DOI: [10.1007/JHEP09\(2016\)072](https://doi.org/10.1007/JHEP09(2016)072). arXiv: [1501.04964](https://arxiv.org/abs/1501.04964) [[hep-ph](#)].

- [264] P. Arnold, “Multi-particle potentials from light-like Wilson lines in quark-gluon plasmas: a generalized relation of in-medium splitting rates to jet-quenching parameters \hat{q} ,” *Phys. Rev. D*, vol. 99, no. 5, p. 054017, 2019. DOI: [10.1103/PhysRevD.99.054017](https://doi.org/10.1103/PhysRevD.99.054017). arXiv: [1901.05475](https://arxiv.org/abs/1901.05475) [[hep-ph](#)].
- [265] R. Baier, A. H. Mueller, D. Schiff, and D. T. Son, “‘Bottom up’ thermalization in heavy ion collisions,” *Phys. Lett. B*, vol. 502, pp. 51–58, 2001. DOI: [10.1016/S0370-2693\(01\)00191-5](https://doi.org/10.1016/S0370-2693(01)00191-5). arXiv: [hep-ph/0009237](https://arxiv.org/abs/hep-ph/0009237).
- [266] B. Schenke, C. Gale, and S. Jeon, “MARTINI: An Event generator for relativistic heavy-ion collisions,” *Phys. Rev. C*, vol. 80, p. 054913, 2009. DOI: [10.1103/PhysRevC.80.054913](https://doi.org/10.1103/PhysRevC.80.054913). arXiv: [0909.2037](https://arxiv.org/abs/0909.2037) [[hep-ph](#)].
- [267] Y. Mehtar-Tani and S. Schlichting, “Universal quark to gluon ratio in medium-induced parton cascade,” *JHEP*, vol. 09, p. 144, 2018. DOI: [10.1007/JHEP09\(2018\)144](https://doi.org/10.1007/JHEP09(2018)144). arXiv: [1807.06181](https://arxiv.org/abs/1807.06181) [[hep-ph](#)].
- [268] J.-P. Blaizot, Y. Mehtar-Tani, and M. A. C. Torres, “Angular structure of the in-medium QCD cascade,” *Phys. Rev. Lett.*, vol. 114, no. 22, p. 222002, 2015. DOI: [10.1103/PhysRevLett.114.222002](https://doi.org/10.1103/PhysRevLett.114.222002). arXiv: [1407.0326](https://arxiv.org/abs/1407.0326) [[hep-ph](#)].
- [269] K. Kutak, W. Placzek, and R. Straka, “Solutions of evolution equations for medium-induced QCD cascades,” *Eur. Phys. J. C*, vol. 79, no. 4, p. 317, 2019. DOI: [10.1140/epjc/s10052-019-6838-9](https://doi.org/10.1140/epjc/s10052-019-6838-9). arXiv: [1811.06390](https://arxiv.org/abs/1811.06390) [[hep-ph](#)].
- [270] M. Rohrmoser, “The TMDICE Monte Carlo shower program and algorithm for jet-fragmentation via coherent medium induced radiations and scattering,” *Comput. Phys. Commun.*, vol. 276, p. 108343, 2022. DOI: [10.1016/j.cpc.2022.108343](https://doi.org/10.1016/j.cpc.2022.108343). arXiv: [2111.00323](https://arxiv.org/abs/2111.00323) [[hep-ph](#)].
- [271] J.-P. Blaizot, E. Iancu, and Y. Mehtar-Tani, “Medium-induced QCD cascade: democratic branching and wave turbulence,” *Phys. Rev. Lett.*, vol. 111, p. 052001, 2013. DOI: [10.1103/PhysRevLett.111.052001](https://doi.org/10.1103/PhysRevLett.111.052001). arXiv: [1301.6102](https://arxiv.org/abs/1301.6102) [[hep-ph](#)].
- [272] V. E. Zakharov, V. S. L’vov, and G. Falkovich, *Kolmogorov spectra of turbulence I: Wave turbulence*. Springer Science & Business Media, 2012.
- [273] R. Baier, Y. L. Dokshitzer, A. H. Mueller, and D. Schiff, “Quenching of hadron spectra in media,” *JHEP*, vol. 09, p. 033, 2001. DOI: [10.1088/1126-6708/2001/09/033](https://doi.org/10.1088/1126-6708/2001/09/033). arXiv: [hep-ph/0106347](https://arxiv.org/abs/hep-ph/0106347).
- [274] K. Golec-Biernat, S. Jadach, W. Placzek, and M. Skrzypek, “Solving QCD evolution equations in rapidity space with Markovian Monte Carlo,” *Acta Phys. Polon. B*, vol. 39, pp. 115–146, 2008, [Erratum: *Acta Phys. Polon.* 40, 213 (2009)]. arXiv: [0708.1906](https://arxiv.org/abs/0708.1906) [[hep-ph](#)].
- [275] R. Enberg, K. J. Golec-Biernat, and S. Munier, “The High energy asymptotics of scattering processes in QCD,” *Phys. Rev. D*, vol. 72, p. 074021, 2005. DOI: [10.1103/PhysRevD.72.074021](https://doi.org/10.1103/PhysRevD.72.074021). arXiv: [hep-ph/0505101](https://arxiv.org/abs/hep-ph/0505101).

- [276] R. Enberg and R. B. Peschanski, “Infrared instability from nonlinear QCD evolution,” *Nucl. Phys. A*, vol. 767, pp. 189–205, 2006. DOI: [10.1016/j.nuclphysa.2005.12.012](https://doi.org/10.1016/j.nuclphysa.2005.12.012). arXiv: [hep-ph/0510352](https://arxiv.org/abs/hep-ph/0510352).
- [277] “Measurement of transverse momentum flow relative to the dijet system in PbPb and pp collisions at $\sqrt{s_{NN}} = 2.76$ TeV,” 2014.
- [278] P. Caucal, E. Iancu., A. H. Mueller, and G. Soyez, “A new pQCD based Monte Carlo event generator for jets in the quark-gluon plasma,” *PoS*, vol. HardProbes2018, D. d’Enterria, A. Morsch, and P. Crochet, Eds., p. 028, 2019. DOI: [10.22323/1.345.0028](https://doi.org/10.22323/1.345.0028). arXiv: [1812.05393](https://arxiv.org/abs/1812.05393) [[hep-ph](https://arxiv.org/abs/hep-ph)].
- [279] K. C. Zapp, “JEWEL 2.0.0: directions for use,” *Eur. Phys. J. C*, vol. 74, no. 2, p. 2762, 2014. DOI: [10.1140/epjc/s10052-014-2762-1](https://doi.org/10.1140/epjc/s10052-014-2762-1). arXiv: [1311.0048](https://arxiv.org/abs/1311.0048) [[hep-ph](https://arxiv.org/abs/hep-ph)].
- [280] G. P. Lepage and S. J. Brodsky, “Exclusive Processes in Perturbative Quantum Chromodynamics,” *Phys. Rev. D*, vol. 22, p. 2157, 1980. DOI: [10.1103/PhysRevD.22.2157](https://doi.org/10.1103/PhysRevD.22.2157).
- [281] S. J. Brodsky and G. P. Lepage, “Exclusive Processes in Quantum Chromodynamics,” *Adv. Ser. Direct. High Energy Phys.*, vol. 5, pp. 93–240, 1989. DOI: [10.1142/9789814503266_0002](https://doi.org/10.1142/9789814503266_0002).
- [282] S. J. Brodsky, H.-C. Pauli, and S. S. Pinsky, “Quantum chromodynamics and other field theories on the light cone,” *Phys. Rept.*, vol. 301, pp. 299–486, 1998. DOI: [10.1016/S0370-1573\(97\)00089-6](https://doi.org/10.1016/S0370-1573(97)00089-6). arXiv: [hep-ph/9705477](https://arxiv.org/abs/hep-ph/9705477).
- [283] W.-M. Zhang and A. Harindranath, “Light front QCD. 2: Two component theory,” *Phys. Rev. D*, vol. 48, pp. 4881–4902, 1993. DOI: [10.1103/PhysRevD.48.4881](https://doi.org/10.1103/PhysRevD.48.4881).
- [284] H. Mellin, *Zur Theorie zweier allgemeinen Klassen bestimmter Integrale, von Hj. Mellin*. Ex officina typographica Societatis litterariae fennicae, 1897.
- [285] H. Georgi and H. D. Politzer, “Electroproduction scaling in an asymptotically free theory of strong interactions,” *Phys. Rev. D*, vol. 9, pp. 416–420, 1974. DOI: [10.1103/PhysRevD.9.416](https://doi.org/10.1103/PhysRevD.9.416).
- [286] D. J. Gross and F. Wilczek, “Asymptotically Free Gauge Theories - II,” *Phys. Rev. D*, vol. 9, pp. 980–993, 1974. DOI: [10.1103/PhysRevD.9.980](https://doi.org/10.1103/PhysRevD.9.980).
- [287] L. Dixon, “Calculating scattering amplitudes efficiently,” *arXiv preprint hep-ph/9601359*, 1996.